Running Dynamic Properties of Small-Radius Railway Wheels

vorgelegt von
Shiping Dongfang
M. Eng.

an der Fakultät V – Verkehrs- und Maschinensysteme
der Technischen Universität Berlin
zur Erlangung des akademischen Grades

Doktor der Ingenieurwissenschaften
– Dr. -Ing. –

genehmigte Dissertation

Promotionsausschuss:

Vorsitzender: Prof. Dr. -Ing. Birgit Milius
Gutachter: Prof. Dr. -Ing. Markus Hecht
Gutachter: dr hab. inż. Bartosz Firlik

Tag der wissenschaftlichen Aussprache: 26. März 2021

Berlin 2021

Acknowledgements

The completion of this dissertation would not have been possible without the guidance and support of the following persons and organizations, towards whom I would like to extend my most sincere gratitude.

My greatest appreciation goes to Prof. Dr.-Ing. Markus Hecht who leads the Chair of Rail Vehicles at Technische Universität Berlin and has taken the role as my mentor for my five years at his department. From the selection of this contemporary and highly relevant topic to the European railway industry to the detailed content discussion and guidance during the research process, from the coordination of industrial projects that support the research in terms of data and resource access outside the department to the organization of computation resources and further funding within the university, Professor Hecht has been along for every step of the way with great patience and readiness to provide guidance, offering insight and advice that ultimately kept me on track for a rather smooth research progress.

This doctoral research is made possible with a four-year funding provided by the China Scholarship Council. A further financial support for the final four months of the research is provided by the Technische Universität Berlin through its STIBET project. I am profoundly grateful for the funding that enabled my stay in Germany as well as to focus on the academic work with little financial concerns.

Much of the research also benefitted from the insightful discussions and technical support with the colleagues at the Chair of Rail Vehicles. Many gridlocks in the logical analysis or the usage of certain methods and software were able to be resolved only with the expertise of the colleagues, who time and again provided inspirations and shared their valuable experience in their respective fields. Special thanks go to my fellow vehicle system dynamics specialists Dr.-Ing. Gernoth Götz, Dr.-Ing. Daniel Jobstfinke, Mirko Leiste, Florian Peche and Márton Pálinkó for the expertise that they selflessly spared in time of need, as well as Jonas Vuitton and Hanno Vetter for their IT support which was instrumental for the extensive simulation work involved in the research.

Special thanks go to Nathalie Korf, a close friend and fellow scientist at Technische Universität Berlin, who proofread the German abstract of this thesis and helped greatly to improve its concision in both linguistic and scientific terms, as well as to Zhiting “Thomasina” Cai, my sister-like friend and fellow railway vehicle engineer, for all the thought exchanges during the preparation and rehearsal of the oral defence as well as the family-like spiritual support.

Also, I would like to explicitly acknowledge my parents Prof. Dr. Yang Dongfang and Danxia Bi not only for their emotional and financial support, but also for their encouragement and advice through the sharing of their own academic experience.

Last but not least, a special expression of gratitude goes towards my best friends Irina Nurutdinova, Fangming Tian, Yingjian Hu, as well as my friends from the Kleines Sinfonisches Orchester (KSO) of Collegium Musicum Berlin with which I played horn during my doctoral period. Their indispensable love and accompaniment, as well as their selfless support in times of distress and depression, each in their most unique and significant ways, kept me ready for challenges along the way.

Abstract

Wheels are components of decisive significance for rail vehicles in terms of properties such as structural strength, running quality and space for loading or interior layout. Using small wheels allows a further lowering of the floor throughout the full length of the vehicle, which exploits more loading space above running gears for freight wagons, enables drive-on/off loading of taller road vehicles for auto transporter wagons and provides room for bi-level gangways for double-deck coaches. However, with smaller wheels, running stability is expected to decrease and the tread becomes more susceptible to wear. It is thus worth investigating whether it is possible to use unconventionally small wheels in favor of their benefits in vehicle capacity increase and layout design without causing an excessive deficit of its running dynamics properties. Understanding the extent of the running dynamics behaviour deterioration associated with smaller wheels and identifying possible remedies are important first steps for this investigation. These constitute the goals of this dissertation: (1) to determine how the running dynamics behaviour of a common rail vehicle changes with wheel radii varying into an unconventionally small range; (2) to test the effect of certain proposed modifications to the running gear in restoring the dynamics performance lost through the use of small wheels.

This dissertation takes a numerical approach, obtaining the behaviour of a selected reference vehicle through conducting time-domain integrations with its multibody simulation (MBS) model with its wheel radius set as a varying parameter. The reference vehicle in question is chosen as a generic freight wagon with Y25 two-axle single-frame bogies. The stability, the curve negotiation, and wear behaviour of the vehicle with wheel radii ranging from 140 mm to 500 mm are analyzed, once for the original vehicle without any corrective modifications to ascertain the hypothetic consequences of using smaller wheels, then once again after two proposed modifications are implemented to assess the effectiveness of the countermeasures both individually and in combination. The specific modifications proposed are the scaling of the wheel profile with a factor dependent on the wheel radius and the use of a radial steering mechanism.

The simulation results indicate that for a Y25 bogie using its original wheel profile, the decrease in wheel size without introducing further modifications causes a significant decrease in the vehicle's non-linear critical speed and a significant increase in tread wear, whereas its theoretically expected benefit on curve negotiation is minimal. The addition of a functioning radial steering mechanism is able to restore the wear and stability behaviour of the small-wheeled vehicle, bringing the three aspects of dynamics performance back into balance. On the other hand, a wheel-radius-dependent scaling of the wheel profile, in which the scaling factor is chosen to be equal to the ratio of the actual wheel radius against the standard wheel radius of the reference Y25 bogie, benefits stability beyond practical demand at the sacrifice of severe deteriorations for curving and wear properties both with and without the simultaneous implementation of the radial steering mechanism.

In the practical sense, the research suggests that small wheels may be applicable for operational railway vehicles in the running dynamics' point of view, since there exists the use of radial steering as a working countermeasure against the performance loss associated with the wheel size reduction.

Keywords: rail vehicles; small wheels; running dynamics; wheel profile modification; radial steering

Zusammenfassung

Eisenbahnräder sind Schienenfahrzeugkomponenten von entscheidender Bedeutung, unter anderem in Bezug auf die Festigkeit, die Laufqualität und der Raum für Ladung oder Innenraumgestaltung. Die Anwendung von kleinen Rädern ermöglicht eine tiefe Bodenhöhe über die gesamte Wagenlänge, wodurch zusätzlicher Raum über den Laufwerken für Güterbeladung genutzt werden kann. Zudem wird das Auf- und Abfahren von größeren Straßenfahrzeugen auf/von einem Eisenbahn-Autotransportwagen sowie die Gestaltung von Durchgängen auf beide Etagen eines Doppelstock-Reisezugwagens ermöglicht. Mit kleineren Rädern muss man hingegen mit Stabilitätsverlust des Schienenfahrzeuges und erhöhter Verschleißanfälligkeit der Räder rechnen. Daher ist es von Interesse, ob es möglich ist, zugunsten der Vorteile von Kapazitätserhöhung und Innenraumgestaltung außergewöhnlich kleine Räder einzusetzen, ohne eine unverhältnismäßig starke Verschlechterung der Laufdynamik des Fahrzeuges. Wichtige erste Schritte hierfür sind sowohl ein Verständnis fürs Ausmaß der Fahrdynamikverschlechterung aufgrund außergewöhnlich kleiner Radgrößen zu entwickeln als auch die Identifizierung von Gegenmaßnahmen. Aus diesen Aspekten leiten sich die zwei Ziele dieser Doktorarbeit ab: (1) zu untersuchen, wie sich die klassischen fahrzeugdynamischen Eigenschaften mit der Radgröße ändern bis zu einem ungewöhnlich kleinen Radradius; (2) zu überprüfen, inwiefern vorgeschlagene Änderungen am Laufwerk der kleinradbedingten Dynamikverschlechterung entgegenwirken können.

Diese Doktorarbeit geht numerisch vor und erzeugt durch Multikörpersimulation (MBS: engl. für „Multibody Simulation“) die laufdynamischen Verhältnisse eines Referenzfahrzeuges mit zweiachsigen Festrahmen-Drehgestellen des Typs Y25, wobei der Radradius zwischen 140 mm und 500 mm variiert. Untersucht werden die Laufstabilität sowie die Bogenfahrt- und Radverschleißverhältnisse des Fahrzeuges, zuerst mit dem ursprünglichen Fahrzeug ohne jegliche Modifizierung am Laufwerk zwecks Ermittlung vermuteter Folgen der Radverkleinerung, dann jeweils nach der Anwendung der beiden vorgeschlagenen Gegenmaßnahmen (sowohl individuell als auch kombiniert) für die Auswertung ihrer Effekte. Die hier vorgeschlagenen Maßnahmen sind zum einen eine radradiusabhängige Skalierung des Radprofils und zum anderen die Anwendung eines Radialeinstellungsmechanismus.

Die Simulationsergebnisse zeigen, dass die Stabilität und das Verschleißverhältnis des Y25-Drehgestells mit ursprünglichem Radprofil mit einer Verkleinerung des Rades deutlich verschlechtern, wohingegen die theoretisch zu erwartende Bogenfahrtverschonung nur geringfügig ist; vorausgesetzt, dass keine weiteren Veränderungen gemacht werden. Ein Radialeinstellungsmechanismus kann die Stabilität und das Verschleißverhältnis ausbessern und einen besseren Ausgleich zwischen den drei Aspekten der Fahrzeugdynamik schaffen. Eine Radprofilskalierung hingegen, mit einem Faktor, der dem Quotienten aus dem aktuell betrachteten und dem ursprünglichen Radradien des Y25-Referenzdrehgestells entspricht, verbessert die Stabilität übermäßig auf Kosten von starken Verschlechterungen der Bogenfahrt- und Verschleißeigenschaften, unabhängig vom Einsatz der Radialeinstellung.

Die Arbeit stellt vor, dass es möglich ist, kleine Räder mit verlässlicher Laufdynamik im Betrieb einzusetzen, da mit der Radialeinstellung eine funktionierende Gegenmaßnahme zur Verschlechterung der fahrzeugdynamischen Eigenschaften durch die Radverkleinerung besteht.

Schlüsselwörter: Schienenfahrzeuge; kleine Räder; Laufdynamik; Radprofilanpassung; Radialeinstellung

Table of Contents

List of Figures

Note: figures in Appendix C – Appendix G are omitted from the list of figures.

List of Tables

List of Notations and Abbreviations

a	Linear acceleration
A	Amplitude of an oscillation
d	Damping coefficient of a suspension element
D_0	Nominal rolling diameter of a wheel
δ_L	Contact angle on left wheel
δ_R	Contact angle on right wheel
Δy	Lateral offset from track centreline
e	Half of the lateral distance between wheel-rail contact points on the left and right wheels of a wheelset in ideally centred position
f	Scaling factor for z-coordinates of modified wheel profile points
γ_i	Wheel-rail contact creepage in direction i
h_{CG}	Height of centre of gravity above rail level
k	Stiffness of a suspension element
K_y	Gravitational stiffness of a wheelset
Λ	Wavelength of a motion or a wave
λ	Conicity of conical-treaded wheelsets
λ_e	Equivalent conicity of a wheelset with non-conical treads (Optional superscript for distinguishing equivalent calculation method)
m	Mass
M_z	Wheel-rail contact spin torque (around z-axis by definition)
ν_z	Wheel-rail contact spin creepage (around z-axis by definition)
P_0	Total quasistatic vertical load on a wheelset (axle load)
Q	Wheel-rail vertical force
R	Curve radius
r_0	Nominal rolling radius of a wheel
r_L	Rolling radius of left wheel of a wheelset
r_R	Rolling radius of right wheel of a wheelset
T_i	Wheel-rail contact creep force in direction i
v	Travel speed of a vehicle
v_c^L	Linear critical speed of a vehicle
v_c^{NL}	Non-linear critical speed of a vehicle
Y	Wheel-rail lateral force
DAE	Differential-algebraic equation
EMU/DMU	Electric multiple unit / diesel multiple unit
FEM	Finite element model
MBS	Multibody simulation
NLVc	Non-linear critical speed
ODE	Ordinary differential equation
PRR	Rail profile
PRW	Wheel profile

1 Introduction

1.1 Motivation

1.1.1 Freight wagons: the need for capacity

A freight vehicle's capacity is not only limited in terms of weight, but also by the available loading volume. Rail freight transport also handles voluminous cargo, which has a relatively low density and exhausts the loading space of the vehicle before reaching the maximum loading mass. For a closed loading space such as that of a box car, a gondola car or a container, the loading volume capacity is obviously characterized by its interior dimensions.

Aside from fully exploiting the available space within the upper part of the rolling stock loading gauge by heightening, lengthening or broadening the carbody, another possibility is to make the space underneath the wagon available for loading cargo. This becomes necessary when the vehicle loading gauge relevant to the local railway system restricts the expansion of the loading space in other directions, but the demand for transporting larger or taller goods and more volume capacity exists. There exist cases of lower space exploitation such as flat wagons with lowered or even hollow floor between the running gears (also referred to as pocket wagons) and gondola cars or open wagons with the so-called "bathtub" carbody structure as shown in Figure 1.1. In some railway systems, low-floor flat wagons and pocket wagons with lower loading planes have enabled loading double-stacked containers or large semitrailers on freight wagons without significant expanding their respective loading gauge profiles in the vertical direction.

Figure 1.1 Examples of lower space usage in freight wagons of China Railways. Above: Class JSQ6 double-deck automobile transport wagon with a low-floor section between the running gears. Below: Class C80 bathtub-shaped coal wagon (exterior and interior), notice the additional cargo room made possible by arching the floor downward on either side of the chassis' central beam.

However, the greatest difficulty lies in exploiting the space above the bogies. Under the condition that the bogie retains the classical singular-frame or three-piece bogie form with ordinary wheelsets, in which the wheelset shafts run across the width of the wagon, the floor in the bogie area must be raised to clear the shafts and even higher on either side to clear the wheels. Thus, the size of the wheels practically determines how low the floor above the bogies can be set for such railway vehicles.

With the example of European freight wagons with Y25 bogies [1], whose wheels have a nominal diameter of 920 mm and EN 13715 - S1002/h30/e30/15% profile [2] with a flange height of 30 mm, the highest point of the wheel stands 920 mm + 30 mm = 950 mm above rail level when vehicle is in standstill on a perfectly centralized position on the track, forcing the floor height above the bogies to go well over 1 m above rail level in most applications (some examples see Table 1.1). Assuming that the wagon has 2 bogies, neither of which protrude longitudinally beyond the length of the floor (ruling out bogies used in articulated wagon configurations), being able to half the nominal wheel diameter would mean allowing the height of the floor over at least the length of two bogie lengths (per bogie 3250 mm in the instance of the Y25 bogie plus approximately 100 mm redundancy clearance, summing to 6700 mm) to drop by an equal amount, namely 460 mm; for a wagon conforming to and maximally exploiting the European G1 dynamic loading gauge, which limits the width of the part of the wagon's cross section between 400 mm and 1170 mm above rail level to 3240 mm [3], the lowering of the floor would create a total of $6700\ \text{mm} \times 460\ \text{mm} \times 3240\ \text{mm} = 9.98568 \times 10^9\ \text{mm}^2$, which is nearly 10 m^3, or circa 1/10 to 1/8 of the total loading volume compared to an average European type T grain gondola car.

Table 1.1 Examples of floor heights of European freight wagons, taken from the product catalogue of the Slovak freight wagon manufacturer Tatravagónka Poprad

Wagon type	Description	Floor height (mm)
Rbnpss	Long goods freight wagon with 2 Y25Ls(s) bogies	1560
Sggrss 80'	Articulated container flat wagon with 3 Y25Ls(s) bogies	1170
Sdggmrss	Articulated pocket wagon with 3 Y25Ls(s)i1 or Y25Ls(s)i1f bogies	1155
Habii(ll)nss	Covered wagon with sliding walls and 2 TVP2007 bogies	1200
Laes	Articulated double-deck car transporter with 3 single wheelsets	640 (lower) 2830 (upper)

A consistently low floor is especially of great significance for automobile transporters, since it allows for easier loading onto and parking of larger automobiles on the wagons. A semi truck or a bus risks vertically extruding the European rolling stock loading gauge if loaded onto ordinary high-floor flat wagons. Though they can be transported on wagons with a low-floor section between the bogies, the alternating high- and low-floor sections either form ledges that prevent loading the road vehicles from the end of the wagon, or a slope which leaves a greater length of the wagon floor at an inconveniently high level above rail level. One existing example of solution is the Rolling Highway (RoLa) wagons produced by Waggonbau Niesky. The Austrian carrier ÖBB Rail Cargo Operator currently operates these wagons. Each wagon has 8 wheelsets with an extraordinarily small maximum nominal wheel diameter of 360 mm and a loading deck height of as low as 410 mm above rail level [4, 5]. This allows trucks to be driven onto the wagon floor from one end, through the entire train to be parked, and off the other end while unloading, significantly simplifying the loading process. ÖBB Rail Cargo Operator allows tractor trailers up to 4 m tall and 2.6 m wide to be transported on RoLa wagons on the routes Wörgl

– Brenner, Wörgl – Trento, Wels – Maribor and Salzburg – Fernetti [6], although a close examination of the available rolling stock loading gauges for the parts of Europe with normal-gauge railways show that such a load is only compatible with the most tolerant GB2 gauge profile and would violate all other loading gauges [3]. As another example, the double-deck automobile transporters of the Sylt Shuttle operated by the German carrier DB allow for loads with a height of 2.7 m and 1.65 m on the upper and lower decks respectively [7]. Referring to the height of common vehicles given by [8], the lower deck only has enough vertical clearance to transport vehicles as large as some smaller compact vans or SUVs. If the floor height can be dropped a further 460 mm through the use of smaller wheels, the lower deck clearance can be enlarged to 2.11 m which would allow loading larger pickup trucks or utility vans.

The types of freight wagons mentioned above see an increase in operational economy through the enabling of a lower floor height throughout the entire length, which can made possible by implementing smaller wheels. Voluminous cargo wagons become more spacious, allowing for the transport of more goods with the use of less wagons. The more convenient loading and unloading of bulky on and off automobile transport wagons saves the use of expensive cranes and specialized loading infrastructure.

1.1.2 Passenger coaches: more seating space and convenient thoroughfare inside the cabin

Although passenger coaches seldom become loaded up to the weight limit and never up to the spatial limit, having more interior room means being able to provide more passenger space for better comfort in normal passenger volume conditions as well as more passenger capacity during peak transit periods. A more regular interior profile and an even-height floor also helps provide more freedom in arranging seats, standing areas and luggage or bicycle areas anywhere within the cabin.

For most double-deck coaches, there also exists the difficulty in fully utilizing the space above bogies. In most cases, the lower deck is lowered between the bogies with staircases built into the transition area between the lower deck and the over-bogie section. From the end of the staircase to the end of the coach, the roof clearance is much higher than that on either the upper or the lower deck, but the vertical interior height is not enough to be separated into two levels. This high roof area is then lowered into a platform for equipment such as air conditioning and pantographs. Figure 1.2 shows some examples of double-deck coaches. Note the length of the single-deck section and concave roof area of the middle deck. If the floor in the single deck section can be lowered, leaving vertical room for another deck to be built above, in other words allowing an extension of the upper deck floor to the end of the coach, more floor area for seating passengers would be provided. The Stadler KISS EMUs' lower deck floor is typically 440 mm above rail level [9], which is already close to the height that could be realized by implementing wheels with diameters around 400 mm without or with minimal local protruding of the floor profile in the wheel area.

Passenger thoroughfare can also be made possible on both decks. As an existing example, the French high-speed EMU TGV Duplex (Figure 1.3) only has gangways on the upper deck, whose floor extends throughout the entire length of the car. The lower deck cannot be walked through, and has one dead end with an equipment chamber and an open end leading to the door area, where the stairs leading to the upper deck is located and a lavatory is built into the bend of the staircase. Though both decks are tall enough for passengers to walk through, additional gangways cannot be added to the lower deck due to

(a)

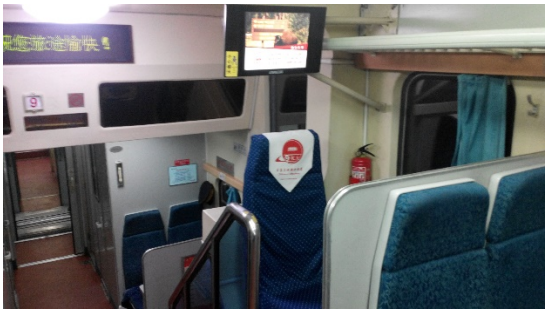

(b)

(c)

(d)

Figure 1.2 Examples of conventional double-deck passenger coaches with interior views of their respective over-bogie sections

(a) China Railway Class SYZ25K double-deck second-class coach
(b) DB Regio Bombardier 4th generation double-deck coach
(c) NS Class VIRM double-deck EMU
(d) CFL Stadler KISS double-deck EMU

the bulky Jacobs bogies and equipment chamber blocking the coaches' ends. However, given that the bogie can be made far smaller and equipment can be otherwise arranged, the space for another lower-level gangway would be made available. Since the lower deck would then have an even floor height throughout the entire length of the coach, as long as the interior arrangement leaves both the gangway and the cabin corridor enough width for wheelchair movement throughout the train, the whole train

throughout its length has the potential to be barrier-free. Mobility impaired passengers would thus no longer be confined within an area of the lower deck only as long as the longitudinal spacing between the two running gears. The prospects of improving the efficiency of interior arrangements with gangways on both levels of double-deck coaches is demonstrated in the dissertation of Künzel [10].

Additionally, having even floor heights on either deck also helps increase the "modularizability" of the interior layout, in which the positioning of seats, multipurpose areas and equipment throughout the cabin can be more flexible. The area over the bogies would no longer need to be specially considered but can be used to arrange cabin modules or full-height equipment chambers like any other area.

(a) (b)

(c) (d)

Figure 1.3 TGV Duplex EMU intermediate car layout
(a) external view of the gangway and entrance areas
(b) entrance area viewed from the upper deck gangway
(c) lower deck cabin seen from the entrance area
(d) gangway viewed from the end of the upper deck cabin

1.1.3 Applicability: dynamical soundness and maintainability

Despite the positive effects on interior space maximization, wheels with small diameters are seldom used in heavy rail and metro vehicles. Wheel diameters below 650 mm (for new wheels) are rare in all applications and almost only seen in leading and trailing wheels in narrow-gauge steam locomotives.

Table 1.2 Nominal wheel diameter of some German tractive stock up to 1995

Steam locomotives			
Class designation	Wheel diameter (mm)		
	Leading	Traction	Trailing
DR 52	850	1400	N/A
DR 03.10	1000	2000	1250
DR 86	850	1400	850
DR 95	850	1400	850
Electric locomotives			
Class designation	Wheel configuration (UIC notation)	Wheel diameter (mm)	
		Traction	Trailing
DR E 04	1'Co1'	1600	1000
DR E 60	1'C	1250	850
DR E 18	1'Do1'	1600	1000
DBAG 155	Co'Co'	1250	N/A
DBAG 110, 113, 751	Bo'Bo'	1250	N/A
DBAG 181.0, 181.2	Bo'Bo'	1250	N/A
DR 99.480[1]	500	850	N/A

Diesel locomotives		
Class designation	Wheel configuration (UIC notation)	Wheel diameter (mm)
DB V 200.0, V 200.1	B'B'	950
DB V 100	B'B'	950
DB 230-232, 234, 754	Co'Co'	1050
DB 344	D	1100
DB 310, 323/324	B	850
Electric multiple units		
Class designation	Wheel diameter (mm)	
	Traction	Trailing
DBAG 401, 402	1040	Not given in the reference
DB 403	1050	N/A
DBAG 450[2]	740	740
DBAG 485	850	N/A
DBAG 480	900	N/A
Diesel multiple units		
Class designation	Wheel diameter (mm)	
	Traction	Trailing
DB VT 11.5 “TEE”	970	900
DB VT 18.16	950	950
DB 610	890	Not given in the reference
DBAG 628.0	760	Not given in the reference
DB 771	900	900
DB 798	900	Not given in the reference

[1] 750 mm gauge
[2] Karlsruhe tram-train class GT8-100C/2S

A 1995 publication provides a summary of technical parameters of powered stock in Germany up to that date [11]. Some typical wheel nominal diameters given therein are collected in Table 1.2.

Even smaller wheels emerged in some European rail vehicles developed shortly after the period mentioned above. According to Riechers [12], in 1996 Talbot rolled out the earliest version of the diesel multiple unit Talent, which uses non-powered Jacobs bogies featuring wheels with a nominal diameter of 630 mm (wear limit 570 mm). This enables a continuous 800 mm low-floor section across cars of the

Figure 1.4 Talent DMU operated by Niederbarnimer Eisenbahn (NEB) in Berlin and Brandenburg, Germany

Figure 1.5 Siemens-DUEWAG RegioSprinter1 operated by Lokalbanen in Copenhagen, Denmark

same unit. Riechers [12] also introduces that in 1995 Siemens-DUEWAG presented its RegioSprinter1 diesel-mechanic multiple unit with three cars, whose middle car is short (carbody length 4100 mm) and sits on one non-powered bogie equipped with 520 mm (wear limit 480 mm) monobloc wheels. The wheels are so small that the wheel body is used in its entirety as a brake disc. The bogie still possesses two levels of suspension, meanwhile allowing for a 530 mm floor height in 75% of the cabin. Figure 1.4 and Figure 1.5 show the two examples respectively, focusing on the small-wheeled bogies and the low floor cabin that result thereof.

The realization of more low-floor section proportion through the use of smaller wheels, on the other hand, results in worse running behaviour of the units, which manifests itself most noticeably in the reduced passenger comfort. Theoretically, passenger discomfort arises from an excess of carbody oscillation acceleration in the lateral and vertical directions. Transitioning between straight and curved track sections, passing switch frogs and running on a track with pronounced irregularity cause excitations to the vehicle system. On the one hand, these excitations trigger direct oscillations within the vehicle, passing upward through the suspension into the carbody to be felt by the passengers, causing discomfort. In 1997, the Berlin-based railroad passenger association published a subjective comparison of six commuter DMUs from the perspective of passenger experience [13] which involved the Talent and the RegioSprinter1. Though the comfort of both units is positively commended, the article does point out that the RegioSprinter1 experiences strong shocks when running over switch frogs and has a hard and uncomfortable curving behaviour. On the other hand, lateral excitations from the track arouse the vehicle to go into the self-excited lateral-yaw-combined oscillation known as hunting motion which, if becoming unstable, causes severe accelerations in the lateral and roll directions. Klingel [14] has shown that the hunting motion ideally follows a wave form trajectory with a wavelength independent of the vehicle's speed of travel but in direct relationship to the rolling radius of the wheel. Reducing the wheel size would thus reduce the wavelength. When the vehicle is travelling at a given speed, the lateral oscillation frequency of the vehicle is thus in inverse relationship to the wavelength. The higher the frequency of an oscillatory motion, the more acceleration the oscillating body undergoes. Thus, a vehicle with a smaller wheelset would be subject to more violent oscillation when hunting motion occurs.

In aspects outside the scope of classical vehicle system dynamics, behaviour has also been perceived as tendentially unpromising for vehicles with smaller wheels.

A smaller wheel diameter is synonymous to a larger curvature on the rolling circle, which tends to reduce the wheel-rail contact patch area, resulting in larger contact stresses on the tread; additionally, the wheel also has a smaller circumference, meaning that the wheel needs to rotate more revolutions to cover the same travelling distance. Both the increased contact stress and the increased number of loading cycles throughout the wheelset's life cycle cause earlier fatigue damage to the tread. UIC 510-2 [15] thus has an axle load limit for wheelsets with different diameters, in which wheelsets with wheel diameters between 330 mm and 390 mm are only permitted a 5 t axle load in normal cases, whereas a wheelset with 920 mm wheels can be loaded up to 20 t or more.

When the wheel becomes smaller, it tendentially becomes increasingly comparable (though still magnitudes larger) in size to gaps in the rail, most notably at rail joints or switch frogs. When passing gaps, a smaller wheel falls deeper into the gap, causing the contact with the edge of the gap in the forward direction to interact with the wheel in a more horizontal direction, thus causing more resistance and

impact to the rolling wheel. This not only impedes vehicle movement but also threatens damage to both the tread and the rail in the gap area. In some European networks, there exist obtuse track crossings similar to switch frogs even in curved track sections. As the wheel's size reduces, the overlapping area of the flange on the rail tends to approach the length of the crossing gap, which for obtuse crossings may be rather large. As a result, the wheelset may not be properly guided in the crossing gap, as the flange is too short to have its leading edge cross over to the other side of the gap before its trailing edge leaves the rear end of the gap or as the wheel yaws reacting to an irregularity. When the crossing is in a track curve, this unguided gap section may result in the loss of necessary guidance force generation required to negotiate the curve, causing a subsequent impact when the flange does bridge over to the rail beyond the gap, or even a rail climb or a catastrophic derailment event. The European rail vehicle acceptance standard EN 14363 [16] includes an informative appendix that recommends an additional assessment of the vehicle's behaviour in obtuse crossings on curves for vehicles that use small wheels.

In the end, the possibility to apply small wheels to railroad vehicles is generally perceived as remote, as a suitable running dynamics behaviour as well as the associated ride comfort cannot be sufficiently guaranteed, the maintenance of the wheel system becomes intensive beyond feasible, and the safety while passing switch or obtuse crossing is questionable. As further regulations regarding vehicle acceptance and operational safety develop, product requirements for wheel systems have factually excluded the use of wheels of extraordinarily small sizes. Though a clearly worded ban does not exist, the additional proof that must be presented and the calculation and testing workload required to provide this evidence in order for newly designed small-wheeled vehicles to receive vehicle acceptance and be legally pronounced fit for operation strongly demotivates manufacturers to develop their rail vehicle products in this direction. Development of small-wheeled solutions becomes burdensome and financially less profitable than solutions with rather conventional designs. This leaves very few exemplars of small-wheeled vehicles on the rail vehicle market, with the RoLa automobile transport wagons mentioned above as one of the few, if not the only, successful example still in operation. Further, since there are neither such products nor the desire by manufacturers to develop these products, there is consequently very little research done investigating the practicability of very small wheel sizes in any viewpoint. Prior knowledge on the behaviour of vehicles with very small wheels or how the wheel size factors into the change of running dynamics behaviour into the very small wheel size ranges is severely limited.

1.2 Goals of this research

With this dissertation, the author intends to explore the running dynamics behaviour of rail vehicles using unconventionally small wheels, specifically for bogies retaining the conventional two-axle, singular-framed form commonly used in European railroads. The running dynamics behaviour to assess is in terms of classical vehicle system dynamics, namely the running stability in terms of critical speed, curve negotiation behaviour of the vehicle in terms of guidance force, track-shift force and risk of flange-climb derailment, as well as wear behaviour in terms of wear number.

Given that the running behaviour theoretically predicts unfavourable for the application of small-radius wheels as mentioned above in Section 1.1.3, this dissertation also intends to explore whether there exists countermeasures against the worsening of dynamics behaviour caused by the use of smaller wheels which would help them regain applicability.

Specifically, this research pursues to fulfill two major purposes:

(1) To quantify the behaviour of running stability, curve passing capability and wheel-rail contact wear associated with a decrease in nominal wheel radius. In other words, the extent of change in each aspect of running dynamics with wheel size is to be determined in quantity for a given vehicle configuration and given running scenarios.
(2) To investigate the effects of two specific countermeasures against the deterioration in running dynamics, namely a modification of the tread geometry and the addition of a radial steering mechanism, and assess whether these measures are able to bring the behaviour of the vehicle back into an applicable range.

It is worth noting that this research alone is unable to directly provide evidence or even a practically feasible recommendation for designing small-wheeled running gears in engineering practice. Due to the lack of participation from the industry and the lack of accumulated research and development experience on this topic mentioned in Section 1.1.3 above, the research is only able to provide a theoretically justifiable prediction of the running dynamics behaviour of small-wheeled two-axle singular-framed bogies with a purely simulation-based method. However, as much detail as possible to the running behaviour of the test vehicle is exploited through the simulation design and documented in this thesis to provide further studies regarding the running dynamics of small-wheeled running gears with information to build upon: tests are done for a range of practical settings for track, curve and centrifugal acceleration parameters, and details such as the stability of the vehicle at any tested speed as well as the wheel or wheelset at which the most critical loading occurs is documented where relevant. Regarding other issues of implementing small wheels such as the wheel material's wear resistance and maintainability, the arrangement of braking mechanisms and heat capacity of the wheelset under braking conditions as well as obtuse crossing passing behaviour, the author acknowledges these aspects as significant constituents of a full applicability analysis but does not aim to clarify these issues in the framework of this research. Further research must be conducted to offer field and track test data which support and complete the assessment in other aspects before this long-discontinued development can be resumed in practice with sufficient security.

2 Prior theoretical and practical knowledge

2.1 Dynamical requirements for rail vehicles

The purpose of the discipline "rail vehicle system dynamics" can be summarized as to solve problems arising from the rail vehicle's oscillating behaviour [17]. This statement can be expanded to any issue regarding the maintenance of desired running behaviour of a vehicle under the influence of forces it is subject to while running. Varying forces coming from the running surface affect the state of motion of vehicle components, and excite oscillation within the multi-body, multi-level and non-linearly suspended multi-dimensional oscillator system which the vehicle mechanically constitutes. How these forces and its resulting oscillatory motions of the vehicle contribute to the vehicle's desired running behaviour, as well as how this influence can be managed from the constructive and operational measures of the vehicle-track system, is ultimately the object of vehicle system dynamics analyses.

The "desired" dynamics behaviour of a rail vehicle depends on the scope of application of the vehicle in question. It is not difficult to intuitively require that rail vehicles remain on track at any time during running, run with limited levels of vibration in the carbody so that passenger comfort or cargo integrity does not become compromised, and be less prone to impact or wear damage. In realistic practice, official technical requirements are drawn specific to each rail transit system that quantify these requirements and specify the limit of operational soundness for each behavioural performance, as well as prescribe design and testing requirements of rail vehicles. Dynamical issues of general concern regardless of region or system include risk of derailment, degree of potential damage to the track and excessive oscillation of the carbody. Conditions of acceptance of rail vehicles for operation are to be experimentally determined as prescribed in standards such as the European EN 14363 [16], Chinese GB 5599-85 [18] and Australian AS7507, AS7508 and AS7509 [19], each with considerations for the local operational backgrounds.

Citing regulations valid for European railway networks as an example, the International Union of Railways (UIC) standard UIC 518 [20] prescribes harmonized rules regarding the requirements that rail vehicles must prove to satisfy by means of a test procedure in order to become approved for revenue service. Specific choice of test methods are given in the standard for different approval applications (new approval or expansion of existing approval, vehicle type, intended range of operation of the vehicle, etc.). During a test run on a selected test track consisting of a given number of typical track sections with different combinations of speed, superelevation deficiency[3] and curve radius and satisfying prescribed track and wheel-rail contact geometric property requirements, statistics of the vehicle's sum of guidance forces per axle, derailment coefficient, real-time vertical wheel-rail force, quasistatic wheel-rail lateral and vertical forces as well as carbody and bogie frame acclelrations in vertical and lateral directions must fall within limit values concerning soundness in safety, track fatigue and running behaviour. For instance, under requirements for safety, the sliding mean of the derailment coefficient taken over a 2 m track length may not exceed 0.8 for a freight wagon; the standard variation of the sum of guidance forces on a wheelset may not exceed a half of the limit value for the sum of guidance forces,

[3] In this dissertation, "superelevation deficiency" will be used to refer to the concept "cant deficiency" in standard terminology. This non-standard referral is intended to avoid confusion between rail cant and superelevation of the entire track, both of which are involved in this thesis.

which equals to the sum of 10 kN and one third of the axle load multiplied by a factor of 0.85 for freight wagons; under requirements for running behaviour, the acceleration measured above the bogie on the carbody of a wagon may not be over 3 m/s² and 5 m/s² in the lateral and vertical directions respectively and their RMS values may not be over 1.3 m/s² and 2 m/s² respectively. These requirements ensure that a vehicle being approved for service is safe to operate on networks whose operating conditions are consistent with the reference levels as are used in the tests. Should the vehicle be intended for operation on networks with worse conditions, additional verifications are required to ensure safety for the particular operation.

The technical specifications for interoperability for freight wagons (WAG TSI) issued by the European Commission Agency for Railways [21] likewise demands that rail vehicles be proven to provide safe movement up to the maximum design speed. It designates that proof should be provided through realistic or simulated test procedures given by the standard EN 14363 [16], which under the scope of vehicle system dynamics evaluates the railway vehicle's running safety, stress loading on track and oscillation behaviour with prescribed tests similar to UIC 518, but additionally covers non-classical-dynamics aspects such as safety of vehicles under longitudinal compressive forces while on an S-curve, investigation of twist coefficient of the carbody, stress loading on switches, obtuse crossing pass-by safety of vehicles with small wheels, etc. Most limit values of indices for dynamics performance given by EN 14363 are consistent with those required by UIC 518, while for some indices limit values are given for more detailed case classifications regarding vehicle type, axle load, load state and test condition.

2.2 The wheel radius' relation to running dynamics

The basic features of rail vehicles include guidance by tracks, the existence of hunting behaviour, low running resistance, capability of being operated in a consist (a connected group of vehicles, also referred to as "rake"), and strict clearance requirements [17]. This summary is meant for "contemporary", "true" rail vehicles as developed in the early 19th century through some 300 years of trial-and-error development [22, 23], whose guidance is realized with two wheels with flanges on the inside (side of each wheel facing the other wheel) rigidly mounted on a common axle in an assembly known most commonly as a wheelset, running on two rails [23]. This is also the type of vehicle of concern in this dissertation. Once the material for the wheels and rails transitioned from wood and stone to cast iron, for which tapering is necessary foundry practice, the wheels obtained conical profiles with the inside end thicker than the outside end, which were observed to aid guidance of the vehicles with less flange engagement, as well as give rise to a smoother passing behaviour in curved track sections. [23, 24] The conicity of the wheels results in a rolling circle diameter difference in the two wheels in case the wheelset is not rolling along the track centreline. Owing to the equal angular rotation velocity of the left and right wheels due to their fixed connection to the common axle, the centre of the wheel with the larger rolling circle a higher linear speed than the other wheel. Redtenbacher provided a geometric illustration of such a rolling situation in 1855 [25], here cited as Figure 2.1 [4]. As a result, the wheelset gyrates back towards the track's centreline as it rolls further along the track, thus neutralizing the rolling circle difference. This behaviour stands as long as no slipping occurs at the wheel-rail contact interfaces. The combination of the wheelset's forward motion and gyration continues as the wheelset laterally overshoots the track centreline and corrects

[4] The diagram elements on the bottom left associated with point *S* are related to a separate figure located below these diagrams in the original literature and are hereto irrelevant.

itself by gyrating in the opposite direction, resulting ultimately in the form of a damped sinusoidal oscillation with a damping that may not necessarily be, as is generally depicted in literatures as Figure 2.2 (Figure 2.1 in [22], Figure 1.2 in [26], Figure 1.3 in [27] etc.). This phenomenon is known as hunting mentioned above in the summary from [17], and is the fundamental cause of the most significant issues which vehicle system dynamics needs to deal with.

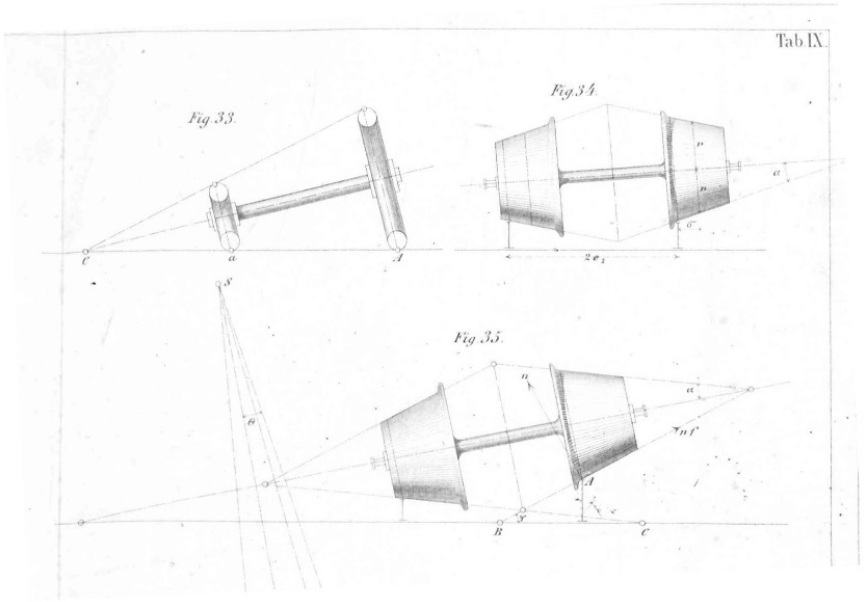

Figure 2.1 Redtenbacher's original illustration to the rolling radius difference of conical wheels of a wheelset

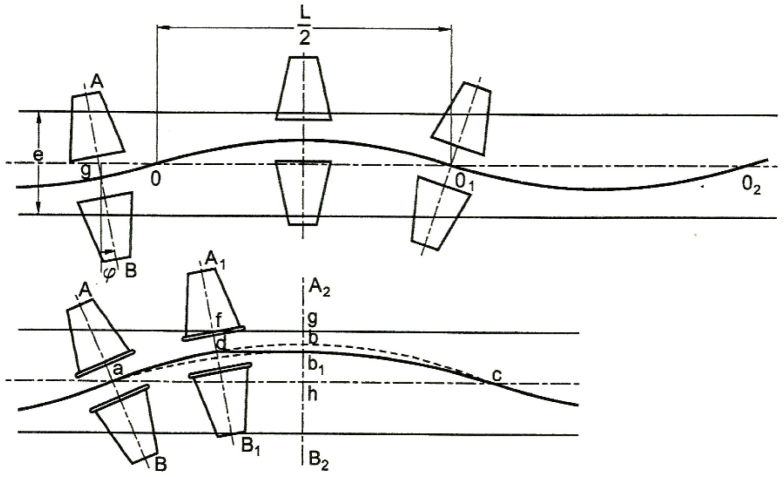

Figure 2.2 Illustration of hunting motion, taken from Knothe [26]; symbol L in the diagram represents the wavelength of the hunting motion, which corresponds to Λ_{WS} in Equation (2.1)

The nominal wheel radius has an influence on the hunting behaviour. The first analytic description of the kinematics of hunting motion given by Klingel in 1883 [14] states that for an unsuspended wheelset with a conical wheel profile free-rolling on a perfect straight track, the translational motion of the wheelset's centre point is a waveform whose wavelength is

$$\Lambda_{WS} = 2\pi\sqrt{\frac{r_0 e}{2\lambda}} \tag{2.1}$$

which indicates a positive correlation between Λ_{WS} and r_0. Based on this equation, Klingel proposes using wheels with large diameters and cylindrical or less conical treads as measures to reduce hunting and improve the motion for then current wagons.

A different way to view the gyrating motion of the wheelset is to view this motion as being similar to that of an oscillating sprung mass [17, 28]. It can be presented as in [17] as follows. For the wheelset's translational motion component, the position where the wheelset centre coincides with track centreline, i.e. where the wheelset's y-coordinate in the track reference frame is 0, is the equilibrium position of this oscillation. Consider a wheelset rolling slowly forward in a hunting motion, omitting wheel-rail contact creep forces and dynamic loads. For any lateral displacement y of the wheelset, the left and right wheel-rail contact patch normal form angles δ_L and δ_R respectively with the track's vertical centre plane (sOz-plane, see Appendix A for the coordinate naming convention used herein) known as contact angles. The wheel-rail contact normal forces on either side can thus be decomposed into a vertical and a lateral component. Of interest for the wheelset's lateral motion component of hunting are the lateral components of wheel-rail normal forces on both sides, here denoted Y_L and Y_R respectively for the left and right sides:

$$\begin{cases} Y_L = \dfrac{P_0}{2}\tan\delta_L \\ Y_R = \dfrac{P_0}{2}\tan\delta_R \end{cases} \tag{2.2}$$

where P_0 is the axle load on this wheelset, and the equation is given in scalar form with all variables being only the magnitudes. From this, now also assuming the directionality definition of the track reference frame in which y-coordinates are considered positive towards the right, the sum of lateral forces acting on the wheelset becomes

$$\Sigma Y = Y_R - Y_L = \frac{P_0}{2}(\tan\delta_R - \tan\delta_L) \tag{2.3}$$

where $(\tan\delta_R - \tan\delta_L)$ is called contact gradient difference. When considering the wheelset's lateral motion as a sprung oscillation, ΣY becomes the restoration force, and the wheelset can be considered to be connected to the track centreline with a single-directional lateral spring with stiffness

$$K_y = \frac{\Sigma Y}{y} = \frac{P_0}{2y}(\tan\delta_R - \tan\delta_L) \tag{2.4}$$

K_y is known as the gravitational stiffness of the wheelset. Note that for a given wheel-rail geometric profile pair, the contact gradient difference $(\tan\delta_R - \tan\delta_L)$ partially dependent on y (wheelset yaw angle also plays a role). A higher $(\tan\delta_R - \tan\delta_L)/y$ and thus a higher K_y indicates a higher height change of the wheelset's centre of gravity with a given amount of lateral offset. For the rolling wheelset, this means that more kinetic energy of its forward motion would be converted to potential energy as the wheelset laterally displaces, thus reducing the kinetic energy associated with the lateral speed of the wheelset. Hence a higher gravitational stiffness is positive for a wheelset's stable motion.

Within a wagon, the wheelsets are constrained by the primary suspension and axle guidance, but are still capable of undergoing hunting motion within the lateral clearance of the axle guidance, and their hunting motion will interfere with that of the carbody and the bogie frame through the suspension and axle

guidance structures. The lateral and yaw motions of the masses within the vehicle thus become a superposition of sinusoidal motions of different amplitudes and frequencies, which Klingel also described.

For running on a straight track, hunting motion is problematic. On the one hand, from a "macroscopic" view on the entire vehicle, the lateral and yawing motion of the vehicle associated with hunting swings the carbody, thus reducing passenger comfort and increasing the likelihood of damage to the cargo and wagon itself. A sinusoidal motion requires restoration forces or restoration torques to achieve, thus the forces between the oscillating bodies connected with fastening joints or suspension elements becomes larger as the hunting motion becomes more violent; furthermore, ride comfort felt by passengers is determined by the acceleration to which the passenger is subjected [26]. A hunting motion with wavelength Λ under speed of travel v has a frequency of $f = v/\Lambda$ and thus a peak acceleration of

$$\hat{a} = A(2\pi f)^2 = \frac{(2\pi v)^2 A}{\left(2\pi\sqrt{\frac{r_0 e}{2\lambda}}\right)^2} = \frac{2\lambda A v^2}{r_0 e} \tag{2.5}$$

which suggests an increase in the maximum lateral acceleration of the hunting vehicle and thus worse ride comfort and the need for more restorative interaction on each oscillating mass of the vehicle with decreasing wheel size. On the other hand, should the amplitude of the lateral oscillation be large enough, the flange of the wheel would impact the rail repeatedly, causing additional wear and increasing the risk of derailment or wheel-rail damage.

What Klingel in his work did not cover is how the amplitude of this sinusoidal motion progresses over time, namely, whether the hunting motion's amplitude increases or decreases as the vehicle continues to run. This issue is known as the running stability of the vehicle. In fact, for a vehicle with suspension, as the suspended masses oscillate in relation to each other, the damping elements in the suspension hinders the relative motion between the masses and dissipate the kinetic energy of the hunting motion, thus counteracting the wheelset's tendency to initiate and amplify the self-driven hunting motion while rolling forward. Should this overall damping be sufficient, the hunting motion will decrease in amplitude and ultimately the lateral and yaw displacements will converge to a constant value, ideally zero, i.e. the vehicle regains the perfect straightforward orientation of running. The self-driven hunting, as mentioned earlier, is only possible under the premise that no slipping occurs at the wheel-rail interfaces. Ultimately, upon an initial deviation of the wheelset from the ideally centred position, tangential wheel-rail contact forces contribute to the conversion of part of the forward motion into the lateral and yaw motions comprising the hunting motion. The damping component of these tangential wheel-rail contact forces decreases with increasing speed of travel v as is explicitly indicated with the formulation of the vehicle's matrix equation of motion (10.2) in [26]. The speed of travel thus influences whether the hunting motion converges or diverges. With the above mentioned equation of motion, once one substitutes the force laws of all suspension elements and relevant wheel-rail contact into the equation, analyses can be performed to indicate that as the speed increases, the hunting oscillation first converges, then diverges as the speed exceeds a certain value v_c known as the critical velocity. Such an analysis can be done either by generating a root locus plot with speed of travel as parameter as is done in [26], Chapter 10.2, from which one can read out the speed at the root locus plot's non-zero intercept with the imaginary axis as v_c, or, as proposed in [17], convert the equation of motion into a residual-form energy equation with the

right hand side containing a term representing the decrement of energy of the lateral and yaw motion components with speed of travel as parameter, from which one can solve for the speed that makes the energy decrement zero (thus being the critical point where the hunting motion's energy neither decreases or increases over time) as v_c. Coming back to the practical scenario, the stable running behaviour of the vehicle, i.e. the hunting motion converges and decreases in amplitude while running, is favourable, as the vehicle tends to maintain centred on the track and its direction of travel oriented along the track centreline, thereby reducing the chance of flange contact and an uneven rolling radius on the two wheels of one wheelset. The stability issue is thus safety-relevant and of concern in standards for vehicle approval [16, 20, 21].

Although Equation (2.1) indicates a direct influence of r_0, e and λ on hunting wavelength Λ, as it neither deals with the development of the hunting motion's amplitude nor indicates the behaviour of the hunting amplitude in relation to vehicle speed, the relationship between non-linear critical speed v_c^{NL} and the parameters r_0, e and λ still remains to be shown. Whereas this relationship is relatively more definite for the linear critical speed v_c^L, in that a larger λ or a smaller e increases v_c^L and the effect of r_0 is ambiguous (as is demonstrated by Knothe in [26], Equations (10.24) and (10.34)), the relationship involving the more practice-relevant and less idealized v_c^{NL}, especially under consideration of realistic, strongly non-linear friction-based damping that is present in many running gears, still remains to be quantified.

On the other hand, the geometric and kinematic basis of the undesirable hunting motion is also the basis of the wheel-rail system's guidance function on curved track, at least on moderate curves before the flange contact becomes inevitable. Redtenbacher's account of this behaviour and its positive effect on curve negotiation [25] was among the first researches to quantify the relationship between lateral wheelset offset from track centreline and the curve radius negotiable by a free-rolling, conical-profiled wheelset under pure rolling conditions:

$$\Delta y_{WS} = \frac{r_0 e}{R\lambda} \tag{2.6}$$

which indicates that the size of the wheel also plays a role in the curving capability of a vehicle: the smaller the wheel radius, the less the wheelset has to deviate from the track centreline to the outside of the curve to complete the curve negotiation under pure rolling. This is of benefit as it reduces flange engagement in the guidance through the curve, reducing the abrasive and impact damage to the wheels and rails.

The conflicting requirements for hunting motion stability maintenance and curve negotiation on vehicle parameters, not only wheel radius or wheel-rail contact geometry parameters but also suspension parameters, allows for vehicle parameter design problems to be formulated as optimization problems, in which a compromise can be found to a certain degree based on the intended application purpose of the vehicle being designed.

2.3 The numeric approach to vehicle dynamics analysis

The theories introduced in Section 2.2 belong primarily to the so-called group of "linear" theories in which assumptions stand that the wheels are have conical treads, the rail profiles are arcs, and the vehicle suspension are all linear in behaviour (where elastic and damping forces are respectively proportional

to the displacement and velocity of the force-exerting elements). This is for a realistic modern rail vehicle not overall true; hollow treads with non-conical profiles, springs and bushings with multistage or even specially-purposed non-linear characteristics, friction elements with stick-slip phenomenon, etc. usually cannot be simplified into linear approximates and still reflect the real behaviour occurring in rail vehicle applications to a satisfactory degree. The mathematical evaluation of a system combining non-linear and linear components as well as components whose behaviour has a wide range of various sensitivities to the same input quantities calls for the use of an iterative, numeric calculation method, usually in the form of a multibody simulation (MBS). [29] gives an account of the development of MBS in rail vehicle applications, as well as the current major fields of analysis in which simulation is involved – running stability, curving behaviour and wheel wear, all of which the current research also concerns, as well as ride quality, structural loading and fatigue, gauging, "virtual" vehicle acceptance testing, wheel-rail interface, track and structures, track access and life cycle cost, longitudinal dynamics, vehicle-vehicle interaction and troubleshooting.

First, the vehicle-track system to be analyzed must be expressed mathematically in the form of equations of motion. This step is known as modelling. A vehicle-track system can be considered as a set of bodies containing certain degrees of freedoms being connected with force elements following certain functions, constrained with geometric, algebraic or control conditions and excited with known motion functions.

For multi-rigid-body systems, the typical, explicit form of system of general non-linear equations as is used by Simpack [30] is given in its user manual as follows:
Kinematic: $\dot{\mathbf{p}} = \mathbf{T}(\mathbf{p})\mathbf{v}$
Momentum: $\mathbf{M}(\mathbf{p})\dot{\mathbf{v}} = \mathbf{f}(\mathbf{p}, \mathbf{v}, \mathbf{c}, \mathbf{s}, t, \mathbf{u}, \boldsymbol{\lambda}) - \mathbf{G}^T(\mathbf{p}, \mathbf{c}, \mathbf{s}, t, \mathbf{u})\boldsymbol{\lambda}$
Dynamic states: $\dot{\mathbf{c}} = \mathbf{f}_c(\mathbf{p}, \mathbf{v}, \mathbf{c}, \mathbf{s}, t, \mathbf{u}, \boldsymbol{\lambda})$
Constraints: $0 = \mathbf{g}(\mathbf{p}, \mathbf{c}, \mathbf{s}, t, \mathbf{u})$
Algebraic states: $0 = \mathbf{b}(\mathbf{p}, \mathbf{v}, \mathbf{c}, \mathbf{s}, t, \mathbf{u}, \boldsymbol{\lambda})$
where $\mathbf{p}$ is the vector of position states of each degree of freedom, $\mathbf{T}$ is the transformation matrix for angles, $\mathbf{v}$ is the DOF state vector on velocity level, $\mathbf{M}$ is the mass matrix, $\mathbf{f}$ are the force and torque equations of force elements, $\mathbf{c}$ is the dynamic state vector of force or control elements, $\mathbf{s}$ is the algebraic state vector on position and acceleration level, $\mathbf{u}$ is the vector of excitation inputs to certain DOFs on position and velocity level, $\boldsymbol{\lambda}$ is the vector of constraint forces and torques, $\mathbf{G}$ the Jacobian matrix of the constraint conditions ($\mathbf{G}(\mathbf{p}, \mathbf{c}, \mathbf{s}, t, \mathbf{u}) = d\mathbf{g}/d\mathbf{p}$), $\mathbf{f}_c$ are the dynamic state equations of force and control elements, $\mathbf{g}$ is the vector of kinematic constraint condition, $\mathbf{b}$ is the vector of algebraic constraint conditions, and t is the time. Note that the momentum equation is essentially equivalent to the equation of motion in Newtonian mechanics $m_i\mathbf{a}_i = \mathbf{F}_i$, $J_i\ddot{\boldsymbol{\theta}}_i = \mathbf{M}_i$ [19]. The specific modelling approach must, however, take into consideration of the purpose of the analysis, and guarantee that the model can be evaluated with reasonable effort and accuracy for that specific purpose; influencing factors include the range of forced frequencies involved [31], the so-called "stiffness" of the problem (whether the problem must consider a wide range of natural frequencies within the dynamical system to be analyzed) [32], the desired precision and tolerance goals, etc. Vohla [33] summarized the types of vehicle and wheel-rail contact models used in fundamental analysis of rail vehicle running dynamics, see Table 2.1.

The bodies in the MBS model may also be considered flexible, in which case the motion and deflection of a body may require more DOFs and internal connections to describe; the "subdivision" of the body

into finer DOFs and the determination of the internal interaction laws is usually done in a separate finite element analysis process. This does not change the topology of the system of equations above.

Table 2.1 Translation of Vohla's summary of fundamental problems in rail vehicle dynamics and their model use, partially excerpted from [33]

Problem type	Low-frequency ("classical") dynamics		High-frequency dynamics
Problem	Curve negotiation	Running on straight track	Wheel polygonalization, rail corrugation, noise
Quantities of interest	Wheel-rail and track-subgrade forces; wear	Running stability; forces during unstable running; comfort	Service life span; maintenance; comfort
Vehicle model	MBS	MBS	MBS + FEM
Wheel-rail contact model	Non-linear, stationary	Linear models possible; stationary	Non-linear, non-stationary

Bodies in a system interact with one another through either forces or constraints. Within the analyzed system, each body (inertial element), each force and constraint connecting the bodies or limiting the relative motion of the bodies as well as active controlled parameters must be individually mathematically described using component-specific theories, and integrated into the system of equations to be solved. Reference [19] provides general mathematical descriptions for some of such vehicle components. By far the most effort in this step is taken with the mathematical representation of forces, constraints and excitations. Theories are already developed for the force and constraint behaviour of most suspension, guidance, coupling, traction and braking components of rail vehicles from the fields of mechanics and material engineering, from which MBS modelling approaches for suspension components and assemblies are investigated and proposed [34–54].

For railway vehicles, the most unique and important interaction to model is the wheel-rail contact force. This is further divided into two subordinate research points: the normal contact problem and the tangential contact problem. The theoretical foundation for the mathematical description of wheel-rail normal contact was laid by Hertz [55], whose theory is still widely used for analysis today where the contact area as well as the elastic deformation of the contacting bodies are very small compared to the bodies' dimensions, and meanwhile the tangential force on the contact area is not pronounced enough to cause deviation in the normal force distribution on the contact area, which is consistent with the most usual wheel-rail contact situation. When analyzing contact with worn profiles or around the gauge corner, where conforming contact occurs over a larger area, or where tangential forces have too strong an influence on contact normal force distribution, Hertz' theory is no longer valid; instead, general elastic contact mechanics theories such as that of Kalker [56] are usually used. These theories take into consideration of the tangential contact forces, which according to Wickens [23] was first realistically modelled by Carter in [57] in which the concept of creep was established. Further improved theories were developed by Johnson [58, 59], who expanded Carter's theory for two-dimensional contact into three-dimensional cases that involved the influence of spin, and by Johnson and Vermeulen [60] who formulated the description of elliptical contact patch with areas of slip and adhesion. Kalker [56, 61, 62] widens the application of tangential contact into situations with non-zero Poisson's ratio, general three-dimensional cases and arbitrary creepage. Models for wheel-rail contact calculations that are suitable for computerized numerical calculation have been proposed by Kalker [56] and Polach [63] among others.

Once the vehicle-track system as well as all external factors are mathematically described as a system of equations with time being an independent variable, a time integration is done to the whole system of equations to find out the state of the system at any given end time point. This is the core step of most MBS tasks; the obtained time history can then be used for various analyses by demand, for instance be transformed into the frequency domain for ride comfort or noise analyses. Most rail-vehicle-related problems already have well-developed and validated iterative solution methods and software kits based on theories like the Newton-Raphson iteration [64] or the Runge-Kutta algorithm [65]. [66] provides an overview of the time integration's use in rail vehicle dynamics applications as well as available solver packages and their functioning principles. Different time integration software packages have different benefits for solving certain types of problems depending on what algorithms or strategies for integration they incorporate. Currently popular integrators include SODASRT2, LSODE, DOPRIS, RADAU5, SOBDF2, all of which belonging to the variable-step-size integrator family and are used for their great capability of handling stiff problems, as well as the fixed-step-size integrator family usually used for real-time simulation [30]. SODASRT2 is the default solver used in the MBS software Simpack as the default for the vast majority of applications. It is a backward differentiation formula integrator with variable step size that was improved on the basis of the DASSL solver [67, 68]. It is suitable for stiff models with constraints and algebraic states (non-dynamic, i.e. not directly related to time, quantities, such as actively controlled force elements or contact positions). The variable step size ensures that the necessary tolerances, either absolute or relative, defined by the user based on the scenario being analyzed are met. The solver rejects a step that does not result in tolerance-satisfying outputs, reduces the step size, and repeats the integration until the tolerances are met. It also allows variable order up to 5 and is stable for cases with non-negative damping in all eigenmodes in the linearized model with orders 1 and 2.

For rail vehicle engineering practice, numerical simulations have been successfully used to analyze rail vehicle dynamics problems such as vehicle running stability against lateral oscillations, curve negotiation performance as well as wear and fatigue. Approaches and test programmes for these specific purposes have been proposed, validated and implemented. This is important for assessing the stabiility of vehicles with non-linear suspensions or friction damping, which accounts for almost all realistic rail vehicles, for which linearization would cause the model to become too inaccurate; hence, time integration is the only possibility [29]. Polach [69] introduced and compared various methods for conducting non-linear stability analysis with numerical simulation, among which the method with single excitation and a series of constant speeds is used in this research for determining the critical speed. Alfi et al. [70] performed numerical non-linear stability analyses to determine the effect of using elastic traction motor mounts on the critical speed. Wang et al. [71] simulated with vehicle-track coupled models to propose a framework of performance matching of wheel-rail dynamic interaction on curved track for modern high-speed railways, analyzing the impact of different track irregularity wavelengths on the wheel load reduction rate of the high-speed train during curve negotiation. Braghin et al. [72] modelled a rail vehicle with an active control device in the longitudinal secondary suspension and evaluated its performance against that of a conventional vehicle during curve negotiation by means of a combination of numerical simulations and line tests. Vohla [33] developed an MBS module for analyzing wheel-rail contact aimed specifically at polygonalization and wear of rail vehicle wheels. Sun et al. [73] performed a simulated case study involving a 78-DOF freight wagon model with a three-piece bogie to investigate the initiation

of corrugation on curved track. The relative ease of preparation, execution and modification with simulated test procedures has also found use in vehicle homologation, leading to a series of research and practice into the so-called "virtual homologation" with MBS rather than testing with actual vehicles and tracks. Mazzola et al. [74, 75], Polach et al. [76], Wilson et al. [77] have investigated in the use of simulation for vehicle acceptance evaluation tests. UIC [20] and EN [16] standards also allow the use of simulation for vehicle acceptance tests; the standardization was supported by findings of the DynoTRAIN research project which is mentioned in [76]. The state of art, circumstances for applicability validation of the use of simulation for vehicle acceptance is summarized by Polach and Evans in [78]. A combination of dynamics simulation and optimization has also been used to find improved designs for rail vehicle and their components. Dongfang [79] conducted a multi-objective optimization of suspension parameters with a surrogate model describing the relation between running dynamics behaviour and suspension parameters obtained from a limited set of simulation results. Liu et al. [80] performed a multi-objective optimization on the design of wheel profile described as a NURBS curve and confirmed the optimization results with MBS.

2.4 Wear and maintenance of dynamical behaviour

The term "wear" used here is meant to refer to the removal of material from surfaces due to relative motion and mechanical interaction in general. [81] defines wear as "the surface damage or removal of material from one or both of two solid surfaces in a sliding, rolling or impact motion relative to one another". Causes for such material removal does not only include only the narrow-sense adhesive or abrasive wear, but also to a large extent rolling contact fatigue, which causes cracks or plastic shifts to develop within the material, contributing to the chunk- or layer-wise non-abrasive detachment of the contacting material under contact stress. Either way, the analysis of wear can be considered as a two-part process: one part deals with the "outside" of the material, in which the forces acting on the contacting surfaces which are relevant for material removal must be identified and their quantities (magnitude, frequency of change, etc.) determined; another analyzes "within" the material, in which the stress resulting from the forces determined in the previous step is related to the quantity of material removal with regard to material properties.

For the second part of wear analysis mentioned above, geometric alteration to the wheel and rail contact profile is of primary concern in wheel-rail wear, as the contact geometry change induces a series of deteriorations in force and motion behaviour of the wheel-rail contact pair. Thus, the material removal is usually characterized volumetrically. Wear laws dealing with wheel-rail contact thus investigate the volume of the worn material in relation to frictional contact indices. The frictional contact indices related to in each theory are different and are to be determined by the first, "outside" part of the wear analysis. For instance, Krause and Poll relate volumetric material wear to the frictional energy dissipated in the wheel-rail contact as $V = CW_f$ with V representing the volume of worn material, C being the wear coefficients with different values for mild and severe wear and W_f as the frictional energy [82], whereas the frictional energy W_f is given by the wear number calculated using the T-γ method, i.e. the sum of the magnitude of wheel-rail creep force components and creep rates in each direction [83], i.e. $|T_x\gamma_x| + |T_y\gamma_y| + |M_z\nu_z|$. In Archard's theory [84] the volumetric material wear is related to the contact normal

force and sliding distance. Under the assumption of hemispherical wear particles of the same radius as the contact areas, Archard gives the wear rate as $W = KP/3a$ where W is characterized by the wear volume per unit sliding distance, K is the material-specific probability of an asperity contact inside the contact patch that results in a material particle being worn off, P is the contact normal force and a is the contact area radius.

Wheel wear is an issue of concern for the maintenance of running quality of rail vehicles because it changes the wheel-rail contact profile geometry, which is crucial for the determination of the running dynamics. It is important that a vehicle maintains the satisfaction of dynamical requirements introduced in Section 2.1 throughout its operating lifespan. Wear on wheelsets over approximately 100,000 km running distance used on type Sgnss wagons with Y25 bogies operated by Rail Cargo Austria has been observed to cause the equivalent conicity to increase significantly, thereby worsening the running behaviour of the vehicle, for instance exhibiting higher lateral acceleration [85]. Extensive research has been completed on the effect, detection and mitigation of the so-called hollow wear of the tread which is responsible for the worsening of dynamical behaviour [86–92]. Optimized tread designs [93–95] help compromise between a hard-to-maintain, easily worn out profile geometry and favourable running dynamics behaviour of the wheelset; [96] provides a survey of the benefits of wheel profile improvements observed with various types of rail systems. Although worn wheels can be reprofiled to restore the tread geometry, the material removal it involves limits the amount of times a wheel can be reprofiled before it reaches the minimum usable size. As an alternative to always restoring the wheel profile geometry to the new state, optimized reprofiling geometries have been investigated which restore the running dynamics with minimal material removal [97].

Aside from optimizing the wheel-rail interface itself, design improvements on other parts of the vehicle contribute to a better wheel-rail wear behaviour as well. The use of radial steering bogies is proven to reduce accumulated tread and rail head wear. In practise at Rail Cargo Austria, the use of the radial steering bogie TVP2007 has been shown to reduce wheel wear to around a third of the level previously observed with Y25 bogies [85]. The TVP NG-DBS bogie, a later development of the TVP-series radial steering bogie which uses the same cross-linkage steering principle as the TVP-2007 but a different cross link geometry and connection positions to the axleboxes, was reported by [98] according to statements from TU Berlin and VTG to reduce rolling-resistance-related energy loss by 107% compared to ordinary Y25 bogies.

3 Methodology

3.1 Overall approach

This research lays the theoretical groundwork with a simulation-based approach, using multibody simulation to investigate the patterns of change in the running dynamics of a chosen typical reference rail vehicle. The unavailability of testing opportunities within the research period makes simulation a reasonable and necessary approach for this investigation.

All investigations are done with one specific type of reference vehicle. It is not intended to investigate the influence from a variation of vehicle type or structure in this research, but rather how the dynamics behaviour of a given vehicle with known running gears changes with the use of small-radius wheels. The choice of the reference vehicle is primarily based on availability of vehicle and running gear data.

As mentioned in Section 1.2, the scope of aspects of running dynamics to investigate in this research are stability, curve negotiation behaviour and wear. Investigation into these aspects are carried out in two different running scenarios. A straight track scenario is used for determining the stability, whereas an S-curve scenario is used for investigating the curving and wear behaviour. Following sections in this chapter will describe the choice of methodology regarding test setup and result analysis for each case in detail.

Some variations of the track gauge and rail cant are included to explore the behaviour of the vehicle on tracks with installation parameter deviations either due to practical inaccuracy or systematic differences. For both test scenarios, the track gauges 1437 mm, 1435 mm, 1432 mm and 1430 mm as well as rail cant 1:40 and no rail cant are considered. Here, the combination of 1435 mm track gauge and 1:40 rail cant is the standard track setting in Germany and is used as a reference track setting. The smaller track gauges represent cases with permissible deviations in the track gauge as is allowed by the German Ordinance on the Construction and Operation of Railways [99], with 1430 mm being the smallest allowed track gauge. Theoretically, smaller track gauges tend to worsen the running dynamics of vehicles. These track gauge values are thus potentially more critical but may still occur, which makes them worthy of consideration. The 1437 mm gauge is a variation to the standard gauge adopted by the Austrian Federal Railways (ÖBB) as the nominal track gauge for new and rebuilt railway lines [100] and is thus additionally considered in this study. Although it theoretically tends to be less critical for running dynamics, its inclusion will provide a description of running property details of practical relevance which may serve later research on operating small-wheeled vehicles on systems that use or may be converted to this track gauge.

To fulfill the first goal mentioned in Section 1.2, the investigation is formulated as a parameter variation test with the nominal wheel radius of the simulated vehicle being the varying parameter. The values of nominal wheel radius considered herein vary from 140 mm to 500 mm at 20 mm increments. Simulations for determining the characterizing indices for each of the dynamical performances mentioned above are conducted for each nominal wheel radius included in the variation range. Relations are then drawn between the dynamical performance index results and nominal wheel radius to complete the quantification.

For the second goal, additional variables are added to the previous parameter variation test: first, radius-dependent wheel profile scaling is used to provide material for the first proposed countermeasure; then, the bogie is given cross links between diagonally positioned axleboxes, converting it into a radial steering bogie, and the same parameter variation investigations both with and without radius-dependent wheel profile scaling are repeated. Section 3.6 describes the detailed approaches conceived for this goal.

The settings of the investigation mentioned above is summarized in Figure 3.1.

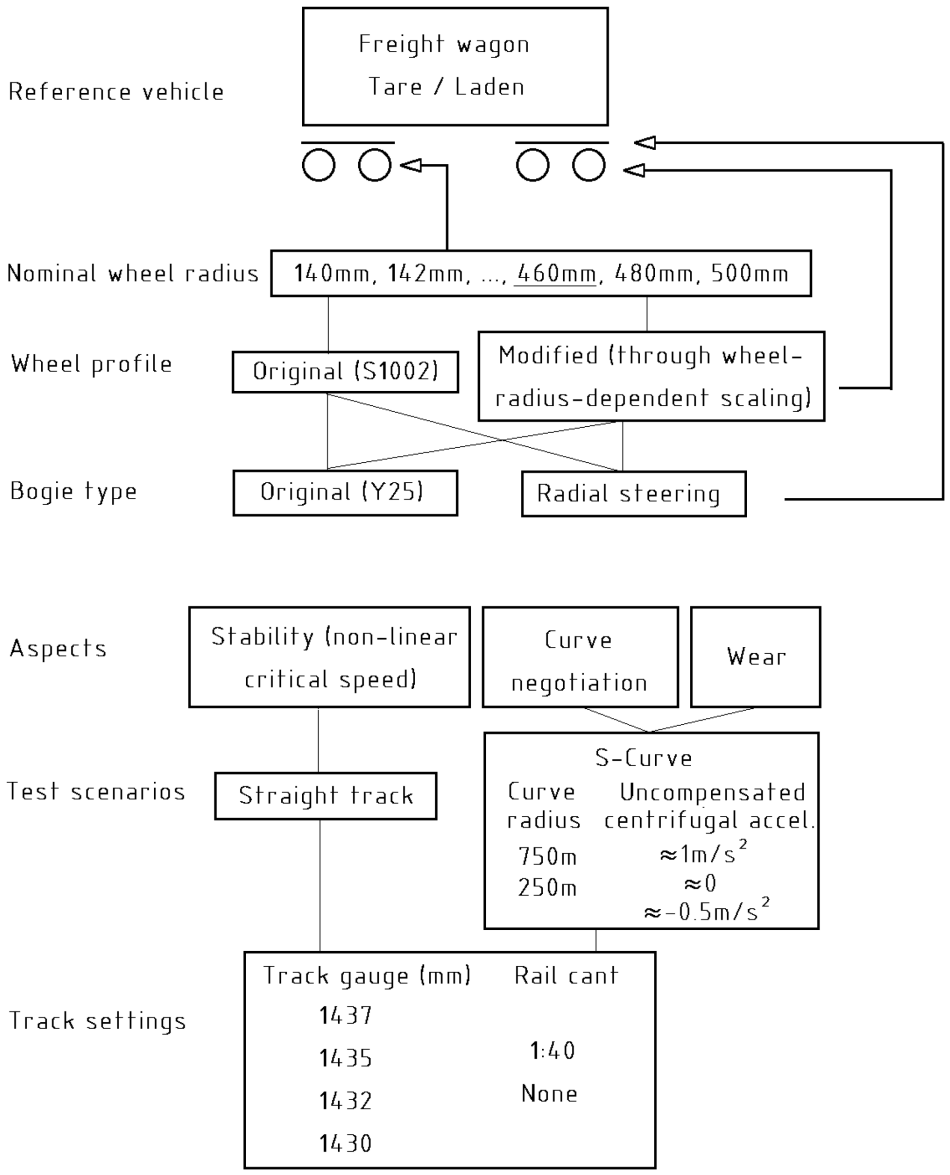

Figure 3.1 Overall settings of this research

All the modelling and simulation tasks are carried out in the MBS software Simpack. Due to the large amount of cases and variations in parameter, simulation by hand is no longer an option. Thus, Simpack's built-in scripting function is used to automatically control scenario changes, reducing the workload to a manageable level. Scripts are specially written to automatically set up the simulation model, simulate with varying case settings and parameter variations as required by the test purpose, launch the simulation

automatically, identify and handle broken simulation runs, as well as post-process simulation results and compile findings into diagram- and table-form outputs.

3.2 Selection of the reference vehicle and bogie

The form as well as dimensional and suspension parameters have a strong influence on the running properties of the bogie. It is thus necessary to select a fixed form or type of bogie and investigate only the behaviour of this specific chosen bogie when small wheels are used. Here, the choice is made based primarily on data and model availability; since no testing possibilities are available throughout the course of the research, it is necessary to choose a bogie for which there exists an MBS model which has been validated for sufficiently realistic behaviour for running dynamics. At the Chair of Rail Vehicles of Technical University of Berlin, an MBS model of the Y25 bogie is available which has been validated for running dynamics investigations under circumstances similar to this research and further matured over a series of separate research and implementation into research projects [101–109]. The model was originally created in MEDYNA and later adapted to Simpack 8. This validated model is used in this research after being adapted to Simpack 9.10, the most current version of Simpack at the time of the beginning of modelling work, and modified to allow for the desired parameter variations that this research involves as well as automation through Simpack Scripting.

Other advantages of using the well-established Y25 bogie as the reference bogie are that most of the construction and suspension data are no longer confidential, as well as that the behaviour of the bogie has been abundantly researched at the Chair of Rail Vehicles and elsewhere, providing reference data on the bogie's running dynamics behaviour for plausibility check in this research.

3.3 Stability assessment

The non-linear behaviour of the vehicle upon passing a track-bound excitation in its actual suspension configuration and with full consideration of the non-linear wheel-rail contact is chosen as the metric for stability evaluation and comparison. An assessment of the linear critical speed, on the other hand, which must be calculated under assumptions of wheel-rail contact quasilinearization and linear elasticity and damping of all suspension elements, is no longer realistically adoptable for freight wagons with running gears incorporating highly non-linear friction damping. It tends to be overoptimistic, producing a stability upper limit far above the speed at which a vehicle starts exhibiting unstable hunting behaviour in realistic running scenarios. This research thus disregards the linear assessment method, and only assesses the stability behaviour based on non-linear critical speed.

The assessment is carried out in a way consistent with that used by Polach in [69]. The method known as "method with single excitation" in the reference is used to generate a readout of the non-linear critical speed for each tested scenario. The vehicle will be placed on level, non-distorted track and given a constant test speed in the initial state of the simulation. The vehicle runs over a short lateral track irregularity functioning as the excitation source shortly after the simulation begins. The lateral displacement of the leading wheelset is observed and its convergence is used as the judgment criterion for stability.

The method described in [69] as "method without excitation", in which the vehicle starts from an unstable initial state and slowly decreases its speed until stability is regained, provides a quick and rough visualization of the system's stabilizing properties, but does not unambiguously provide the non-linear

critical velocity, as the exact speed v at which the lateral displacement y starts to steadily decrease is not determinable from the v-y diagram that this method outputs; also, the method it produces tend to be lower than other methods, for instance by simulating with the vehicle running on rough track with increasing speed and documenting the speed at the emergence of hunting [29]. This is due to the Höpf bifurcation [69, 110] that occurs with the non-linear vehicle system. At speeds between the linear and non-linear critical speeds, whether the lateral displacement diverges or converges over time is dependent on the amplitude of the initial excitation. When the excitation amplitude is large, the system is attracted towards a diverging, unstable periodic solution, and when the excitation amplitude is small the system behaves as stable. When using the method with decreasing speed, the vehicle starts from an unstable running state and goes through each speed state with a hunting motion with the maximum possible amplitude under flange-rail geometric constraints as the initial hunting for this speed state, which would draw the system towards instability in case the current speed is lower than v_c^L but higher than v_c^{NL}, thus registering the system as stable only after the current speed has become lower than the v_c^{NL}. Compared with the method with increasing speed, in which the vehicle enters each speed state with a non-maximum excitation, the system may behave as stable well after exceeding v_c^{NL} and the first observed speed with instable behaviour may less accurately reflect the non-linear critical speed, being higher than the actual v_c^{NL}. Whereas the method with decreasing speed theoretically has the capability of determining the value of v_c^{NL}, the accuracy decreases with the increase in deceleration, as the speed difference between the actual occurrence of the stabilization and the emergence of an observable converging behaviour in the hunting curve must be extremely small in order for the speed registered at the observation of hunting motion convergence to be close enough to the actual non-linear critical speed. The low deceleration of the vehicle, however, stretches the simulation runtime, and the long period of simulating the vehicle's unstable running is extremely demanding on calculation resources and calculation time due to the extensive existence of non-linear elements in the model. These factors render the method impractical for a determination of the non-linear critical speed. The method is thus only used for preliminary purposes and not for generating a comparable performance index for stability. When applied, it is also the leading wheelset of the vehicle whose behaviour is used as the judgment criterion, as with the previously mentioned method.

As the stability of non-linear vehicles can vary depending on the amplitude of the excitation due to bifurcation, it is important that the amplitude of the track excitation input for non-linear stability assessment should be chosen sufficiently large to avoid overestimating the critical speed, which in practical situations gives rise to more serious consequences than an underestimation. Here, the excitation amplitude is set as the largest possible within the flangeway clearance geometric constraint, namely through a periodically occurring ±9 mm lateral track irregularity in the form of a sinusoidal function with a fixed wavelength. In this way, the system tends to become attracted towards the instability branch of a Höpf bifurcation in the case the speed being tested lies between the non-linear and linear critical speeds, namely within the unstable saddle cycle shown in Figure 3.2, causing behaviour to be registered as unstable and the current speed as overcritical, which ultimately avoids a "false positive" judgment on stability in this speed range. Although it is still possible that the 9 mm excitation amplitude used is still insufficient to drive the system into the unstable bifurcation branch, a larger excitation amplitude would not be realizable within flange guidance constraints: the flange would have climbed the rail or the wheelset would even have derailed if a higher wheelset lateral offset from the track centreline were to exist.

Thus, the potential instability under such conditions is irrelevant for rolling stock applications. Note that this choice of initial excitation is harsher than that chosen in most existing simulation-based stability tests and would generate a lower reading of the critical speed than with the methodology in other literature. The readings from this research, however, can be seen as more accurate, as they have a lower likelihood of being influenced by "false positive" readings in the unstable saddle cycle and being far higher than the system's actual non-linear critical speed.

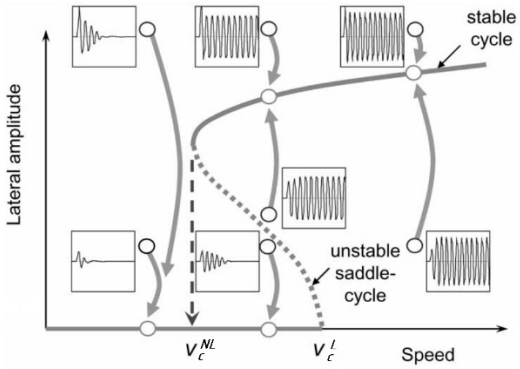

Figure 3.2 Bifurcation diagram of a wheelset's hunting behaviour after running over a lateral excitation from the track, cited from [69] with symbols modified as is designated in this thesis

A convergence of the lateral displacement of the leading wheelset may occur at very slow rates. Mathematically, this still indicates stability, but in the practical context, it still indicates prolonged hunting with similar levels of wear, kinetic energy loss and excessive lateral acceleration in its duration as unstable hunting, and the eventual convergence may be practically undetectable within a finite observation duration. With this taken into consideration, the oscillation convergence is not judged with its mathematical definition $\lim_{t\to\infty} y(t) = c$, but rather with $\left|\lim_{t\to\tau} y(t) - c\right| \leq \varepsilon$, namely whether the oscillation amplitude (without considering the static offset c) diminishes below a certain finite small threshold value ε after a reasonably long but finite time τ. This judgment criterion is realized with a QSA script clause in Simpack-Post executed during the post processing of the time integration results which automatically judges whether a simulation run exhibits stability or instability.Here ε is taken as 1 mm. The lowest speed at which instability occurs is judged as the critical speed and recorded as a relation of the nominal wheel radius.

3.4 Curve negotiation behaviour assessment

3.4.1 Determination of test conditions

The ability to negotiate curves encompasses a wide range of scenarios with different curve radii, superelevation levels and passing speeds. These combinations result in different levels of uncompensated centrifugal acceleration of the vehicle that needs to be counteracted by additional wheel-rail lateral forces. The increased guidance force during curve passing also increases the risk of derailment, track shift and wheel-rail wear intensification which are ultimately the aims of curve negotiation behaviour assessment.

The European rail vehicle acceptance standard EN 14363 specifies under its Section 7.3 "Performing on-track tests" tests for determining the dynamic running behaviour on tracks with four different types

of curve radii (straight track or very large curve radii, large curve radii, small curve radii and very small curve radii) [16]. Here, two different values of curve radius R are chosen for the investigations, namely 250 m and 750 m, respectively corresponding to "test category 4 – very small curve radii" and "test category 2 – large curve radii". Test tracks used for the simulations described in the following text are referred to as "CAT4" and "CAT2" respectively after their corresponding test categories in EN 14363.

In realistic vehicle acceptance tests conforming to EN 14363, only high-speed passing scenarios are required to be examined: for large curve radii the test speed must be no less than the maximum allowable speed of the vehicle, and for small and very curve radii the superelevation deficiency must be no less than 0.7 times the admissible superelevation deficiency value (130 mm for freight wagons). While the increase of wheel-rail guidance force on outer wheels due to an excess of curve passing speed is self-explanatory, it must also be noted that in reality trains often need to pass superelevated curves at slower rates than the prescribed speed, causing the train to slip towards the inside of the curve and the flanges on the inner wheels to grind against the inner rails, which, like curve negotiation at excessive speeds, may also pose a risk of derailment or high wheel-rail force emergence. For vehicles with reduced wheel sizes, the extent of this risk is unknown and difficult to estimate from prior theoretical and practical experience, which necessitates the inclusion of these cases within the simulation tests in this study. Thus, the simulations will cover curve passing scenarios for each test curve with three values of uncompensated centrifugal acceleration Δa, namely a positive, a negative and a zero value, where the zero value case functions as a best-case comparison reference. Note that a positive uncompensated centrifugal acceleration describes the vehicle negotiating the curve at an excessive speed, or, in other words, a situation of superelevation deficiency. In the case with 1:40 cant, standard 1435 mm gauge, S1002 wheel profile and UIC60E2 rail profile, these values are specifically chosen as 1 m/s², 0 m/s², and -0.5 m/s². These accelerations are achieved through a calculated combination of track superelevation in the curve and passing speed of the vehicle.

The superelevation for each curve radius is chosen based on [111], Section 6.2 as the smaller of the two values given in Table 5 "Upper limit for the superelevation D_{lim}" (which is taken as 160 mm under "general, normal limit") and Table 6 "Upper limit for the superelevation $D_{R,lim}$ as function of the curve radius" (calculated by $D_{R,lim} = \frac{R - 50\ \mathrm{m}}{1.5\ \mathrm{m/mm}}$), i.e. the largest superelevation achievable that satisfies both upper limits. Each simulation test track setup uses its largest achievable superelevation value in the test curve. The only exception is the case of passing a 750 m-radius curve ("category 2 curve") with uncompensated centrifugal acceleration 1 m/s², which can only be achieved with a much higher speed than the maximum operational speed of a freight wagon if superelevation in the curve is set as the upper limit value above. For this case, the superelevation is decreased to allow the vehicle to achieve the desired uncompensated centrifugal acceleration with its maximum operational speed.

Based on the curve radius and superelevation, the vehicle's curve passing speed v required to achieve each of the three target values of uncompensated centrifugal acceleration can be calculated with simple mechanics and equations of uniform circular motion.

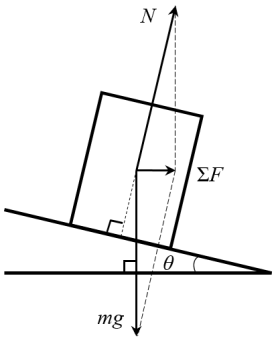

Figure 3.3 Force analysis of a vehicle negotiating a superelevated round curve with constant speed

Consider a vehicle (considered as one rigid entity) with mass m passing a curve with radius R and superelevation D with constant rate of speed v while being subject to a net wheel-rail force perpendicular to the track plane, see Figure 3.3. Let this running scenario be referred to as "ideal curving". As the vehicle neither climbs up nor slips down the superelevation during curve negotiation, the vector sum of forces on the vehicle has no vertical component and lies solely in the horizontal direction, functioning as the centripetal force. As gravity mg is vertical, ΣF is perpendicular to mg, thus

$$\Sigma F = mg \tan\theta \tag{3.1}$$

From the vehicle's uniform circular motion in the horizontal plane,

$$\Sigma F = ma = m\frac{v^2}{R} \tag{3.2}$$

where a is the vehicle's centripetal acceleration while negotiating the curve.

Also, from the definition of superelevation given in [111], Section 3.11, we have

$$\sin\theta = \frac{D}{e} \tag{3.3}$$

where e is the span between left and right wheel-rail support points. Its value is dependent on wheel and rail profiles as well as the attitude of the wheelset on the track. Here the European S1002-wheel-on-UIC60-rail pairing is assumed. As in ideal curving the wheelset maintains a nearly centered and radial attitude on the track, the value of e in for a centred wheelset 1500 mm can be used here. Thus, when $D = 160$ mm, $e = 1500$ mm, with D being measured in the vertical direction and e along the superelevated slope, we have

$$\begin{aligned} &\sin\theta = \frac{160\text{ mm}}{1500\text{ mm}} \approx 0.1067 \\ &\Rightarrow \theta \approx \arcsin 0.1067 = 0.1069 \\ &\Rightarrow \tan\theta \approx \tan 0.1069 = 0.1073 \end{aligned} \tag{3.4}$$

so that $\sin\theta$, $\tan\theta$ and θ can still be considered approximately equal for the actual case with standard gauge and $D \leq 160$ mm.

A substitution of the variables yields the property of ideal curving as

$$\frac{v^2}{R} \approx g\frac{D}{e} \tag{3.5}$$

so that the passing speed at zero uncompensated centrifugal acceleration on the curve in question can be determined by

$$v \approx \sqrt{\frac{gDR}{e}} \tag{3.6}$$

For cases where the vehicle has excessive speed v^*, the uncompensated centrifugal acceleration Δa can be described as the vector difference between the centripetal acceleration required for the vehicle to complete the aforementioned ideal curving and that required to complete the uniform circular motion with the said excessive speed; in other words, how much the centripetal acceleration provided by the horizontal component of the net wheel-rail force which is perpendicular to the superelevated track plane lacks in order to enable a uniform circular motion on the said curve with the higher speed v^*. Its magnitude is thus calculated as

$$\Delta a = \frac{v^{*2}}{R} - \frac{v^2}{R} \approx \frac{v^{*2}}{R} - g\frac{D}{e} \tag{3.7}$$

In reality, this additional centripetal acceleration is provided by the increased horizontal component of force N, which no longer remains perpendicular to the track surface but inclines further inward. This is caused partly by the vehicle's slight outward offset on the curved track, which shifts wheel-rail contact points on both sides and changes the orientation of the wheel-rail contact forces that compose force N, and partly by the wheel load redistribution that changes the magnitude of the wheel-rail contact forces.

Thus, the test velocities required to achieve a certain desired value for Δa can be calculated for each defined curve with known R, D and e values:

$$v^* = \sqrt{\left(\Delta a + g\frac{D}{e}\right)R} \tag{3.8}$$

Note that the superelevation in ideal curving cases D defined here is in fact identical to the definition of "compensated superelevation" in [111], Section 3.12, represented in Equation (1), Section 6.3 as D_{EQ}.

There is also direct correspondence and convertibility between the uncompensated centrifugal acceleration mentioned above and the superelevation deficiency defined in [111], Sections 3.13 and 6.3. It is explained below so that the test conditions regarding uncompensated centrifugal acceleration and superelevation deficiency can be unified in the following text.

Let the variable in the analysis above be shifted from passing speed ("passing a given curve with a higher speed") to superelevation. When the speed v is fixed, the superelevation that enables ideal curving at this speed, or the D_{EQ} in [111], Equation (1), is unambiguously determined. From the analysis of ideal curving above, using the variable notation as in the standard,

$$v \approx \sqrt{\frac{gD_{EQ}R}{e}} \tag{3.9}$$

$$\Longrightarrow D_{EQ} = \frac{v^2 e}{gR} \tag{3.10}$$

where v is the vehicle's speed given in m/s. Note that in the standard the vehicle's speed V is given in km/h, $V = v \cdot 3.6\ (\mathrm{km/h})/(\mathrm{m/s})$. Let the variables carry units as given in the standard, namely D_{EQ}, e in mm and R in m. Substituting these into the equation above, we have

$$D_{EQ} = \frac{1500\ \mathrm{mm}}{9.81\ \mathrm{m/s^2} \cdot R}\left(\frac{V}{3.6\ (\mathrm{km/h})/(\mathrm{m/s})}\right)^2 \approx 11.8\ \mathrm{mm{\cdot}m{\cdot}h^2/km^2} \cdot \frac{V^2}{R} \tag{3.11}$$

which is consistent with the substitution of D_{EQ} involved in Equation (1) in the standard. Thus, for the case with standard gauge, S1002 wheels and UIC60 rail, the parameter $q_E = 11.8\ \mathrm{mm{\cdot}m{\cdot}h^2/km^2}$ in [111], Equation (1) is explained.

When the superelevation D is smaller than D_{EQ}, the corresponding centripetal acceleration required for the vehicle to negotiate the curve at the same speed v remains unchanged ($a = v^2/R$), but it can no longer be sufficiently provided by the horizontal component of a force N acting perpendicular to the track surface while keeping the magnitude vertical component still equal to the gravity of the vehicle. With the current superelevation, represented in terms of superelevation deficiency as $D = D_{EQ} - I$, we now have

$$\theta \approx \frac{D}{e} = \frac{D_{EQ} - I}{e} \tag{3.12}$$

so that the centripetal acceleration that could be provided by the horizontal component of force N if it were acting perpendicular to the track surface is only

$$a^* = \frac{mg\tan\theta}{m} \approx g\theta = g\frac{D_{EQ} - I}{e} \tag{3.13}$$

whereas the condition $\sum F = N\sin\theta = G\tan\theta$ from the fact that the vehicle does not climb up of slip down the superelevated curve is implemented.

From here, the uncompensated centrifugal acceleration of the vehicle during the negotiation of a curve with superelevation deficiency I is in magnitude

$$\begin{aligned} \Delta a &= \frac{v^2}{R} - g\frac{D_{EQ} - I}{e} = \frac{v^2}{R} - g\frac{\frac{v^2 e}{gR} - I}{e} \\ &= I\frac{g}{e} \end{aligned} \tag{3.14}$$

This unifies the representations "uncompensated vehicle centrifugal acceleration" and "superelevation deficiency". The two quantities are thus directly convertible. Here, both are used interchangeably to express the centrifugal effects in test conditions.

The test track model in the simulations is set up as an S-curve, with an initial straight section, a positive-radius curve incorporating the test curve parameters explained above, an intermediate straight section, a negative-radius curve which is an exact inversion of the previous curve, and a final straight overshoot section. The two round curves are given transition curves at each end with lengths chosen based on requirements in [111], Sections 6.6, 6.7.1 and 6.8 regarding the distance derivative of superelevation, time derivative of superelevation and time derivative of superelevation deficiency respectively.

Table 3.1 lists all test cases involved with the appropriate test speed as well as the resultant superelevation deficiency and uncompensated centrifugal acceleration calculated with e = 1.5 m. Note that for the cases with varied track gauge and rail cant, as well as for non-standard S1002 wheel profiles paired with the same rail profile, the uncompensated centrifugal accelerations deviate slightly due to a change in wheel-rail nominal contact point positions and thus a change in the value of e. Among all combinations of track gauge, rail cant and wheel profile that this research concerns, e is found to vary in the range [1.4672 m, 1.5168 m] (see also Appendix H). The variation of e affects the second term in the equation for uncompensated centrifugal acceleration $\Delta a \approx \frac{v^{*2}}{R} - g\frac{D}{e}$ introduced above, from which a deviation in the calculated Δa can be determined for each given superelevation value. This deviation in calculated Δa is listed in the last row in Table 3.1. As can be seen, the deviation is insignificant and is thus not recalculated with each change of track or wheel profile setting.

Table 3.1 Overview of curve test cases

Test case	CAT2 Δa_+	CAT2 Δa_0	CAT2 Δa_-	CAT4 Δa_+	CAT4 Δa_0	CAT4 Δa_-
Curve radius R (m)	750 (EN 14363:2016 §7.3, test category 2)			250 (EN 14363:2016 §7.3, test category 4)		
Superelevation D (mm)	10	100 (EN 13803:2017 §6.2)		133 (EN 13803:2017 §6.2)		
Transition curve length (m)	75 m (EN 13803:2017 §6.6, §6.7.1, §6.8)			58 m (EN 13803:2017 §6.6, §6.7.1, §6.8)		
Test speed v (km/h)	100	79.75	38.5	77	53.25	34.75
Uncompensated centrifugal acceleration Δa (m/s²)	0.963	0.000	-0.502	0.958	0.003	-0.499
Superelevation deficiency I (mm)	147.333	0.065	-76.679	146.516	0.505	-76.336
Deviation range of Δa due to change of track gauge, rail cant and wheel profile (m/s²)	+0.001 -0.001	+0.007 -0.015		+0.010 -0.019		

3.4.2 Assessment criteria

The indexes for curving performance used here are taken from classical dynamics: wheel-rail lateral force, sum of lateral forces on wheelset, and derailment coefficient. These are the same parameters that are assessed in practice for vehicle acceptance for revenue service in EN 14363.

As diverse combinations of vehicle speed and superelevation deficiency are considered, the vehicle may pass the curve with different attitudes whereas different wheels or wheelsets may become the most critically loaded in different cases. It is thus necessary to assess the curving performance indexes for all wheels and wheelsets, since existing accounts on the behaviour of small-wheeled vehicles are rare in

available research literature, making it difficult to estimate which wheel or wheelset may be the most critical. In order to gain some knowledge of the vehicle's attitude and the most stress-loaded wheel or wheelset, this information is also assessed and used as supplement in the result summary.

The time history of each index in the simulation tests are recorded and presented in both raw and smoothed forms. The smoothing is done first by transforming the time history into a displacement function and then applying a sliding mean filter with 2 m window length and 0.5 m window shift step size. Also, the maximum absolute value of these performance indexes over all wheels or wheelsets are extracted from the smoothed time histories and recorded for cross-comparison and applicability determination based on comparison with limit values given in standards.

3.5 Wear assessment

The simulation results for curve negotiation assessment are also great materials for the wear assessment and comparison of wear behaviour of the test vehicles with different wheel sizes and across different scenarios. Curve-passing cases with positive and negative uncompensated centrifugal accelerations on small-radius curves (CAT4) are the most critical cases in terms of wear, since they are more likely require flange contact to provide the necessary lateral forces to counteract the uncompensated centrifugal accelerations and have high chances of two-point contact emerging across the gauge corner due to the large lateral wheelset offset.

The wear number, calculated by the T-γ method, is used here as the wear performance index. The wear number for each wheel is interpreted as time history and also integrated over the distance covered by each wheelset to obtain the wear work done by the wheelset in the whole simulation process.

It is to be noted that each curve-passing scenario also contains straight-track segments where wheel-rail wear occurs at a non-critical level of severity and transition curves which are too short for wear to accumulate pronouncedly despite the stronger wheel-rail interaction. Also, test tracks with curves belonging to different test categories have different transition curve lengths (see Table 3.1) and thus different total lengths, and some simulation runs may break off prematurely (for a description of broken runs which occurred in this research, their treatment and influence, see Appendix C), both of which result in different total covered distances by the test vehicle as well as each of its wheels in different simulation runs. For more focus on the most critical wear scenario and better mutual comparability across different simulation cases, the wear data is further processed as follows. Only the subtotal of wear work within the round curve section of the first curve is extracted for each single wheel. This total work is then divided by the distance covered by the wheel, which gives the wear work per meter round curve for each wheel. This result physically represents the so-called "effective value" of the wear number of each wheel in the round curve, or specifically, an equivalent constant wear number that would produce the same amount of wear work with the wheel rolling through the round curve as the actual, fluctuating wear number observed in the simulations. Finally, the "effective values" of each wheel are summed to obtain the "effective" wear number of the whole vehicle, or the wear work done per unit distance by the whole vehicle. This is the quantity ultimately used for cross-case comparisons.

3.6 Countermeasure implementation and effectivity assessment

3.6.1 Tread geometry modification: radius-dependent wheel profile flattening

The equivalent conicity, in later research works more often replaced by the more general rolling radius difference function, is one of the three basic conditions of a wheelset's automatic centring effect and hunting motion, and thus becomes one of the most influential factors of running dynamics performance. This is a pure geometric parameter related to the wheel-rail profile pairing which can be manipulated by modifying either the wheel or the rail profile. Here, in order to adjust this parameter, the wheel profile's radial dimensions, or z-coordinates in the commonly used descriptive reference system as shown in Figure 3.4, is scaled to various factors within the tread section while maintaining the flange unaltered. The gauge corner is given a transitional scaling factor varying from 1 on the flange end to the desired scaling factor f on the tread end in a quadratic manner. The profile modification scheme is illustrated with the S1002 profile drawing given by [2] in Figure 3.4.

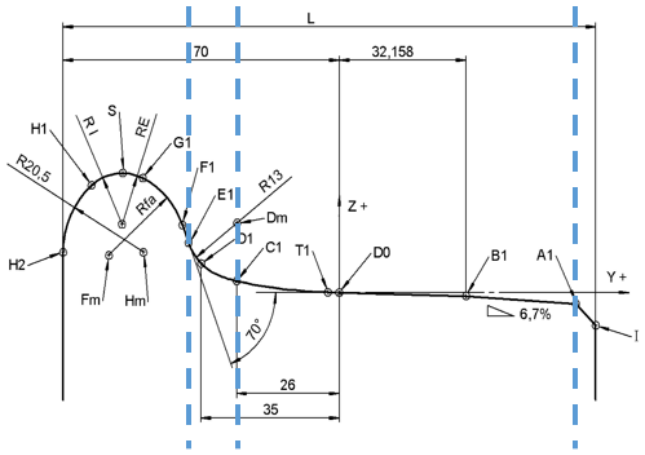

Section	Description	Z-coordinate scaling
I-A1	Chamfer	Omitted
A1-C1	Tread	By uniform factor f
C1-E1	Gauge corner	Parabolic transition: C1-end: by factor f E1-end: by factor 1
E1-H2	Flange	By factor 1

Figure 3.4 Wheel profile scaling scheme

The scaling factor f is first set as a fixed value of 70% as a rough comparison to the original profile (see Figure 3.5), then as a function of the wheel radius value which relates to the actual countermeasure intended to be investigated. The former 70% scaling is intended as a preliminary investigation for probing the sensitivity of running dynamics behaviour to tread flatness change for the whole range of nominal wheel radii in question. In the latter functional setting, two further f-$r_0$correspondences are considered. First, upon realizing the opposite effects of a reduction in wheel size and a decrease in tread conicity on running stability, a typical case of f that decreases with decreasing r_0 is devised so as to observe and quantify the compensation effect of the worsening stability due to reduced wheel size. Here, f is set as the ratio between the current wheel radius r_0 and the standard Y25 bogie's wheel radius $r_{0,standard} =$ 460 mm, i.e. $f = \frac{r_0}{r_{0,standard}}$. For brevity, this case is abbreviated "MAT" for "matching f-r_0 pairing order" in latter text. Figure 3.6 shows these profile forms in comparison. Subsequently, the pairing order between the wheel radii and scaling factors is reversed; for instance, the smallest tested wheel with 140 mm nominal radius is given a wheel profile with the radial dimension scaled by 500/460 on the tread, which, in case MAT, is paired with the largest tested wheel with 500 mm radius. Thus, the scaling factor can be expressed in terms of the scaling factor of the wheel radius as $f = \frac{640\ mm - r_0}{r_{0,standard}}$. This case is abbreviated "INV" for "inverted f-r_0 pairing order" in latter text. In fact, only case MAT is intended to be

the proposed countermeasure of wheel-radius-dependent wheel profile modification. Case INV is meant as an extreme comparison case rather than a viable practical countermeasure: the smallest wheel sizes, which are ultimately of the most concern in this research, are tested in combination with no profile modification, with decreased conicity (case MAT) and with increased conicity (INV), forming a relatively complete comparison set that indicates the behaviour of small wheels with different conicity settings.

Table 3.2 provides an overview of the profile scaling factor used for each MAT and INV profile modification case. The values of the equivalent conicity λ_e^{3mm} (calculated over ±3 mm distance from nominal rolling circle) of each modified profile under track settings with 1435 mm track gauge and 1:40 rail cant are also given as a reference to the profiles' properties in a classical dynamics' sense.

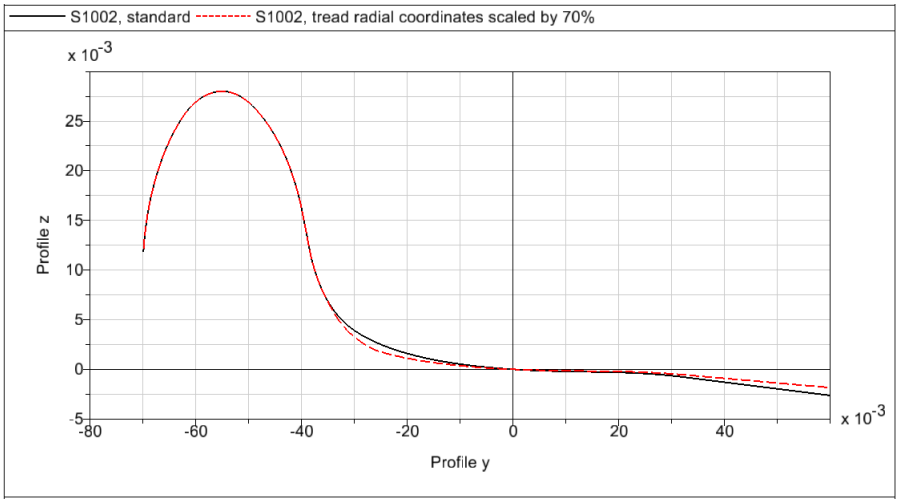

Figure 3.5 70% fixed factor scaling of the S1002 profile

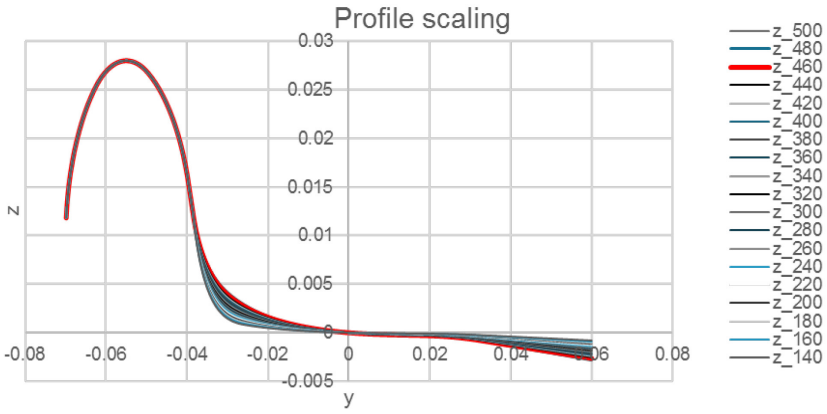

Figure 3.6 Radius-dependent scaling of the S1002 profile; the numbers given in the legend are the corresponding nominal wheel radii in millimetres to each curve in the case with positive radius-scaling factor correlation (Case MAT)

The full set of simulations described previously are repeated for each scaled profile and the same analyses are conducted, forming comparison sets within the results corresponding each chosen wheel radius value. This comparison helps determine whether the modification to the profile flatness has an effect on running dynamics performance and quantify the effect.

Table 3.2 Scaling factors and equivalent conicity values of radius-dependently scaled wheel profiles (read out from Simpack model, track gauge 1435 mm, rail cant 1:40)

Nominal wheel radius r_0 (mm)		Scaling factor f	Equivalent conicity λ_e^{3mm}
Case MAT	Case INV		
500	140	1.087	0.113850
480	160	1.043	0.092996
460	180	1.000	0.076954
440	200	0.957	0.063863
420	220	0.913	0.052958
400	240	0.870	0.043975
380	260	0.826	0.036637
360	280	0.783	0.030656
340	300	0.739	0.025811
320	320	0.696	0.021884
300	340	0.652	0.018670
280	360	0.609	0.016030
260	380	0.565	0.013820
240	400	0.522	0.011937
220	420	0.478	0.010313
200	440	0.435	0.008887
180	460	0.391	0.007620
160	480	0.348	0.006485
140	500	0.304	0.005450
(Profile with fixed scaling factor 70%)		0.700	0.022191

3.6.2 Radial steering mechanism

Theoretically, a reduction in wheel size benefits a vehicle's curving behaviour, though the extent of this positive effect is not clearly estimated. The previous countermeasure, namely flattening the wheel profile for smaller wheels, reduce the wheelset's conicity and thereby weakens the automatic centring effect necessary for smooth curving. This can be counteracted by the use of a radial steering mechanism. This is the basis for the choice of using a radial steering mechanism as a countermeasure. With the simulation tests devised as explained here, especially the cases where both tread geometry modification and radial steering are implemented, the extent of the above-mentioned compensation effect can be observed and quantified.

As described by literature [26], Chapter 11.2.1, when considering the mutual movements of the two wheelsets in a conventional two-axle bogie, the lateral and longitudinal primary suspension stiffness can be equivalently transformed with respect to wheelbase and lateral span of primary springs into an inter-wheelset bending stiffness and an inter-wheelset shear stiffness, given with symbols as is used in the original literature as follows:

$$c_b = e_x^2 c_x \tag{3.15}$$

$$c_s = \frac{e_x^2 c_x c_y}{e_x^2 c_x + b^2 c_y} \tag{3.16}$$

where c_b and c_s are the inter-wheelset bending and shear stiffnesses respectively, c_x and c_y are the actual primary suspension stiffness components in the longitudinal and lateral directions respectively, e_x is the half-distance between attachment points of longitudinal springs and b is a half of the wheelbase. These two parameters determine the interaction between the two wheelsets in radial steering. From this formulation, the principle for an effective realization of self-steering[5] finds its theoretical basis. In literature [26], Chapter 14.4 states that low values of c_b is beneficial for good curving behaviour, whereas Chapter 11.2.6 shows that for low values of c_b a higher c_s is helpful for maintaining the critical speed, although a simultaneous low c_b and high c_s is not achievable without introducing a direct connection between the wheelsets. Consistent to this theory, Wickens explains in [112] that steering linkages or yaw relaxation of wheelsets are effective measures of achieving passive radial steering on steady-state curves.

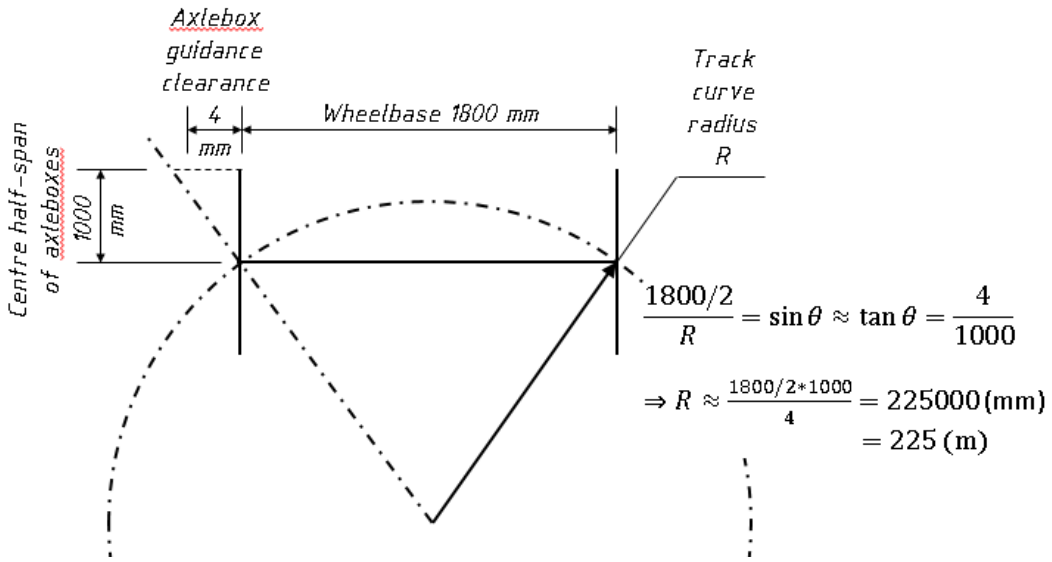

Figure 3.7 Calculation of the minimum curve radius on which the radial attitude of wheelsets is possible for a Y25 bogie

Here, a passive, self-steering mechanism is added to the original bogie in the form of cross links between diagonally located axleboxes within the same bogie. To ensure that all changes in running behaviour with the modified bogie are associated with the addition of the radial steering system itself, no other changes are done to the bogie model. This is unlike the actual redesigning of the Y25 bogie into passive steering variants such as the TVP2007 or SUSTRAIL, where the longitudinal clearance between the axlebox and guidance brackets has been increased to allow a larger wheelset yaw angle; the minimal longitudinal clearance between the axlebox and the guidance bracket is 4 mm [107], which would allow the bogie to assume a radially steered attitude on curves with a radius no smaller than 225 m (assuming that the centre pivots lie over the track's centreline), see Figure 3.7. The bogie is thus geometrically

[5] "Self-steering" is to be understood as being able to facilitate the passive radial steering of the wheelsets without the involvement of any structure that does not belong to the bogie, such as the carbody or the frame of a neighbouring bogie. Not to be confused with "active steering".

capable of assuming the radially steered attitude on all test curves involved here, whose radii are all greater than 225 m, even without increasing the longitudinal axlebox guidance clearance. With this self-steering bogie model, the same simulation tests mentioned previously are performed first with the standard S1002 wheel profile, then with the wheel-radius-dependent scaled profiles.

4 MBS preparatory work for the simulation approach

This chapter explains the process and considerations of the preparation of the simulation models needed for the running dynamics assessment.

The multibody modelling and simulation setup work consists of the following tasks. First, a vehicle model is to be prepared which is capable of adapting variable wheel radius and wheel profile as well as switching on and off radial steering of the bogies. Then, based on each of the required test purposes, corresponding realizable test tracks should be chosen (straight track for stability, S-curve for curve negotiation and wheel-rail contact analysis), the parameters defined and the tracks accordingly modeled. Last, the parameter variation routine for automatically launching simulations and performing post-processing is to be scripted and tested.

4.1 Vehicle MBS model

As track and field testing is impossible in the framework of this research, establishing a new running gear model is impractical, as no validation tests can be done to ensure that the newly created model's behaviour sufficiently resembles reality. The running gear model is thus adopted from a previous project conducted by TU Berlin [108] in which a model of the Y25 freight wagon bogie was created in Simpack 8 and validated. The model is restored and rebuilt in Simpack 2019 to allow for a smooth run in the current available version of the simulation tool and modified to realize the required changes in model states (such as with different vehicle loading states or with the investigated parameters varied), as well as provide the necessary interfaces with the vehicle model. The visual rendering of the rebuilt model in Simpack 2019 is shown in Figure 4.1.

Figure 4.1 MBS model of the whole vehicle in Simpack 2019

4.1.1 Complete vehicle (parent model)

The parent model is the site where the submodels for the carbody and the bogies to be described in the next sections are assembled and positioned within the track reference frame. Vehicle modelling parameters are defined in the submodels, although the varying parameters are given as substitution variables stored directly within the parent model, overwriting the original parameters defined in the submodels.

The complete vehicle model is also where the tracks for all test purposes are modelled and corresponding solver settings are set up. Ultimately, the simulation process control scripts only access the parent model, modifying the vehicle parameters and choosing the required track and corresponding solver settings based on the purpose of the simulation.

Figure 4.2 shows the topology of the complete vehicle, taken from the 2D representation of the model in Simpack directly. Each grey block represents a substructure defined in a submodel, and the shaded border represents the global reference frame onto which the track system is fixed. The 0-DOF joints linking the bogies to the carbody are between the carbody and the so-called "dummy structures", which belong to the bogie submodel but is actually a fixed part on the carbody. Its purpose is to enable placing the carbody-side application points and bodies of the secondary suspension within the bogie submodel, thereby making the carbody and bogie submodels more independent and increasing their interchangeability. This can be explained by Figure 4.5 in Section 4.1.2.

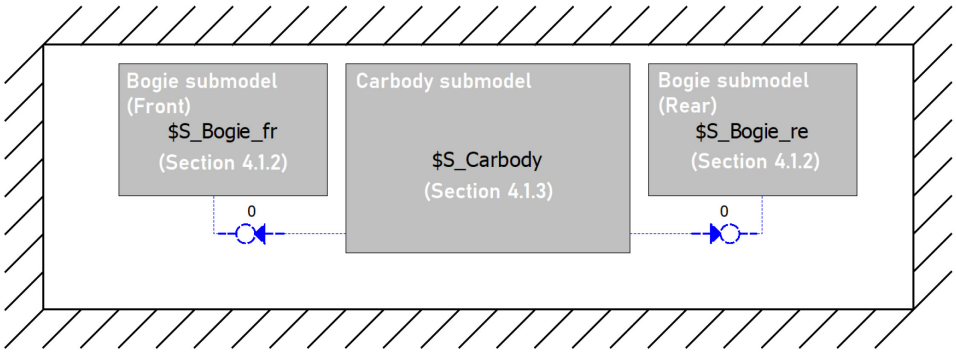

Figure 4.2 Complete vehicle model topology

The whole vehicle's axle load and static vertical wheel load are important parameters regarding the determination of limit values for dynamics behaviour indices, as is regulated in EN 14363 [16]. The wheel size and vehicle load state will change during the scenario variations involved in the investigations, causing the overall mass of the vehicle to change, thus altering the axle load. The change of wheelset mass and the laden and tare masses of the carbody are explained respectively in Sections 4.1.2 and 4.1.3 below. The axle load of the complete vehicle is given in Table 4.1 for all variations of the model.

4.1.2 The bogie submodel

The model of the Y25 model adopted from Schelle [108] is visualized in Simpack as in Figure 4.3. This model is further adopted from Hanneforth and Fischer in [113], in which it is given as in Figure 4.4 below. It is modelled in Simpack with such a topology as illustrated in Figure 4.5 (rear wheelset omitted for conciseness). Features of the original bogie modelled in Simpack 8 from [108] have been retained where possible so as to avoid compromising the proven validity of the model.

Table 4.1 Complete vehicle's mass, axle load and nominal static vertical wheel-rail force for all variations

r_0 (mm)	Total vehicle mass (t)		Axle load (t)		Static vertical wheel-rail force P_{F0} (kN)	
	TARE	LADEN	TARE	LADEN	TARE	LADEN
500	26.30	89.50	6.57	22.37	32.25	109.75
480	26.05	89.25	6.51	22.31	31.94	109.44
460	25.81	89.01	6.45	22.25	31.64	109.14
440	25.57	88.77	6.39	22.19	31.36	108.86
420	25.35	88.55	6.34	22.14	31.09	108.59
400	25.14	88.34	6.28	22.08	30.82	108.32
380	24.93	88.13	6.23	22.03	30.57	108.07
360	24.74	87.94	6.18	21.98	30.34	107.84
340	24.55	87.75	6.14	21.94	30.11	107.61
320	24.38	87.58	6.09	21.89	29.89	107.39
300	24.21	87.41	6.05	21.85	29.69	107.19
280	24.06	87.26	6.01	21.81	29.50	107.00
260	23.91	87.11	5.98	21.78	29.32	106.82
240	23.77	86.97	5.94	21.74	29.15	106.65
220	23.64	86.84	5.91	21.71	28.99	106.49
200	23.53	86.73	5.88	21.68	28.85	106.35
180	23.42	86.62	5.85	21.65	28.71	106.21
160	23.32	86.52	5.83	21.63	28.59	106.09
140	23.23	86.43	5.81	21.61	28.48	105.98

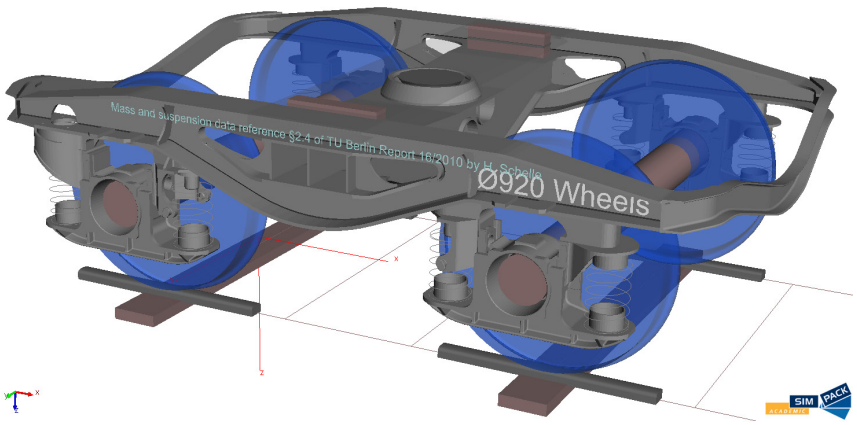

Figure 4.3 MBS model of the Y25 bogie in Simpack

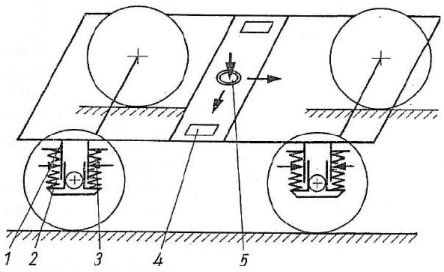

Figure 4.4 Assembly of the Y25 bogie model by Hanneforth and Fischer [113]
1 and 3 – axle guidance; 2 – primary suspension; 4 – side bearers; 5 – centre pivot

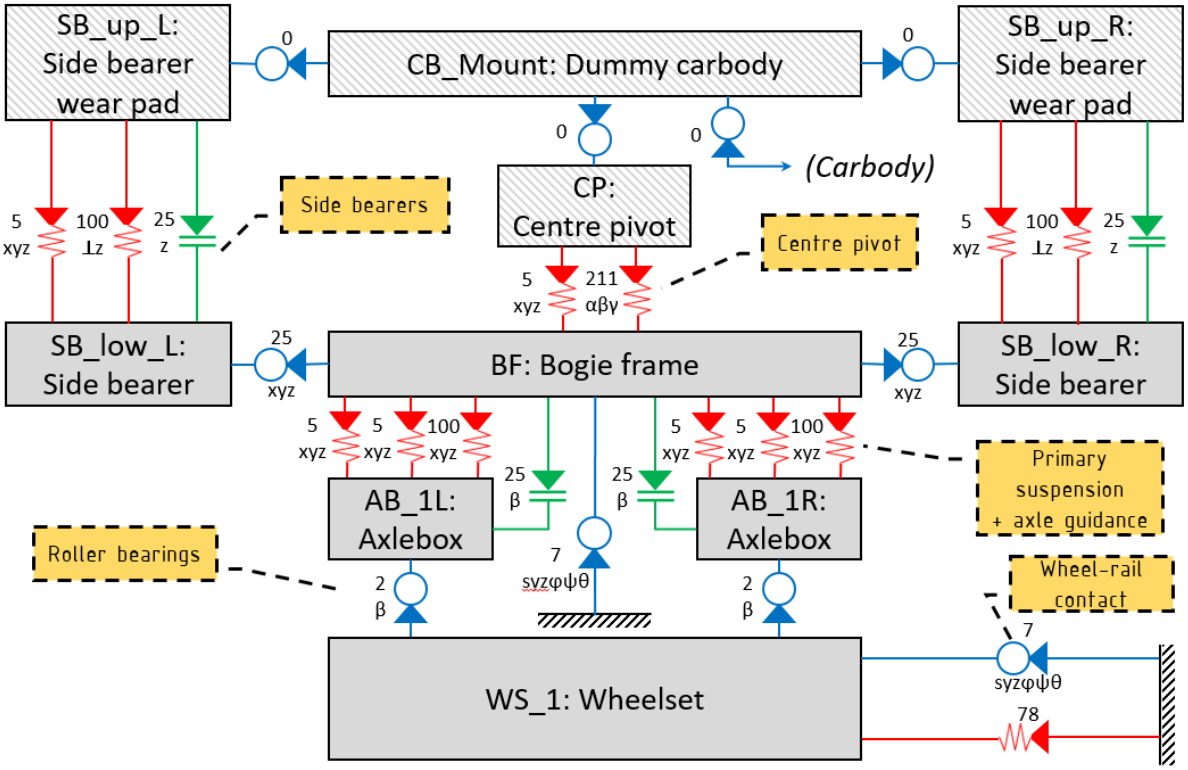

Figure 4.5 Bogie model topology

The most significant changes in the model are the variable wheel radius as well as the associated changes in the height of all bodies above the wheelsets and the wheelset's mass properties.

Since wheel size variation does not alter any suspended masses or suspension parameters, the relative positions of suspended masses do not alter and the loaded lengths of suspension elements remain unaffected. Thus, the height of all suspended bodies whose position is given in reference to the global coordinate system *Isys* (namely the bogie frame, as well as the carbody which belongs to a different substructure), given in the model by the z-coordinates in their joints, must be uniformly reduced by the wheel radius increment in comparison to the standard 460 mm wheel radius used in the original model

(achieved in the model by adding the radius increment value, since the z-axis points downward, giving bodies located higher a smaller z-position coordinate value).

The mass and moments of inertia of the wheelset affect the force-acceleration behavioural characteristics, thus their changes due to wheel size variation is not negligible. The mass properties are directly related to the wheelset's density, which can be considered uniform for a conventional steel-made wheelset, and its volume. The relation between wheelset volume and wheel radius is dependent on the wheelset's cross-section through its axis. In order to work with an unambiguous wheelset-volume-versus-wheel-radius relationship, some simplifications are made. The axle is considered to be a uniform cylinder whose radius remains fixed at 80 mm for all wheel sizes. The wheel is assumed to have a web with a rectangular cross-section 60 mm in width and a variable length which is the sole source of change for the wheel's actual radius. As this infers, the wheel possesses fixed forms for the hub and the rim that do not change with the wheel size. Both the rim and the hub are assumed to be 135 mm thick (cross-sectional width) and 20 mm tall (cross sectional length; for the rim, this is measured from nominal rolling point to the bottom of the rim). To complete the determination of mass properties corresponding to each nominal wheel radius, a 3D geometrical model of the wheelset is created in the CAD modelling software Inventor 2017. The aforementioned wheel cross-section is sketched, from which a rotational solid body is created representing a single wheel. Figure 4.6 shows the sketch of the wheel's cross-section, in which h is the actually varying web length that determines the wheel's nominal radius r_0. Then, an axle as mentioned above is modelled and assembled with two wheels into a wheelset, see Figure 4.7. The assembly is given a uniform density of 7.85×10^3 kg/m³ for steel, from which the mass and the moments of inertia are calculated for any nominal wheel radius. The calculated results can be read out in Inventor from the assembly's "iProperties". The values of mass and principle moments of inertia about centre of mass of the wheelset for each nominal wheel radius read out from Inventor are listed in Table 4.2. The axes are defined as shown by the coordinate symbol in Figure 4.7. The products of inertia calculated by Inventor are all close to 0, as can be anticipated from the highly symmetric form of the body, and thus omitted.

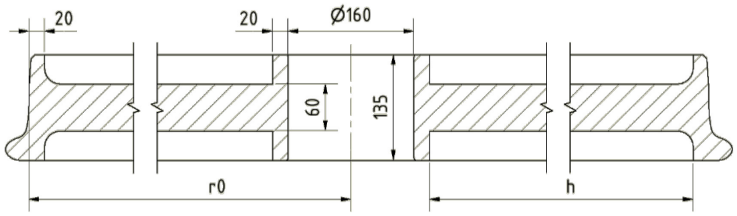

Figure 4.6 Simplified wheel cross-section with variable nominal radius

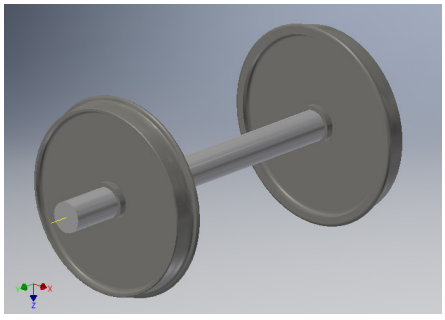

Figure 4.7 Simplified wheelset geometric model for mass property determination. Current figure shows wheels with the original nominal diameter Φ920 mm

The generated wheelset CAD model has a larger mass and greater moments of inertia around its rolling axis, which presents a more critical wheel-rail interaction condition, compared to the original model.

Table 4.2 Mass properties of the wheelset for each chosen nominal wheel radius

Wheel radius r_0	Mass m	Principle moments of inertia about centre of mass		
		I_{xx}	I_{yy}	I_{zz}
0.500	1,200.233	675.191	122.959	675.191
0.480	1,137.441	631.547	105.627	631.547
0.460	1,077.016	590.182	90.206	590.182
0.440	1,018.958	551.024	76.550	551.024
0.420	963.268	514.002	64.521	514.002
0.400	909.946	479.050	53.984	479.050
0.380	858.991	446.104	44.811	446.104
0.360	810.404	415.102	36.881	415.102
0.340	764.184	385.987	30.077	385.987
0.320	720.331	358.703	24.287	358.703
0.300	678.846	333.197	19.407	333.197
0.280	639.729	309.420	15.336	309.420
0.260	602.979	287.324	11.982	287.324
0.240	568.597	266.865	9.256	266.865
0.220	536.582	248.003	7.074	248.003
0.200	506.934	230.699	5.362	230.699
0.180	479.654	214.917	4.046	214.917
0.160	454.742	200.625	3.063	200.625
0.140	432.197	187.792	2.351	187.792
Note: all values are given in SI units				

To simulate the effects of wheel profile scaling, separate wheel profile files are created, each containing one profile as shown in Figure 3.6 in the form of coordinate pairs. During the simulation of the first countermeasure, these profiles are accordingly applied to all wheels. To simulate the effects of implementing radial steering, a cross-link mechanism is added to a copy of the model. The links are modelled as massless, free bodies and are each bound to diagonally-positioned axleboxes with Type 5 force elements with stiff settings. Note that links do not exert forces each other; visually the detail of how the links divert from each other is omitted. Also omitted is the geometry of the extended adapters on axleboxes to which the links are connected. This model is otherwise fully interchangeable with the original Y25 bogie model and is switched onto the parent model for the simulations regarding the second envisaged countermeasure. The radial steering bogie model is shown in Figure 4.8.

4.1.3 The carbody submodel

The carbody model is entirely retained from the original MBS model, which already possesses the desired features such as having two swappable sets of mass properties to represent both a loaded and a tare wagon. The only adaptation is the use of the so-called communicator elements which were not available in Simpack 8 to allow the automatic positioning of the bogies on desired positions on the carbody upon integration of the substructures.

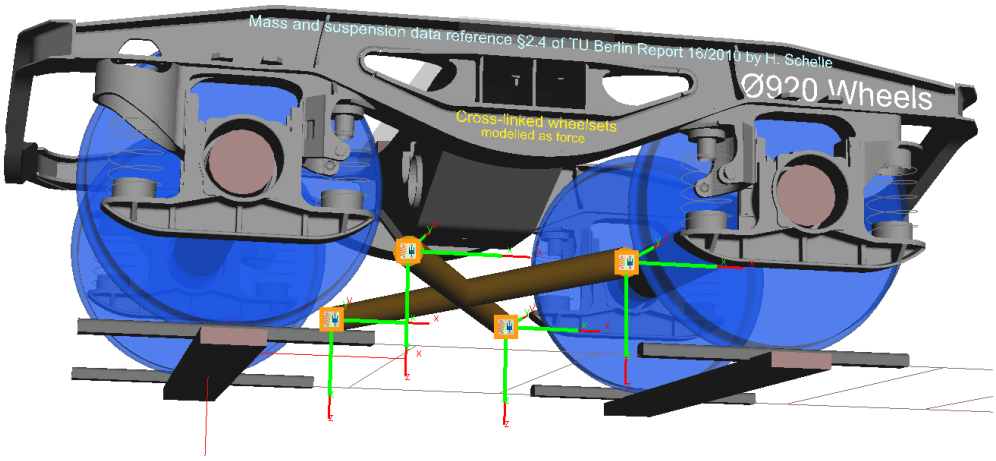

Figure 4.8 MBS model of the radial steering bogie

The mass properties of the carbody considered in both loading states are given in Table 4.3.

Table 4.3 Carbody mass properties

Loading state	Mass m	Principle moments of inertia about centre of mass			Centre of mass height above wheelset axis h_{CG}
		I_{xx}	I_{yy}	I_{zz}	
Tare	16600	2.42×10^{4}	2.95×10^{5}	2.91×10^{5}	1.36
Laden	79800	1.02×10^{5}	1.03×10^{6}	9.92×10^{5}	1.90
Note: all values are given in SI units					

4.2 Modelling of necessary testing conditions

This part of the work involves the all other important modelling aspects than the vehicle, including tracks, rails, solver settings, as well as elements for simulation process and post-processing control. Their different setups and combinations correspond to different aspects of running dynamics behaviour to be assessed, as already covered in detail in Chapter 3. These conditions are integrated within the complete vehicle model as well as into the process control scripts.

4.2.1 Stability

As mentioned in Section 3.3, the stability assessment criterion used is reduced from mathematical convergence of the leading wheelset's lateral offset as time reaches infinity to whether the lateral displacement consistently falls within a small threshold after a finite running time. Here, the solver settings are set up for the simulation to include 65 s of running with all speeds; in other words, the so-called "model time" is set as 65 s. A so-called "wall clock time" of 1 h is also set, meaning that the solver will abort a simulation run that has lasted more than 1h in real calculation time, thus avoiding corrupt runs holding up the simulation process. During the post-processing of the stability simulation results, the post-processing script uses type 112 filters "threshold count" to check the lateral displacement data for exceedance of the threshold [-1 mm, 1 mm] within the time frame [55 s, 65 s]. Should any exceedance occur, the behaviour is considered unstable. The post-processing script also checks if the simulation aborted before the model time reached 56 s, one second after the threshold time frame begins, in which case the

result data is considered to be insufficient for a reliable determination of stability and needs to be rerun with adjusted solver settings.

The straight test track modelled is 6000 m long, which is sufficient for the simulation to run for the 65 s fixed model time duration with any speed without the vehicle overshooting the end of the track. Between 25 m and 50 m from the beginning of the track, the excitation to drive the vehicle system into initial hunting is applied in the form of a lateral track offset irregularity. This irregularity is defined with a distance-domain harmonic function $y = 0.009 \sin 0.2\pi s_I$ with the lateral offset y given in mm and the distance along track from the start of the irregular track section s_I in m. The 9 mm amplitude of the irregularity function is consistent with the maximum flangeway clearance and is used to ensure the system's behaviour tending towards instability in Höpf bifurcations and avoid overestimating the nonlinear critical speed, as mentioned previously in Section 3.3. The irregular track section is placed well ahead of the entire vehicle in the initial state, in which the leading wheelset is positioned 10.83 m from the track's start point, so that the vehicle starts on a perfect straight track and enters the irregular section with a stable attitude. The first and last 5 m of the irregular section are smoothed to avoid excessive impact that may not be characteristic of a realistic irregularity passing scenario. Figure 4.9 shows the graphic of the initial irregularity exported from Simpack.

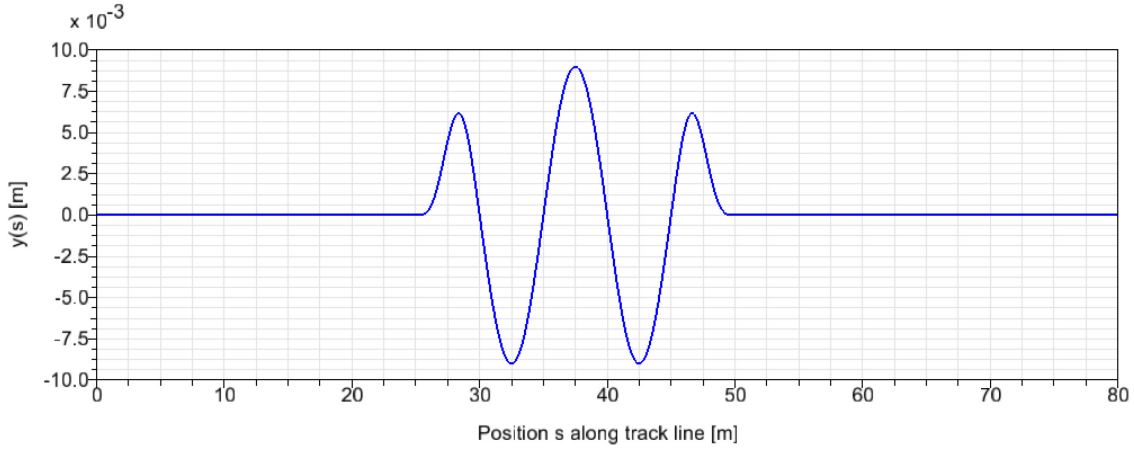

Figure 4.9 Initial excitation for stability simulations

The vehicle is given each test speed in turn and one time integration is performed with each given speed. The speed is applied as the vehicle's initial speed at solver start, meaning that the vehicle is considered to be already carrying the given speed at time 0 as opposed to being instantaneously accelerated from a different speed (in practice 0 or the end speed of the previous time integration) at time 0. The pre-processor script is in charge of assigning each chosen test speed to the model and starting the time integration.

4.2.2 Curving

Two separate track models are set up in the complete vehicle model for the two chosen curve radii. Within each track model, an S-curve is laid out using the track layout parameters calculated in Section 3.4.1, see Figure 4.10. The parameters are entered into the track modelling element as substitution variables. During the script-controlled test condition switching process, the substitution variables holding the vehicle speed and track superelevation are given values that achieve the desired uncompensated superelevation deficiency specified in Section 3.4.1. The pre-processing script also selects the curve

radius to be tested in turn by activating the track model with the desired radius and deactivating the other. The end result in Simpack is shown in Figure 4.11. Only the CAT2 curve is shown; the CAT4 curve has only radius and superelevation value differences.

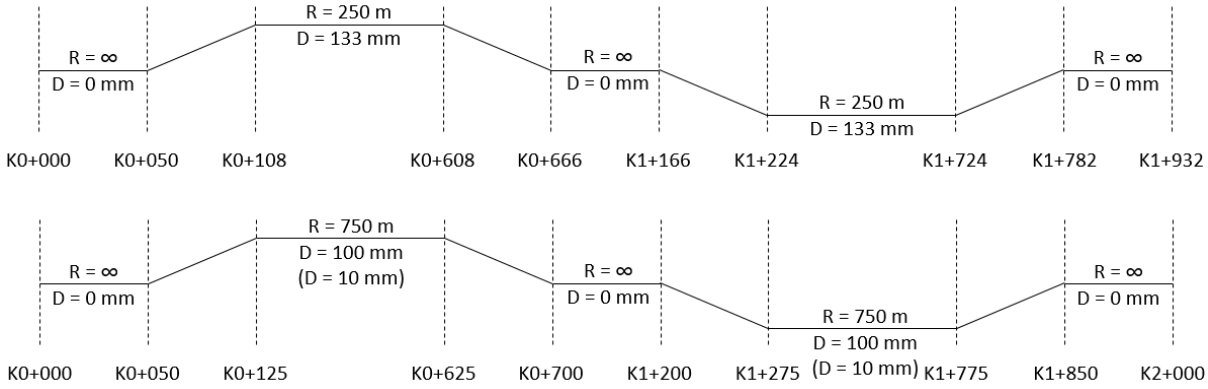

Figure 4.10 Track layouts modelled for the two curve radii (above: CAT4 curve; below: CAT2 curve). Transition curves have clothoid radius transitions and linear superelevation transitions. Track segment endpoint positions are given in kilometric point form

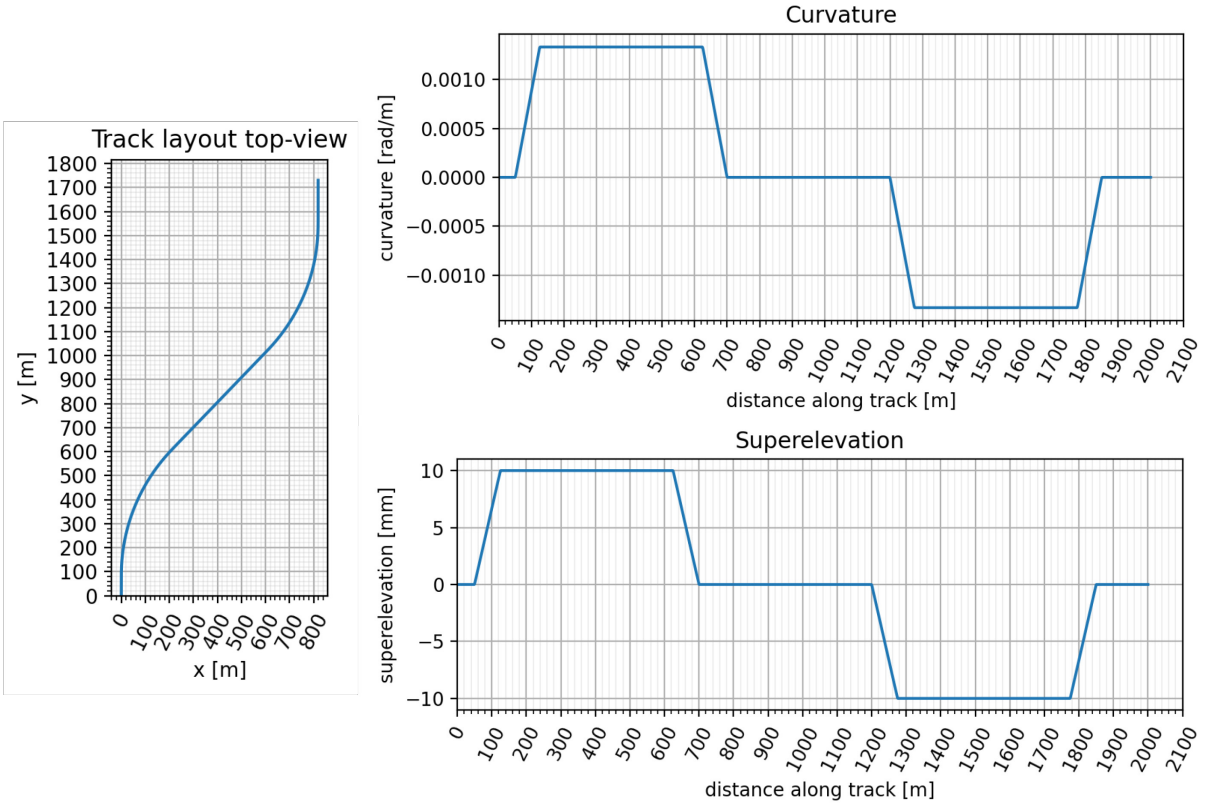

Figure 4.11 Track layout plots from Simpack for the CAT2 test track

The curved track is not given any excitations, as effects of track irregularity are not intended to be considered.

The simulation is designed to terminate once the test vehicle's first wheelset reaches the end of the track. This is realized by using a force element type 234 "stop integration", which is in fact a control element for the simulation process, set up to trigger a forced time integration stop when the leading wheelset's

s-coordinate (position of the centre point of the wheelset along track) becomes larger than the total length of the current track (1932 m for the CAT4 curve track and 2000 m for the CAT2 curve track). This spares the effort of calculating a suitable simulation end time to put into the solver while still enabling the simulation to run only until the vehicle clears the curved track segments of concern without redundant run time.

5 Running dynamics assessment for running gears with reduced wheel size

In this chapter and the next, the large amount of simulation results are summarized and visualized in respect to the two research purposes stated in Section 1.2. This chapter deals with the first research question, namely, presents a quantifiable visualization of the extent of change of a vehicle's stability, curve passing ability and wear from simulation results. The second research question of whether the compromised dynamical behaviour can be compensated will be dealt with in the next chapter.

5.1 Stability

5.1.1 Organization of available results

The simulation produces the time history of the lateral displacement of the vehicle's leading wheelset for each test scenario, stored in both tabular and image form exported directly from Simpack-Post. As an example, available results for the so-called "standard scenario" with the original Y25 bogie, 460 mm-radius wheels and S1002 wheel profile on a test track with the so-called "reference track setting" (1435 mm gauge and 1:40 rail cant as mentioned in Section 3.1) are given in Figure 5.1. The emergence and decline of the wheelset offset's unstable (diverging) behaviour, which may occur multiple times at different amplitudes as the vehicle's speed increases, can be seen here. Because the initial track irregularity that excites the vehicle has a spatially fixed wavelength, as the speed at which the vehicle runs over this irregularity increases, the frequency of the excitation also increases and passes different modal eigenfrequencies of the lateral oscillatory system that the vehicle comprises, triggering oscillatory behaviour of different modes. The stability of the system at each speed, as is judged by the Simpack-Post QSA script automatically with the criteria described in Section 3.3, can be read out from an annotation below the respective time history plots as shown in Figure 5.2.

Figure 5.1 Leading wheelset lateral displacement time history curves for test case with Y25 bogie, S1002 wheel profile, standard gauge, 1:40 rail cant and 460 mm nominal wheel radius, arranged in descending order of test speed with increment 2 km/h

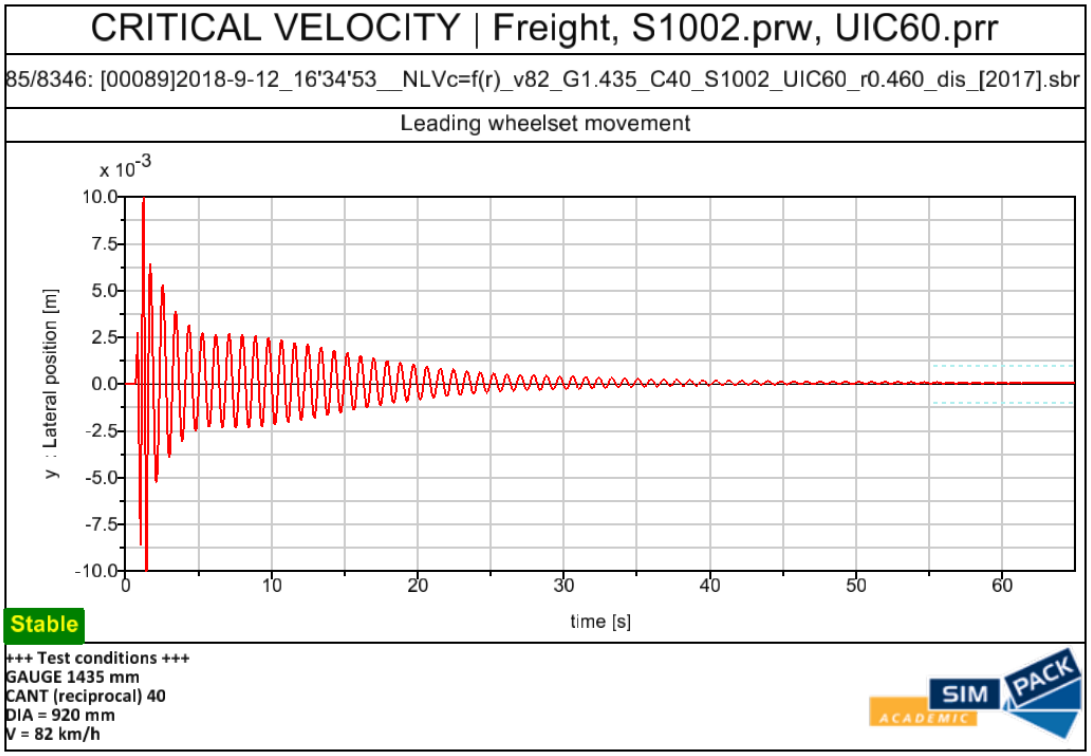

(a)

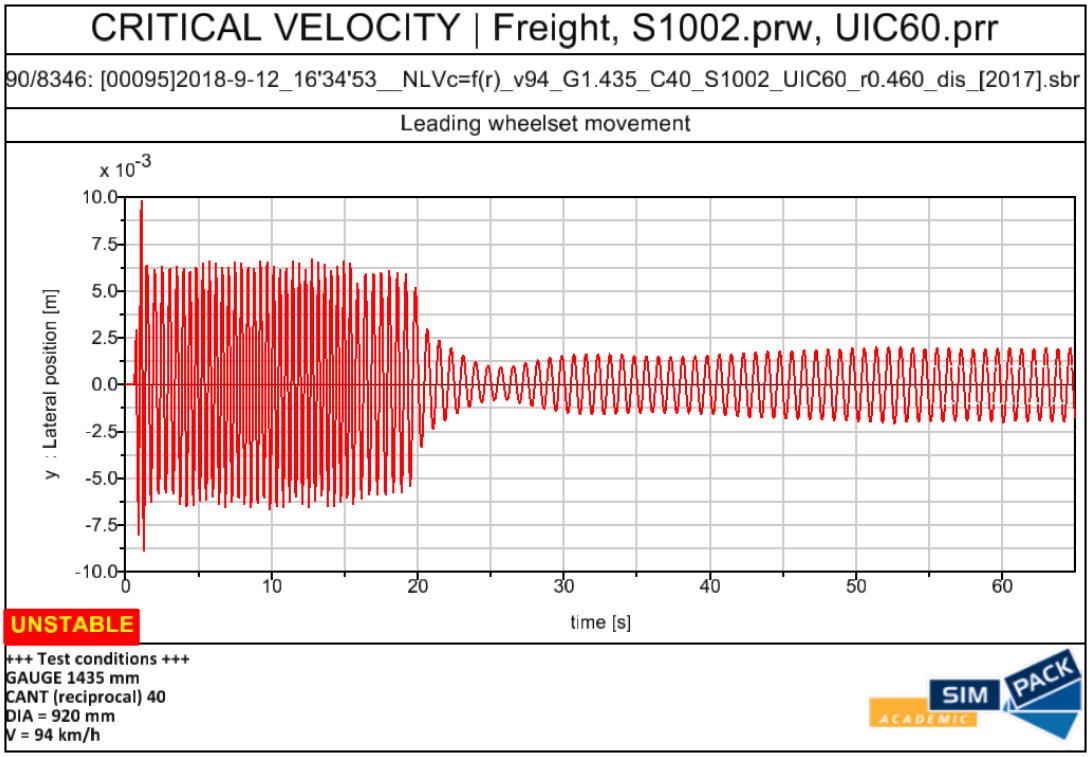

(b)

Figure 5.2 Time histories of leading wheelset lateral displacement with automatic stability judgment (a) example of a stable behaviour (at 82 km/h); (b) example of an unstable behaviour (at 94 km/h)

The stability at each test speed is logged in a summary table along with the respective test conditions, of which an excerpt is shown in Figure 5.3, from which the critical speed for each test case (combination of track gauge, rail cant, bogie type and wheel profile) can then be read as the lowest speed that exhibits an unambiguous unstable leading wheelset displacement behaviour over time. In this example scenario (which is the standard scenario mentioned above), the critical speed is read as 88 km/h.

Gauge(mm)	Cant(reciprocal)	r0(mm)	v(km/h)	Stability	Observation
1435	40	460	50	Stable	
1435	40	460	52	Stable	
1435	40	460	54	Stable	
1435	40	460	56	Stable	
1435	40	460	58	Stable	
1435	40	460	60	Stable	
1435	40	460	62	Stable	
1435	40	460	64	Stable	
1435	40	460	66	Stable	
1435	40	460	68	Stable	
1435	40	460	70	Stable	
1435	40	460	72	Stable	
1435	40	460	74	Stable	
1435	40	460	76	Stable	
1435	40	460	78	Stable	
1435	40	460	80	Stable	
1435	40	460	82	Stable	
1435	40	460	84	Stable	

Gauge(mm)	Cant(reciprocal)	r0(mm)	v(km/h)	Stability	Observation
1435	40	460	86	Stable	
1435	40	460	88	UNSTABLE	
1435	40	460	90	Stable	
1435	40	460	92	UNSTABLE	
1435	40	460	94	UNSTABLE	
1435	40	460	96	Stable	
1435	40	460	98	UNSTABLE	
1435	40	460	100	UNSTABLE	
1435	40	460	102	UNSTABLE	
1435	40	460	104	Stable	
1435	40	460	106	Stable	
1435	40	460	108	Stable	
1435	40	460	110	Stable	Stabilized off-centre
1435	40	460	112	UNSTABLE	
1435	40	460	114	UNSTABLE	
1435	40	460	116	UNSTABLE	
1435	40	460	118	Stable	
1435	40	460	120	UNSTABLE	

Figure 5.3 Summary table for the stability of all speeds tested within one test case

For each test case, the stability of the vehicle for all tested wheel radii at each speed is mapped out in a colour-coded v-r_0 plot. An example is seen in Figure 5.4 in Section 5.1.2 below. The observed stability behaviour of the vehicle with each value of nominal wheel radius r_0 running at each speed is indicated by a specific colour given to the corresponding point in the v-r_0 plot. The colour code is defined in Table 5.1. A line connecting the plot points corresponding to the lowest speed at which instability occurs for each nominal wheel radius is drawn to highlight the non-linear critical speeds read out from the current set of simulations as well as show its trend against varying r_0. The read-out value of non-linear critical speed for each nominal wheel radius r_0 is also shown above the plot, aligned with the respective vertical grid line for each r_0.

It is to be noted how the critical speed is to be read out concerning an observed instability at the lowest tested speed 50 km/h and a consistent observation of stability up to the highest tested speed 120 km/h. Recall that the definition of non-linear critical speed assumed in this research is the lowest speed at which instability is first observed. Note that an instability occurring at the lowest tested speed (50 km/h) does not rule out instability occurring at an even lower, untested speed, and hence such an observation must be interpreted as that the vehicle's non-linear critical speed is less than or equal to 50 km/h. Likewise, when the vehicle exhibits stability for all speeds up to the tested speed, the lowest speed at which instability occurs cannot be determined any more accurately than that it is greater than 120 km/h. Such an observation must be interpreted as the vehicle's non-linear critical speed is greater than 120 km/h.

5.1.2 Assessment of stability behaviour variation in relation to nominal wheel radius

5.1.2.1 Behaviour with reference track settings (1435 mm gauge, 1:40 rail cant)

Stability results mapped in Figure 5.4 indicate that under reference track settings, a regular Y25 bogie with S1002 wheel profile running on standard track experiences a reduction in non-linear critical speed with reducing wheel radius in an approximately linear v_C^{NL}-r_0 relation, with v_C^{NL} reducing by circa 2 km/h for every 20 mm of reduction in r_0. By the stability criteria assumed herein, the original Y25 reference bogie with r_0 = 460 mm is observed to possess a critical speed of v_C^{NL} = 88 km/h.

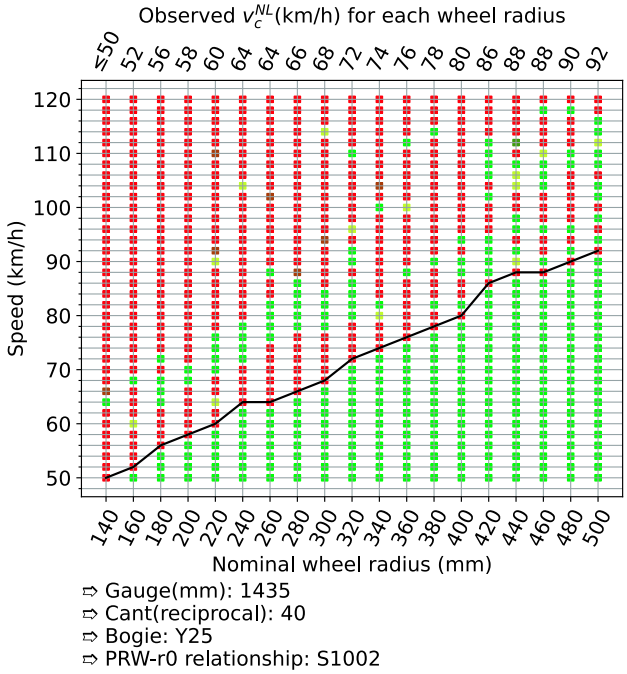

Figure 5.4 Stability observation of the Y25 bogie with S1002 wheel profile on standard (1435 mm gauge, 1:40 rail cant) track

Table 5.1 Colour legend for plot points in stability maps

Plot colour	Indication	
Bright green ■	Stable	Automatically determined by script
Dark green ■		Visually determined from a partially finished simulation run
Yellow green ■		"Off-centre" stabilization (converging to a non-zero displacement)
Bright red ■	Unstable	Automatically determined by script
Dark red ■		Visually determined from a partially finished simulation run
Grey ■	Inconclusive (broken simulation run or result unavailable)	

5.1.2.2 Behaviour on track with different track gauge and rail cant settings

Stability maps for both 1:40 and no rail cant are shown in Figure 5.5 and Figure 5.6 respectively, both in side-by-side comparison across the four gauges.

With different track gauges, the vehicle's change of stability behaves with the same general trend in which a smaller wheel radius gives rise to a lower non-linear critical speed. However, for a given nominal wheel radius, the critical speed does not take on a monotonous correlation to varying gauge. With the case r_0 = 460 mm for instance, the critical speeds for 1430 mm, 1432 mm, 1435 mm and 1437 mm gauge are respectively 96 km/h, 94 km/h, 88 km/h and 96 km/h for 1:40 rail cant and 90 km/h, 90 km/h, 82 km/h and 80 km/h for no rail cant. The situation becomes more complex with smaller wheels, as will be analyzed below.

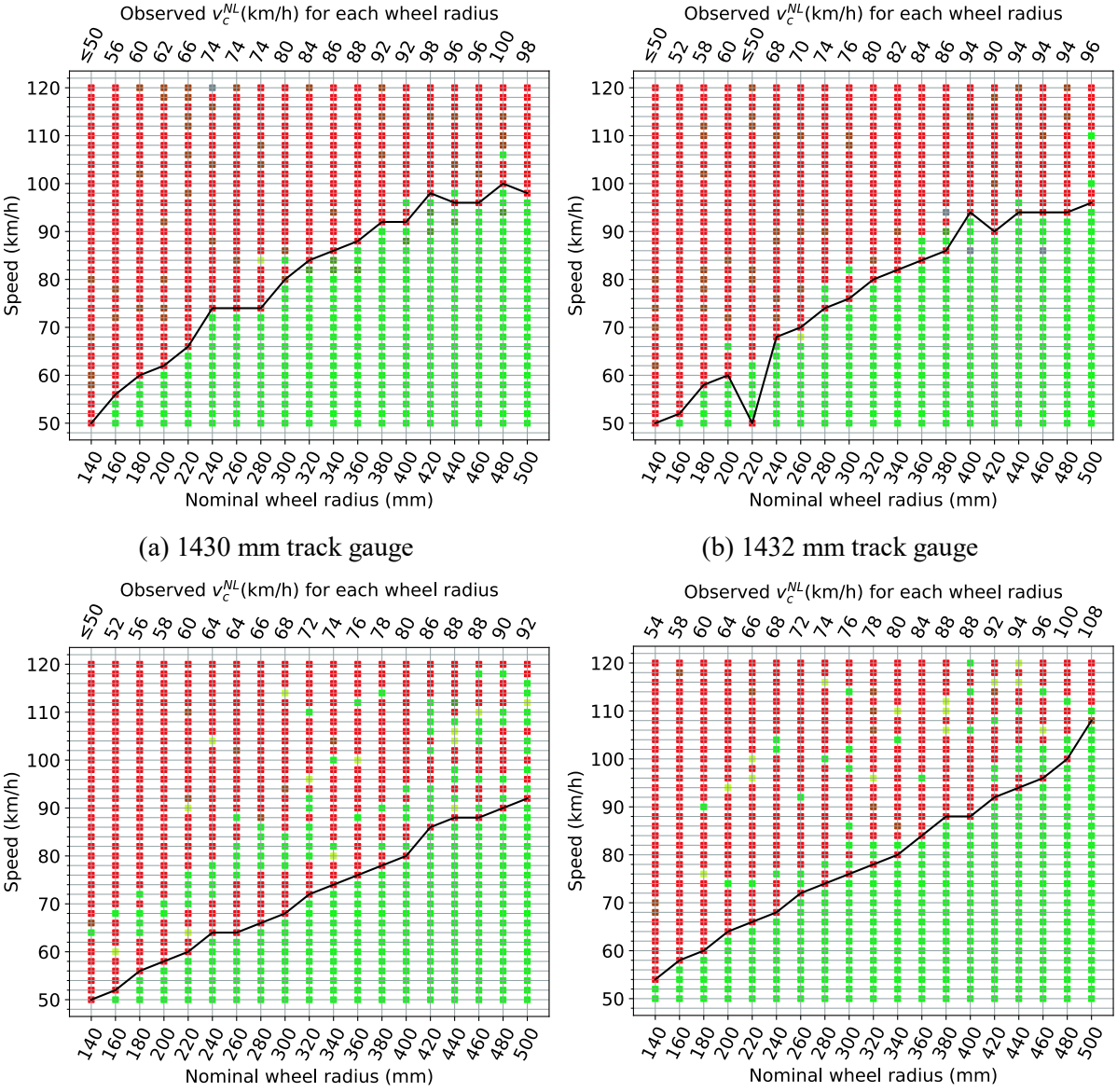

(a) 1430 mm track gauge

(b) 1432 mm track gauge

(c) 1435 mm track gauge

(d) 1437 mm track gauge

Figure 5.5 Comparison of the stability behaviour across different track gauges with rail cant 1:40

Whereas the single instability observed for 1432 mm gauge, 1:40 rail cant, r_0 = 220 mm at 50 km/h in Figure 5.5 (b) seems like an outlier, a view at the leading wheelset's lateral displacement time history for speeds 50 km/h – 56 km/h indicate that the instability is the beginning of the combination of different modes of oscillation. At 54 km/h and 56 km/h beats become distinctly visible, suggesting a superposition of two oscillations with different frequencies, see Figure 5.7. A closer look at the motion time histories of all major bodies in the front half of the vehicle – wheelsets 1 and 2, bogie 1, and carbody – shows that the beat frequency of wheelset 1's lateral motion (0.13 Hz) is approximately equal to the difference of the dominant frequencies of wheelset 1's own dominant oscillation frequency (1.40 Hz) and that of the carbody (1.27 Hz), as is shown in Figure 5.8. This observed process of beat development indicates that the consistent instability occurring at speeds at 64 km/h is in fact the secondary hunting, with the carbody's motion contributing strongly to the behaviour. The observation that the vehicle was already unstable at 50 km/h before the motion of the carbody became pronounced enough to cause discernable

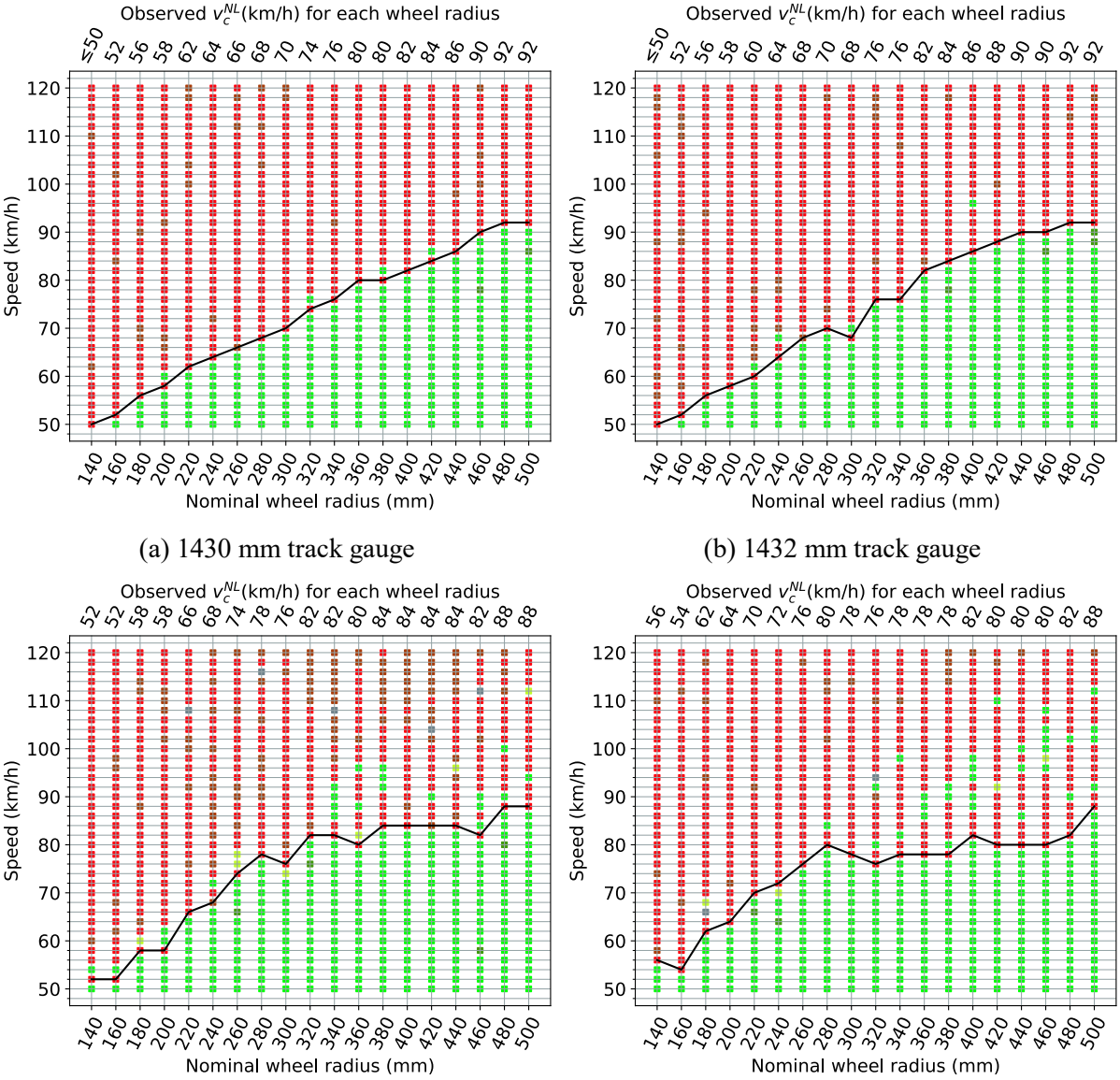

(a) 1430 mm track gauge

(b) 1432 mm track gauge

(c) 1435 mm track gauge

(d) 1437 mm track gauge

Figure 5.6 Comparison of the stability behaviour across different track gauges with no rail cant

beats after being superposed to the wheelset motion indicates that the wheelset's primary hunting motion is already unstable. For nominal wheel radii smaller than 220 mm, the same phenomenon may also have occurred at speeds lower than 50 km/h, which are not within the scope of the conducted sets of simulations and thus not observable. Ultimately, this observation brings the observed values of v_c^{NL} for nominal wheel radii below 220 mm into question: the actual non-linear critical speeds for these wheel radii may likewise be lower than 50 km/h due to the same possibility of pronounced primary hunting.

Note how this analysis above indicates that for larger nominal wheel radii, such as the case of r_0 = 460 mm mentioned, the first-appearing instability under 1435 mm and 1437 mm gauges are not occurring with the same oscillation mode as that under 1432 mm gauge. With the former two gauges, the re-stabilizing behaviour at higher speeds indicate that the first-observed instability is occurring with the primary hunting of the wheelsets only, whereas with the latter there is primary hunting instability occurring at much lower speeds with small wheels that diminish as the wheels increase in size, and for larger wheels the first-observed instability is in fact occurring under the influence of secondary hunting.

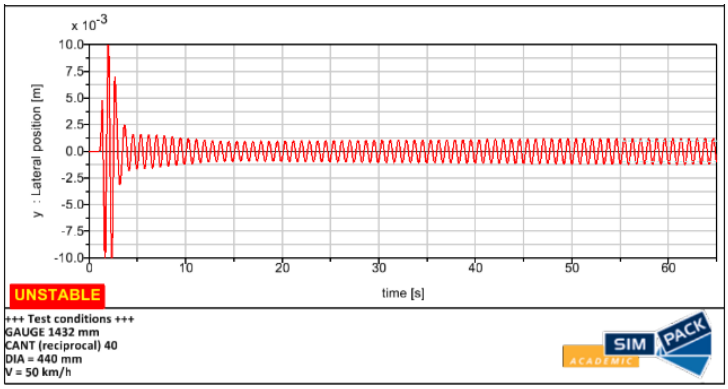

(a) 50 km/h

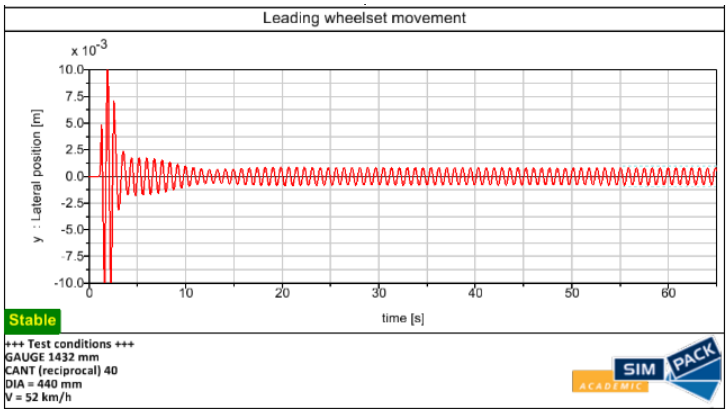

(b) 52 km/h

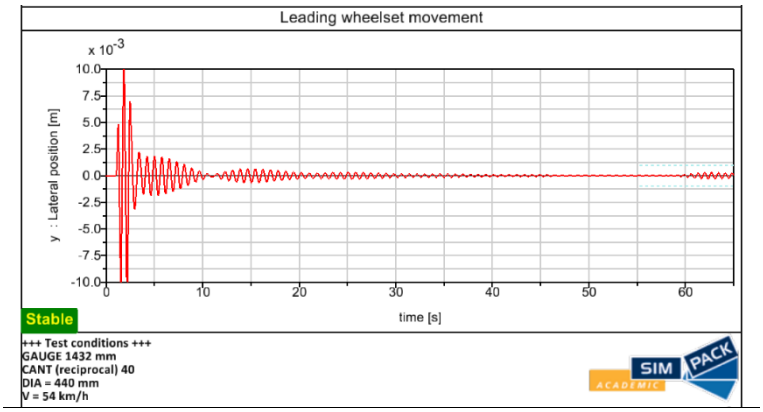

(c) 54 km/h

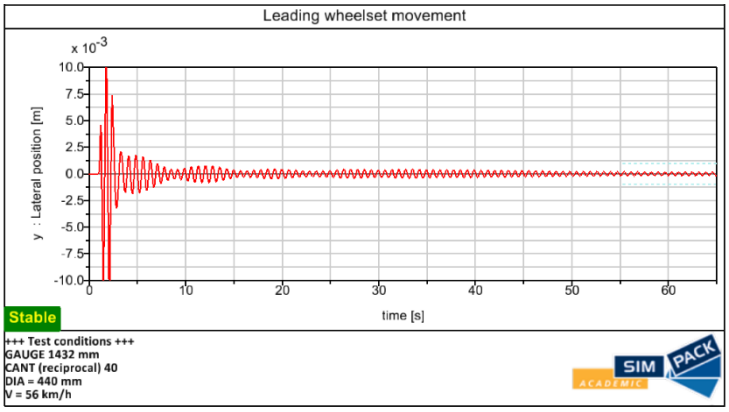

(d) 56 km/h

Figure 5.7 Emergence of beats observed with speeds 50 km/h-56 km/h for the simulation case with 1432 mm gauge, 1:40 rail cant, Y25 bogie, S1002 wheel profile and 220 mm nominal wheel radius

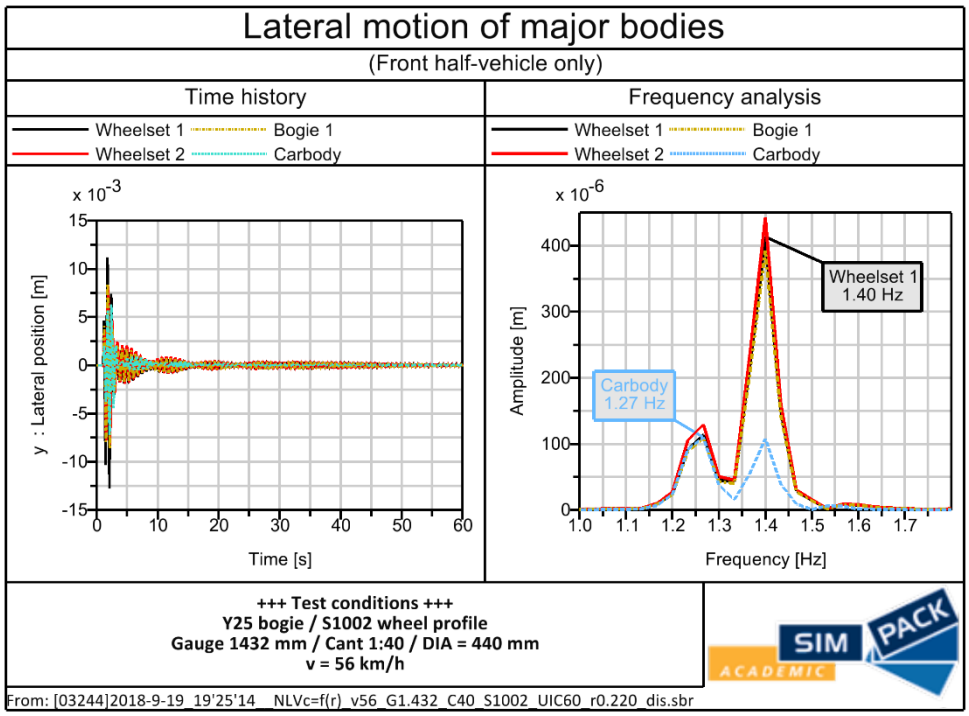

(a)

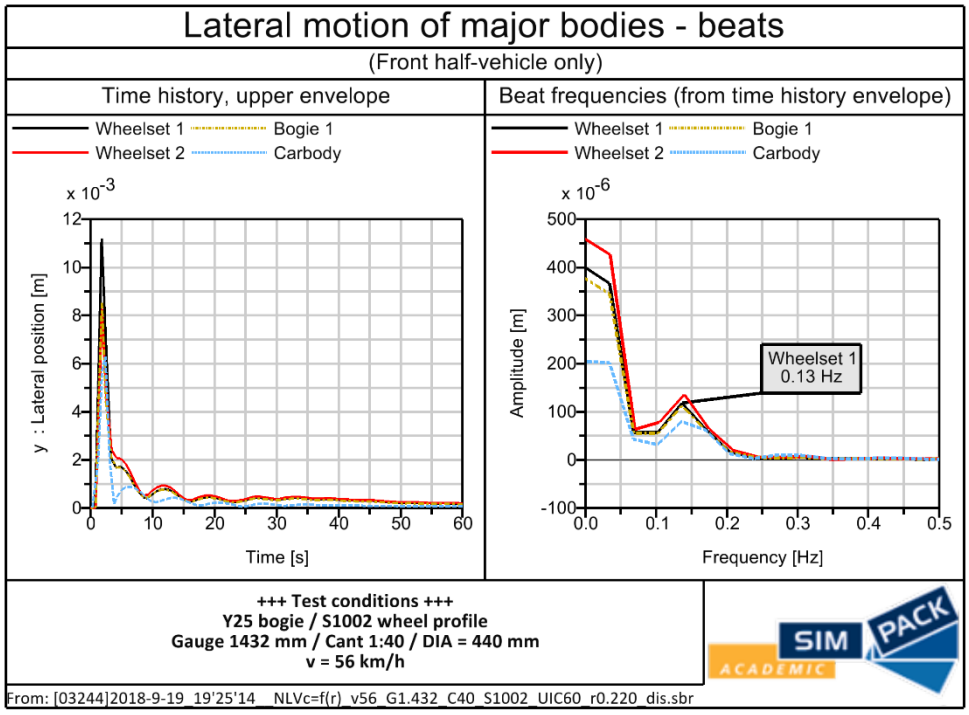

(b)

Figure 5.8 Dominant frequencies of the lateral motions of the carbody and wheelset 1 (a) compared with beat frequency of the motion of wheelset 1 (b)

This further indicates that small wheels which have not undergone any further modifications are incapable of gaining the necessary stability for operation on tracks with narrow gauges. A similar behaviour is found in later simulations involving profile modifications in Chapter 6. It is seen that the re-stabilization of the vehicle in some settings attribute to the influence of carbody motion. However, unlike the case mentioned above, this behaviour does not affect the readout of the critical speed in most of the cases, and thus a detailed analysis for every occurrence of re-stabilization does not need to be conducted.

The observations show that with a vehicle with realistic nonlinearities considered, neither the equivalent conicity λ_e nor the gravitational stiffness mentioned in Section 2.2 alone are sufficient in predicting the trend of non-linear critical speed for any given wheel size. Table 5.2 lists the equivalent conicity λ_e^{3mm} of the S1002 wheel profile in all gauge and rail cant conditions, calculated over ±3 mm offset from the respective contact position on the tread. The critical speed readouts from each track setting are compared in Figure 5.9, with the conicity given for each track setting. Additionally, the contact gradient difference for each lateral offset of the wheelset under each track setting is read out from Simpack-Pre and plotted in Figure 5.10, in which the slope of each curve is proportional to the gravitational stiffness under each track setting. It can be seen that neither appears to have a direct and deterministic relation to whether a certain track setting may result in a higher non-linear critical speed or whether primary hunting instability may become distinct for any nominal wheel radius. Note that according to Figure 5.10, when viewing the contact gradient difference at ±3 mm wheelset offset (same as the offset amplitude used for determining the equivalent conicity in this research) and sorting the track settings by value of $(\tan\delta_R - \tan\delta_L)\,|_{y=3\text{ mm}}$, the sort order is the same as when sorted by λ_e^{3mm} as is shown in Table 5.2. It is thus seen that for the herein involved S1002-UIC60E2 wheel-rail profile geometry pairing, a track setting that results in a higher conicity also gives rise to a higher gravitational stiffness. Since a high conicity is detrimental for stability and a high gravitational stiffness is beneficial for stability, as is explained in Section 2.2, the same track setting causes the conicity and gravitational stiffness to change in directions with opposite effects on the stability of the vehicle, and it cannot be determined which factor has the dominant influence for this specific wheel-rail profile geometry pairing. Furthermore, the influence from the non-linearity in the primary suspension, etc. on the vehicle's behaviour after receiving the specific initial excitation used herein is not quantifiable. This observation stresses the necessity of choosing the simulation-based approach for the purpose of this research. How exactly each profile pair affects the conicity and gravitational stiffness as well as how these two factors affect the critical speed of the vehicle is another research topic that will not be covered in this thesis.

Table 5.2 Equivalent conicity over 3 mm amplitude of the S1002 wheel profile under different track gauge and rail cant settings. The number given in circles after each value of λ_e is the sort sequence in descending order of value (1 as the smallest and 8 as the largest)

Gauge (mm) / Rail cant	1430	1432	1435	1437
None	0.367393 ⑧	0.262172 ⑦	0.163463 ⑤	0.121177 ③
1:40	0.216384 ⑥	0.131178 ④	0.076954 ②	0.053556 ①

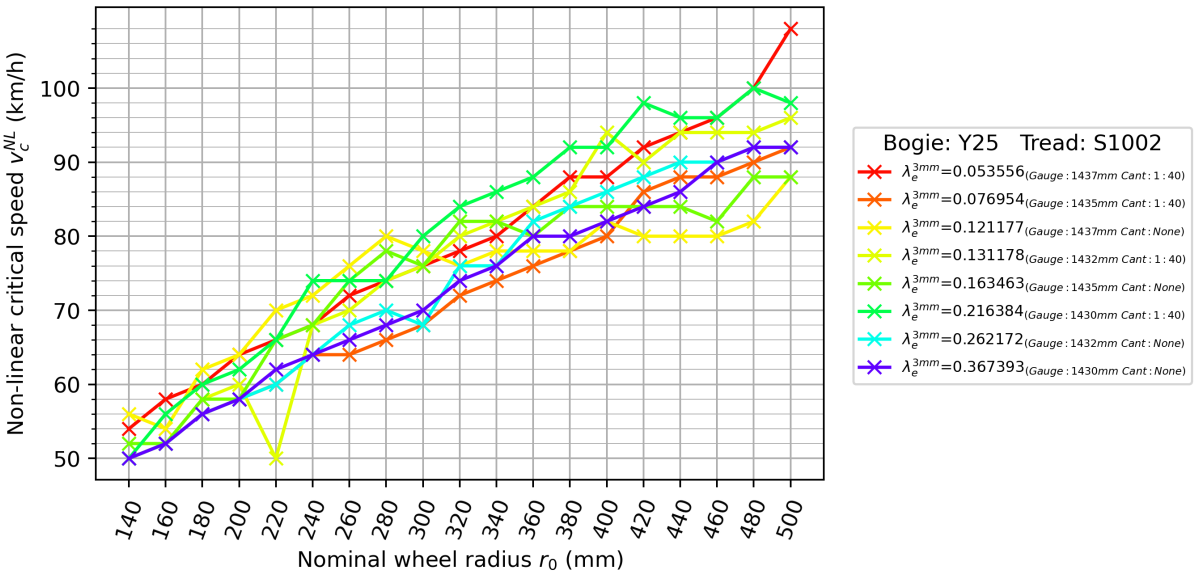

Figure 5.9 v_c^{NL}-r_0 relation of the Y25 bogie with S1002 wheel profile, compared with regard to equivalent conicity

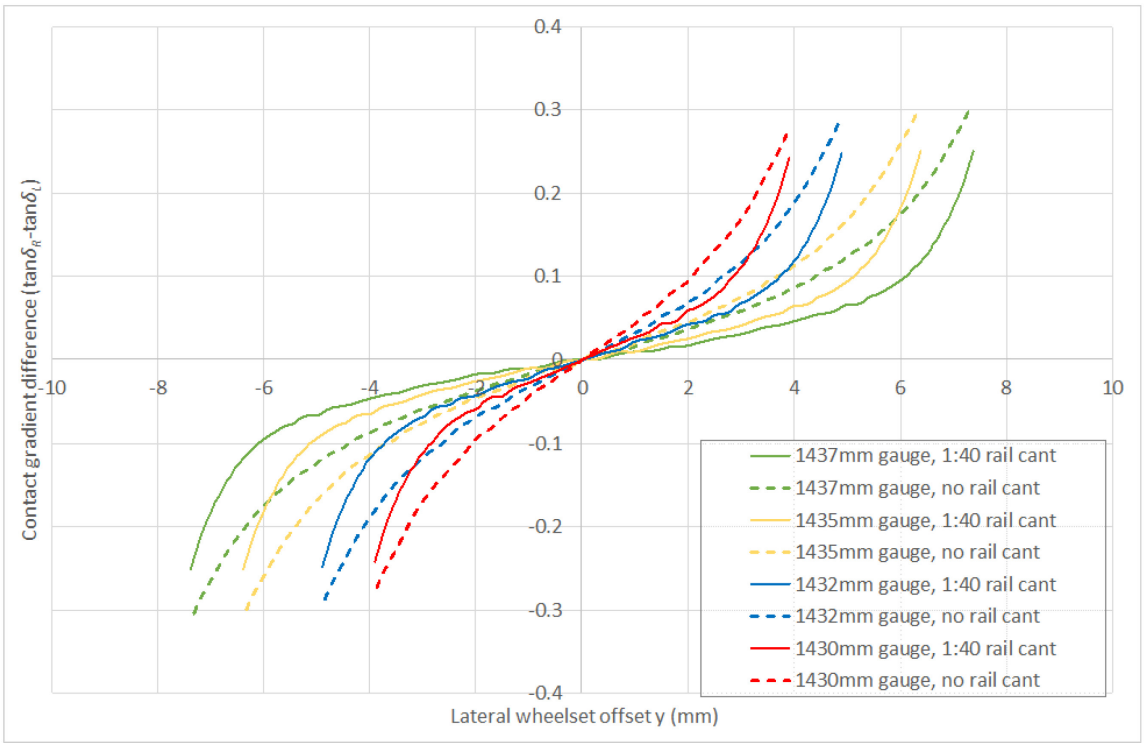

Figure 5.10 Contact gradient difference against lateral wheelset offset of the Y25 bogie with S1002 wheel profile for all track settings

5.2 Curve negotiation

5.2.1 Organization of available results

From the curve-passing time integration results, which are available in the form of time-history curves, the maximum magnitudes of all three curve negotiation performance indices (wheel-rail lateral force Y, sum of wheel-rail lateral forces on one wheelset ΣY, derailment coefficient Y/Q) among all wheels (for

Y and Y/Q) or wheelsets (for ΣY) are recorded in a summary table as $|Y|_{max}$, $|\Sigma Y|_{max}$ and $|Y/Q|_{max}$, together with the number indicating the position (defined as in Appendix A) of the wheel or wheelset at which the maximum is observed. The summarized magnitude peak values are then plotted against nominal wheel radius r_0 in each track, curve, superelevation deficiency and vehicle load state setting, with the location (wheel or wheelset number) where the largest magnitude occurs for each nominal wheel radius r_0 marked above the plot lined up to the vertical grid line corresponding to each r_0 value. The maximum magnitude of each performance index represent the most critical situation occurring within all vehicle-track interfaces of the same vehicle and are thus the ultimate quantities of concern for the dynamics behaviour of the vehicle, whereas their location of occurrence as well as the individual curve-passing time history plots themselves offer supplementary information to the vehicle's attitude and behaviour while negotiating the curve necessary for understanding the actual process of curving and plausibility of questionable observations.

Simulations are done for all combinations of the following setting parameters:

- Track gauge: 1437 mm, 1435 mm, 1432 mm, 1430 mm
- Rail cant: 1:40, none
- Track curve (referred to in following text by their corresponding curve passing test category given in EN 14363): R = 750 m (CAT2), R = 250 m (CAT4)
- Superelevation level: deficient ($I > 0$), ideal ($I \approx 0$), excessive ($I < 0$); respectively abbreviated as Δa_+, Δa_0, Δa_-
- Vehicle load state: tare, laden

This totals to 96 different cases, each with a set of simulation results for all 19 nominal wheel radii involved, making the number of simulations 1824.

Here, the 96 sets of simulation results are visualized with each combination of vehicle load state, track gauge and rail cant settings constituting a separate diagram and each combination of track curve radius and level of uncompensated centrifugal acceleration settings plotted as an individual line-connected scatter plot in each diagram. This way the results can be organized rather concisely without impeding the presentation of the results as is needed for the first research goal.

Due to the large quantity of diagrams, all simulation result summary plots (maximum magnitude of curve passing behaviour indices against nominal wheel radius) are collected in Appendix C.

5.2.2 Assessment of curve negotiation behaviour variation in relation to nominal wheel radius

Notable observations from the curve passing result summary plots are explained in this section respectively for each curve negotiation performance index (wheel-rail lateral force, sum of lateral wheel-rail forces on one wheelset and derailment coefficient).

5.2.2.1 Wheel-rail lateral force

Here, the behaviour of the vehicle on the 750m-radius (CAT2) and 250m-radius (CAT4) curves will be described respectively in this sequence, followed by an overall remark concerning both curves regarding the safety in terms of wheel-rail lateral force.

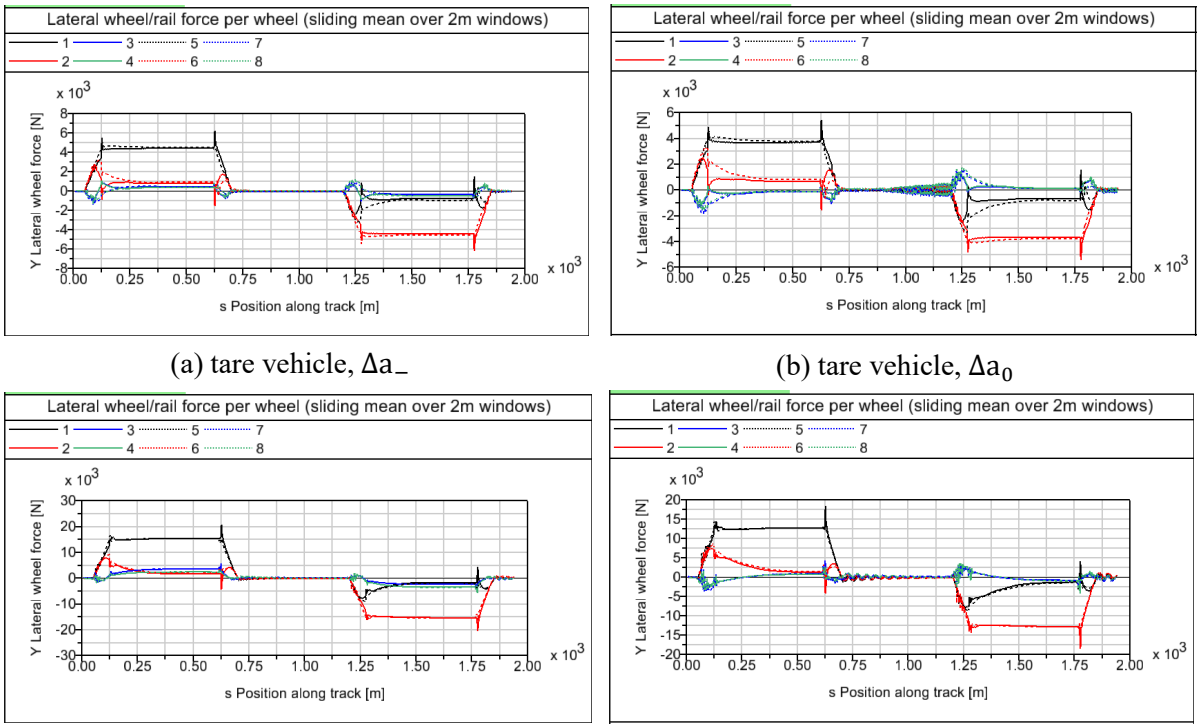

(a) tare vehicle, $\Delta a_{\_}$

(b) tare vehicle, Δa_0

(c) laden vehicle, $\Delta a_{\_}$

(d) laden vehicle, Δa_0

Figure 5.11 Lateral wheel-rail forces against displacement along track. Conditions: Y25 bogie, S1002 wheel profile, r_0=140 mm, 1435 mm gauge, 1:40 rail cant, CAT2 curve

When the test vehicle, either laden or tare, passes the CAT2 curve, it is observed for all track gauge-rail cant combinations that when the superelevation deficiency is non-positive, the maximum magnitude of Y occurring among all wheel-rail pairs of the vehicle decreases monotonously as the wheel size reduces. The reduction of the necessary wheel-rail guidance force in order to complete the curving process indicates an improvement in curving performance which is achieved with the use of smaller wheels. A negative superelevation deficiency, i.e. a slower pass, results in higher wheel-rail lateral forces than a near-zero superelevation deficiency; in both cases the wheel with the highest wheel-rail force is on the leading wheelset. A view of the plot of wheel-rail lateral force Y over position along track for each wheel (derived directly from the time history plot) shows that the inside wheels of both bogies' leading wheelsets (wheels 1 and 5 for the first, right curve; wheels 2 and 6 for the second, left curve) indeed endure more lateral force than other wheels, with the peak occurring at the end of the round curve, see the example with the smallest simulated wheel in Figure 5.11; the same is also observed for other values of r_0.A distinctively different behaviour is observed for the case of deficient superelevation, or fast passing of a curve. In the middle of the tested range for r_0 values, $|Y|_{max}$ almost remains constant for all track gauge-rail cant combinations, varying only in a small range of approximately 5 kN to 6 kN in tare state and 16 kN to 21 kN in laden state of the vehicle, with the wheels that experience the greatest Y always belonging to the rearmost wheelset (wheels 7 or 8). For the largest simulated wheel sizes, a larger $|Y|_{max}$ may occur at a wheel belonging to the front wheelsets of one of the bogies, which decreases with decreasing r_0 until it reaches the above-mentioned range. On the smaller end of the range of tested r_0 values, the $|Y|_{max}$ increases again for track gauge-rail cant combinations that give rise to a smaller equivalent conicity, where one of the rear wheelsets of the two bogies becomes the heaviest loaded. This increase of $|Y|_{max}$ can be very drastic, reaching 59 kN for a laden vehicle and 27 kN for a tare vehicle, in both load states occurring with track gauges 1435 mm and with uncanted rails. A look at the Y-s

diagrams of the two cases with 1435 mm gauge show that the vehicle is already in the state of unstable hunting during the curve passing at the given speed of 100 km/h, see Figure 5.12. The almost "filled" appearance in certain sections of the wheels' Y-s curves indicate very steep and very rapid fluctuations in the wheel-rail lateral forces in these sections. This fluctuation as well as the high amplitudes of the lateral wheel-rail forces indicate violent wheel-rail impact, which arises from the entry of each wheelset into the first transition curve and carries through the entire passing of the round curve. Recall from Section 5.1.2 that the non-linear critical speed under the said conditions is 52 km/h. Whereas the front wheelsets of both bogies are constrained by flange guidance during the curve negotiation and have less room to hunt, the two rear wheelsets undergo violent hunting and repeated flange-rail impact as the bogies pivot about the front outer wheels, especially after entering the straight track section in the middle of the S-curve.

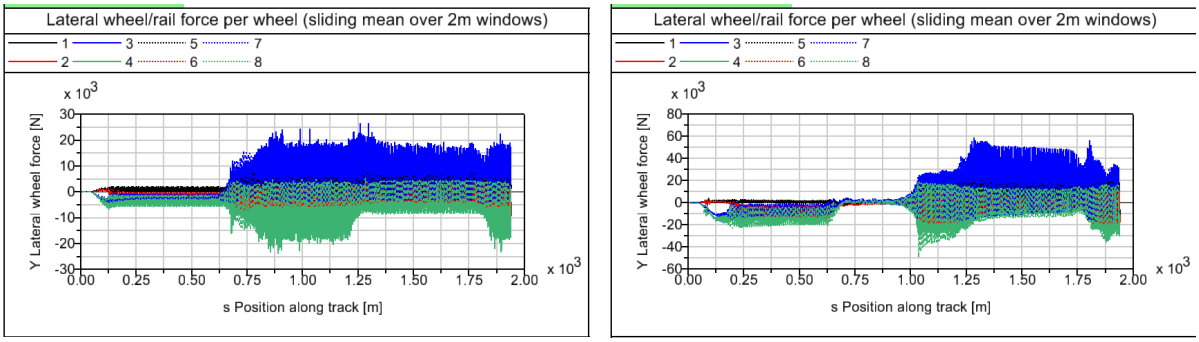

(a) tare vehicle (b) laden vehicle

Figure 5.12 Lateral wheel-rail forces against wheelset displacement along track in a situation where instability occurs during curve passing. Conditions: Y25 bogie, S1002 wheel profile, r_0=140 mm, 1435 mm gauge, 1:40 rail cant, CAT2 curve, Δa_+

The effect of track gauge and rail cant on $|Y|_{max}$ is observed to be minimal. $|Y|_{max}$ levels are similar for all four track gauges and both rail cant settings, although a larger gauge and 1:40 rail cant can be seen to slightly reduce $|Y|_{max}$.

When the test vehicle passes the CAT4 curve, a generally decreasing trend of $|Y|_{max}$ with decreasing r_0 is observed for both load states and all three superelevation deficiency levels. Unlike with the CAT2 curve where slow-passing always causes the highest $|Y|_{max}$ (provided no hunting instability occurs), here, for a tare vehicle, negotiating the curve with positive superelevation deficiency with any gauge, any rail cant and any wheel size almost always results in a higher $|Y|_{max}$ than with near-zero or negative superelevation deficiency. With the laden vehicle, a notable observation is made regarding the slow-passing of a vehicle with smaller wheels, which was designed into this investigation due to lack of prior research: for each combination of track gauge and rail cant, as r_0 decreases, the $|Y|_{max}$-r_0 curve for negative superelevation deficiency transcends the other two curves and becomes the curve with the highest $|Y|_{max}$ among the three cases of superelevation deficiency for r_0 < 220 mm in all track gauge and rail cant settings. This shows that the reduction in wheel size worsens the behaviour of a heavy vehicle negotiating a superelevated curve at low speeds, making slow-passing the most risky curve passing scenario in terms of wheel-rail lateral loading. As is also observed with the CAT2 curve, the effect of the track gauge and rail cant is insignificant.

The quasistatic guidance force (lateral wheel-rail force) is limited by EN 14363 [16] with regard to stress loading on the track as permissible up to 60 kN. Result summary plots of the laden vehicle (a tare vehicle

gives rise to a smaller wheel-rail lateral force and is of no concern when considering track loading limits) in Figure C.10 - Figure C.17 show that this value is approached with larger wheels during the fast passing of a small-radius curve. Note that the lateral force value shown in the plots are peak values of the magnitude of wheel-rail lateral force that usually occurs at the end of the round curve where quasistatic curving occurs; the actual quasistatic guidance force is lower than this value. A smaller wheel results in a smaller $|Y|_{max}$ farther away from the limit value, which represents a safer curve passing situation in terms of track loading; that is, as long as it does not induce the instable hunting motion within the curve as is seen in Figure 5.12, otherwise the limit value may be exceeded even on a large-radius curve, for which the curve negotiation itself is obviously not the cause of the exceedance, thus ruling the situation out of the scope of curve analysis. For the smallest wheel radii, although a wider track gauge only has a marginal effect in reducing $|Y|_{max}$, the gauge increase does cause the tendency of in-curve stability loss to first increase due to the enlarged flangeway clearance and weakened lateral constraint on the wheelset by flange contact, then decrease due to the larger gauge's contribution to a higher critical speed. When no instability occurs, the Y level is always lower for the CAT2 curve as can be easily imagined, making the negotiation of a large-radius curve a non-critical scenario.

5.2.2.2 Sum of wheel-rail lateral forces for each wheelset

The wheel radius appears to have a less significant and less regular influence on the maximum magnitude of the sum of lateral wheel-rail forces of each wheelset $|\Sigma Y|_{max}$ when the uncompensated centrifugal acceleration is near-zero or negative. For the small-radius CAT4 curve, $|\Sigma Y|_{max}$ is observed to have a non-monotonous decreasing pattern with decreasing r_0 for both tare and laden vehicles; for the large-radius CAT2 curve, $|\Sigma Y|_{max}$ only slightly drops as the wheel becomes smaller for either loading state.

The fast-passing scenario is found to be critical for small wheels. On curves of both categories, a sharp increase in $|\Sigma Y|_{max}$ begins when the wheel radius decreases beyond a certain point. In a tare vehicle, this increase is due to the vehicle going into unstable hunting on the curve, as is seen by the sudden increase of $|\Sigma Y|_{max}$ by around 10 kN on either side of the discontinuity in the $|\Sigma Y|_{max}$-r_0 curve. For 1432 mm gauge, 1:40 rail cant as well as 1435 mm gauge, 1:40 rail cant, in which the vehicle does not go into instability for all wheel radii, the $|\Sigma Y|_{max}$ increase is not observed. However, a less drastic $|\Sigma Y|_{max}$ increase with decreasing r_0 is also seen for the laden vehicle where no unstable hunting occurs during curve passing. In Figure 5.13, a view of the ΣY-s plots of the example case of a laden vehicle with r_0 = 220 mm on 1432 mm gauge track with 1:40 rail cant shows no lasting hunting motion during the course of curve negotiation, although the vehicle is running over the critical speed and exhibits instability in both rear wheelsets either in the intermediate straight track section or upon entering the curve, ruling out unstable curve passing as the cause of the $|\Sigma Y|_{max}$ increase.

5.2.2.3 Derailment coefficient

On the CAT2 curve, the behaviour of the maximum value of derailment coefficient within the entire vehicle in relation to nominal wheel radius for each load state, track gauge and rail cant is very similar to that of the lateral wheel-rail force: for ideal or excessive superelevation a smaller wheel always corresponds to a lower derailment coefficient, for deficient superelevation the derailment coefficient stays

low and barely varied until the nominal wheel radius becomes very small, with which the derailment coefficient may spring up abruptly due to the curving run becoming unstable.

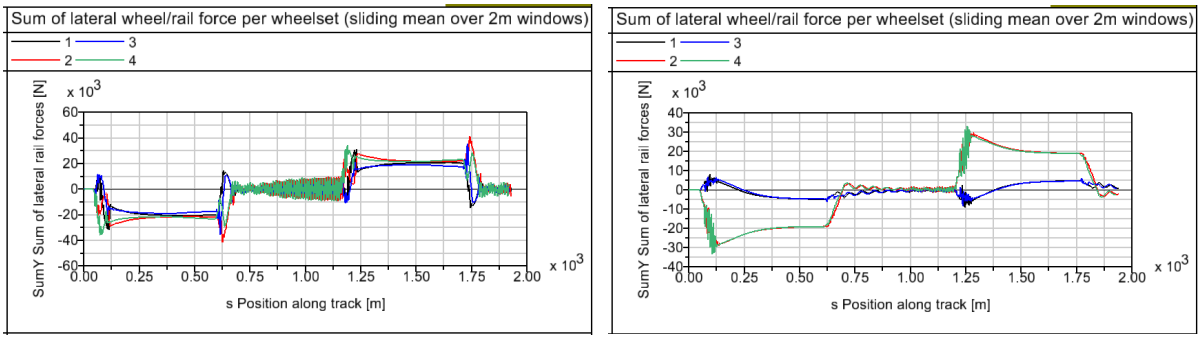

(a) CAT4 curve (b) CAT2 curve

Figure 5.13 Sum of lateral wheel-rail forces on wheelset against displacement along track. Conditions: laden vehicle, Y25 bogie, S1002 wheel profile, r_0 = 220 mm, 1432 mm gauge, 1:40 rail cant

On the CAT4 curve, the derailment coefficient exhibits a decreasing trend with decreasing wheel size, and for the smallest wheel radii, an upward jump in the derailment coefficient also occurs in some fast-passing cases similar to $|Y|_{max}$ and $|\Sigma Y|_{max}$ described above. Unlike the behaviour of $|Y|_{max}$, in which a positive Δa results in higher $|Y|_{max}$ compared to passing with near-zero or negative Δa in most cases, a negative Δa always causes a higher $|Y/Q|_{max}$ than the other two superelevation deficiency levels unless the nominal wheel radius is small enough to cause unstable hunting in the fast-pass scenario.

5.3 Wear

Figure 5.14 and Figure 5.15 show the test vehicle's wear work per unit distance in the first round curve in the tare and laden states respectively.

The general pattern of all the plots indicate that the reduction of the nominal wheel radius intensifies the wear, even though the curving behaviour of the vehicle is improved with decreased wheel size. However, with the vehicle in tare state, 1:40 rail cant and large track gauges, the wear number decreases again with decreasing wheel size for very small wheel sizes, except when negotiating the CAT4 curve with deficient superelevation.

The CAT2 curve is obviously non-critical from the aspect of wear, having only a fraction of the effective wear work observed with running on the CAT4 curve. In the subsequent wear analysis of other test cases, the CAT2 curve will no longer be included. Likewise, simulation results with the tare vehicle will also be omitted in upcoming analyses due to their insignificance in wear number levels observed.

When the vehicle is in the tare state, it can be observed that with gauge and rail cant combinations with larger equivalent conicities (as in Figure 5.14 (f)-(h), see Table 5.2 for actual λ_e values), a slower pass through the curve causes more wear than a fast pass for almost all values of r_0. Recall from Section 3.4.1 that the magnitude of uncompensated lateral acceleration used here for the superelevation excessive case (slow pass, uncompensated acceleration is centripetal) is around a half of that for the superelevation deficient case (fast pass, uncompensated acceleration is centrifugal). The intensification of wear is thus related more strongly with uncompensated centrifugal acceleration magnitude when the uncompensated centrifugal acceleration is negative. For smaller equivalent conicities, the effective value of

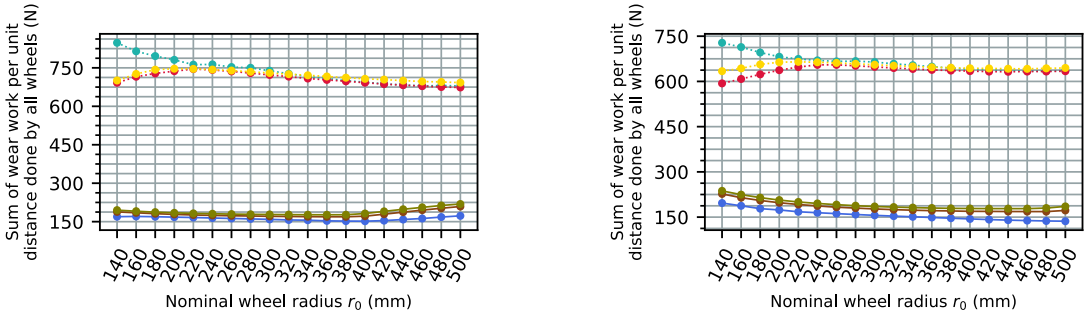

(a) 1437 mm track gauge, 1:40 rail cant

(b) 1437 mm track gauge, no rail cant

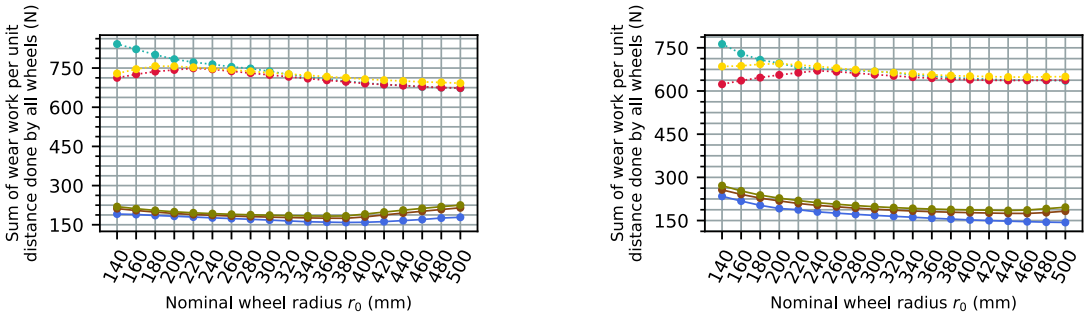

(c) 1435 mm track gauge, 1:40 rail cant

(d) 1435 mm track gauge, no rail cant

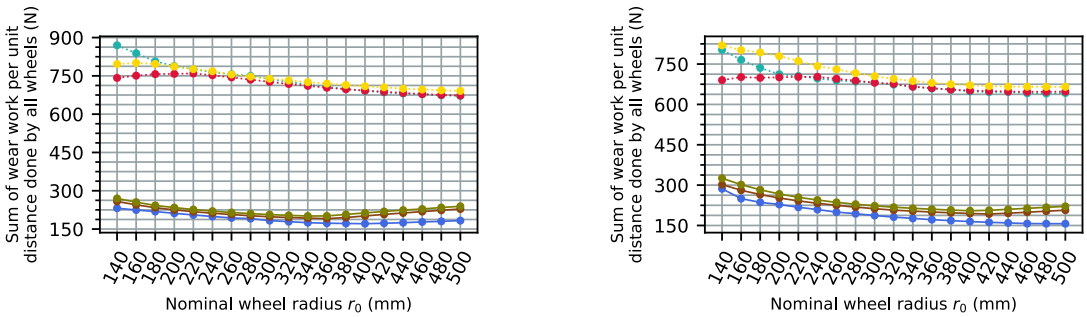

(e) 1432 mm track gauge, 1:40 rail cant

(f) 1432 mm track gauge, no rail cant

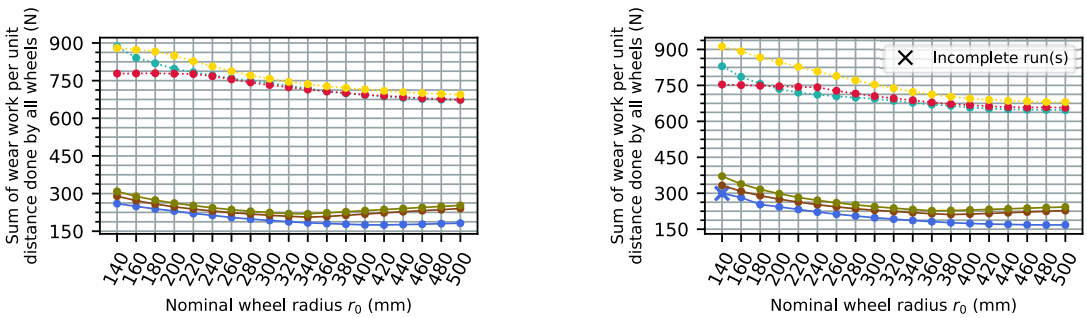

(g) 1430 mm track gauge, 1:40 rail cant

(h) 1430 mm track gauge, no rail cant

Figure 5.14 Wear analysis of a tare vehicle with different combinations of track gauge and rail cant

Constants: Y25 bogie, S1002 wheel profile

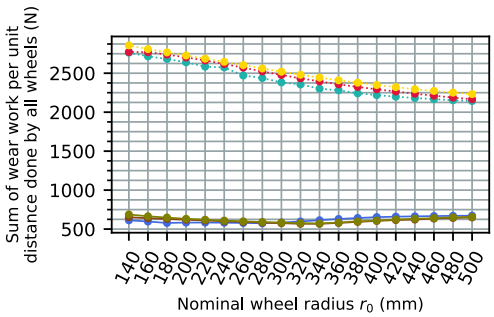

(a) 1437 mm track gauge, 1:40 rail cant

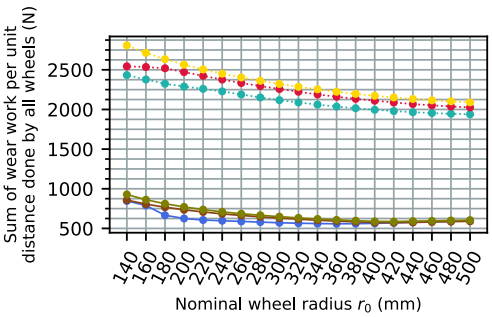

(b) 1437 mm track gauge, no rail cant

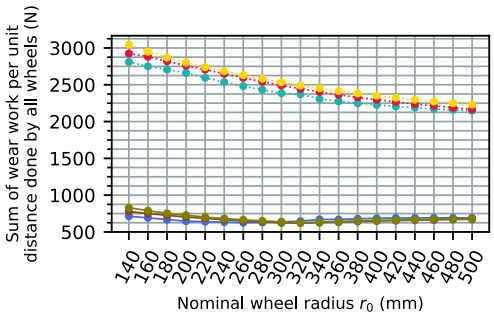

(c) 1435 mm track gauge, 1:40 rail cant

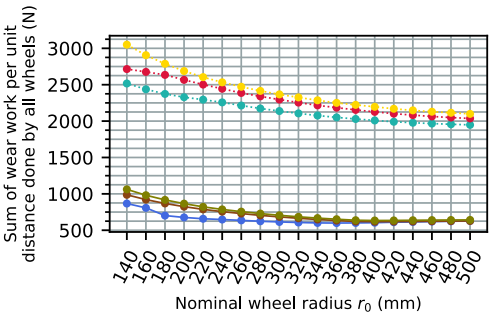

(d) 1435 mm track gauge, no rail cant

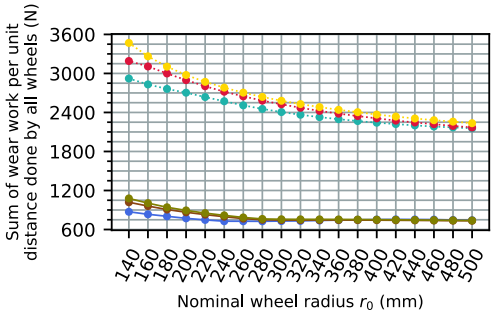

(e) 1432 mm track gauge, 1:40 rail cant

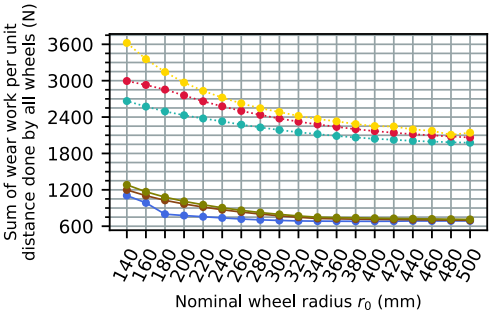

(f) 1432 mm track gauge, no rail cant

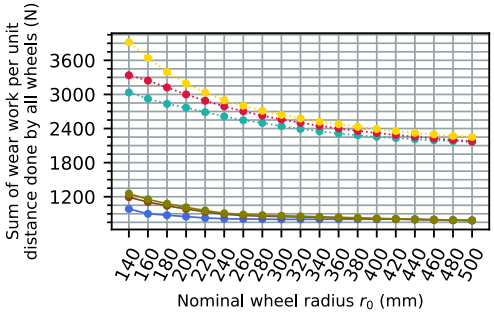

(g) 1430 mm track gauge, 1:40 rail cant

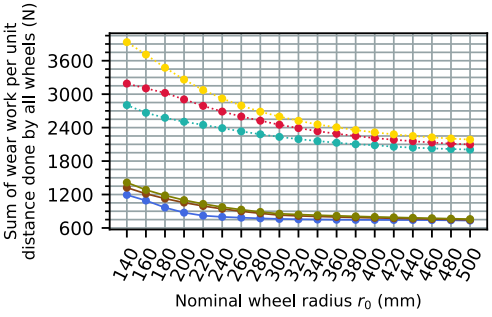

(h) 1430 mm track gauge, no rail cant

Figure 5.15 Wear analysis of a laden vehicle with different combinations of track gauge and rail cant

Constants: Y25 bogie, S1002 wheel profile

wear caused by curve negotiation with deficient superelevation exceeds that caused with excessive superelevation as the wheel size decreases, although the level of wear is noticeably lower than cases with higher λ_e. In the laden state, fast curving becomes the case that causes the least wear for any tested nominal wheel radius, whereas slow pass becomes the most critical case. The least favourable situation occurs with the laden vehicle with the smallest, r_0 = 140 mm wheels negotiating the CAT4 curve with excessive superelevation.

The increasing pattern of wear against decreasing wheel size can be attributed to the decrease in contact patch size during curving and the resulting contact stress increase. To show this, three simulations with different nominal wheel radii are selected from the case shown in Figure 5.15 (h), plot curve CAT4 $\Delta a\_$ (the previously identified most critical case from the aspect of wear) for viewing the wheel-rail contact patch area. Selected are simulations with r_0 = 140 mm, r_0 = 300 mm and r_0 = 500 mm. The contact patch areas on both the tread and the flange are read out from simulation results and plotted in Figure 5.16. In the first round curve, the inner wheels have the largest tread contact patch; due to the superelevation excess, the outer wheels undergo a decrease in contact patch size. The contact patch on the inner wheel treads have areas up to approximately 100 mm² for r_0 = 140 mm, 140 mm² for r_0 = 300 mm and 165 mm² for r_0 = 500 mm. Flange contact is still observed mainly on the outer wheels despite the excessive superelevation; the contact patch area on the outer wheel flanges measure up to 2 mm² to 3 mm², and slightly decreases as r_0 increases. As the wheel load in the three cases of r_0 is minimal and negligible for a laden vehicle, the decrease in contact patch size is responsible for the contact stress increase on the tread, which worsens the wear behaviour.

5.4 Summary of notable observations

From the observations and their analysis made in this chapter, the following conclusions can be drawn on the change in running dynamics behaviour of a typical vehicle equipped with Y25 bogies and S1002 wheel profile as the nominal wheel radius is made variable:

- The use of smaller wheels reduces the non-linear critical speed of the vehicle
- The cross-influence between oscillating bodies in the vehicle may give rise to discontinuous relations between non-linear critical speed and nominal wheel radius
- The use of relatively small wheels improve the curving behaviour of the vehicle
- The use of smaller wheels cause low-speed passing of curves to be less safe compared to high-speed passing, especially on small-radius curves
- The use of smaller wheels threatens the wear behaviour of the vehicle, especially for a heavier or laden vehicle
- The rate of change of non-linear critical speed and wear are generally more sensitive than the rate of change of curving performance to the decrease in nominal wheel radius
- Track settings do not influence the critical speed of the vehicle with any deterministic tendency for any wheel size

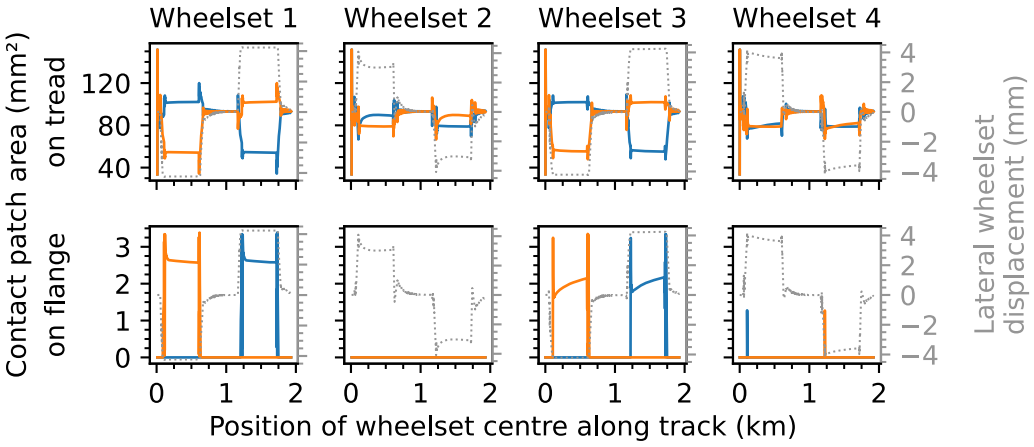

(a) r_0 = 140 mm

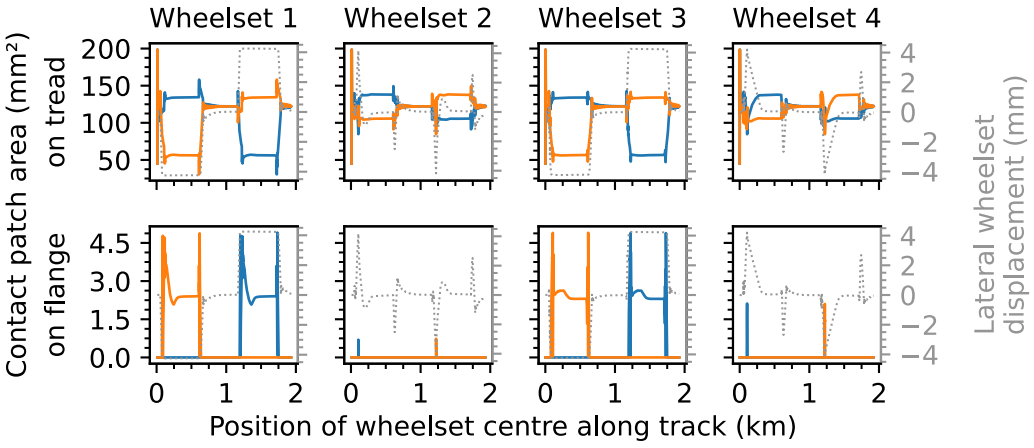

(b) r_0 = 300 mm

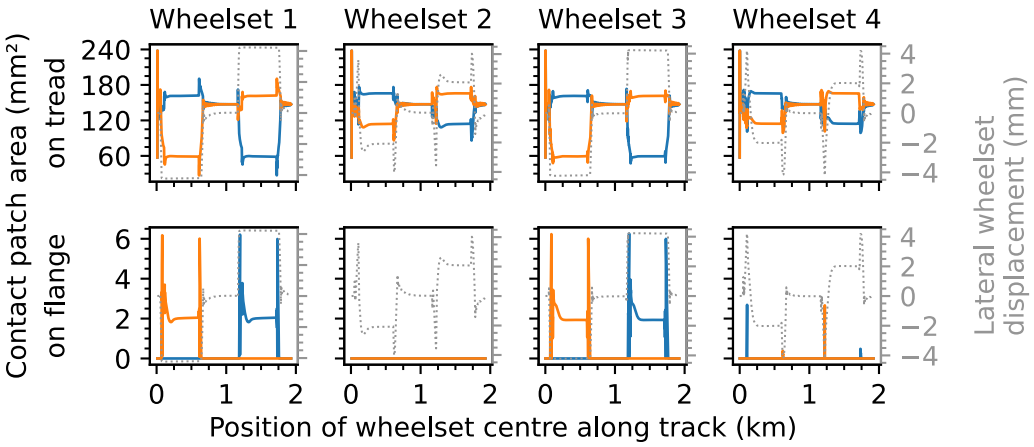

(c) r_0 = 500 mm

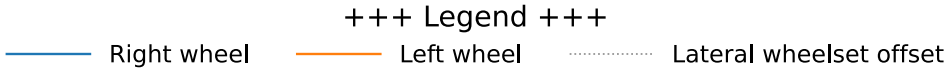

Figure 5.16 Wheel-rail contact patch area on tread and flange
Conditions: Y25 bogie, S1002 wheel profile, laden vehicle, 1430 mm gauge, no rail cant, CAT4 curve, negative superelevation deficiency

6 Running dynamics reassessment after implementing improvements

Here, the results from the simulation runs with modified wheel profiles and retrofitted radial steering mechanism are analyzed and compared against the results from simulations done with each track setting but with the original Y25 bogie and S1002 wheel profile presented in the previous chapter. Thus for each track setting, the case with Y25 bogie and S1002 wheel profile is effectively used as the control case, and will be referred to as such in upcoming text.

To begin with, these comparisons aim at determining whether the devised countermeasures are effective. More importantly, the change of dynamics behaviour is investigated for a specific relation between wheel profile scaling factor and nominal wheel radius both with and without the implementation of a cross-linkage radial steering mechanism. Once the effectiveness of these remedies against running dynamics deterioration with smaller wheels have been indicated with this comparative analysis, the applicability of smaller wheel sizes can be ascertained.

6.1 Effect of implementing radius-dependent profile scaling

6.1.1 Preliminary investigation with constant 70% scaling factor

Results from this preliminary investigation indicate that the scaling of the wheel profile in the wheel's radial direction has a notable effect on the dynamic behaviour of the vehicle, and tends to bring the behaviour associated with smaller wheel sizes into an overall more suitable range.

Analysis of each behaviour of concern is expanded and described in detail in the following sections.

6.1.1.1 Stability

Results of the stability simulations involving the exploratory flattening of the tread by scaling the wheel profile with factor 70% are shown in Figure 6.1 and Figure 6.2 respectively for 1:40 rail cant and no rail cant.

An increase in critical speed is observed for almost all cases compared to the results obtained from previous simulations without tread flattening (Figure 5.5 and Figure 5.6). For instance, the behaviour improvement with the reference track settings (1435 mm gauge, 1:40 rail cant) is rather significant, especially for wheel radii larger than 340 mm, in which the v_c^{NL} exceeds 120 km/h; on the other end of the wheel radius range, even the smallest wheel considered with a nominal radius of 140 mm obtains a critical speed of 74 km/h, which without the profile scaling would have been achieved with a wheel radius of at least 340 mm. This significant benefit of the preliminary flattening of the wheel profile shows that it is worthwhile to consider wheel profile scaling as a valid countermeasure against the adverse effects of using smaller wheels in terms of improving the stability of the wheels within the operational speed range.

It is also noticed that this particular wheel profile causes the influence of track settings on the non-linear critical speed to take on a clearer trend. A wider track gauge in this case unambiguously results in a higher non-linear critical speed. The influence of rail cant is more complex in that it affects the dimin-

ishing behaviour of the primary hunting. It is noticed that for tracks with no rail cant, the division between primary and secondary instabilities becomes pronounced, especially for 1432 mm gauge, with which the "band of stable runs" in the v-r_0 diagram occurs for all cases of r_0 and both frontiers of the band run along monotonously increasing v-r_0 curves. For 1430 mm gauge, when the wheels are very small, the wheelset tends to oscillate in an unstable manner underneath the bogie frame, registering a narrow band of primary instability at lower speeds which diminishes as the nominal wheel radius exceeds 240 mm. This diminution causes an upward-jumping discontinuity in the observed v_c^{NL}-r_0 relation. On the other hand, with the widening of the track gauge, the band of instability becomes narrower and diminishes with 1437 mm gauge.

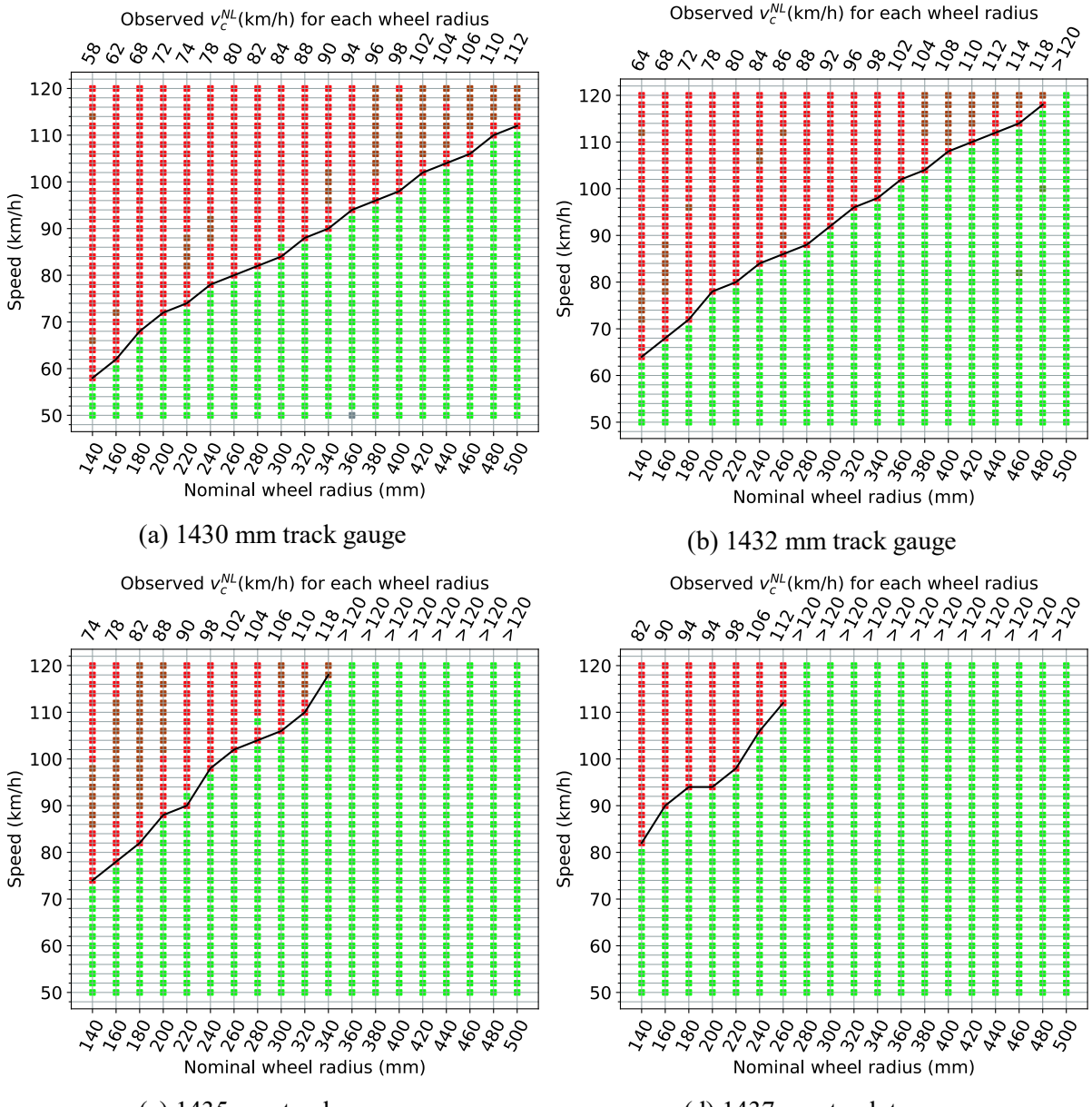

(a) 1430 mm track gauge

(b) 1432 mm track gauge

(c) 1435 mm track gauge

(d) 1437 mm track tgauge

Figure 6.1 Stability behaviour on track with 1:40 rail cant, wheel profile scaled with factor 70%

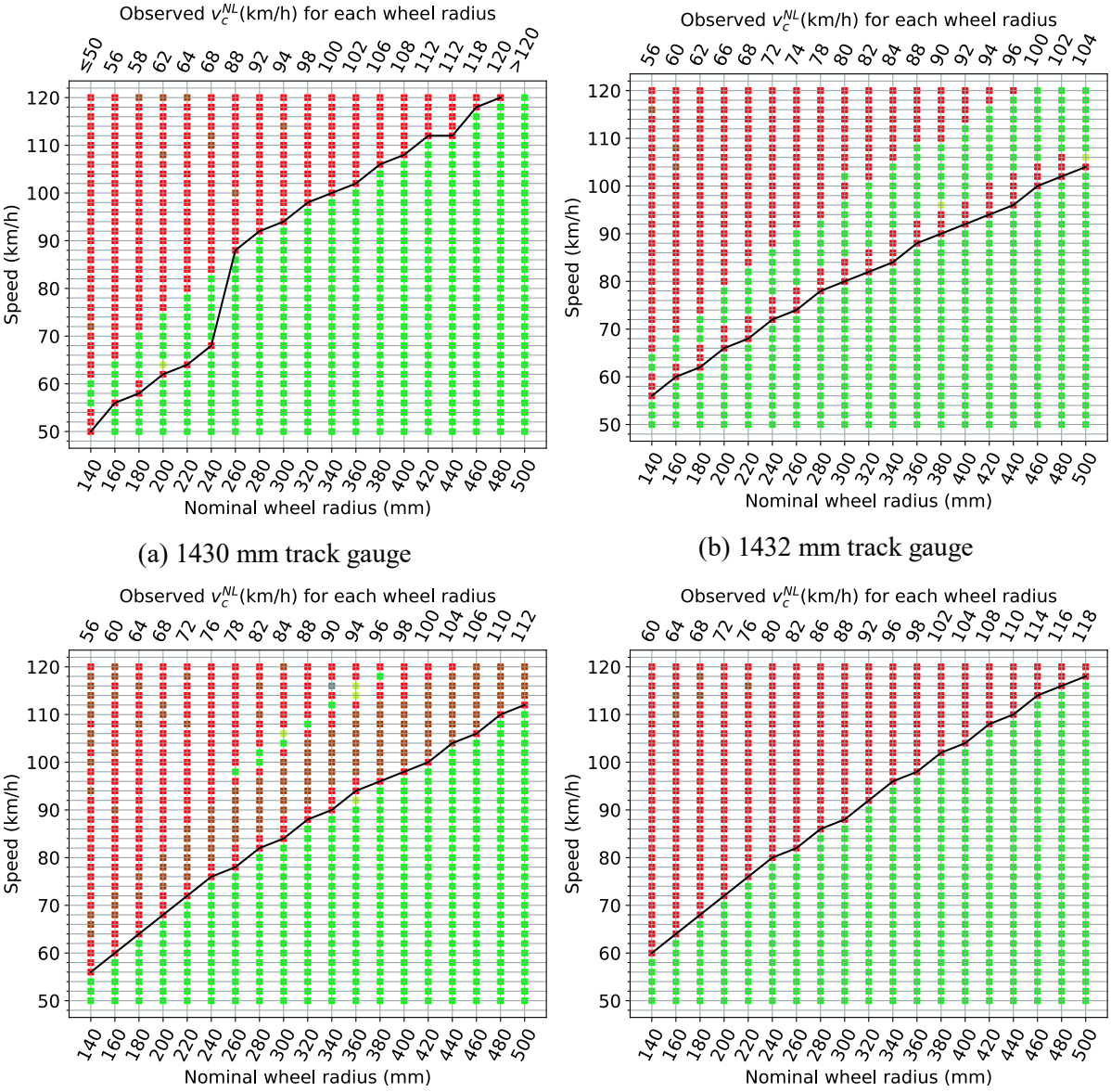

(a) 1430 mm track gauge

(b) 1432 mm track gauge

(c) 1435 mm track gauge

(d) 1437 mm track gauge

Figure 6.2 Stability behaviour on track with no rail cant, wheel profile scaled with factor 70%

6.1.1.2 Curve negotiation

In Appendix D, all result summary plots for curve negotiation done with the said scaled profile are shown. Different from the curve summary plots in Appendix C is that the plots herein are organized such that the behaviour observed with the original and scaled profiles are always in direct comparison within the same diagram rather than comparing in terms of curve category and superelevation deficiency.

On the large-radius CAT2 curve, when other conditions are held the same, most simulations with the scaled wheel profile exhibit elevated levels of $|Y|_{max}$ and $|Y/Q|_{max}$ compared to those with the original S1002 profile. This indicates that the flatter profile generally causes the curve negotiation behaviour to worsen. One notable exception is those with the smallest wheel radii, with which the vehicle using the original wheel profile lost stability when negotiating the curve with positive superelevation deficiency. The scaling of the profile makes the vehicle become less likely to lose stability due to the reduced conicity and reduces the level of wheel-rail lateral force and derailment coefficient magnitudes even in

the case of hunting within the curve. Another exception is observed with the laden vehicle with the smallest nominal wheel radii on tracks no rail cant, negotiating the curve with near-zero or negative superelevation deficiency. In these cases, $|Y|_{max}$ and $|Y/Q|_{max}$ can become lower with the scaled profile than with the original profile; the narrower the gauge, the larger the maximum wheel radius with which the behaviour of the scaled profile becomes better than that of the original profile. For $|\Sigma Y|_{max}$, the level during fast-curving is generally lower for the scaled profile, whereas the influence of profile scaling on the $|\Sigma Y|_{max}$ level with the other two cases of superelevation deficiency is less consistent across the entire r_0 range, although the change in $|\Sigma Y|_{max}$ value due to profile scaling is not significant overall.

On the small-radius CAT4 curve, $|Y|_{max}$ and $|Y/Q|_{max}$ are observed to generally increase due to the profile scaling when the nominal wheel radius is small. The increase is especially significant for fast-pass scenarios. The loss of stability with the smallest wheel radii is no longer observed with the scaled profile. The rate of change of $|Y|_{max}$ and $|Y/Q|_{max}$ in relation to r_0 decreases in general, indicating a weaker sensitivity to the change in wheel size. Notable is that the derailment coefficient changes into an increasing trend with reducing r_0 for tare state and 1:40 rail cant for a large part of the r_0 range as the profile is scaled, making smaller wheels more prone to derailing. Also, for a wider range of wheel radii towards the larger end of the investigated range, the lateral wheel-rail force would exceed the 60 kN limit given by EN 14363, whereas smaller nominal wheel radii result in safer guidance force values; whereas it is to be noted that the 60 kN does not apply to $|Y|_{max}$ but rather the quasistatic guidance force within the round curve, as is already mentioned in Section 5.2.2.1. As even the $|Y|_{max}$ values for the smallest wheels are below the limit, there still remains enough safety redundancy. The change in $|\Sigma Y|_{max}$ is also less consistent with the scaled profile, varying with multiple parameters such as rail cant and wheel size; however, when the uncompensated centrifugal acceleration is positive, $|\Sigma Y|_{max}$ becomes almost always monotonously decreasing with r_0 when using scaled profiles, and generally exhibits lower levels than those achieved by the original wheel profile with small wheel sizes.

The effect of track gauge and rail cant for the scaled profile remains insignificant in all three performance indicators, except with the fast-curving scenarios in which loss of running stability causes performance indicator values to spike with the smallest wheel radii.

6.1.1.3 Wear analysis

Cases previously identified as non-critical for wear are omitted for the effect analysis of wheel profile scaling. Here, only cases with CAT4 curve and laden vehicle are considered.

A comparison between the wear observed with the original S1002 profile and the 70% scaled profile for all gauge-cant combinations is given in Figure 6.3. A general worsening tendency is observed with the profile scaling, which is more pronounced for wider track gauge and for 1:40 cant. When rail cant is not present, the wear during curving with excessive superelevation may even be less with the flattened profile than with the original. With the smallest wheels, the scaled profile exhibits less sensitivity to track gauge and higher sensitivity to rail cant than the original profile.

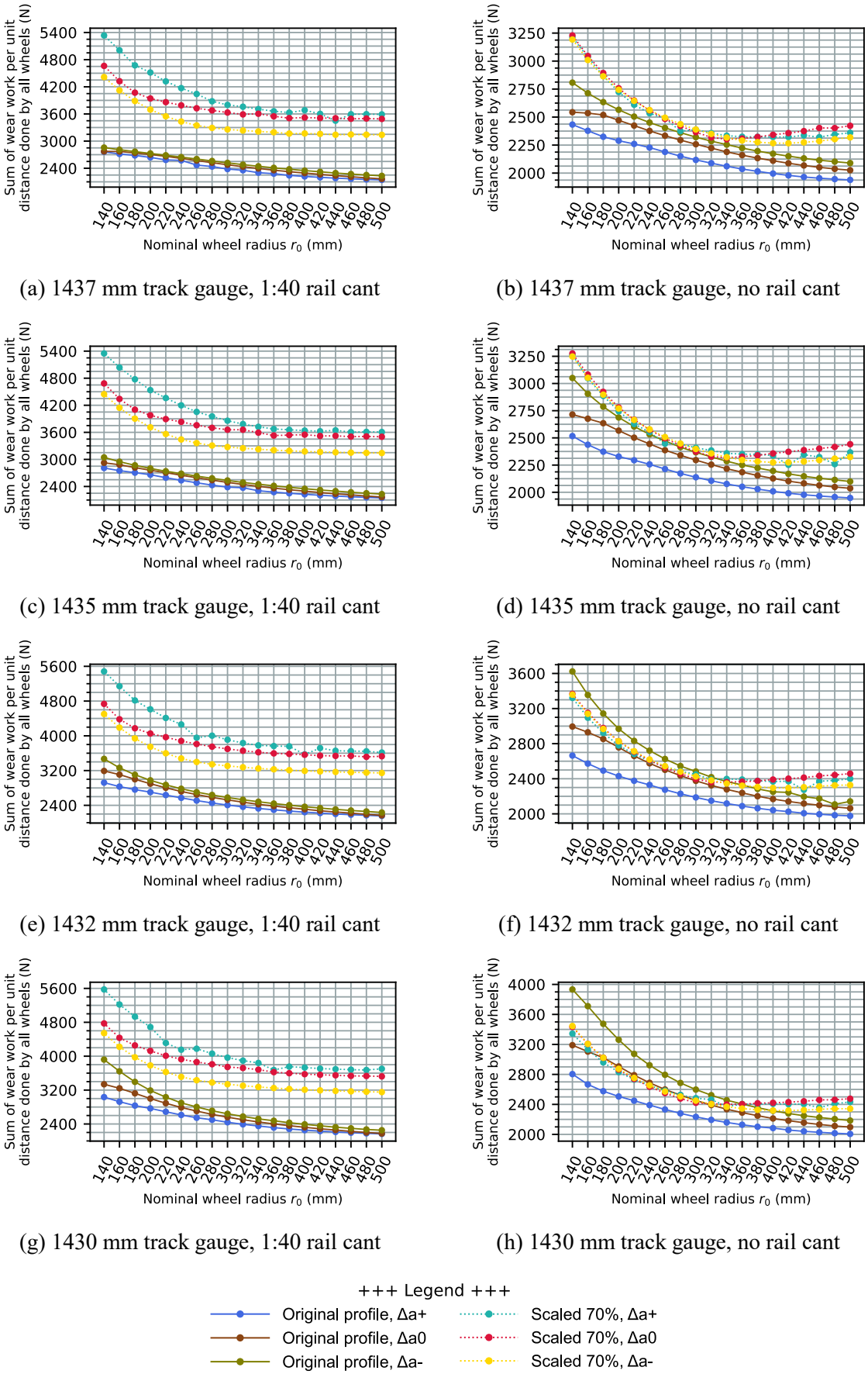

(a) 1437 mm track gauge, 1:40 rail cant

(b) 1437 mm track gauge, no rail cant

(c) 1435 mm track gauge, 1:40 rail cant

(d) 1435 mm track gauge, no rail cant

(e) 1432 mm track gauge, 1:40 rail cant

(f) 1432 mm track gauge, no rail cant

(g) 1430 mm track gauge, 1:40 rail cant

(h) 1430 mm track gauge, no rail cant

Figure 6.3 Wear comparison between original and 70% scaled profiles: laden vehicle, Y25 bogie, CAT4 curve

6.1.2 Case MAT: r_0-dependent wheel profile scaling with same factor as r_0's scaling factor

This case represents the first actually viable countermeasure envisaged for recovering the vehicle's worsening overall behaviour. The simulation results summarized and analyzed in this section indicate that this countermeasure effectively improves the critical speed of the vehicle stricken by the smaller nominal wheel radius, whereas the curving behaviour is severely compromised, resulting in heavy wheel-rail lateral loading when passing small-radius curves. The use of this countermeasure without further changes is questionable due to the worsened wheel-rail guidance capability.

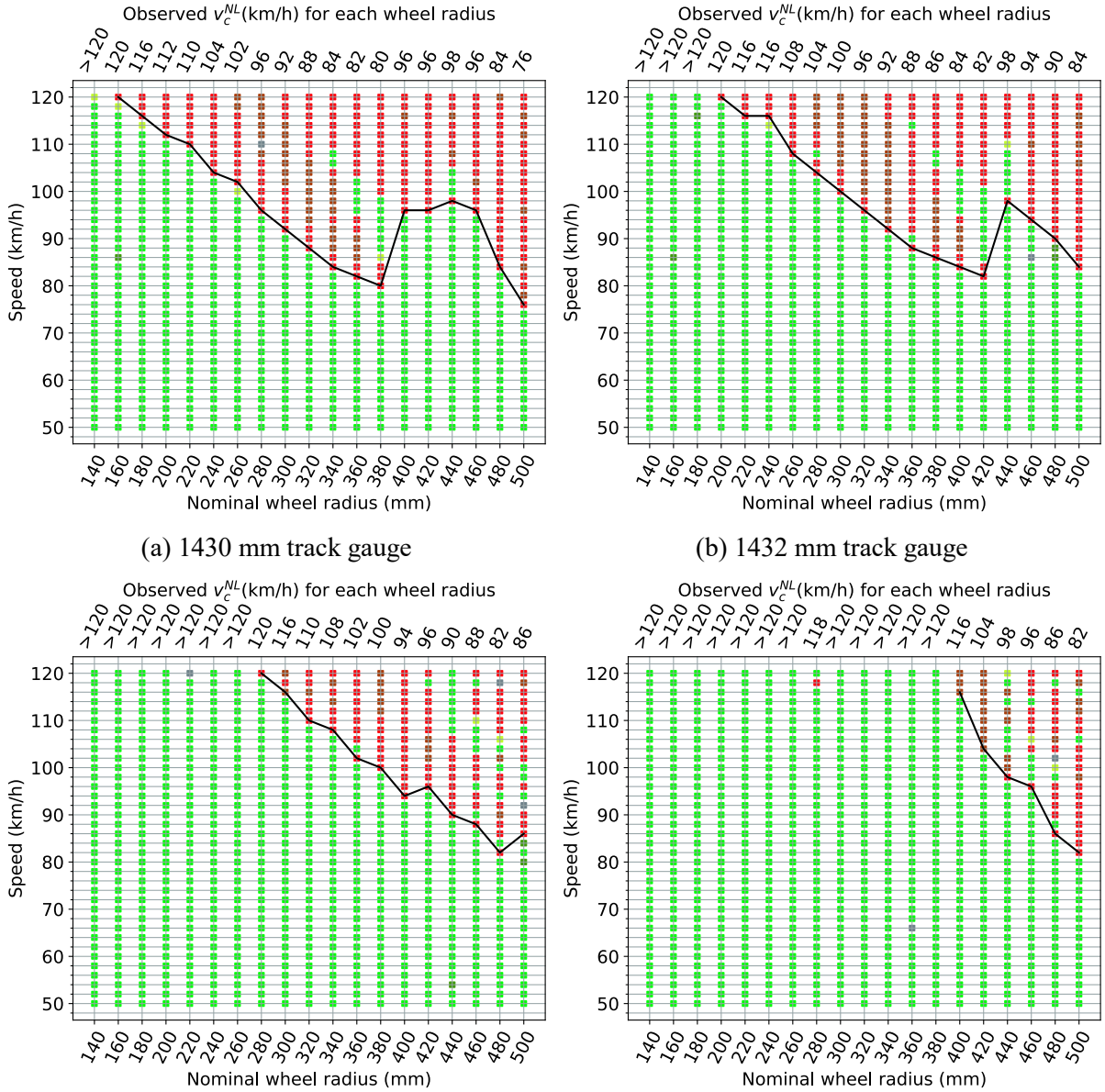

(a) 1430 mm track gauge

(b) 1432 mm track gauge

(c) 1435 mm track gauge

(d) 1437 mm track gauge

Figure 6.4 Stability behaviour on track with 1:40 rail cant, case MAT

6.1.2.1 Stability

Stability-wise, the most notable observation in case MAT is that the non-linear critical speed no longer has an overall decreasing tendency with decreasing wheel radius. The frontier between unstable and stable simulation runs now exhibit an increasing tendency as the wheel size reduces. The elimination of the rail cant is shown to cause the rate of change of v_c^{NL} against r_0 to decrease.

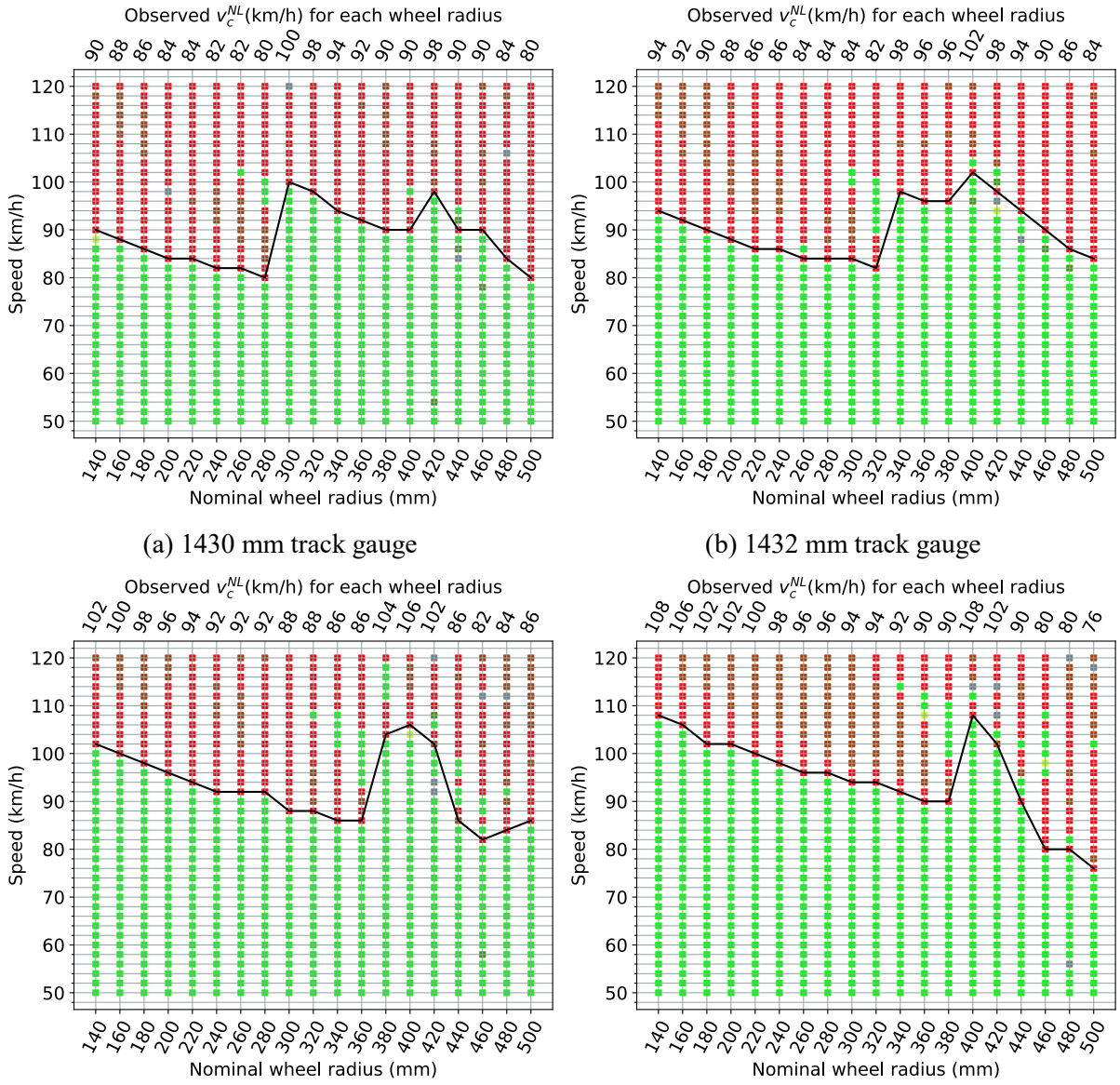

(a) 1430 mm track gauge

(b) 1432 mm track gauge

(c) 1435 mm track gauge

(d) 1437 mm track gauge

Figure 6.5 Stability behaviour on track with no rail cant, case MAT

The influence of track gauge on the critical speed also becomes more unambiguous in the smaller end of the range of nominal wheel radius. In this range the v_c^{NL}-r_0 is in a monotonous decreasing correlation. A wider track gauge tends to raise the non-linear critical speed of the vehicle.

For smaller track gauges and rails set up with no cant, the previously observed second frontiers of instability also occur. They also run in a generally negative correlation to the nominal wheel radius, forming breaks in the line connecting the simulation runs exhibiting the critical speeds, as is seen in Figure 6.4 (a), (b) and all three plots in Figure 6.5. Such breaks even occur twice in track settings with narrower gauges and less rail cant.

For smaller wheel radii, which now have flatter treads due to the profile scaling, the critical speed becomes much higher than before the profile modification, most notably with reference track setting (1435 mm gauge, 1:40 rail cant), in which wheels with a nominal radius smaller than 280 mm are able to reach non-linear critical speeds over 120 km/h, see Figure 6.4 (c).

By comparing the results here with those described in Section 5.1.2 (see also Figure 6.18 for a side-by-side comparison), it is observed that the effect of profile scaling on critical speed overpowers that of wheel size reduction. The non-linear critical speed of the vehicle is observed to be much stronger dependent on tread conicity than on wheel size itself. As the primary practical concern in reducing the wheel size is the loss of stability at operational speeds (whereas the curving behaviour is expected to improve and not of concern), the observations made here suggest that the wheel profile scaling by wheel size scaling factor applied in this set of simulations is potentially effective for mitigating the applicability detriments associated with the use of smaller wheels.

6.1.2.2 Curve negotiation

Appendix E shows the curve negotiation behaviour results from Case MAT simulations, compared with behaviour observed in the control case ("standard scenario") without profile modification.

On the CAT2 curve, the maximum lateral wheel-rail force and derailment coefficient magnitudes of smaller wheels become significantly elevated for case MAT. As the wheel size decreases, the lateral wheel-rail loading for both the tare and the laden vehicle in the fast-passing scenario eventually exceeds the other two superelevation deficiency cases, making fast-curving the most critical case for wheels with a smaller radius combined with a flatter wheel profile. For a tare vehicle, the derailment coefficient is of more interest than the wheel-rail lateral force due to the smaller wheel-rail vertical force, whereas for a laden vehicle the lateral wheel-rail force is the more interesting index. Here it is seen that, when considering all cases of uncompensated centrifugal acceleration altogether, the r_0-dependent profile scaling causes the tare vehicle to almost always have a higher $|Y/Q|_{max}$ associated with smaller values of r_0 than that observed with large-wheeled vehicles with the original S1002 profile, though still remaining around 0.4, well below the flange-climb limit as is suggested by Nadal's theory, whereas for the laden vehicle, small wheels combined with wheel profile scaling do not exhibit the highest $|Y|_{max}$ values compared with all cases of r_0 and Δa with the original wheel profile. The maximum magnitude of sum of lateral wheel-rail forces on wheelsets even undergoes a consistent decrease in the fast-passing scenario with either load state as well as near-zero and negative uncompensated centrifugal acceleration levels with the laden vehicle. The passing of large-radius curves with the implementation of this countermeasure is thus not critical.

On the CAT4 curve, the sum of lateral wheel-rail forces is observed in most cases to change slightly from the behaviour with the control case for the tare vehicle, with the largest difference compared to the control case being less than 2 kN for any r_0 (excluding cases involving the smallest wheel radii where the control case loses stability), raising no cautions. For the laden vehicle, the overall $|\Sigma Y|_{max}$ level decreases for near-zero and negative superelevation deficiency, whereas for positive superelevation deficiency the overall level increases (again excluding the cases where the control case loses stability with very small wheels). From this aspect, the fast-passing behaviour on tight curves worsens with the use of profiles scaled to r_0-dependent factors, increasing the track shift force for a wide range of wheel sizes. The derailment coefficient undergoes a drastic increase with the implementation of profile case MAT, almost doubling in some situations for the tare vehicle and becoming almost always over 0.6 for a nominal wheel radius less than 400 mm. The tare vehicle also exhibits an increasing tendency of $|Y/Q|_{max}$ with decreasing wheel size for any uncompensated centrifugal acceleration level, whereas the laden vehicle exhibits this only for fast-passing. The lateral wheel-rail force behaves rather critical for the fast-

passing scenario of the laden vehicle, in which $|Y|_{max}$ increases with decreasing r_0 and is almost always over 60 kN. In the tare state, the value of $|Y|_{max}$ also significantly increases for any superelevation deficiency compared to the control case. The observations of both $|Y/Q|_{max}$ for the tare vehicle and $|Y|_{max}$ for the laden vehicle indicate significantly compromised curve negotiation behaviour of the scaled wheel profile.

On both curves and with both loading states, the effect of track gauge and this specific wheel profile modification remains insignificant.

6.1.2.3 Wear

As previously explained, the analysis will only be done for the laden vehicle running on the tighter CAT4 curve. The simulation result summary plots are laid out in the same fashion as with the 70%-downscaled profile in Section 6.1.1.3, see Figure 6.6.

It can be observed that the wear number during the negotiation of a round curve remains in a negative correlation to wheel radius as is seen in the control case with the original S1002 wheel profile. The downscaling of the wheel profile's radial coordinates for the smaller wheel sizes causes the wear exacerbate in comparison to the wear level of the wheel of the same size with the unscaled profile. The profile flattening for the smaller wheels also significantly increases the criticality of the fast-passing scenario: on the smaller end of the nominal wheel radius range, the sequence of uncompensated centrifugal acceleration level observed wear number in descending order is Δa_+, Δa_0, Δa_- without exception for case MAT, which is the opposite of that seen with the original S1002 profile. Taking the example of the smallest r_0=140 mm wheel, the worst case with profile scaling (Δa_+) can exhibit an effective wear number value more than double that seen in the worst case without profile scaling (Δa_-). This shows that the countermeasure of profile scaling is highly detrimental in terms of wear, worsening the already exacerbated wear situation caused by the decrease of wheel size at an even higher rate. Compared to the fixed-factor scaling mentioned in the previous section, the wear behaviour in case MAT is more consistent across the different track gauge and rail cant settings.

6.1.3 Case INV: r_0-dependent wheel profile scaling with inverted f-r_0 matching order

The stability simulations in this test case, as seen in Figure 6.7 and Figure 6.8, exhibit generally ascending v_c^{NL}-r_0 relations for all six track settings involved. Compared with the control case with S1002 profile, the rate of increase of v_c^{NL} with increasing r_0 is much larger. On the track with 1:40 rail cant, a test vehicle with a wheel radius larger than 360 mm is able to remain good stability for any speed up to 120 km/h with all three gauge settings. On the smaller end of the wheel radius range, the stability already worsened by the use of smaller wheels is exacerbated by the higher conicity, giving rise to very low critical speeds.

Note that in Figure 6.7 (a) and (b) the lower of the two frontiers where the vehicle transitions from stability to instability after a speed increase may stretch further below the lower range of the plot at 50 km/h as r_0 decreases before breaking off as in Figure 6.8 (a) and (b); further simulations for lower speeds are necessary to confirm this. Thus, on the left side of the plot location where the jump in the black line connecting the lowest speeds with observed unstable vehicle behaviour occurs, the plot points on the

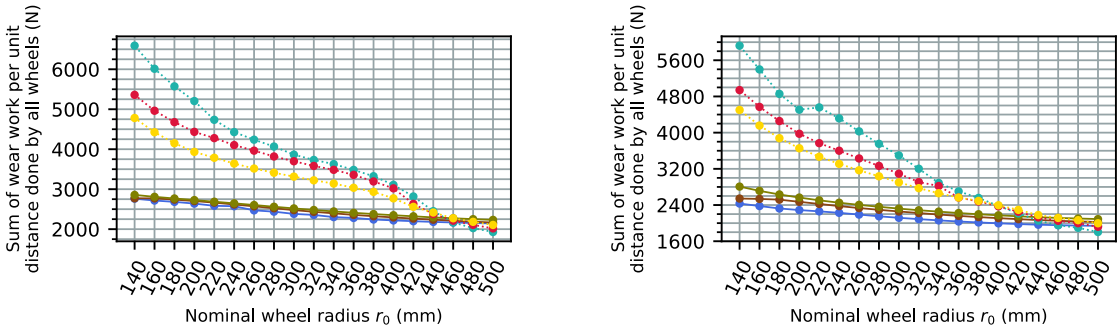

(a) 1437 mm track gauge, 1:40 rail cant

(b) 1437 mm track gauge, no rail cant

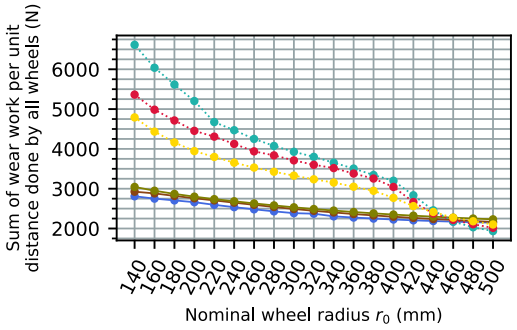

(c) 1435 mm track gauge, 1:40 rail cant

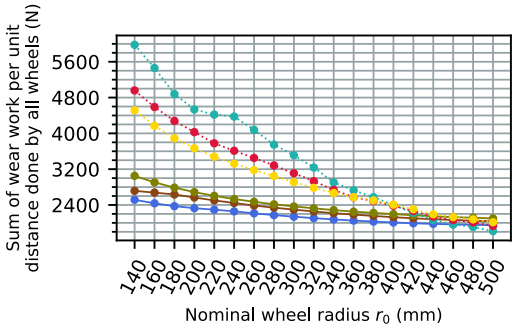

(d) 1435 mm track gauge, no rail cant

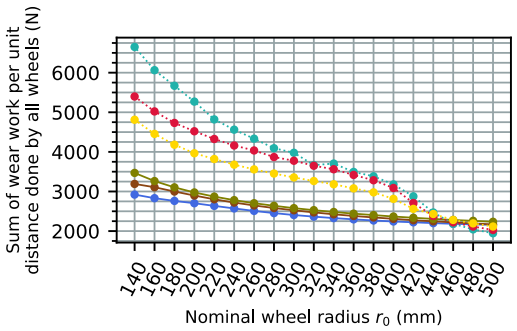

(e) 1432 mm track gauge, 1:40 rail cant

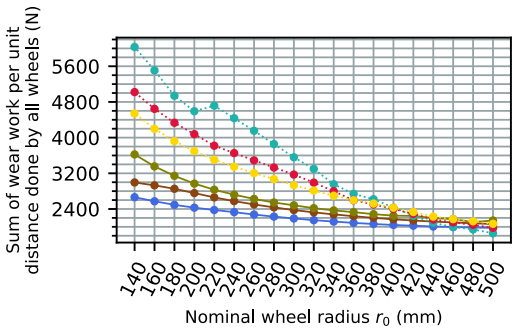

(f) 1432 mm track gauge, no rail cant

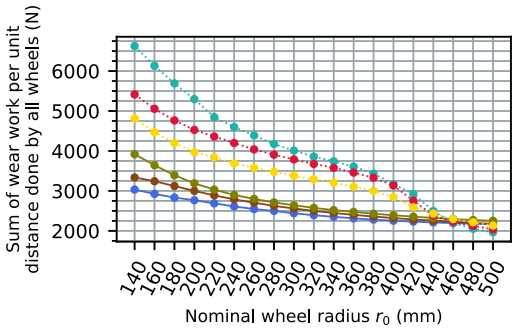

(g) 1430 mm track gauge, 1:40 rail cant

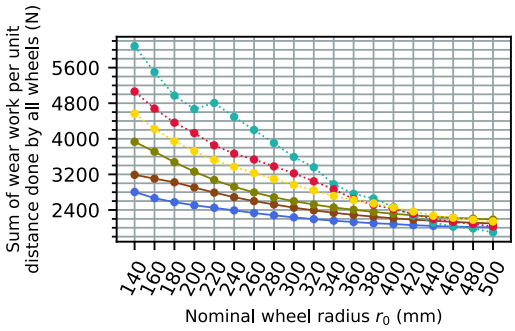

(h) 1430 mm track gauge, no rail cant

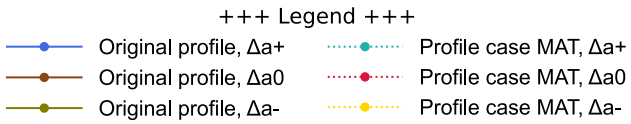

Figure 6.6 Wear comparison between original and modified profiles (case MAT): laden vehicle, Y25 bogie, CAT4 curve

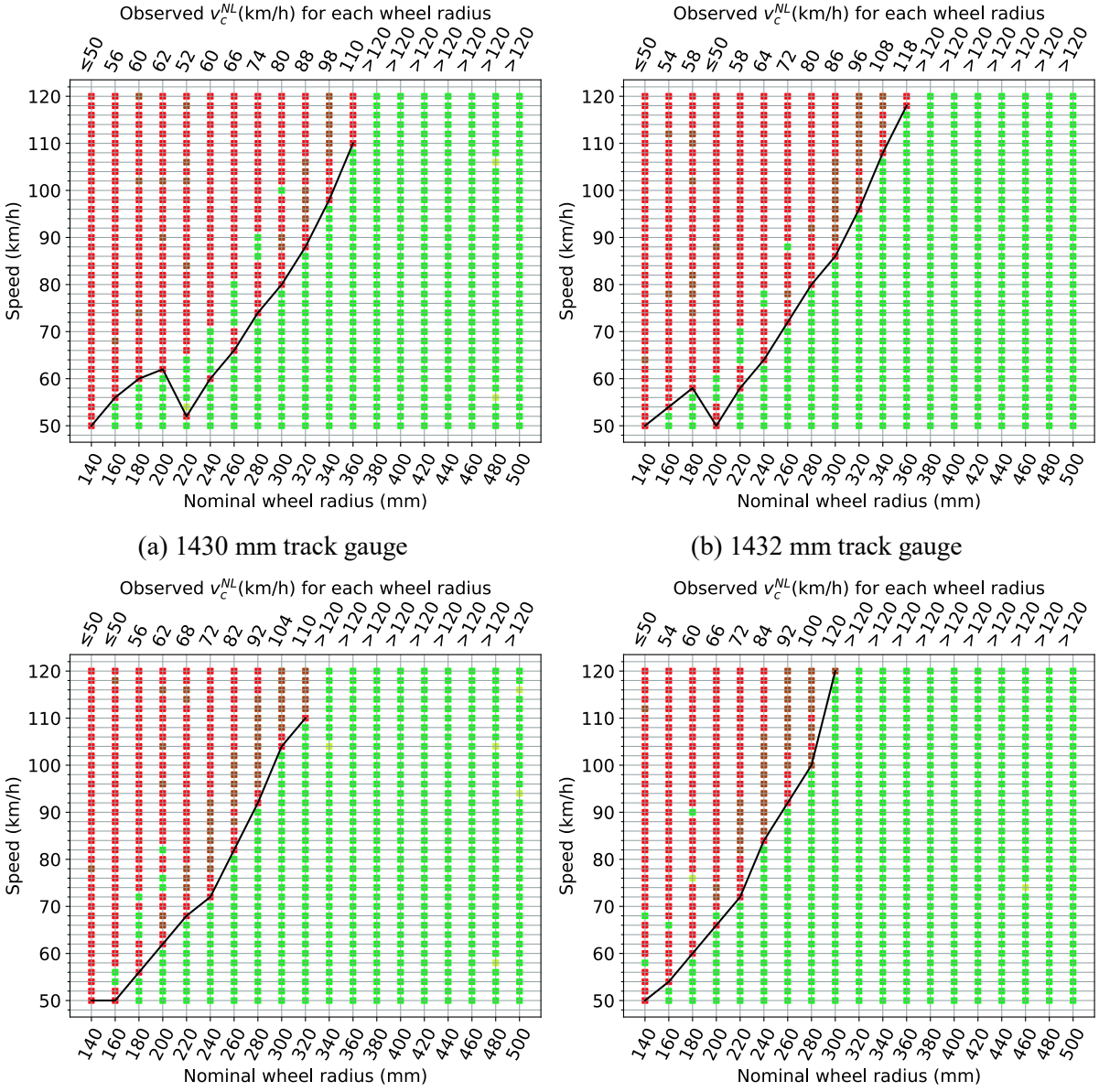

(a) 1430 mm track gauge

(b) 1432 mm track gauge

(c) 1435 mm track gauge

(d) 1437 mm track gauge

Figure 6.7 Stability behaviour on track with 1:40 rail cant, case INV

black line do not necessarily correspond to the non-linear critical speeds, as there possibly exist unobserved lower speeds at which the vehicle behaves as unstable.

By viewing case MAT and case INV results together, it can be seen that the wheel profile scaling factor f plays a much more dominant role in influencing v_c^{NL} compared to r_0. A higher critical speed is associated with a greater wheel profile scaling factor in both cases. Both large and small wheels are capable of achieving high critical speeds with a flatter profile. In theory, in the extreme case of completely flat (cylindrical) treads hunting would not occur at all the critical speed is theoretically infinitely high, regardless of the wheel radius. It is thus not difficult to imply the higher sensitivity of critical speed to tread flatness, characterized by equivalent conicity.

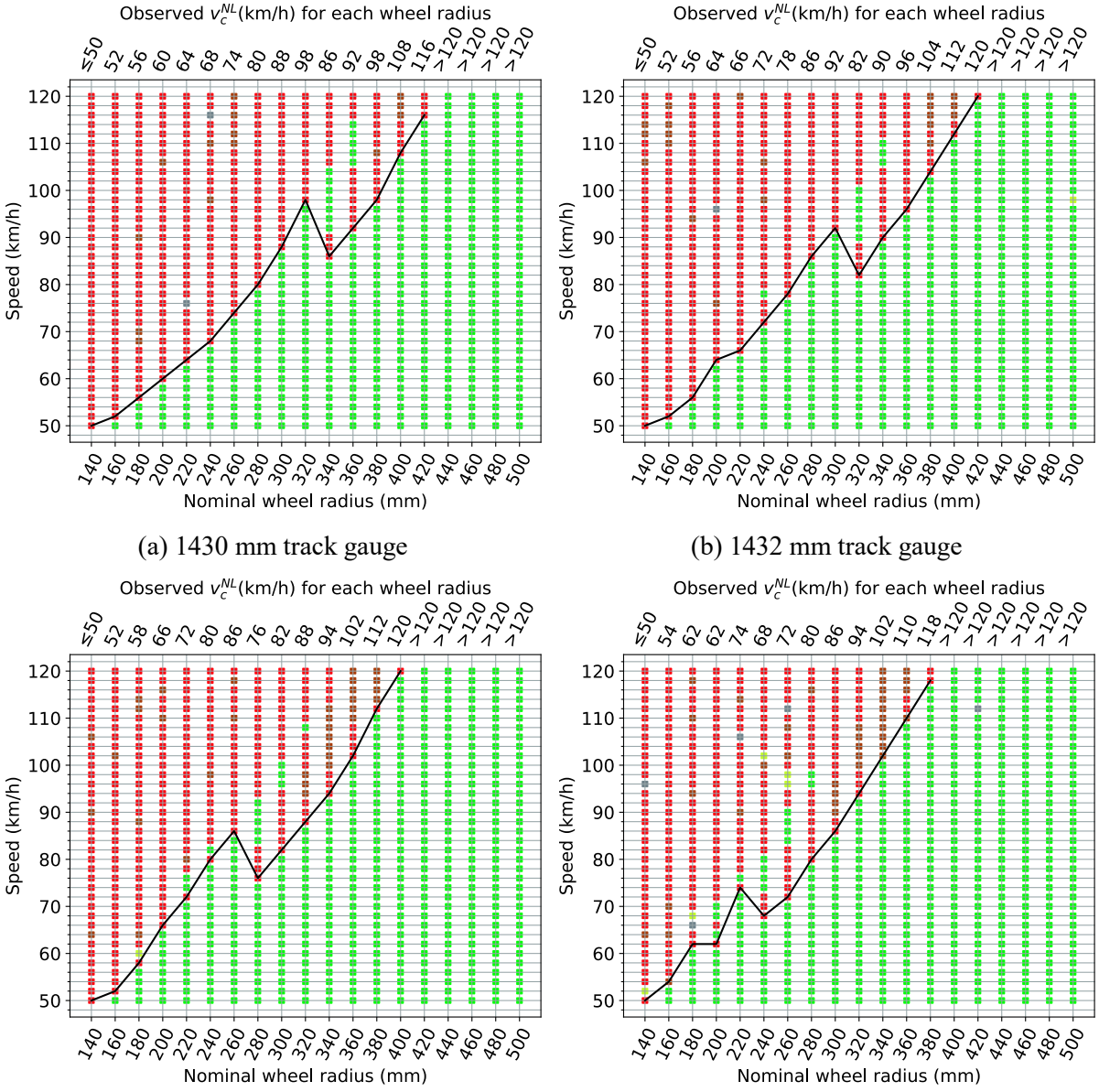

(a) 1430 mm track gauge

(b) 1432 mm track gauge

(c) 1435 mm track gauge

(d) 1437 mm track gauge

Figure 6.8 Stability behaviour on track with no rail cant, case INV

As case INV is not meant as a viable countermeasure, the curve behaviour analysis is simplified in which the degree of compromise to curving performance is not made. Large-radius wheels in case INV and small-radius wheels in case MAT, both of which are associated with very flat wheel profiles with the smallest scaling factors, tend to exhibit significant elevations in $|Y|_{max}$ and $|Y/Q|_{max}$ values. The highest values of these two quantities in the worst case scenario in each combination of gauge, cant, load state and curve category are similar between cases MAT and INV. The change of $|\Sigma Y|_{max}$ remains as previously observed in other cases non-consistent with the use of profile case INV.

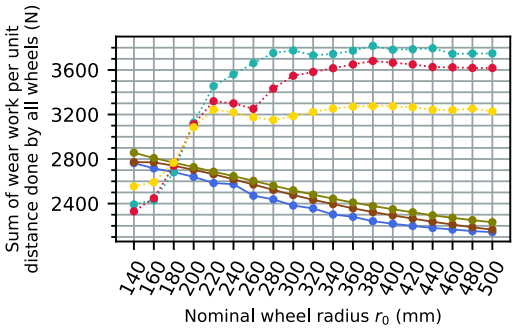

(a) 1437 mm track gauge, 1:40 rail cant

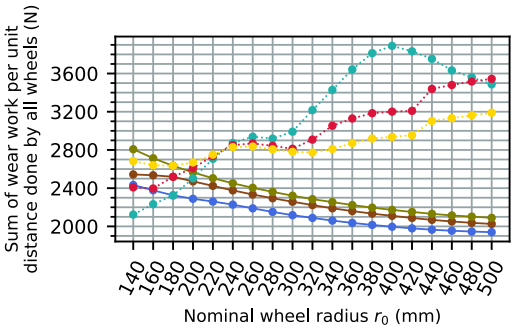

(b) 1437 mm track gauge, no rail cant

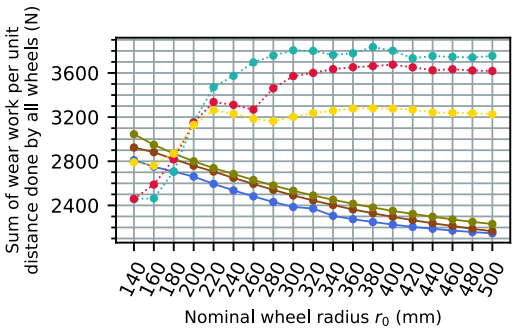

(c) 1435 mm track gauge, 1:40 rail cant

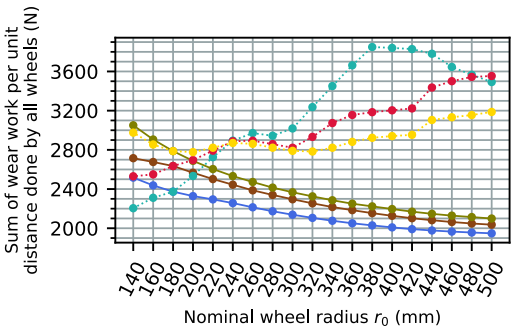

(d) 1435 mm track gauge, no rail cant

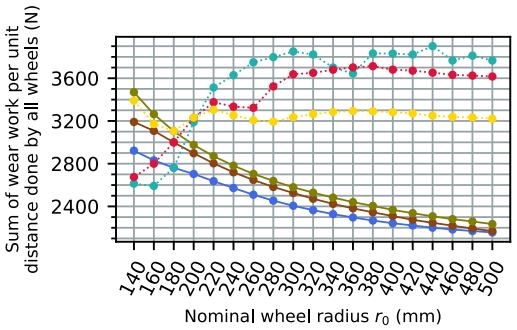

(e) 1432 mm track gauge, 1:40 rail cant

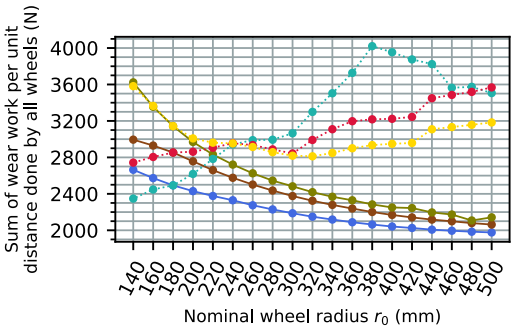

(f) 1432 mm track gauge, no rail cant

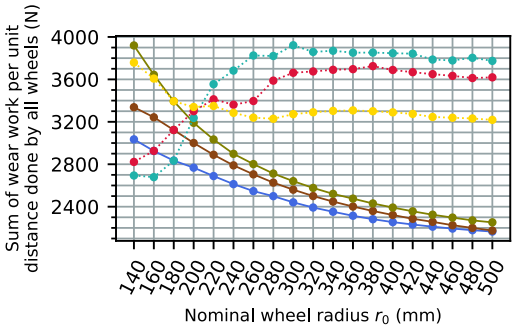

(g) 1430 mm track gauge, 1:40 rail cant

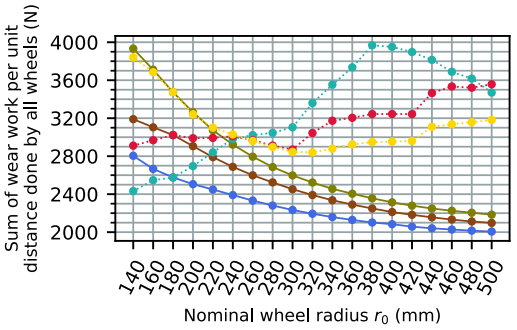

(h) 1430 mm track gauge, no rail cant

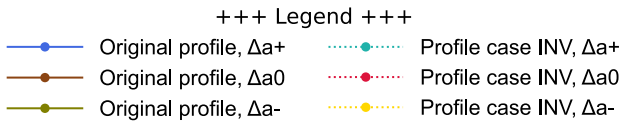

Figure 6.9 Wear comparison between original and modified profiles (case INV): laden vehicle, Y25 bogie, CAT4 curve

The wear behaviour in case INV is plotted in Figure 6.9 for a laden vehicle on the CAT4 curve. A useful finding that can be observed here is again the effect of the wheel profile's scaling factor, or the equivalent conicity of the wheel-rail pair associated with the scaling of the wheel profile, on the wear behaviour of the vehicle. Curves of wear number results with the same uncompensated centrifugal acceleration levels can be used to determine the effect of the scaling factor: points with the same r_0 differ only in scaling factor, and the point on the curve with the greater scaling factor has a smaller wear number. However, this difference is not as pronounced for slow-passing of the curve with the smallest wheels.

6.2 Effect of implementing a radial steering mechanism

This section analyzes the efficacy of the radial steering mechanism for correcting the behavioural decays caused by the use of small wheels both alone without using modified wheel profiles as well as in combination with wheel profile modification in terms of critical speed, curve negotiation and wear respectively in separate sections.

6.2.1 Problem with realization of radial steering and necessary model modification

Upon review of the completed simulation results done with the radial steering bogie model as is described in Section 3.6.2 in which only a pair of cross links are added between diagonally positioned axleboxes, it is noticed that the behaviour of the bogie does not correspond the theoretically expected improvement in curving but rather worsens. Taking the simulation scenario "1435 mm track gauge, 1:40 rail cant, CAT4 curve, vehicle laden" for example, the behaviour of the radial steering bogie is shown in Figure 6.10. Here, even with the standard wheel radius which would correspond to the case of a Y25 bogie and its radial steering variant, the wheel-rail lateral interaction is worsened after the introduction of the radial steering mechanism, which indicates that the radial steering bogie is less capable of smooth curving than the original bogie. A view at the stability behaviour of the radial steering bogie in Figure 6.11 (here only showing the result for the reference track setting) and their comparison against Figure 5.5 (c) show that the critical speed behaviour against wheel radius changed only slightly and had an increasing tendency after the radial steering is introduced. Both observations contradict known behaviour of the radial steering bogie and brings the plausibility of the results into question.

An observation of the wheelsets' yaw angles shown in Figure 6.12 also indicate that the cross links added between the front and rear wheelsets were not able to cause effective radial steering of the wheelsets. The conditions under which these observations are made are: nominal wheel radius r_0 = 460 mm (standard size for the Y25 bogie), curve negotiated with deficient superelevation (case Δa_+). Note that the yaw angle is measured with reference to the s-coordinate (as defined in Appendix A), which is the tangential direction of the track centreline. A higher absolute value of the yaw angle thus represents a higher deviation of the rolling direction from the track's tangential direction, which corresponds to a less radial attitude of the wheelset and a worse curve negotiation smoothness. These yaw angles are thus effectively the angles of attack of each wheelset. On the large-radius CAT2 curve, the cross links cause the angles of attack of the rear wheelsets of each bogie to exceed those of the front wheelsets; the maximum absolute value of the wheelset yaw angles become slightly greater than that observed with the non-steering bogie. On the small-radius CAT4 curve, the front wheelsets of the bogies with cross links exhibit larger yaw angles than without cross links. This indicates that the implementation of cross links

between wheelsets without involving other modifications worsens the radial steering capability of the Y25 bogie.

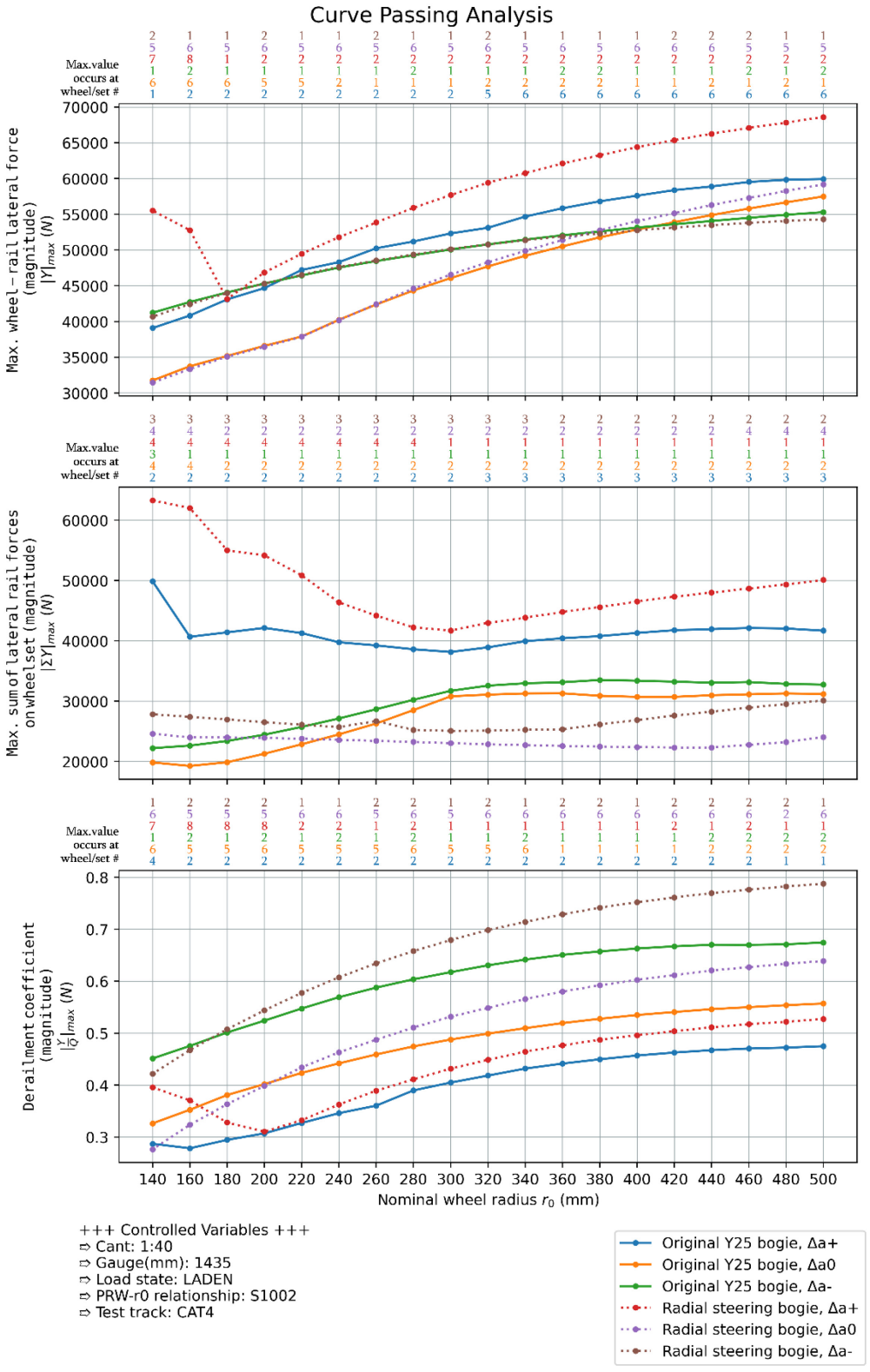

Figure 6.10 Curving behaviour observed with the original radial steering bogie model on CAT4 curve with 1435 mm track gauge and 1:40 rail cant, vehicle laden

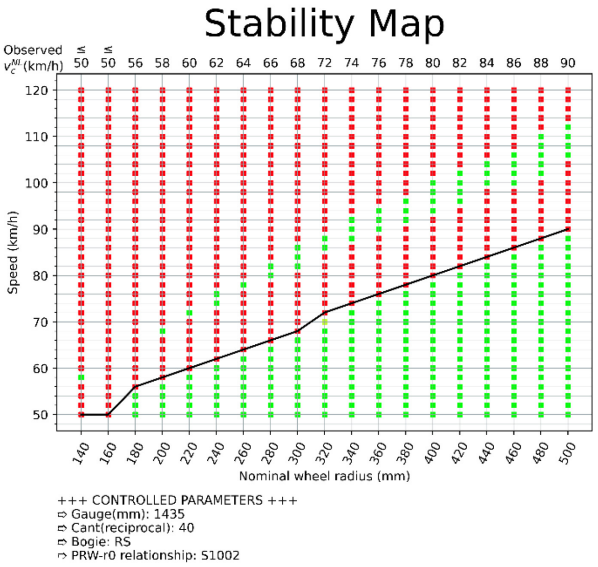

Figure 6.11 Observed stability behaviour of the radial steering bogie on track with 1435 mm gauge, 1:40 rail cant, S1002 profile, simulated with the original model without primary yaw relaxation

Scheffel [114] states that yaw constraints lower than acceptable to flexible suspensions are required for optimised curving performance. Theoretically, the cross links enable the inter-wheelset shear stiffness and bending stiffness (introduced in Section 3.6.2) to be mutually independent, which would allow the simultaneous realization of an inter-wheelset bending stiffness low enough to allow good curving behaviour and an inter-wheelset shear stiffness high enough to maintain stability which would be impossible to achieve with solely suspension tuning. In this specific case, it can be suspected that the longitudinal component of the primary suspension, which was retained from the Y25 bogie, is too high to enable radial steering. Even with the cross link, the wheelsets are too strongly constrained by the rigid guidance brackets against yawing away from each other into the radial attitude. Thus it is impossible to realize radial steering without involving additional changes to the bogie model other than the cross link mechanism.

In order to realize a working radial steering mechanism so that the observation of behavioural changes of the vehicle with different wheel sizes for a radial steering bogie becomes possible, the model of the radial steering bogie is modified so that the primary longitudinal stiffness is set as a constant 4.8×10^5 N/m, which is consistent with the overall shear stiffness (in the lateral or longitudinal direction) of the Y25 bogie's primary suspension for one axlebox with only the outer spring active according to [108] (each coil has shear stiffness 2.4×10^5 N/m, each axlebox has 2 spring packs in parallel configuration in the primary suspension). This would be the softest longitudinal primary suspension setting achievable with original components. This is effectively a yaw-relaxation for the wheelsets, another valid measure for implementing self-steering as is introduced by Wickens [112] among other sources.

Here, the longitudinal primary stiffness modification is done without discussing the details of how this can be done in a realistic bogie; note that this investigation is focused on determining what the vehicle's dynamical behaviour would be if the radial steering were realized, and not aimed at providing a realistic way to facilitate a radial steering mechanism.

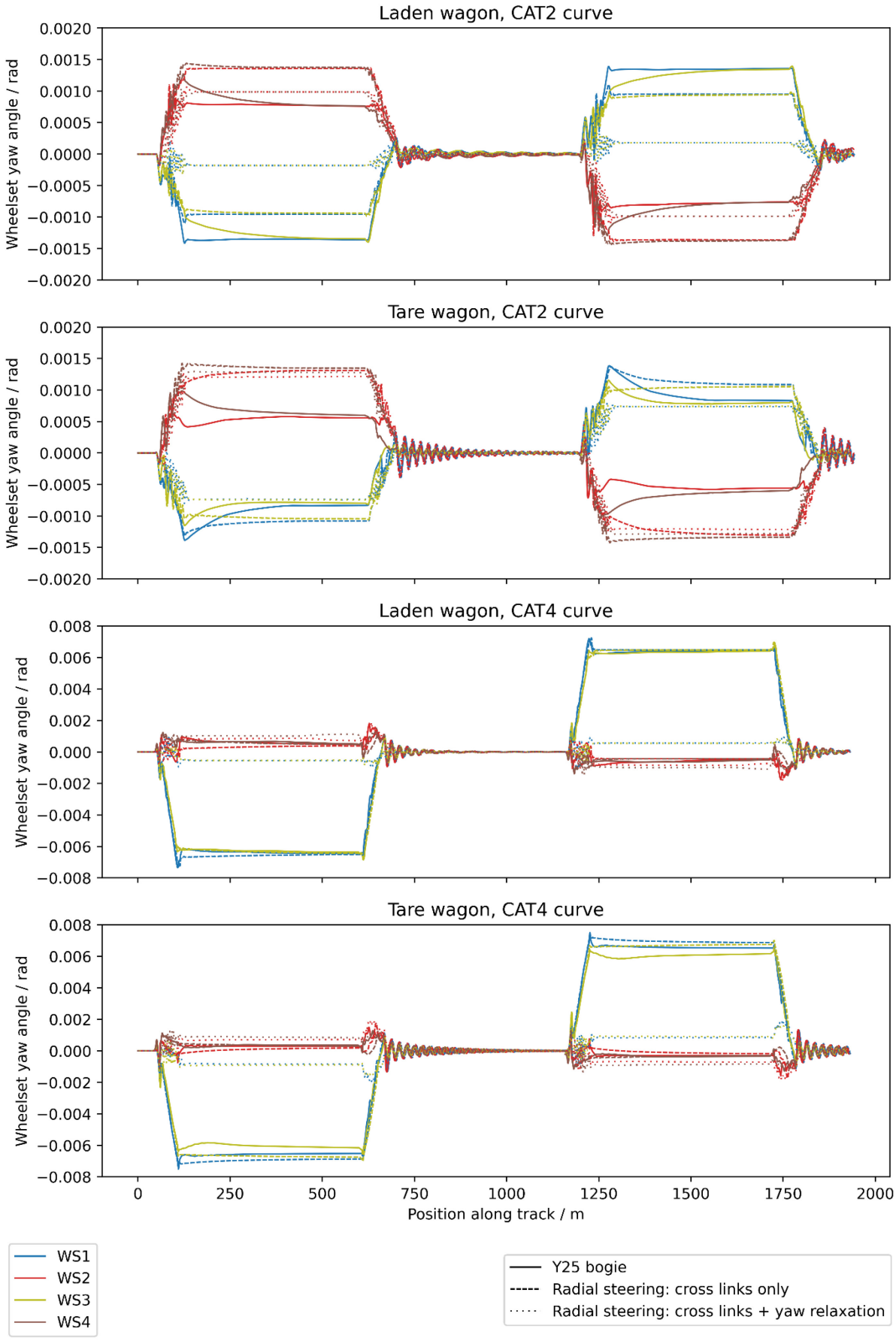

Figure 6.12 Comparison of wheelset yaw angles while negotiating the S-curve test track for bogies with and without radial steering

The same simulations are carried out with the vehicle model now being equipped with the newly-modified radial steering bogie with both cross links and yaw relaxation. From Figure 6.12 it is visible that in this exemplary case with r_0 = 460 mm and superelevation deficiency, the wheelsets now exhibit much smaller angles of attack on a tight (CAT4) curve compared with the original Y25 bogie, which is consistent with the theoretical effects of the use of radial steering bogies. This indicates that this modification to the radial steering bogie model is able to achieve a working radial steering action. The final results regarding the behaviour of the vehicle with radial steering bogies are thus drawn from simulations done using this cross-braced and yaw-relaxed bogie model.

6.2.2 Stability

The stability maps for the revised radial steering bogie model are given in Figure 6.13 to Figure 6.16.

A comparison between stability test results between the revised radial steering bogie and the original Y25 bogie, namely between Figure 6.13 and Figure 5.5 for 1:40 rail cant as well as between Figure 6.14 and Figure 5.6 for no rail cant, indicates a much more significant dependency of the critical speed for the radial steering bogie on the equivalent conicity that the track gauge-rail cant combination facilitates. When the conicity is smaller, a significant increase of critical speed is observed with the radial steering bogie, as is the case with 1435 mm gauge and both rail cants for instance (compare Figure 6.13(c) and Figure 5.5(c)); when the conicity is larger, critical speeds tendentially drop for all tested nominal wheel radii for the radial steering bogie. This is also supported by the results in wheel profile modification case MAT: compared with Figure 6.4 and Figure 6.5 with the Y25 bogie, the results shown in Figure 6.15 and Figure 6.16 with the revised radial steering bogie indicate a clear tendency of critical speed increase with decreasing wheel radius, which in case MAT is associated with a decrease of the wheel profile's conicity (recall Table 3.2).

Of practical interest regarding the use of small wheels, however, the critical speed of the radial steering bogie does not exhibit a significant decrease in comparison to the original bogie in most track settings even without the involvement of wheel profile modification, and even improves on standard gauge tracks with either rail cant setting. The only exceptions are the two track settings with the largest equivalent conicity. This finding supports the use of radial steering bogies as a viable combination to the use of small wheels for the bogie, albeit with the side effect that the stability becomes highly sensitive to minute track gauge and rail cant deviations. When the wheel profile is additionally scaled as in Case MAT, the increasing v_c^{NL}-r_0 relation reverses into a much steeper decreasing relation, which results in a drastic critical speed increase with smaller wheels: wheels with a nominal radius of less than 300 mm are able to gain a critical speed higher than 120 km/h in any of the tested track settings.

6.2.3 Curve negotiation

Appendix G collects curve simulation result summary plots of simulations with the revised radial steering bogie. Each plot corresponds to one combination of track setting, curve and vehicle loading state. Results of simulations with the original S1002 wheel profile as well as with wheel profile modification (case MAT) are plotted in these plots in direct comparison against the control case without either countermeasure in each plot. From these results, the following notable observations can be made on the effects of implementing a radial steering mechanism:

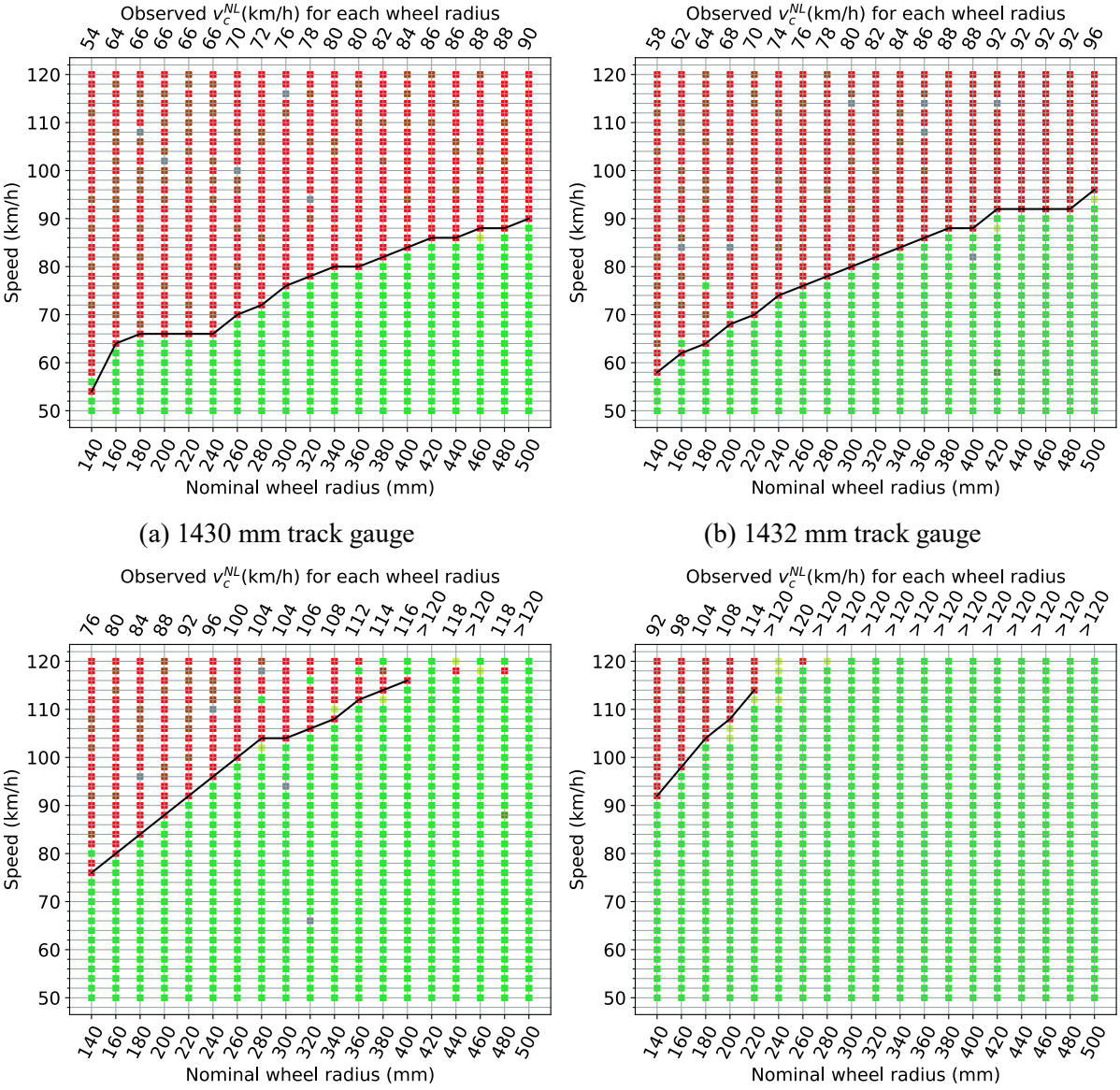

(a) 1430 mm track gauge

(b) 1432 mm track gauge

(c) 1435 mm track gauge

(d) 1437 mm track gauge

Figure 6.13 Stability behaviour of the radial steering bogie with additional yaw relaxation on track with 1:40 rail cant, S1002 wheel profile

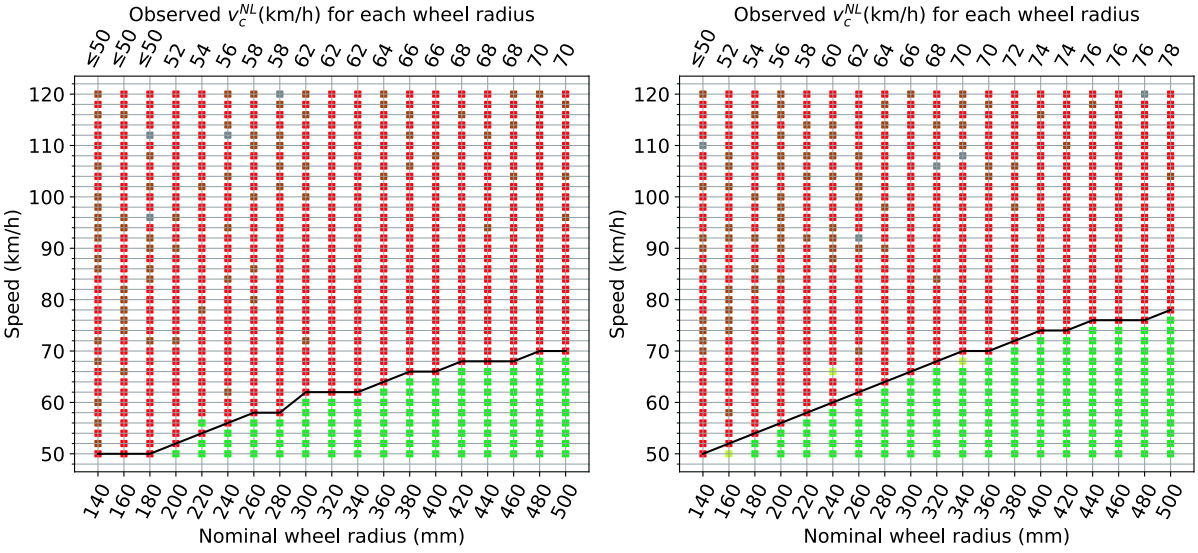

(a) 1430 mm track gauge

(b) 1432 mm track gauge

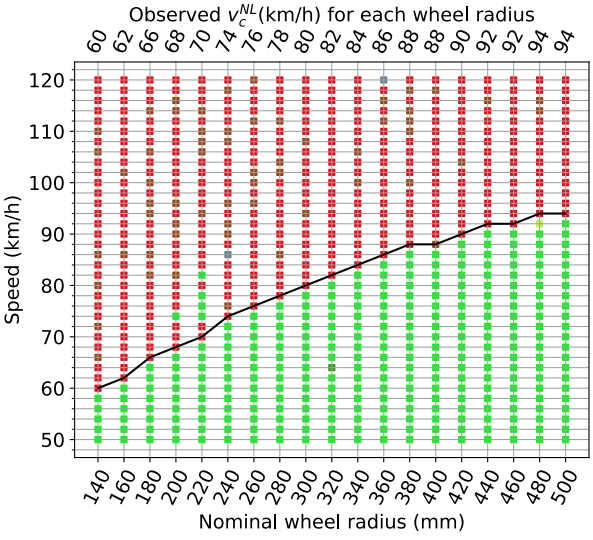

(c) 1435 mm track gauge

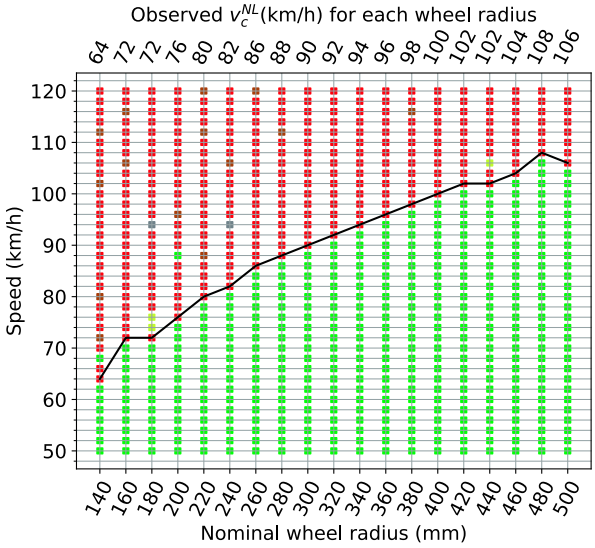

(d) 1437 mm track gauge

Figure 6.14 Stability behaviour of the radial steering bogie with additional yaw relaxation on track with no rail cant, S1002 wheel profile

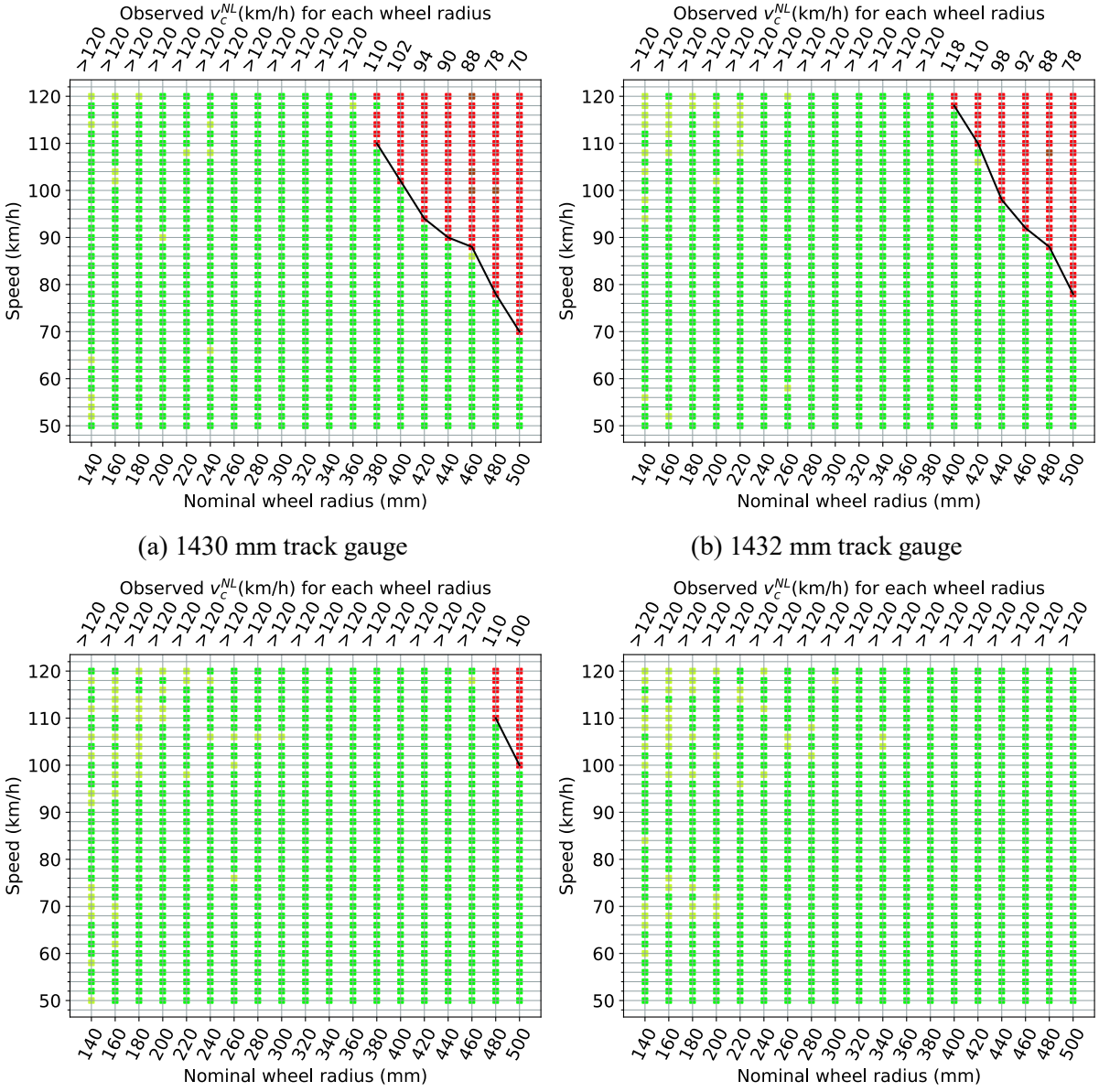

(a) 1430 mm track gauge

(b) 1432 mm track gauge

(c) 1435 mm track gauge

(d) 1437 mm track gauge

Figure 6.15 Stability behaviour of the radial steering bogie with additional yaw relaxation on track with 1:40 rail cant, case MAT

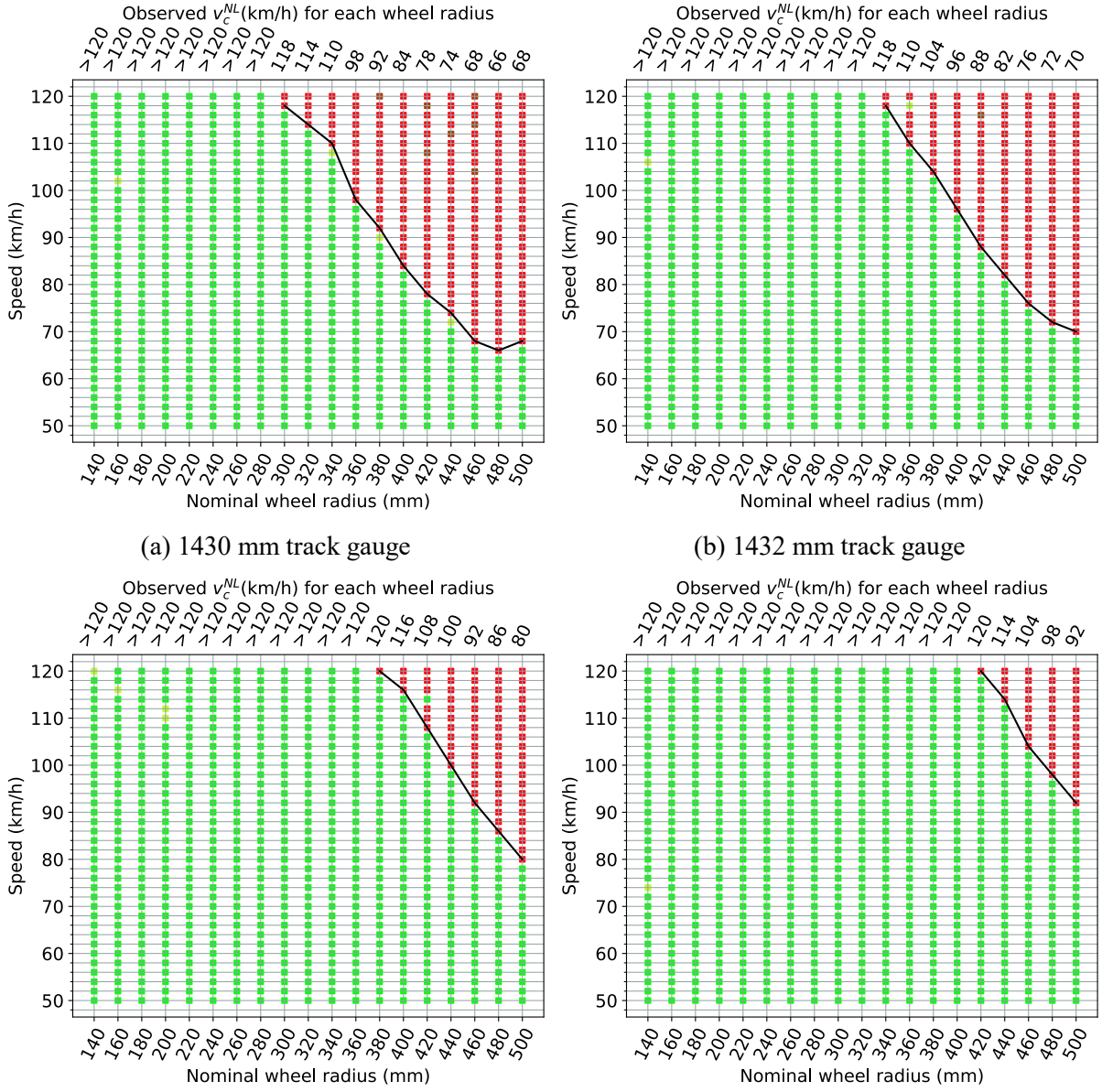

(a) 1430 mm track gauge

(b) 1432 mm track gauge

(c) 1435 mm track gauge

(d) 1437 mm track gauge

Figure 6.16 Stability behaviour of the radial steering bogie with additional yaw relaxation on track with no rail cant, case MAT

First, the radial steering bogie generally exhibits less risk of derailment and a smaller wheel-rail lateral force peak value at lower superelevation deficiencies. For the more difficult situation of a laden wagon, regardless of the track curve radius and combination of track gauge and rail cant, the $|Y|_{max}$-r_0 and $|Y/Q|_{max}$-r_0 plot curves for the radial steering bogie generally runs underneath the same plot curves with the unaltered bogie and profile. The curves for the radial steering bogie without tread modification exhibit only slight variations for different values of r_0; those with the additional wheel-radius-dependent profile scaling generally exhibit a slight worsening of behaviour with decreasing wheel size due to the less slanted and less guidance-capable profiles, although even in the worst cases the values of the maximum wheel-rail lateral force and derailment coefficient are comparable with those in the control case, posing no increased risk.

Second, a combination of radial steering and wheel profile scaling exacerbates the wheel-rail lateral loading for small-wheeled vehicles in the most critical scenario of a laden vehicle negotiating a tight

curve at high superelevation deficiency. The profile scaling causes both $|Y|_{max}$ and $|Y/Q|_{max}$ to elevate significantly with decreasing wheel radius, especially with the addition of r_0-dependent tread flattening, in which case for some medium-sized wheels the wheel-rail lateral force may approach 70 kN on track setups with an originally smaller equivalent conicity (1:40 rail cant). For most wheel sizes smaller than the original wheel size of r_0=460 mm, with the combination of both countermeasures, the peak value of the wheel-rail guidance force $|Y|_{max}$ exceeds the 60 kN limit as is given in EN 14363 [16], although this is not to be interpreted as a definite inapplicability of the said situations, since on the one hand the 60 kN limit value given in the standard is the quasistatic value measured within the round curve and not the peak value occurring usually upon exiting the transition curve measured in this research, and on the other hand this research has not taken practical track irregularities into consideration. This worsening tendency also occurs with the derailment coefficient, although the derailment coefficient observed with the radial steering bogie during the negotiation of a tight curve with deficient superelevation still remains lower than that observed with the original Y25 bogie and S1002 wheel profile in its worst case scenario (with excessive superelevation), making the fast curving of the radial steering bogie a less critical usage scenario than the slow curving of the stiffer Y25 bogie.

Third, during fast curving, the maximum sum of lateral forces on a wheelset $|\Sigma Y|_{max}$ becomes elevated with the implementation of radial steering in most cases, but the additional r_0-dependent wheel profile scaling can effectively drop the $|\Sigma Y|_{max}$ level, thereby reducing the risk of track shift damages. This effect is especially obvious on the CAT2 curve and with a tare wagon. Specifically for small-wheel applications, namely for wheels with a nominal radius smaller than 240 mm, the behaviour of $|\Sigma Y|_{max}$ on the CAT4 curve with a laden wagon is observed to be more track-friendly. As a side note, the profile scaling also reduces the likelihood of the vehicle losing stability during fast curving when using very small wheels, whereas when no profile scaling is used in combination with the radial steering, instability also tends to occur even with larger wheel sizes, notably with the laden vehicle on the CAT2 curve with no rail cant.

Finally, the variation of track gauge involved in this experiment once again does not cause significant changes in the behaviour of any of the curving performance indices. For instance, curve negotiation plots yielded from a track gauge of 1437 mm and a track gauge of 1435 mm when other variables are held the same exhibit barely discernable differences in range of values and trend.

6.2.4 Wear

The wear behaviour of the modified radial steering bogie is summarized and compared against the control case in Figure 6.17. The wear reduction effect of implementing the radial steering mechanism is significant when no wheel profile modification is done; all wear curves of the radial steering bogie remain below those of the Y25 bogie for all nominal wheel radii. Note also that the effective wear number of the radial steering bogie with the smallest wheel radii are normally lower than that of the Y25 bogie with the largest wheel radii. However, with radial steering enabled, fast curving becomes the most wear-intensive scenario, whereas with the original bogie slow curving exhibits the worst wear.

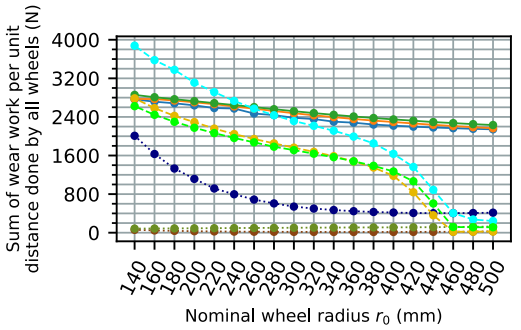

(a) 1437 mm track gauge, 1:40 rail cant

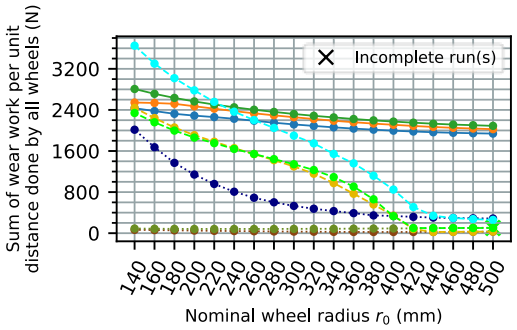

(b) 1437 mm track gauge, no rail cant

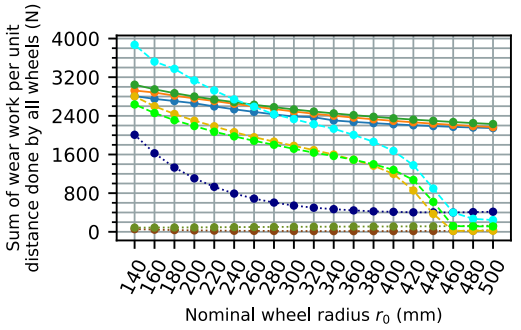

(c) 1435 mm track gauge, 1:40 rail cant

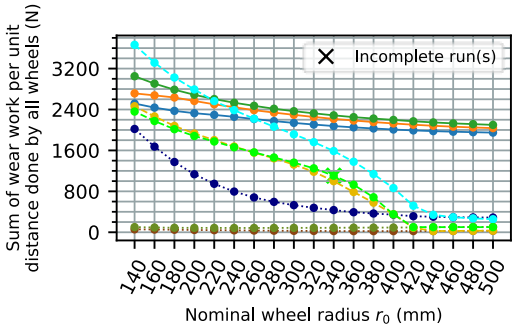

(d) 1435 mm track gauge, no rail cant

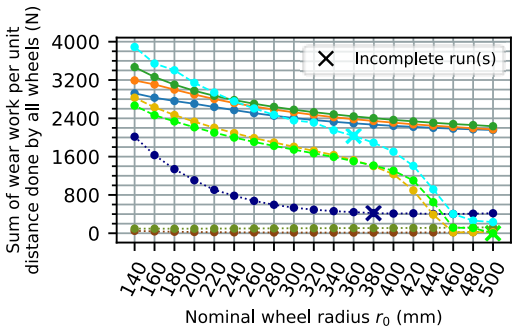

(e) 1432 mm track gauge, 1:40 rail cant

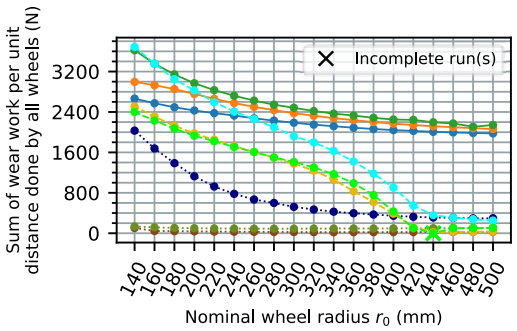

(f) 1432 mm track gauge, no rail cant

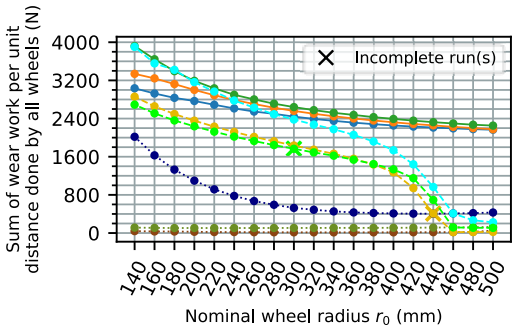

(g) 1430 mm track gauge, 1:40 rail cant

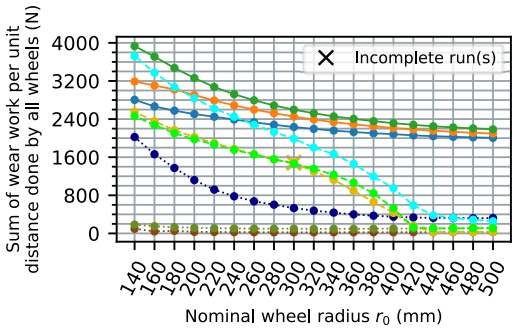

(h) 1430 mm track gauge, no rail cant

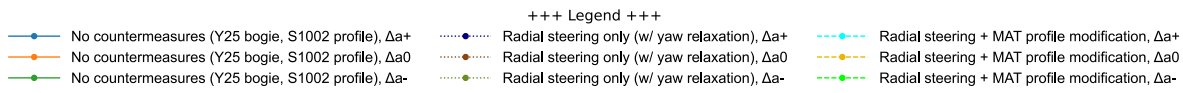

Figure 6.17 Wear behaviour of the radial steering bogie both with and without combination with wheel profile modification case MAT, laden vehicle, CAT4 curve

The additional r_0-dependent wheel profile scaling significantly worsens the wear behaviour as wheel size decreases compared to applying only the radial steering mechanism, whereas the smallest wheels can exhibit even more wear during curve negotiation with superelevation deficiency than observed with the original bogie and wheel profile during curve negotiation with superelevation excess. Considering the equivalent conicity of the respective wheel-rail pairs, it can be seen that the profile scaling affects settings with originally smaller λ_e more significantly. For lower uncompensated centrifugal accelerations the wear behaviour improves in comparison to the control case with the standard bogie and wheel profile.

6.3 Summary of countermeasure effectiveness

The observed influence of the use of a wheel-size-dependent wheel profile and the implementation of radial steering on the vehicle's dynamics behaviour with small nominal wheel radii is herein summarized from the separate tests described in the sections above, focusing on the results plotted on the left side of the respective diagrams with the smaller r_0 values. From the result summaries, the effectiveness of each countermeasure and their combination against running behaviour deterioration due to the use of very small wheels is assessed.

6.3.1 Stability

- Wheel-size-dependent wheel profile scaling with factor $f = \frac{r_0}{r_{0,standard}}$ used alone: effective
- Radial steering mechanism used alone: effective for on standard-gauge tracks; effectiveness diminishes with increase of equivalent conicity of original wheel-rail pair
- Used in combination with wheel profile scaling with factor $f = \frac{r_0}{r_{0,standard}}$: effective, critical speed significantly enhanced for small wheels
- Non-linear critical speed generally benefits more unambiguously from track settings with smaller equivalent conicity values after either countermeasure is implemented

For a clearer overview, a comparison of the stability behaviour of the vehicle before and after implementing countermeasures is summarized in Figure 6.18.

6.3.2 Curve negotiation

- Wheel-size-dependent wheel profile scaling used alone: causes critical worsening of the curving behaviour on tight curves; behaviour also worsens for large-radius curves but remains uncritical
- Radial steering mechanism used alone: effective for reducing risk of derailment; ineffective in terms of stress loading on the track, both on each rail and with respect track shifting
- Used in combination with wheel profile scaling: ineffective – guidance force increases, derailment risk increases for each superelevation deficiency although not exceeding the worst case across all superelevation deficiency settings seen with the original bogie; track shift risks increase
- With usage of radial steering mechanism for small-wheeled bogies: an addition of profile scaling with the above-mentioned f exhibits less risk of track shift at a sacrifice of safety against derailment

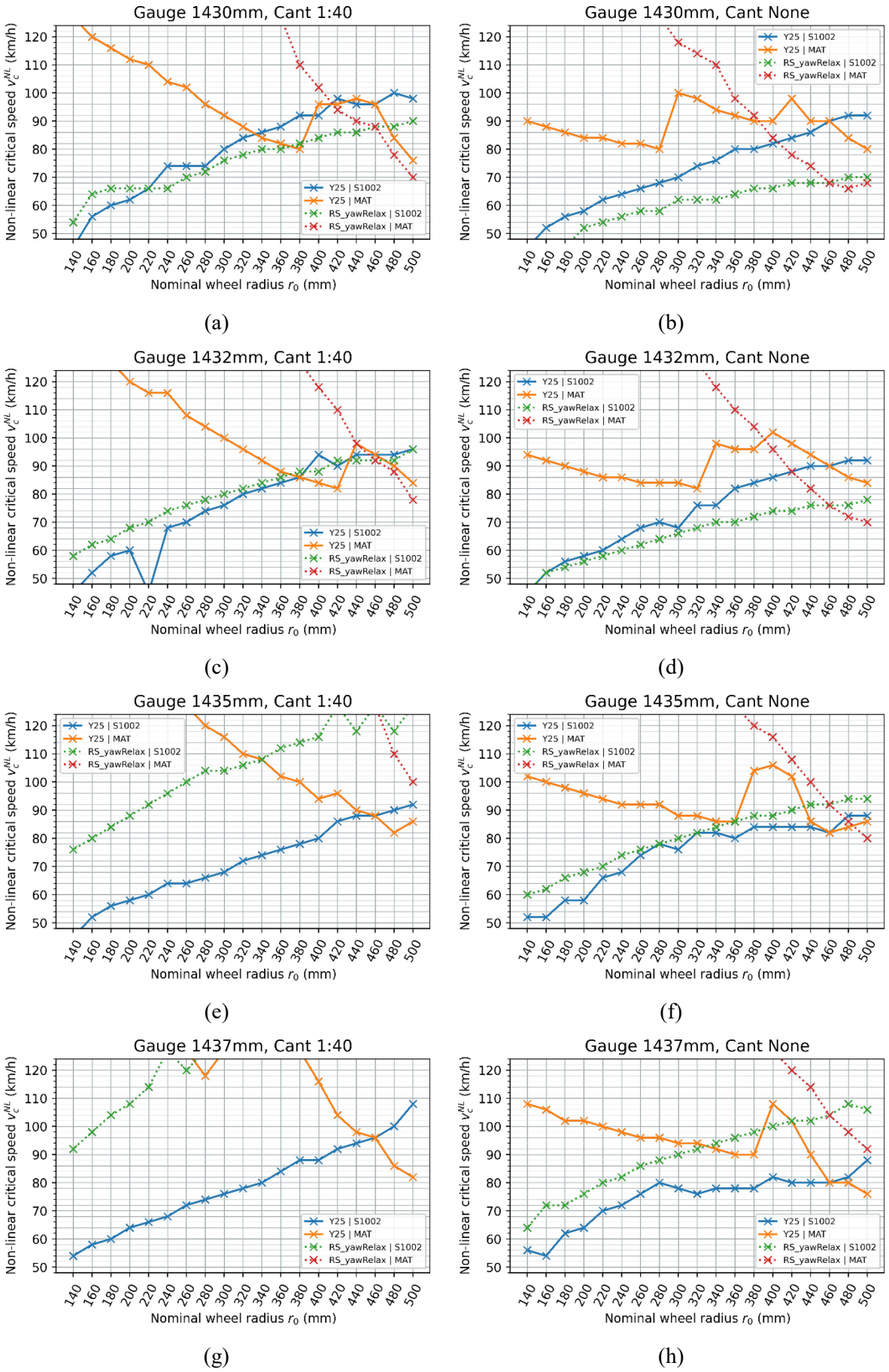

Figure 6.18 Cross-comparison of stability behaviour with and without each countermeasure for each track setting

6.3.3 Wear

- Wheel-size-dependent wheel profile scaling used alone: results in exacerbated wear intensification with decreasing wheel size
- Radial steering mechanism used alone: effective, especially for curving with lower or negative uncompensated centrifugal acceleration; less wear seen with the smallest wheels than the Y25 bogie with the largest wheels under the same running condition
- Used in combination with wheel profile scaling with factor $f = \frac{r_0}{r_{0,standard}}$: ineffective for smaller wheels (with r_0 < 280 mm for most track gauge and rail cant combinations)

7 Conclusion, retrospect and outlook

The first accomplishment of this dissertation is the completion of the investigation of the running dynamics behaviour of a reference freight wagon with two two-axle bogies in the form of the Y25 bogie with wheel radius varying between 140 mm and 500 mm through an MBS-based approach. The behaviour of stability, curve negotiation and wear of the vehicle when using wheels much smaller than the reference bogie's original 920 mm-diameter wheels but without further modification have been quantifiably clarified for the reference vehicle. Simulation results indicate that the reduction of wheel size causes a worsening of the vehicle's stability and wheel-rail wear behaviour and an improvement of curving behaviour. Overall the improvement of curving behaviour is minimal and of no practical significance, whereas the non-linear critical speed is no longer able to maintain above 80 km/h with a wheel with a diameter smaller than 600 mm, and the wear observed with the smallest wheels increases up to around 150% to 200% that with the largest wheels under the same conditions.

Secondly, this dissertation has investigated the recovery effect against the above-mentioned running behaviour deterioration through introducing two specific countermeasures, namely a specific wheel profile downscaling with a factor $f = \frac{r_0}{r_{0,standard}}$ and the implementation of a radial steering. The countermeasures are implemented both individually and in combination. The results indicate that the implementation of radial steering helps the small-wheeled vehicle recover much of the performance lost through the decrease in wheel size, given that the settings do not give rise to high equivalent conicity under operational wheel-rail profile pairings; that is to say, a larger track gauge is significantly beneficial, as well as a rail cant properly chosen for the wheel-rail profile pairing used. Where curving is not critical for operation, the wheel-radius-dependent wheel profile scaling is also helpful in terms of increasing stability of the small-wheeled vehicle, although the vehicle sacrifices the ability to negotiate curves even with excessive superelevation or slow passing speed. The adjustment effect of the wheel profile scaling is much more significant than that of the radial steering implementation, and as a result a combination of both measures tends to bring the behaviour of the vehicle into the tendency of drastic stability increase and drastic curving performance decrease that wheel profile scaling brings forth alone.

The interesting finding of this research is that there exists the use of radial steering as a measure to make two-axle singular-frame bogies suitable for use with very small wheels, thereby making use of its advantage in lowering the floor height throughout the entire vehicle. The investigations conducted in this research are apparently yet to be supported by on-track tests for a more definite validation of the results. Note also that the simulations are done without considering noise factors such as track irregularity or wheel out-of-roundness, nor is the behaviour of small-wheeled wagons operating in a consist considered. This research thus only theoretically sheds light upon the vehicle's intrinsic dynamics behaviour when the wheel size is drastically reduced. Should on-track tests with practical considerations support the findings of this research, further optimization work can be done to find a small-wheeled bogie design that best suits the needs of potential operators with demand for low-floor freight wagons. Further wheel profile scaling schemes which provide a more balanced behavioural adjustment to the vehicle with a potentially less severity in its influence on curve negotiation and wear also deserve deeper investigation. Its realization would mean that even if wheels are worn down in operation, they may be reprofiled according to their new wheel radius after wear and reprofiling with a radius-dependent profile that provides the most running property compensation, thus extending the service life on operational wagons.

Appendix A Naming of degrees of freedom used in this thesis

The coordinate system used here is assumed to be identical to that used in Simpack 2019, and thus the naming of the degrees of freedom are defined in consistency with Simpack conventions.

For vehicle:

Longitudinal: x, with the positive direction being in the direction of travel unless otherwise specified;
Lateral: y, with the positive direction to the right side of the vehicle;
Vertical: z, with the positive direction pointing towards the track (downwards).

The rotational degrees of freedom about each translational coordinate axis are named as follows:
α for rotation about x-axis;
β for rotation about y-axis;
γ for rotation about z-axis,
with the direction following the right-hand rule.

Additionally for track:

Tangentially along track centreline: s, with the positive direction pointing away from the track's starting point.

See Figure A.1.

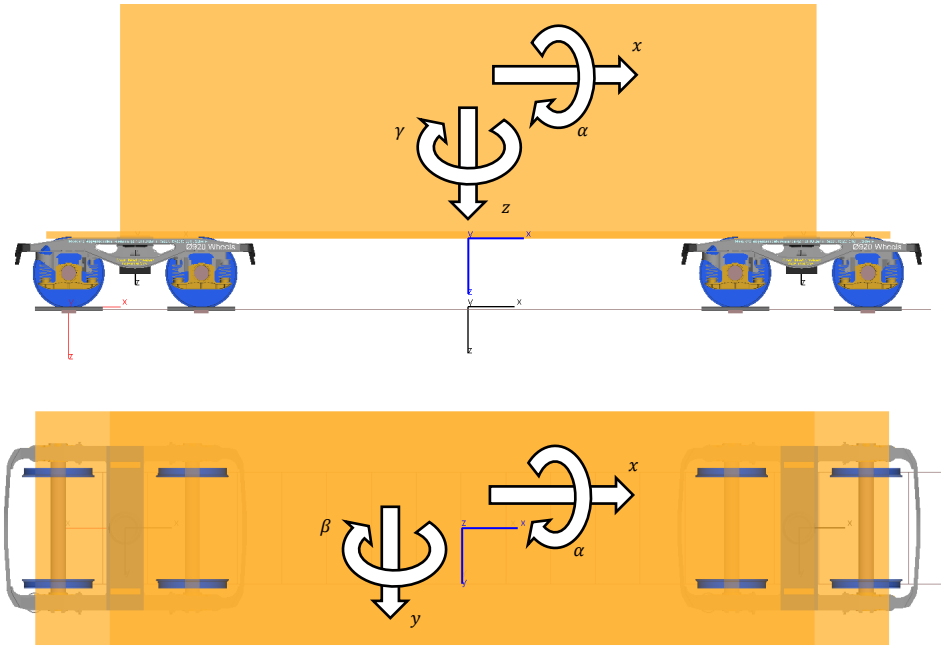

Figure A.1 Naming of degrees of freedom for the vehicle and the track (as shown with white arrows added to the image)

Appendix B Positional numbering scheme for vehicle components

Whereas the standardized convention in Europe for numbering the position of recurring components on railway vehicles is alphanumeric, with the number representing longitudinal sequence and letter representing the side at which the component is located [115], this dissertation opts against this convention and instead adopts a purely numeric positional numbering scheme when referring to wheels and wheelsets. The reason is that a purely numeric index eases the programming effort of scripts, especially in the case of iterating actions over all components. In realistic railroading practice, this is the standard vehicle component position numbering scheme used by China Railways

The position of a recurring vehicle component is numbered in this dissertation as follows:

- The vehicle is observed with the observer facing the vehicle's End 1 from the outside
- Components distributed along the longitudinal axis of the vehicle are numbered in ascending order of distance from the observer, i.e. from End 1 to End 2
- For components distributed on either side of the longitudinal axis of the vehicle, those located on observed left side of the axis are given odd numbers, those located on the observed right side of the axis are given even numbers, respectively numbered in ascending order of distance from the observer

As all components of concern in this research are left-right-symmetrically arranged (with no component occurring more times on one side than the other), the component numbering following the above mentioned rules results in a continuous set of sequence numbers for the same type of component. This purely numeric, continuous numbering allows components to be referenced easily with numeric indices in the programme scripts.

In this dissertation, the vehicle's End 1 is supposed as the front end of the vehicle in respect to the direction of travel. In reality, End 1 is either defined as the direction in which the brake cylinder piston pushes out for vehicles with a single brake cylinder for the whole vehicle, or specified by the manufacturer for vehicles that do not possess a single brake cylinder (eg. caliper-mounted cylinders).

Specifically relevant to this dissertation, the wheels and wheelsets are numbered as shown in Figure B.1.

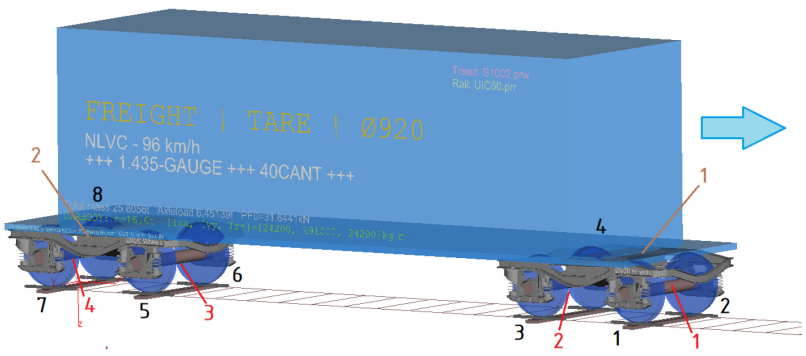

Figure B.1 Positional numbering of vehicle components used in this dissertation
Blue arrow indicates direction of travel
Brown: bogie numbers; red: wheelset numbers; black: wheel numbers

Appendix C Curve negotiation simulation results before implementing either countermeasure

A total of 16 plots are shown, each corresponding to a combination of vehicle load state, track gauge and rail cant.

Each line plot as well as each row of numbers representing the wheel or wheelset with which the highest magnitude of each curve negotiation performance indicator is observed for the current nominal wheel radius (annotated above each plot) represents a combination of track curve radius and superelevation deficiency. This correspondence is indicated with the legend given by Figure C.1. Similar colours and line styles help group together same controlled settings. For example, in this appendix, blue, red and yellow denote respectively deficient, ideal and excessive superelevation, with the curve category distinguished with different line styles. As the location of maximum performance index magnitude occurrence is only indicated with numbers and does not involve lines, the different curve categories are additionally assigned different darknesses of colour so that the location numbers above each plot can be sufficiently distinguished and corresponded to each simulation setting combination.

For each value of nominal wheel radius r_0, if there exist simulations in which the test vehicle's wheelset number 4 cleared one but not both of the test curves, the result is indicated with a different plot marker "×". This is caused by the vehicle's unstable behaviour occurring in these simulations, as mentioned in Section 5.2.2.1 and Figure 5.12, which results in frequent flange-to-rail impacts or multiple-point contacts which calls for substantially more calculation time and constant reduction of the integration step sizes of the SODASRT2 variable step size integration solver. The calculation and time resources available for this research are insufficient to ensure that all simulations completely run through. However, it is ensured that in all simulations the test vehicle cleared the first curve of the S-shaped test track so that the result yielded from the vehicle negotiating the right-hand curve is complete. Nonetheless, given the left-right symmetry of the vehicle's geometry and mass, such results are able to adequately portray the curve negotiation behaviour of the vehicle.

The form of the curve negotiation simulation result plots in subsequent appendices takes after the form shown in this appendix, with the legend for all plots in the same appendix given as the first figure within each appendix.

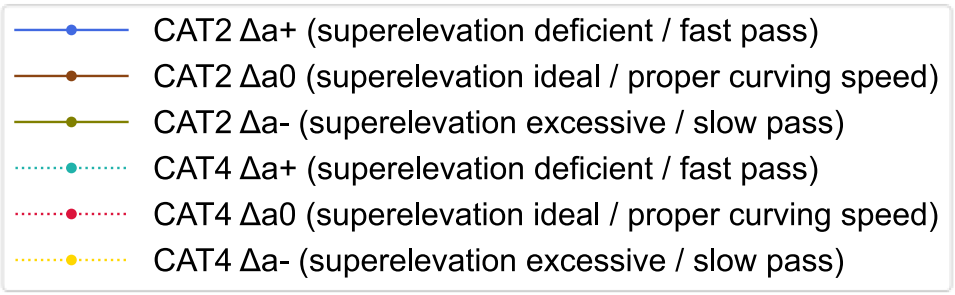

Figure C.1 Legend of all plots in this appendix

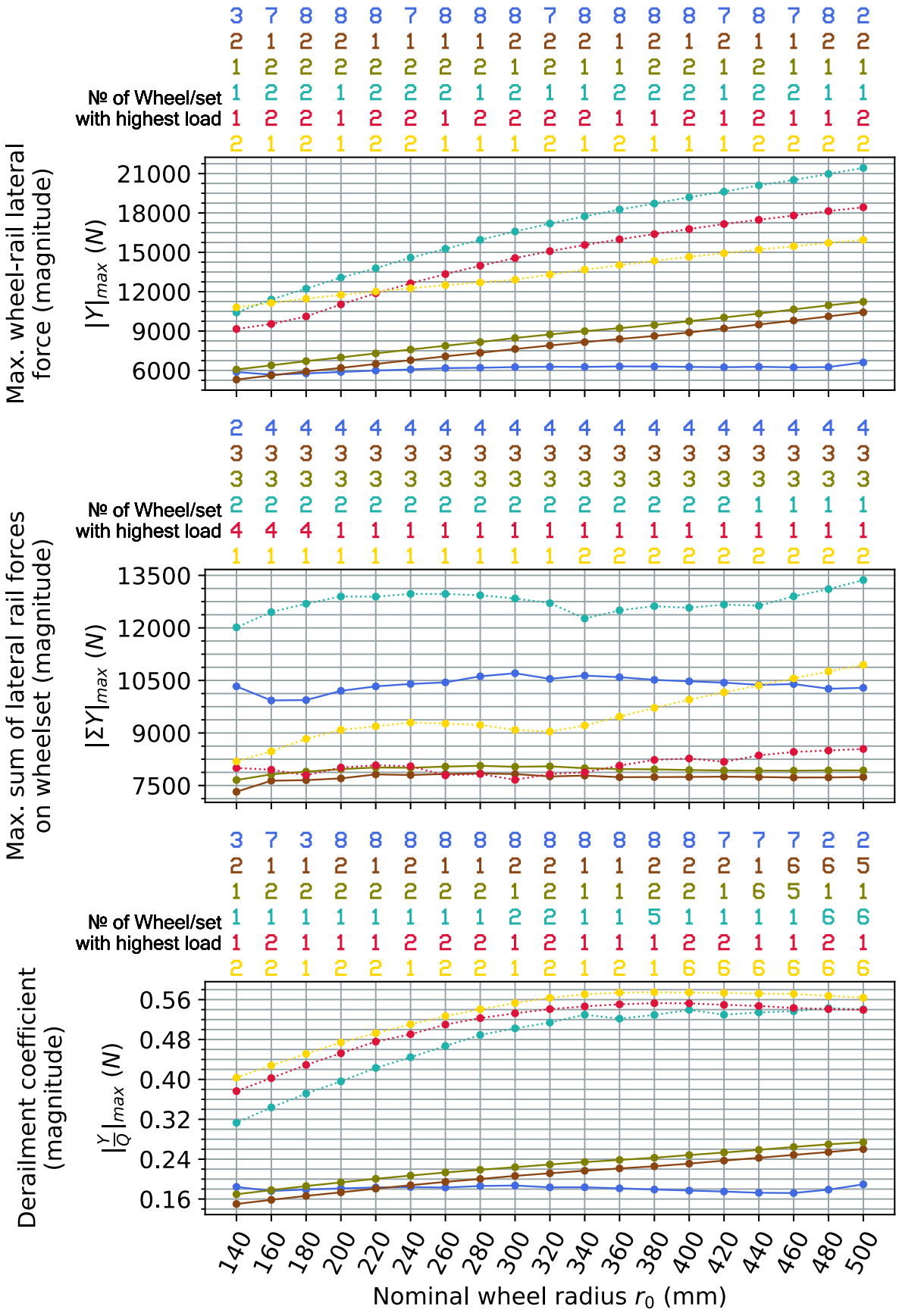

Figure C.2 Tare vehicle on a track with 1437 mm gauge and 1:40 rail cant

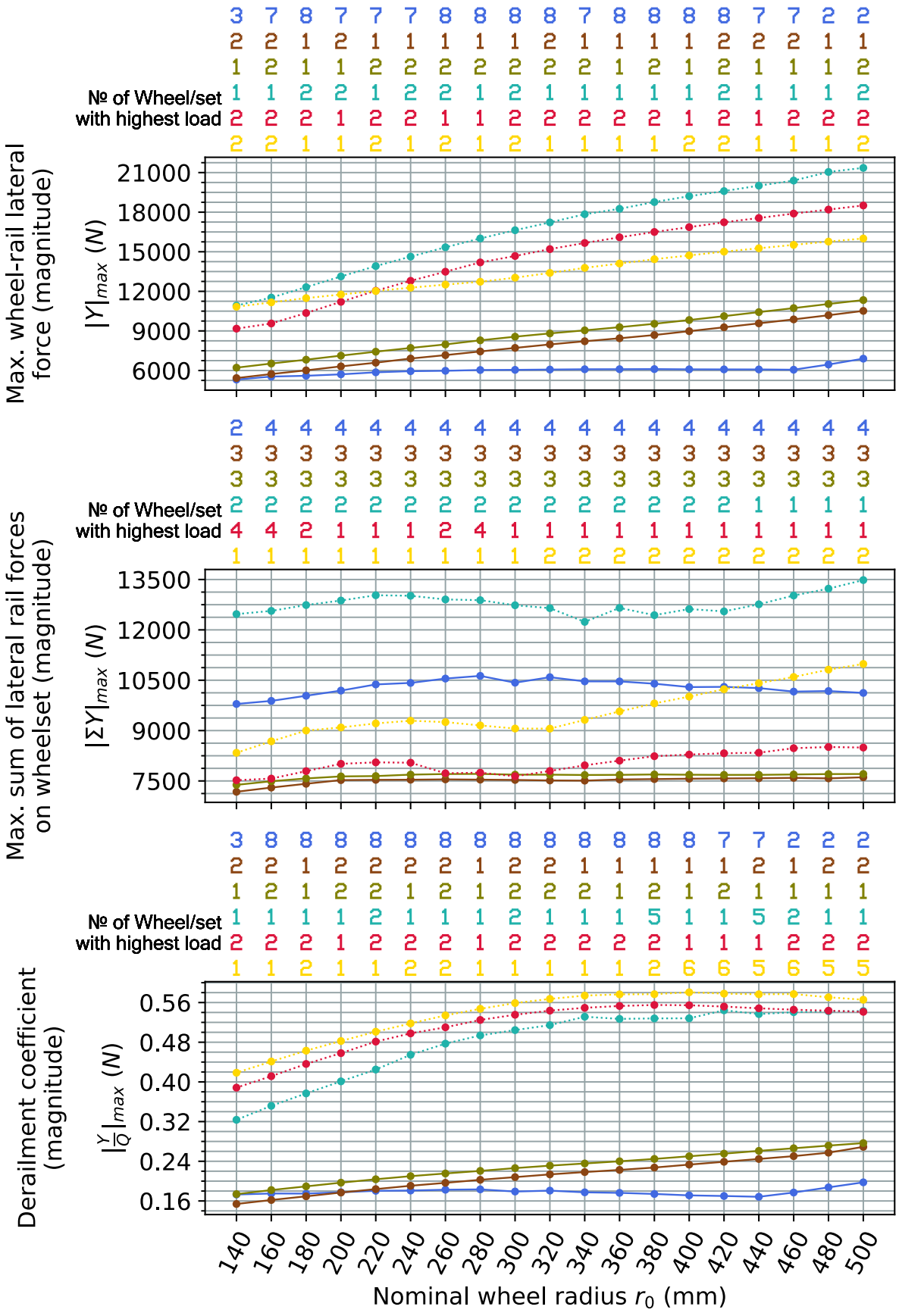

Figure C.3 Tare vehicle on a track with 1435 mm gauge and 1:40 rail cant (reference track setting)

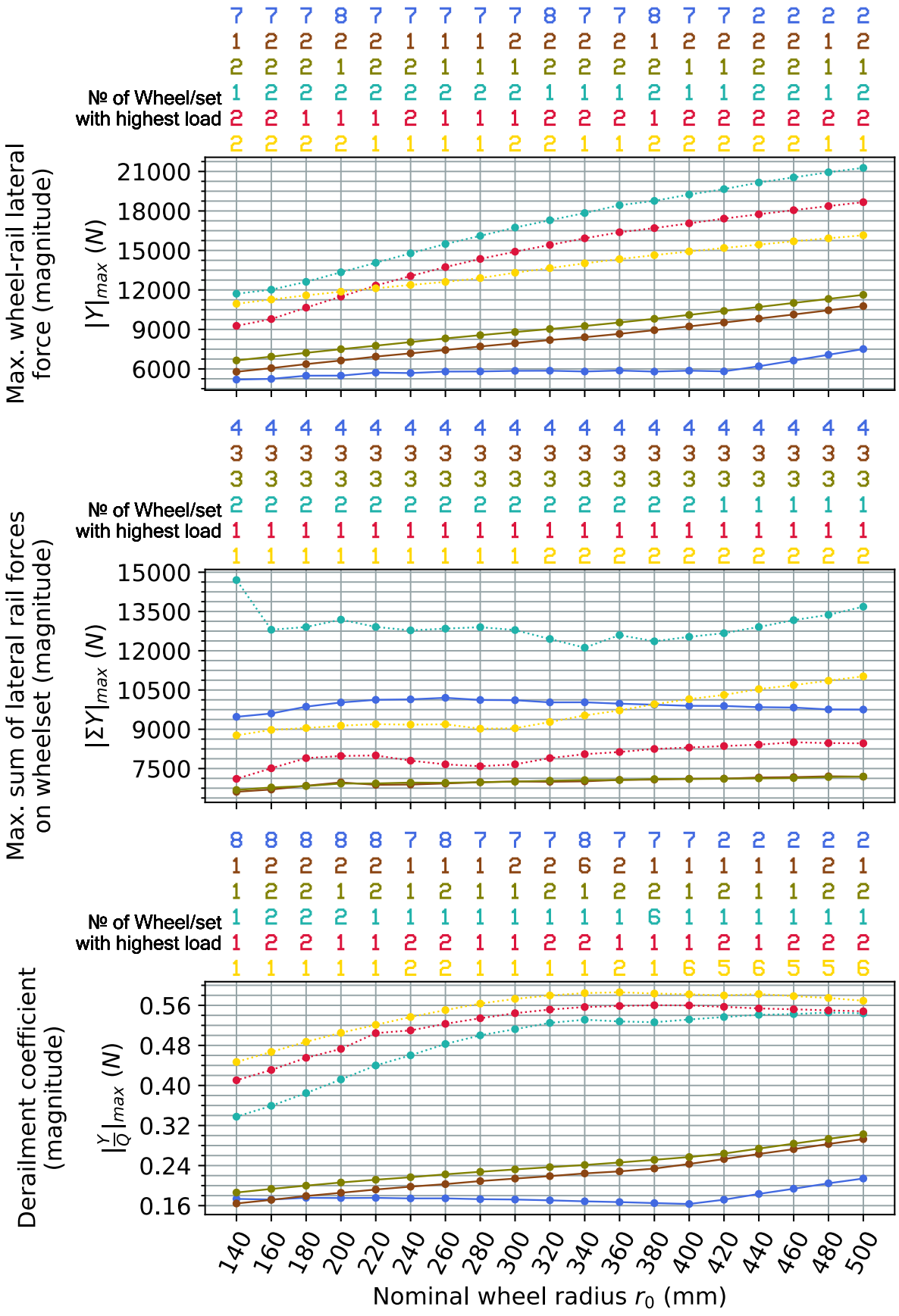

Figure C.4 Tare vehicle on a track with 1432 mm gauge and 1:40 rail cant

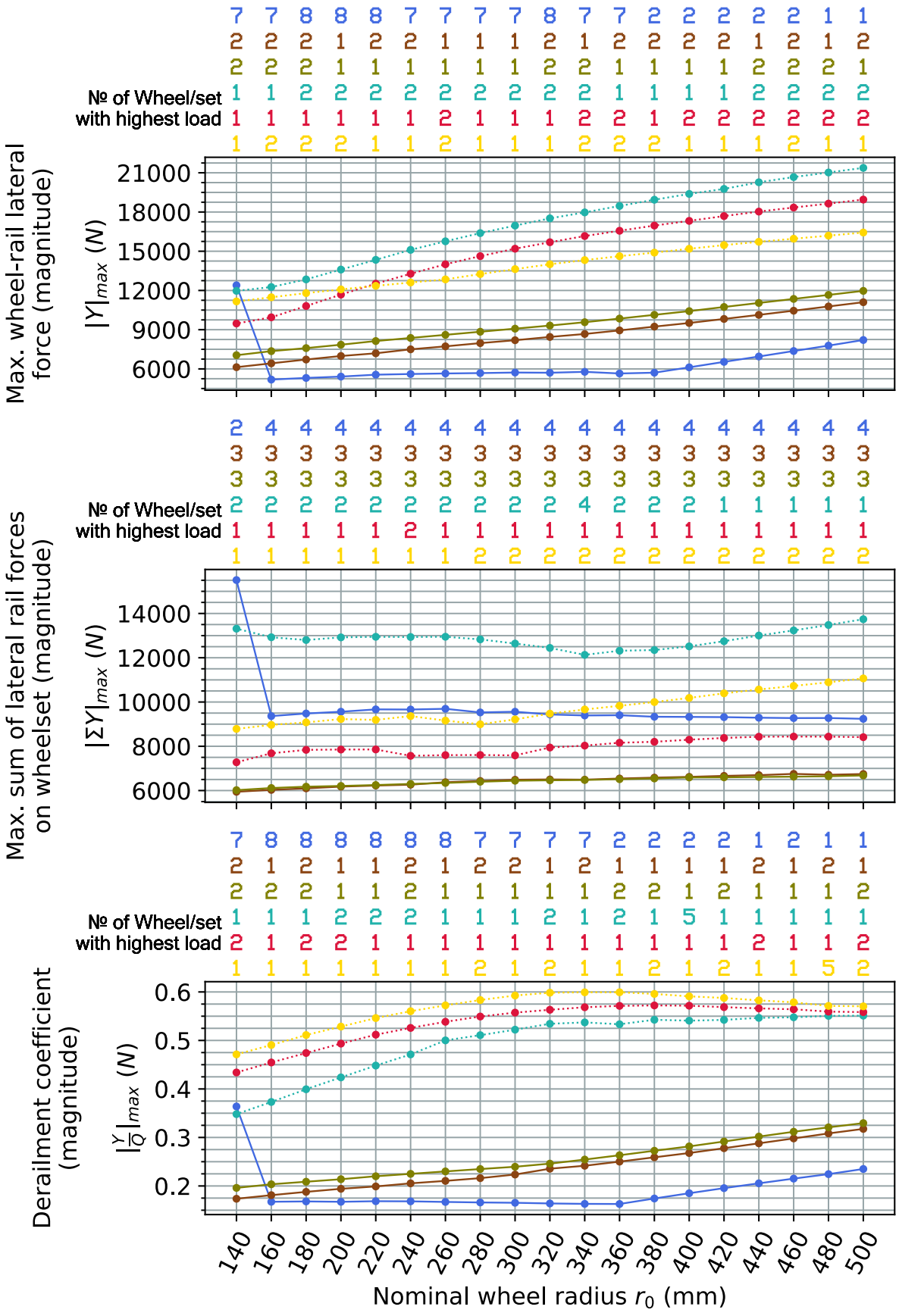

Figure C.5 Tare vehicle on a track with 1430 mm gauge and 1:40 rail cant

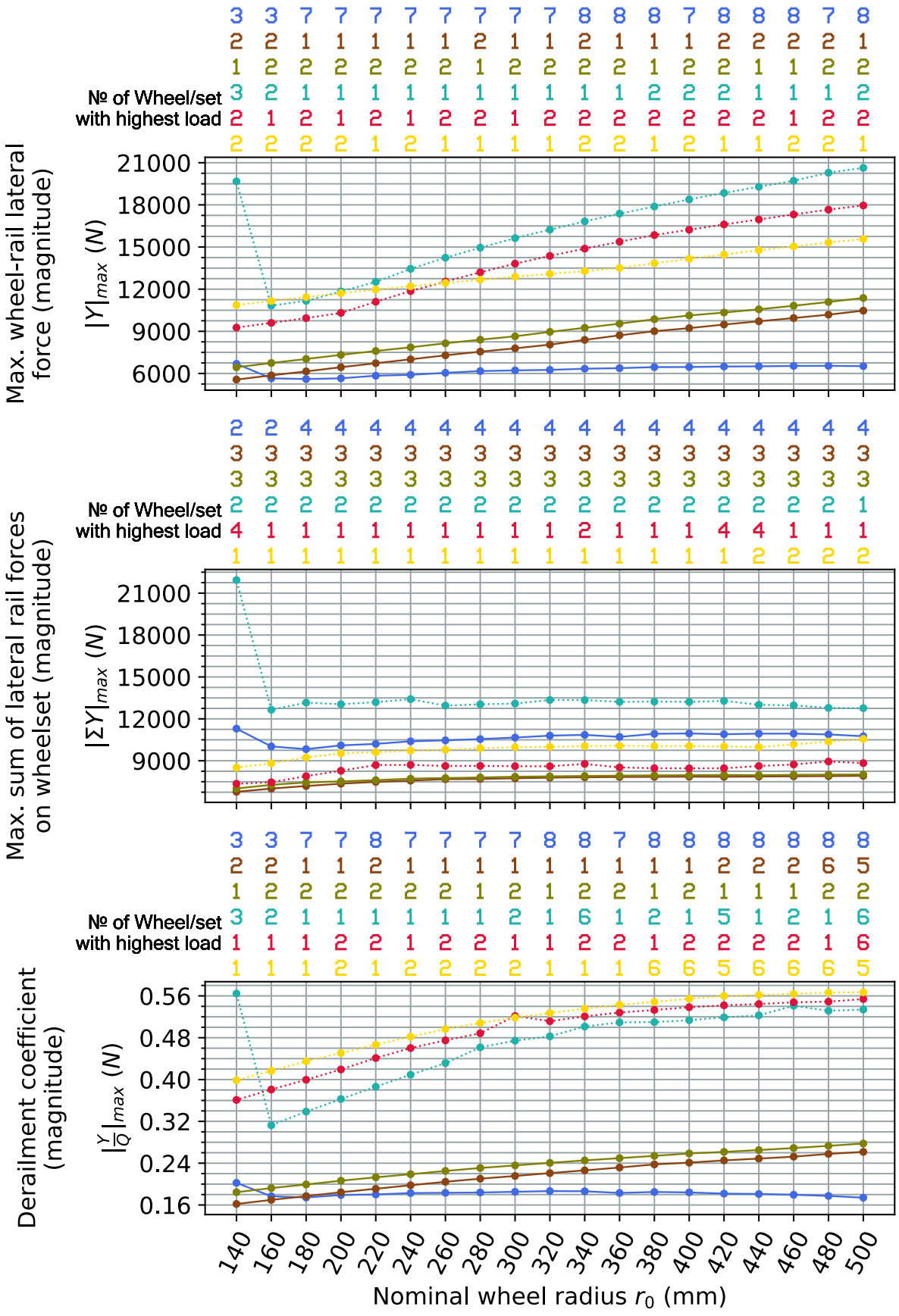

Figure C.6 Tare vehicle on a track with 1437 mm gauge and no rail cant

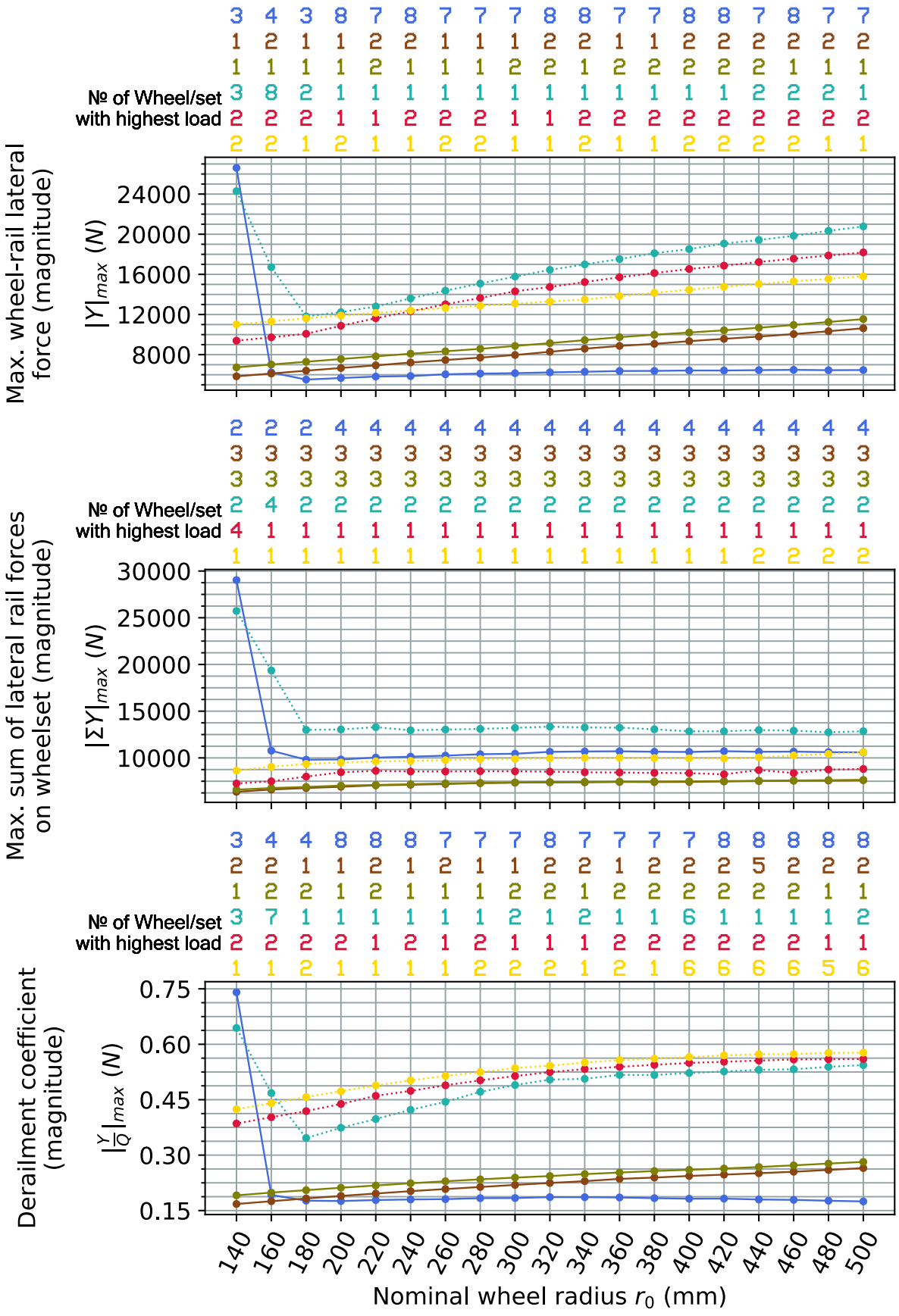

Figure C.7 Tare vehicle on a track with 1435 mm gauge and no rail cant

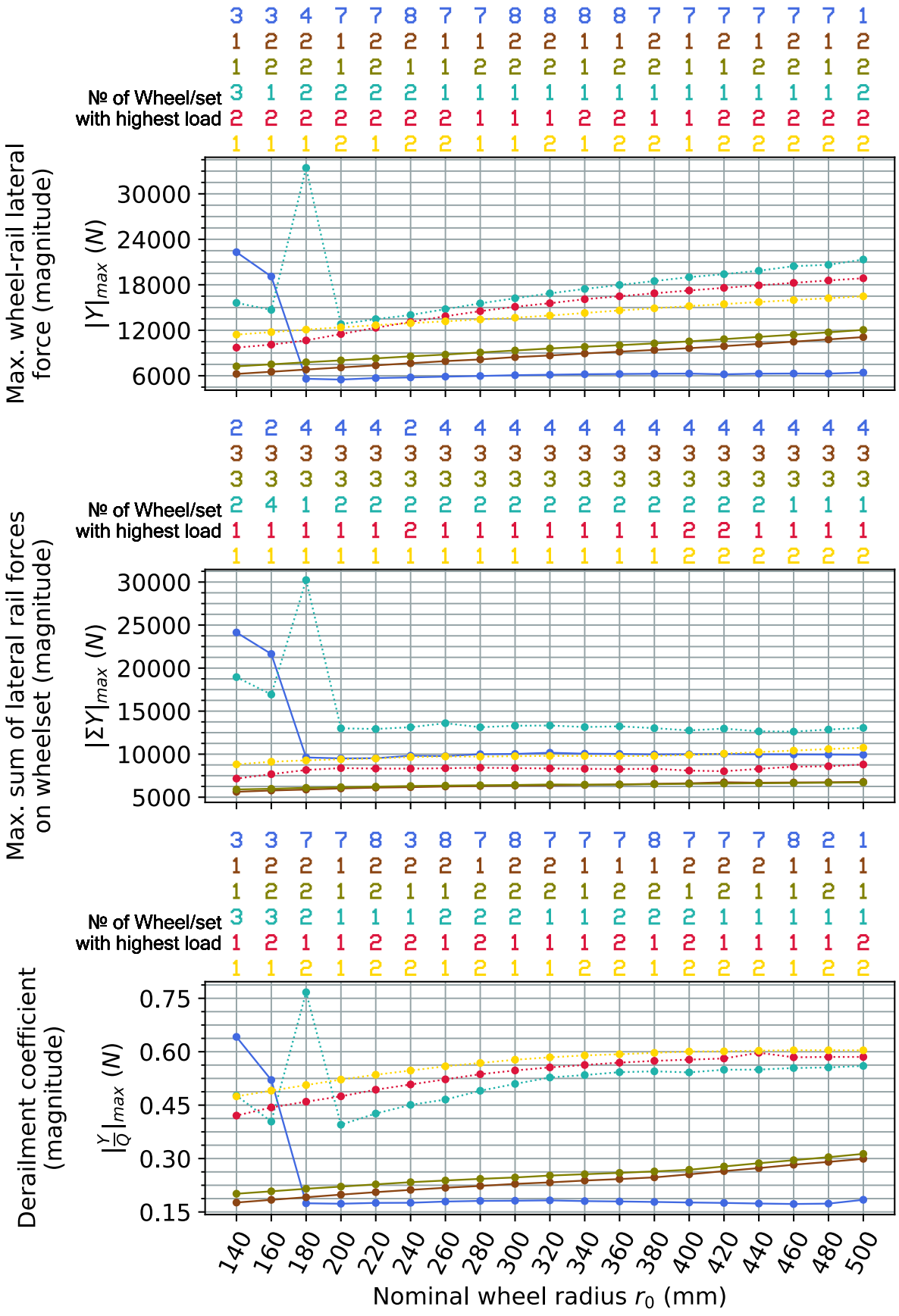

Figure C.8 Tare vehicle on a track with 1432 mm gauge and no rail cant

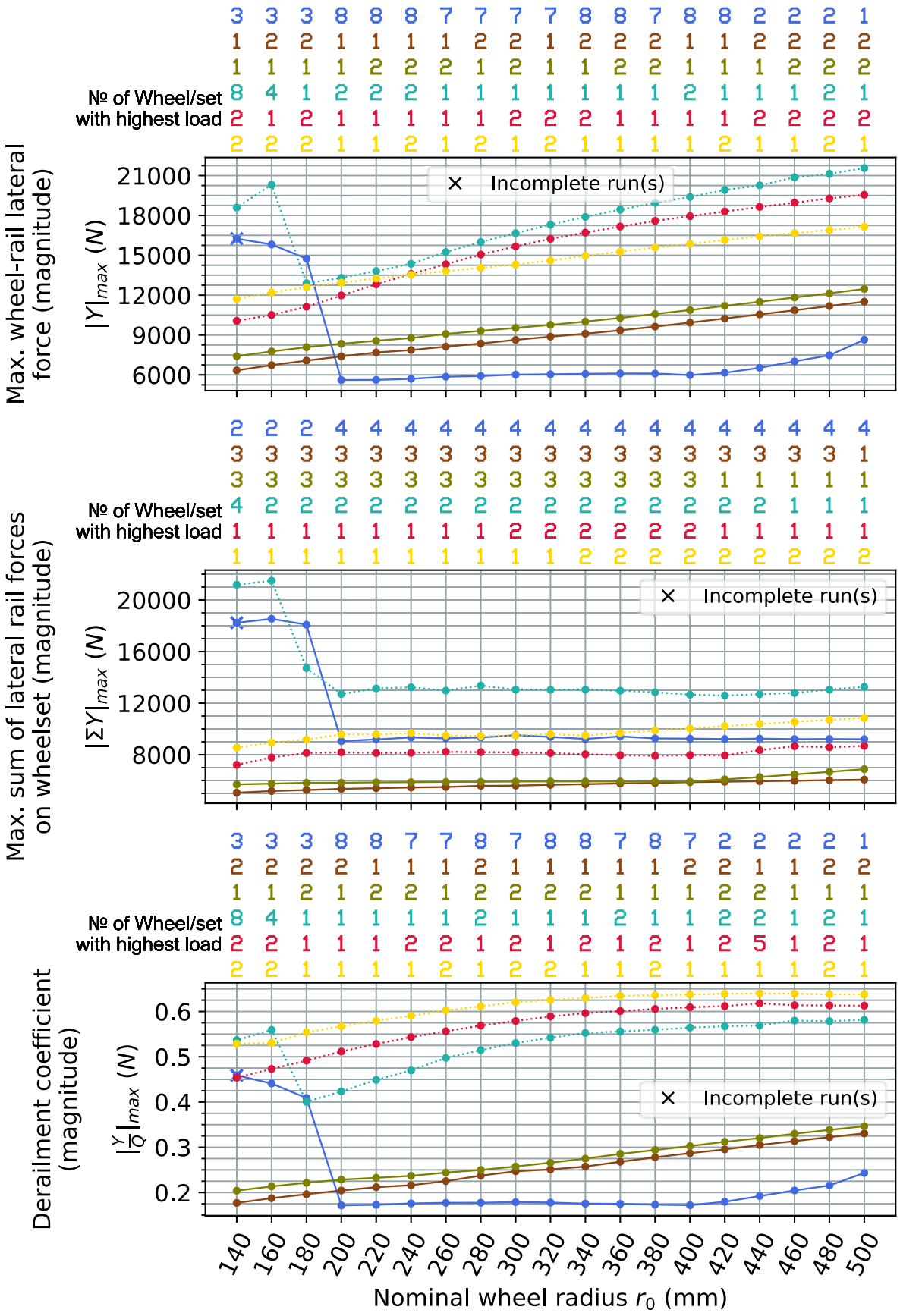

Figure C.9 Tare vehicle on a track with 1430 mm gauge and no rail cant

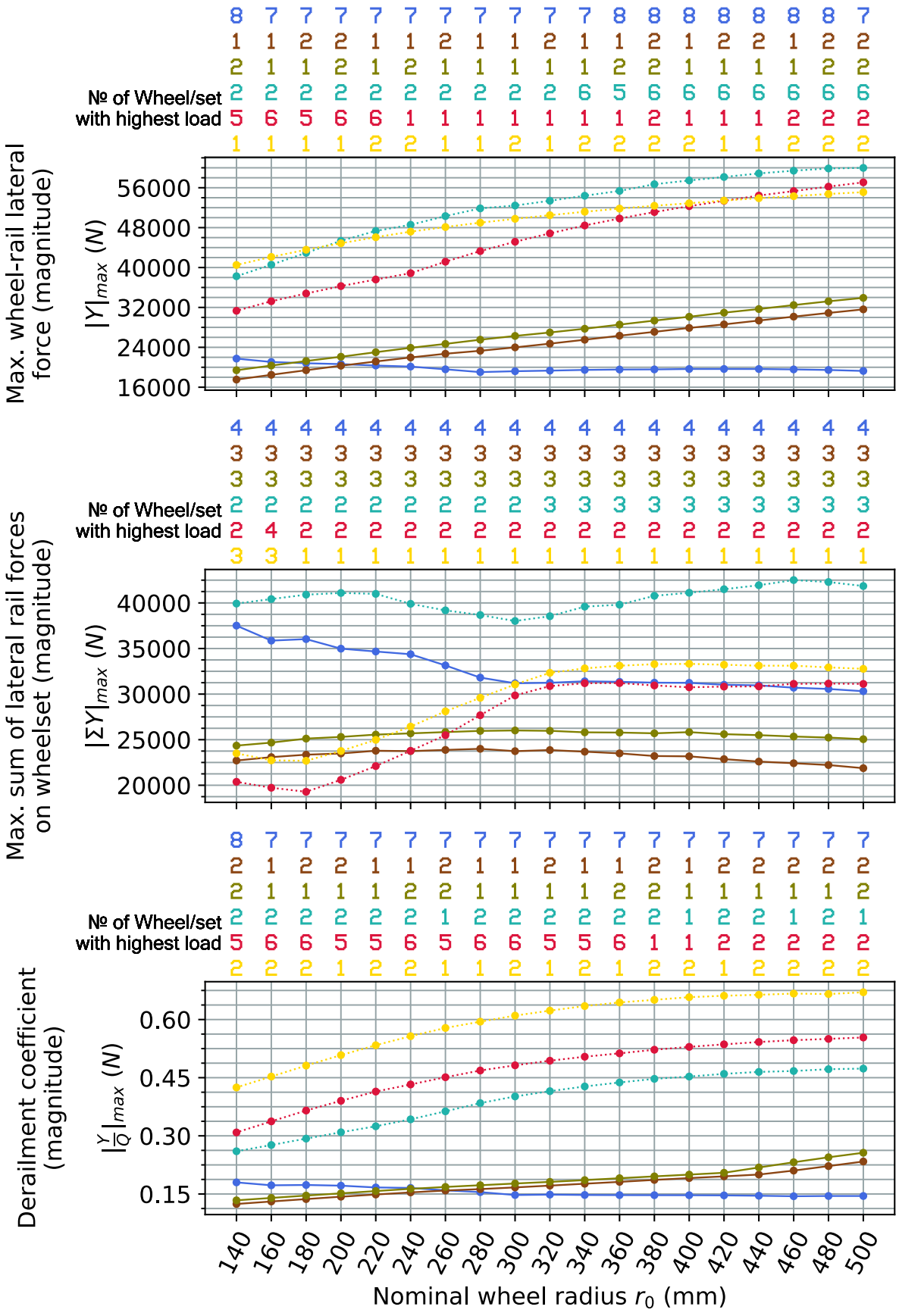

Figure C.10 Laden vehicle on a track with 1437 mm gauge and 1:40 rail cant

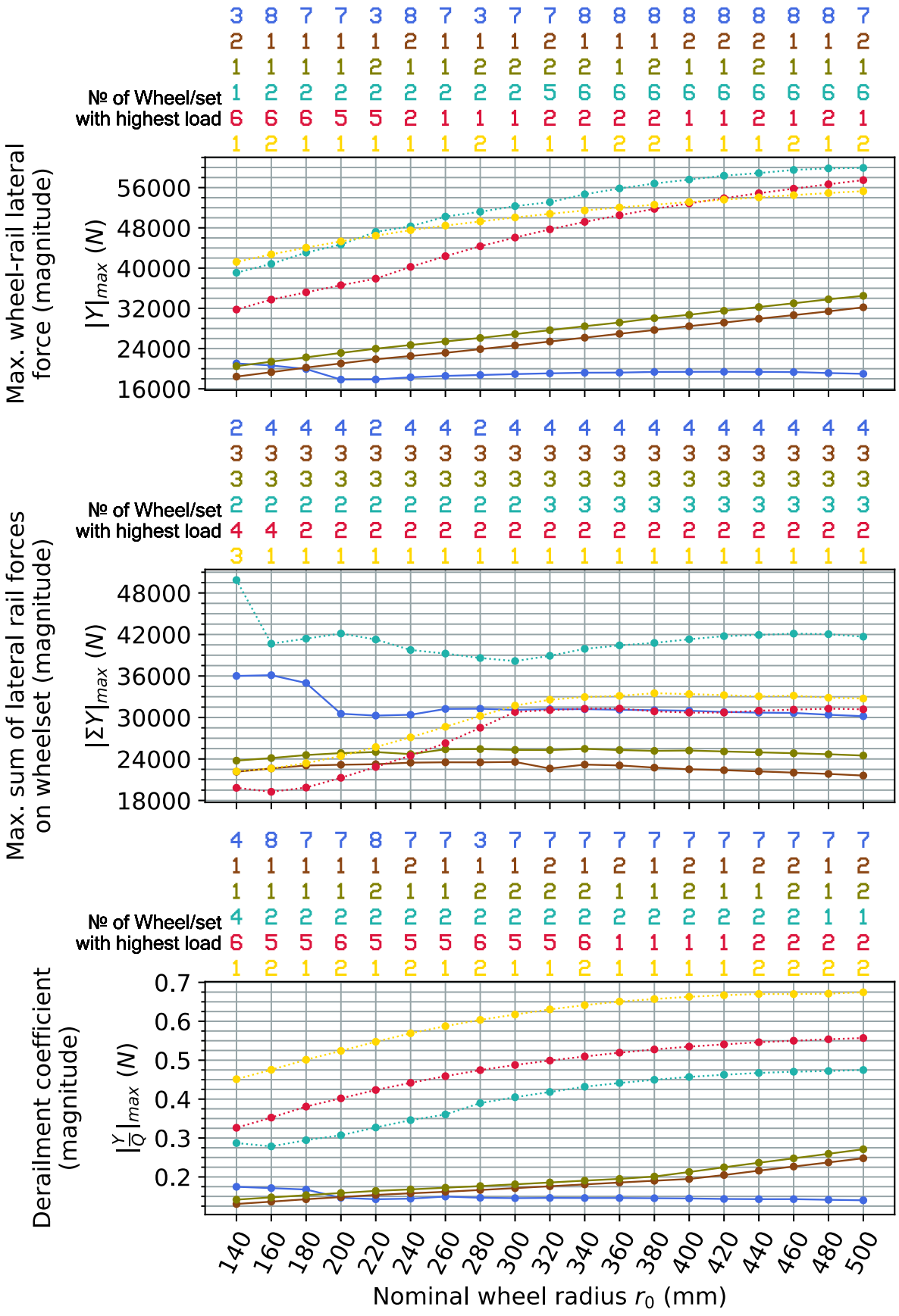

Figure C.11 Laden vehicle on a track with 1435 mm gauge and 1:40 rail cant (reference track setting)

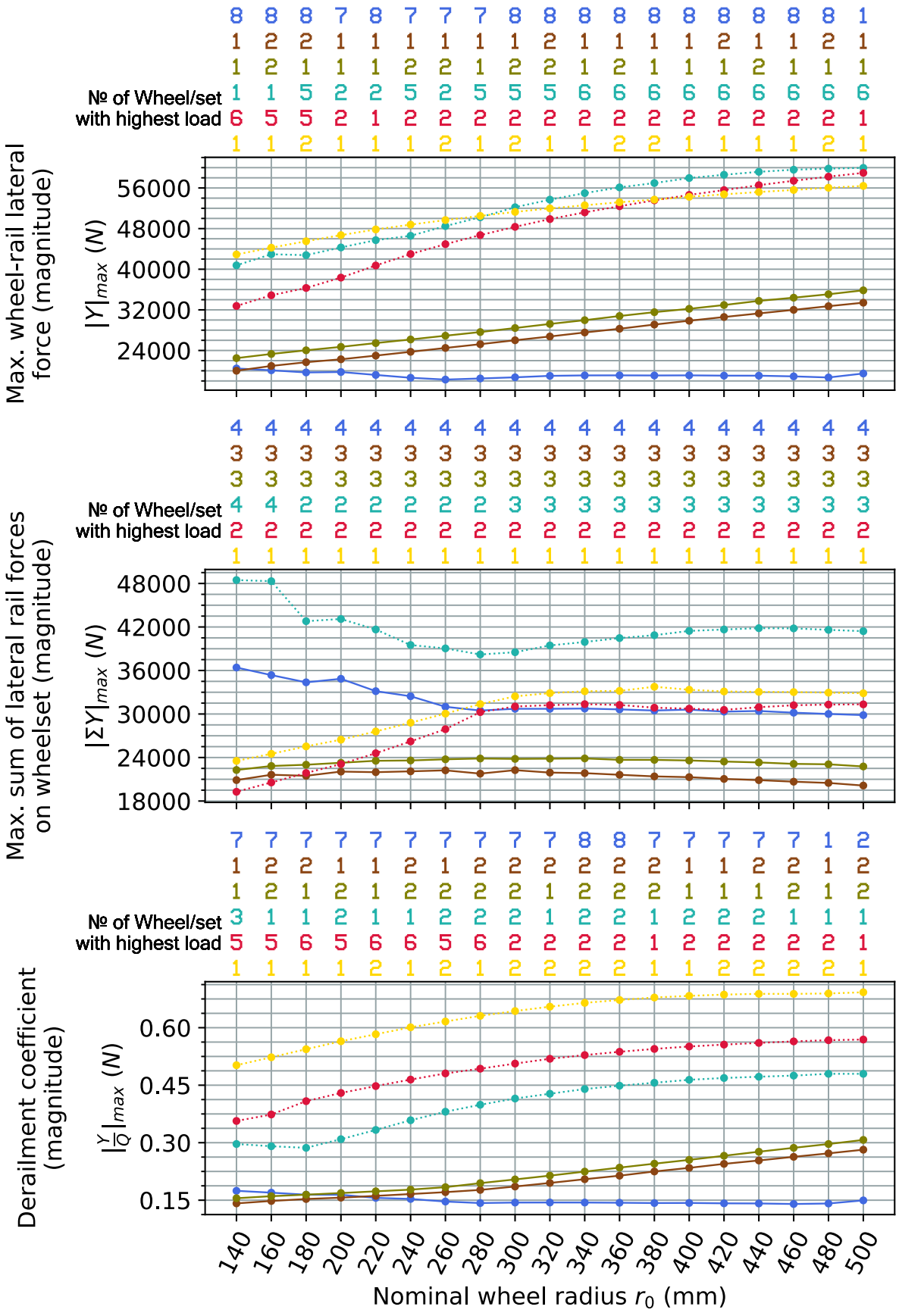

Figure C.12 Laden vehicle on a track with 1432 mm gauge and 1:40 rail cant

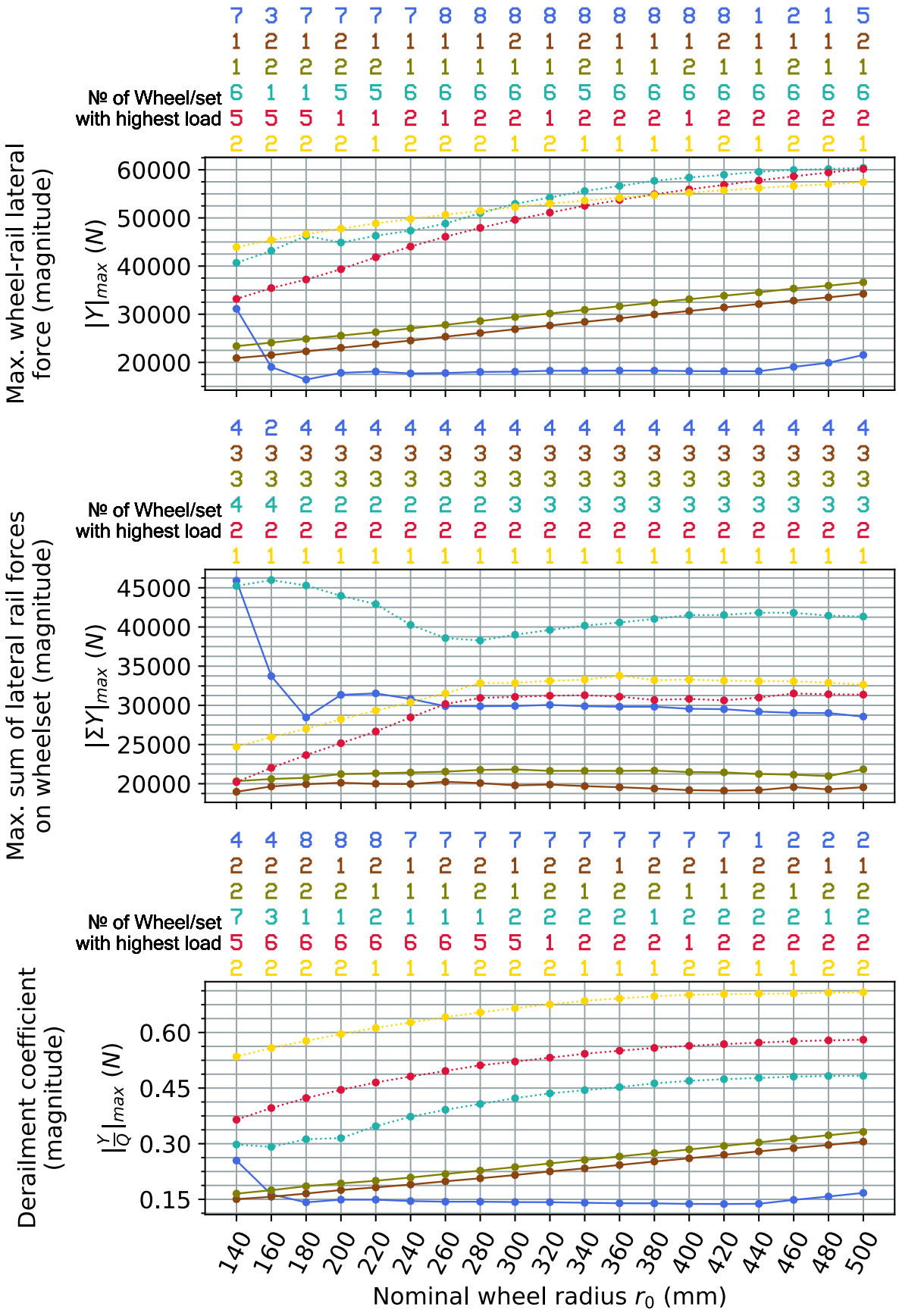

Figure C.13 Laden vehicle on a track with 1430 mm gauge and 1:40 rail cant

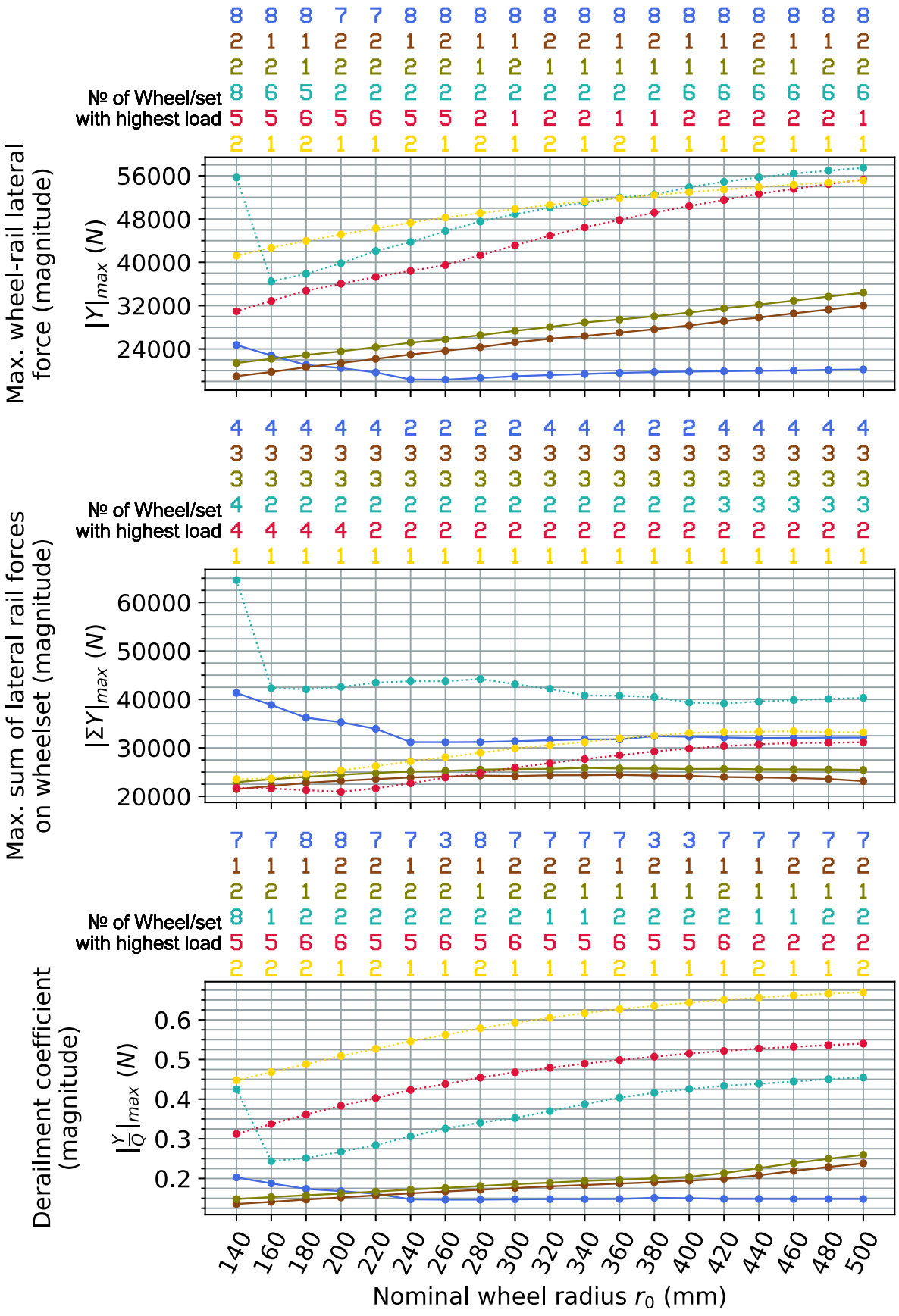

Figure C.14 Laden vehicle on a track with 1437 mm gauge and no rail cant

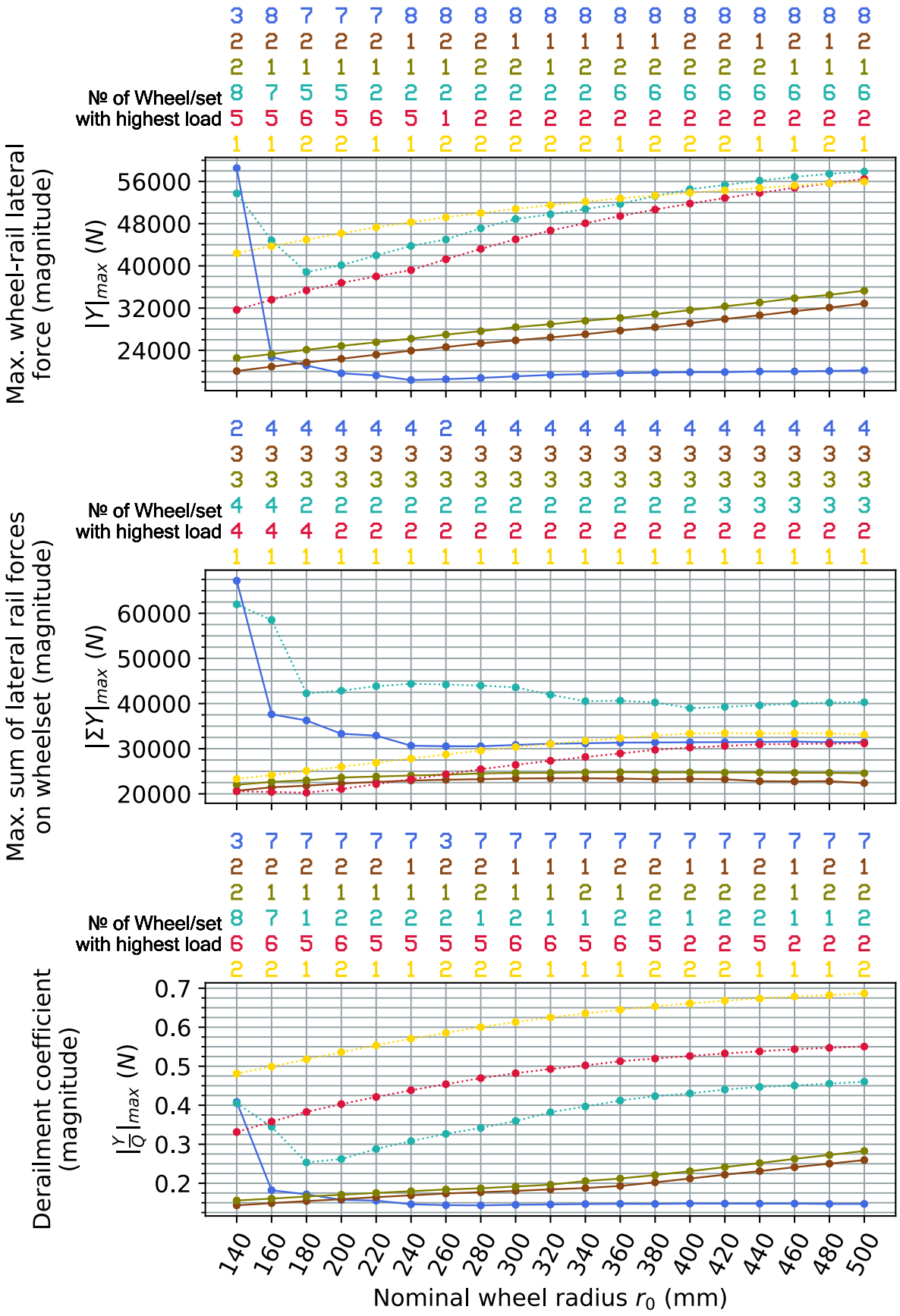

Figure C.15 Laden vehicle on a track with 1435 mm gauge and no rail cant

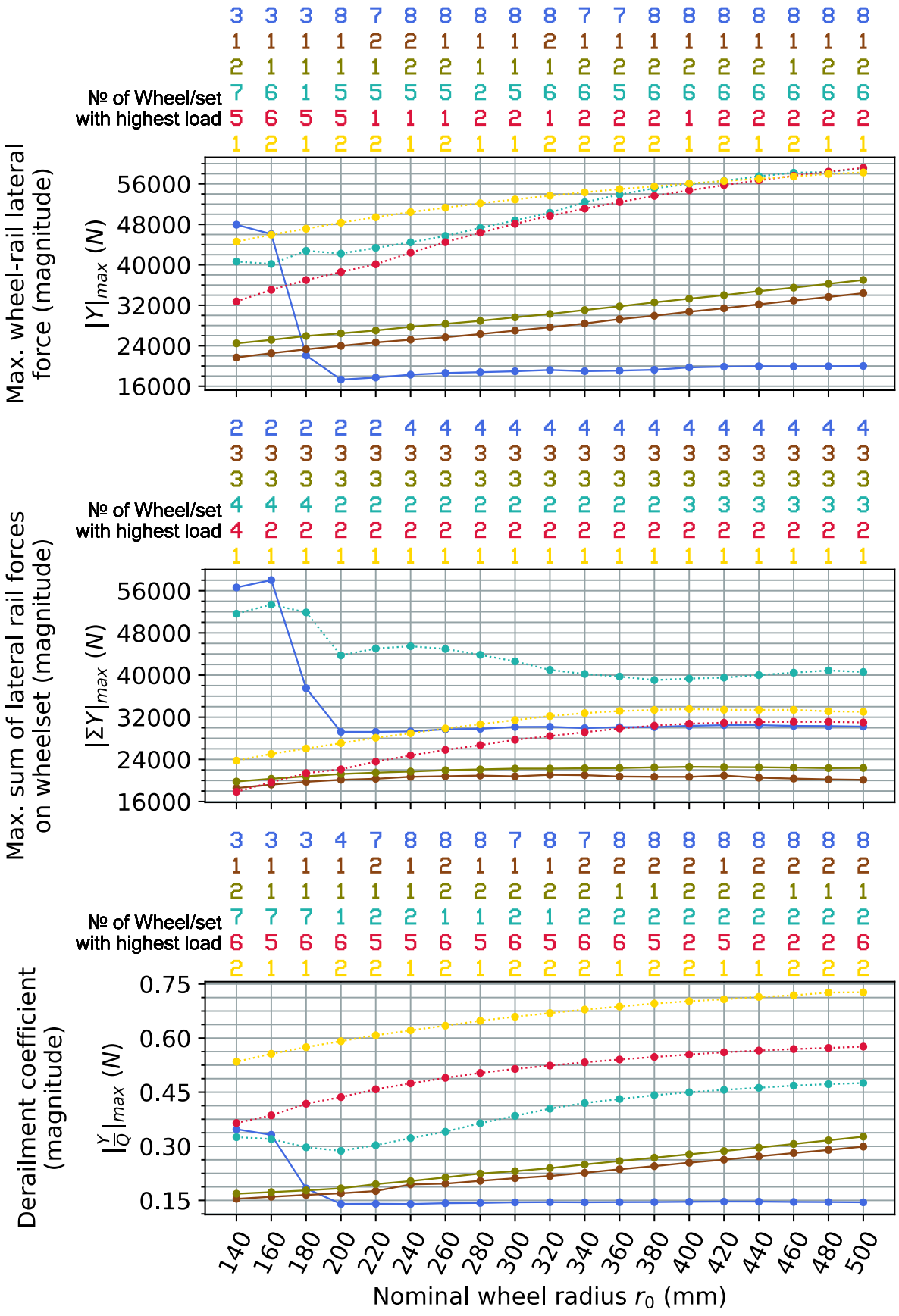

Figure C.16 Laden vehicle on a track with 1432 mm gauge and no rail cant

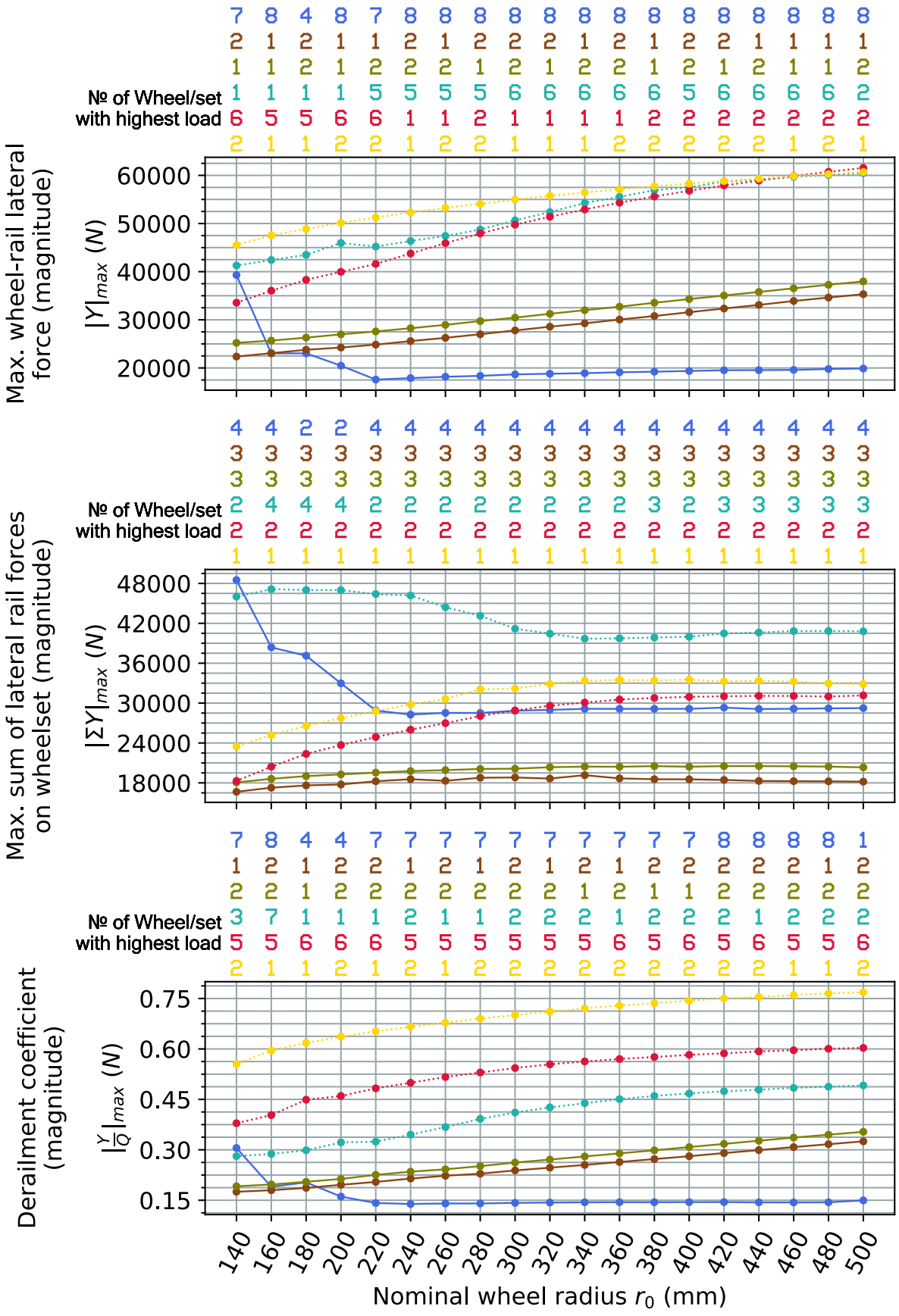

Figure C.17 Laden vehicle on a track with 1430 mm gauge and no rail cant

Appendix D Curve negotiation simulation results after scaling the S1002 wheel profile's radial coordinates by 70%

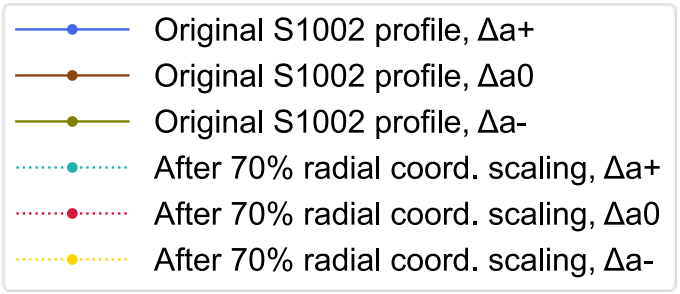

Figure D.1 Legend of all plots in this appendix

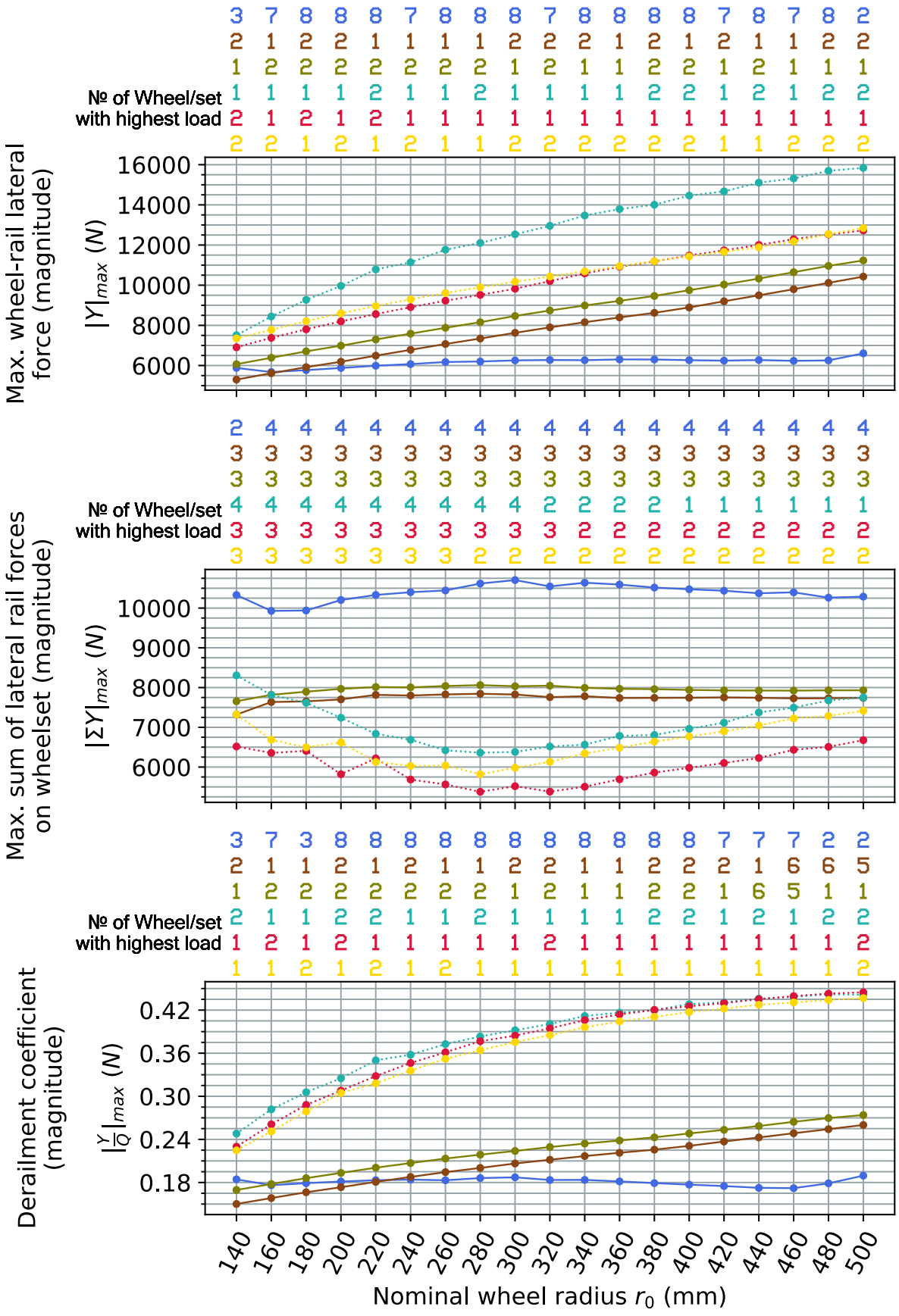

Figure D.2 Tare vehicle on a track with 1437 mm gauge and 1:40 rail cant, CAT2 curve

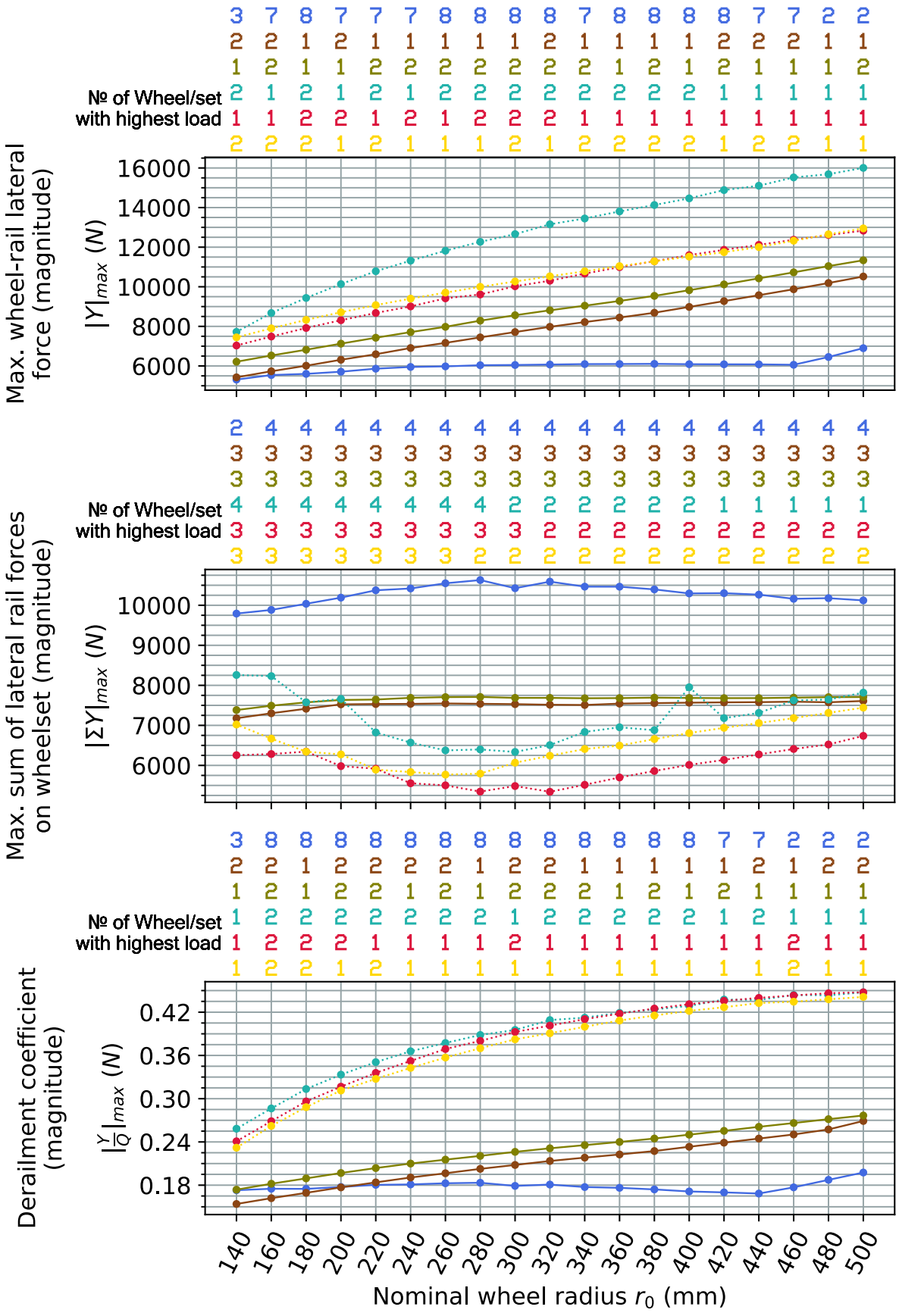

Figure D.3 Tare vehicle on a track with 1435 mm gauge and 1:40 rail cant (reference track setting), CAT2 curve

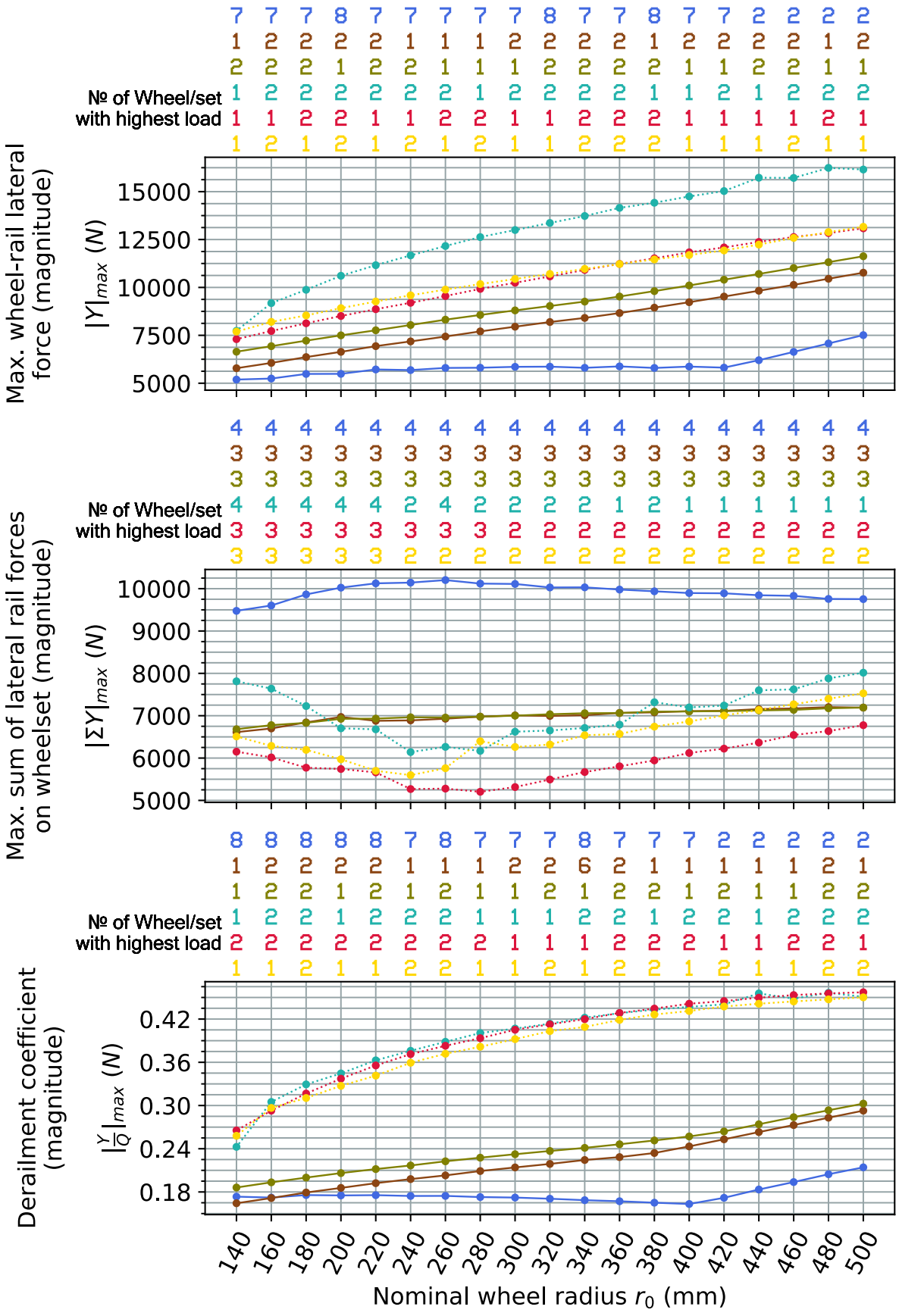

Figure D.4 Tare vehicle on a track with 1432 mm gauge and 1:40 rail cant, CAT2 curve

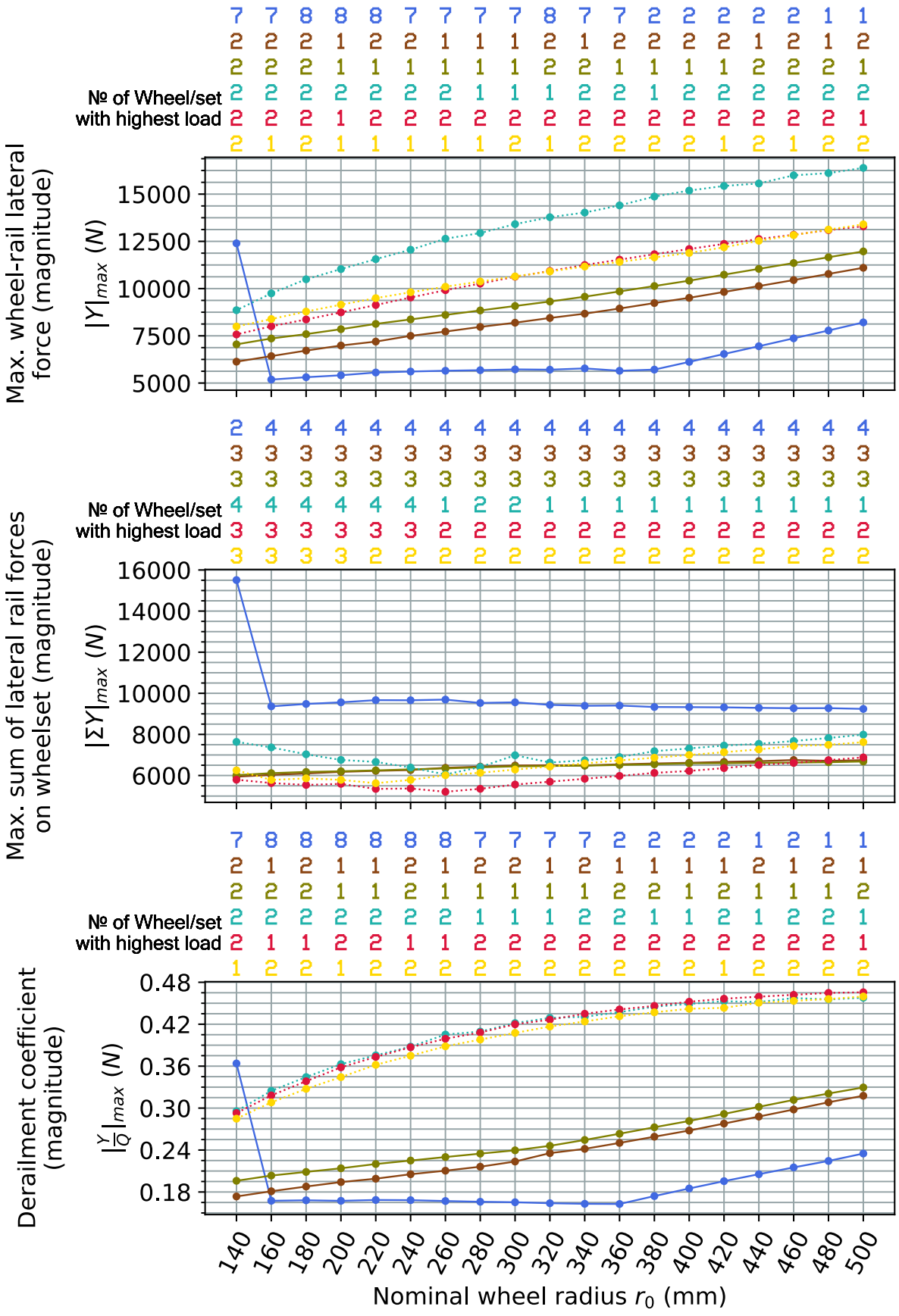

Figure D.5 Tare vehicle on a track with 1430 mm gauge and 1:40 rail cant, CAT2 curve

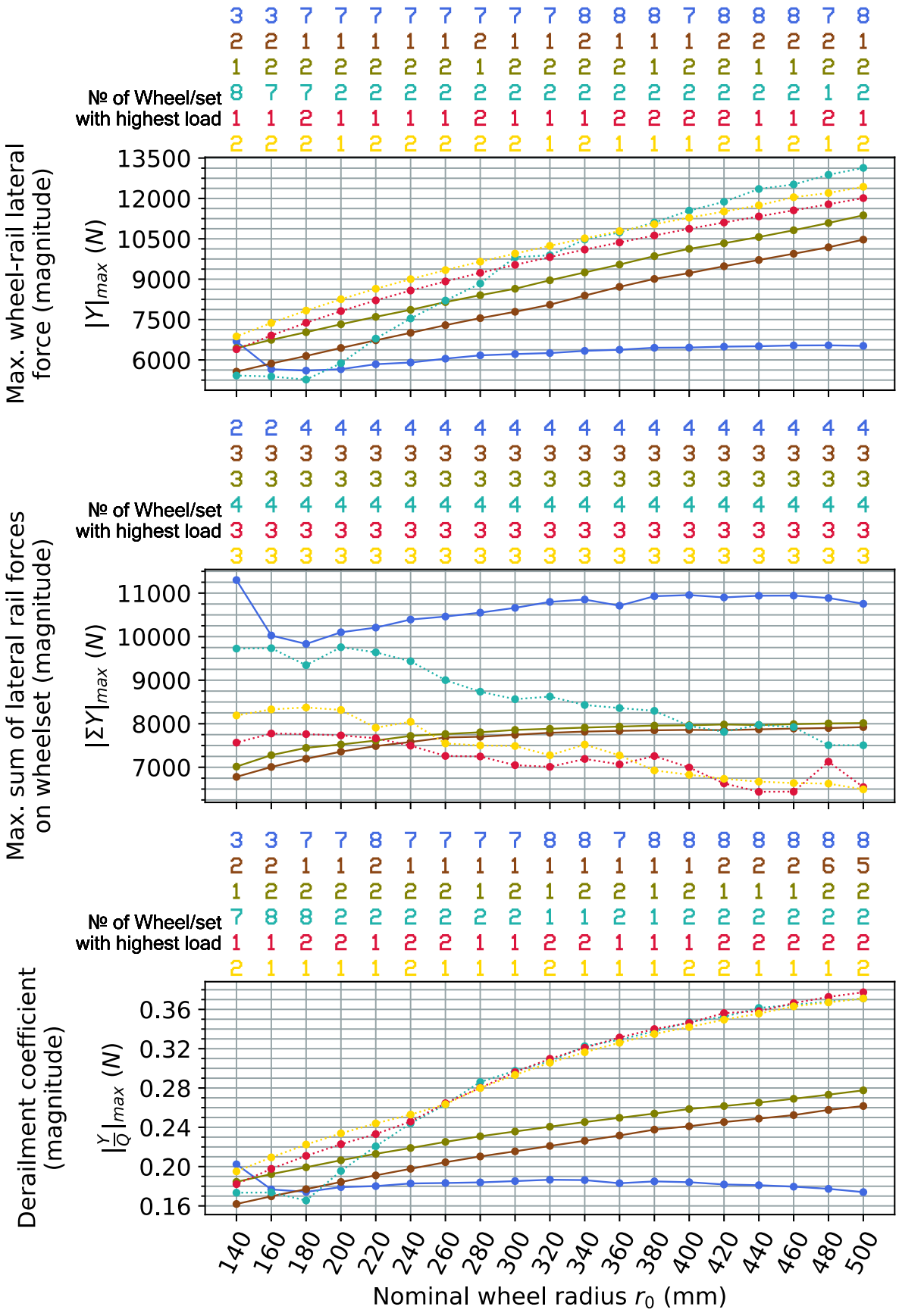

Figure D.6 Tare vehicle on a track with 1437 mm gauge and no rail cant, CAT2 curve

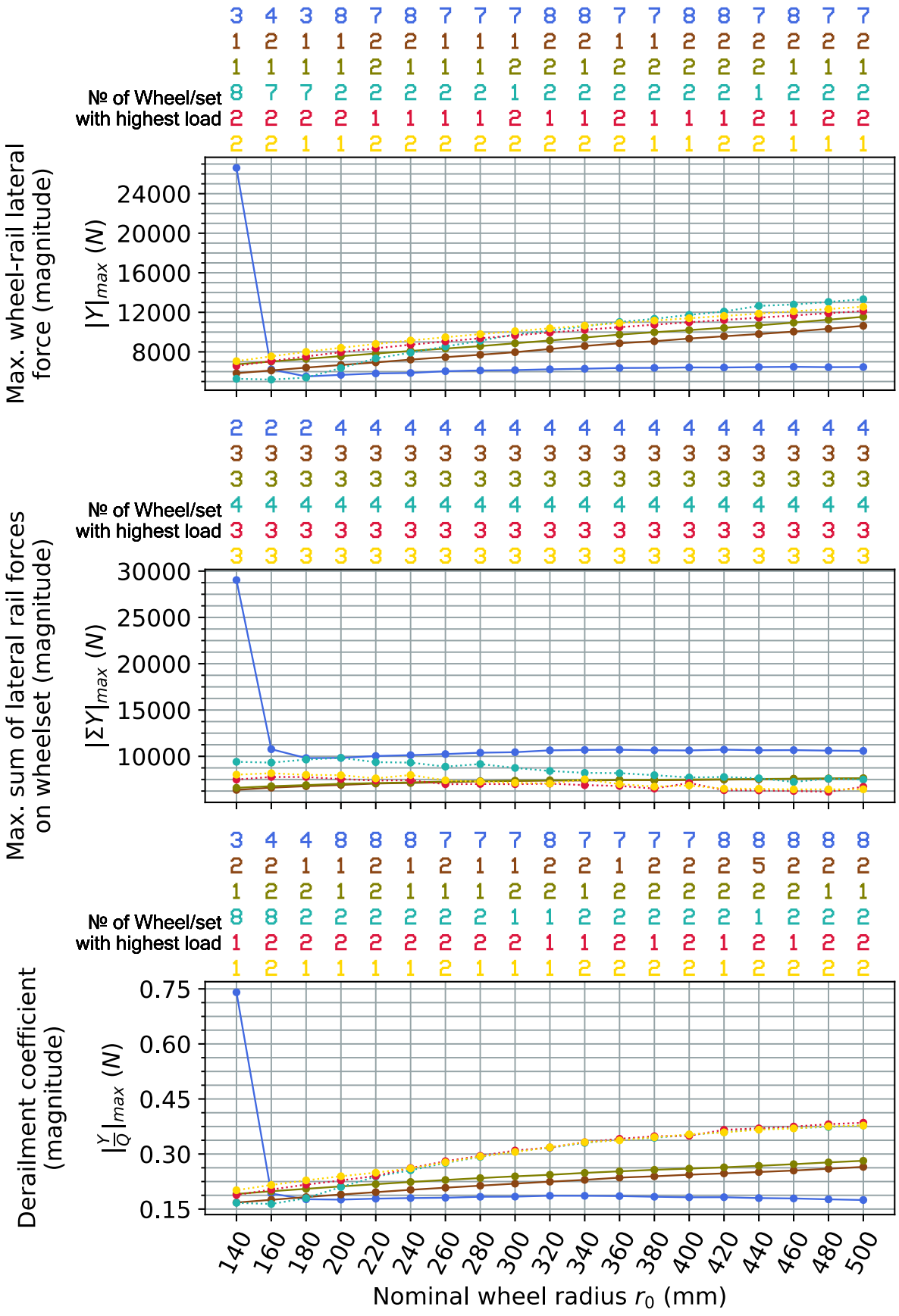

Figure D.7 Tare vehicle on a track with 1435 mm gauge and no rail cant, CAT2 curve

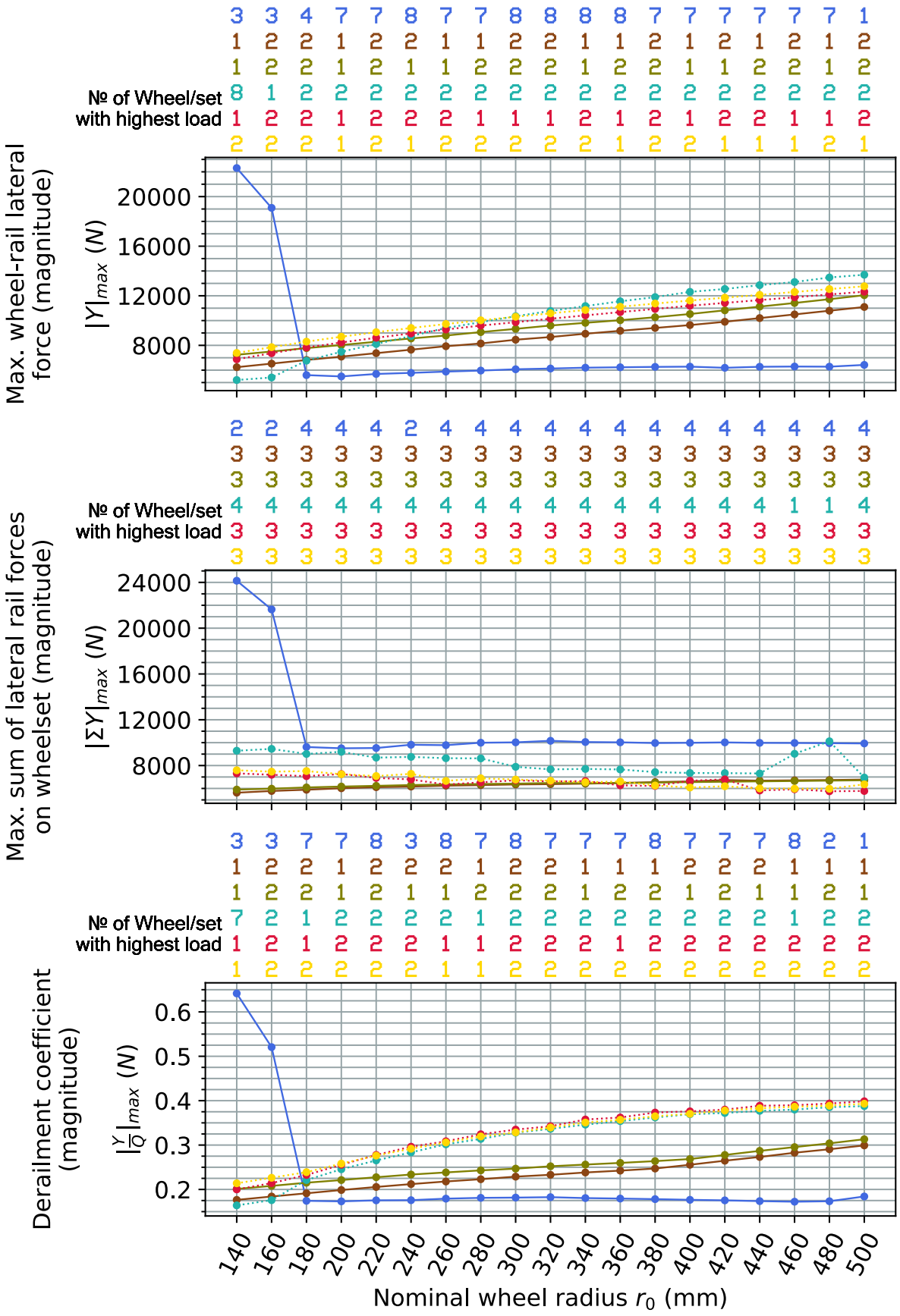

Figure D.8 Tare vehicle on a track with 1432 mm gauge and no rail cant, CAT2 curve

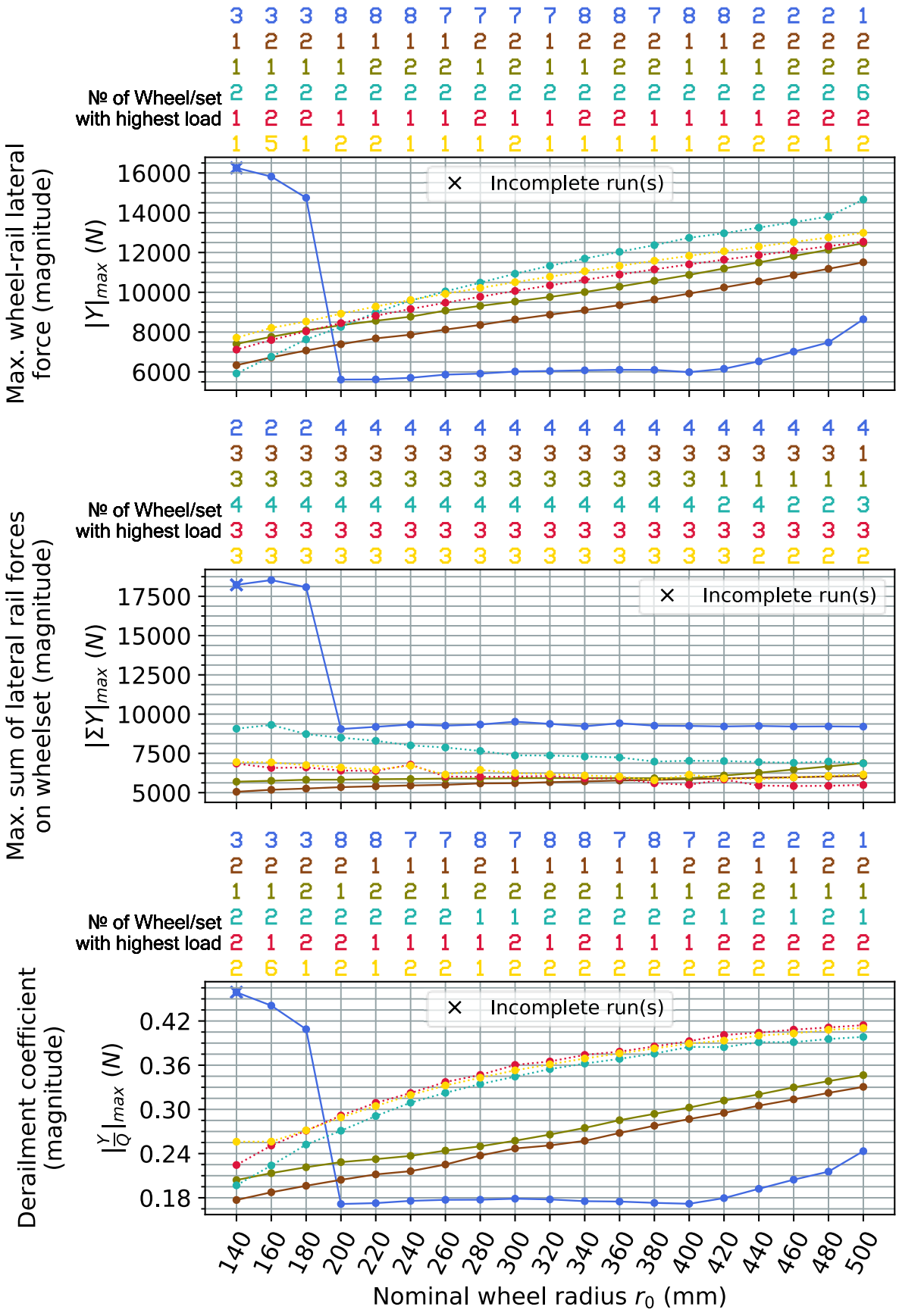

Figure D.9 Tare vehicle on a track with 1430 mm gauge and no rail cant, CAT2 curve

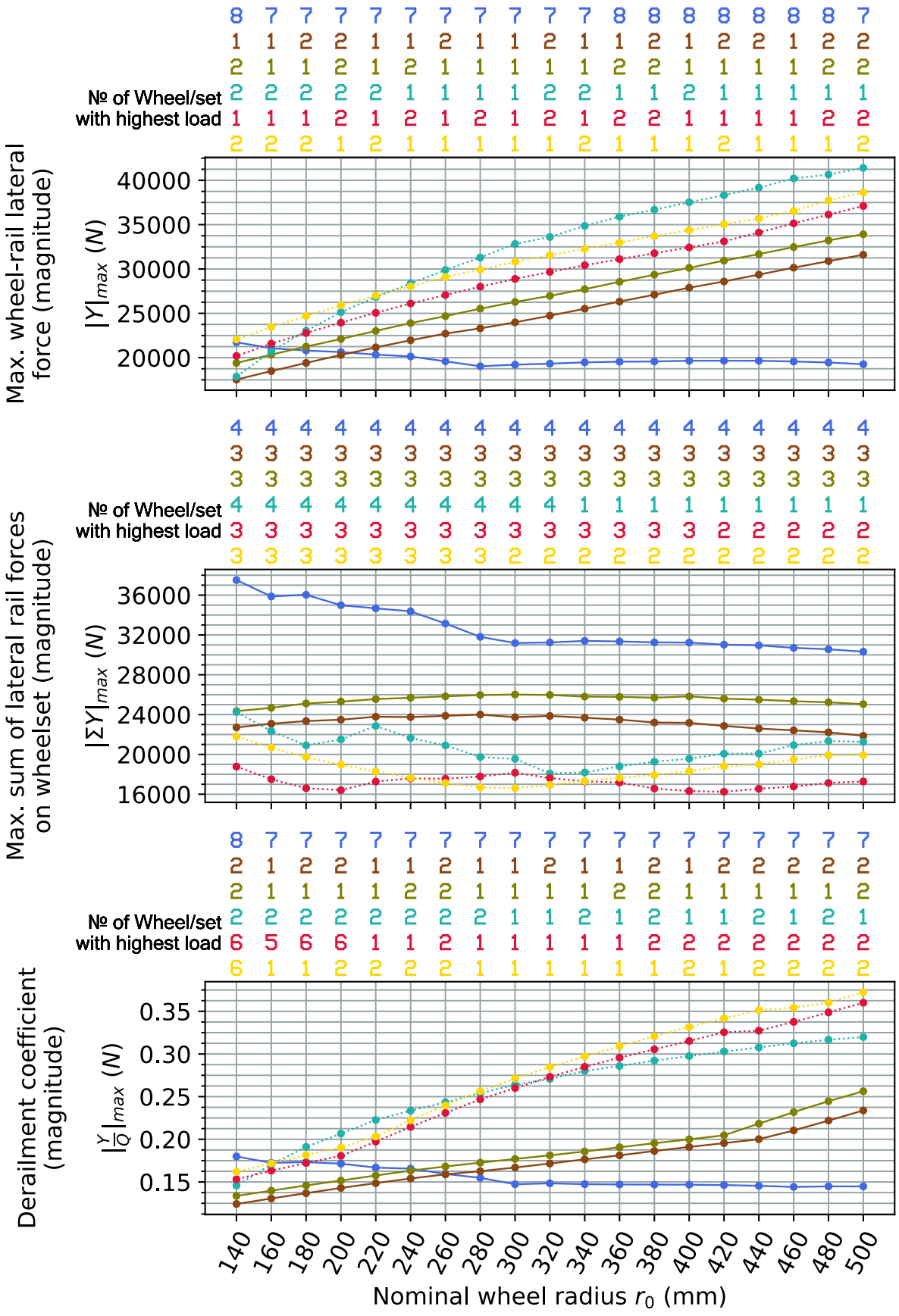

Figure D.10 Laden vehicle on a track with 1437 mm gauge and 1:40 rail, CAT2 curve

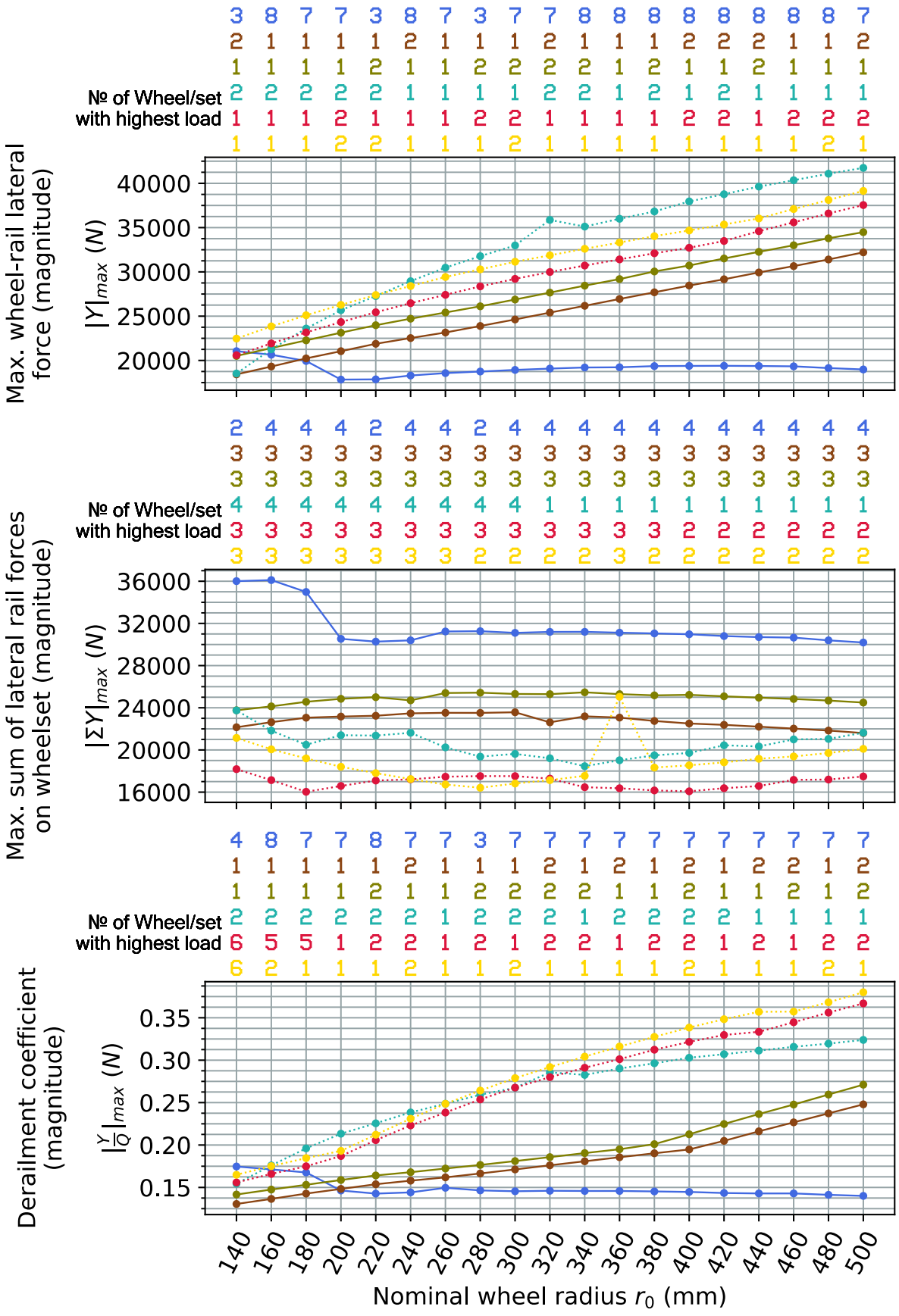

Figure D.11 Laden vehicle on a track with 1435 mm gauge and 1:40 rail cant (reference track setting), CAT2 curve

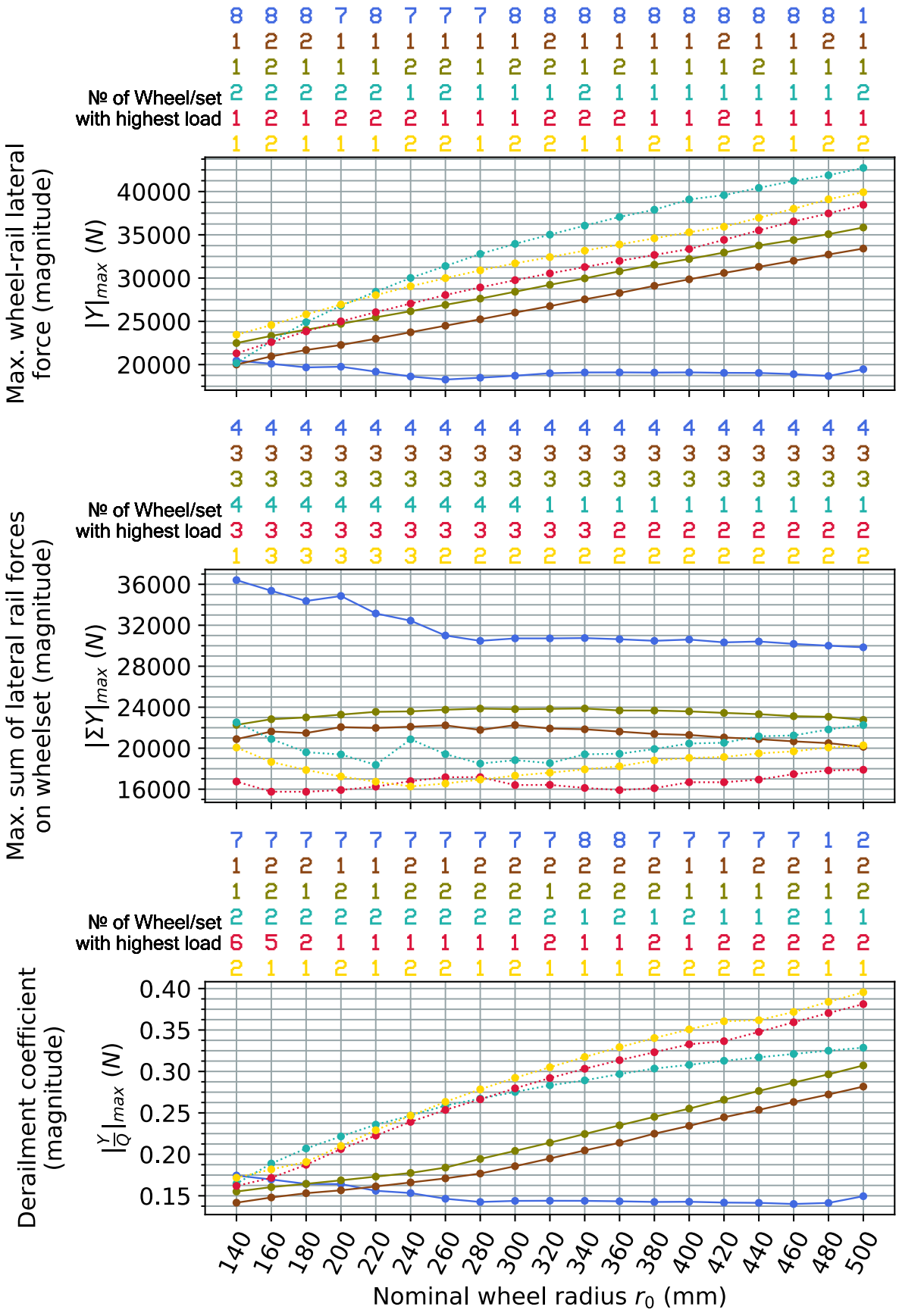

Figure D.12 Laden vehicle on a track with 1432 mm gauge and 1:40 rail cant, CAT2 curve

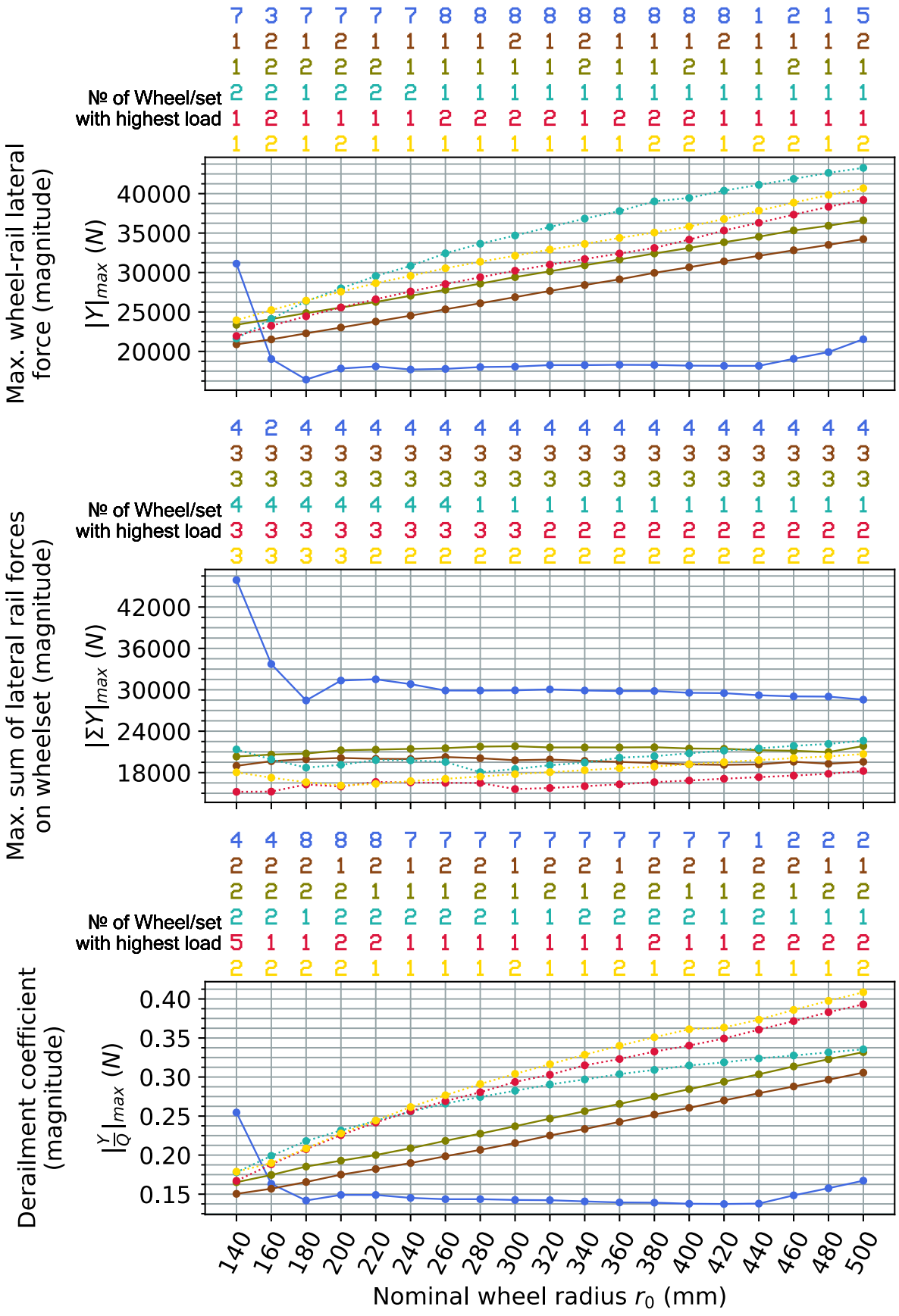

Figure D.13 Laden vehicle on a track with 1430 mm gauge and 1:40 rail cant, CAT2 curve

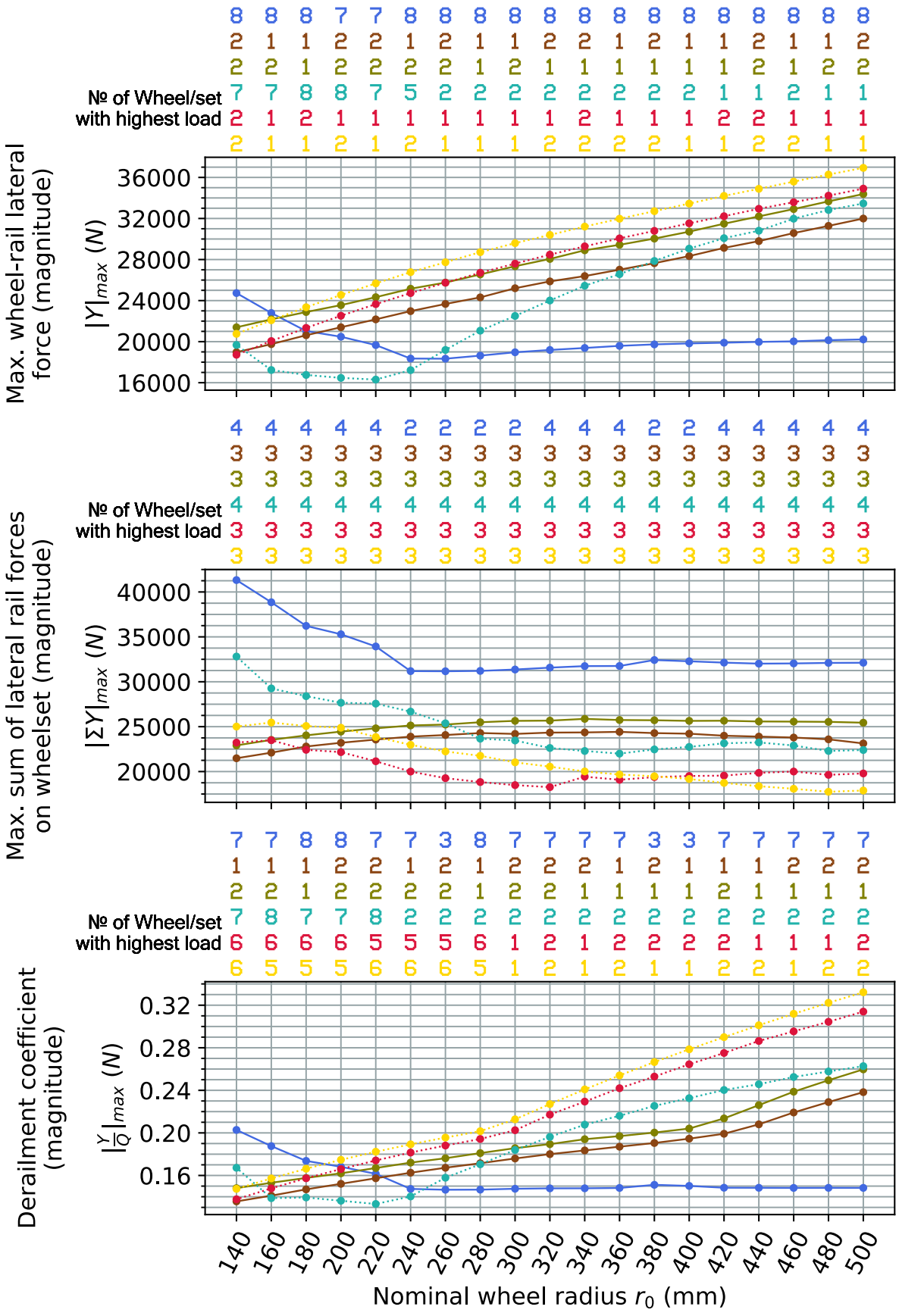

Figure D.14 Laden vehicle on a track with 1437 mm gauge and no rail cant, CAT2 curve

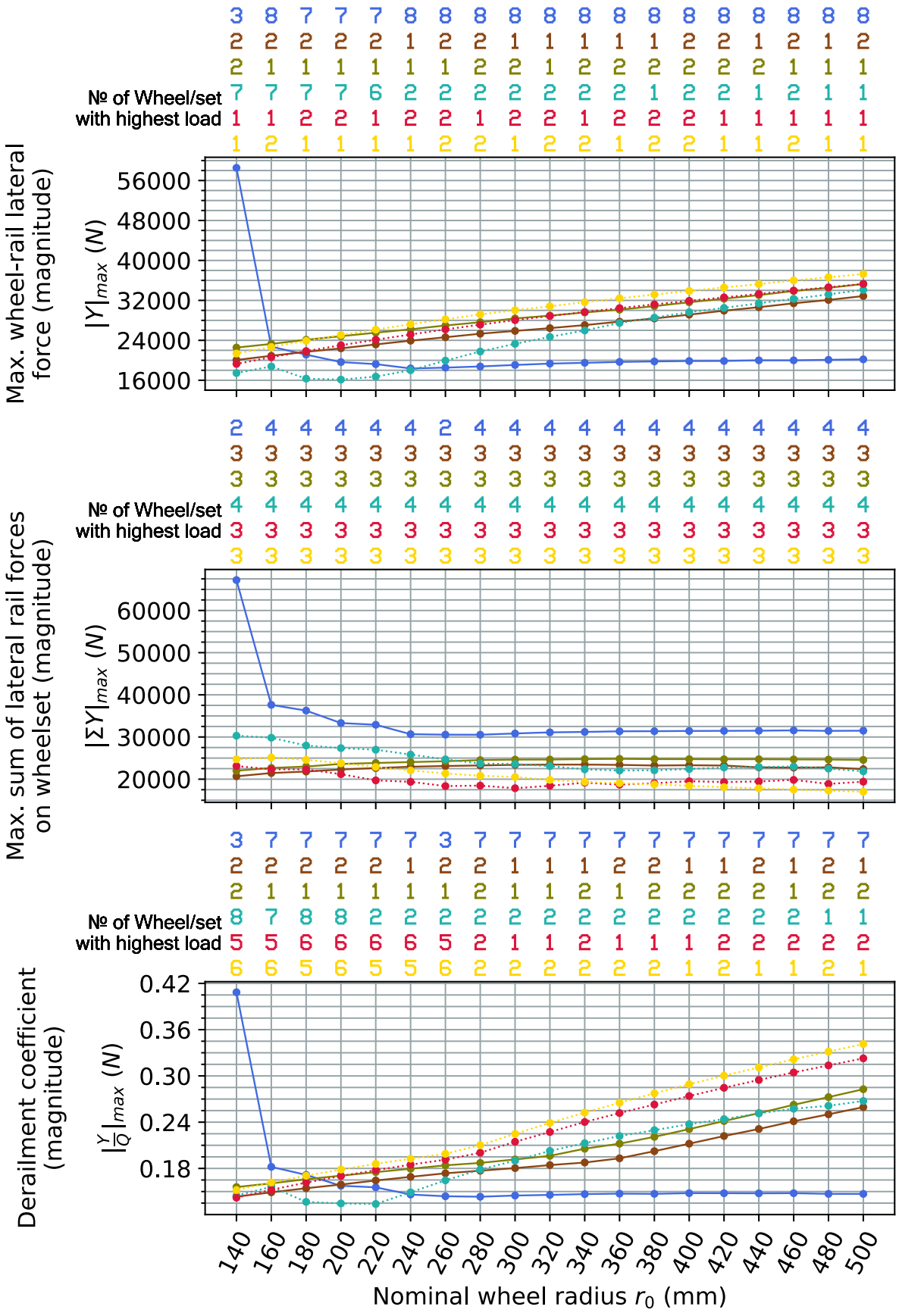

Figure D.15 Laden vehicle on a track with 1435 mm gauge and no rail cant, CAT2 curve

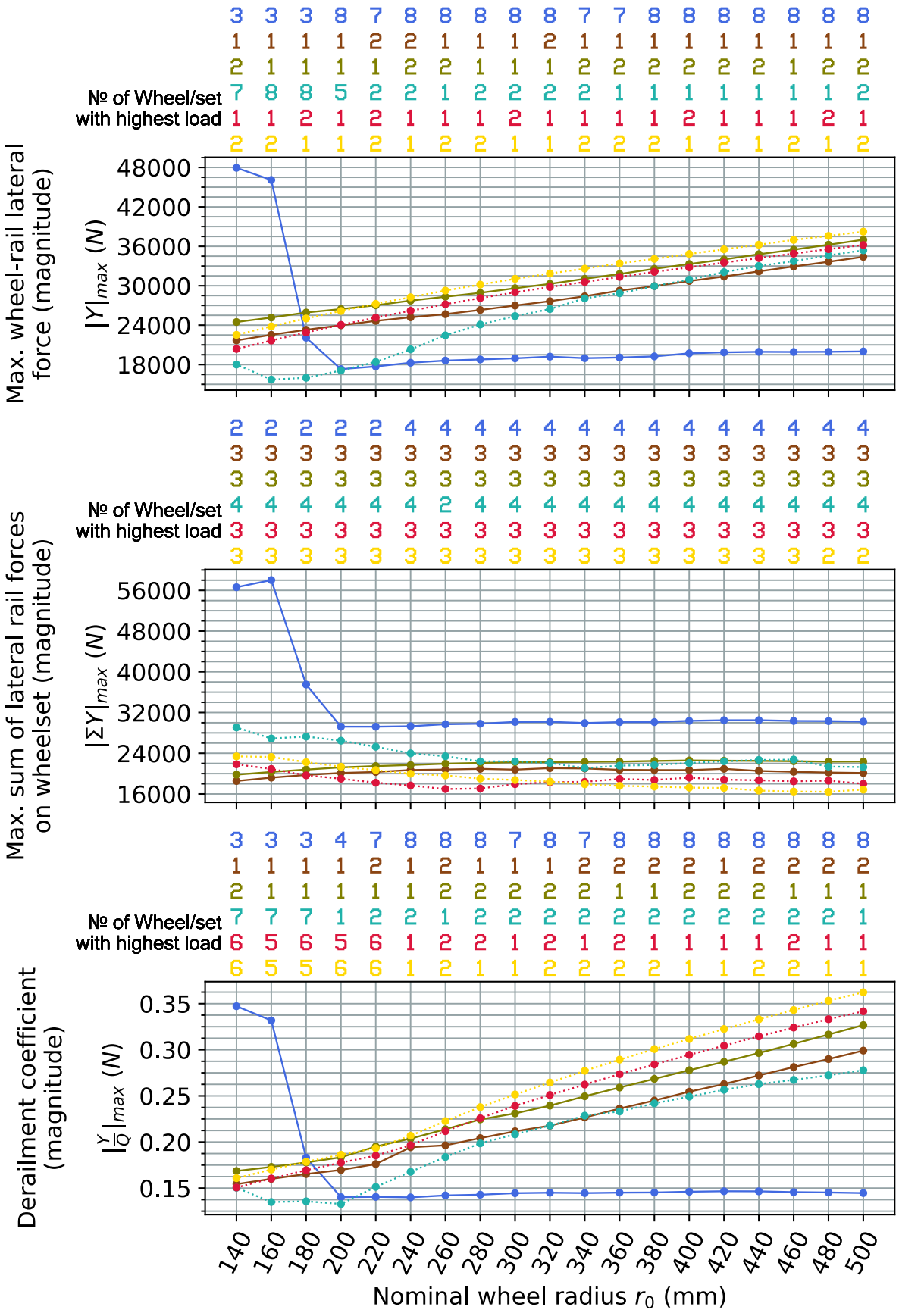

Figure D.16 Laden vehicle on a track with 1432 mm gauge and no rail cant, CAT2 curve

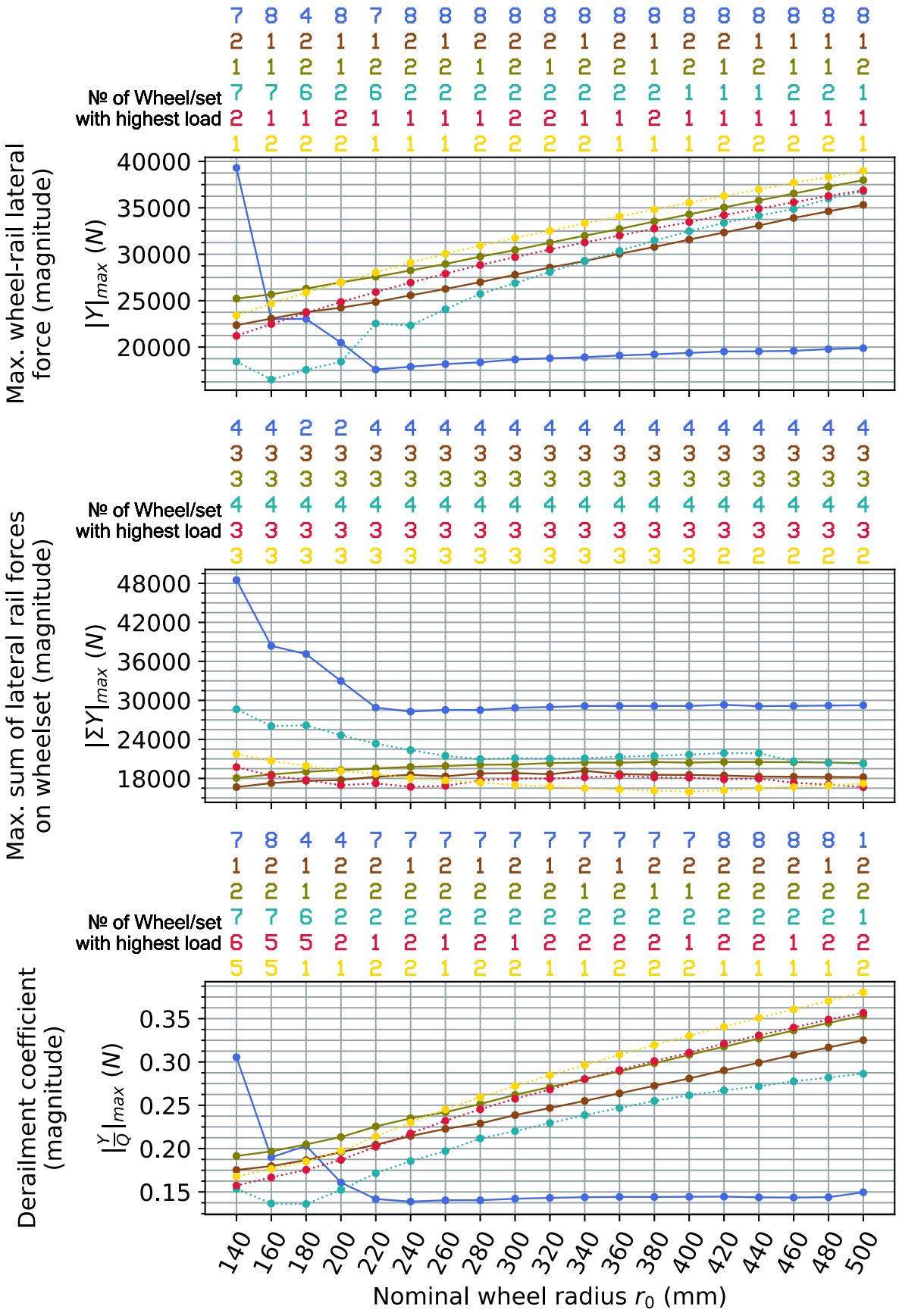

Figure D.17 Laden vehicle on a track with 1430 mm gauge and no rail cant, CAT2 curve

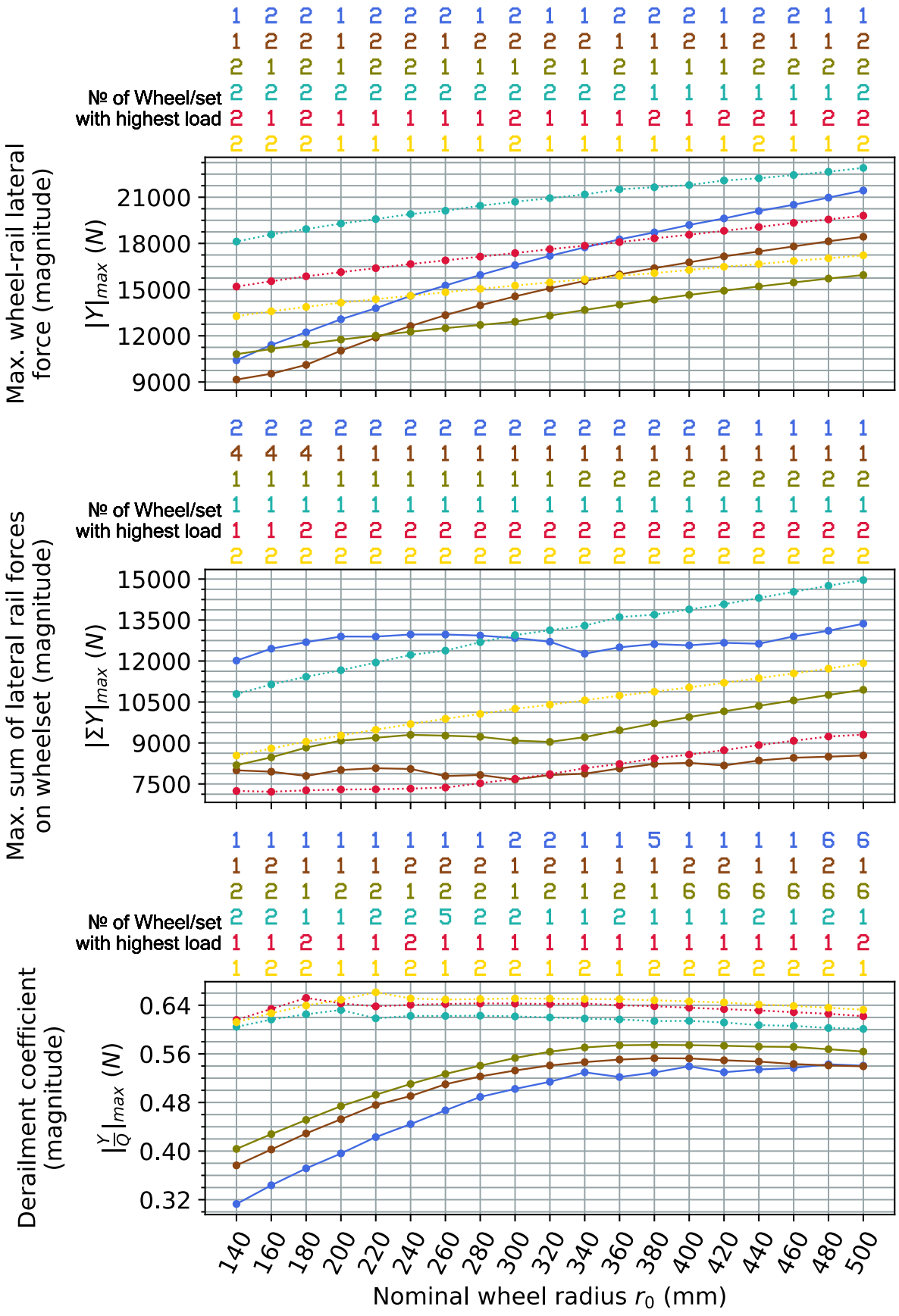

Figure D.18 Tare vehicle on a track with 1437 mm gauge and 1:40 rail cant, CAT4 curve

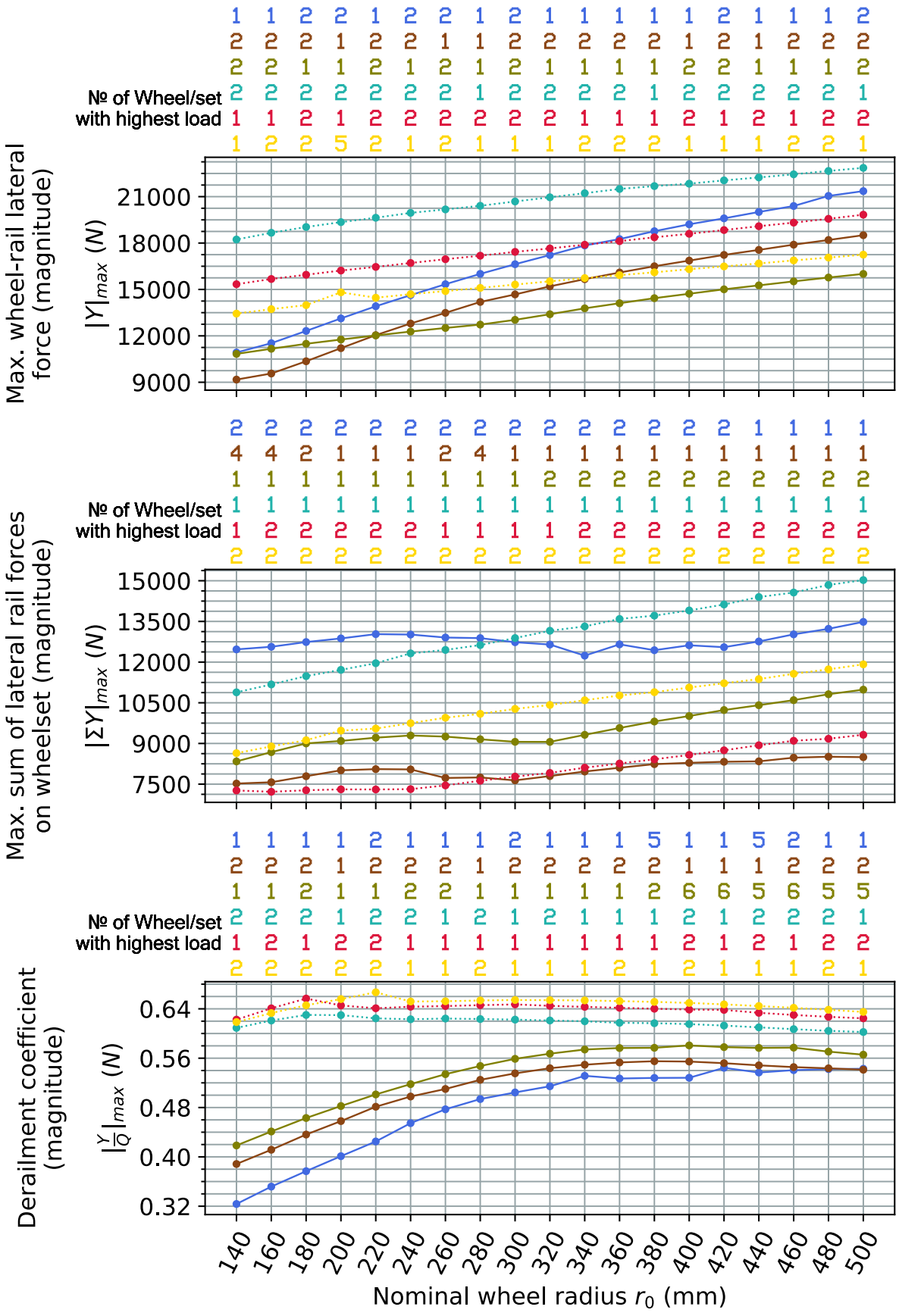

Figure D.19 Tare vehicle on a track with 1435 mm gauge and 1:40 rail cant (reference track setting), CAT4 curve

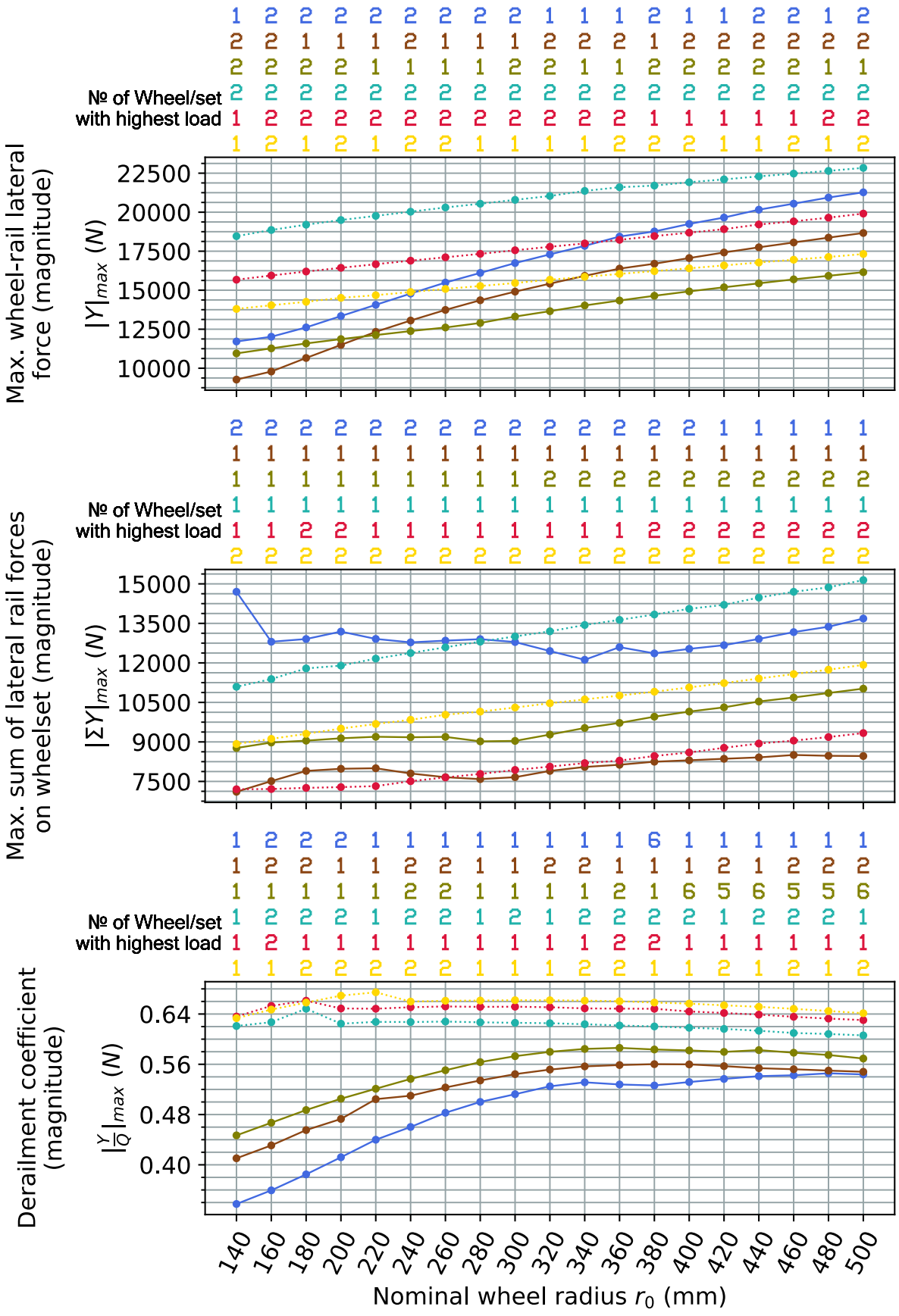

Figure D.20 Tare vehicle on a track with 1432 mm gauge and 1:40 rail cant, CAT4 curve

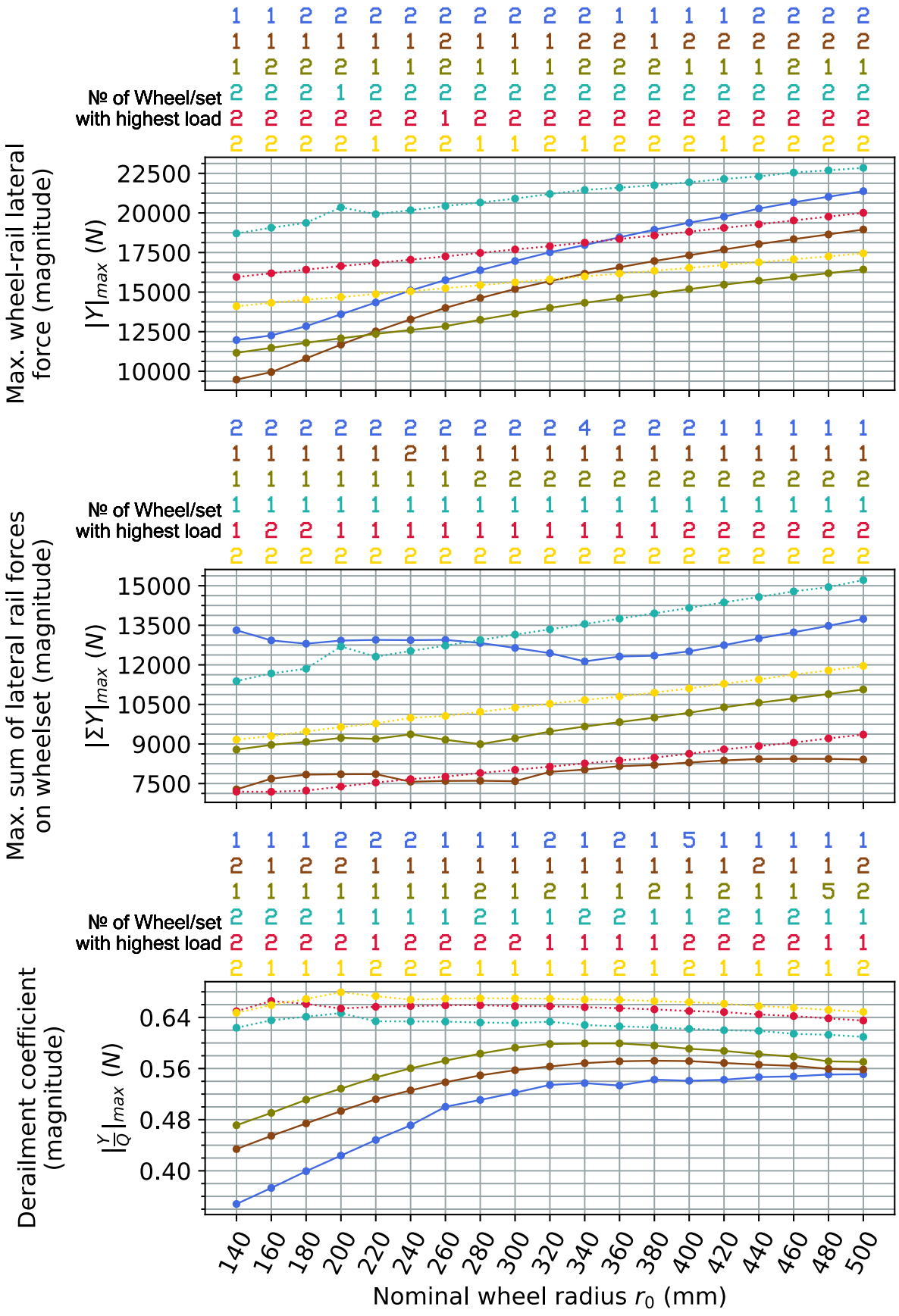

Figure D.21 Tare vehicle on a track with 1430 mm gauge and 1:40 rail cant, CAT4 curve

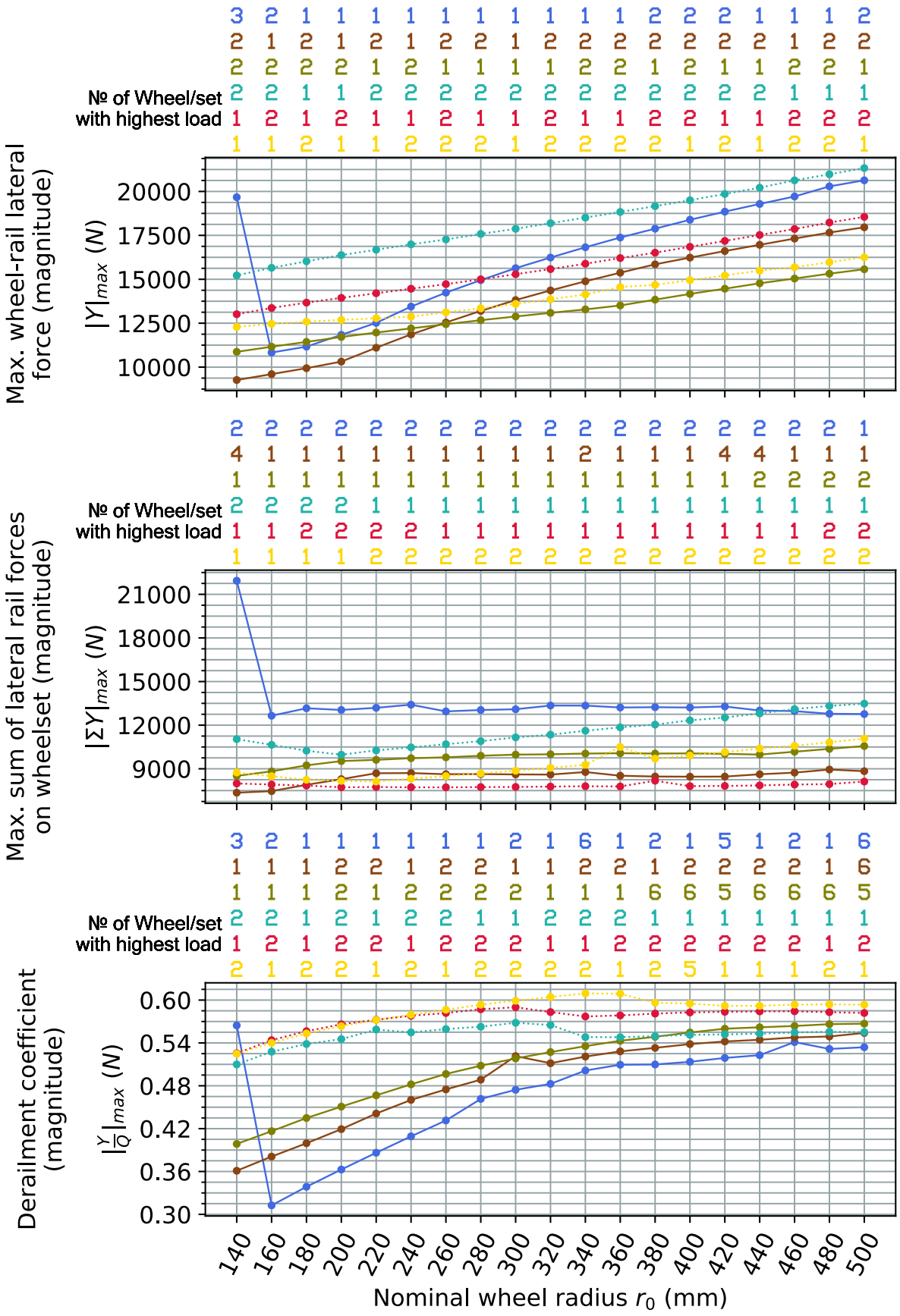

Figure D.22 Tare vehicle on a track with 1437 mm gauge and no rail cant, CAT4 curve

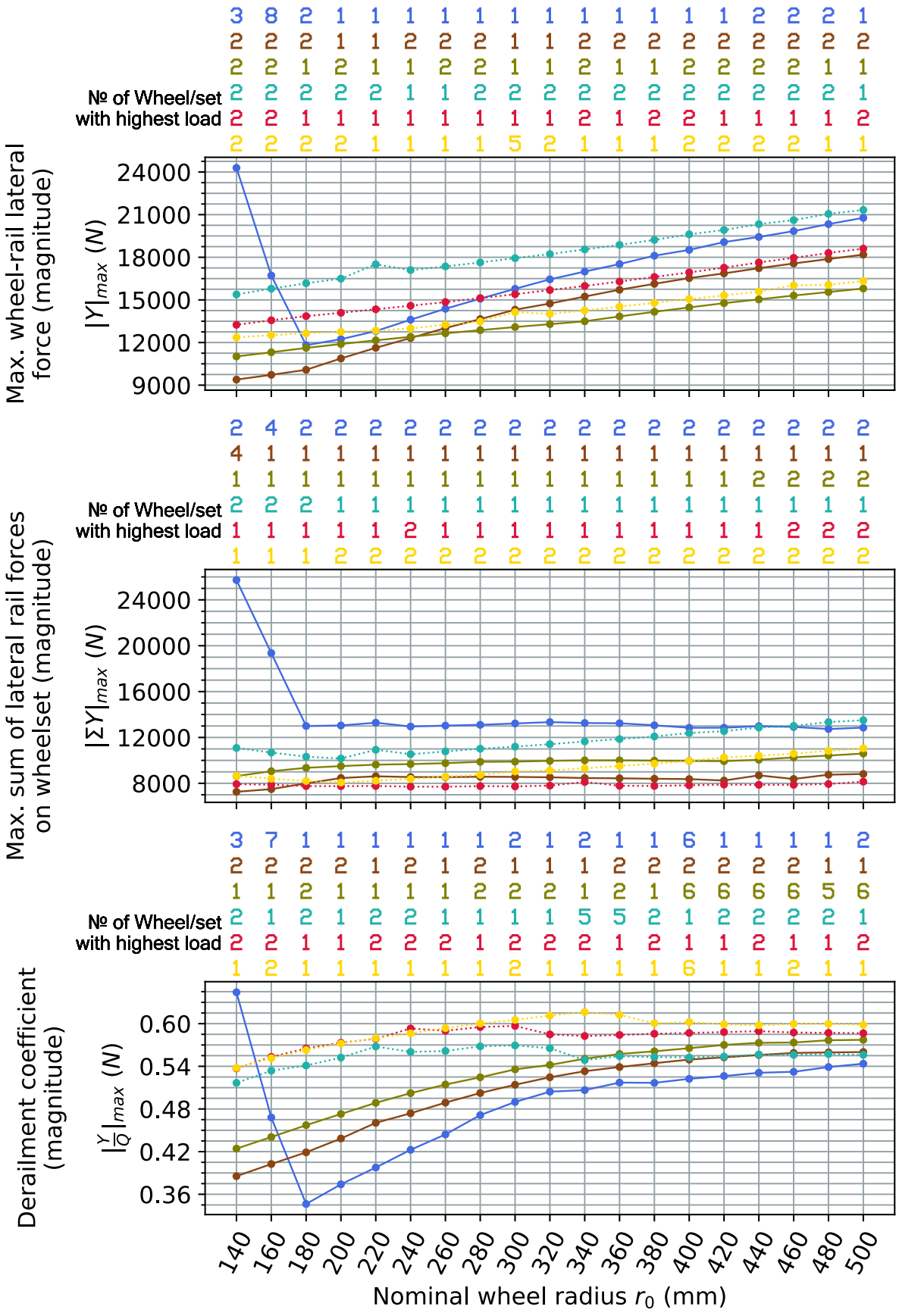

Figure D.23 Tare vehicle on a track with 1435 mm gauge and no rail cant, CAT4 curve

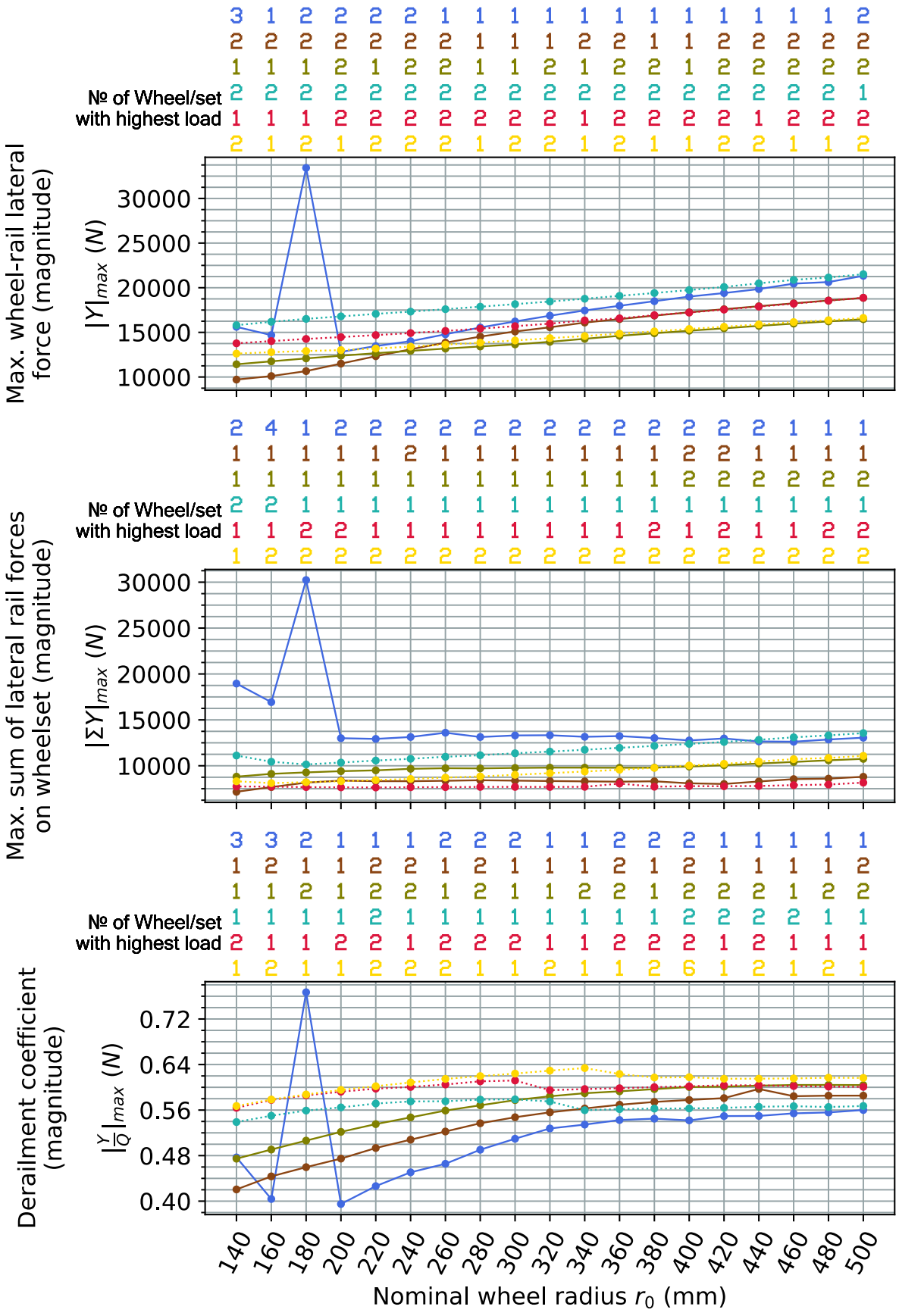

Figure D.24 Tare vehicle on a track with 1432 mm gauge and no rail cant, CAT4 curve

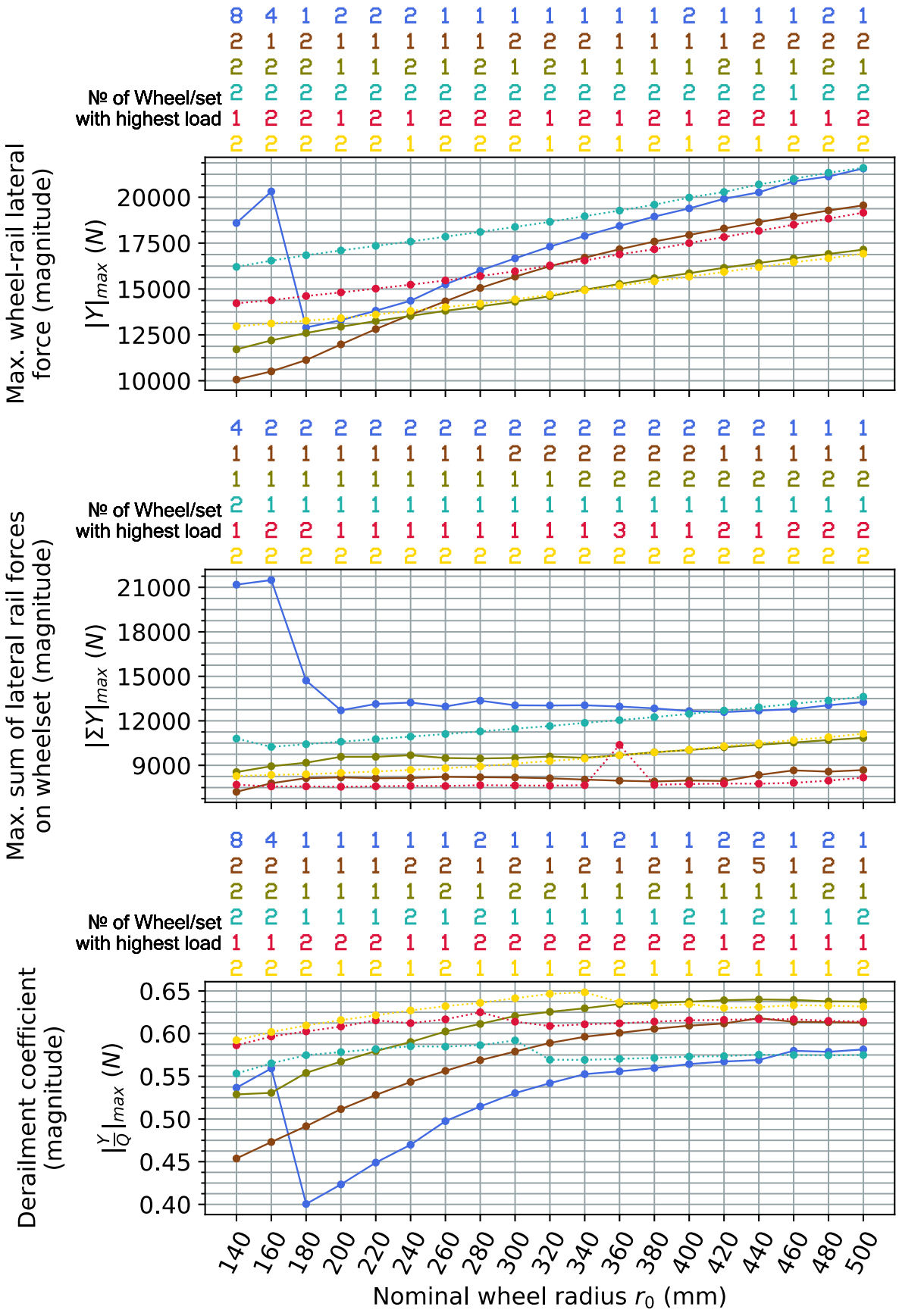

Figure D.25 Tare vehicle on a track with 1430 mm gauge and no rail cant, CAT4 curve

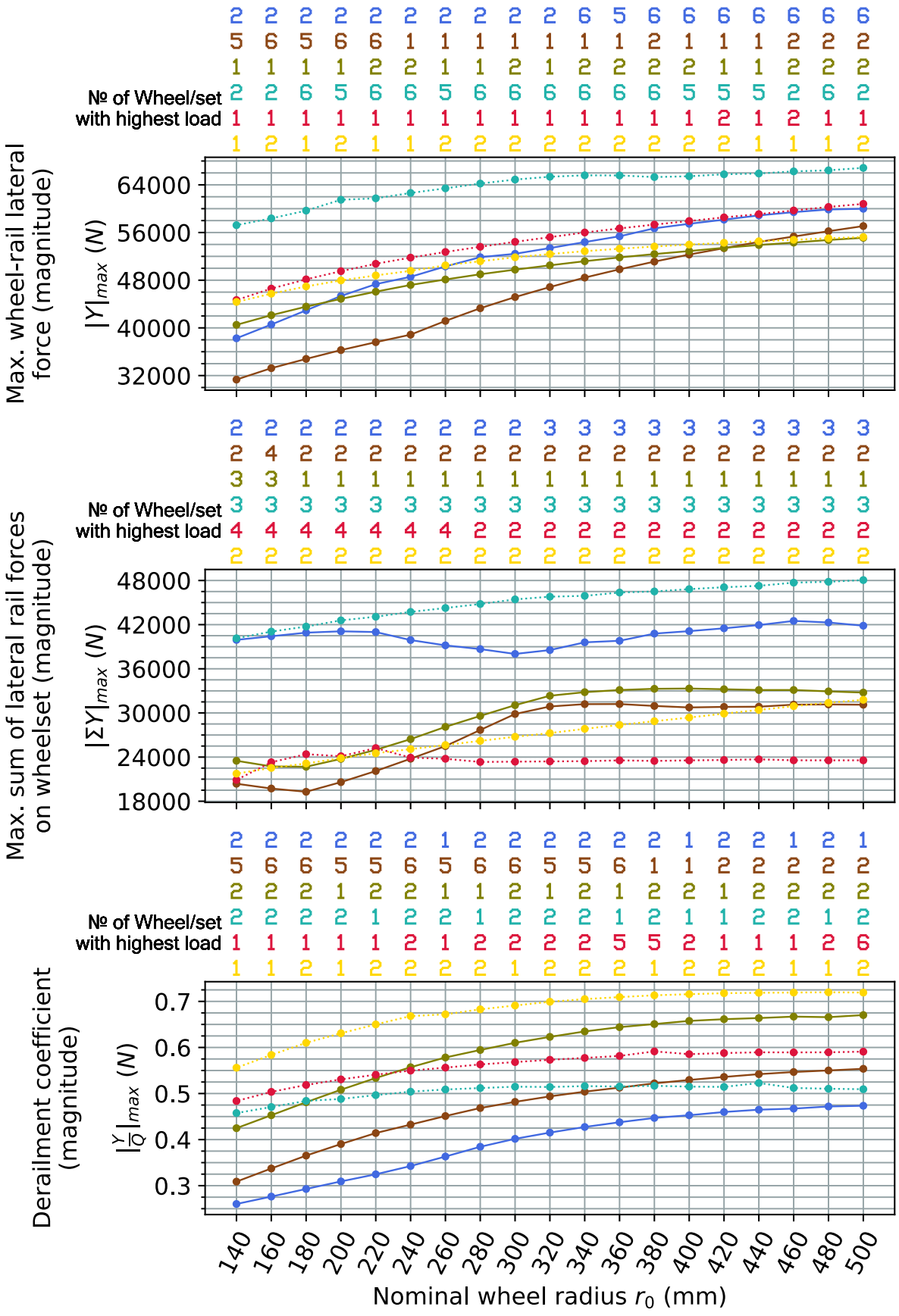

Figure D.26 Laden vehicle on a track with 1437 mm gauge and 1:40 rail cant, CAT4 curve

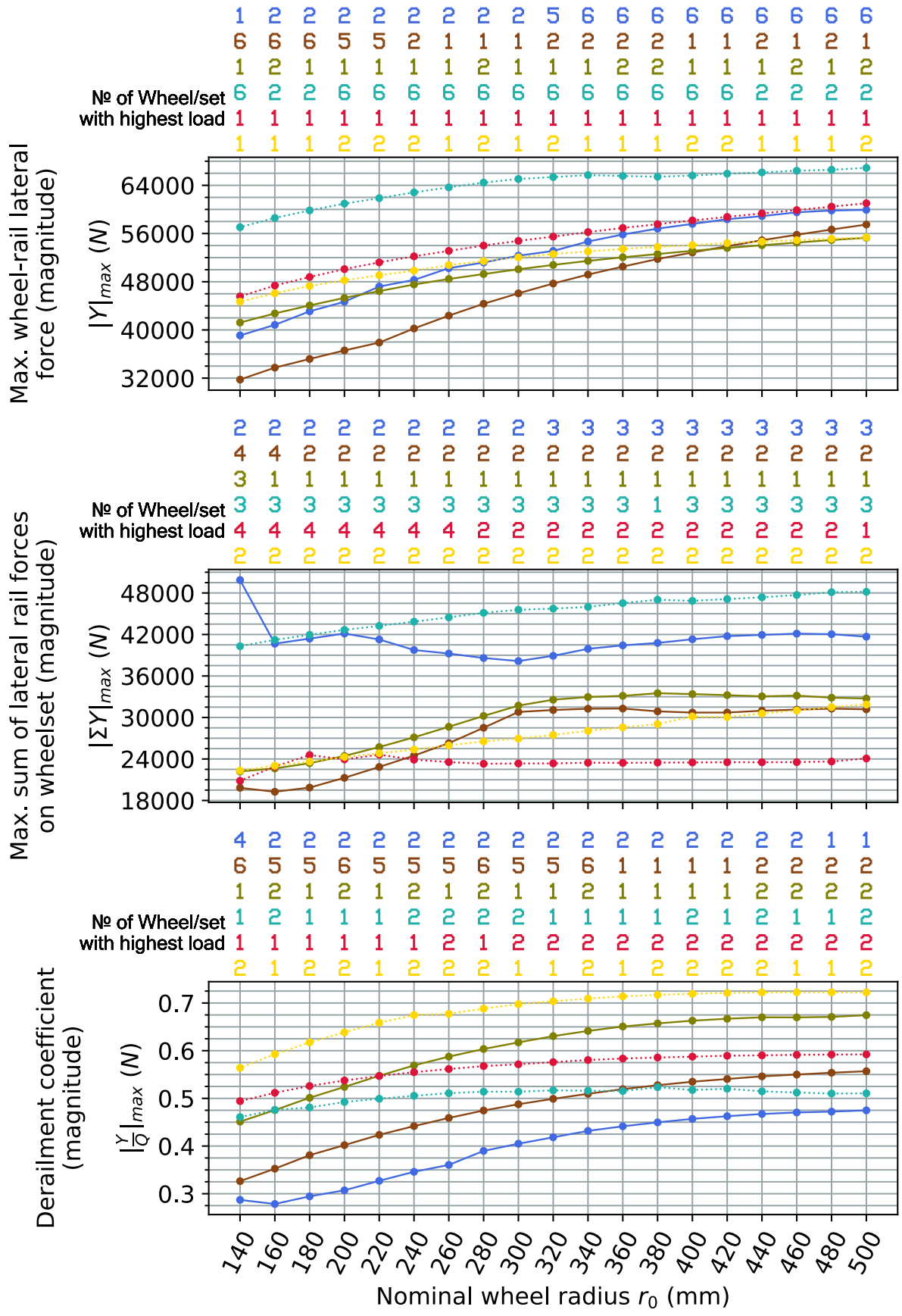

Figure D.27 Laden vehicle on a track with 1435 mm gauge and 1:40 rail cant (reference track setting), CAT4 curve

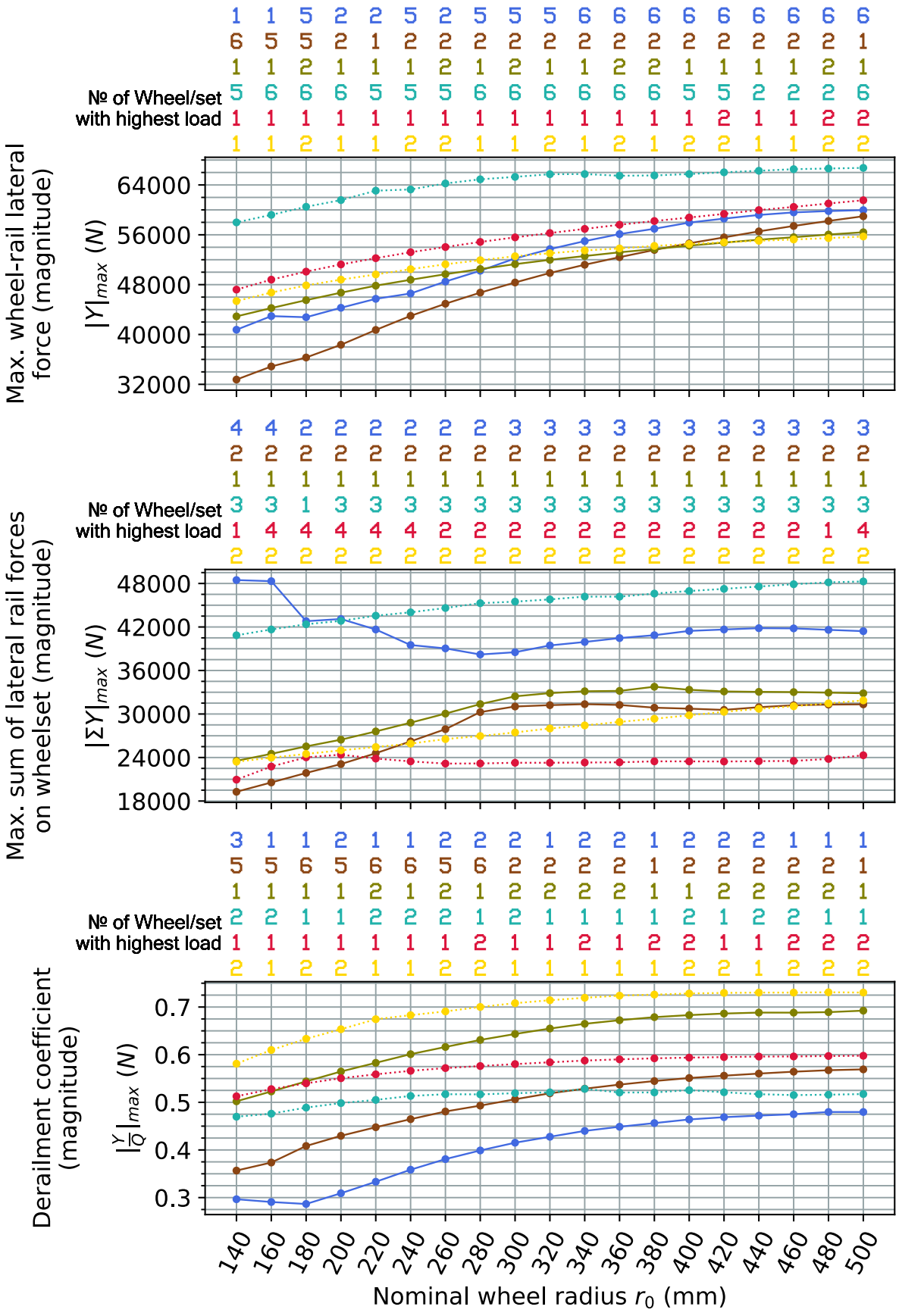

Figure D.28 Laden vehicle on a track with 1432 mm gauge and 1:40 rail cant, CAT4 curve

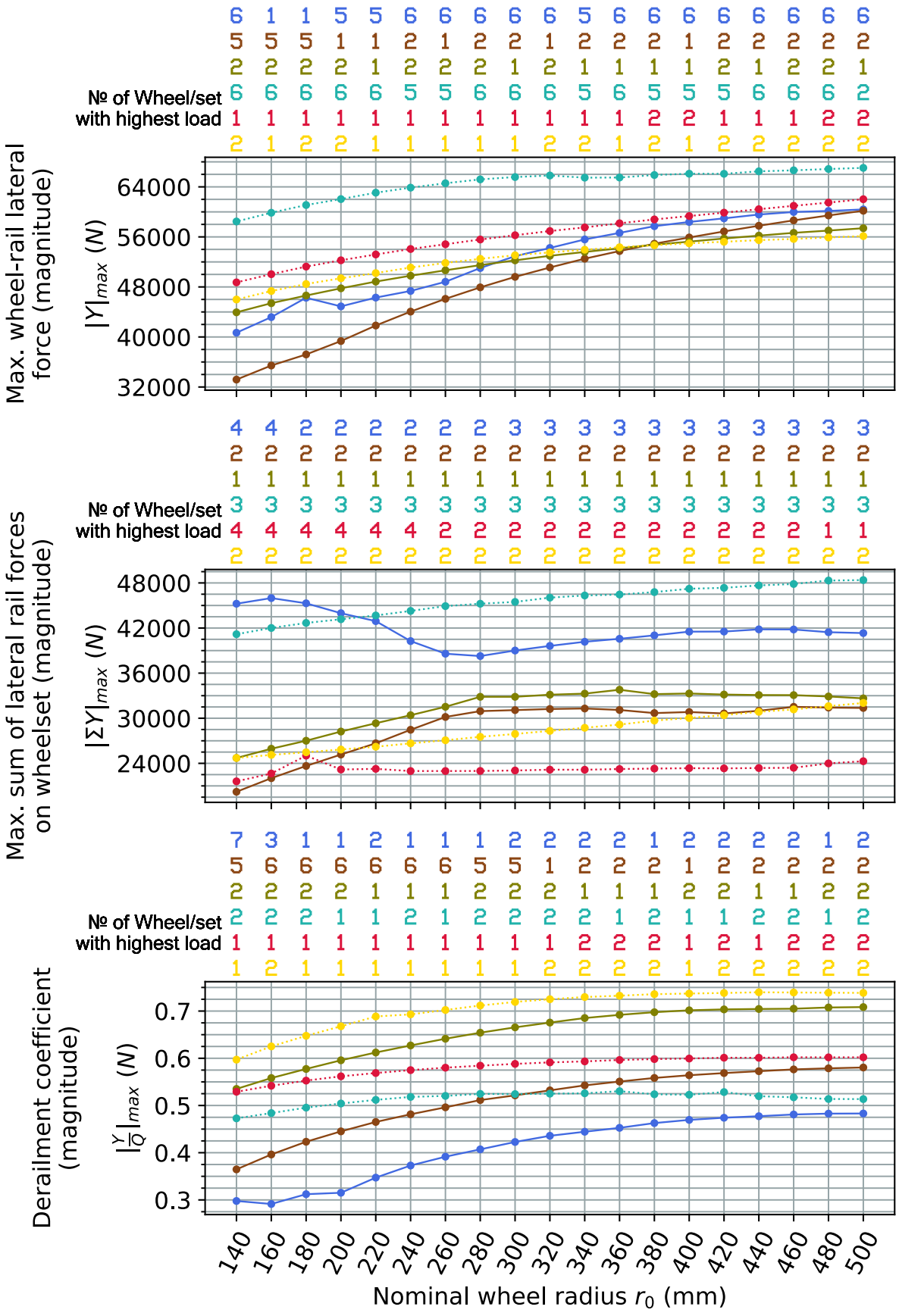

Figure D.29 Laden vehicle on a track with 1430 mm gauge and 1:40 rail cant, CAT4 curve

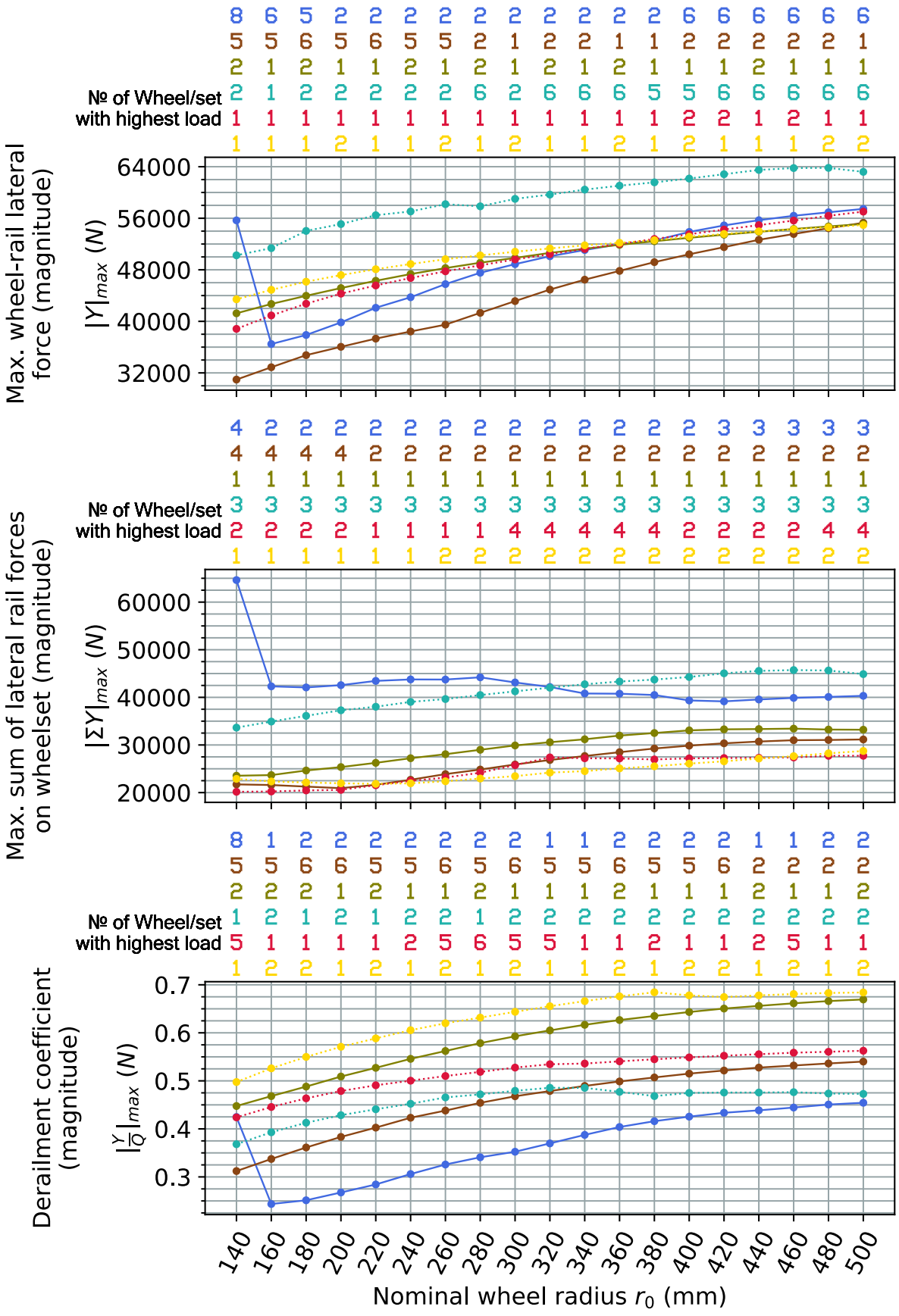

Figure D.30 Laden vehicle on a track with 1437 mm gauge and no rail cant, CAT4 curve

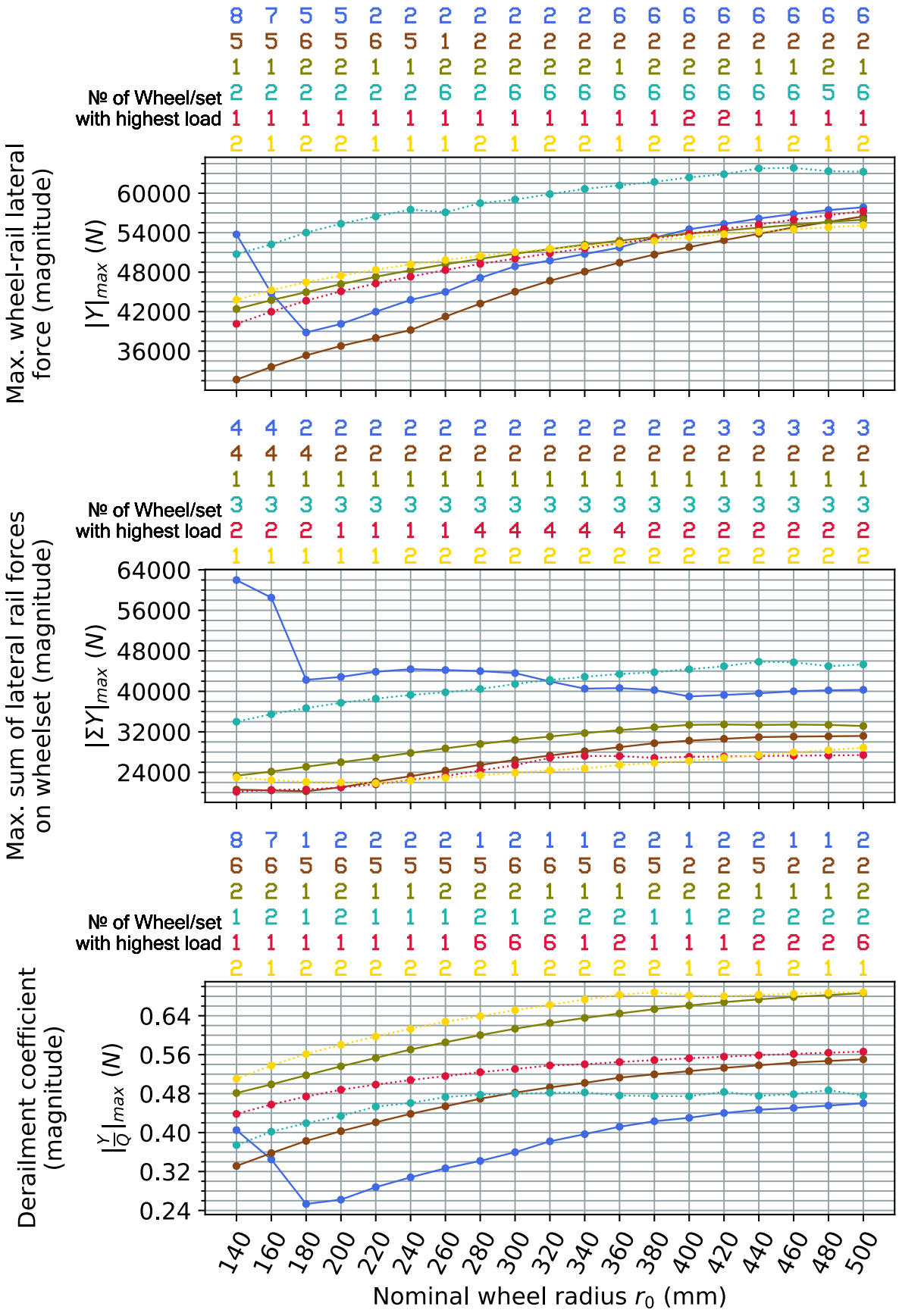

Figure D.31 Laden vehicle on a track with 1435 mm gauge and no rail cant, CAT4 curve

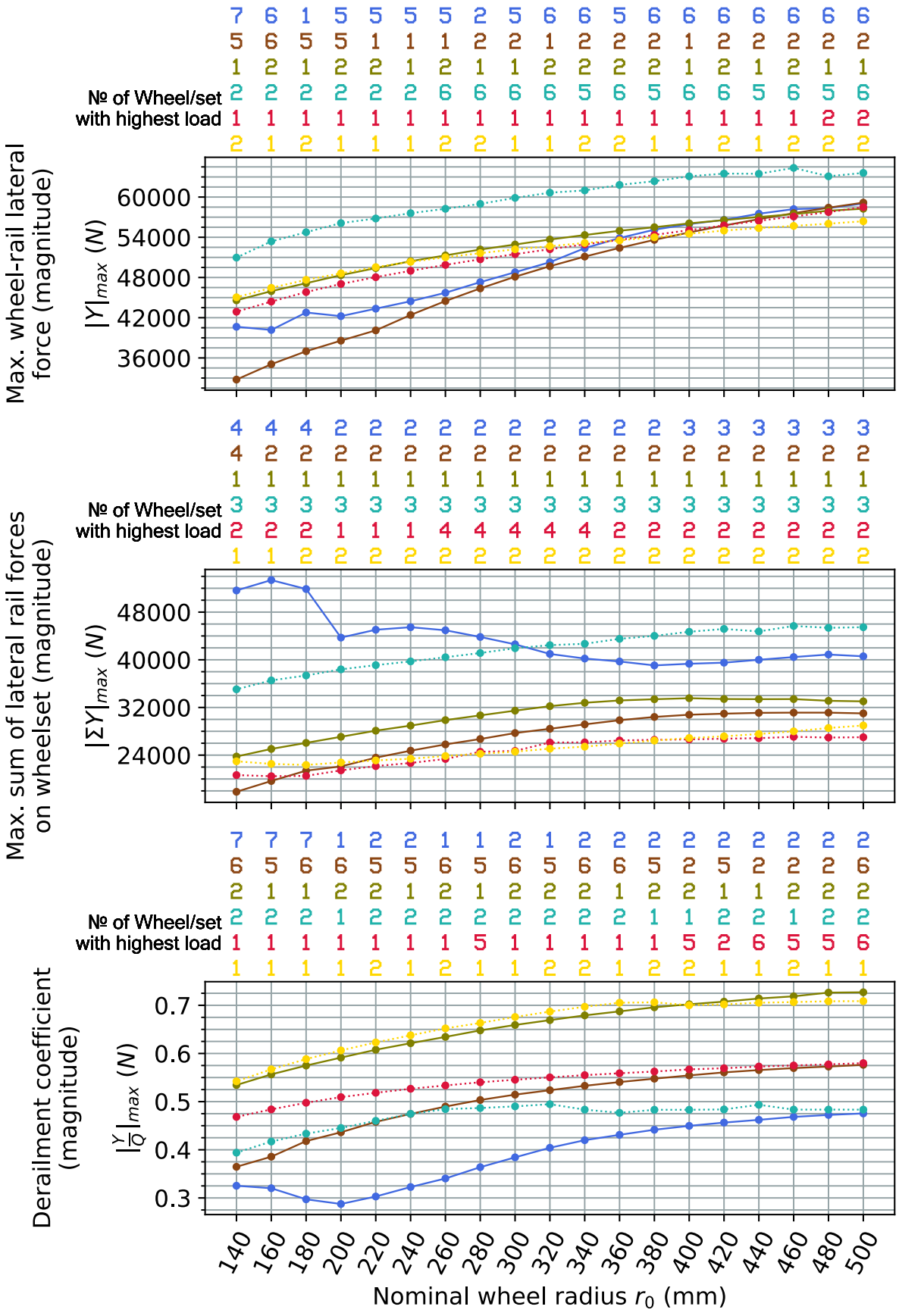

Figure D.32 Laden vehicle on a track with 1432 mm gauge and no rail cant, CAT4 curve

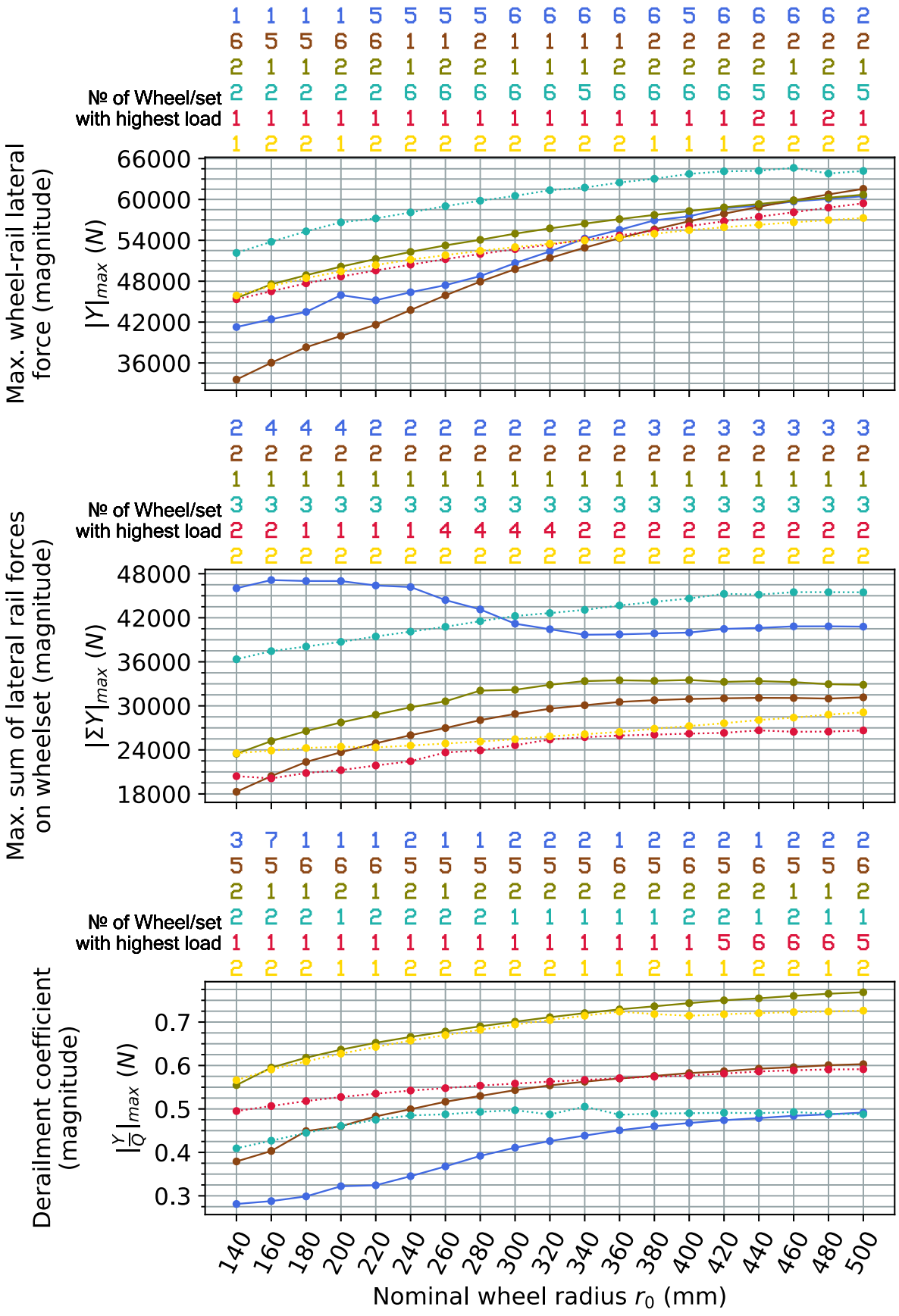

Figure D.33 Laden vehicle on a track with 1430 mm gauge and no rail cant, CAT4 curve

Appendix E Curve negotiation simulation results with wheel profile modification case MAT

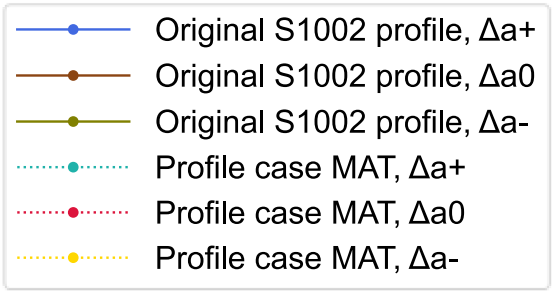

Figure E.1 Legend of all plots in this appendix

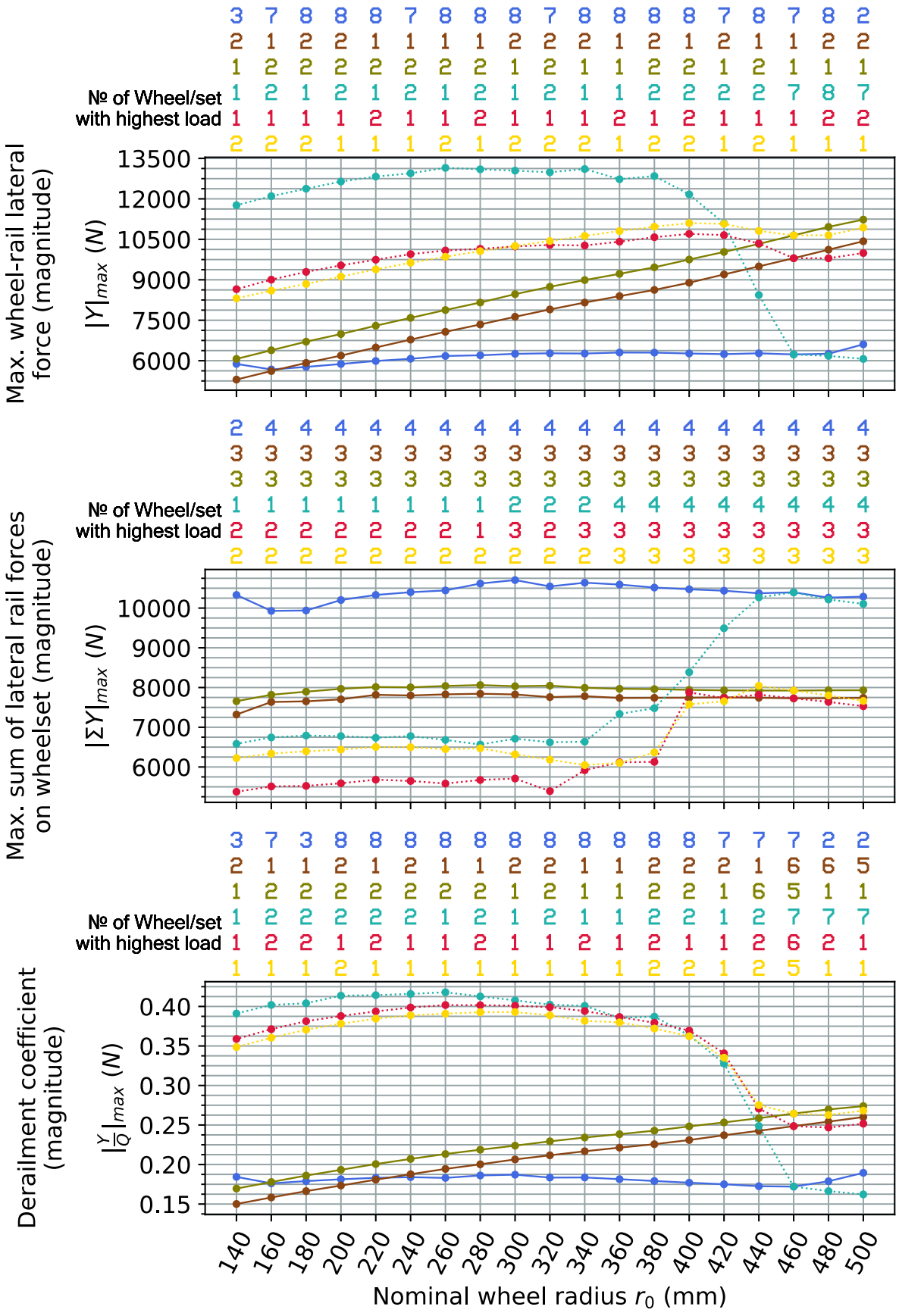

Figure E.2 Tare vehicle on a track with 1437 mm gauge and 1:40 rail cant, CAT2 curve

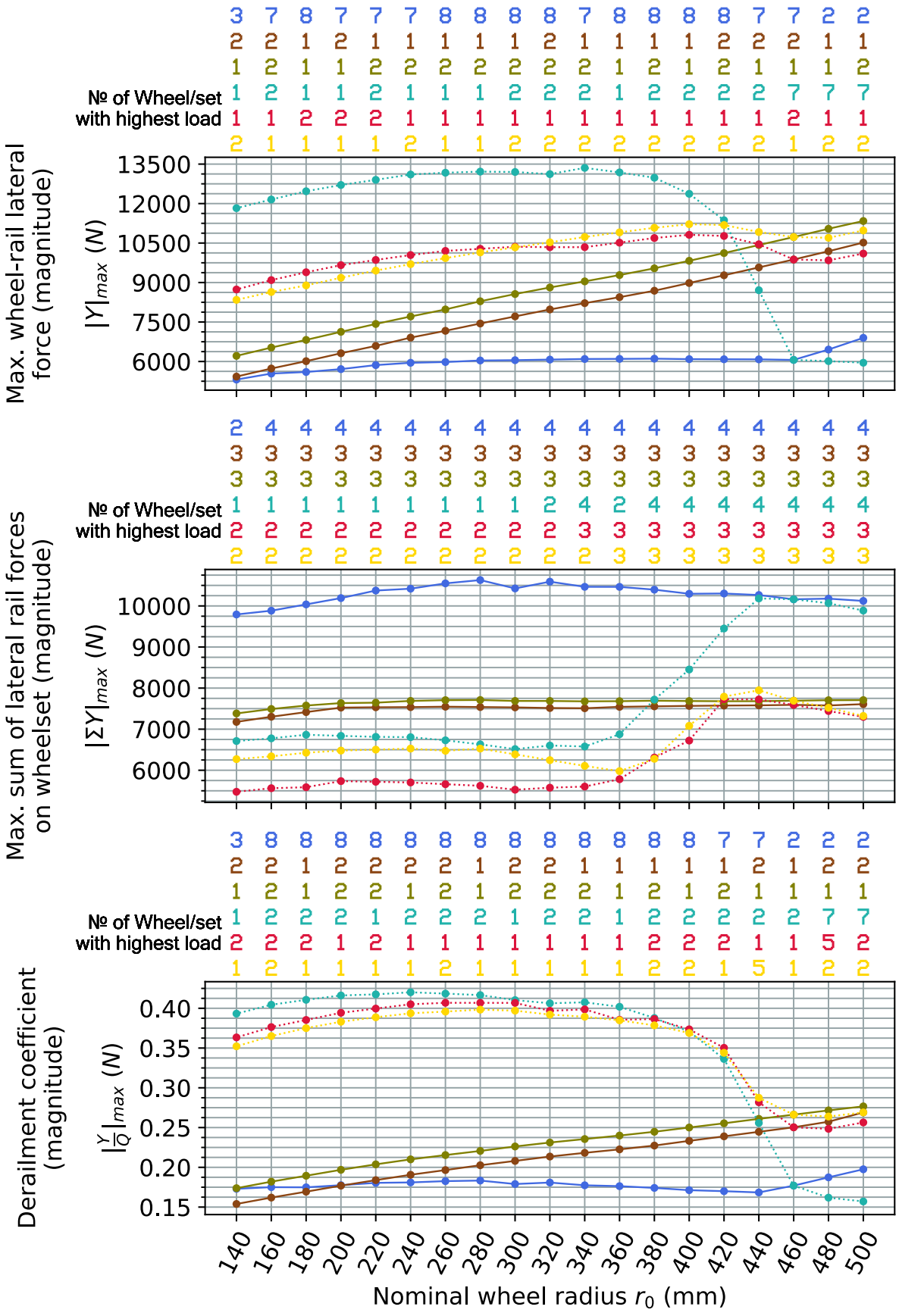

Figure E.3 Tare vehicle on a track with 1435 mm gauge and 1:40 rail cant (reference track setting), CAT2 curve

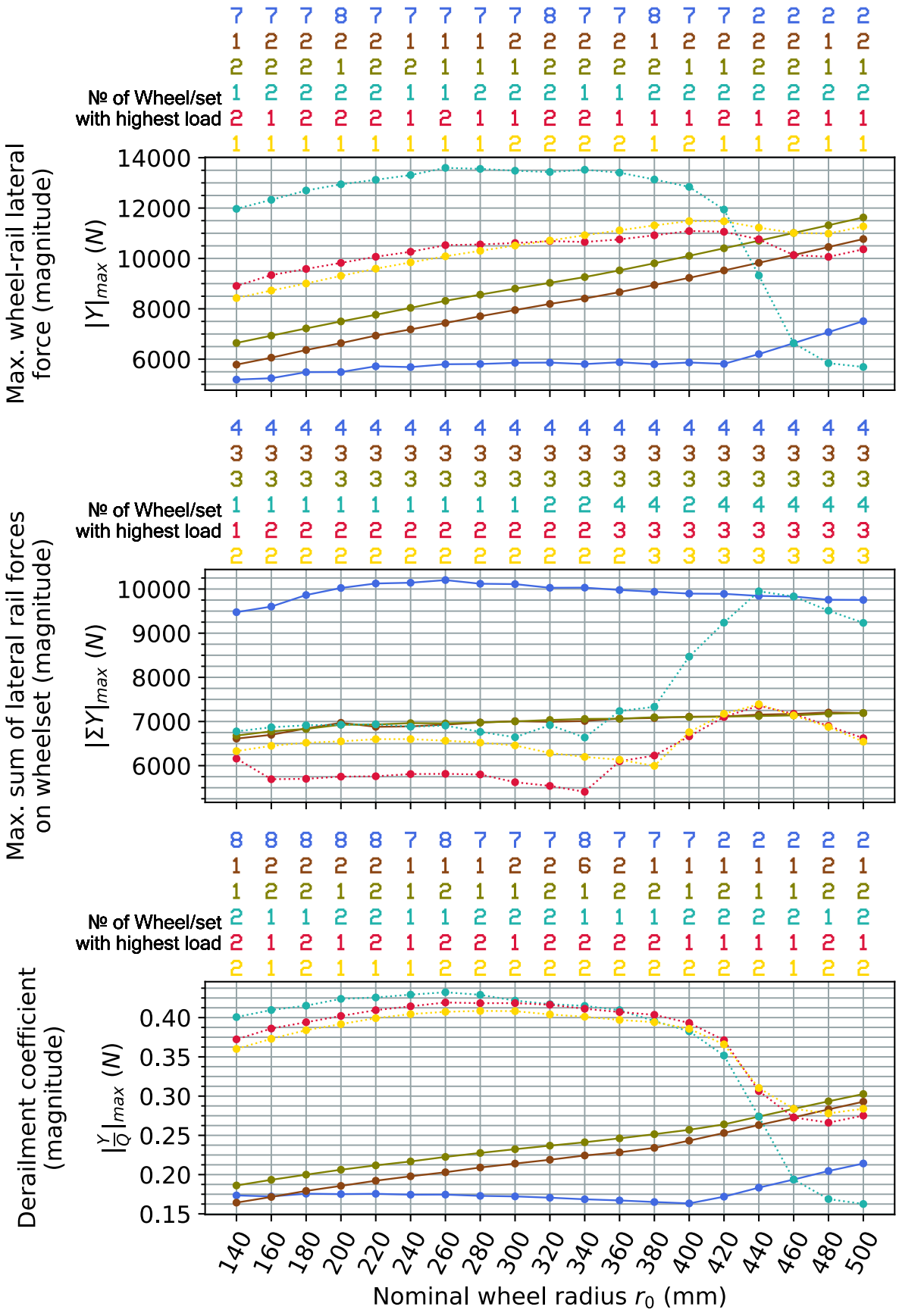

Figure E.4 Tare vehicle on a track with 1432 mm gauge and 1:40 rail cant, CAT2 curve

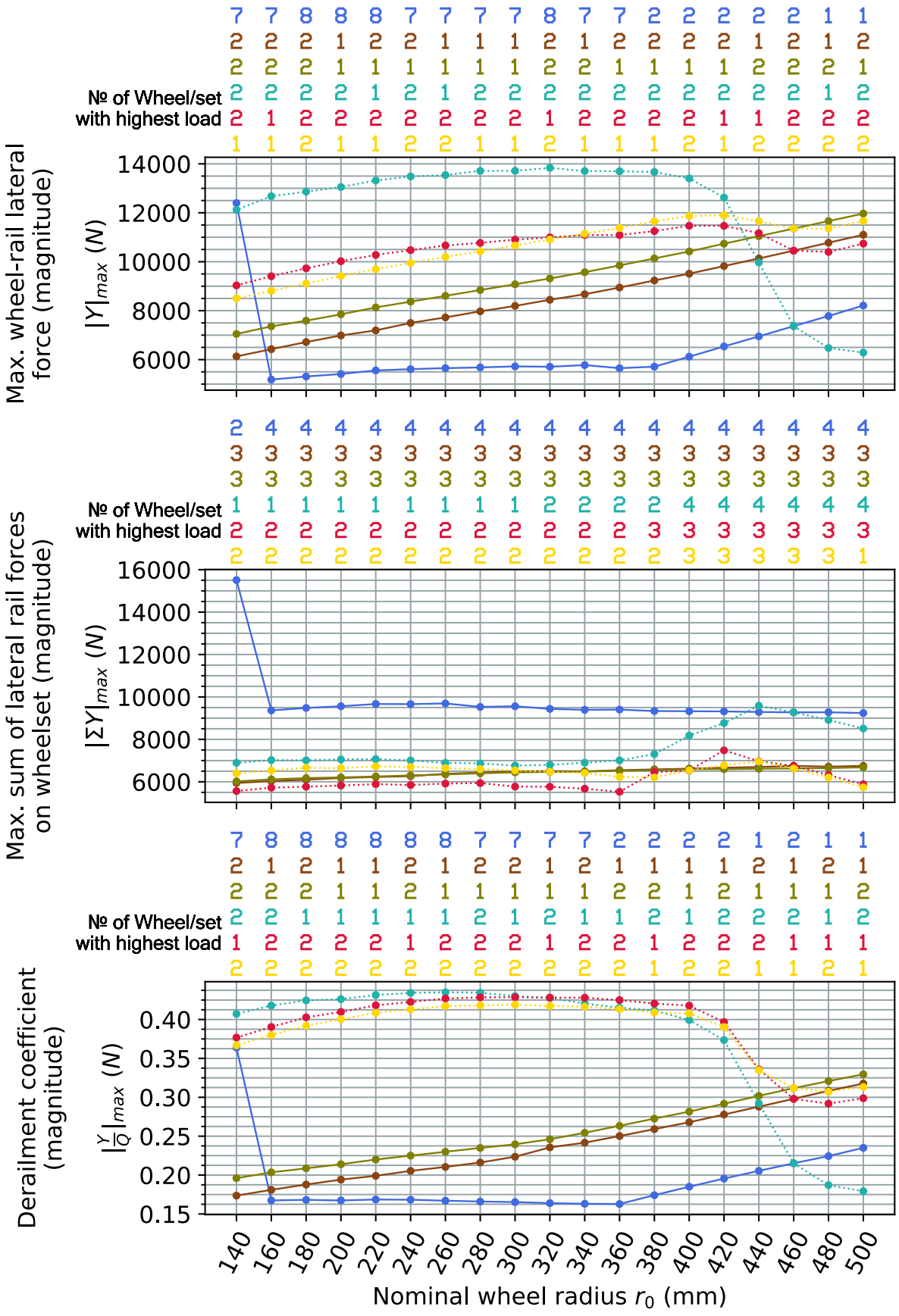

Figure E.5 Tare vehicle on a track with 1430 mm gauge and 1:40 rail cant, CAT2 curve

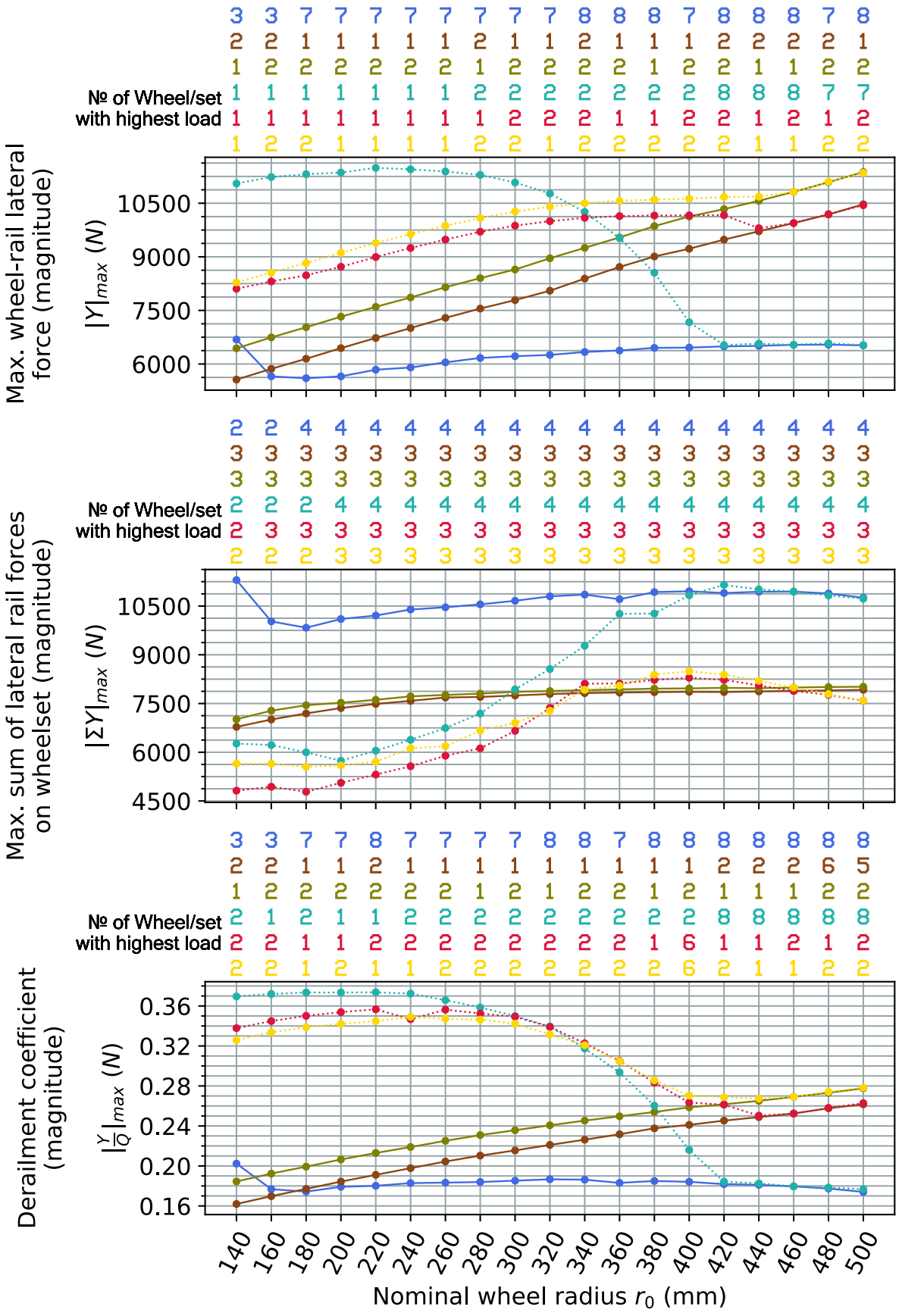

Figure E.6 Tare vehicle on a track with 1437 mm gauge and no rail cant, CAT2 curve

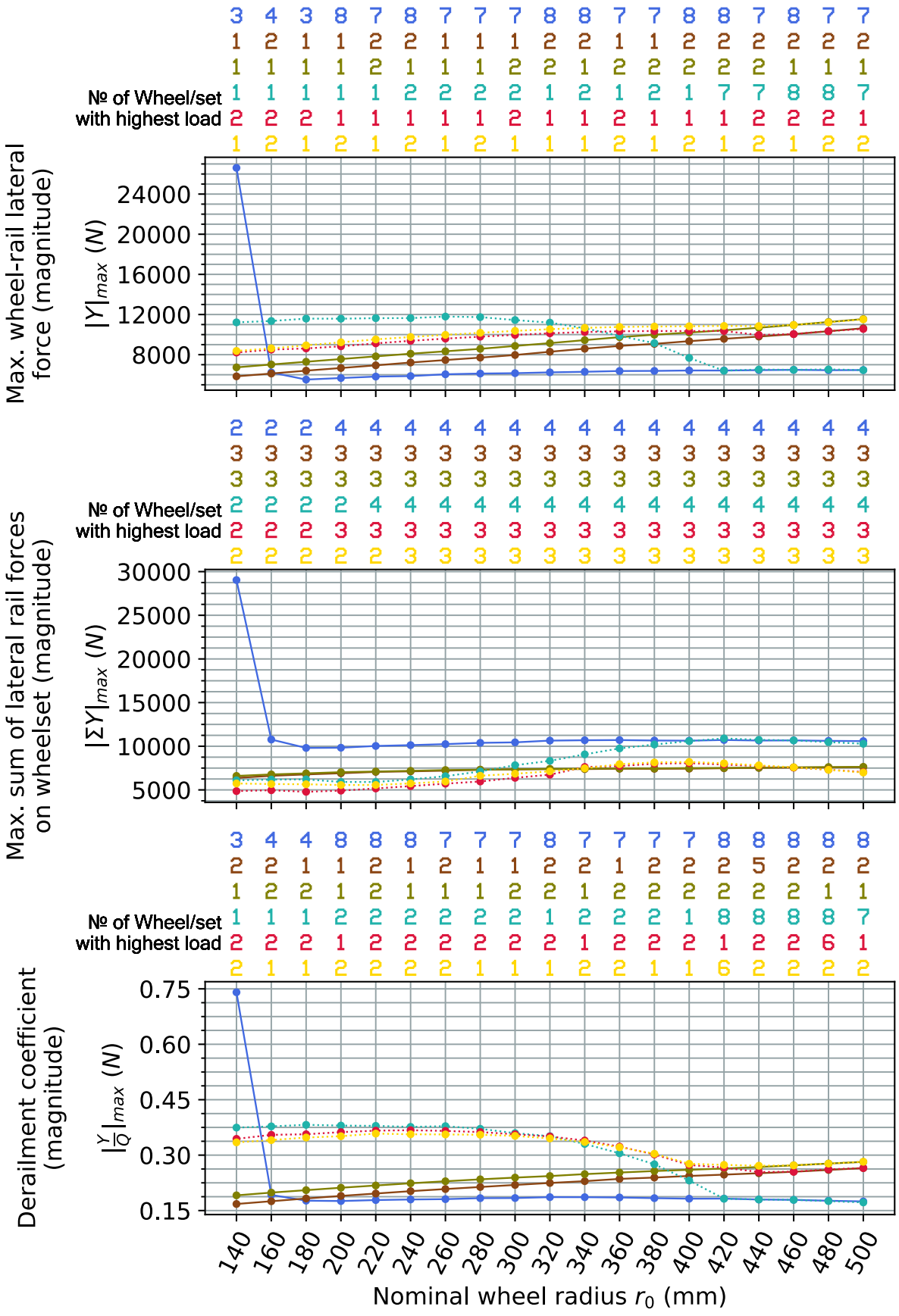

Figure E.7 Tare vehicle on a track with 1435 mm gauge and no rail cant, CAT2 curve

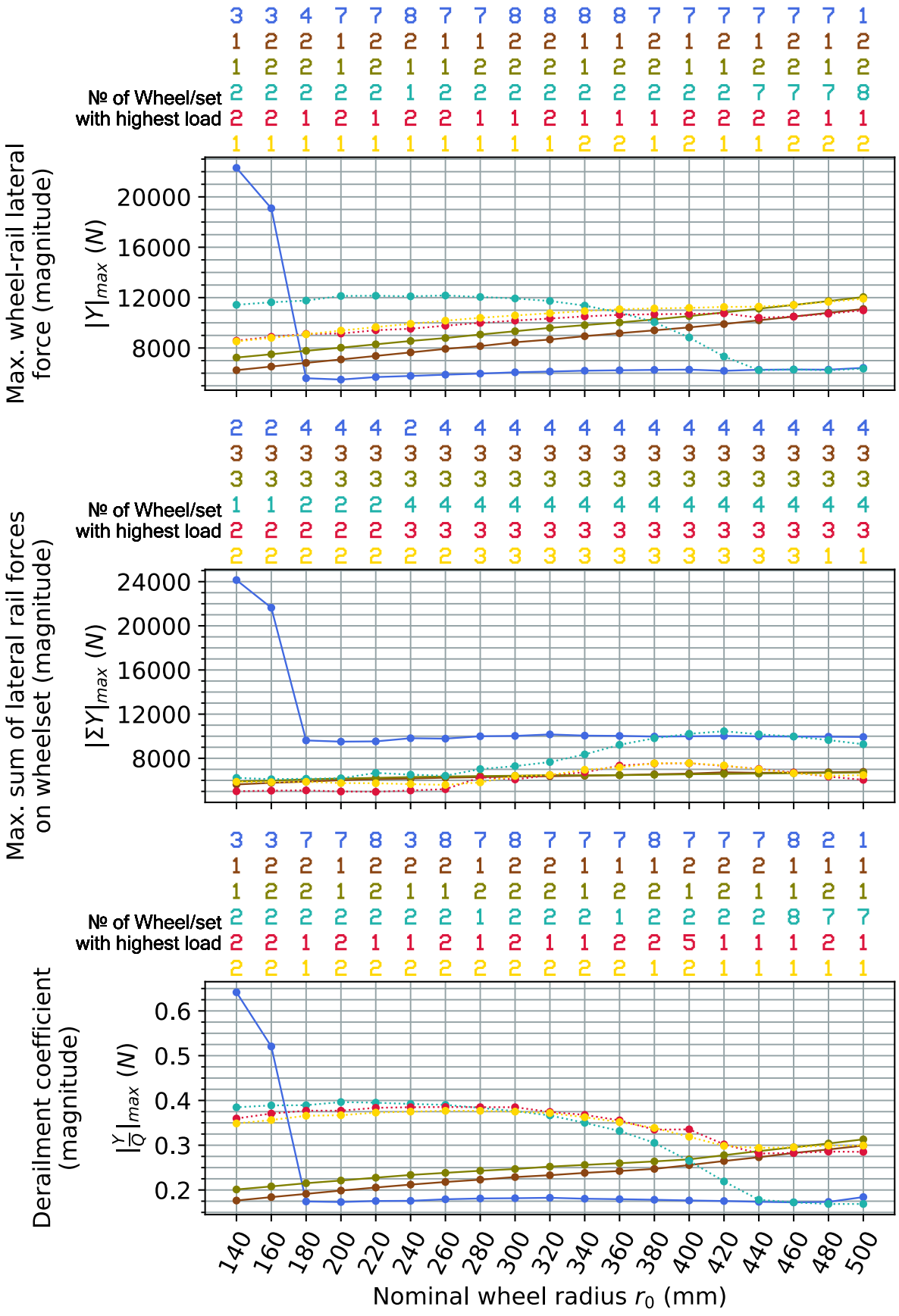

Figure E.8 Tare vehicle on a track with 1432 mm gauge and no rail cant, CAT2 curve

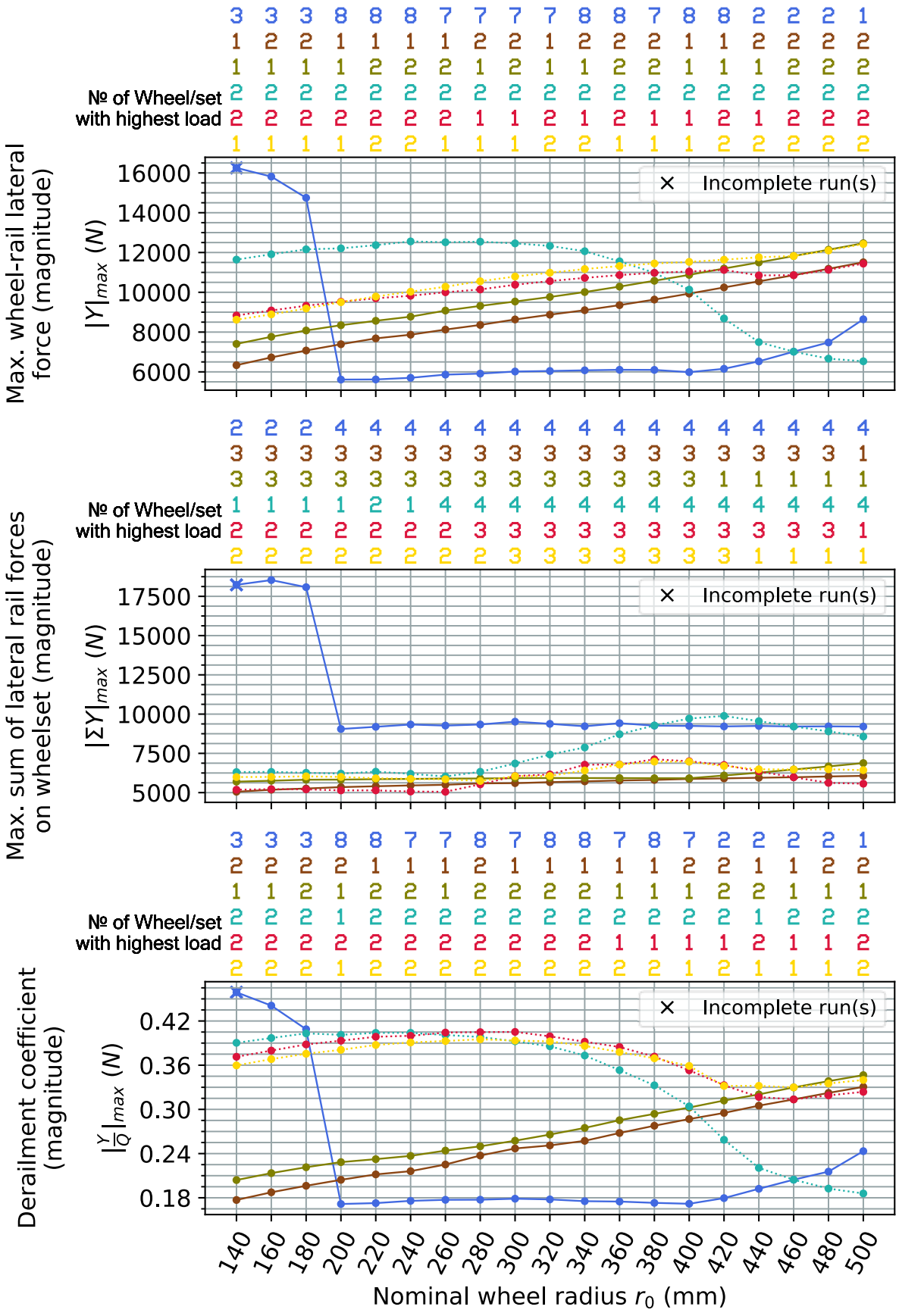

Figure E.9 Tare vehicle on a track with 1430 mm gauge and no rail cant, CAT2 curve

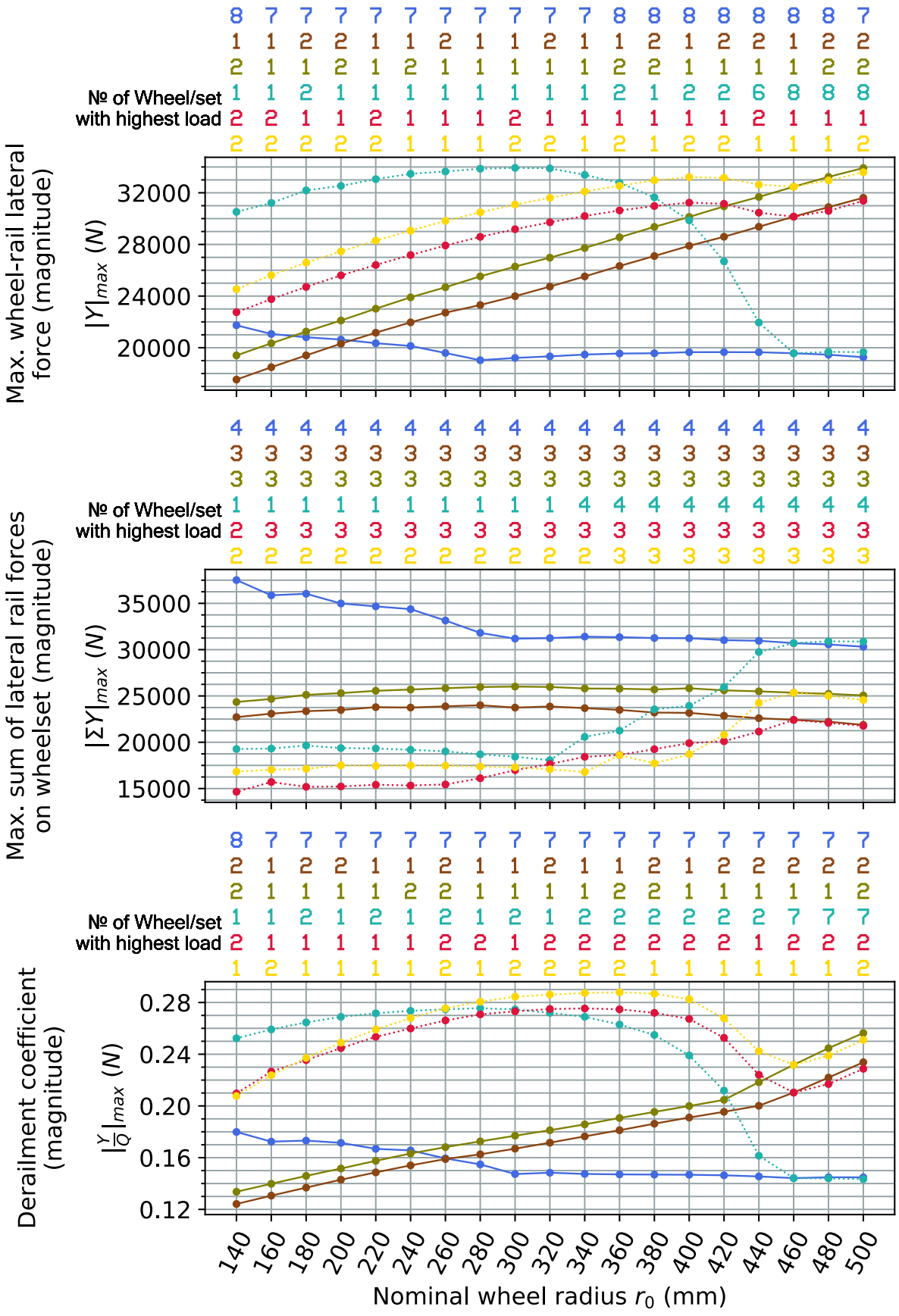

Figure E.10 Laden vehicle on a track with 1437 mm gauge and 1:40 rail cant, CAT2 curve

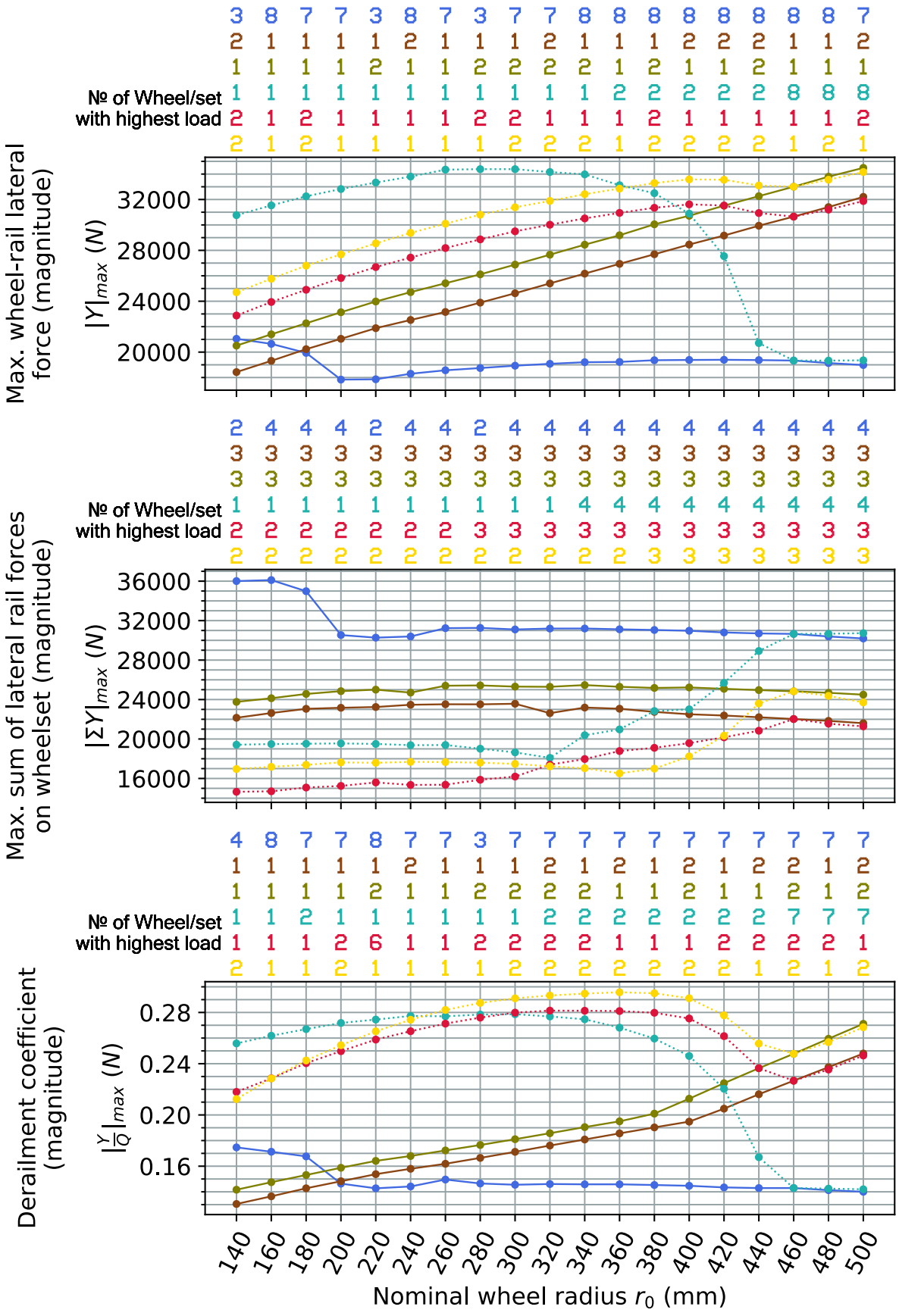

Figure E.11 Laden vehicle on a track with 1435 mm gauge and 1:40 rail cant (reference track setting), CAT2 curve

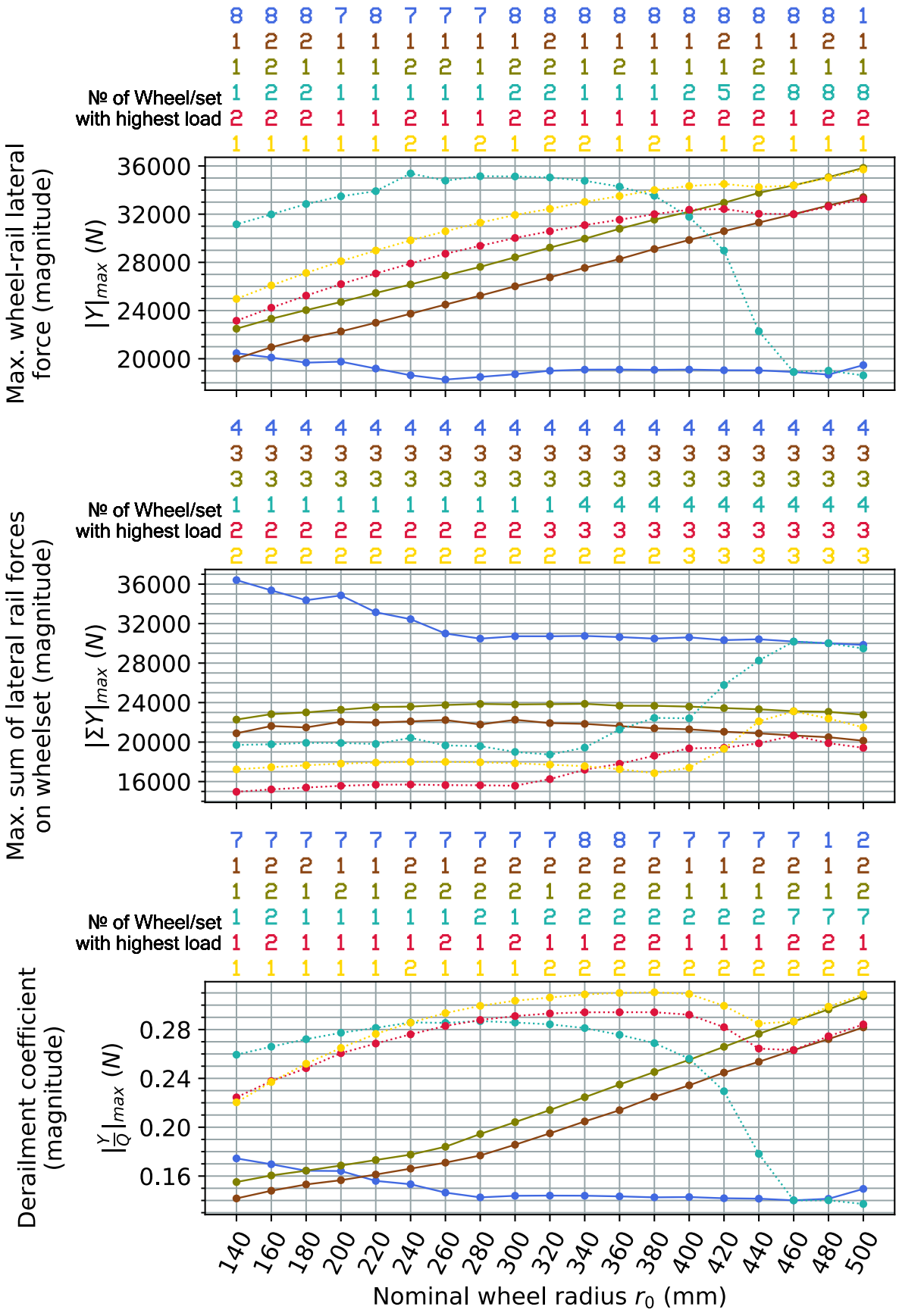

Figure E.12 Laden vehicle on a track with 1432 mm gauge and 1:40 rail cant, CAT2 curve

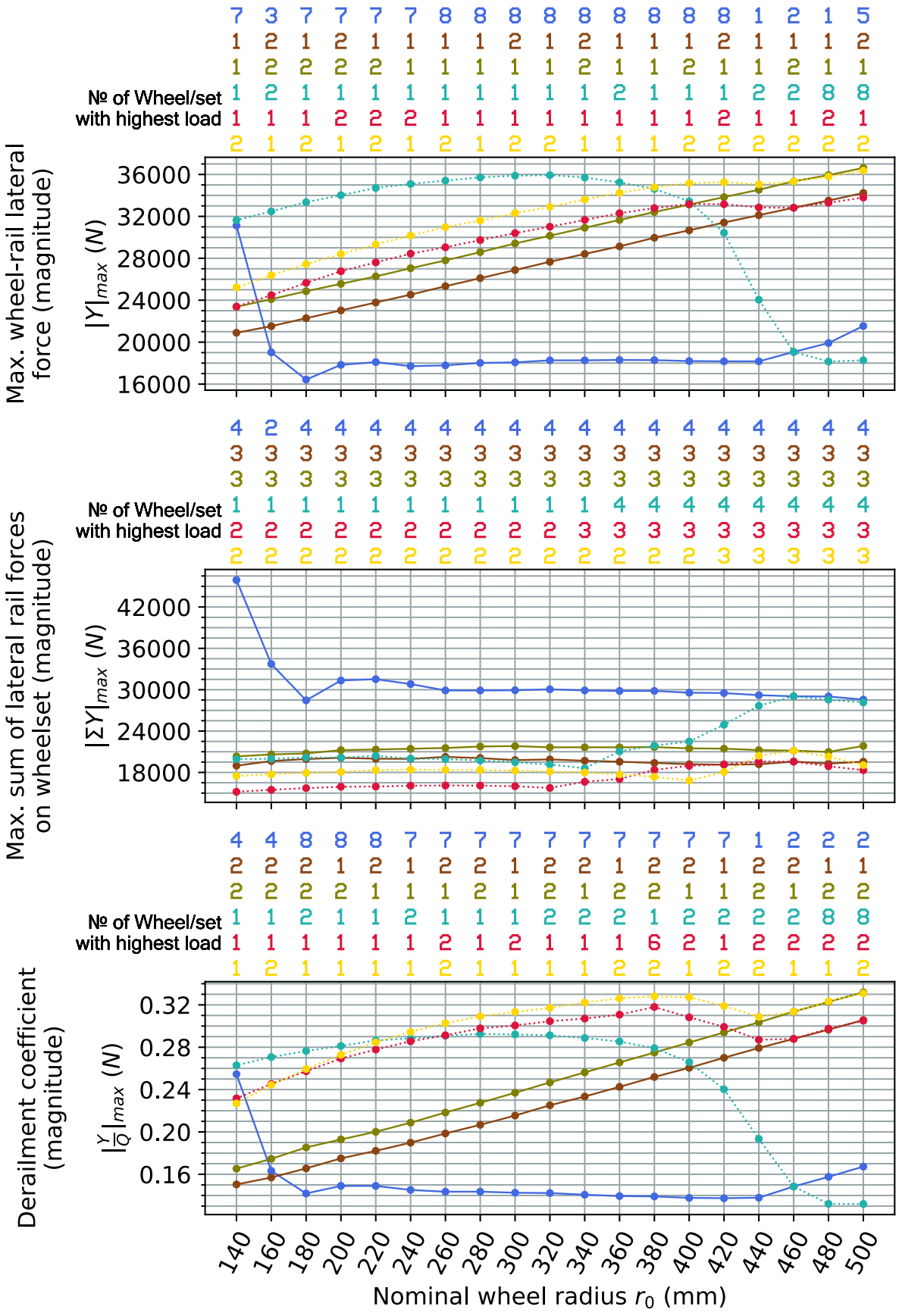

Figure E.13 Laden vehicle on a track with 1430 mm gauge and 1:40 rail cant, CAT2 curve

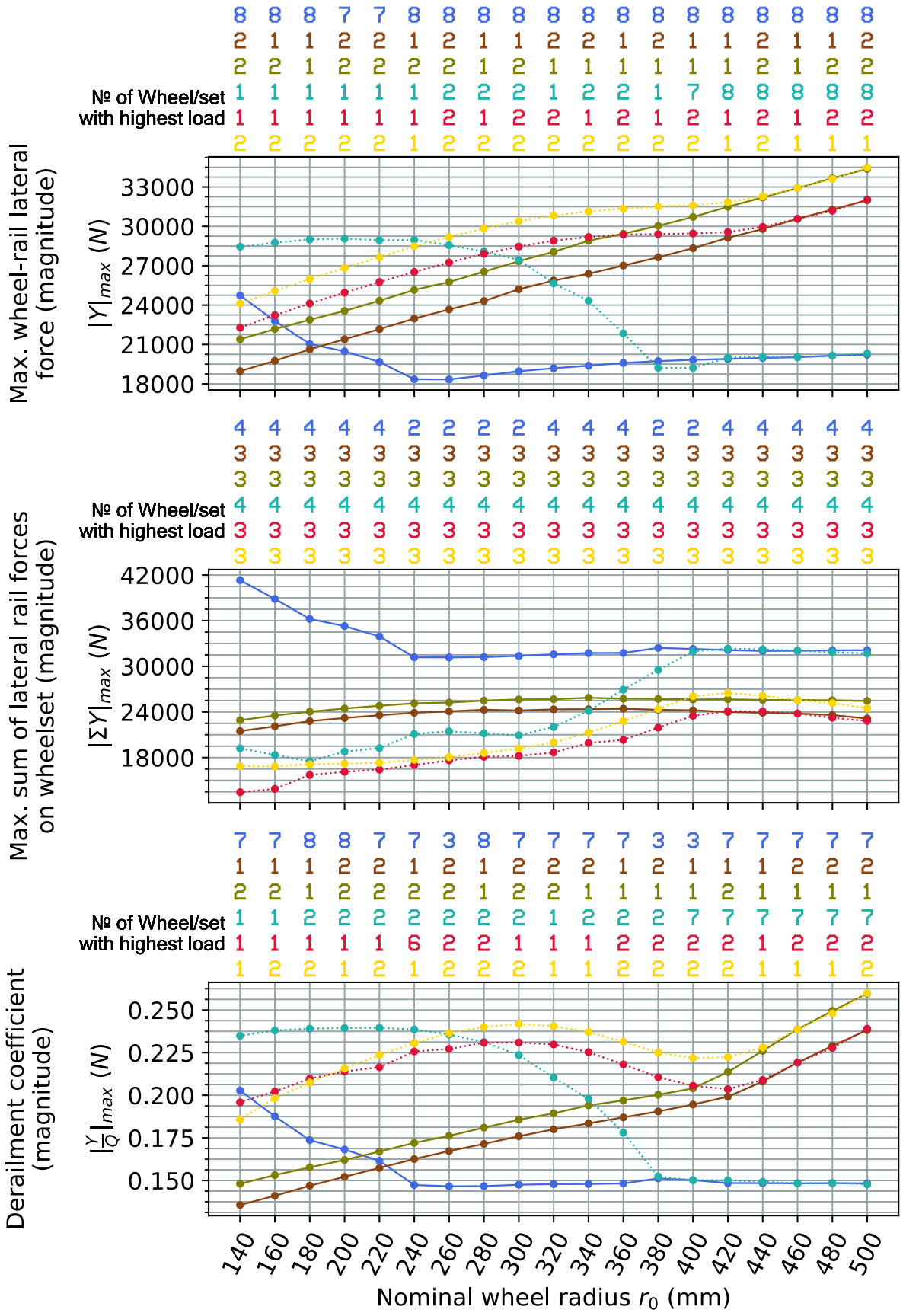

Figure E.14 Laden vehicle on a track with 1437 mm gauge and no rail cant, CAT2 curve

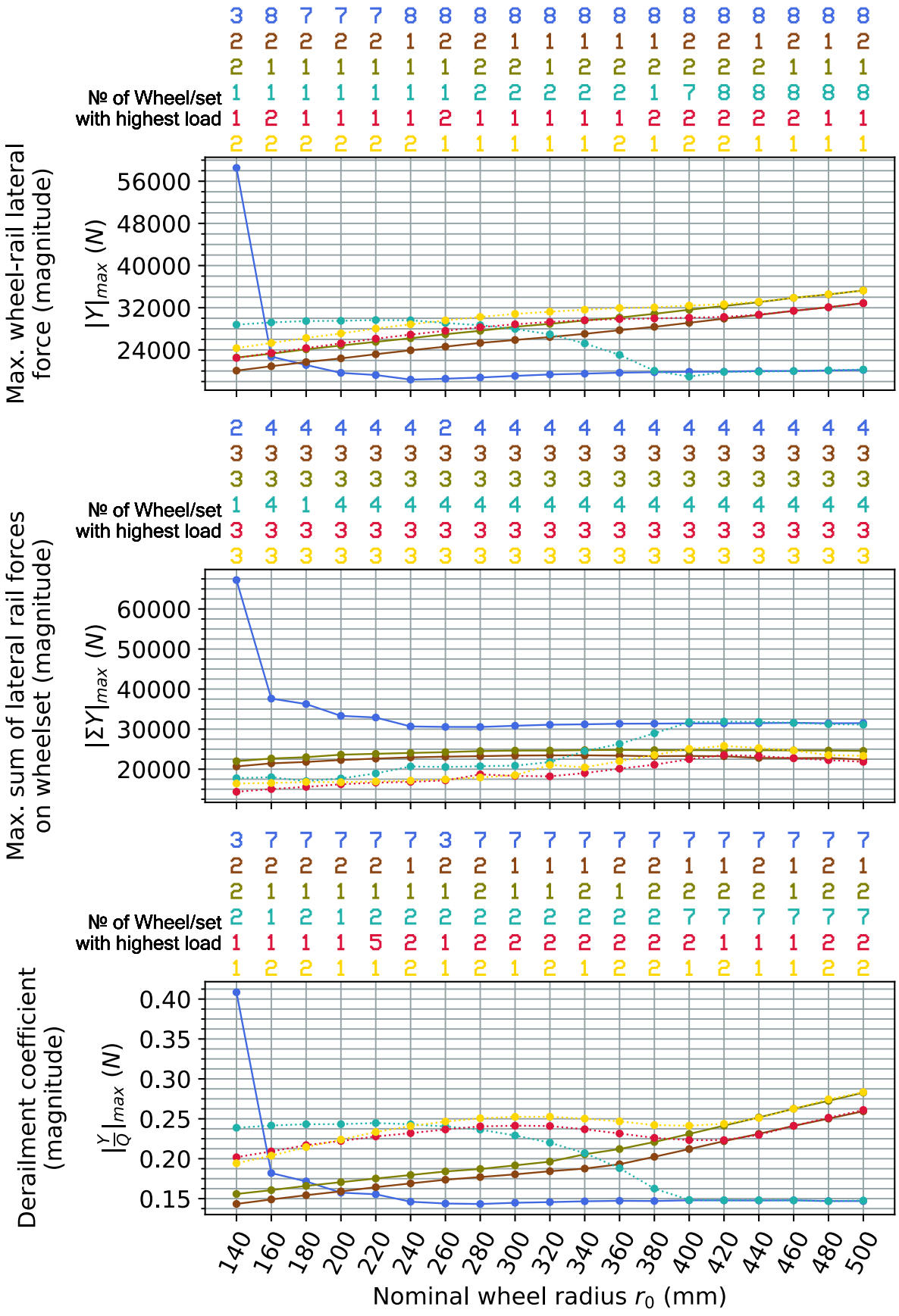

Figure E.15 Laden vehicle on a track with 1435 mm gauge and no rail cant, CAT2 curve

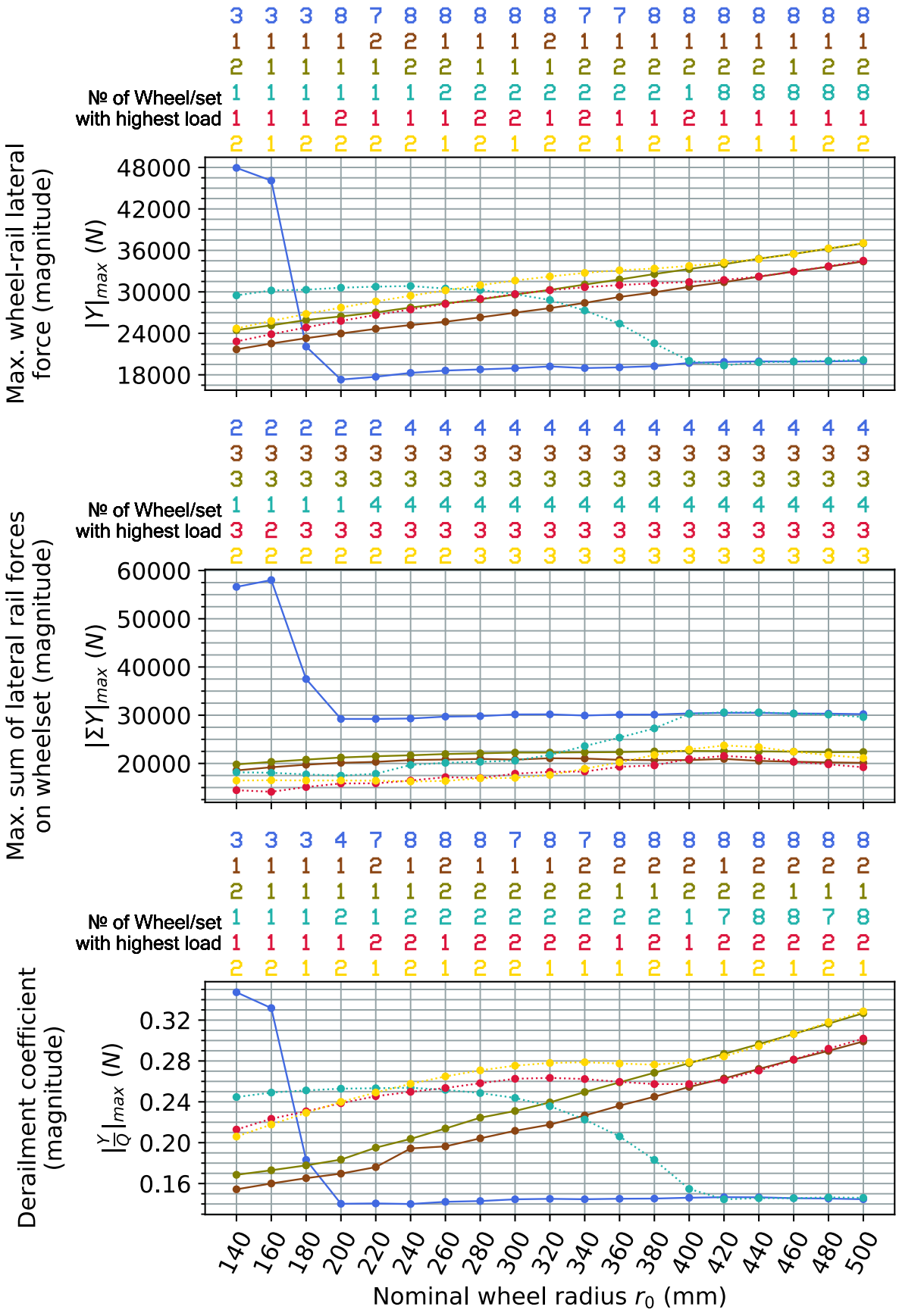

Figure E.16 Laden vehicle on a track with 1432 mm gauge and no rail cant, CAT2 curve

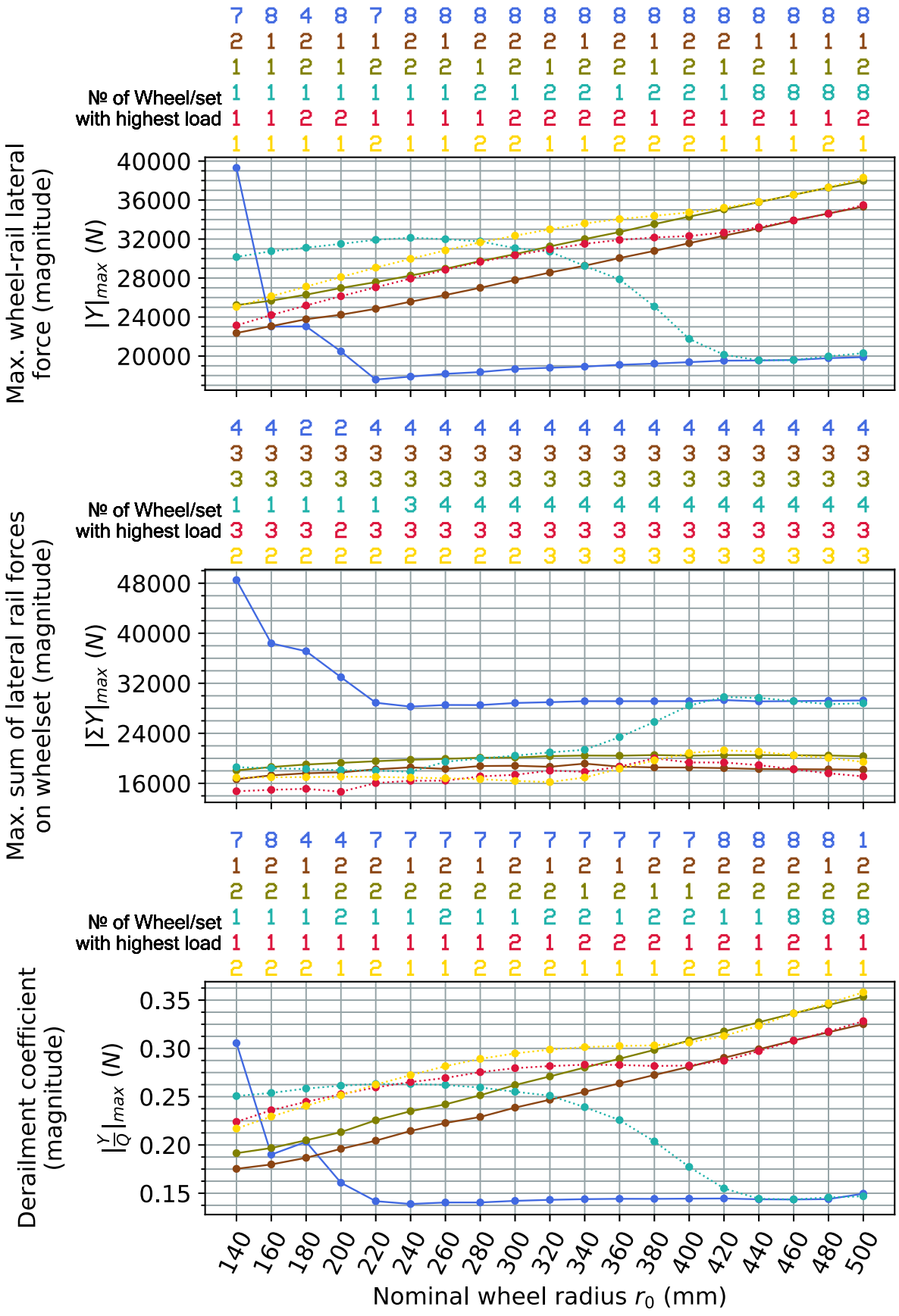

Figure E.17 Laden vehicle on a track with 1430 mm gauge and no rail cant, CAT2 curve

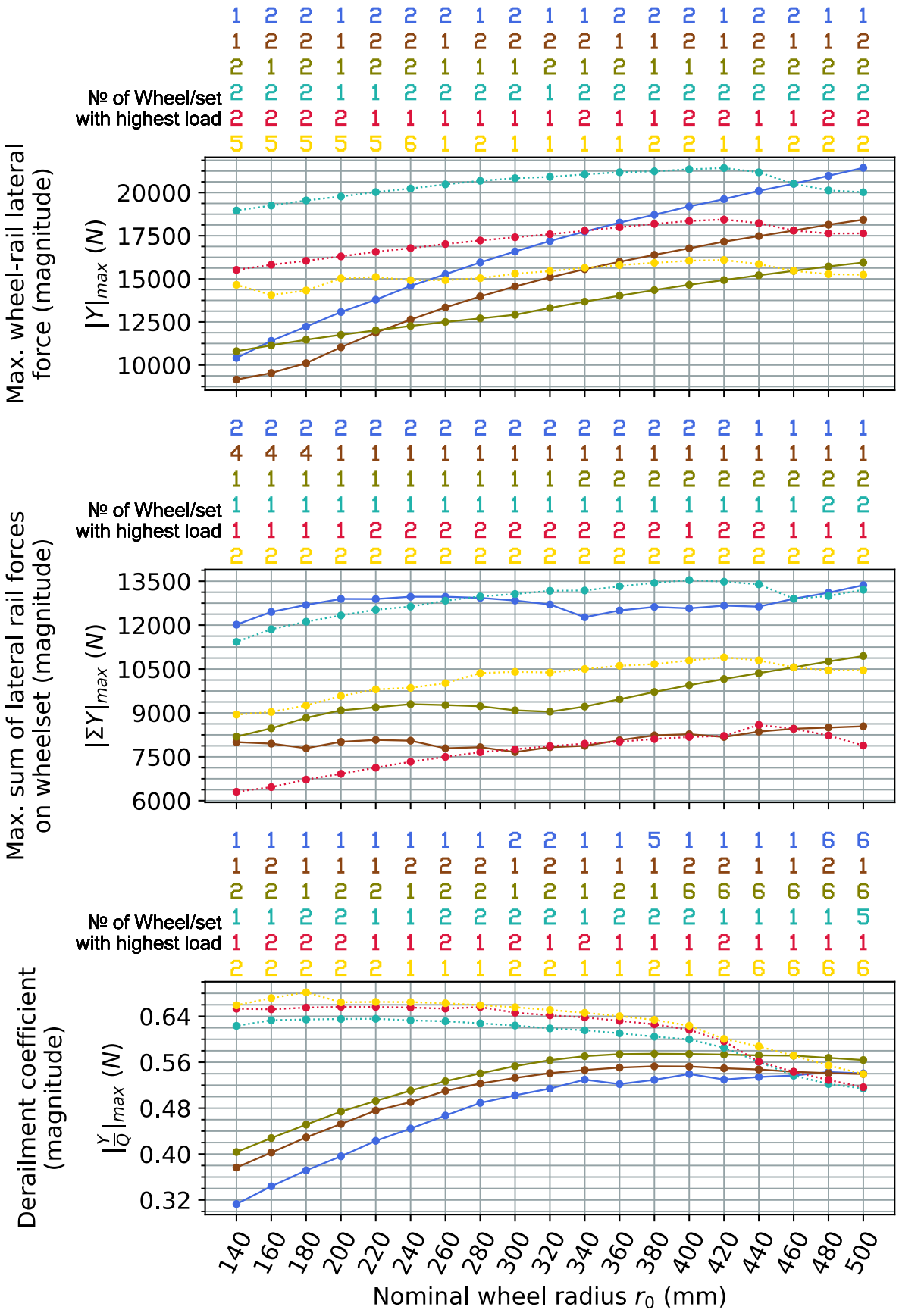

Figure E.18 Tare vehicle on a track with 1437 mm gauge and 1:40 rail cant, CAT4 curve

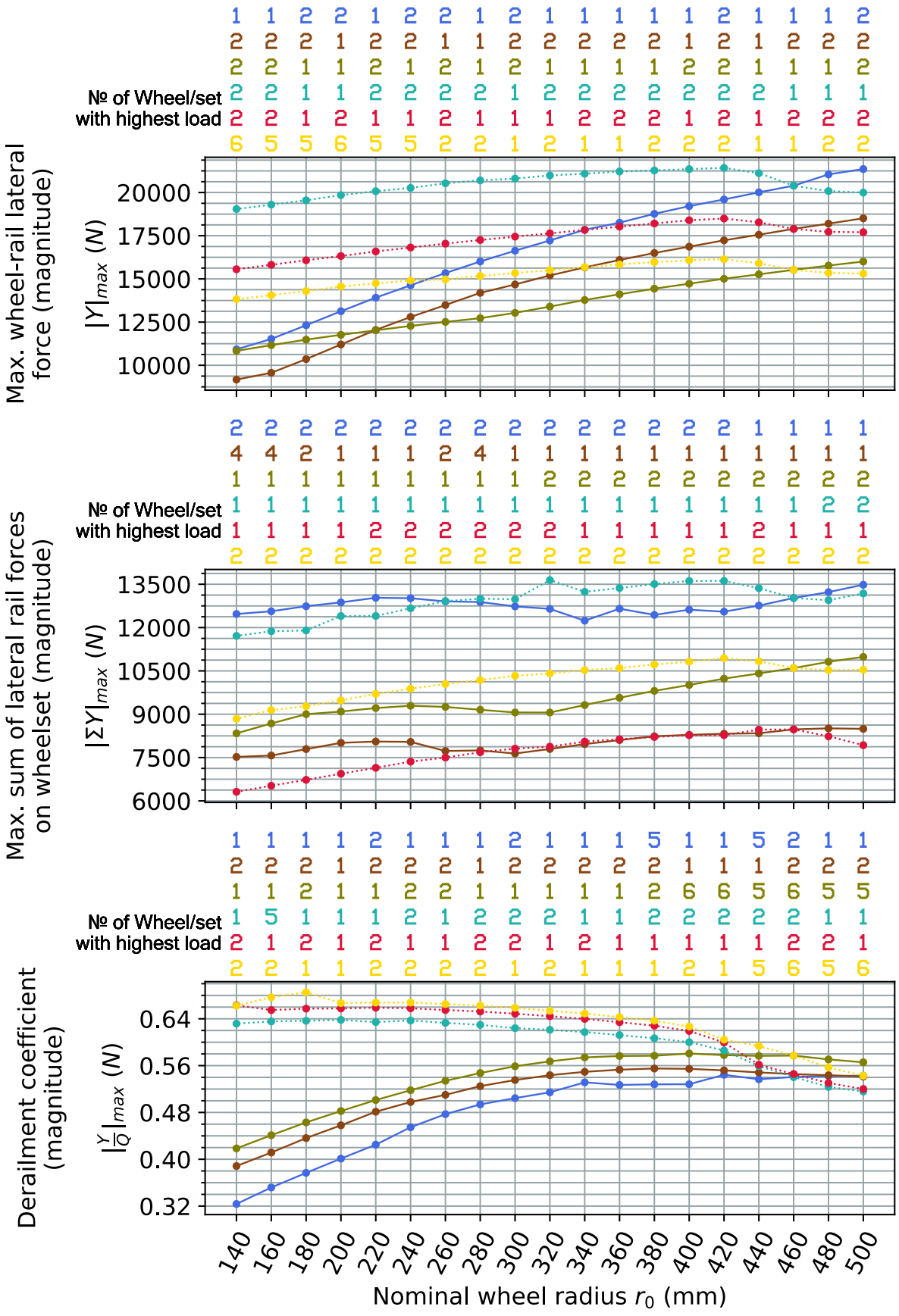

Figure E.19 Tare vehicle on a track with 1435 mm gauge and 1:40 rail cant (reference track setting), CAT4 curve

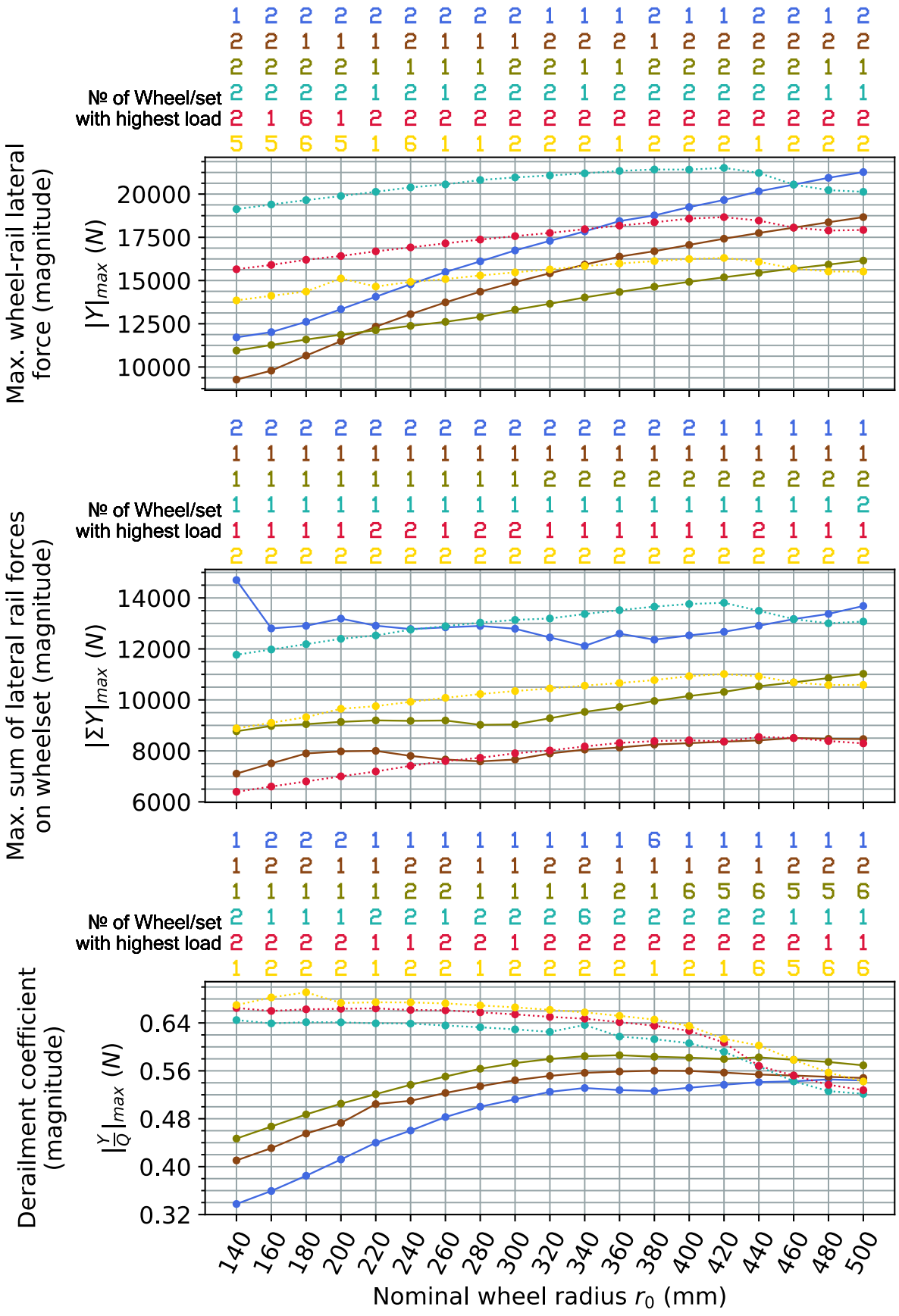

Figure E.20 Tare vehicle on a track with 1432 mm gauge and 1:40 rail cant, CAT4 curve

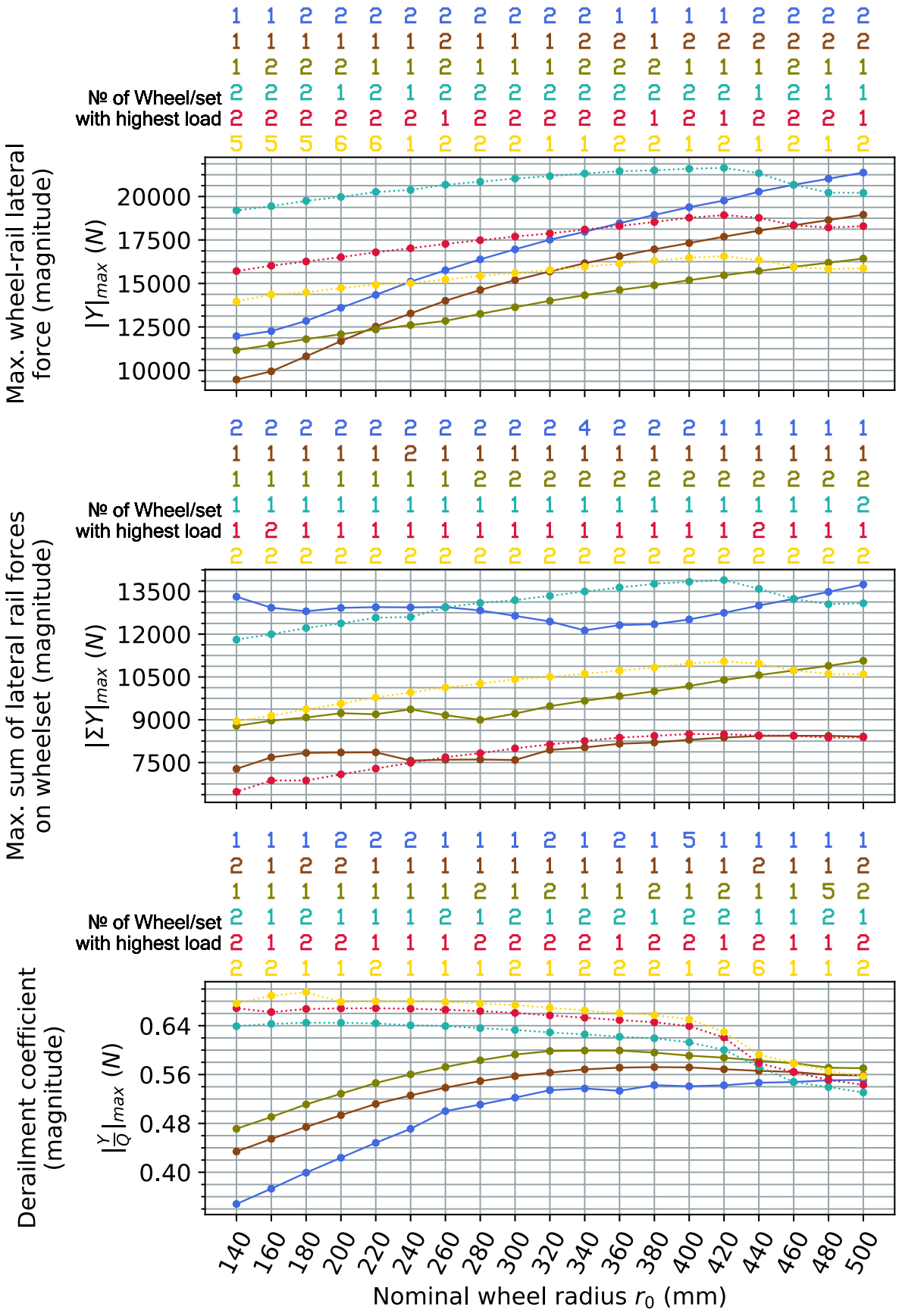

Figure E.21 Tare vehicle on a track with 1430 mm gauge and 1:40 rail cant, CAT4 curve

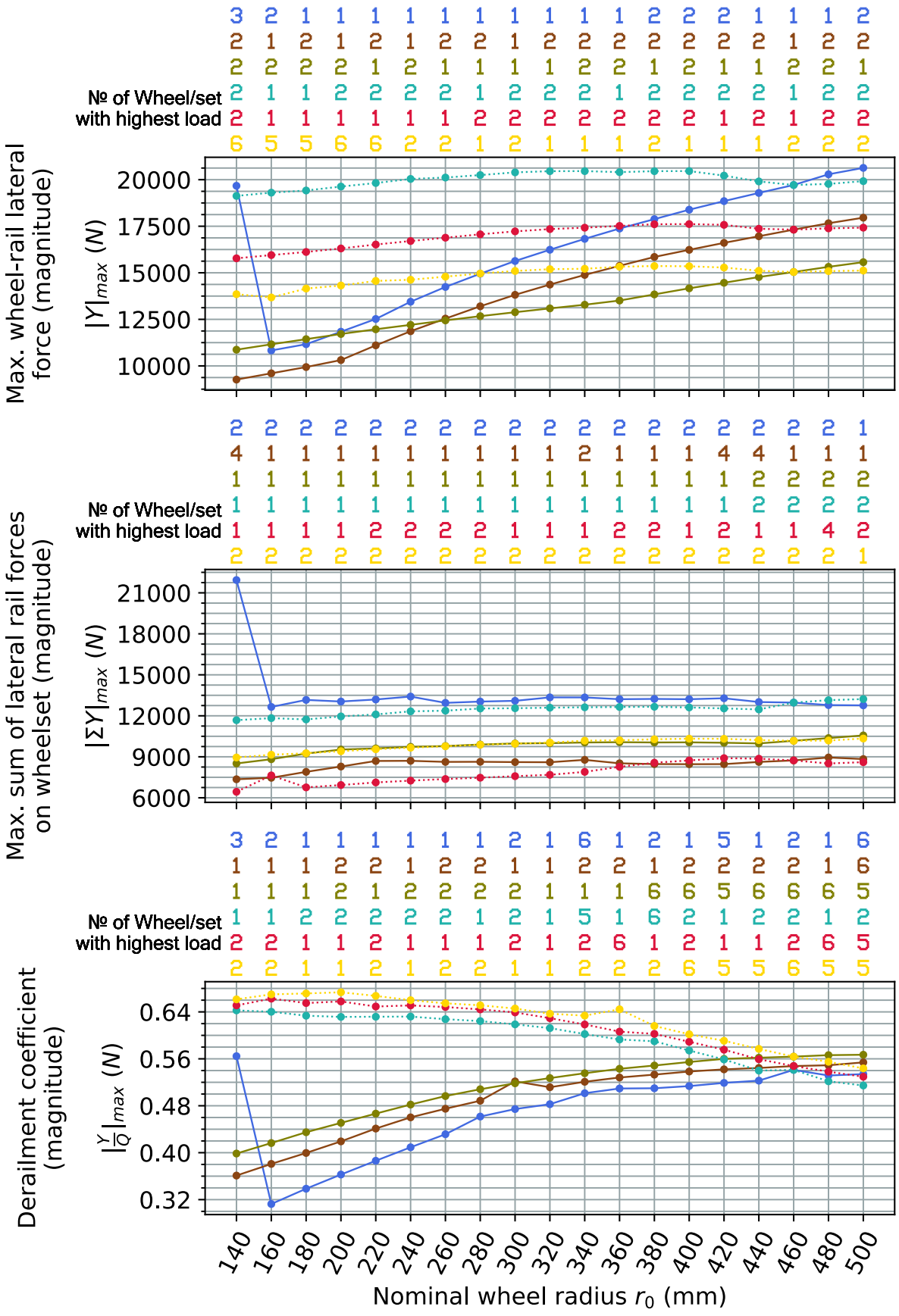

Figure E.22 Tare vehicle on a track with 1437 mm gauge and no rail cant, CAT4 curve

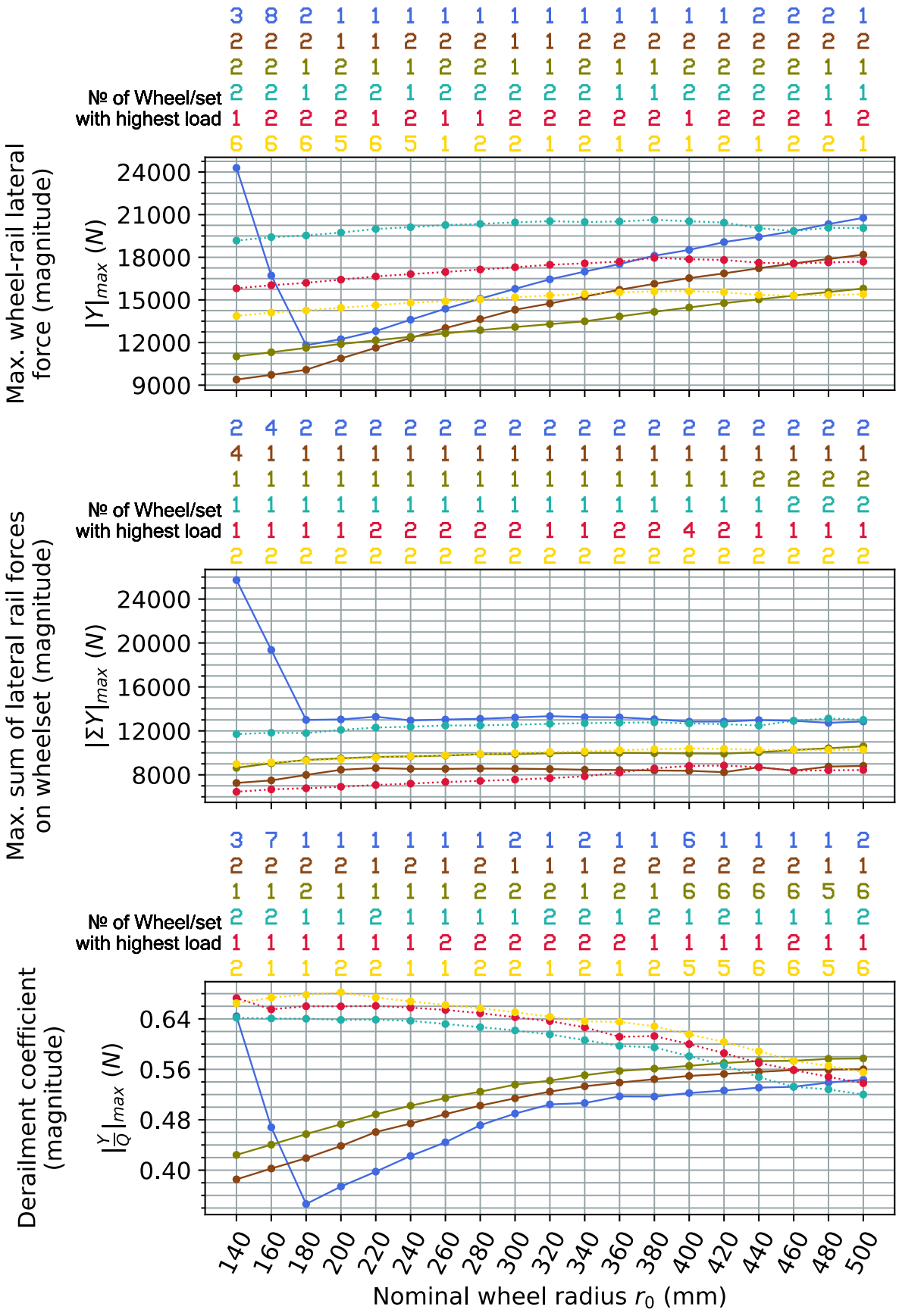

Figure E.23 Tare vehicle on a track with 1435 mm gauge and no rail cant, CAT4 curve

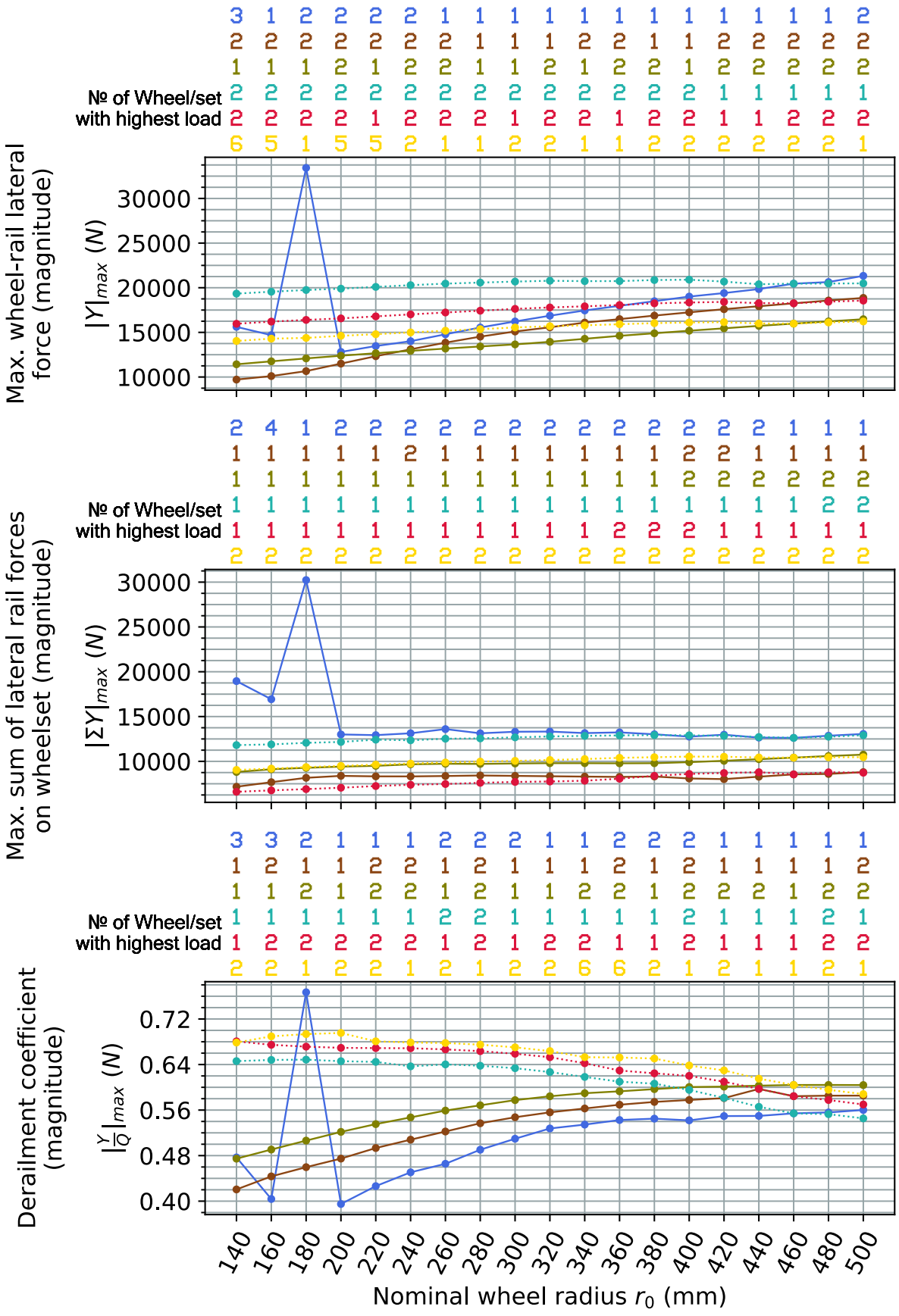

Figure E.24 Tare vehicle on a track with 1432 mm gauge and no rail cant, CAT4 curve

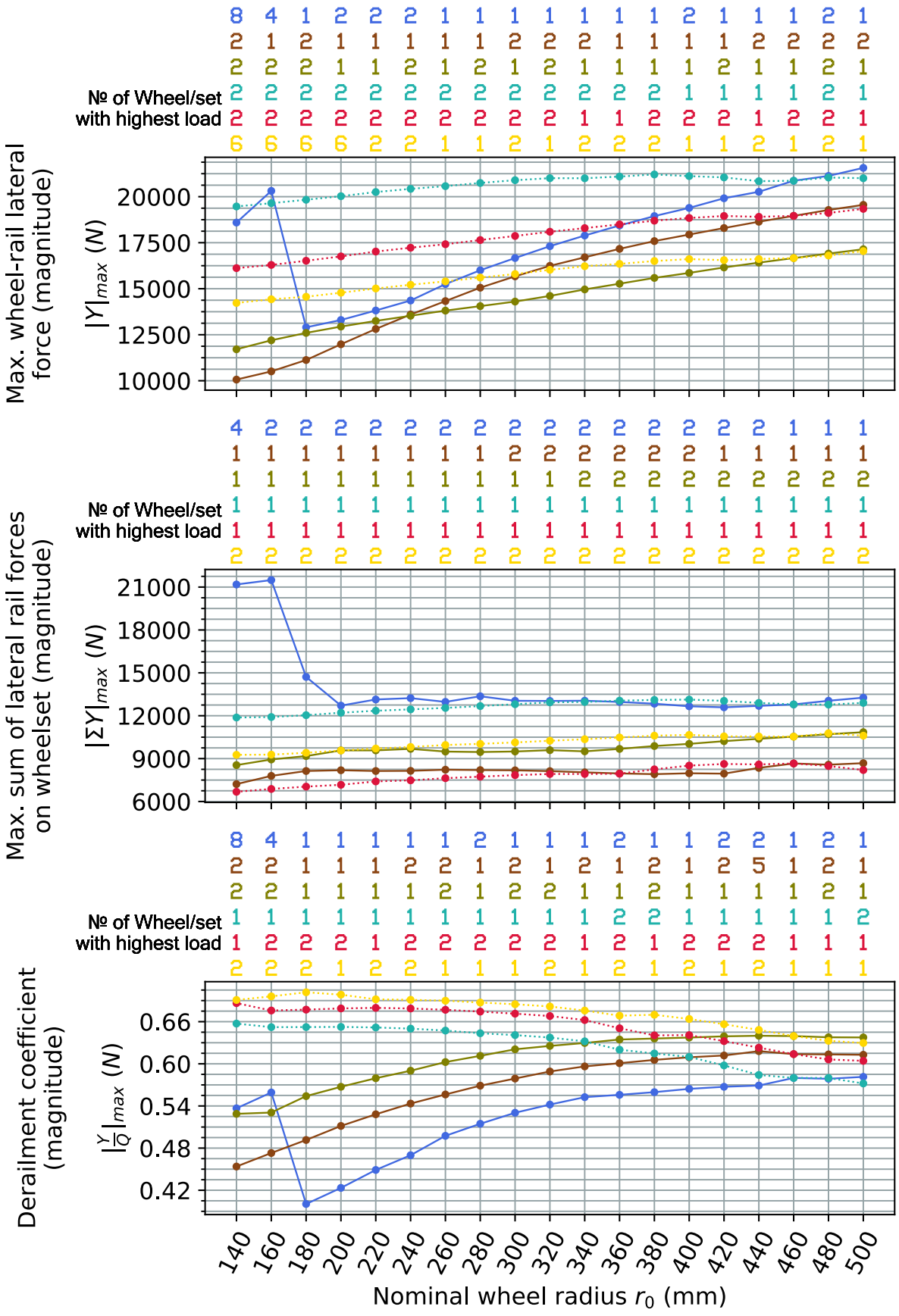

Figure E.25 Tare vehicle on a track with 1430 mm gauge and no rail cant, CAT4 curve

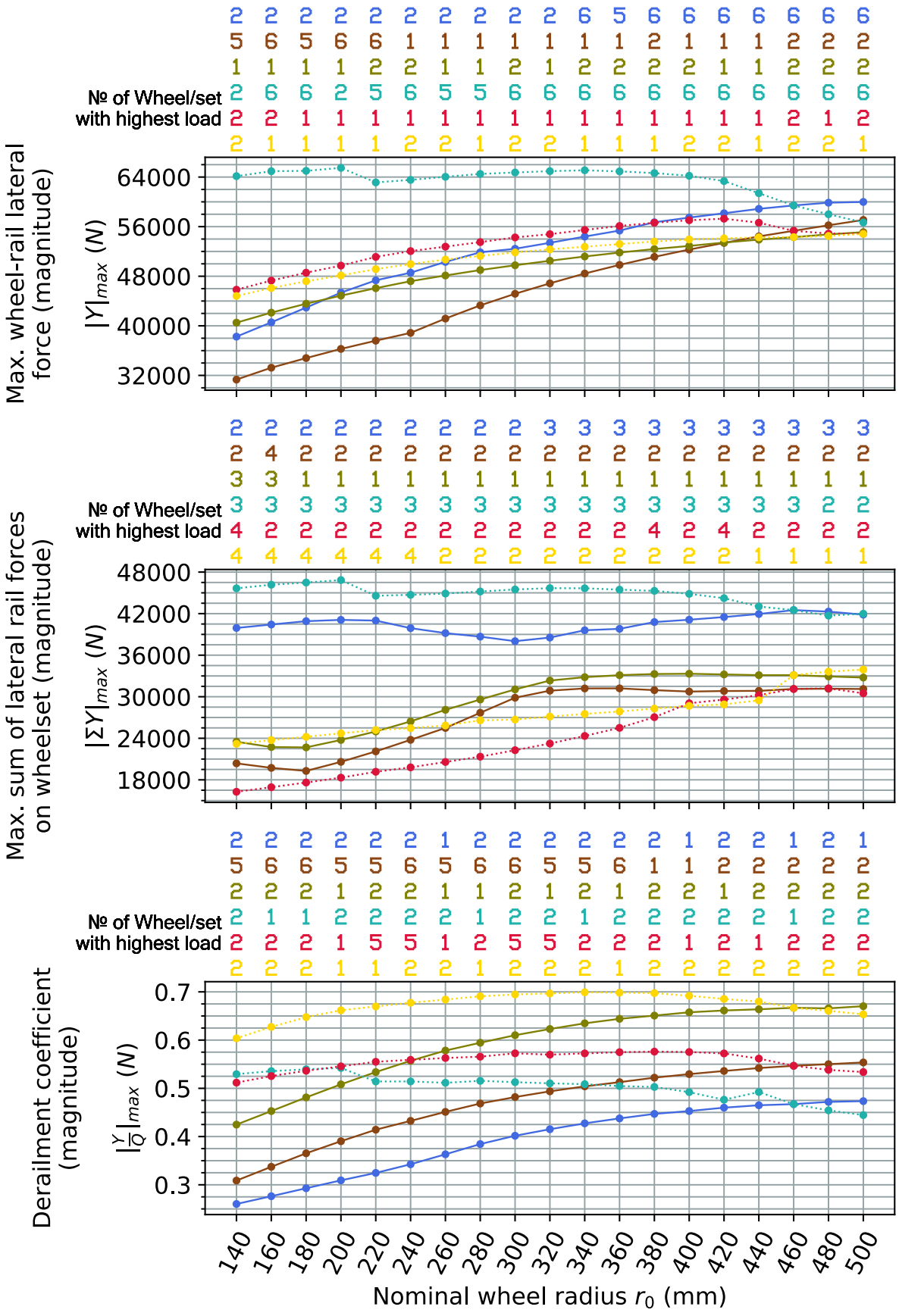

Figure E.26 Laden vehicle on a track with 1437 mm gauge and 1:40 rail cant, CAT4 curve

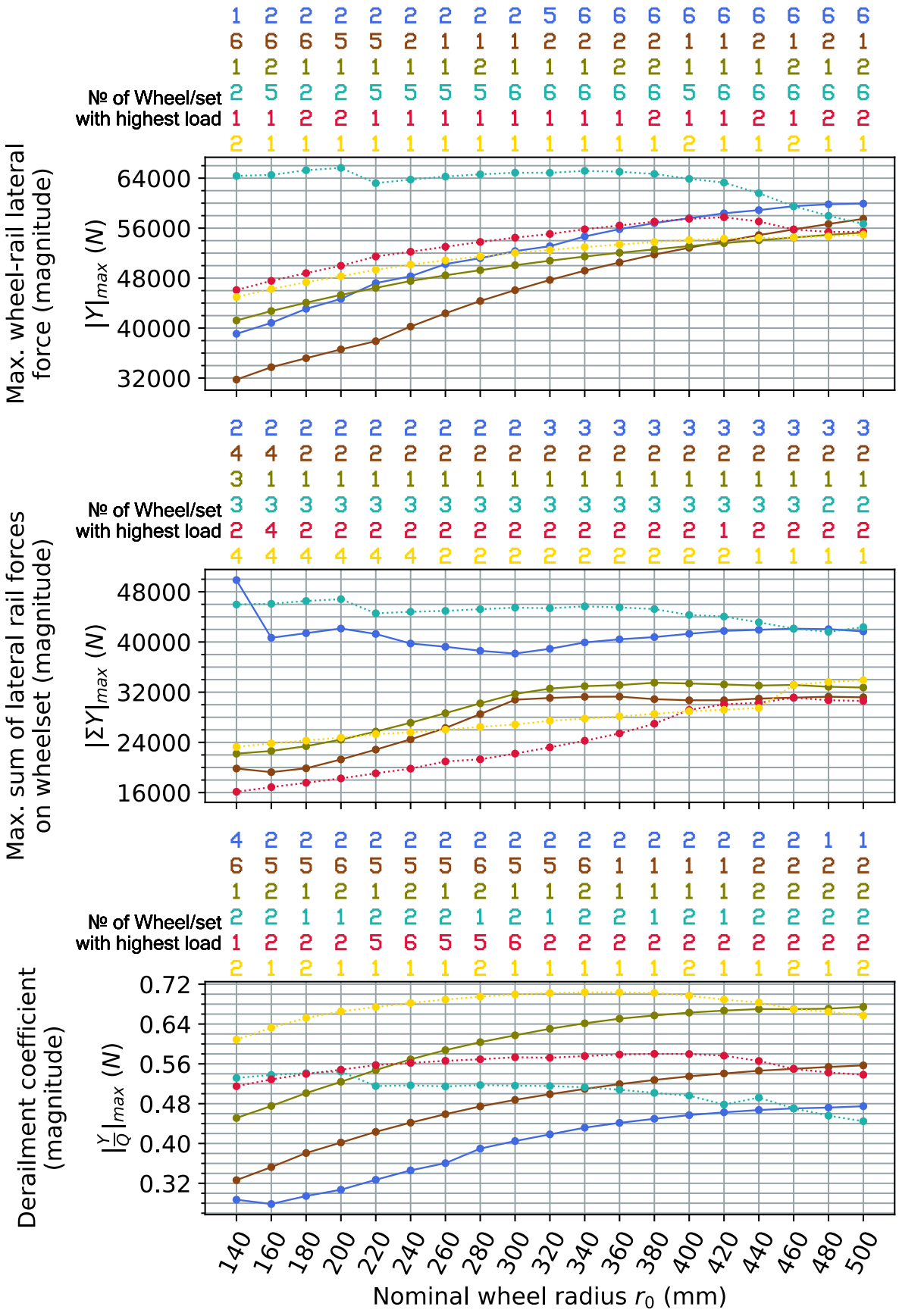

Figure E.27 Laden vehicle on a track with 1435 mm gauge and 1:40 rail cant (reference track setting), CAT4 curve

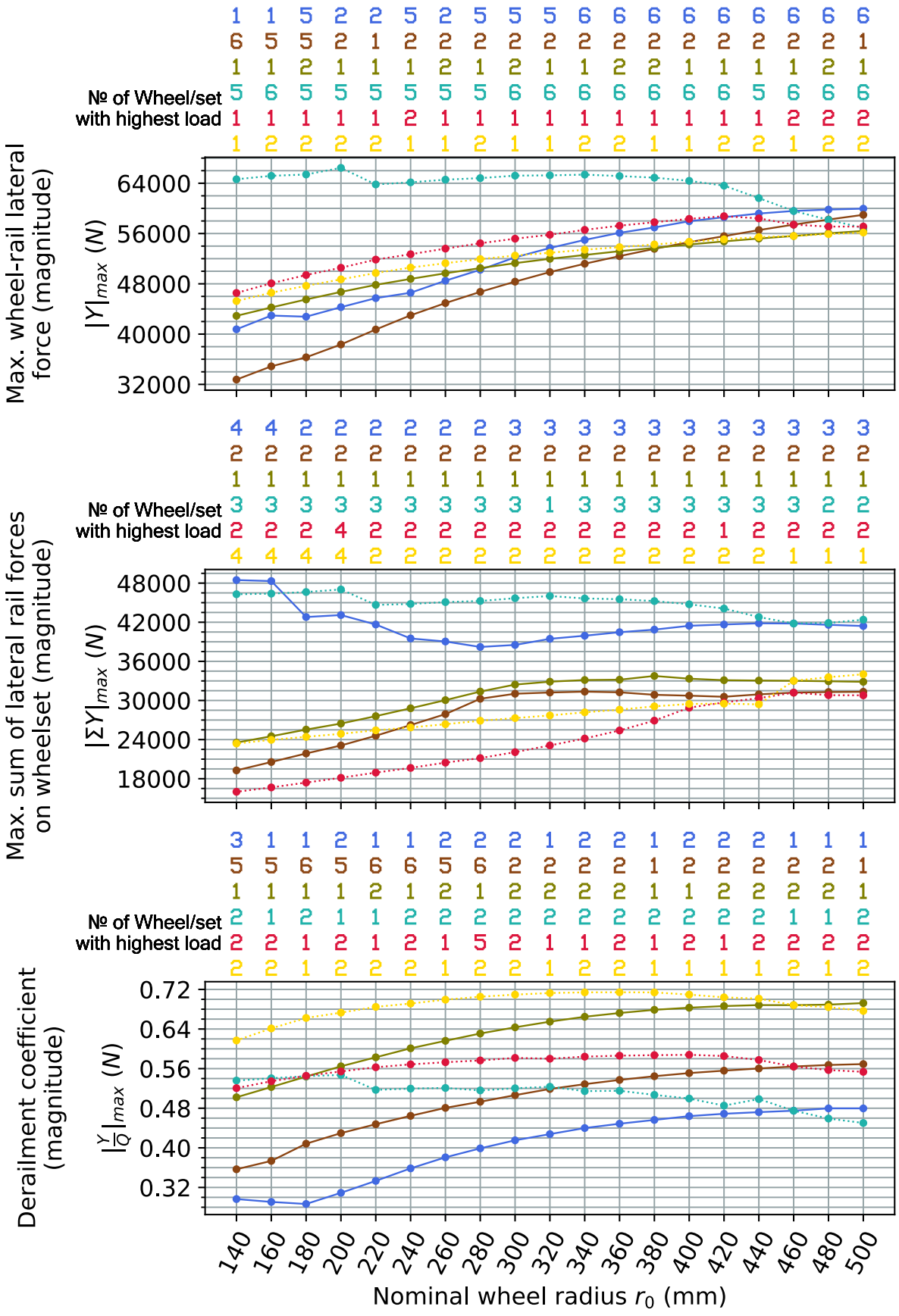

Figure E.28 Laden vehicle on a track with 1432 mm gauge and 1:40 rail cant, CAT4 curve

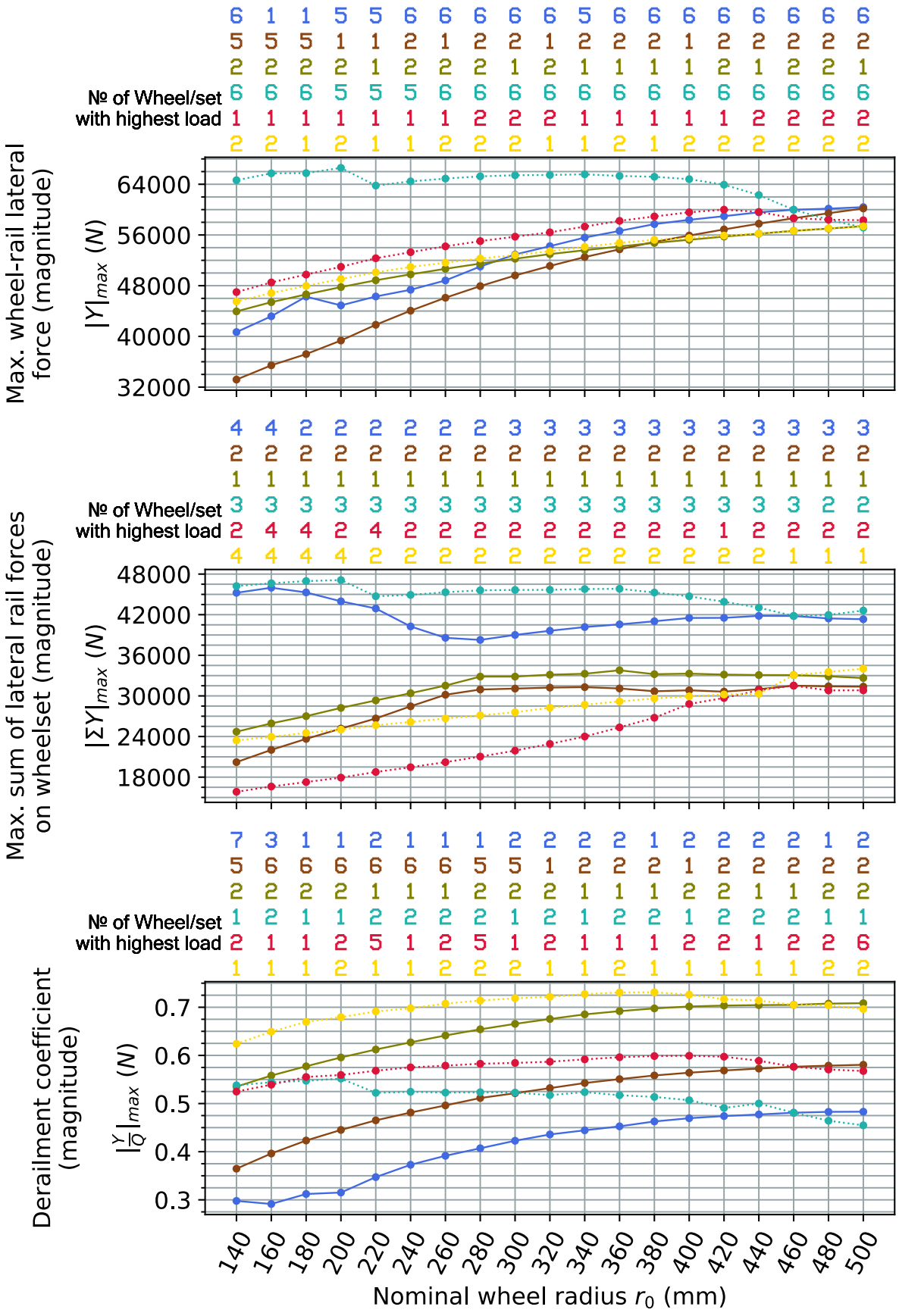

Figure E.29 Laden vehicle on a track with 1430 mm gauge and 1:40 rail cant, CAT4 curve

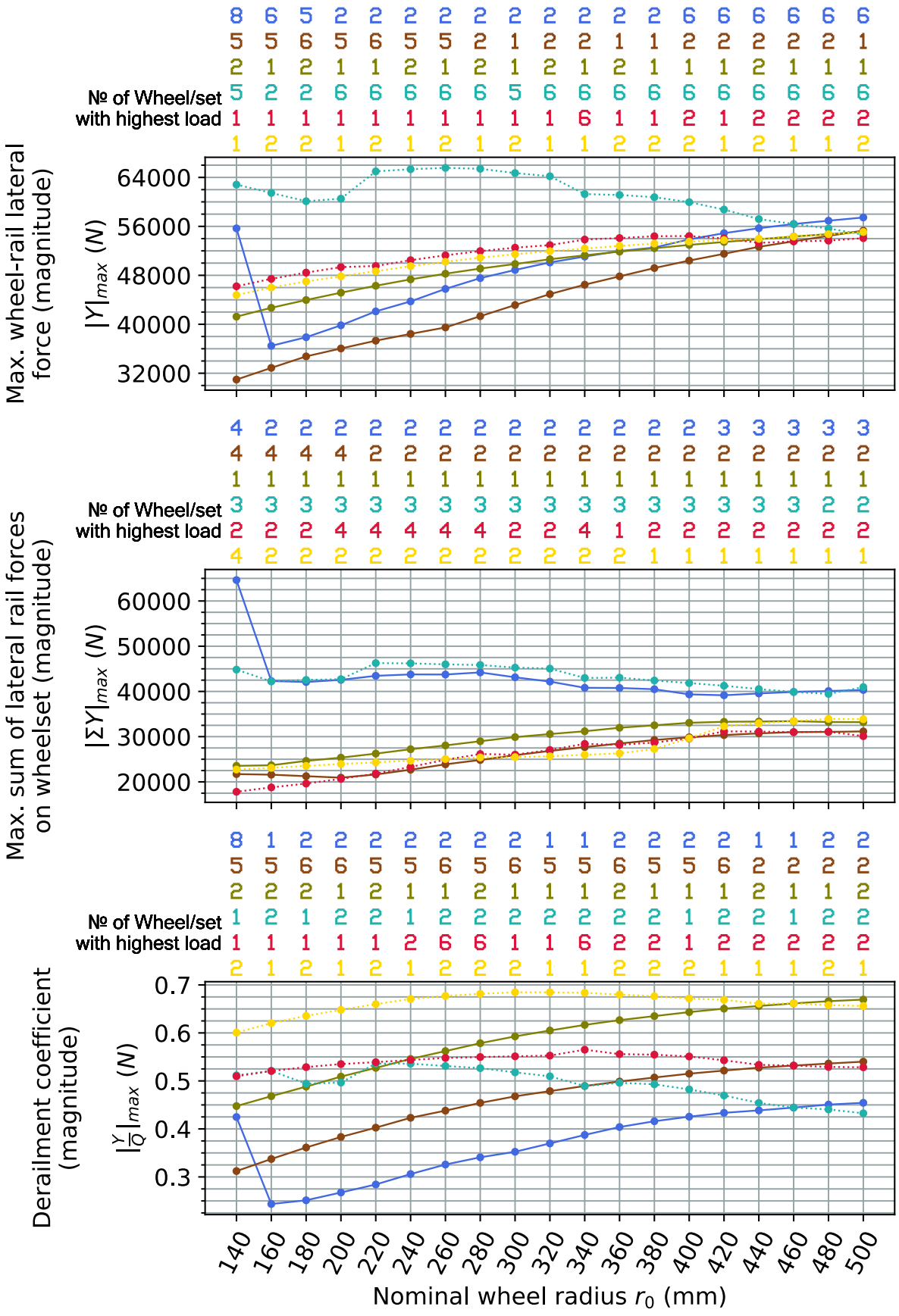

Figure E.30 Laden vehicle on a track with 1437 mm gauge and no rail cant, CAT4 curve

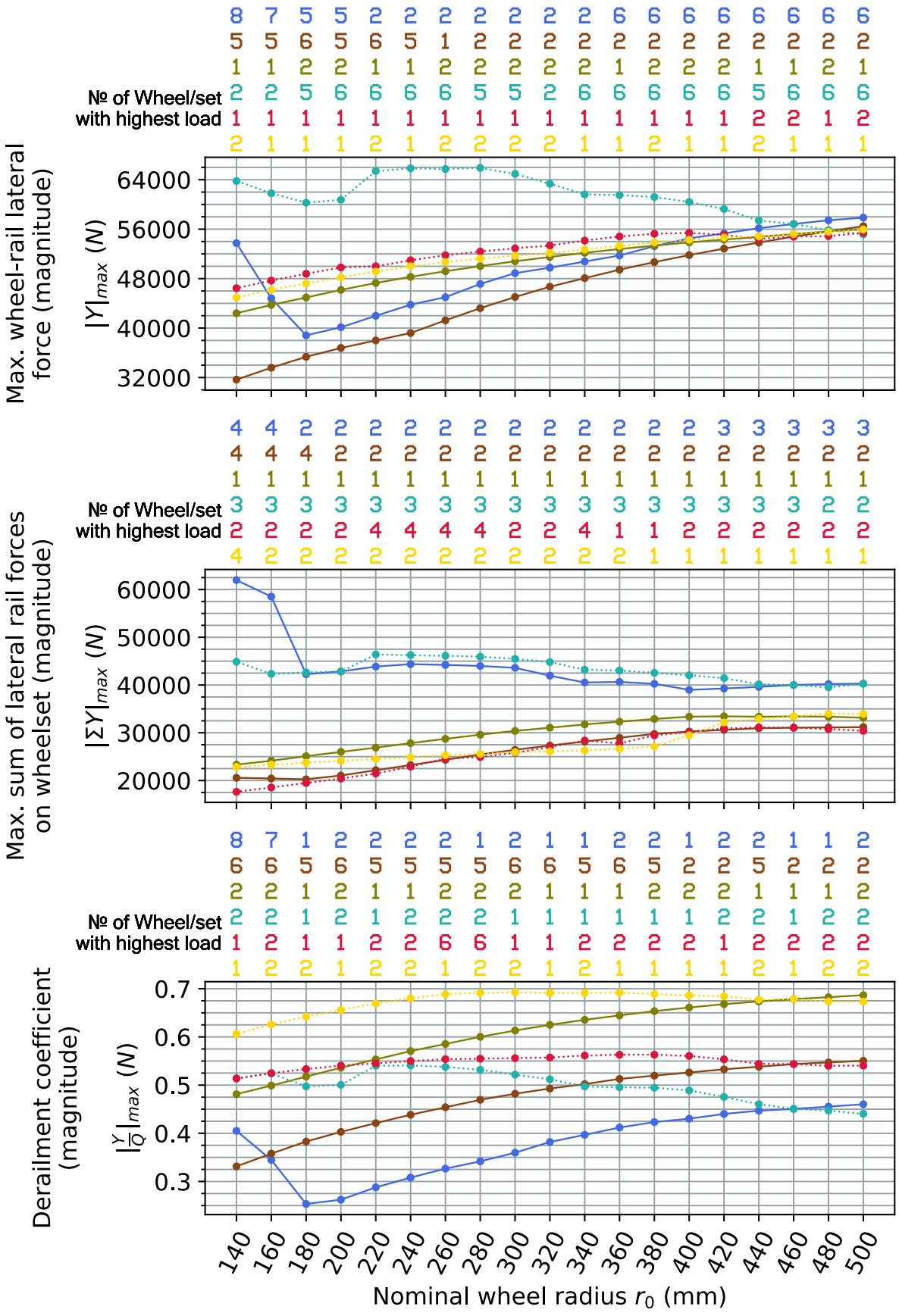

Figure E.31 Laden vehicle on a track with 1435 mm gauge and no rail cant, CAT4 curve

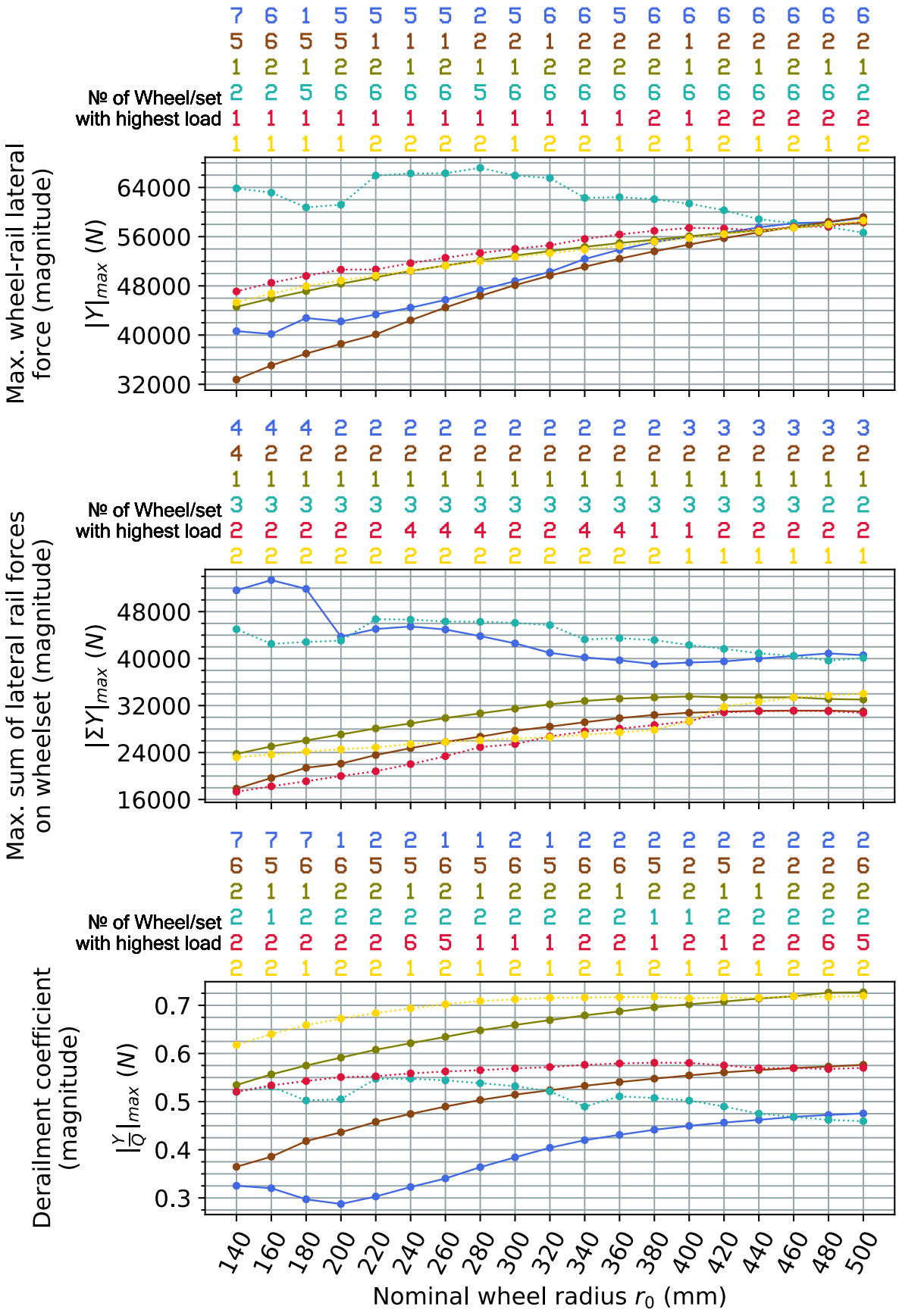

Figure E.32 Laden vehicle on a track with 1432 mm gauge and no rail cant, CAT4 curve

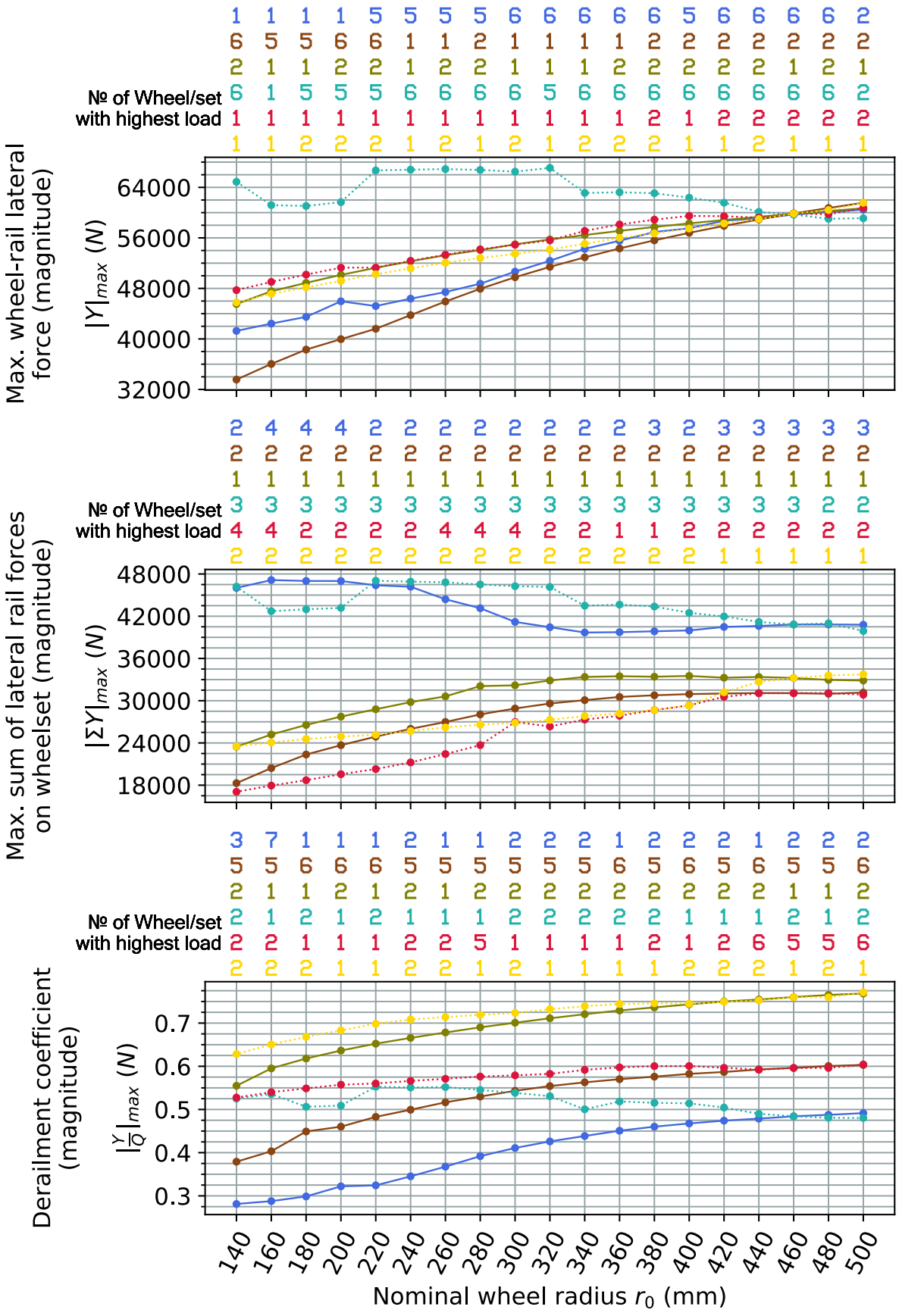

Figure E.33 Laden vehicle on a track with 1430 mm gauge and no rail cant, CAT4 curve

Appendix F Curve negotiation simulation results with wheel profile modification case INV

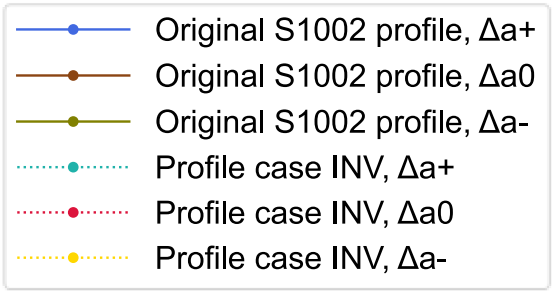

Figure F.1 Legend of all plots in this appendix

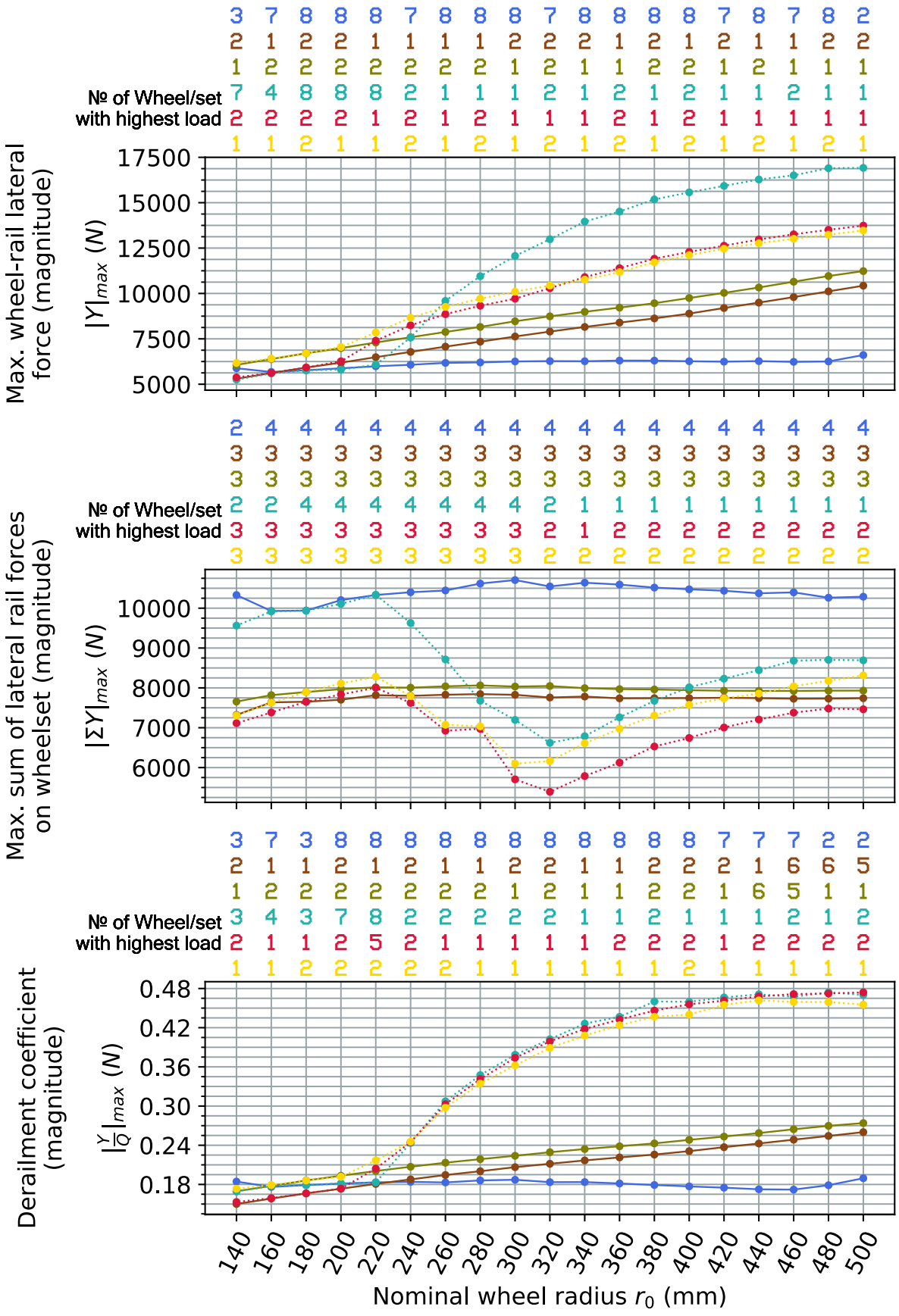

Figure F.2 Tare vehicle on a track with 1437 mm gauge and 1:40 rail cant, CAT2 curve

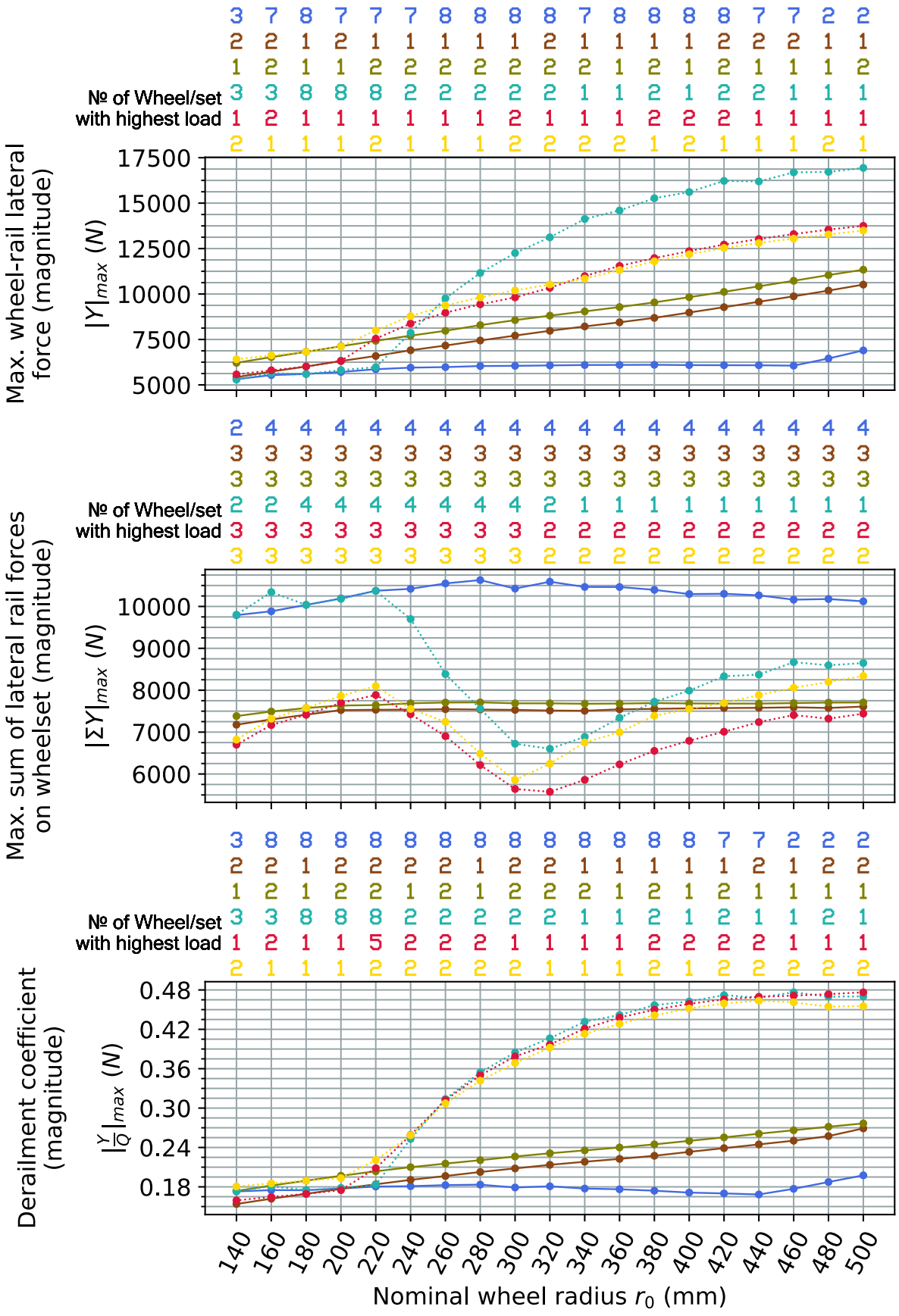

Figure F.3 Tare vehicle on a track with 1435 mm gauge and 1:40 rail cant (reference track setting), CAT2 curve

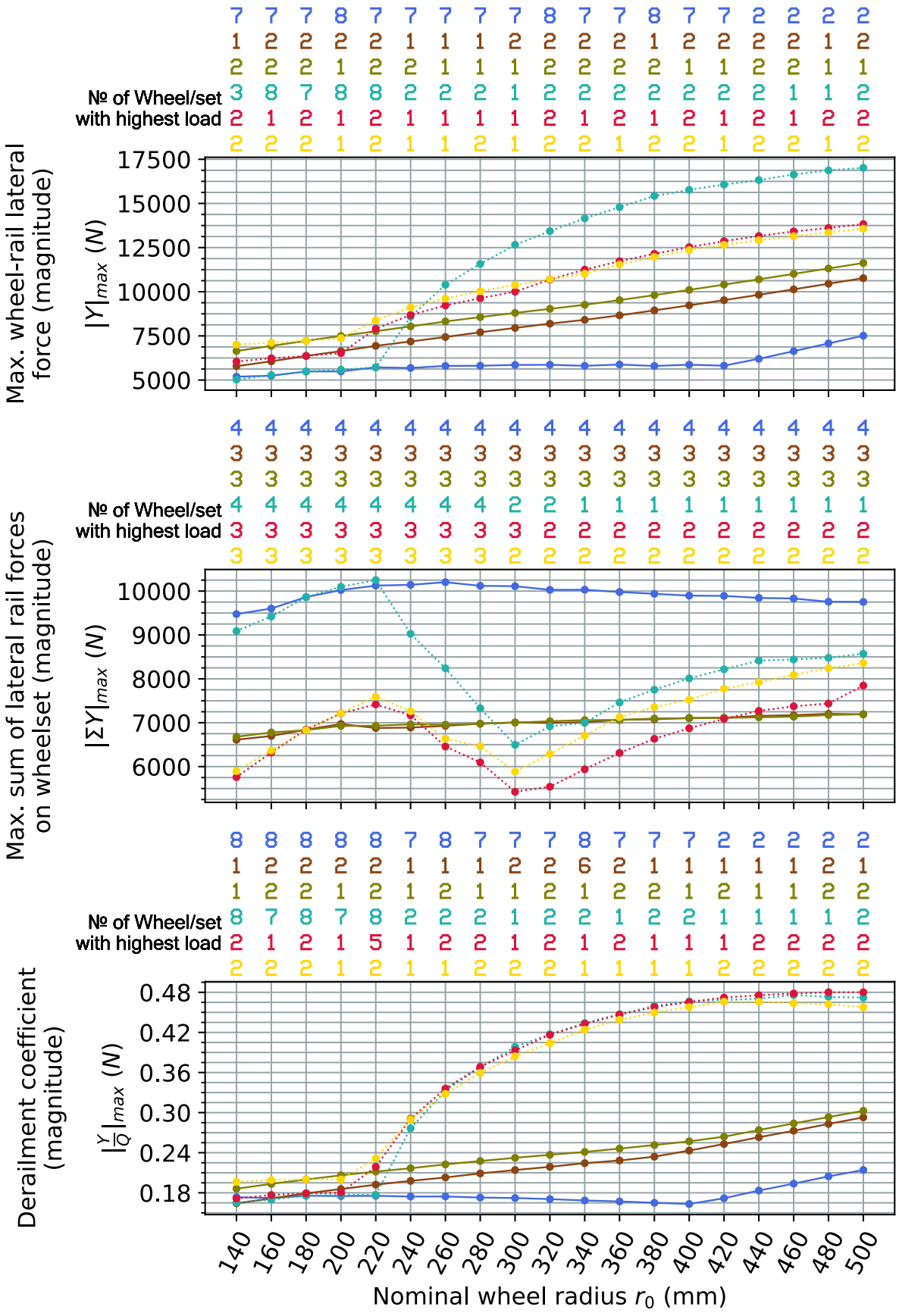

Figure F.4 Tare vehicle on a track with 1432 mm gauge and 1:40 rail cant, CAT2 curve

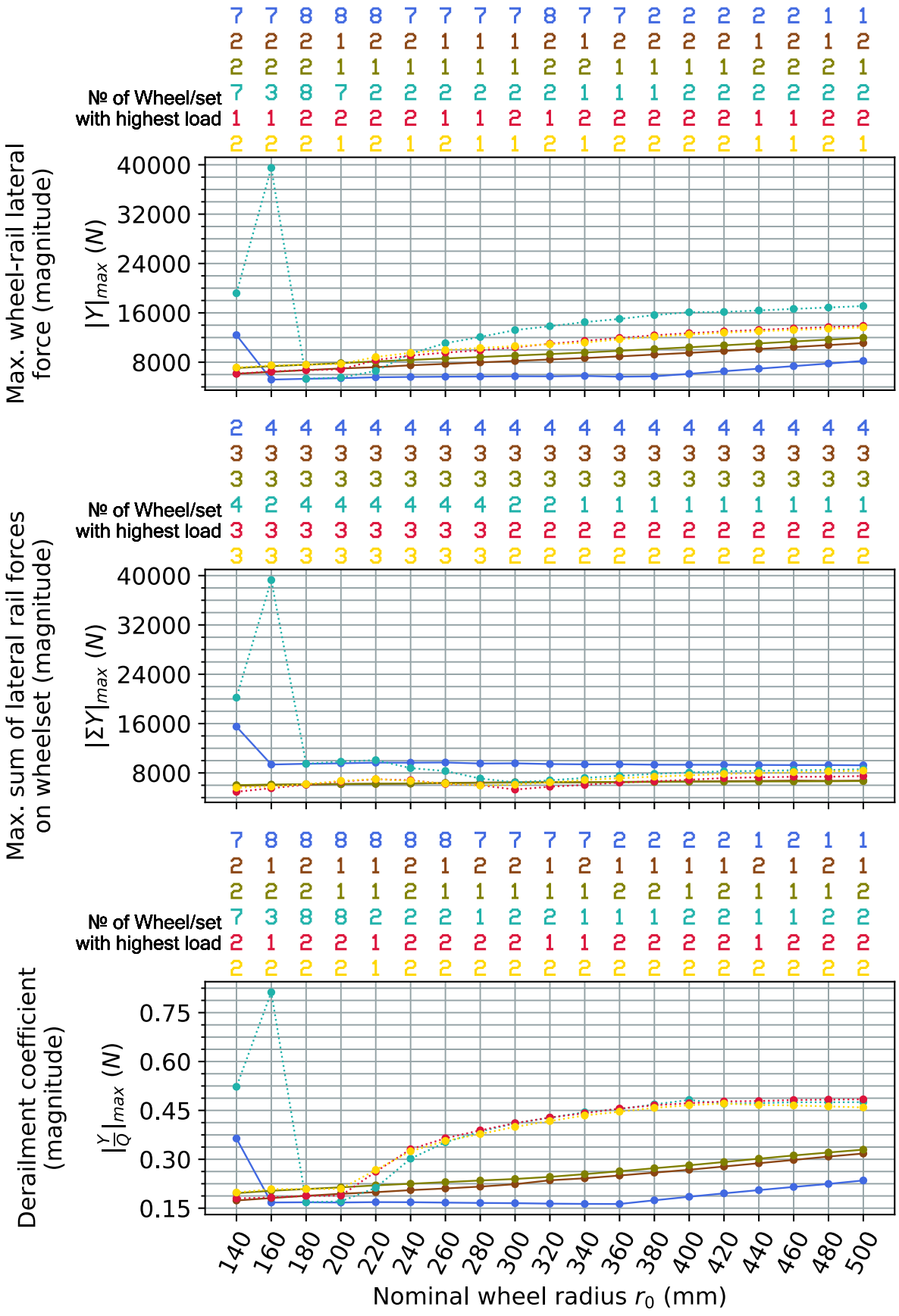

Figure F.5 Tare vehicle on a track with 1430 mm gauge and 1:40 rail cant, CAT2 curve

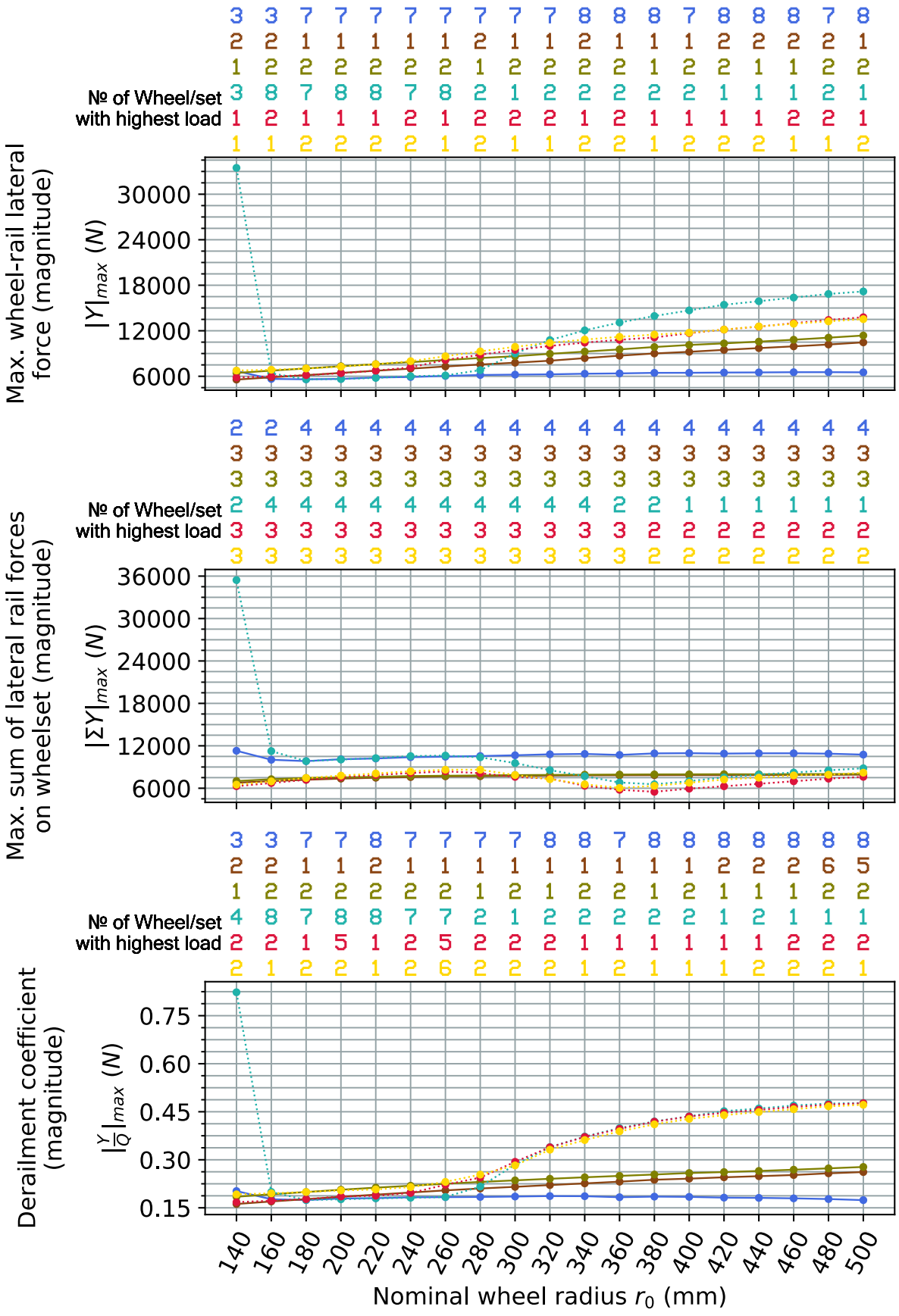

Figure F.6 Tare vehicle on a track with 1437 mm gauge and no rail cant, CAT2 curve

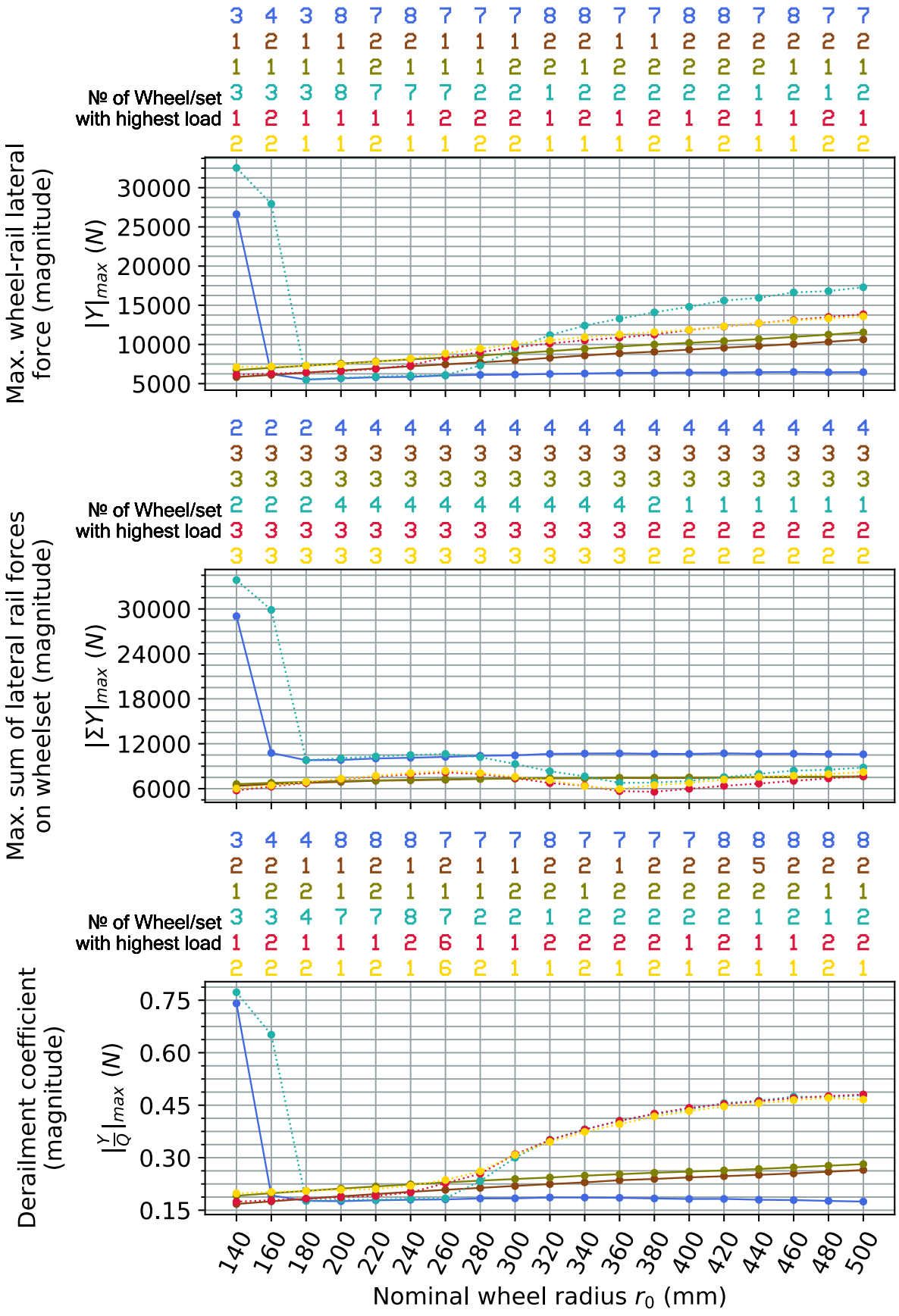

Figure F.7 Tare vehicle on a track with 1435 mm gauge and no rail cant, CAT2 curve

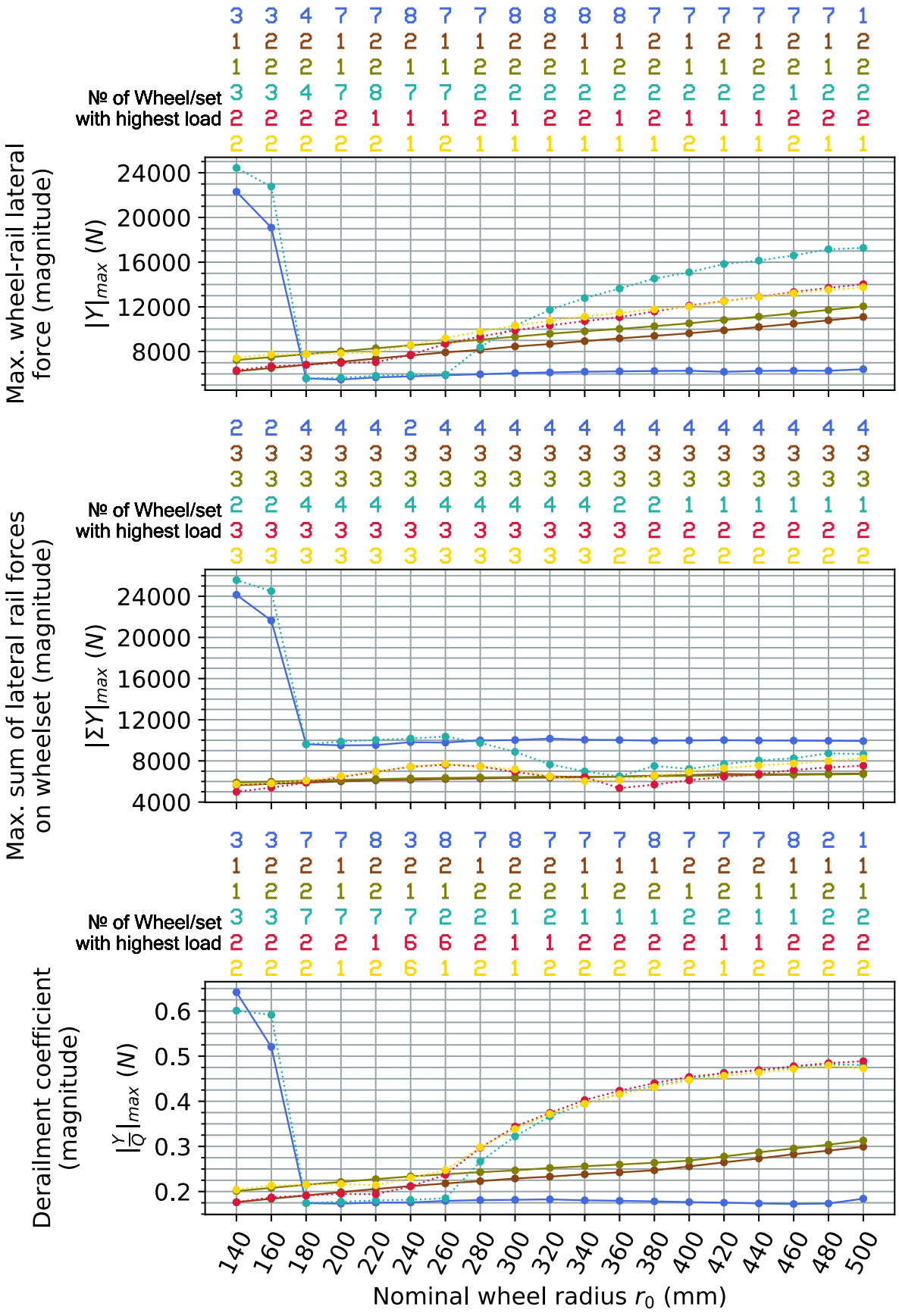

Figure F.8 Tare vehicle on a track with 1432 mm gauge and no rail cant, CAT2 curve

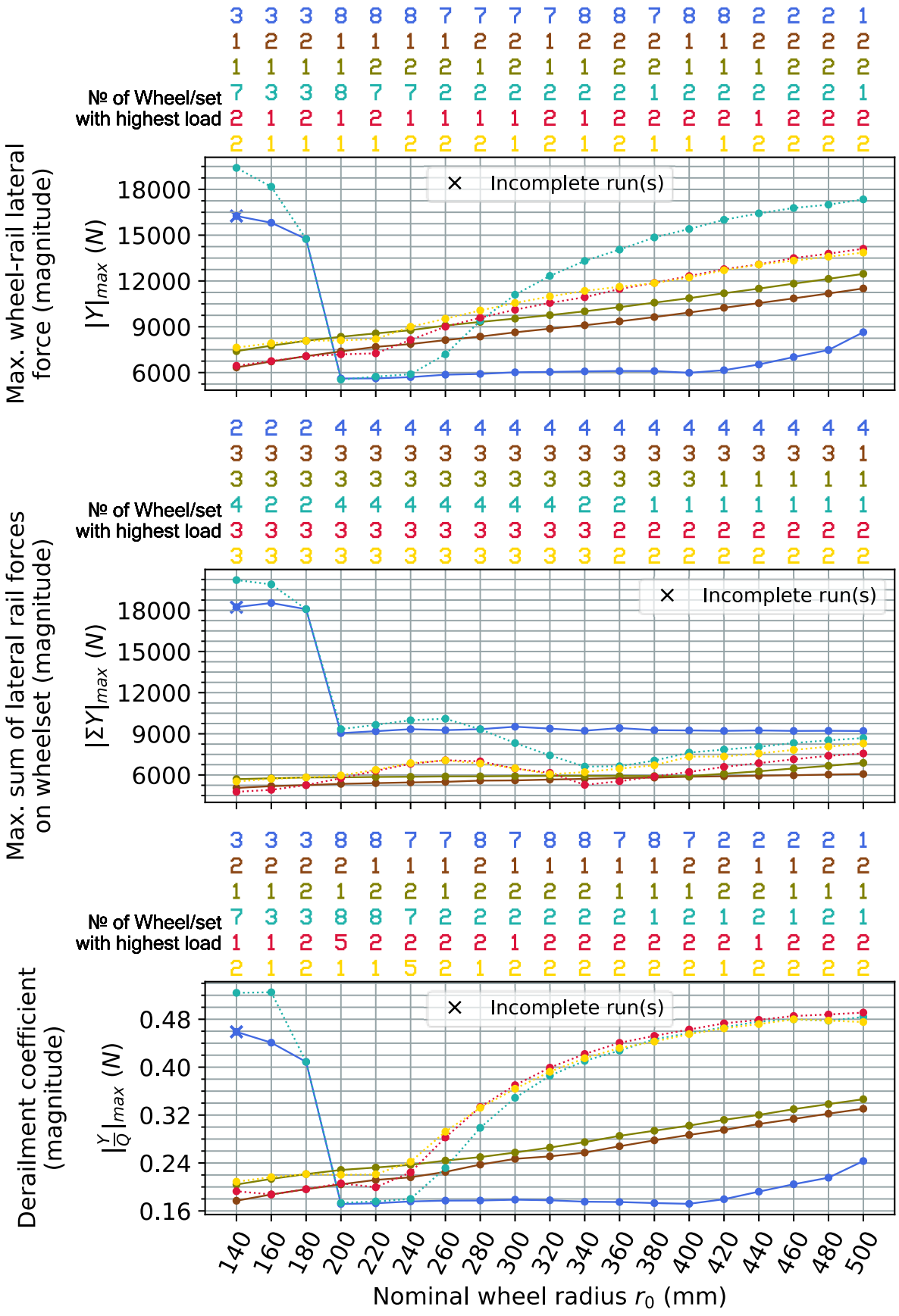

Figure F.9 Tare vehicle on a track with 1430 mm gauge and no rail cant, CAT2 curve

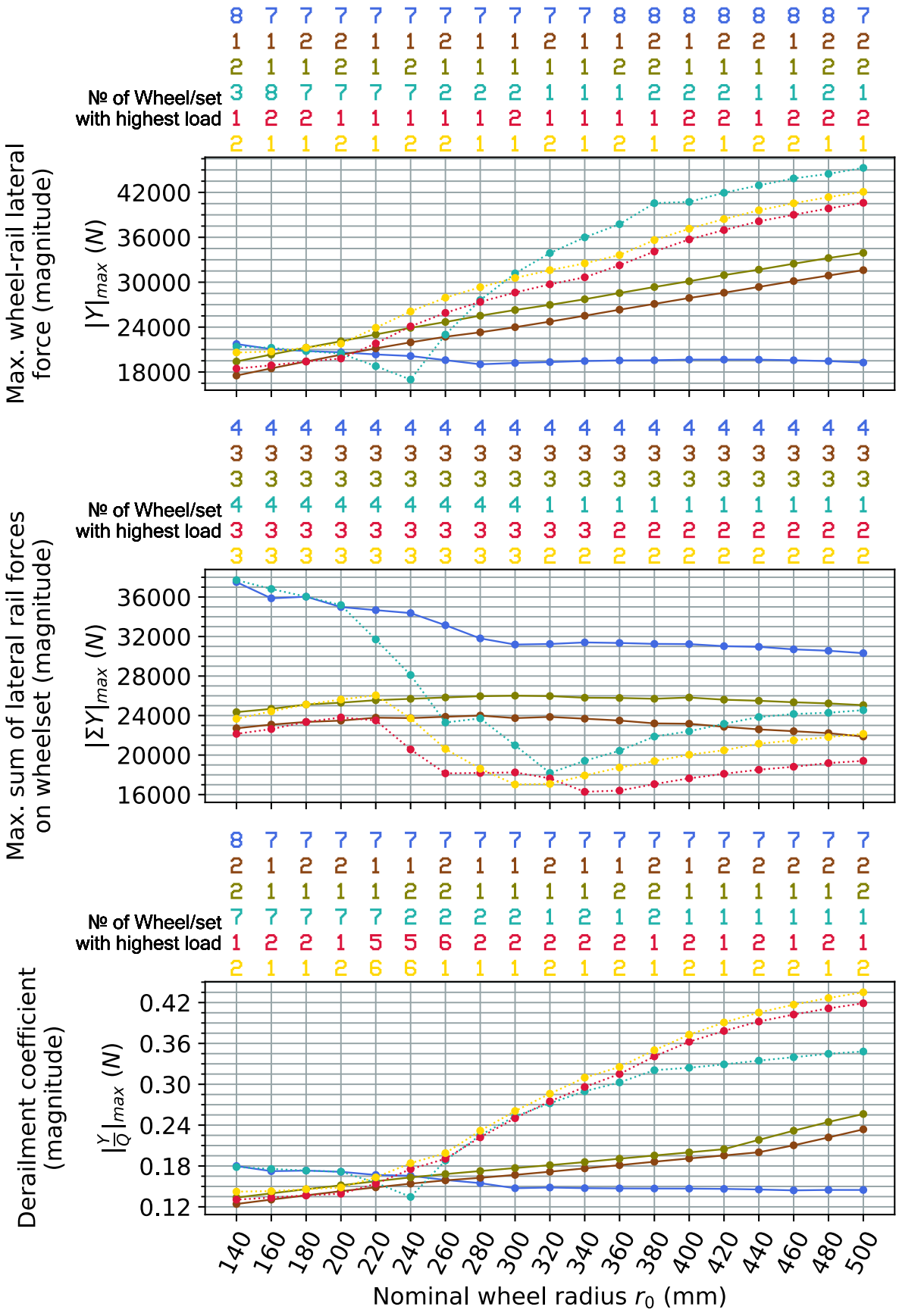

Figure F.10 Laden vehicle on a track with 1437 mm gauge and 1:40 rail cant, CAT2 curve

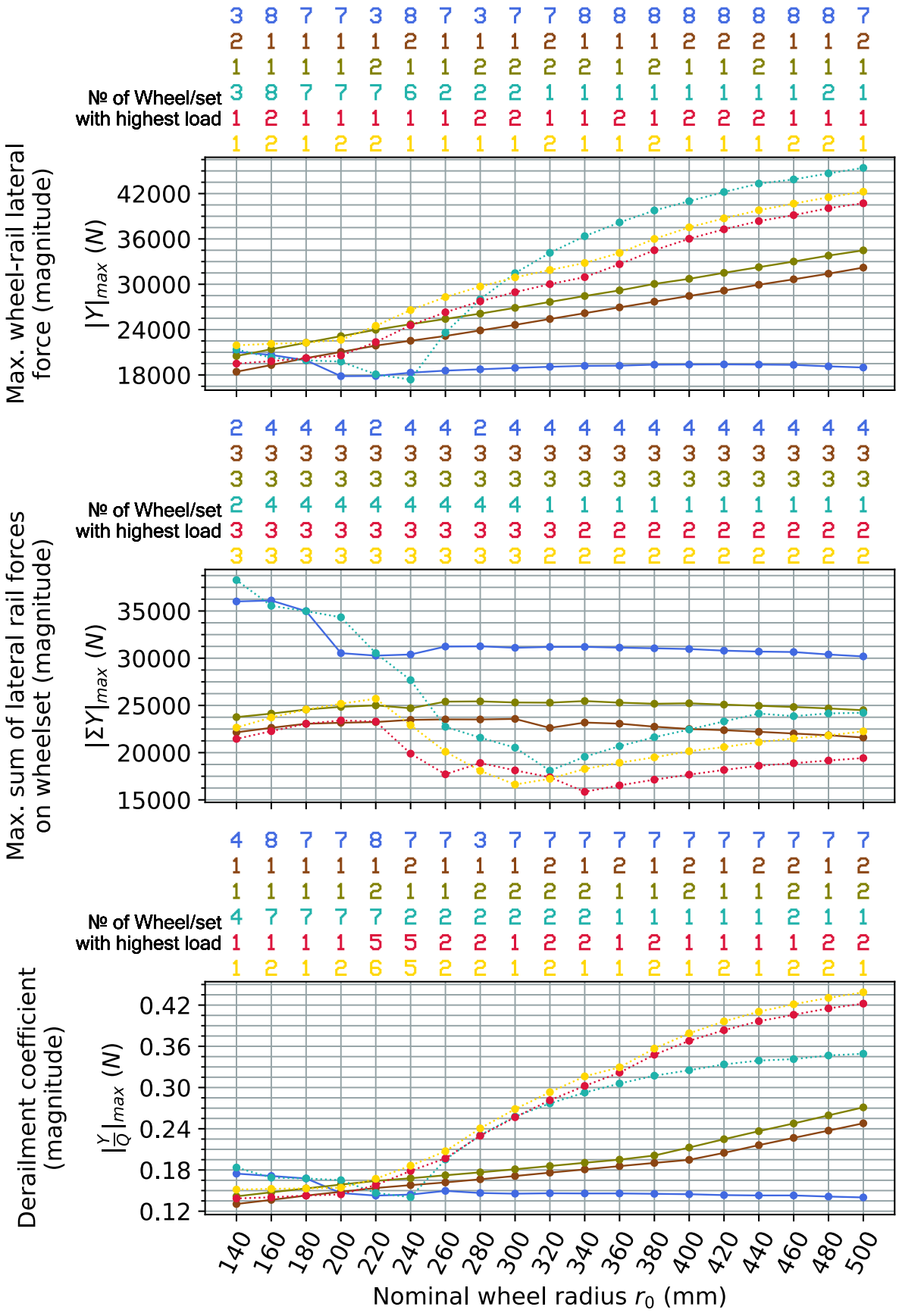

Figure F.11 Laden vehicle on a track with 1435 mm gauge and 1:40 rail cant (reference track setting), CAT2 curve

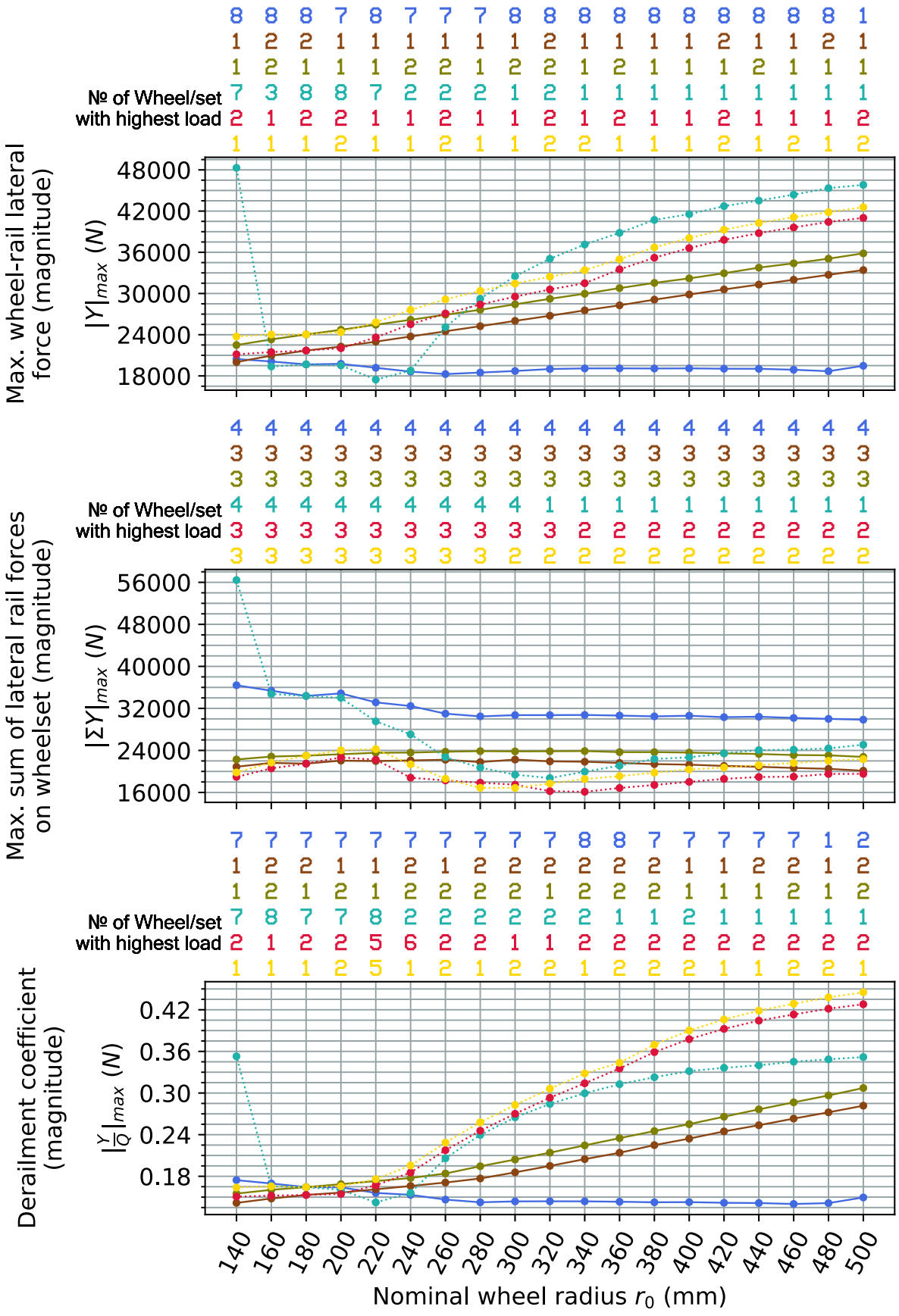

Figure F.12 Laden vehicle on a track with 1432 mm gauge and 1:40 rail cant, CAT2 curve

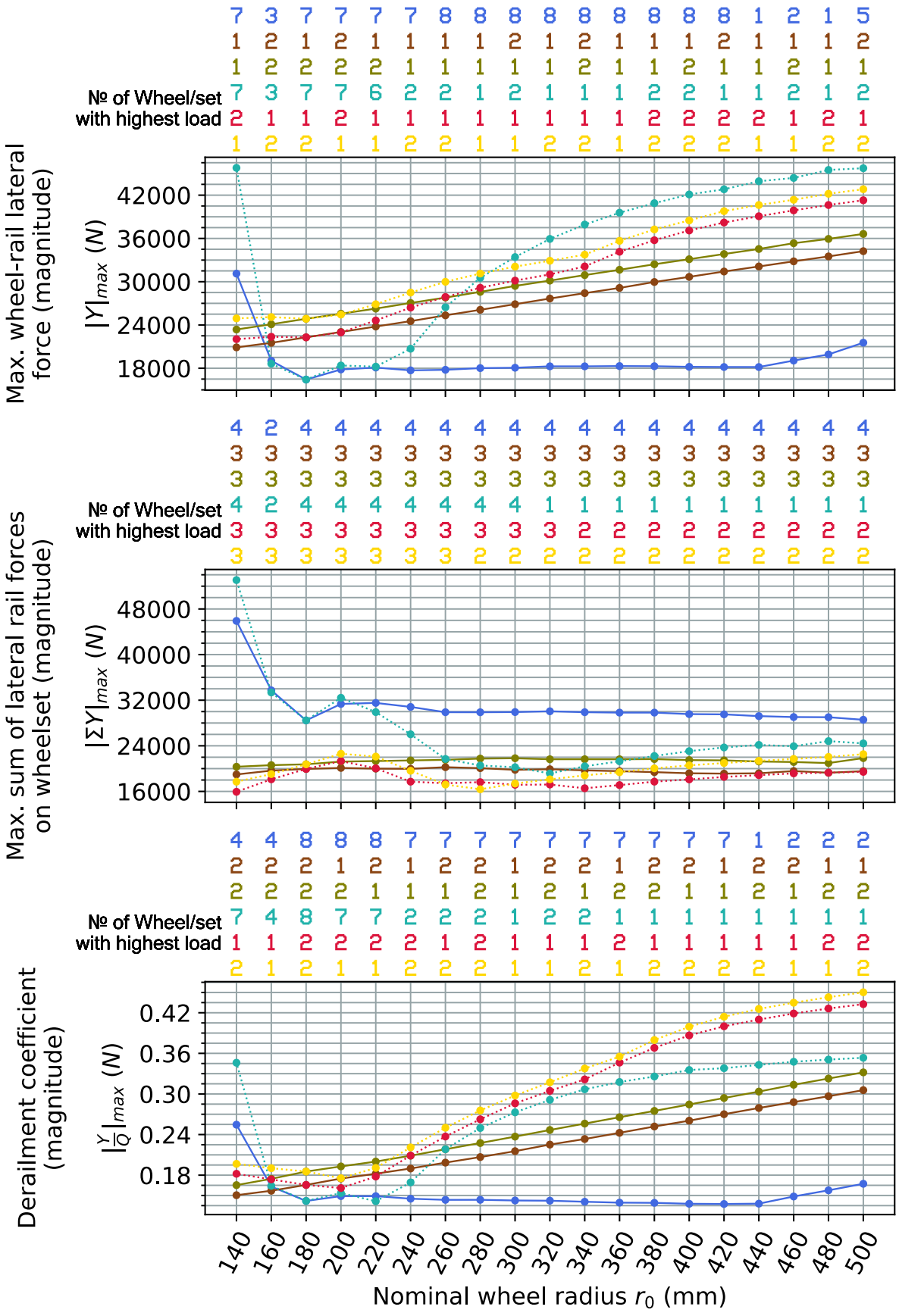

Figure F.13 Laden vehicle on a track with 1430 mm gauge and 1:40 rail cant, CAT2 curve

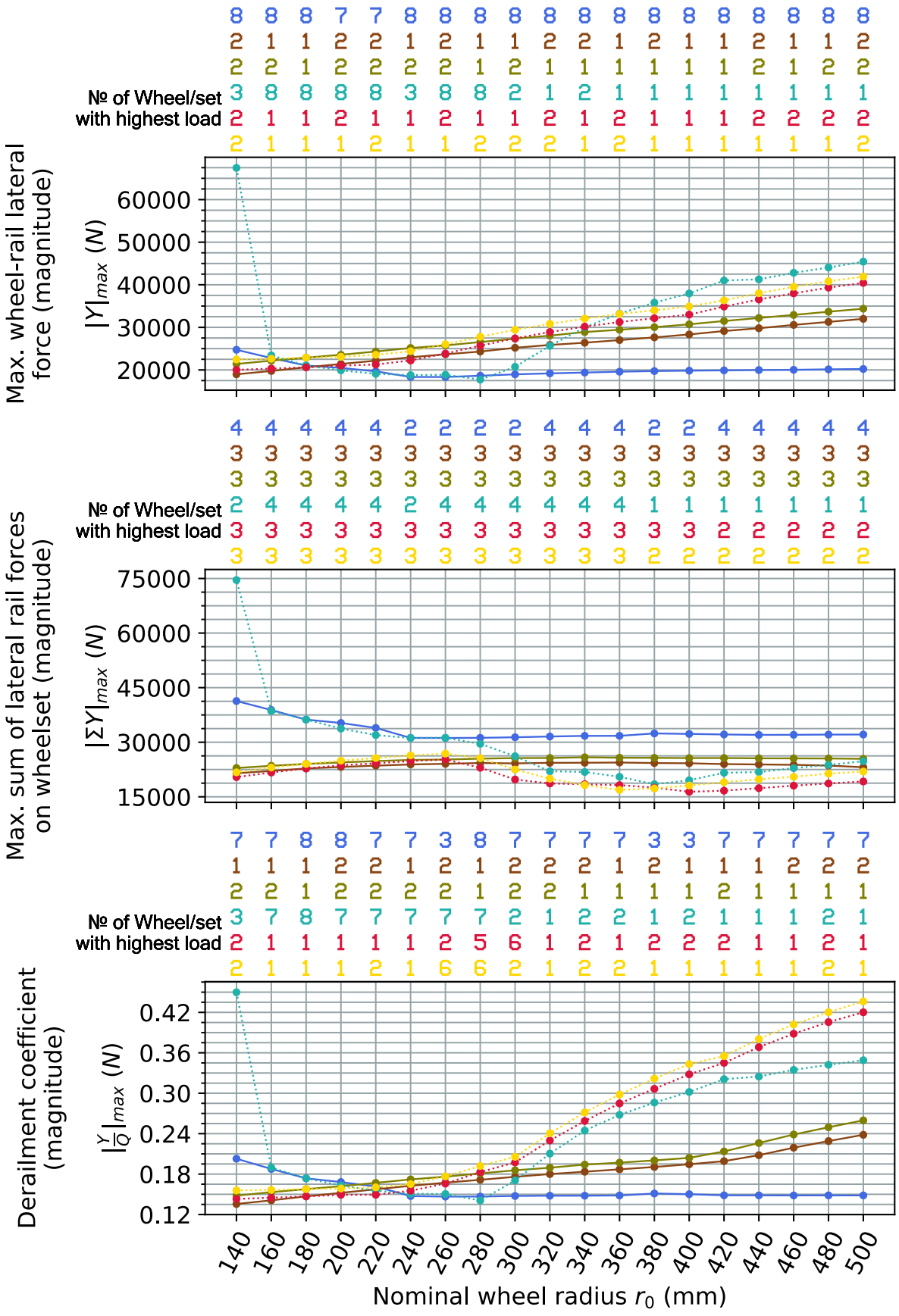

Figure F.14 Laden vehicle on a track with 1437 mm gauge and no rail cant, CAT2 curve

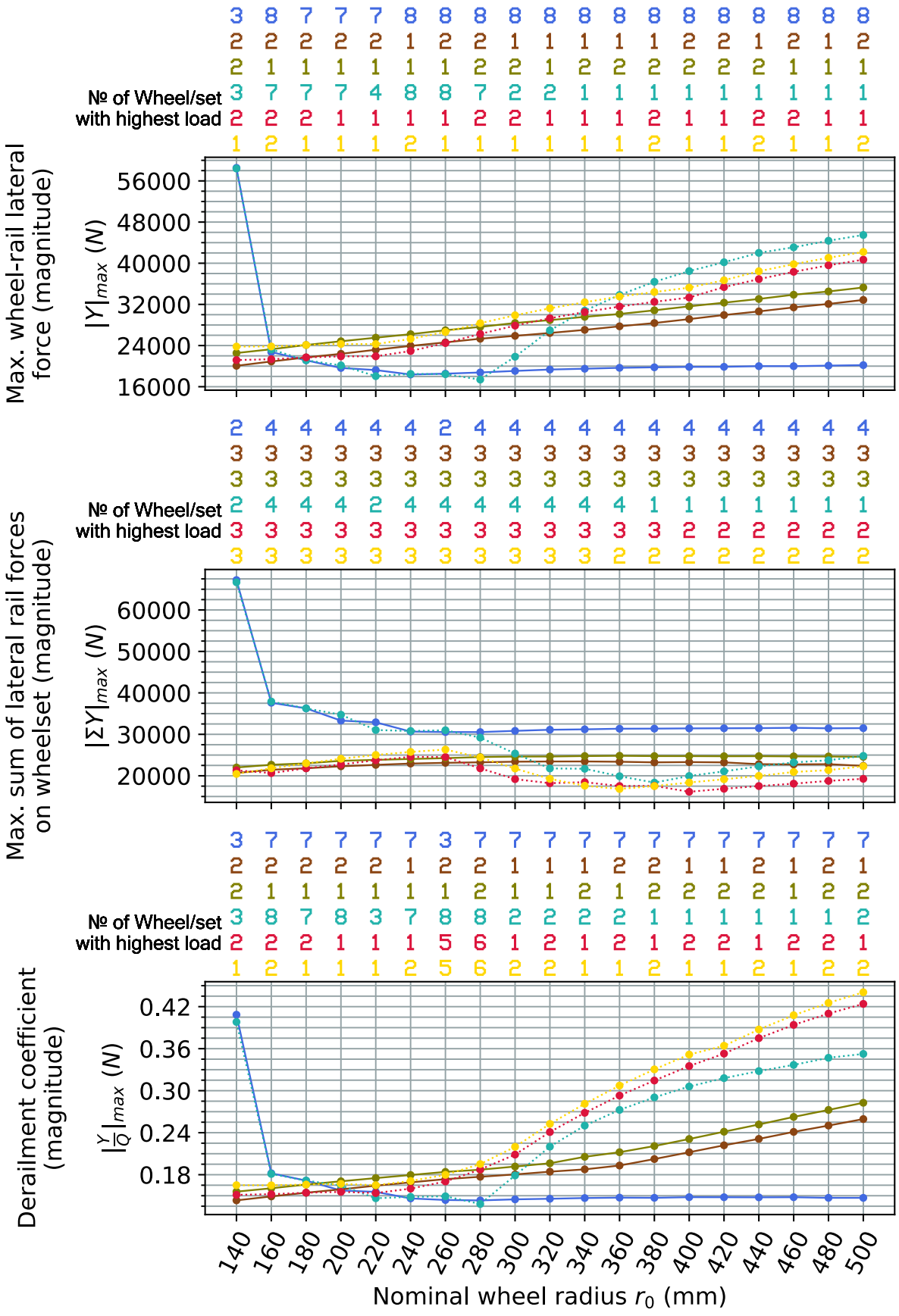

Figure F.15 Laden vehicle on a track with 1435 mm gauge and no rail cant, CAT2 curve

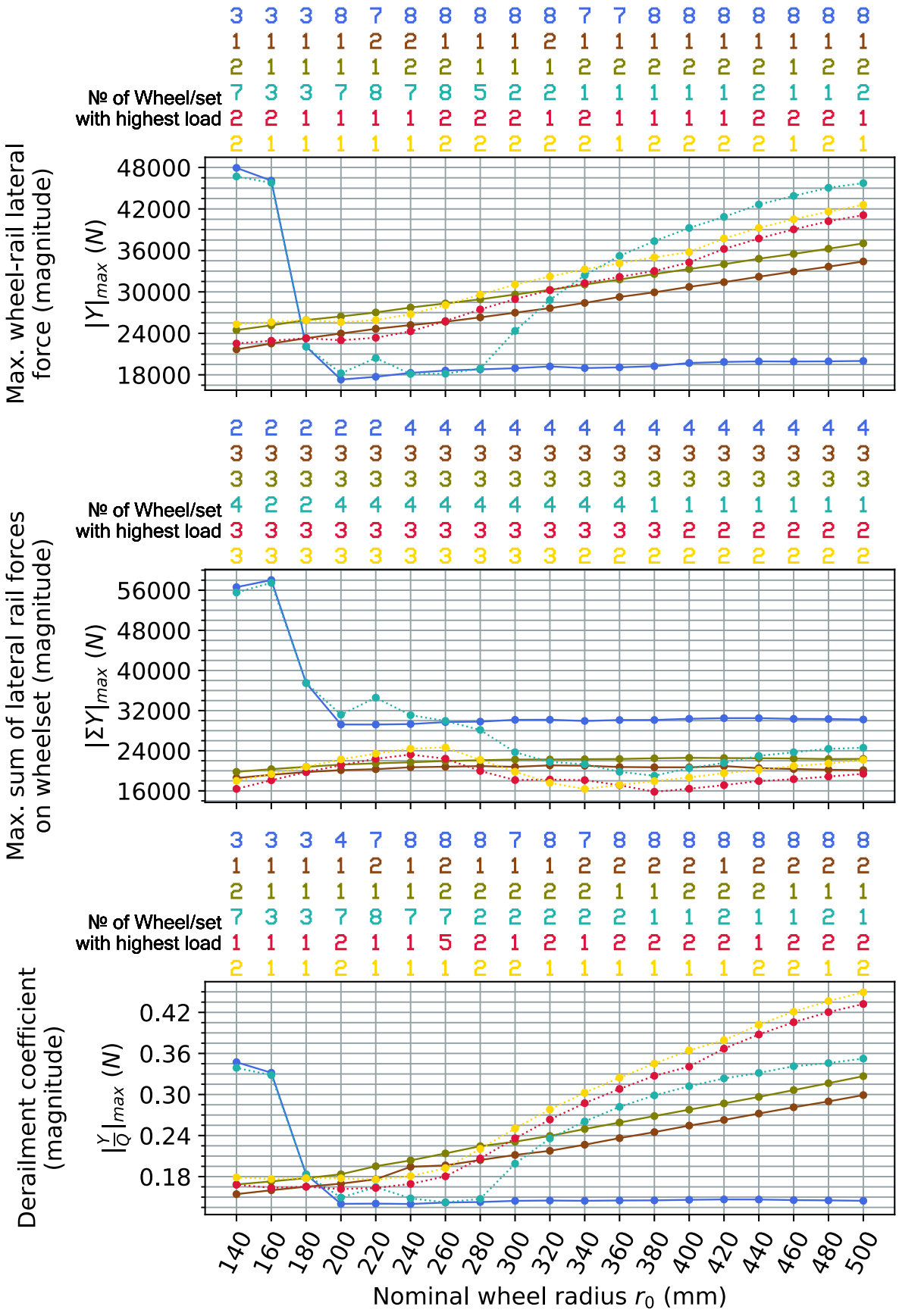

Figure F.16 Laden vehicle on a track with 1432 mm gauge and no rail cant, CAT2 curve

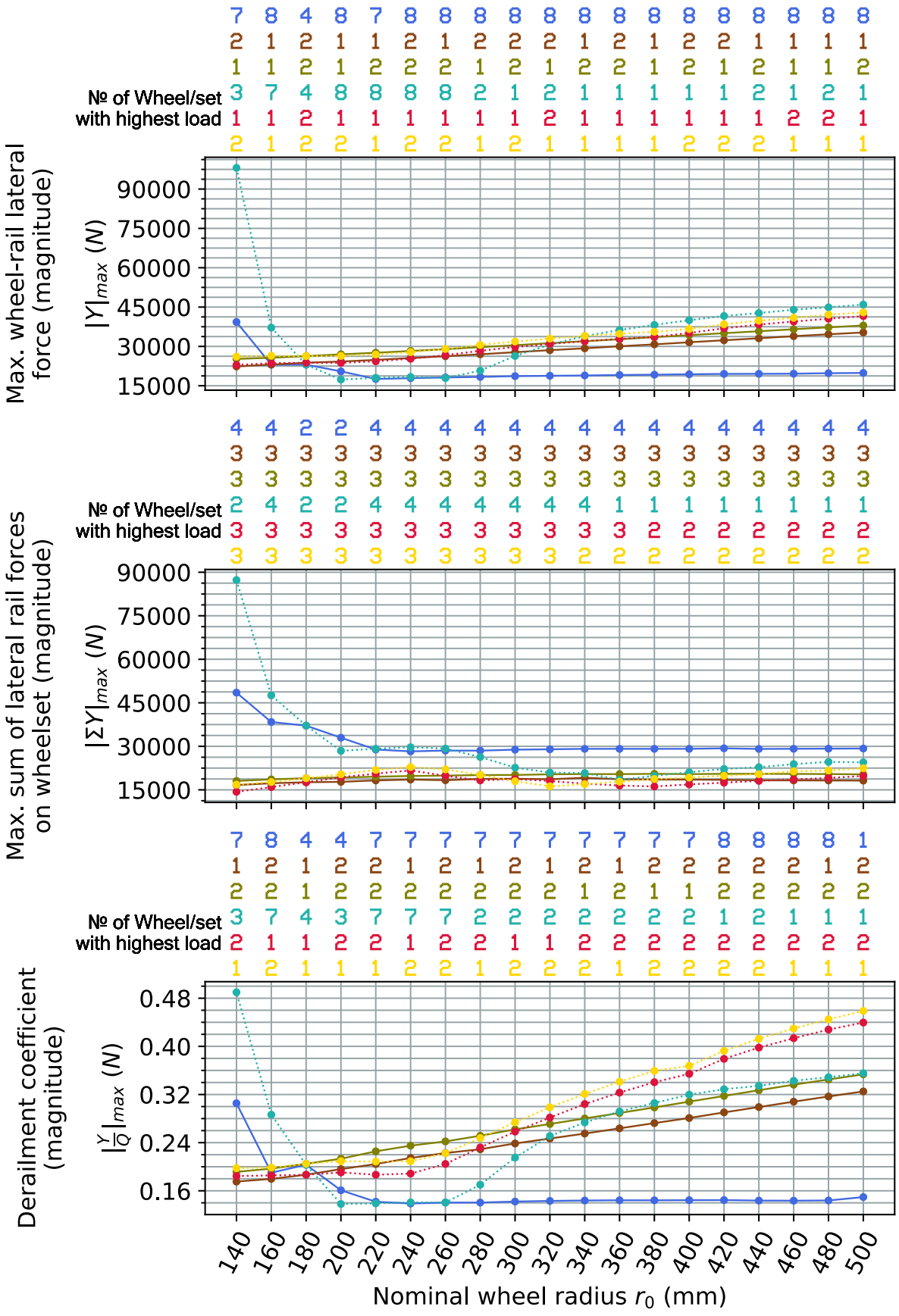

Figure F.17 Laden vehicle on a track with 1430 mm gauge and no rail cant, CAT2 curve

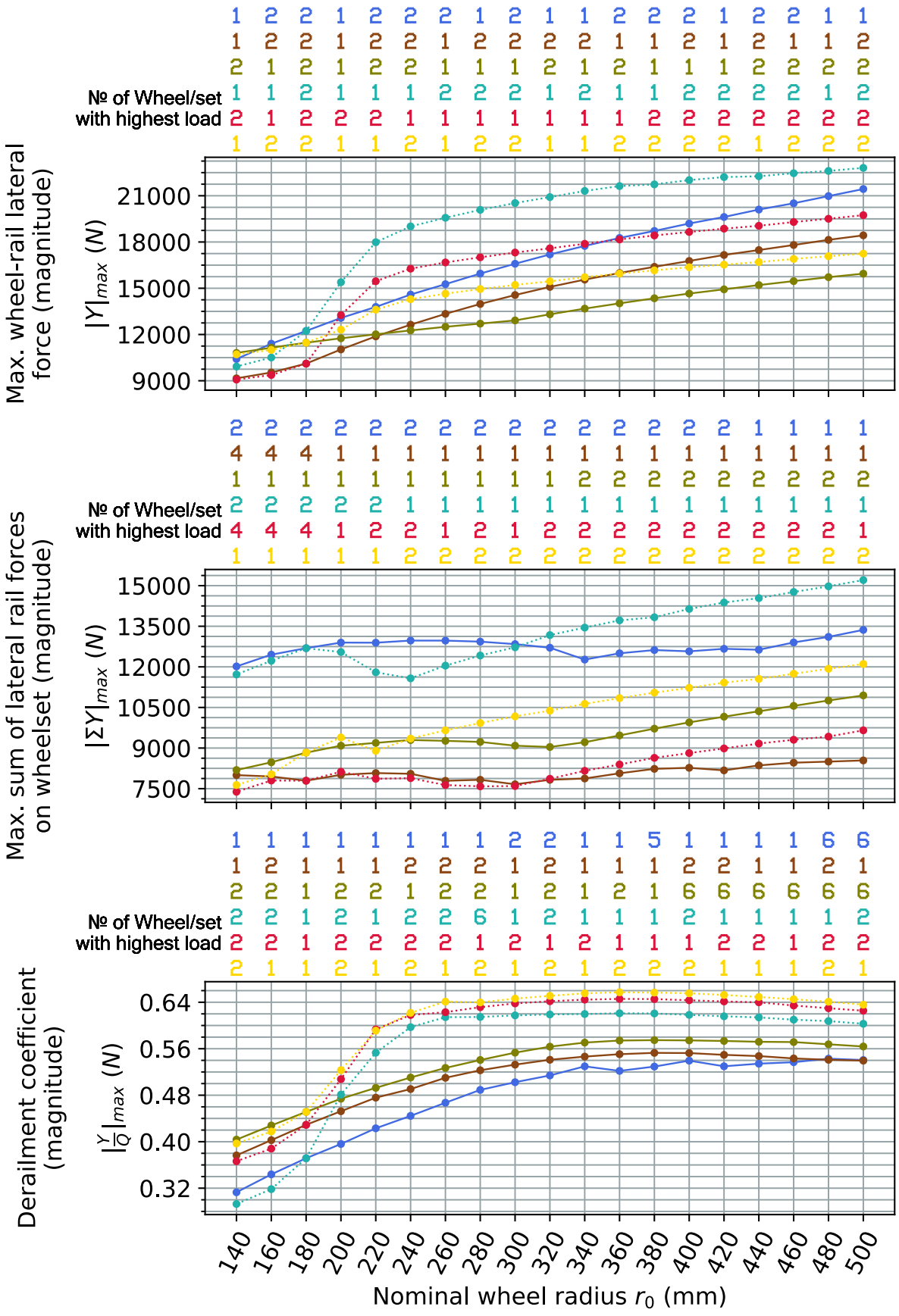

Figure F.18 Tare vehicle on a track with 1437 mm gauge and 1:40 rail cant, CAT4 curve

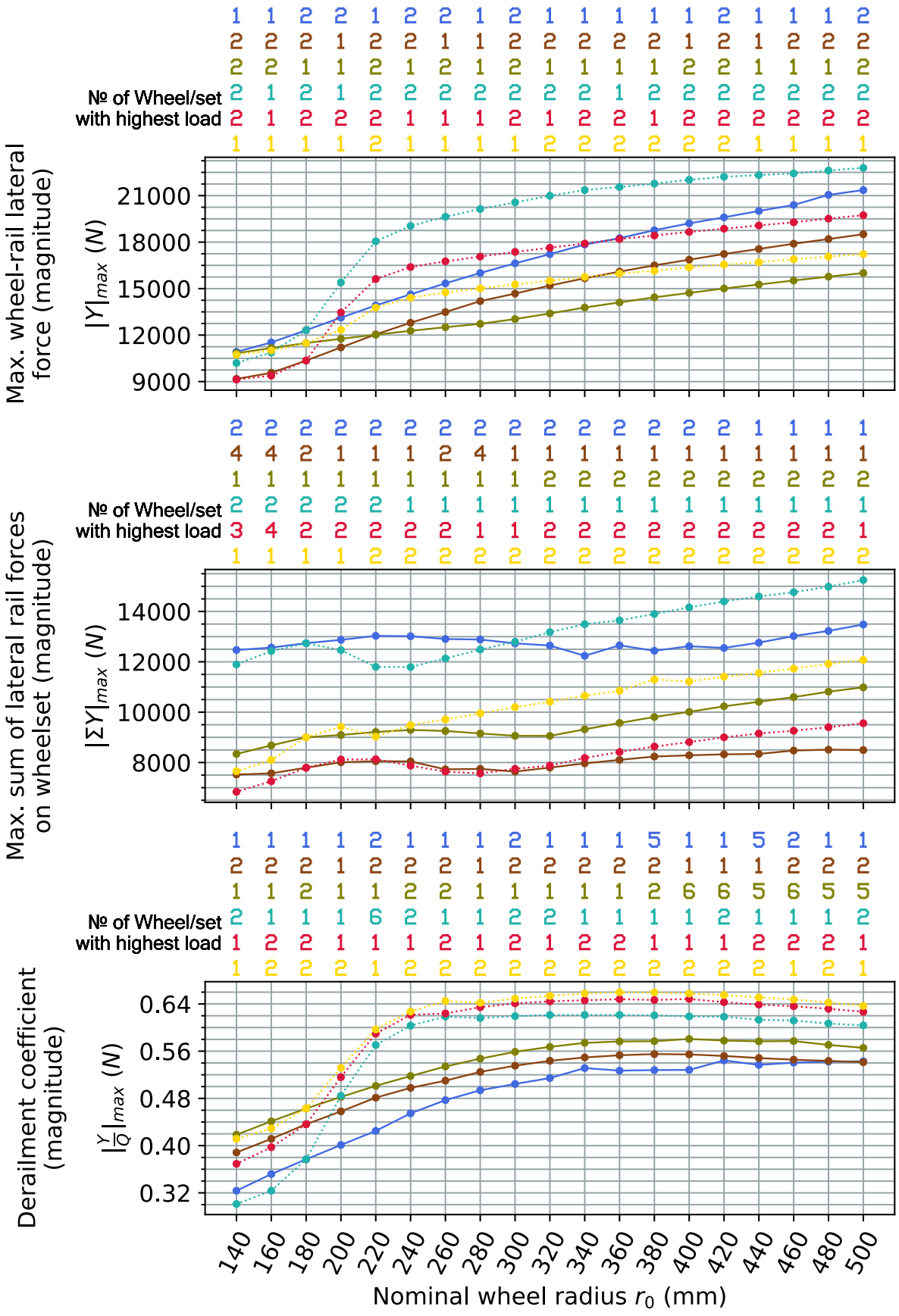

Figure F.19 Tare vehicle on a track with 1435 mm gauge and 1:40 rail cant (reference track setting), CAT4 curve

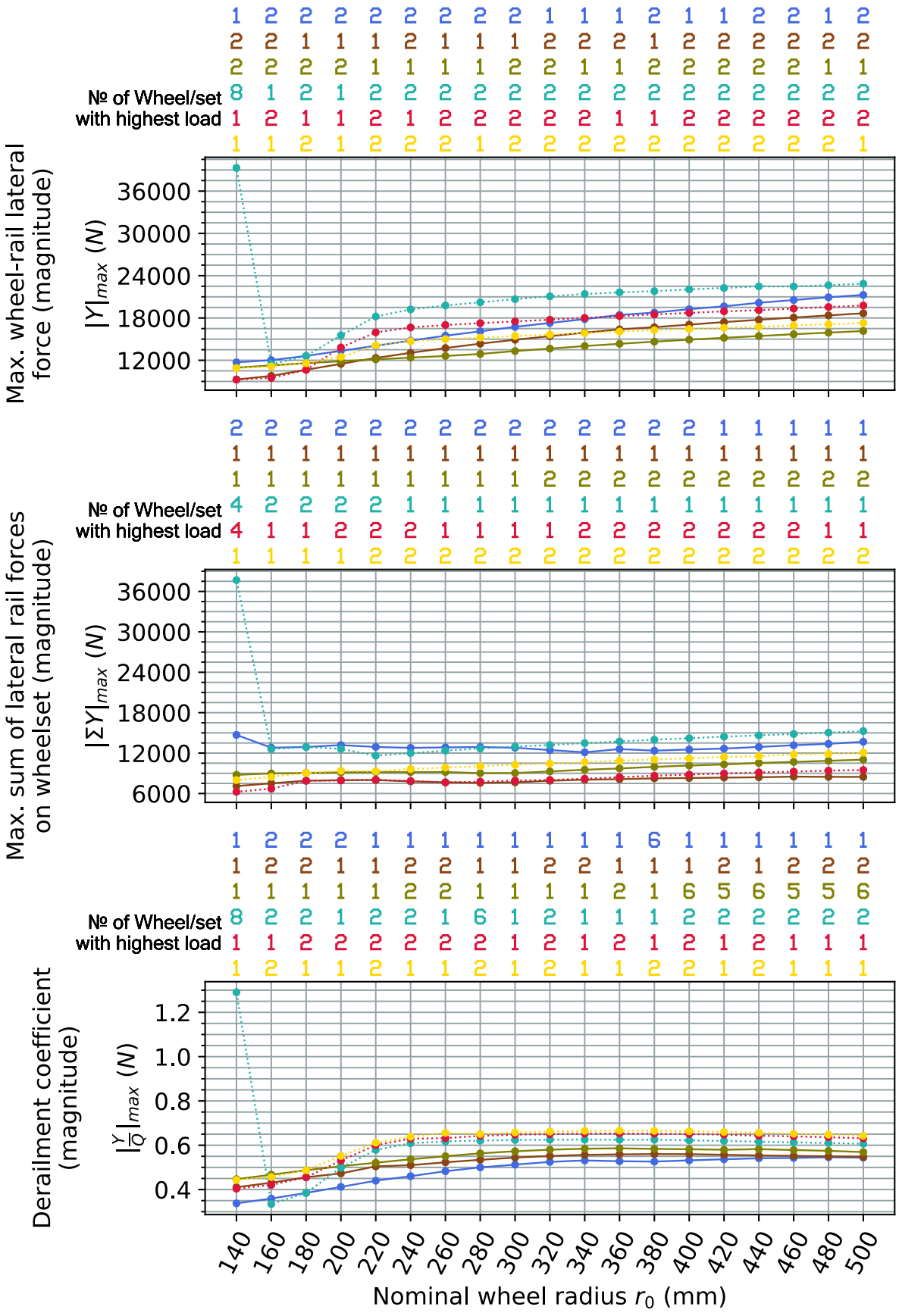

Figure F.20 Tare vehicle on a track with 1432 mm gauge and 1:40 rail cant, CAT4 curve

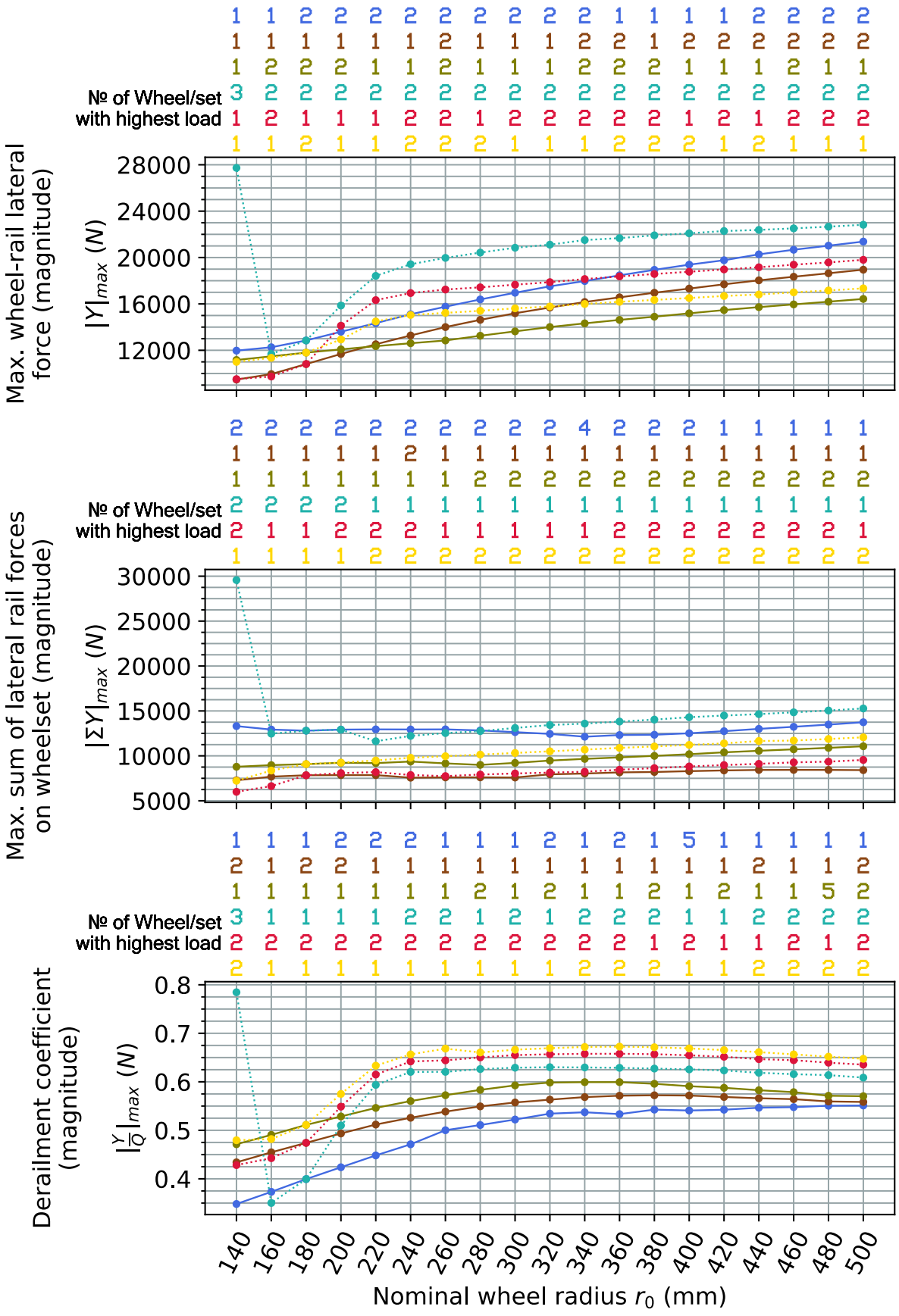

Figure F.21 Tare vehicle on a track with 1430 mm gauge and 1:40 rail cant, CAT4 curve

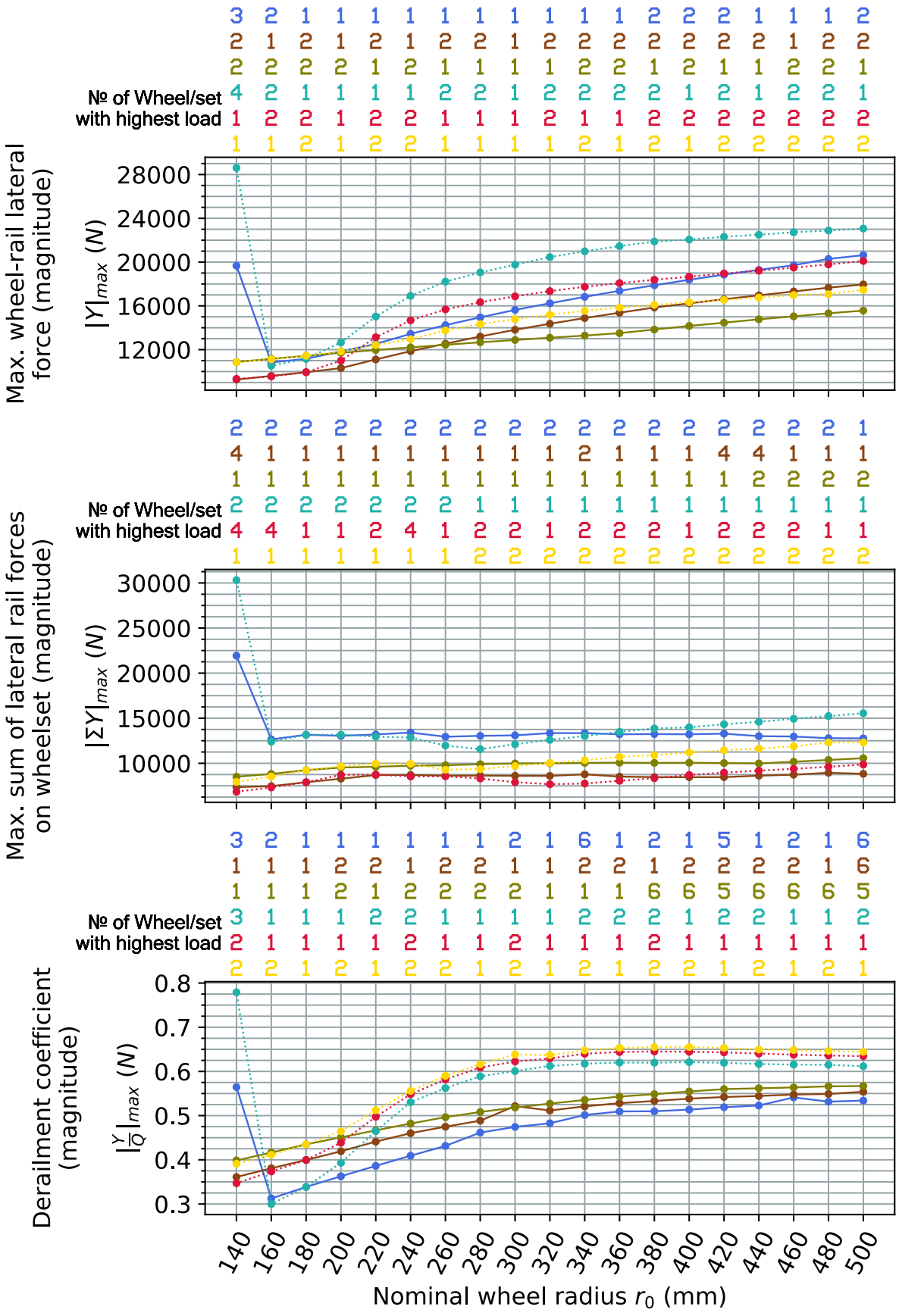

Figure F.22 Tare vehicle on a track with 1437 mm gauge and no rail cant, CAT4 curve

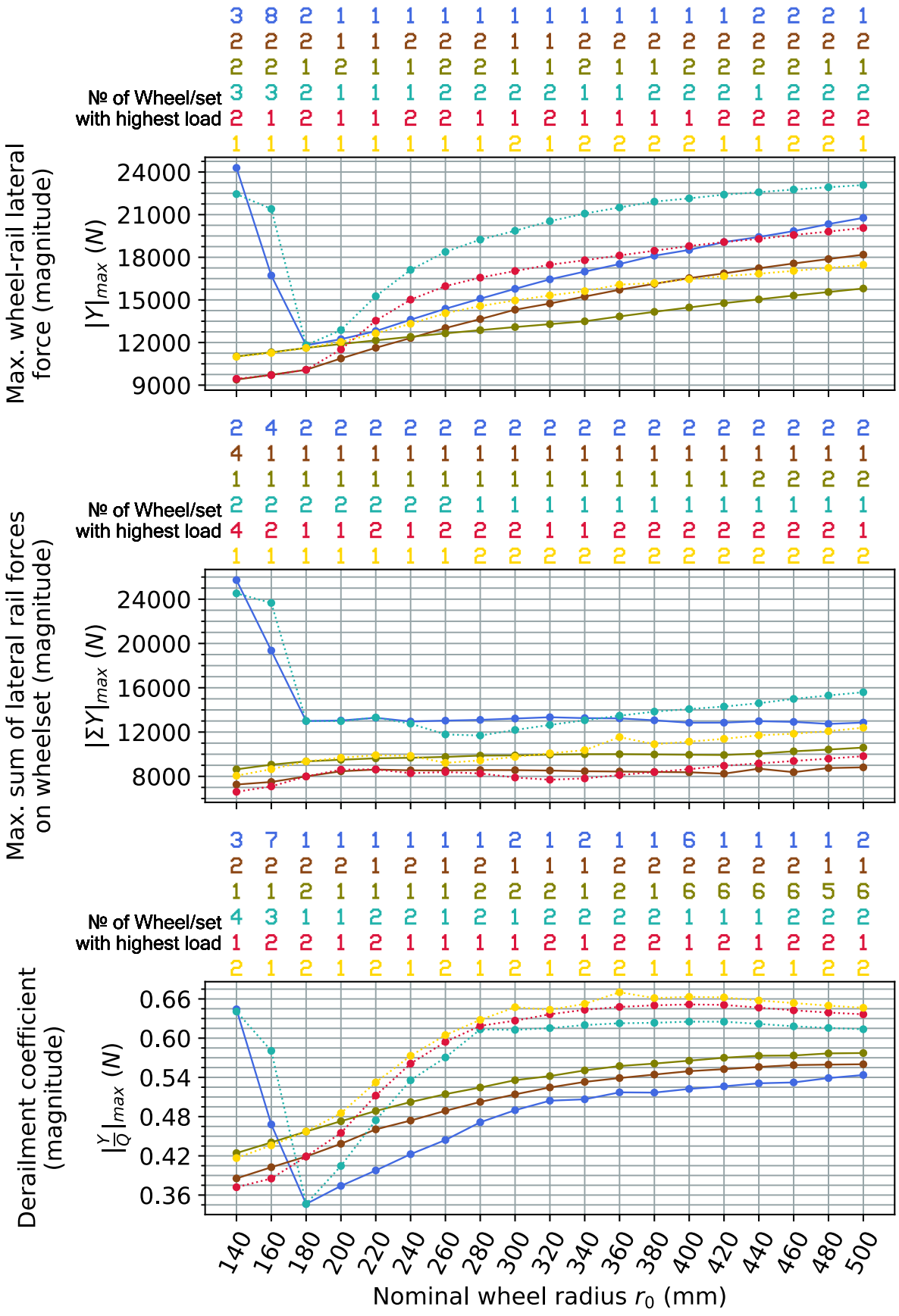

Figure F.23 Tare vehicle on a track with 1435 mm gauge and no rail cant, CAT4 curve

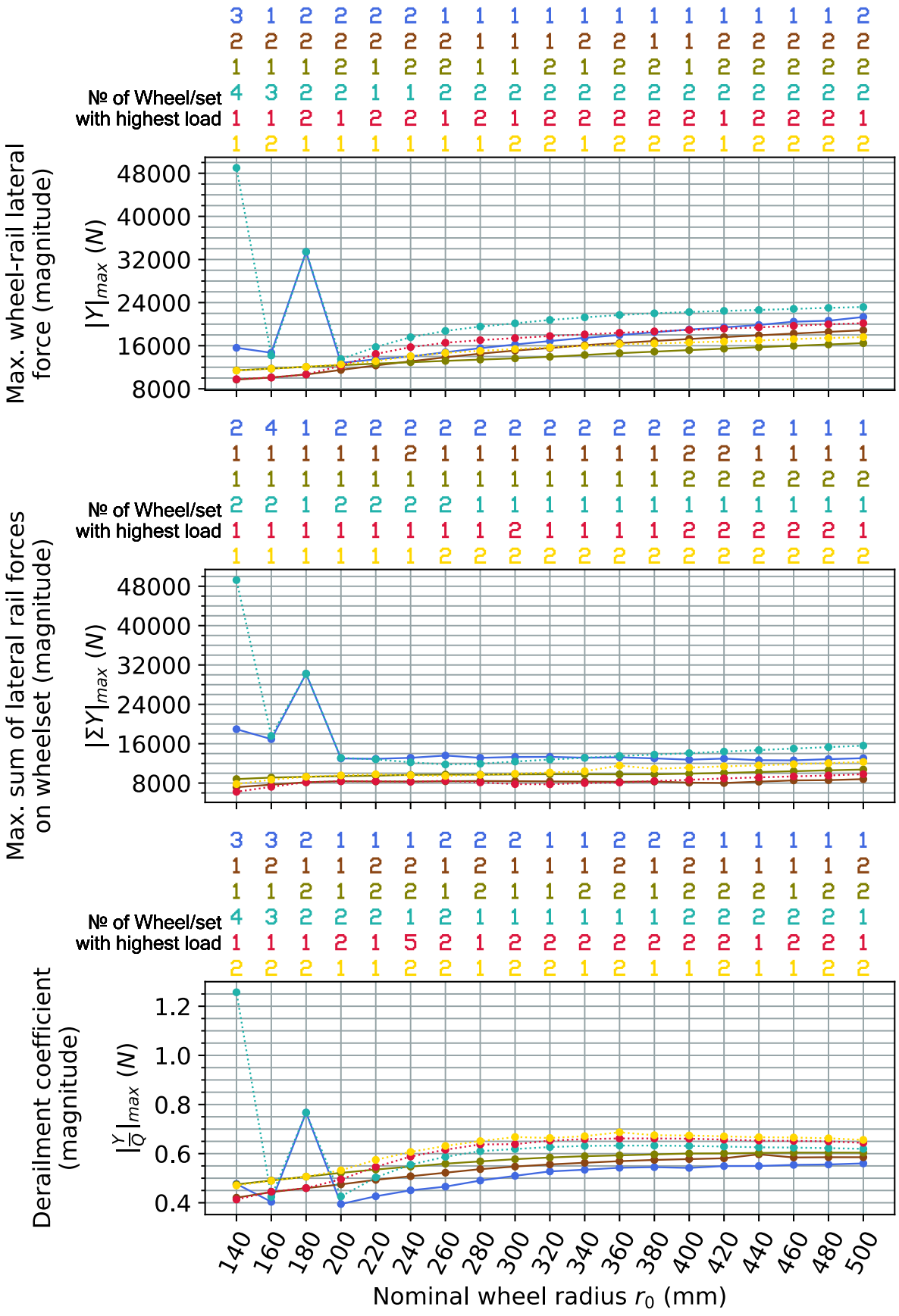

Figure F.24 Tare vehicle on a track with 1432 mm gauge and no rail cant, CAT4 curve

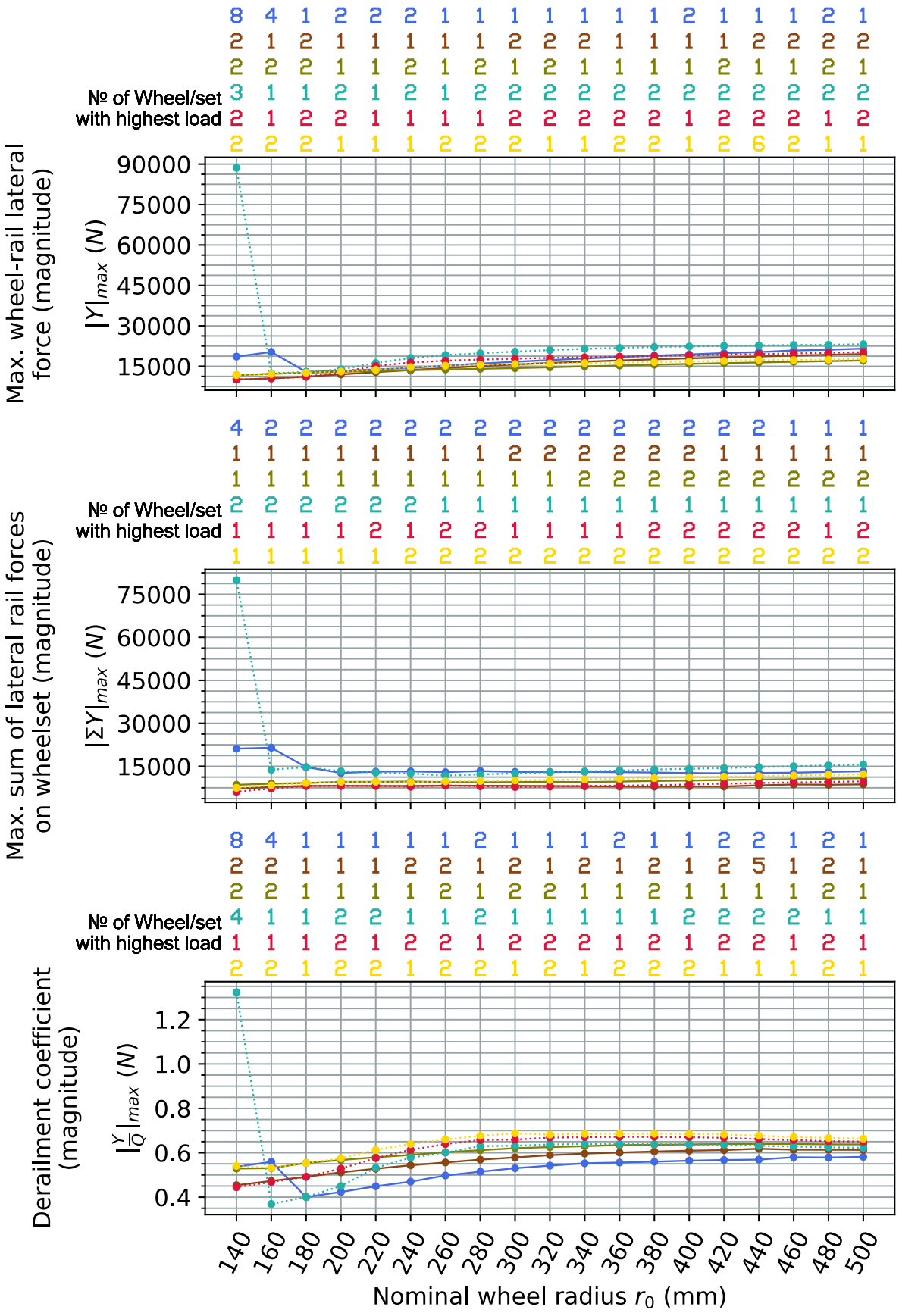

Figure F.25 Tare vehicle on a track with 1430 mm gauge and no rail cant, CAT4 curve

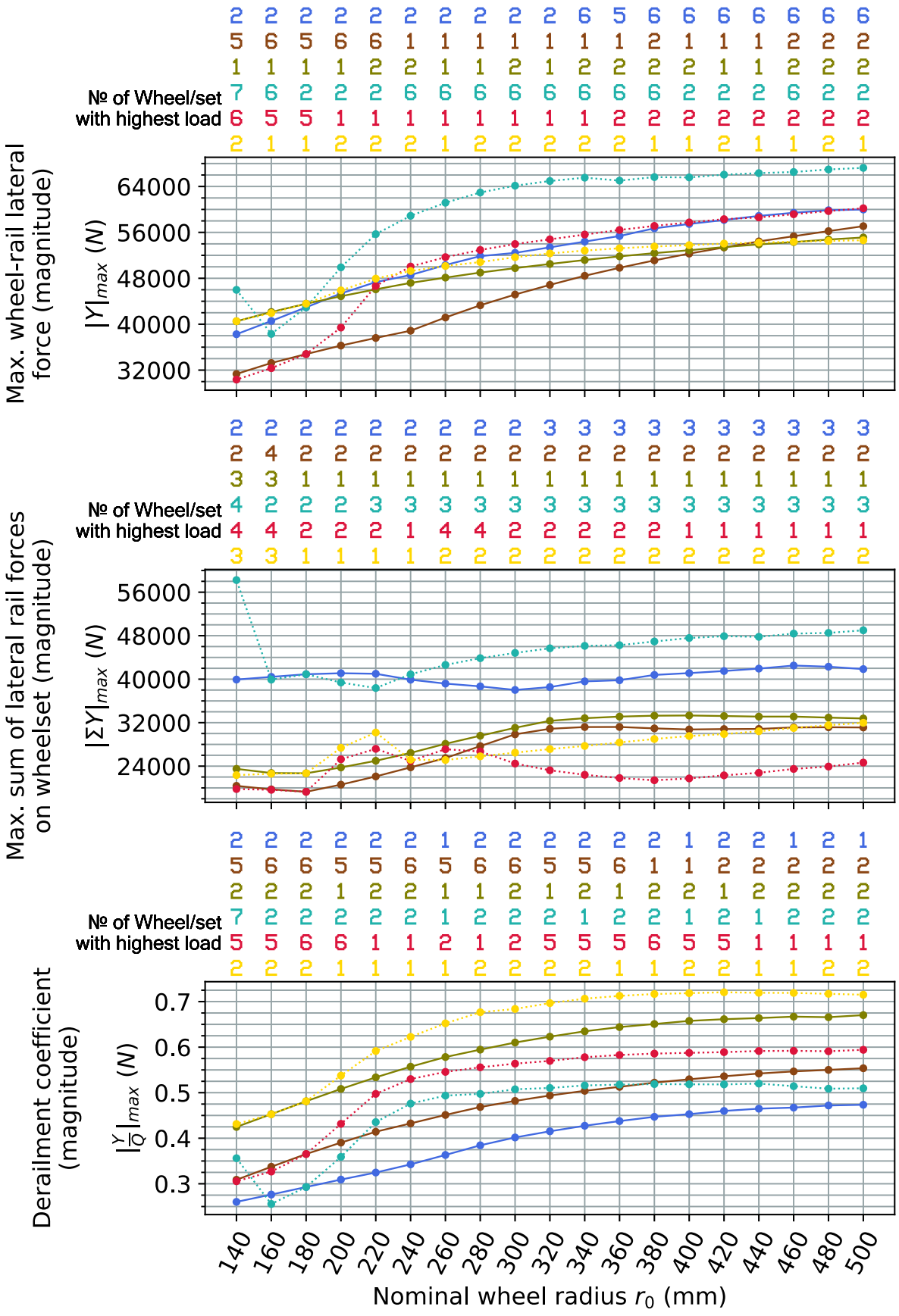

Figure F.26 Laden vehicle on a track with 1437 mm gauge and 1:40 rail cant, CAT4 curve

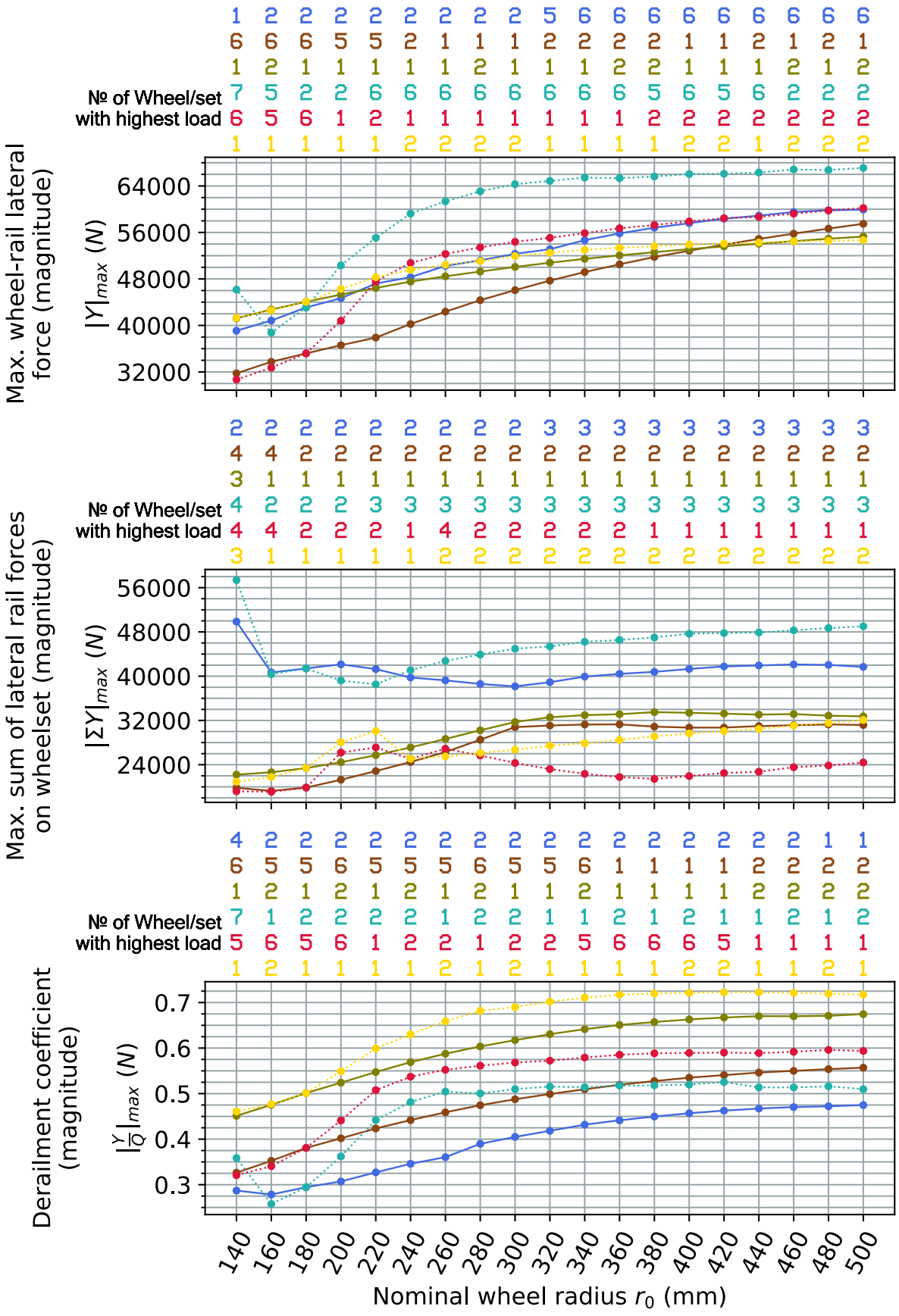

Figure F.27 Laden vehicle on a track with 1435 mm gauge and 1:40 rail cant (reference track setting), CAT4 curve

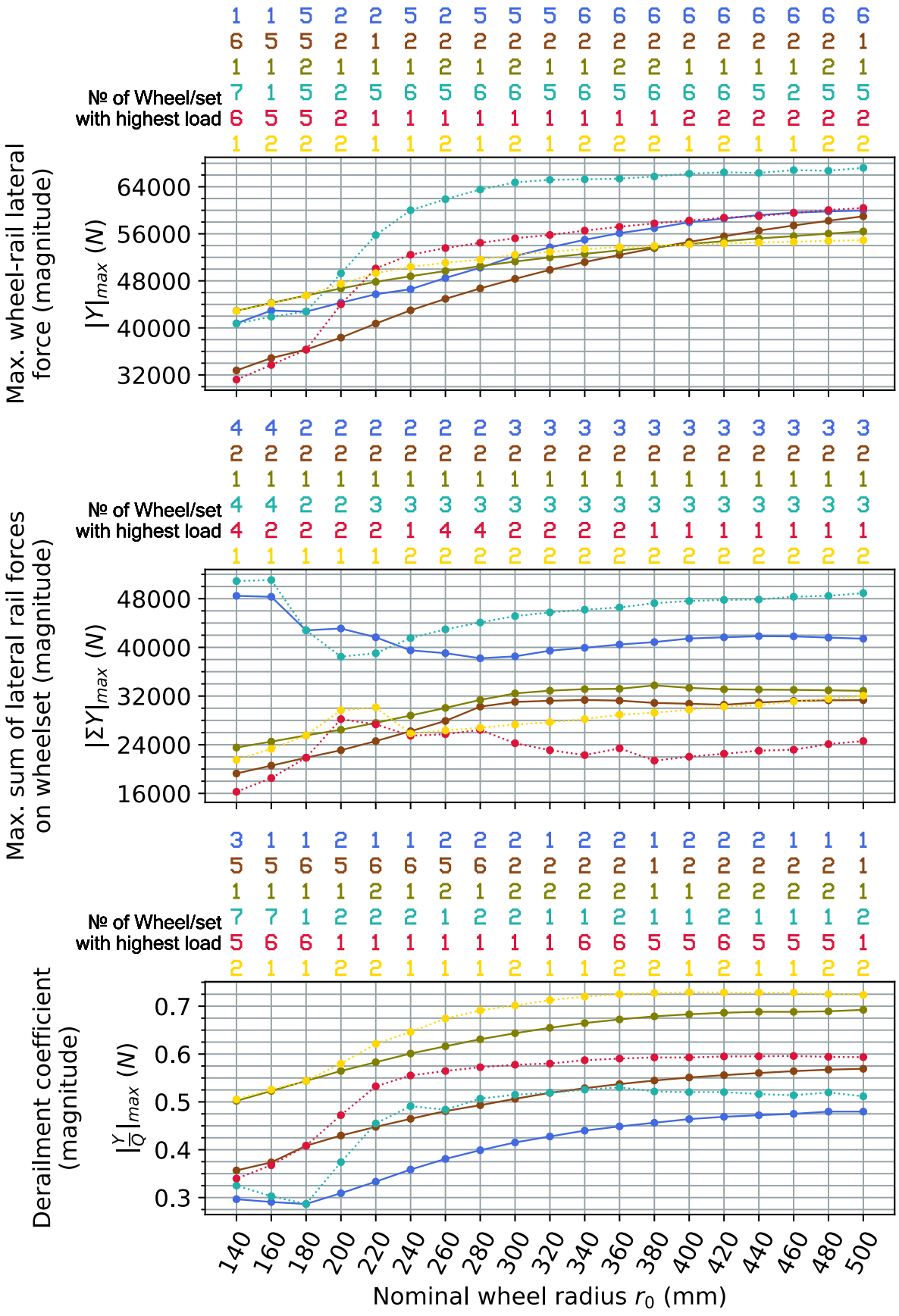

Figure F.28 Laden vehicle on a track with 1432 mm gauge and 1:40 rail cant, CAT4 curve

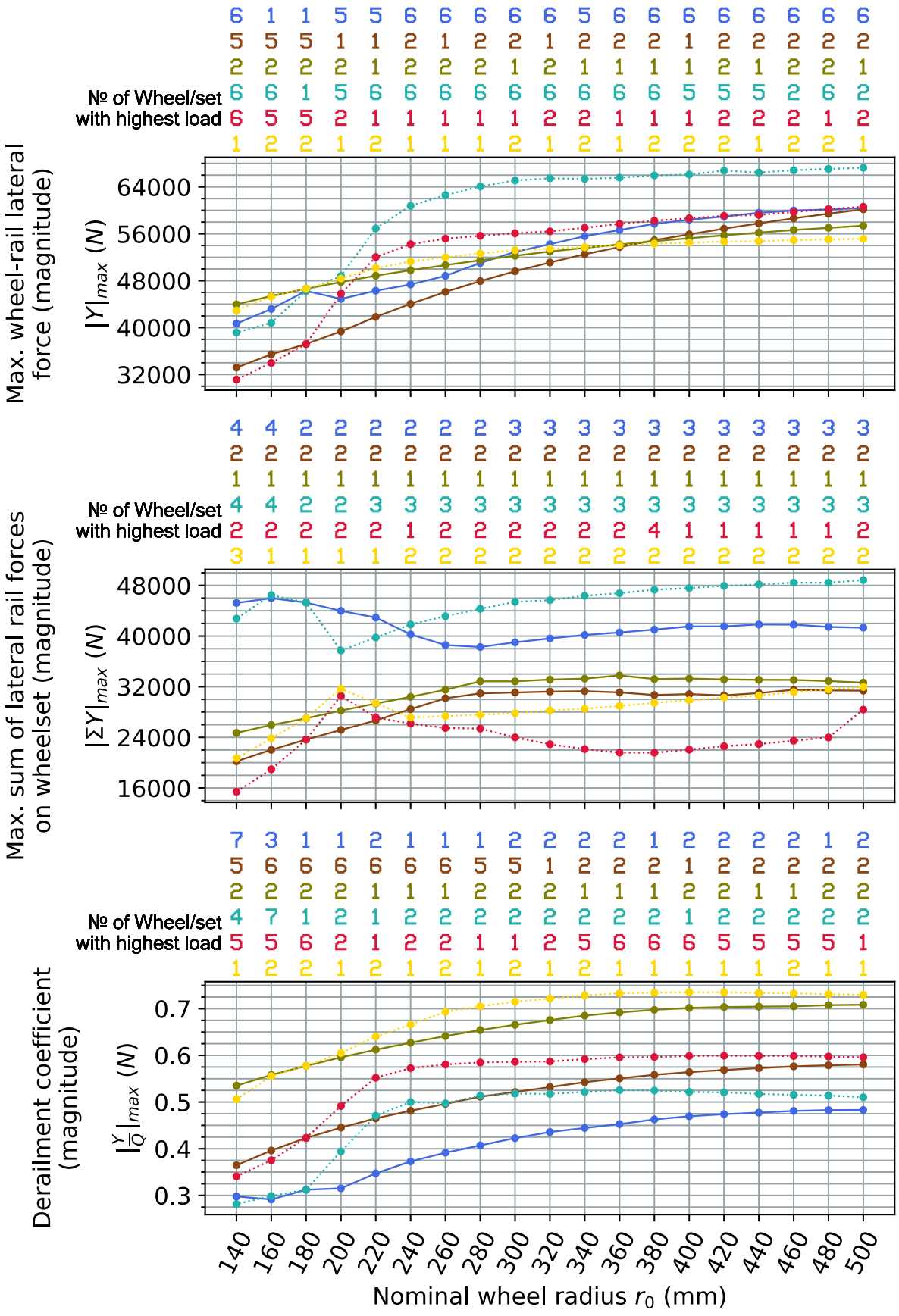

Figure F.29 Laden vehicle on a track with 1430 mm gauge and 1:40 rail cant, CAT4 curve

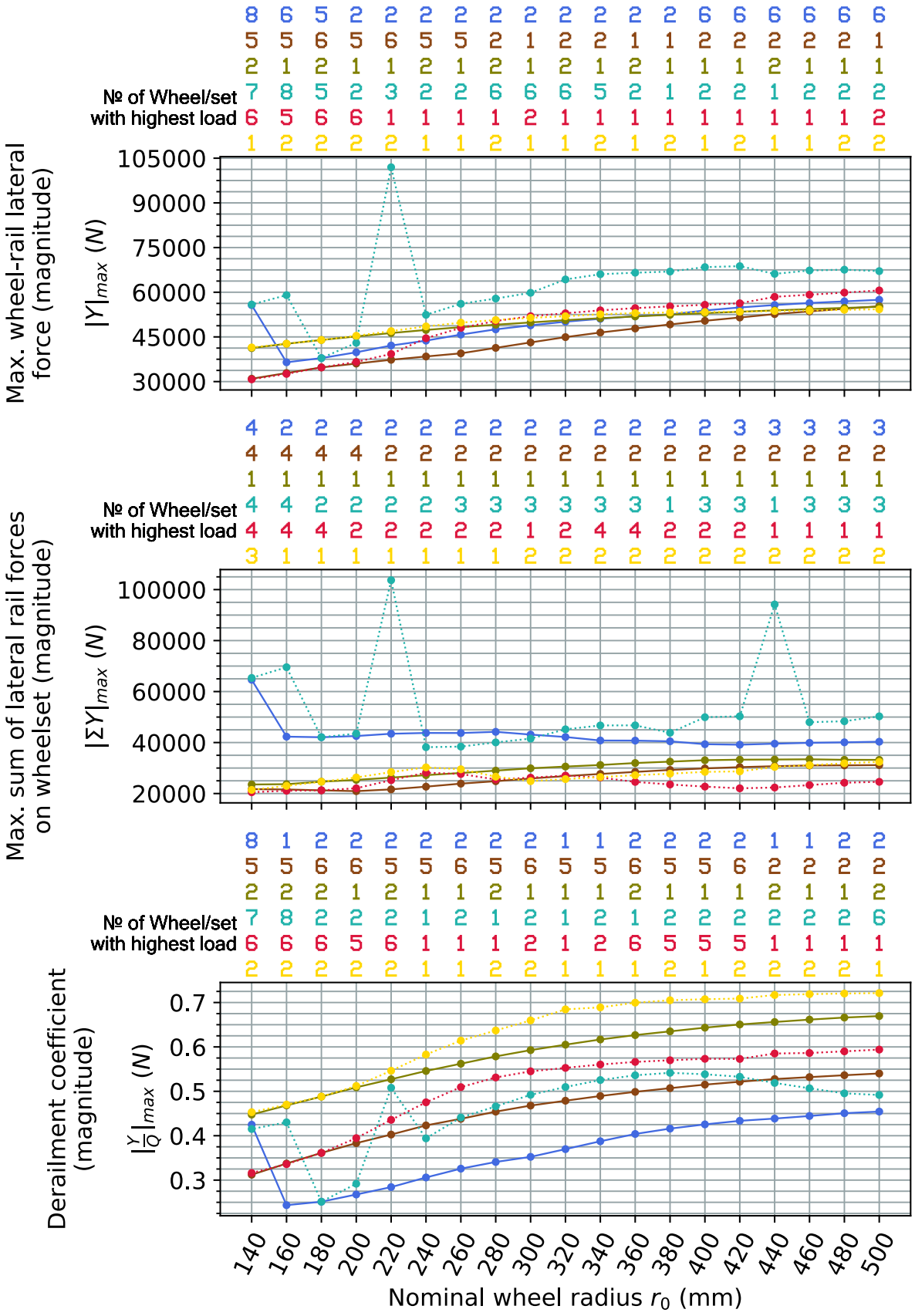

Figure F.30 Laden vehicle on a track with 1437 mm gauge and no rail cant, CAT4 curve

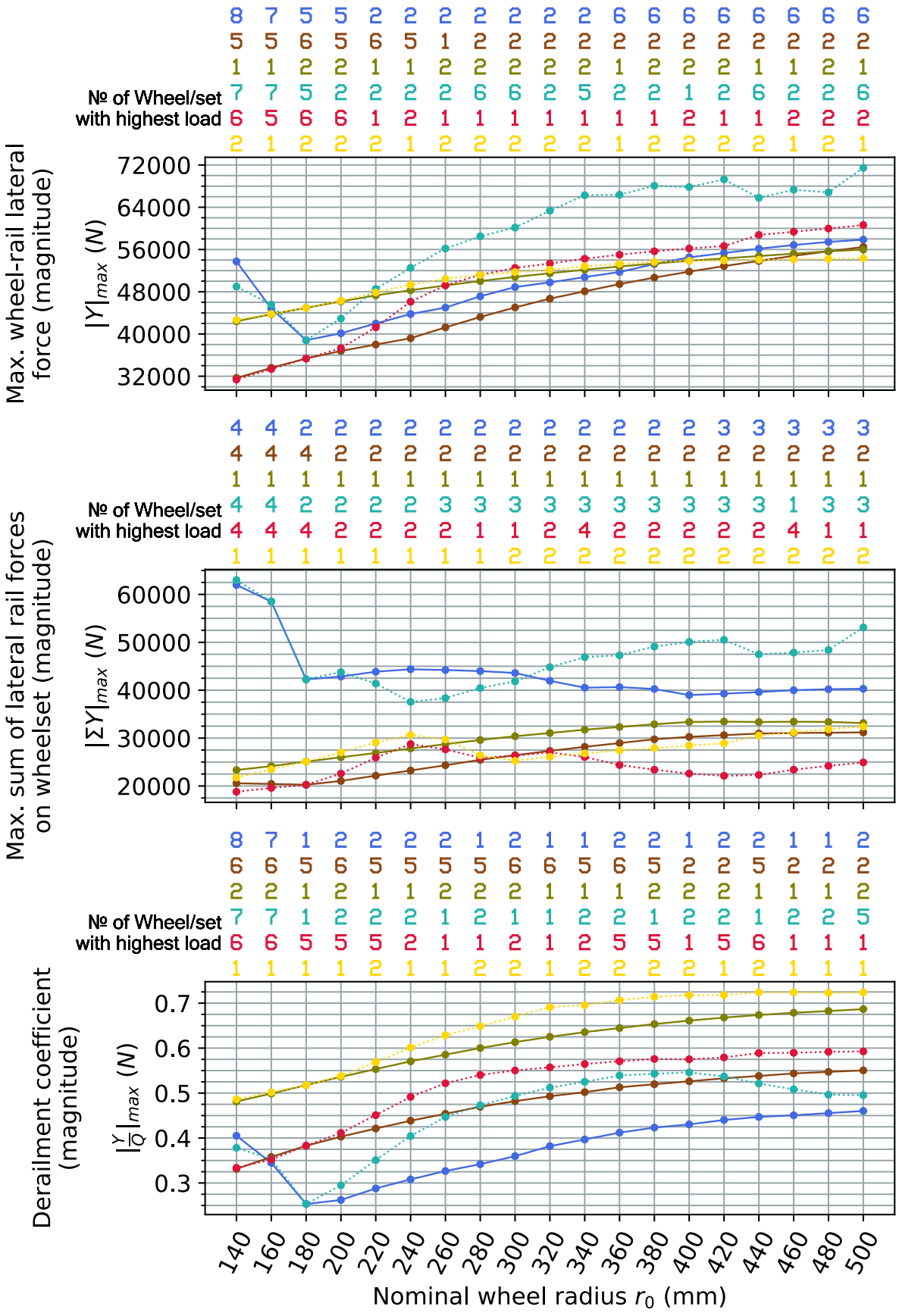

Figure F.31 Laden vehicle on a track with 1435 mm gauge and no rail cant, CAT4 curve

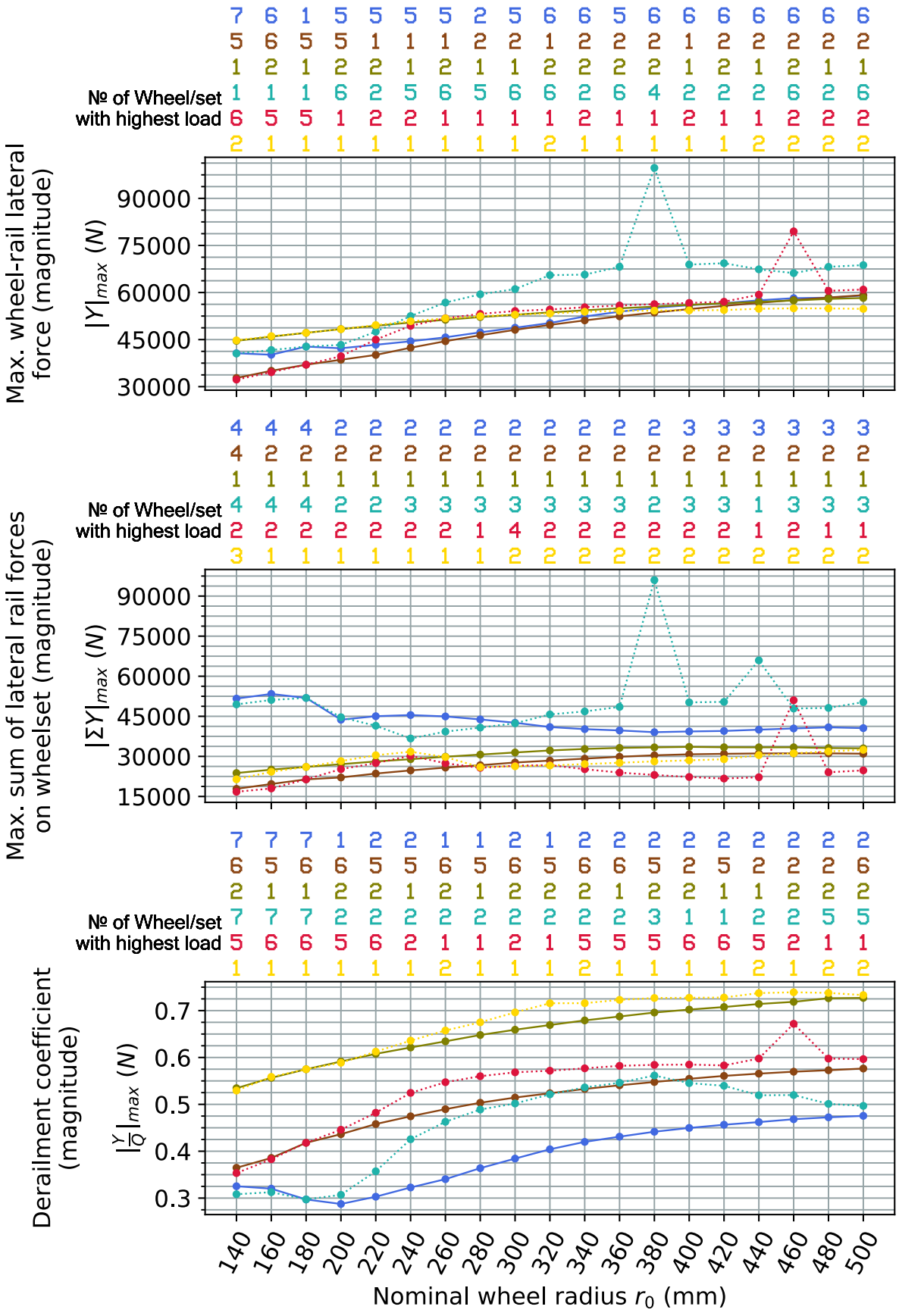

Figure F.32 Laden vehicle on a track with 1432 mm gauge and no rail cant, CAT4 curve

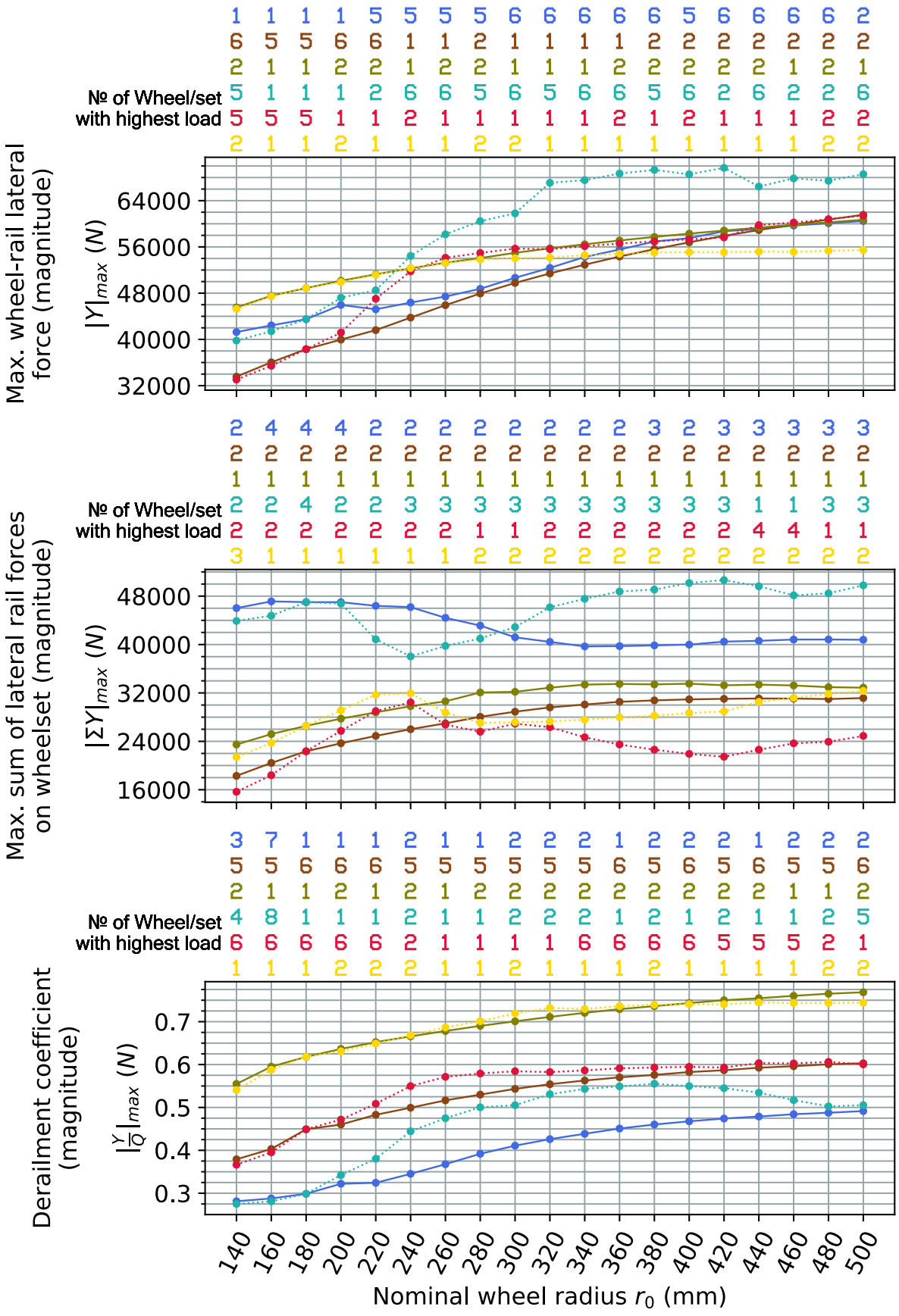

Figure F.33 Laden vehicle on a track with 1430 mm gauge and no rail cant, CAT4 curve

Appendix G Curve negotiation simulation results with implementation of radial steering

The revised radial steering bogie model with additional yaw relaxation is used. Results both with and without simultaneous profile modification (case MAT) are compared against the control case.

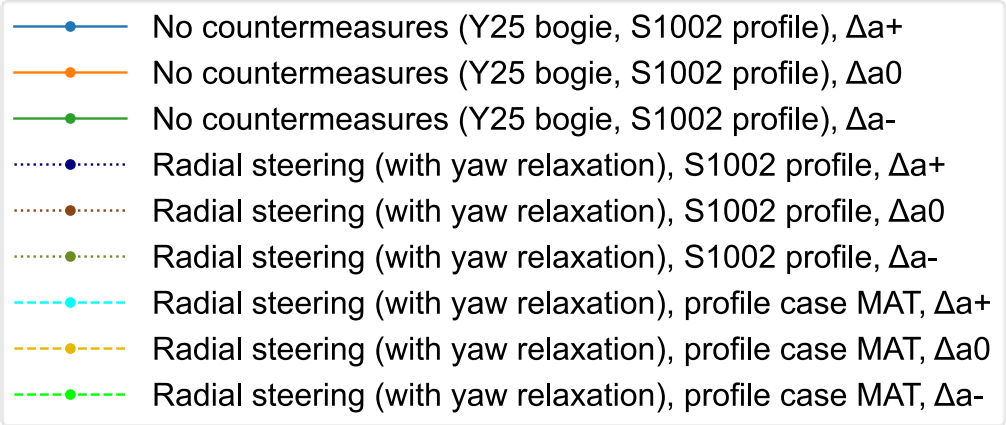

Figure G.1 Legend of all plots in this appendix

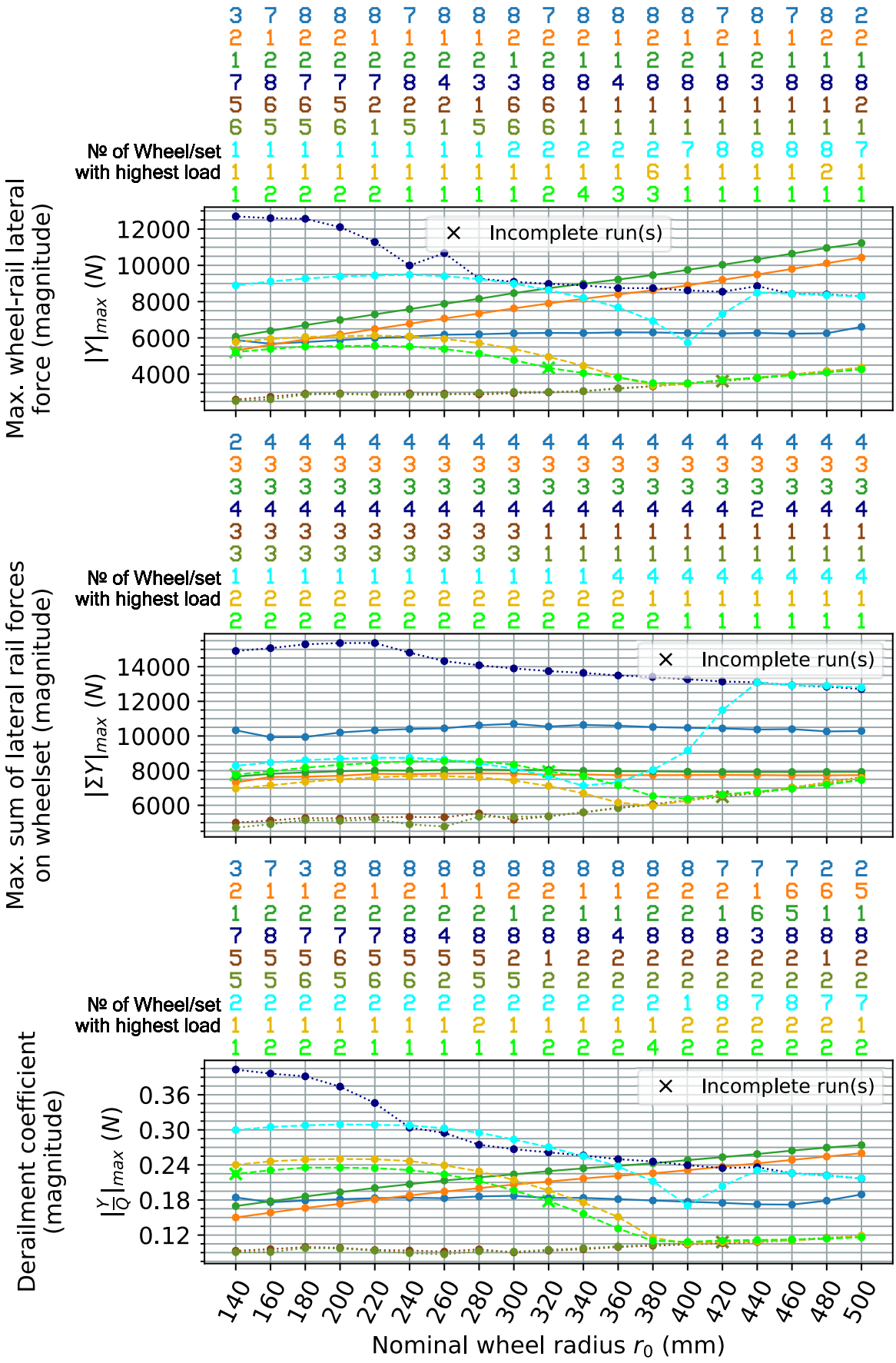

Figure G.2 Tare vehicle on a track with 1437 mm gauge and 1:40 rail cant, CAT2 curve

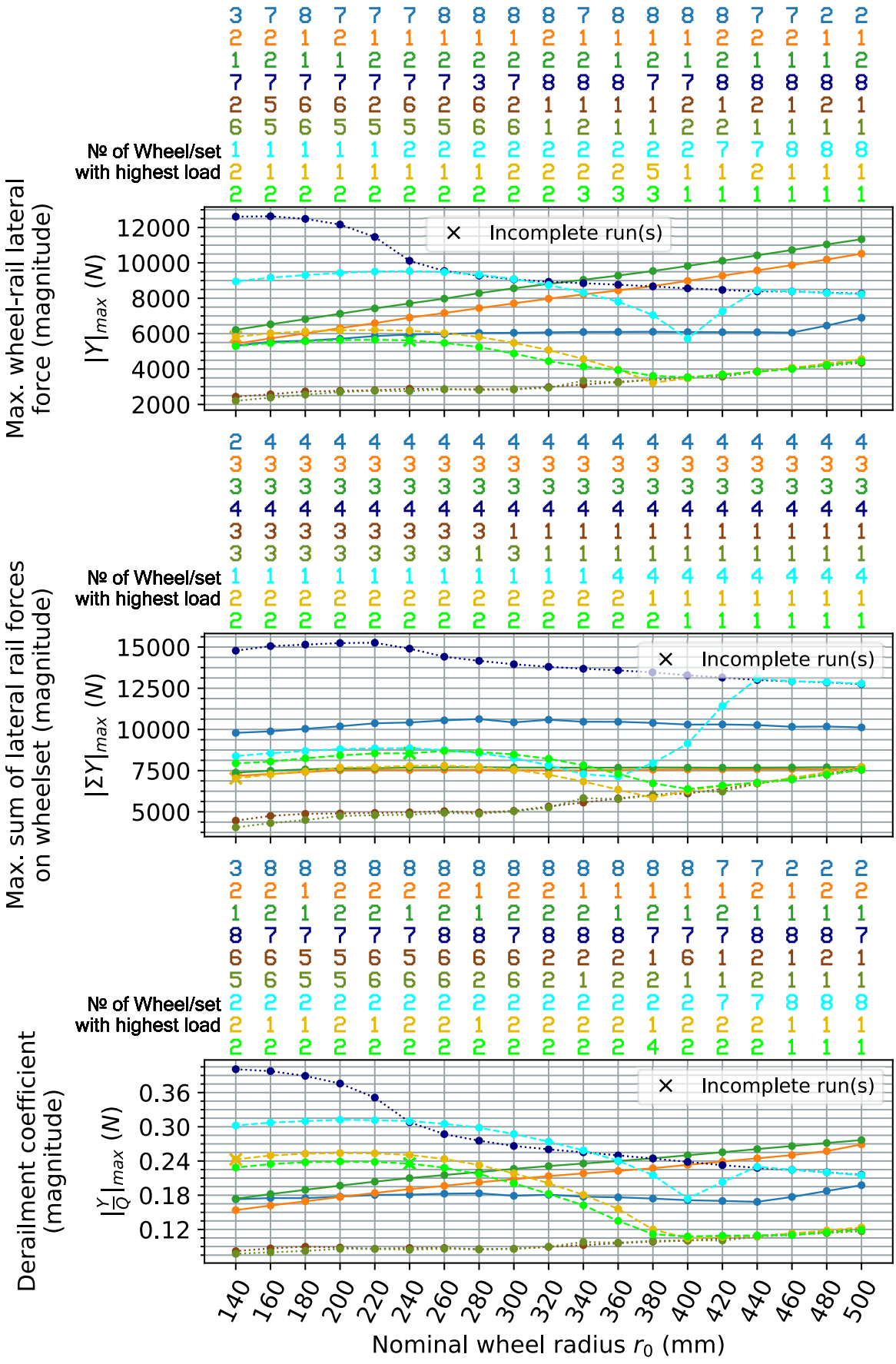

Figure G.3 Tare vehicle on a track with 1435 mm gauge and 1:40 rail cant (reference track setting), CAT2 curve

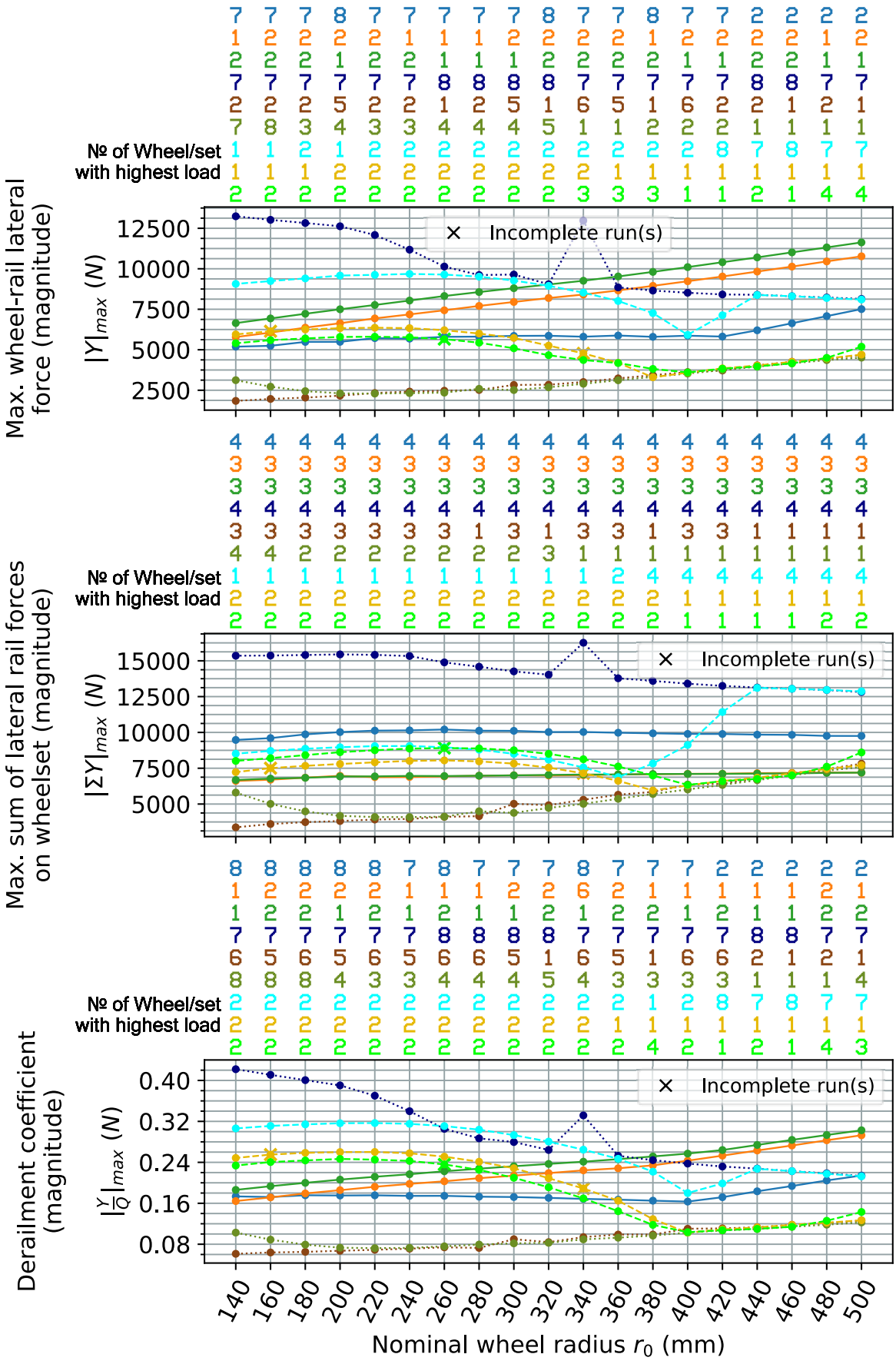

Figure G.4 Tare vehicle on a track with 1432 mm gauge and 1:40 rail cant, CAT2 curve

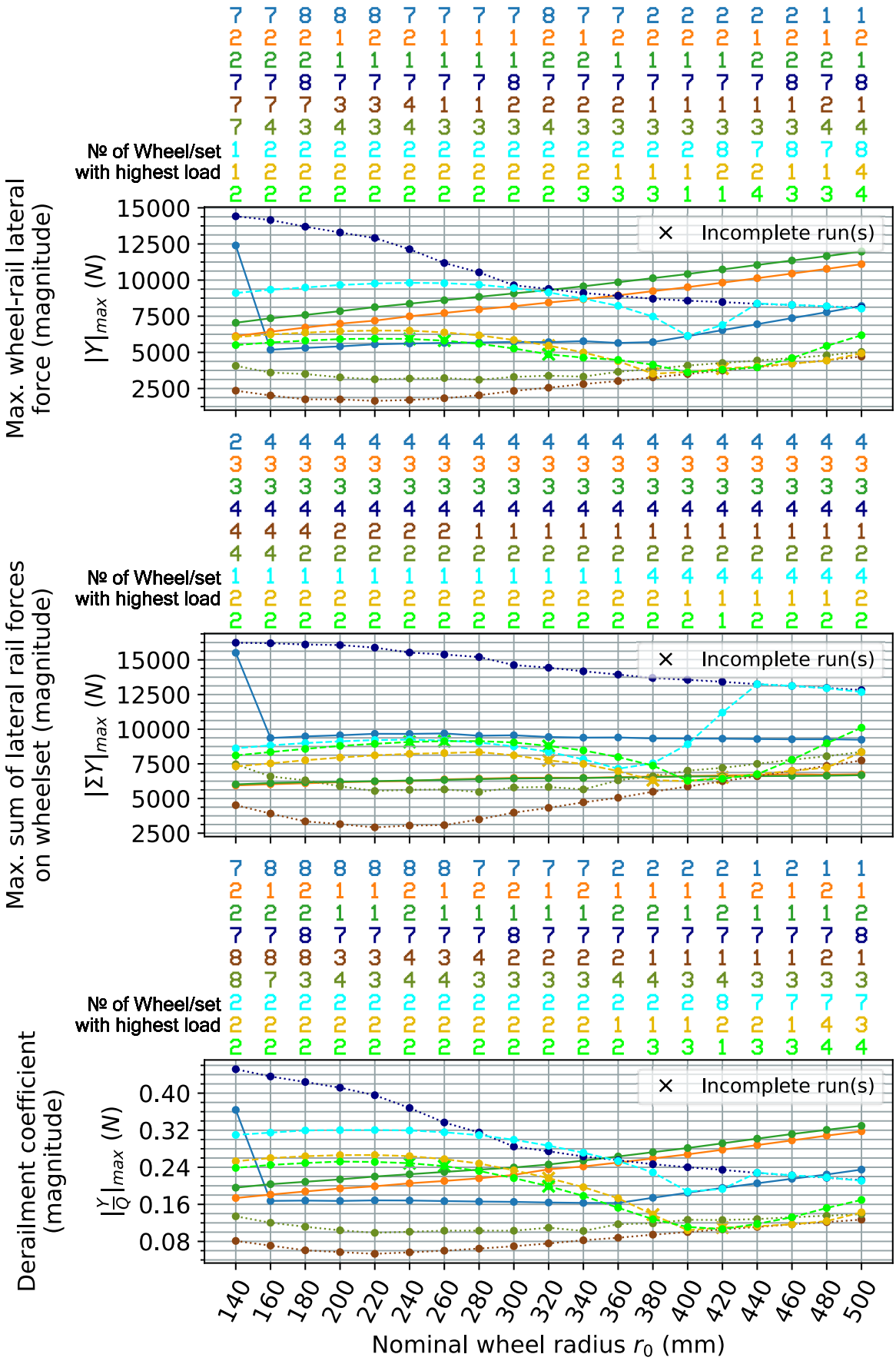

Figure G.5 Tare vehicle on a track with 1430 mm gauge and 1:40 rail cant, CAT2 curve

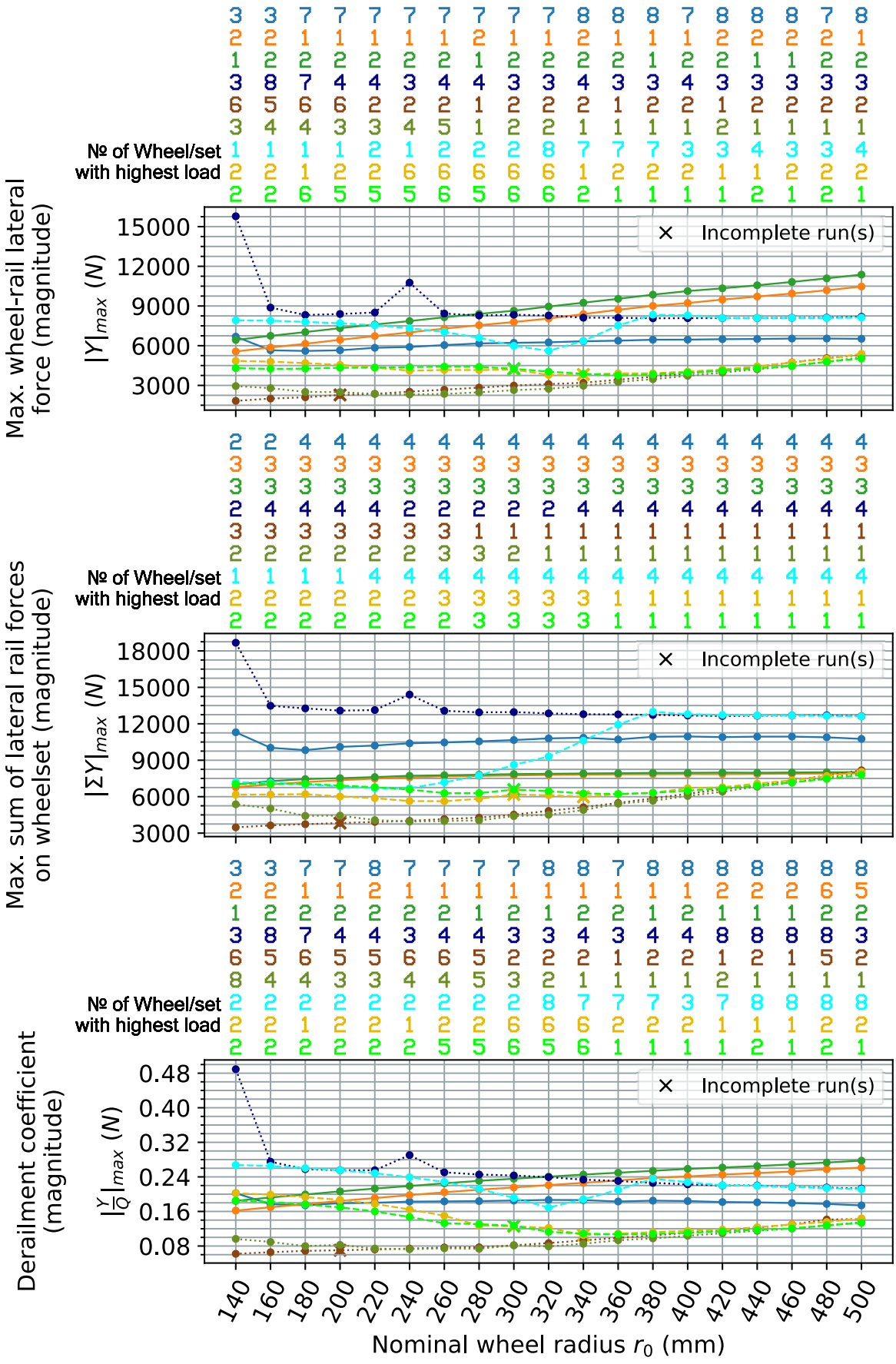

Figure G.6 Tare vehicle on a track with 1437 mm gauge and no rail cant, CAT2 curve

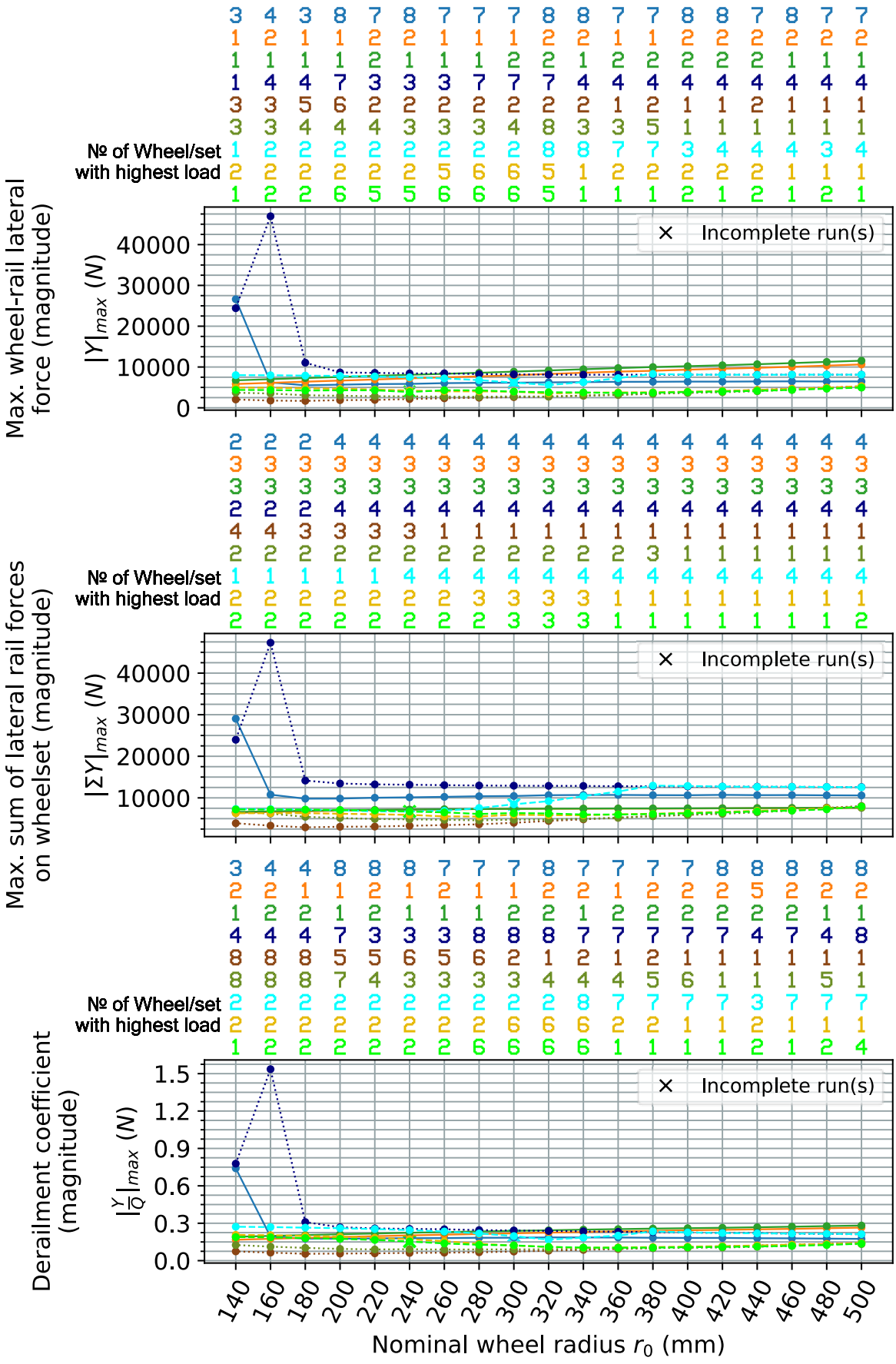

Figure G.7 Tare vehicle on a track with 1435 mm gauge and no rail cant, CAT2 curve

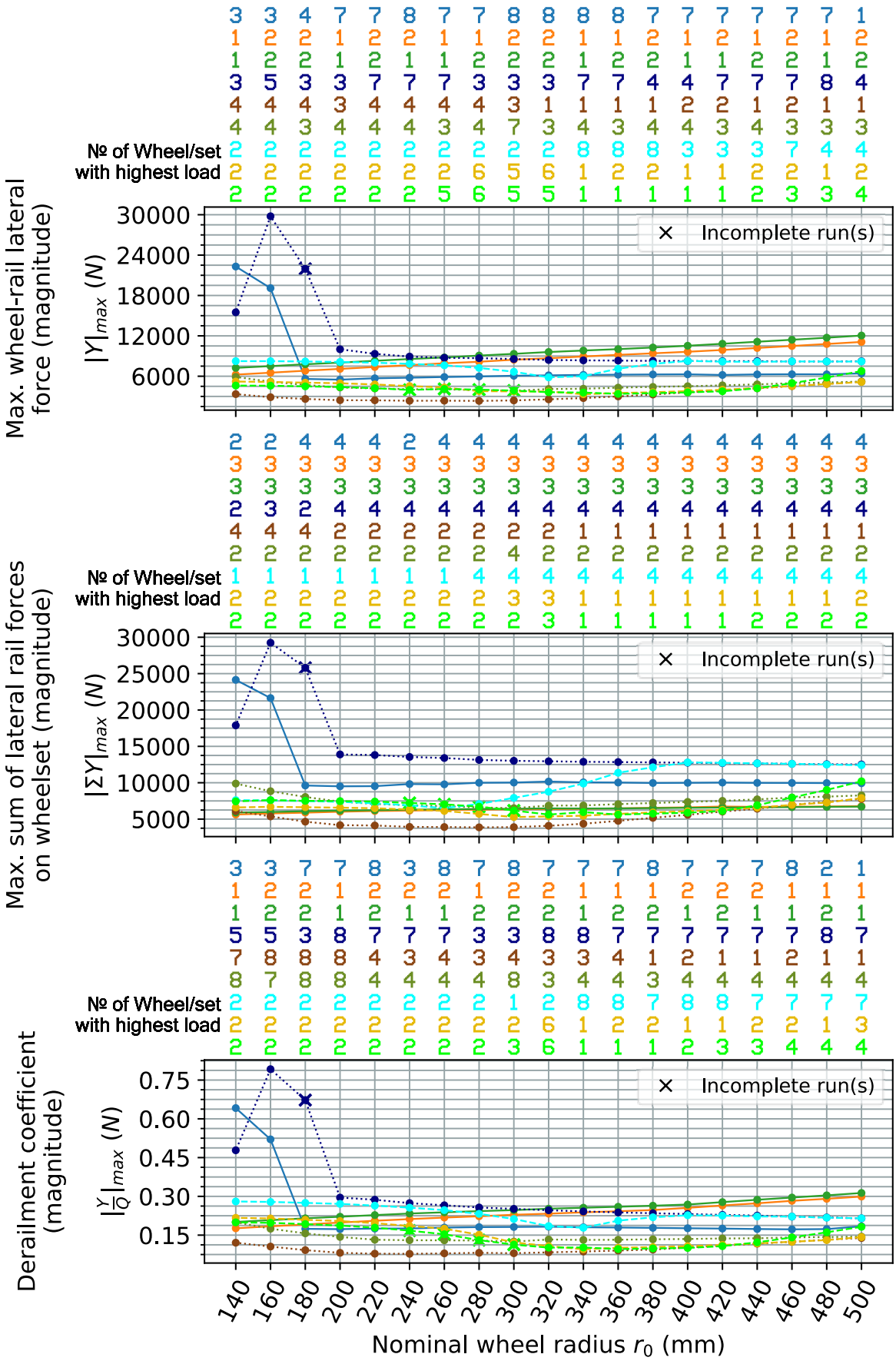

Figure G.8 Tare vehicle on a track with 1432 mm gauge and no rail cant, CAT2 curve

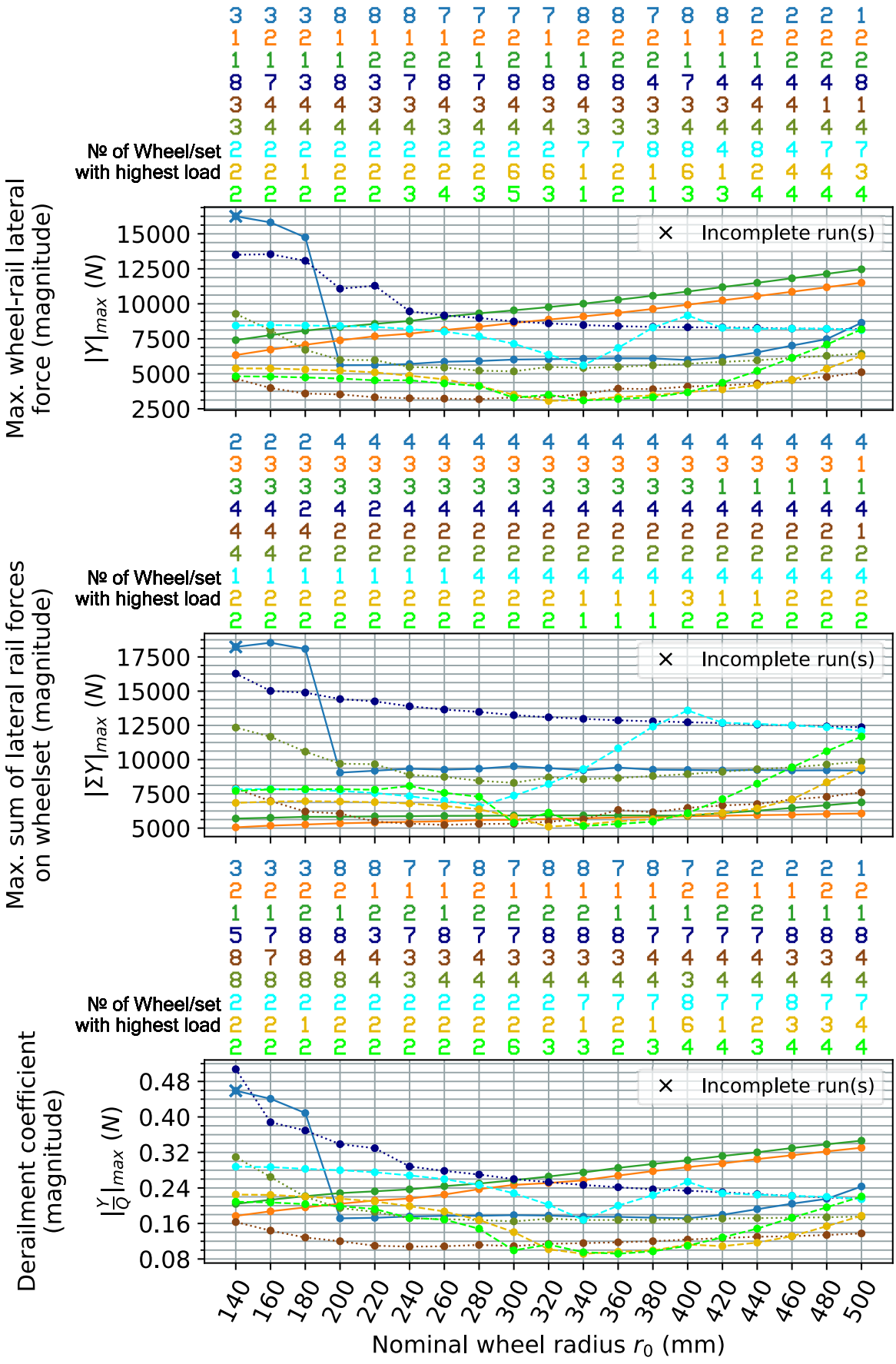

Figure G.9 Tare vehicle on a track with 1430 mm gauge and no rail cant, CAT2 curve

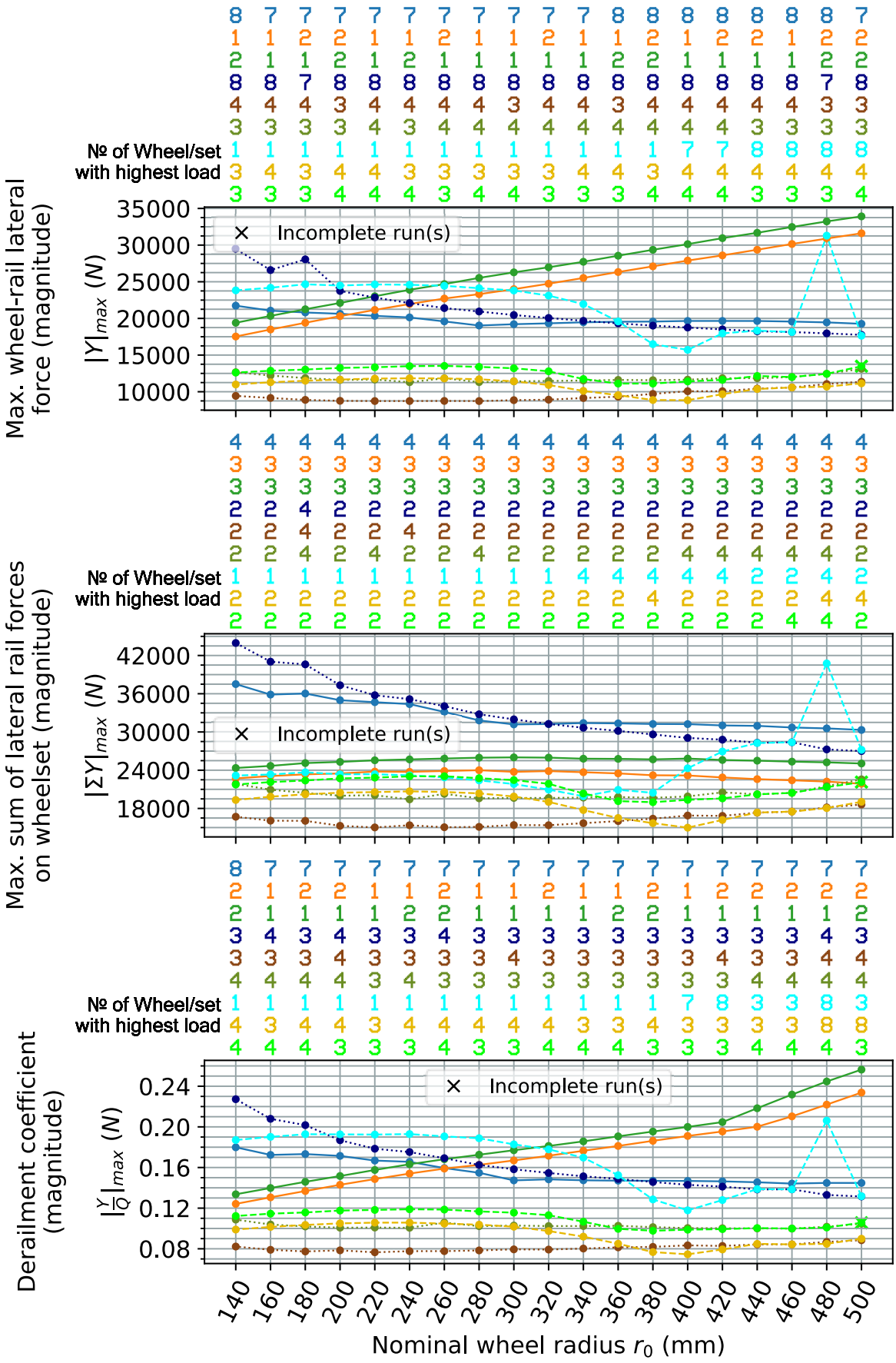

Figure G.10 Laden vehicle on a track with 1437 mm gauge and 1:40 rail cant, CAT2 curve

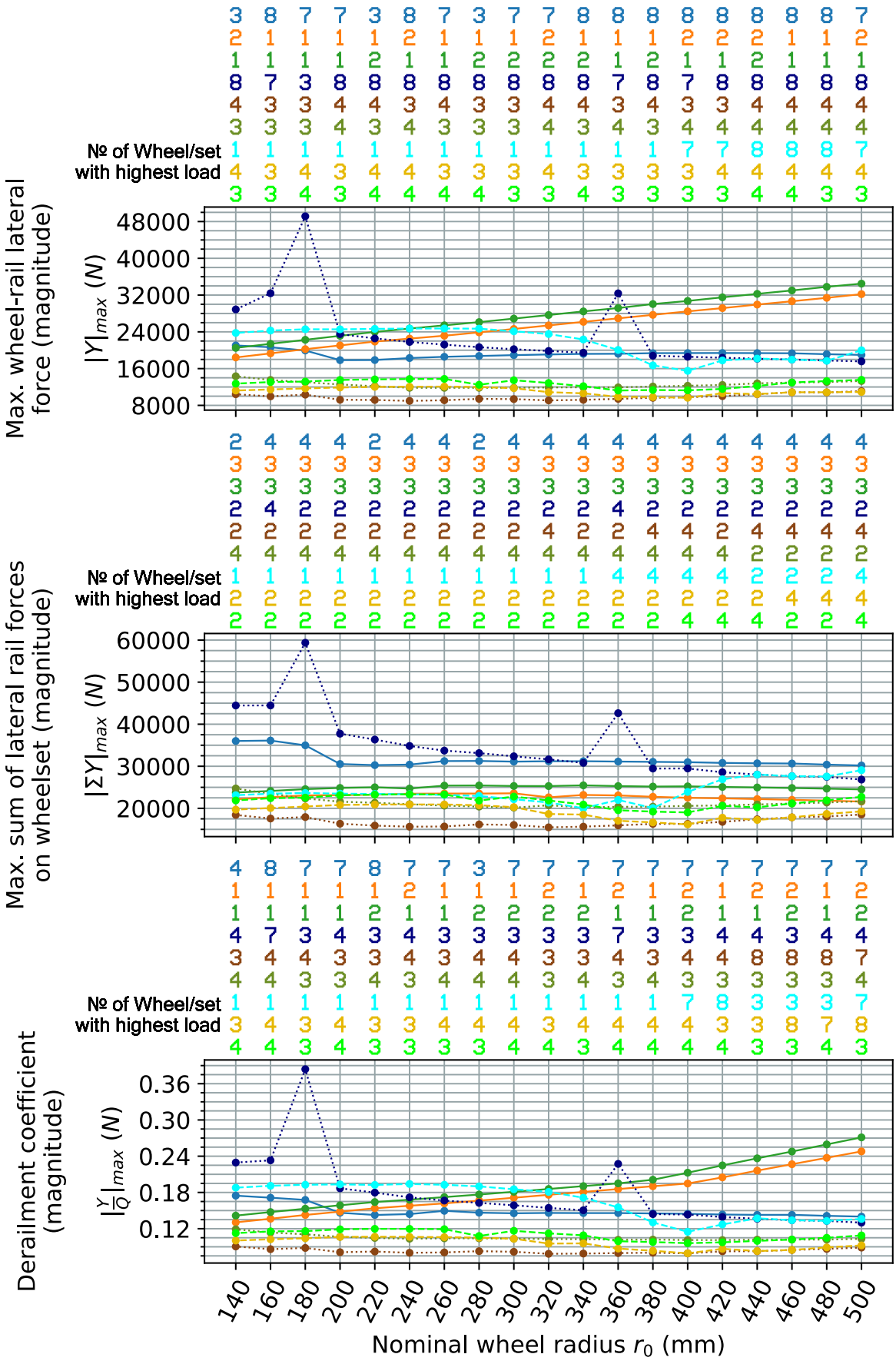

Figure G.11 Laden vehicle on a track with 1435 mm gauge and 1:40 rail cant (reference track setting), CAT2 curve

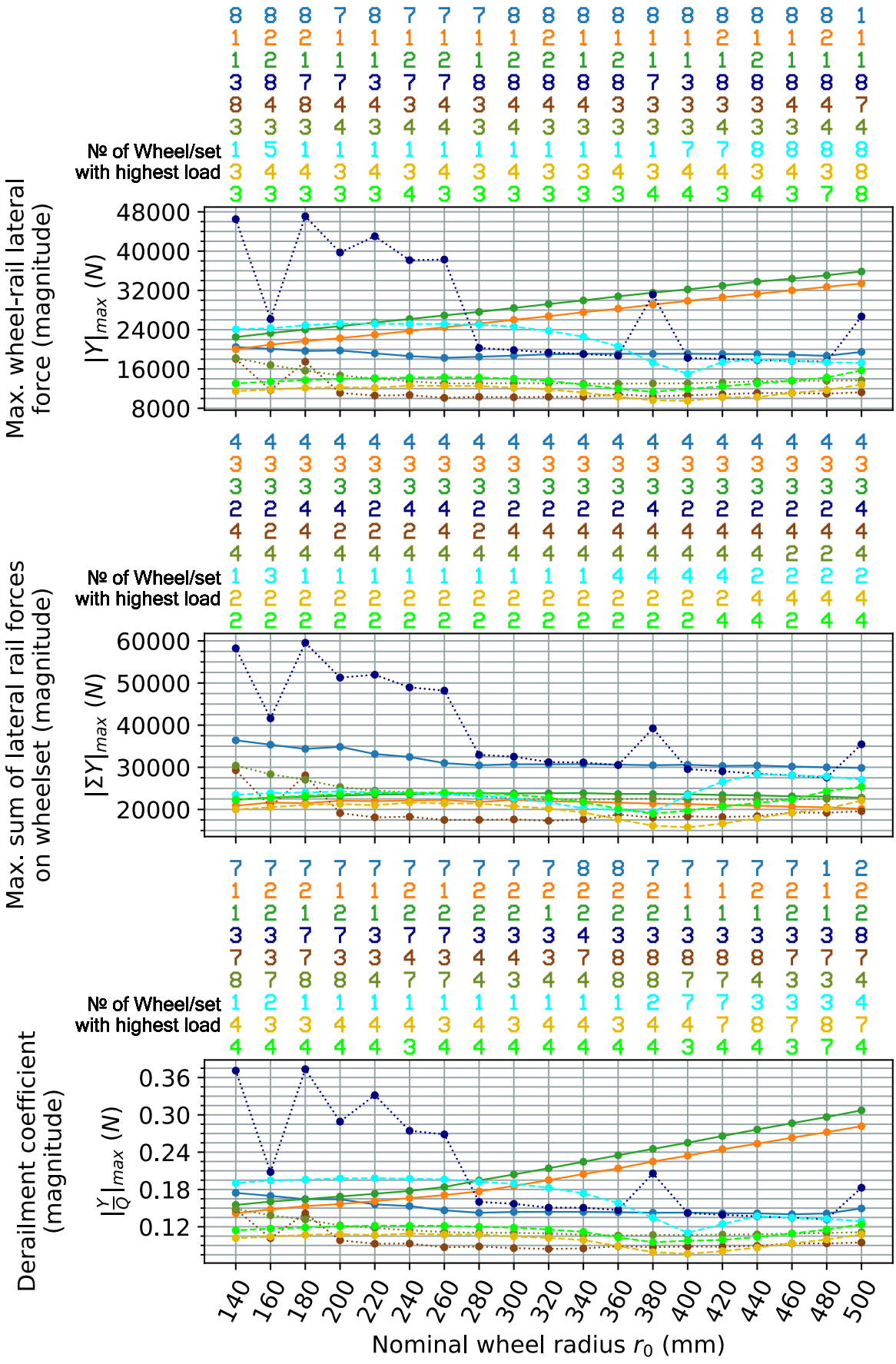

Figure G.12 Laden vehicle on a track with 1432 mm gauge and 1:40 rail cant, CAT2 curve

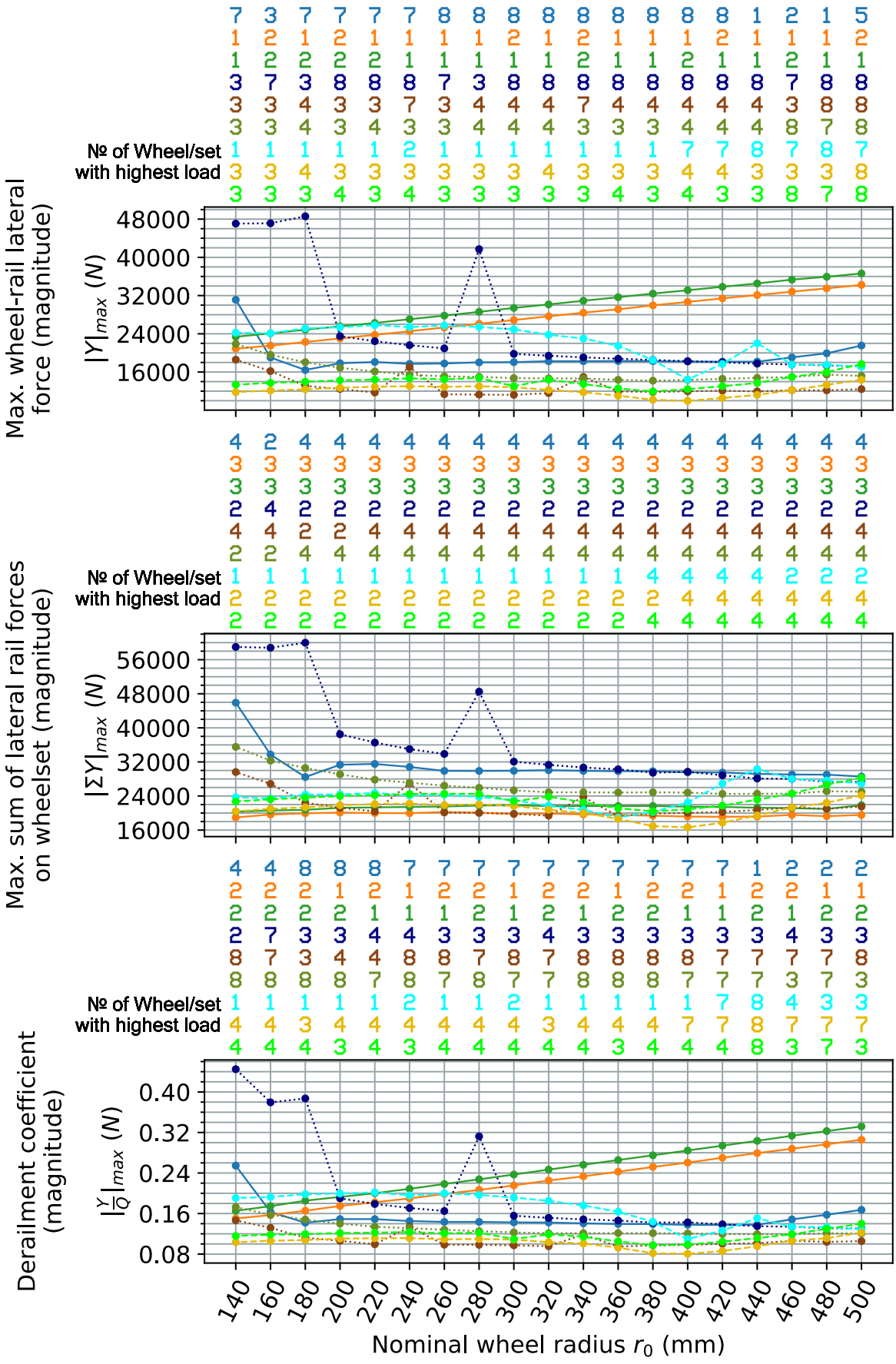

Figure G.13 Laden vehicle on a track with 1430 mm gauge and 1:40 rail cant, CAT2 curve

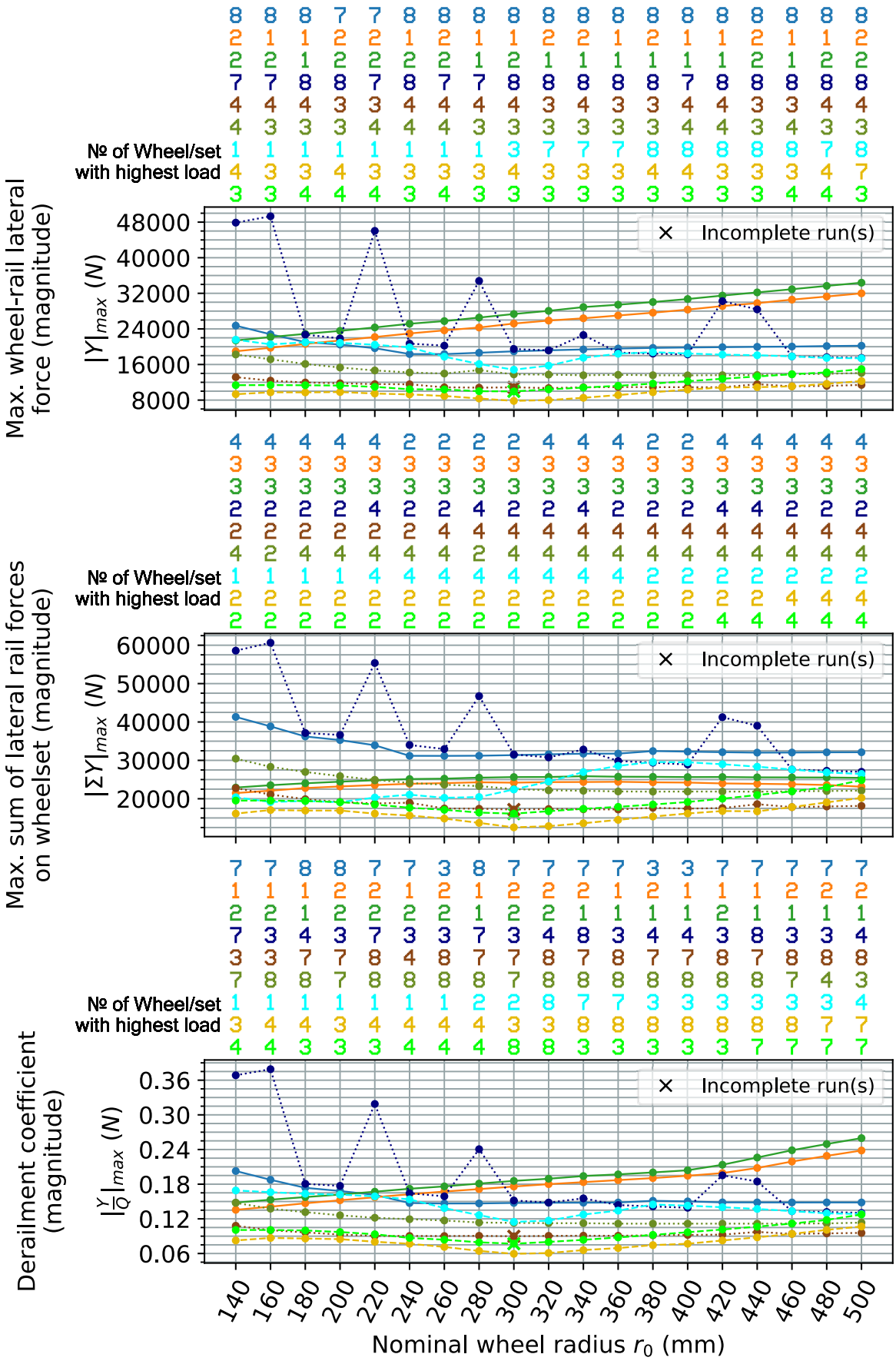

Figure G.14 Laden vehicle on a track with 1437 mm gauge and no rail cant, CAT2 curve

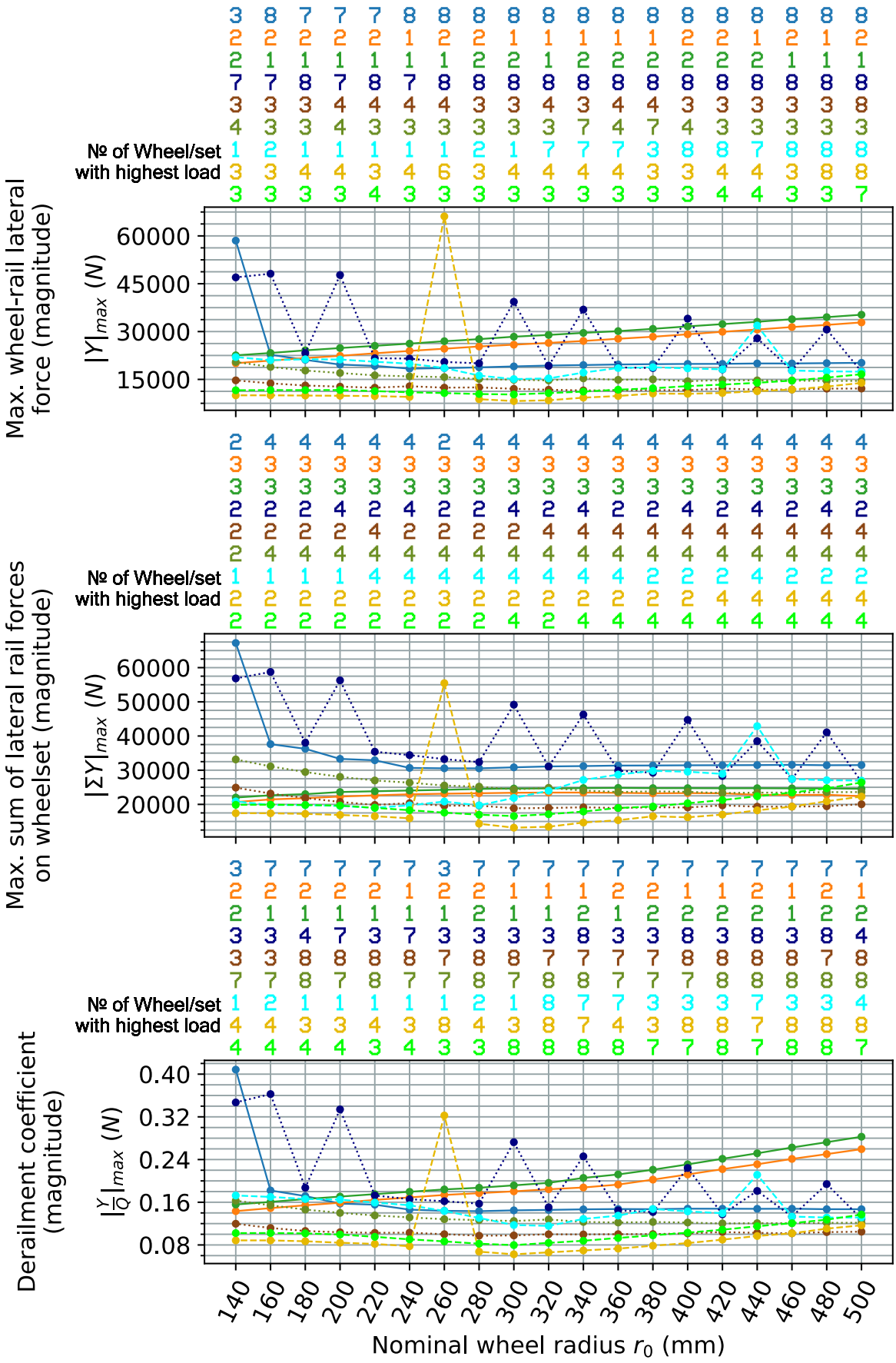

Figure G.15 Laden vehicle on a track with 1435 mm gauge and no rail cant, CAT2 curve

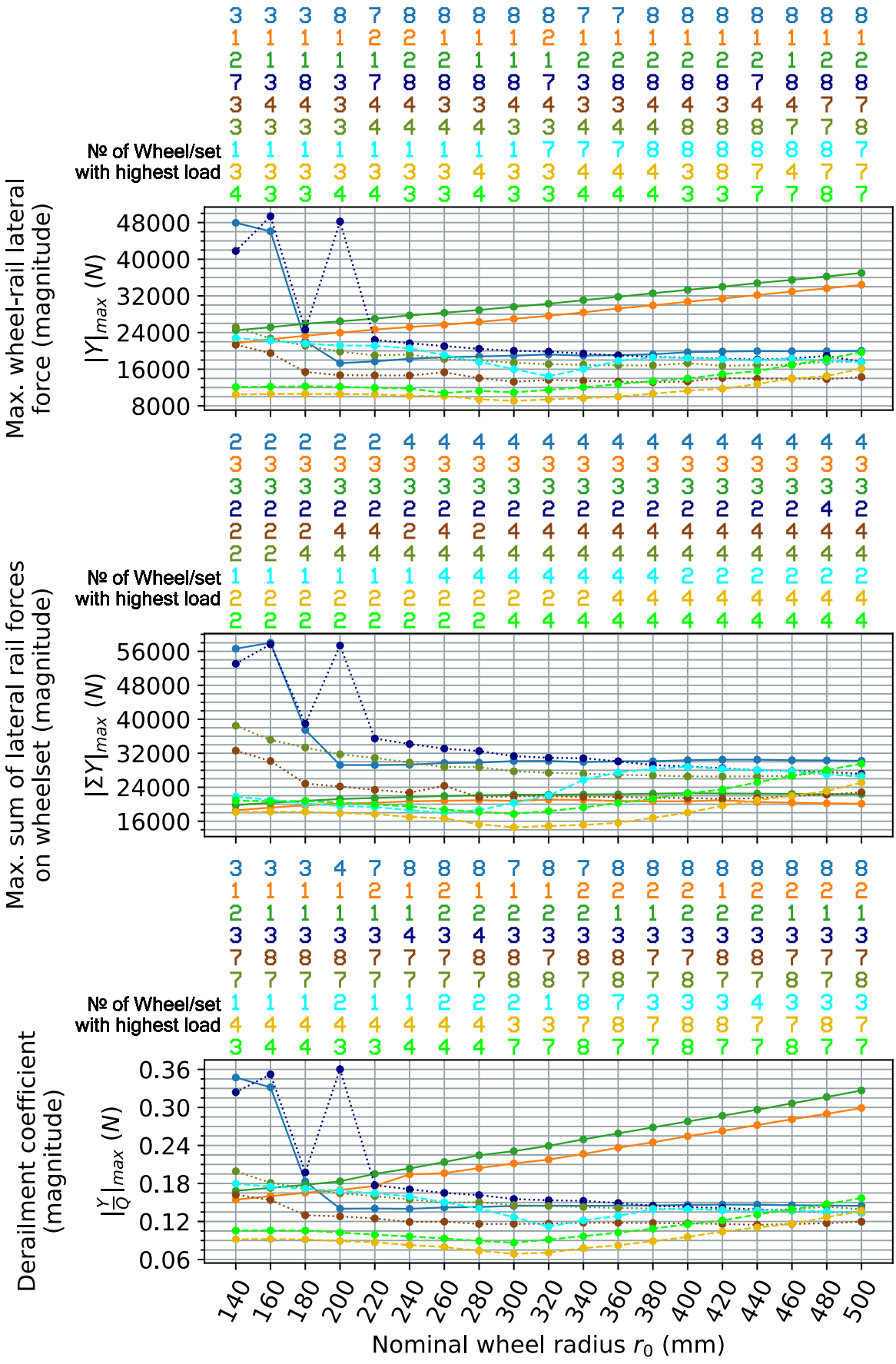

Figure G.16 Laden vehicle on a track with 1432 mm gauge and no rail cant, CAT2 curve

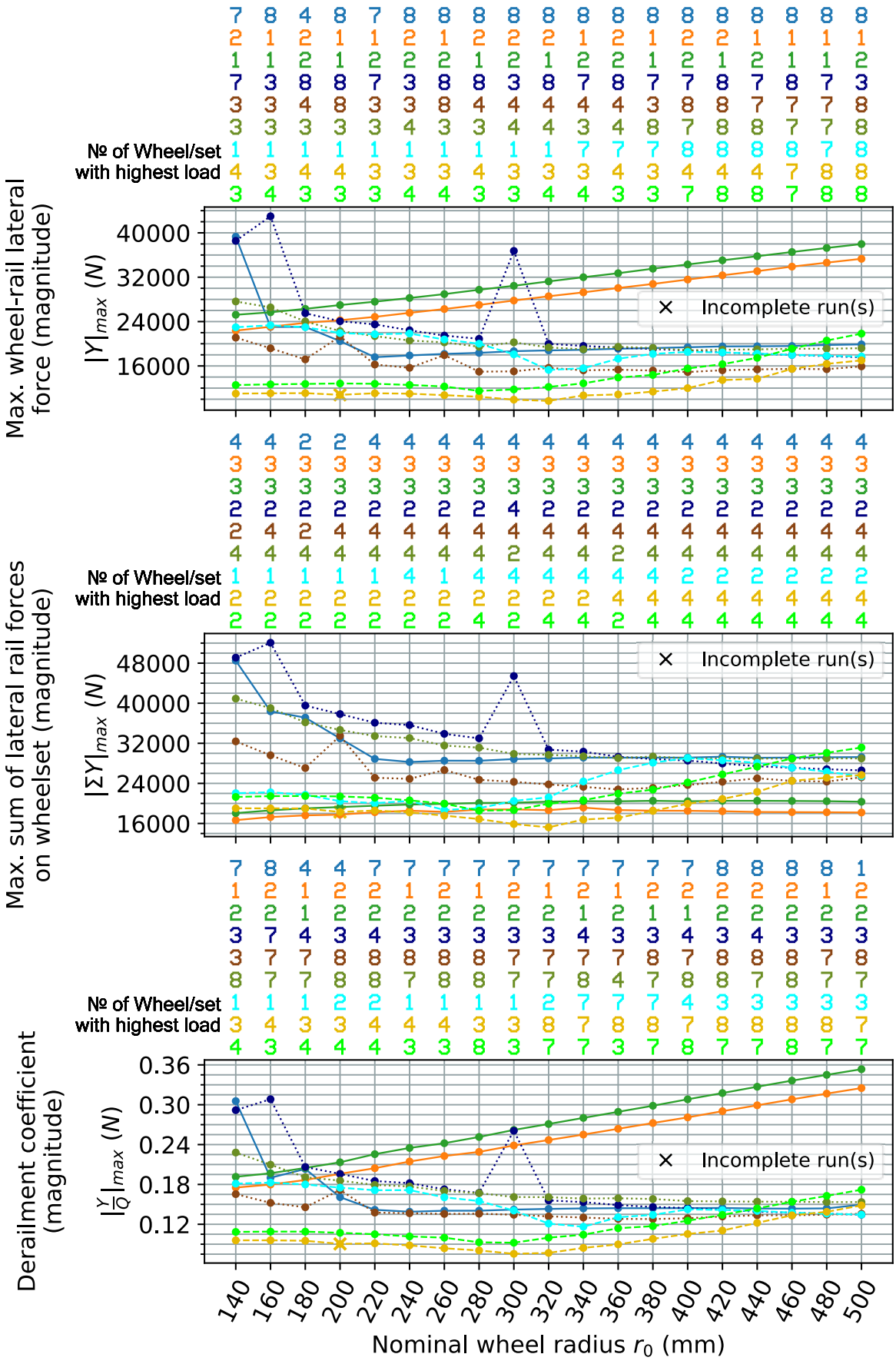

Figure G.17 Laden vehicle on a track with 1430 mm gauge and no rail cant, CAT2 curve

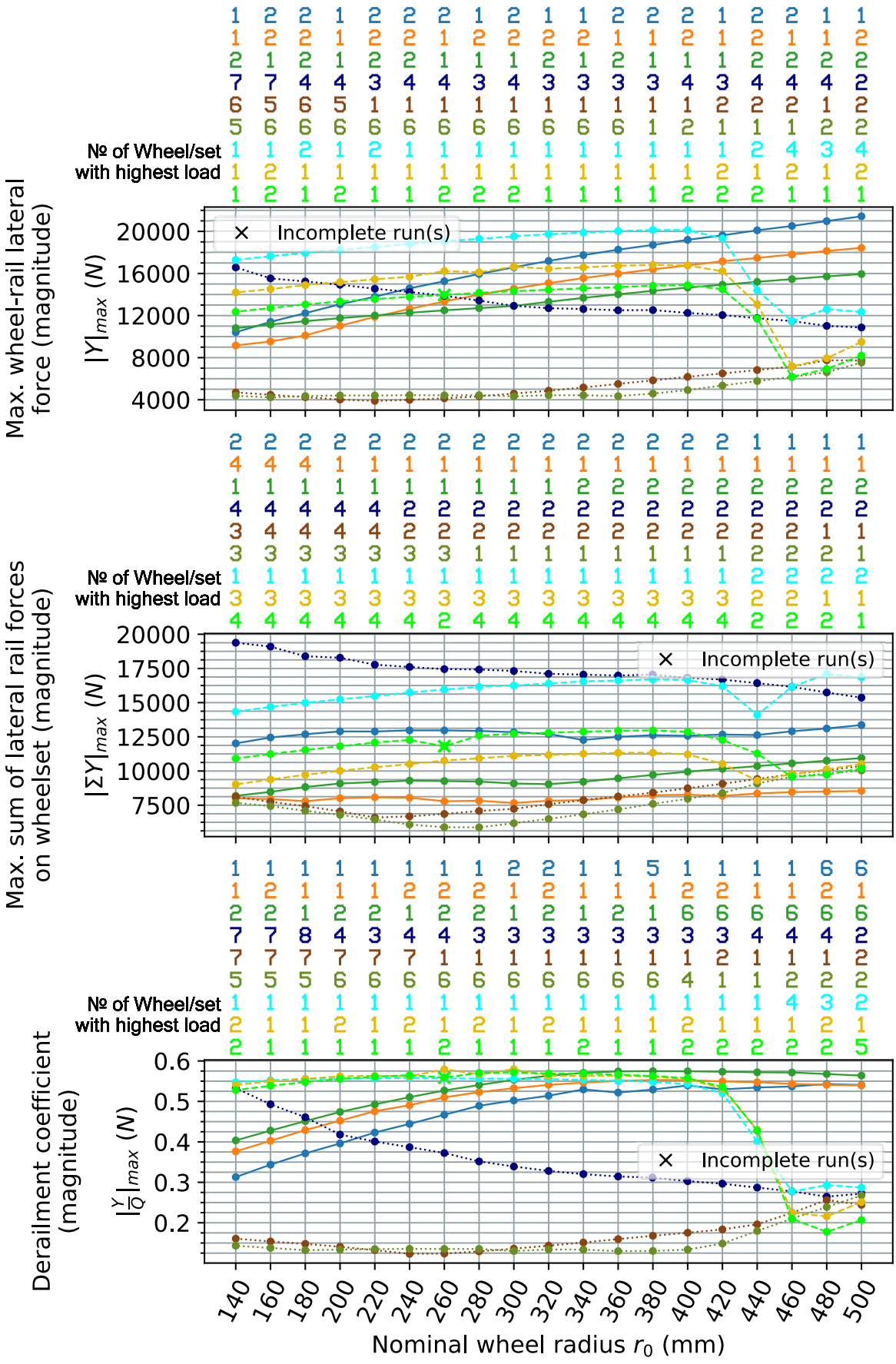

Figure G.18 Tare vehicle on a track with 1437 mm gauge and 1:40 rail cant, CAT4 curve

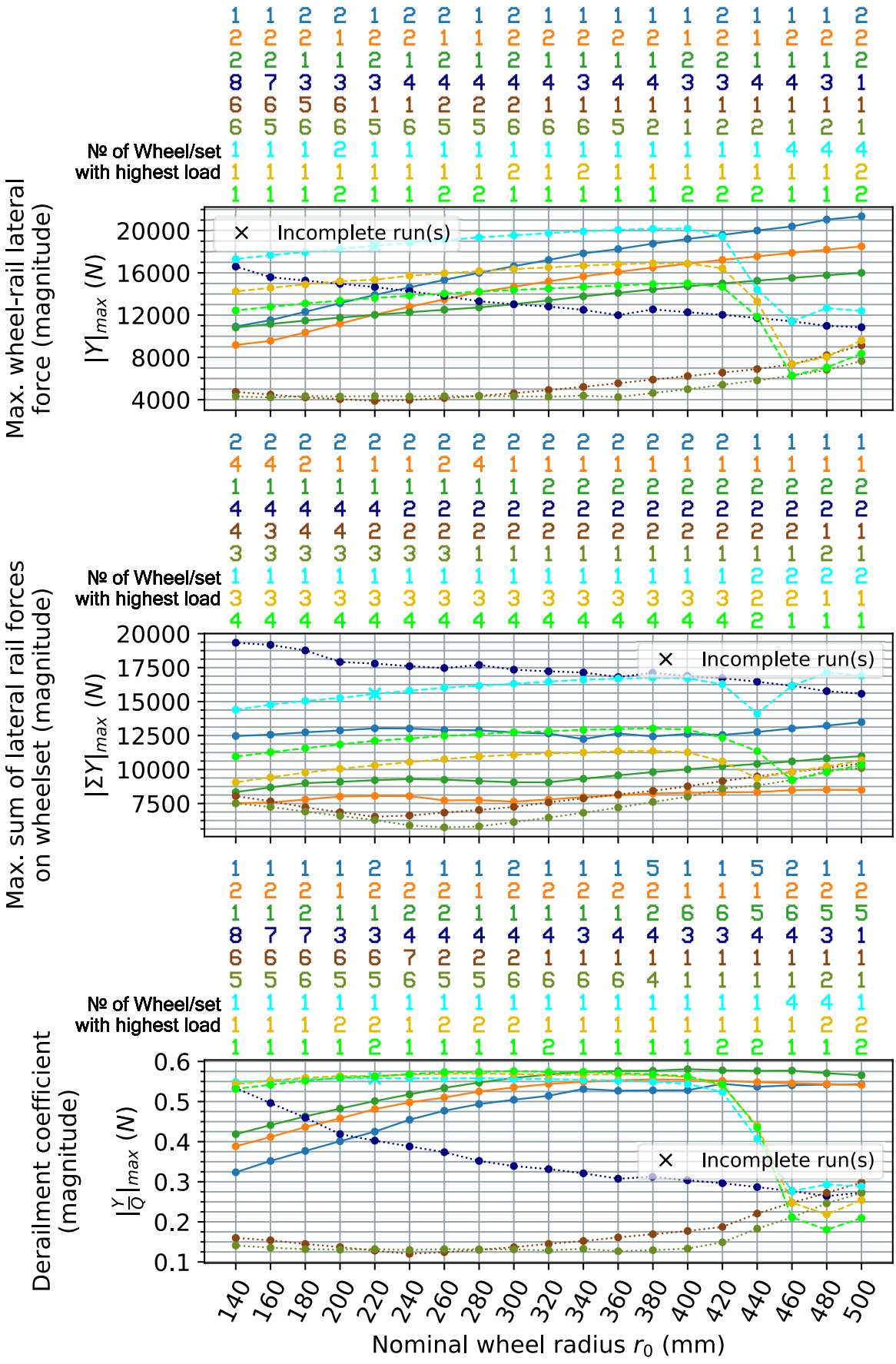

Figure G.19 Tare vehicle on a track with 1435 mm gauge and 1:40 rail cant (reference track setting), CAT4 curve

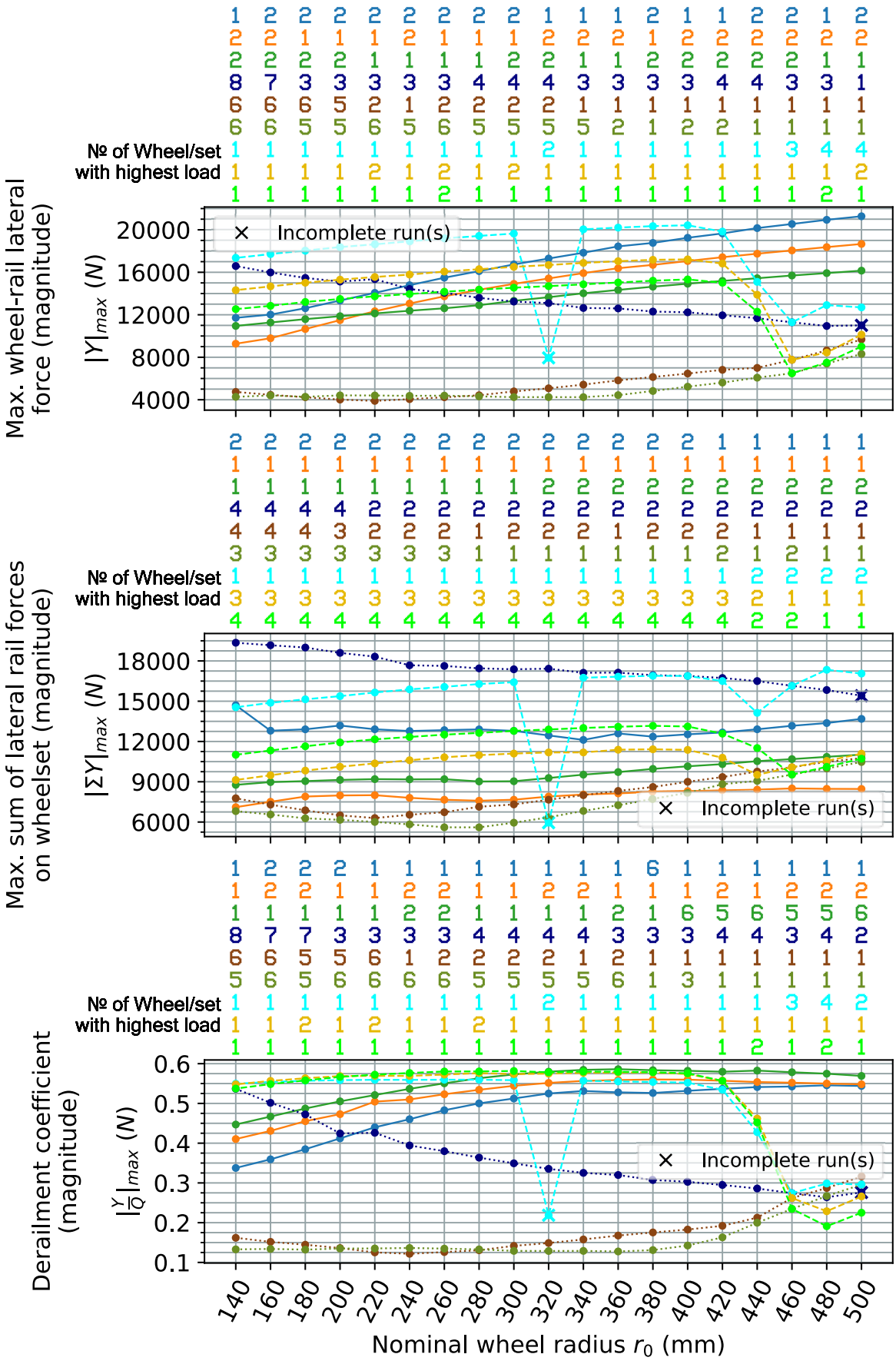

Figure G.20 Tare vehicle on a track with 1432 mm gauge and 1:40 rail cant, CAT4 curve

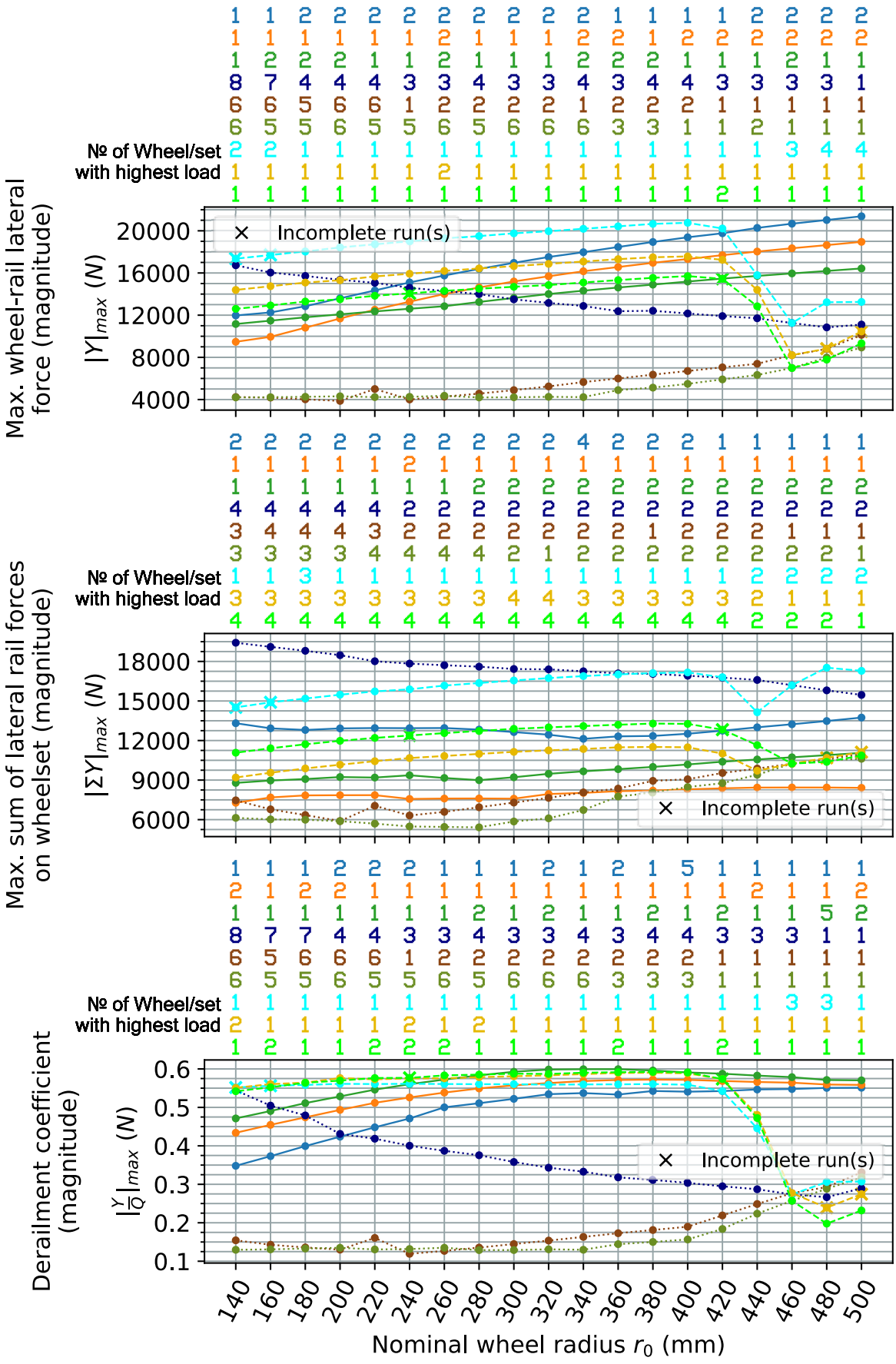

Figure G.21 Tare vehicle on a track with 1430 mm gauge and 1:40 rail cant, CAT4 curve

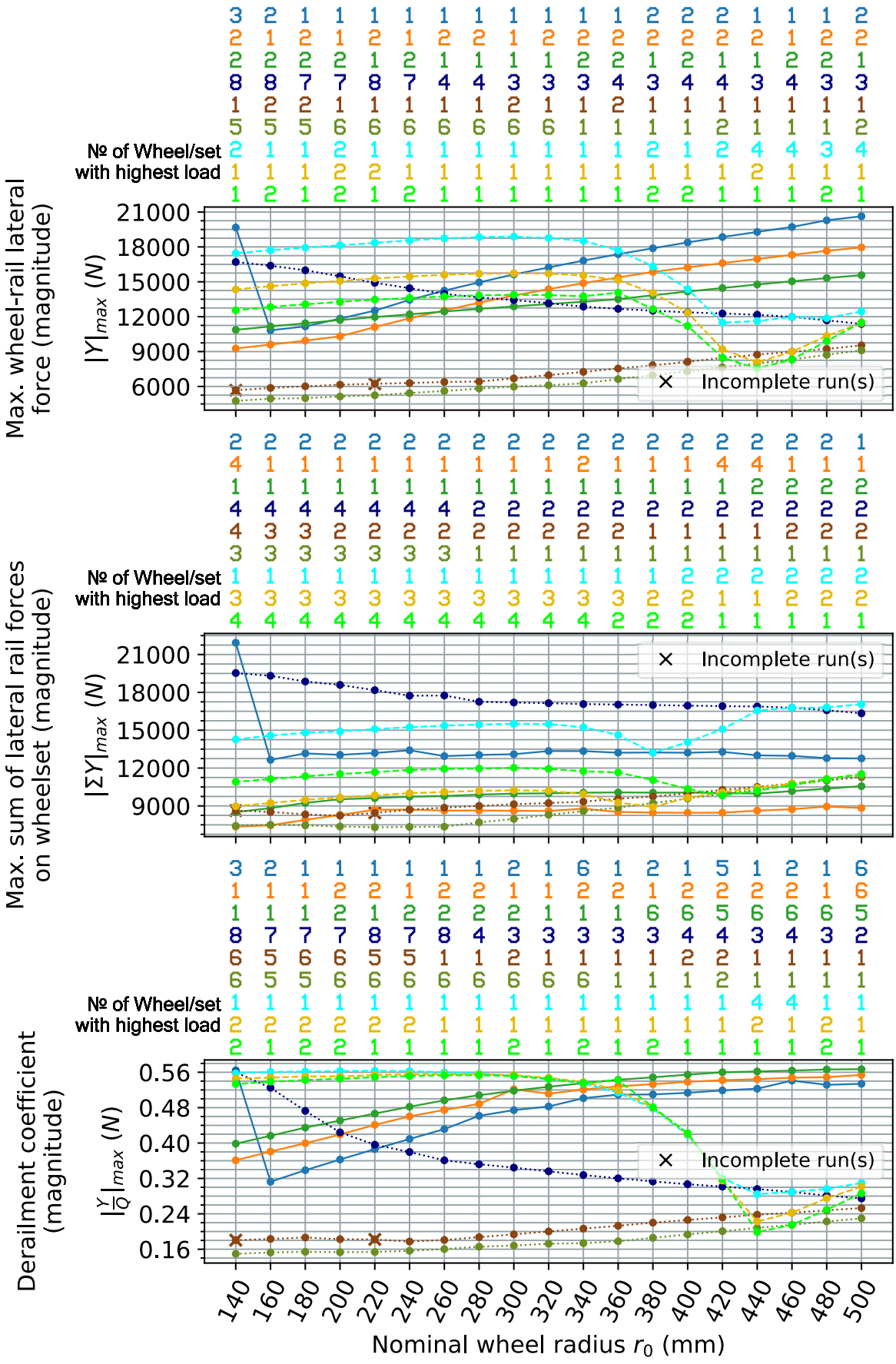

Figure G.22 Tare vehicle on a track with 1437 mm gauge and no rail cant, CAT4 curve

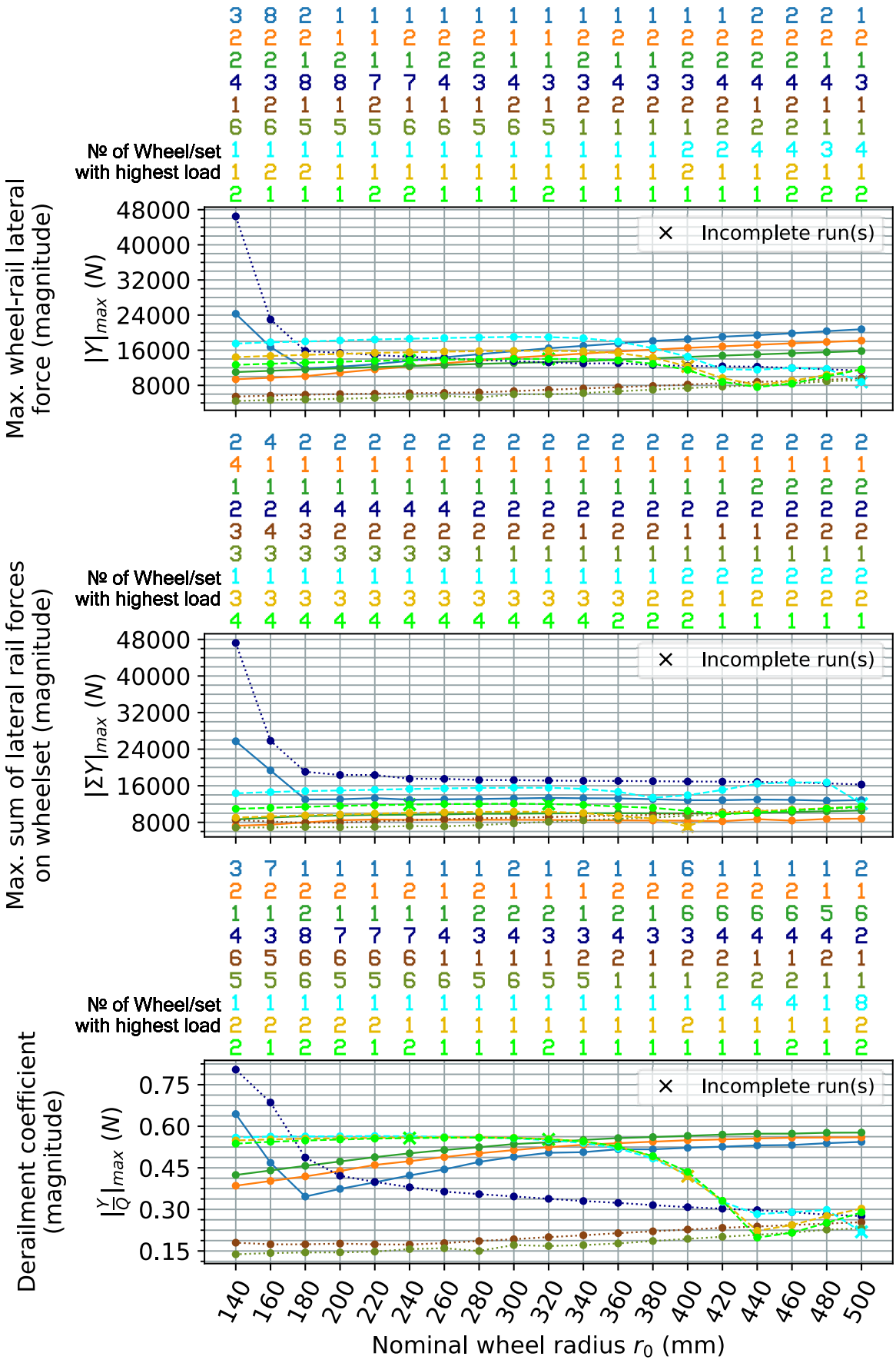

Figure G.23 Tare vehicle on a track with 1435 mm gauge and no rail cant, CAT4 curve

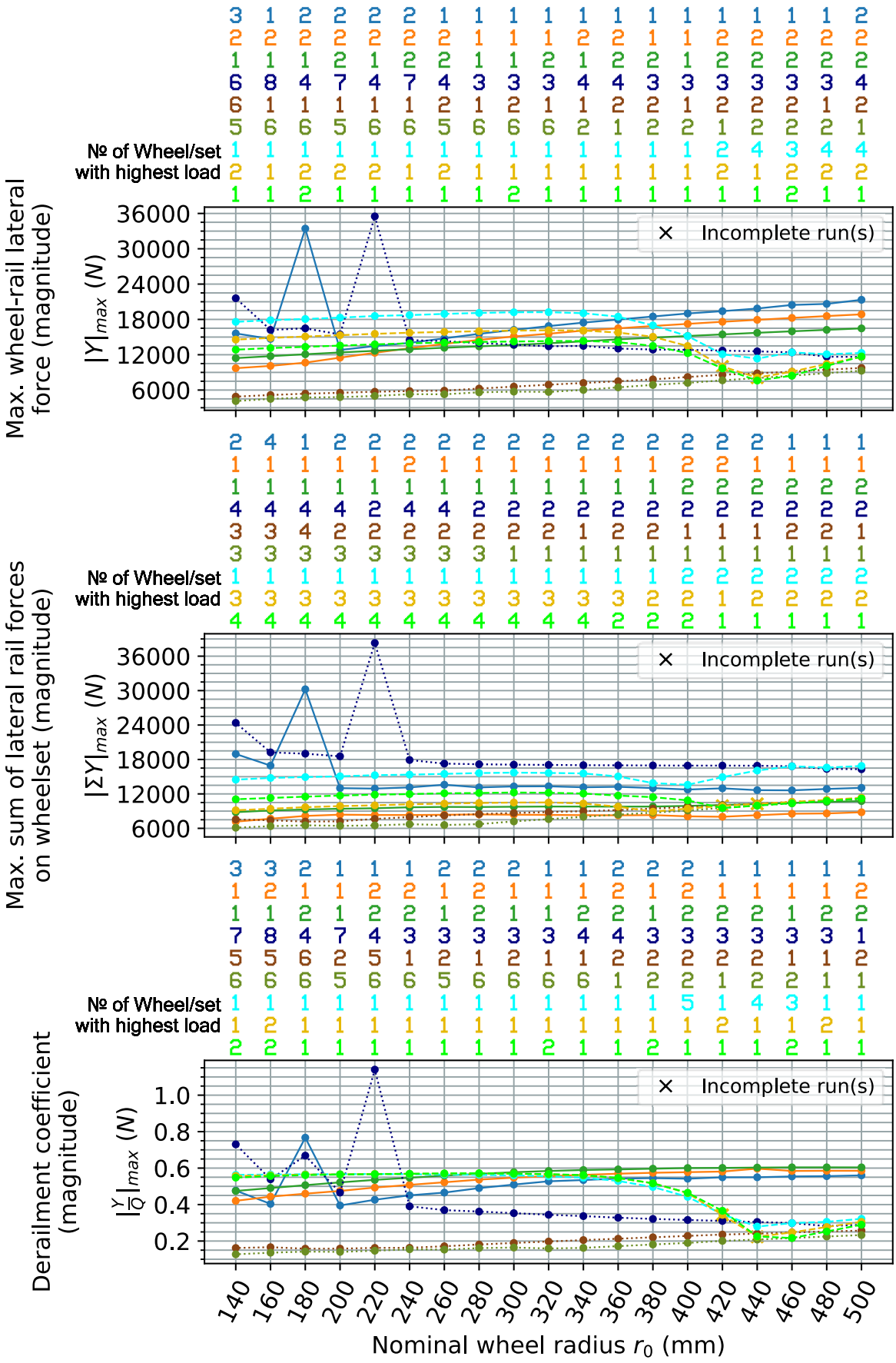

Figure G.24 Tare vehicle on a track with 1432 mm gauge and no rail cant, CAT4 curve

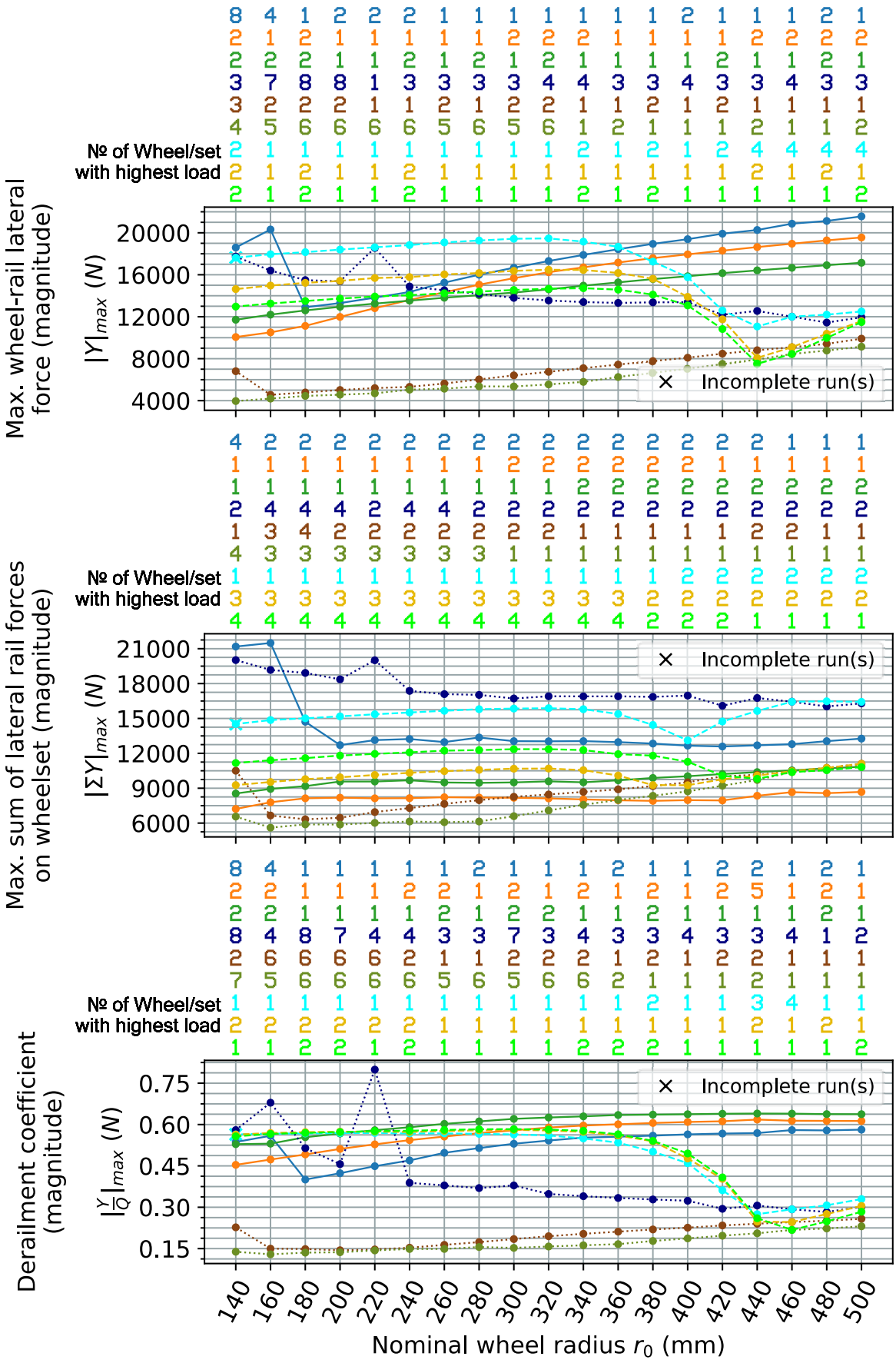

Figure G.25 Tare vehicle on a track with 1430 mm gauge and no rail cant, CAT4 curve

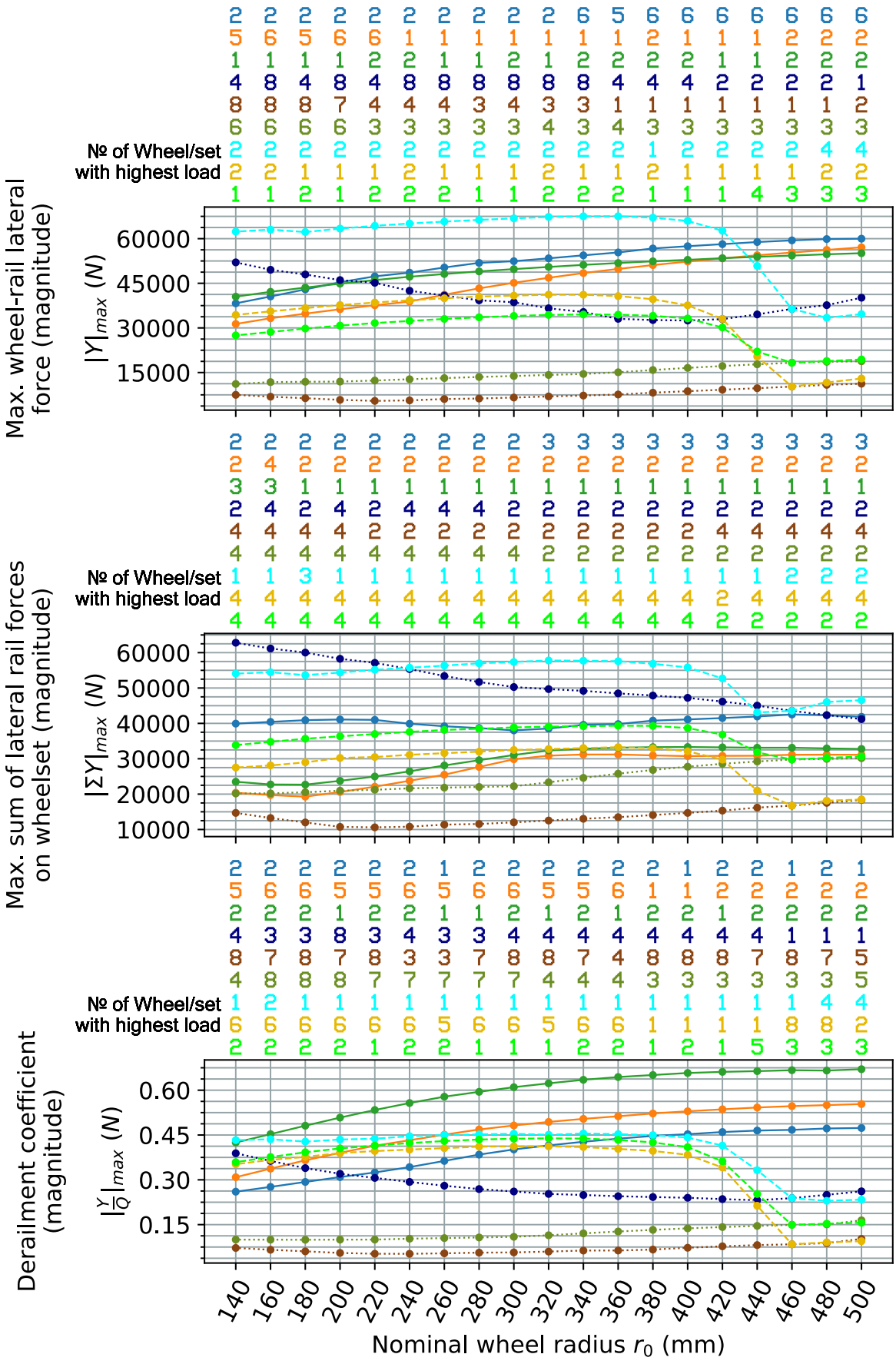

Figure G.26 Laden vehicle on a track with 1437 mm gauge and 1:40 rail cant, CAT4 curve

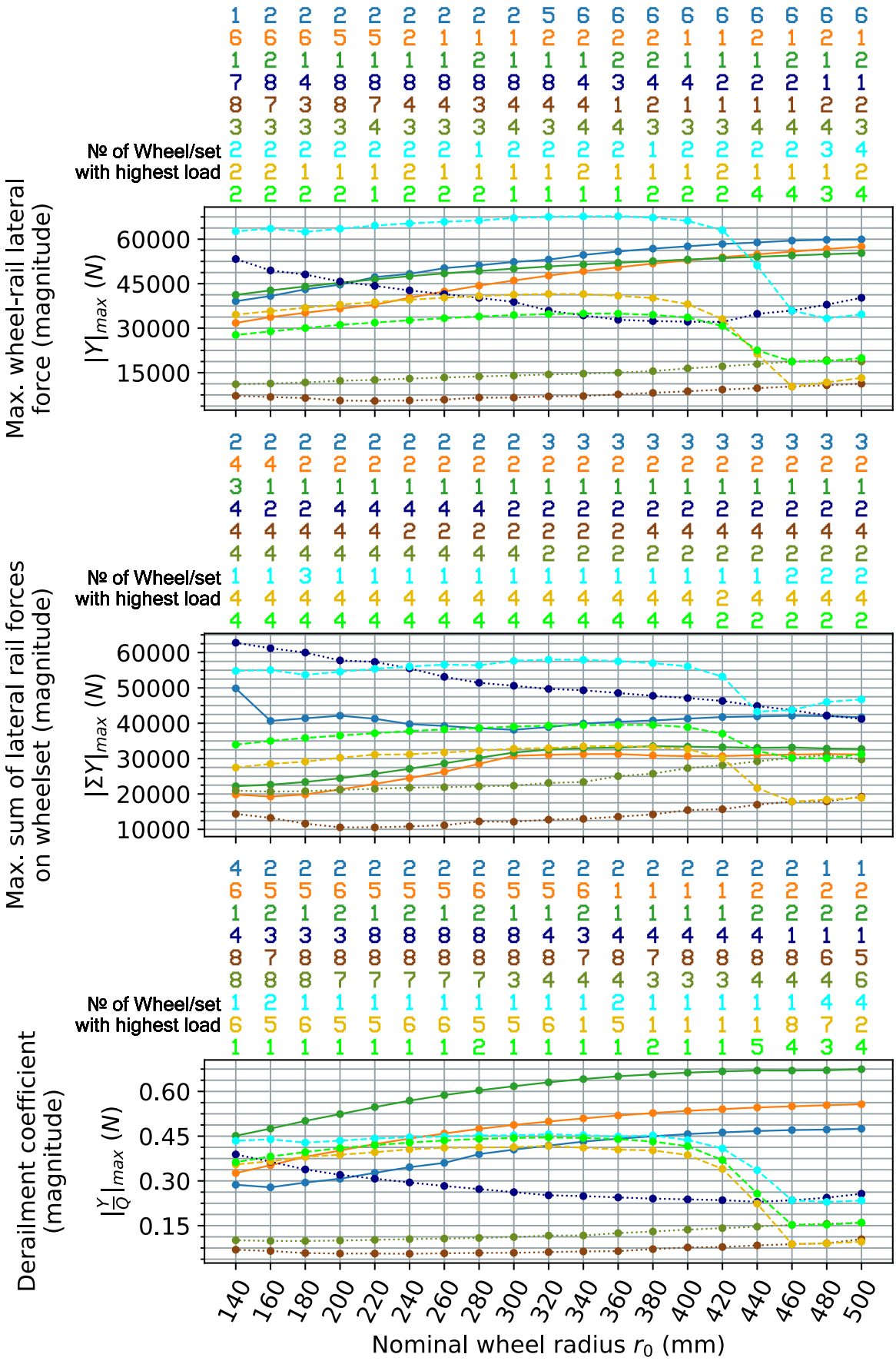

Figure G.27 Laden vehicle on a track with 1435 mm gauge and 1:40 rail cant (reference track setting), CAT4 curve

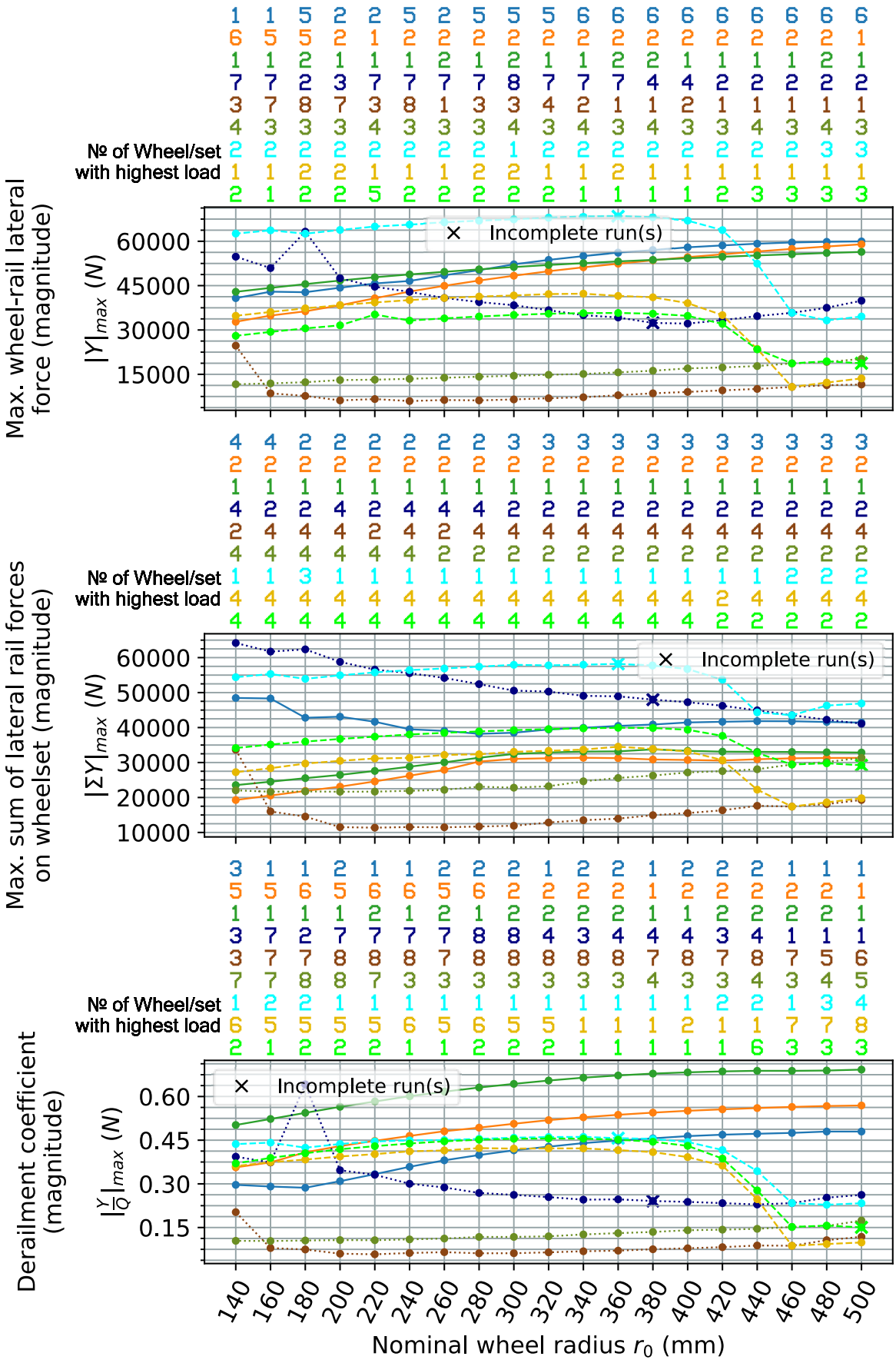

Figure G.28 Laden vehicle on a track with 1432 mm gauge and 1:40 rail cant, CAT4 curve

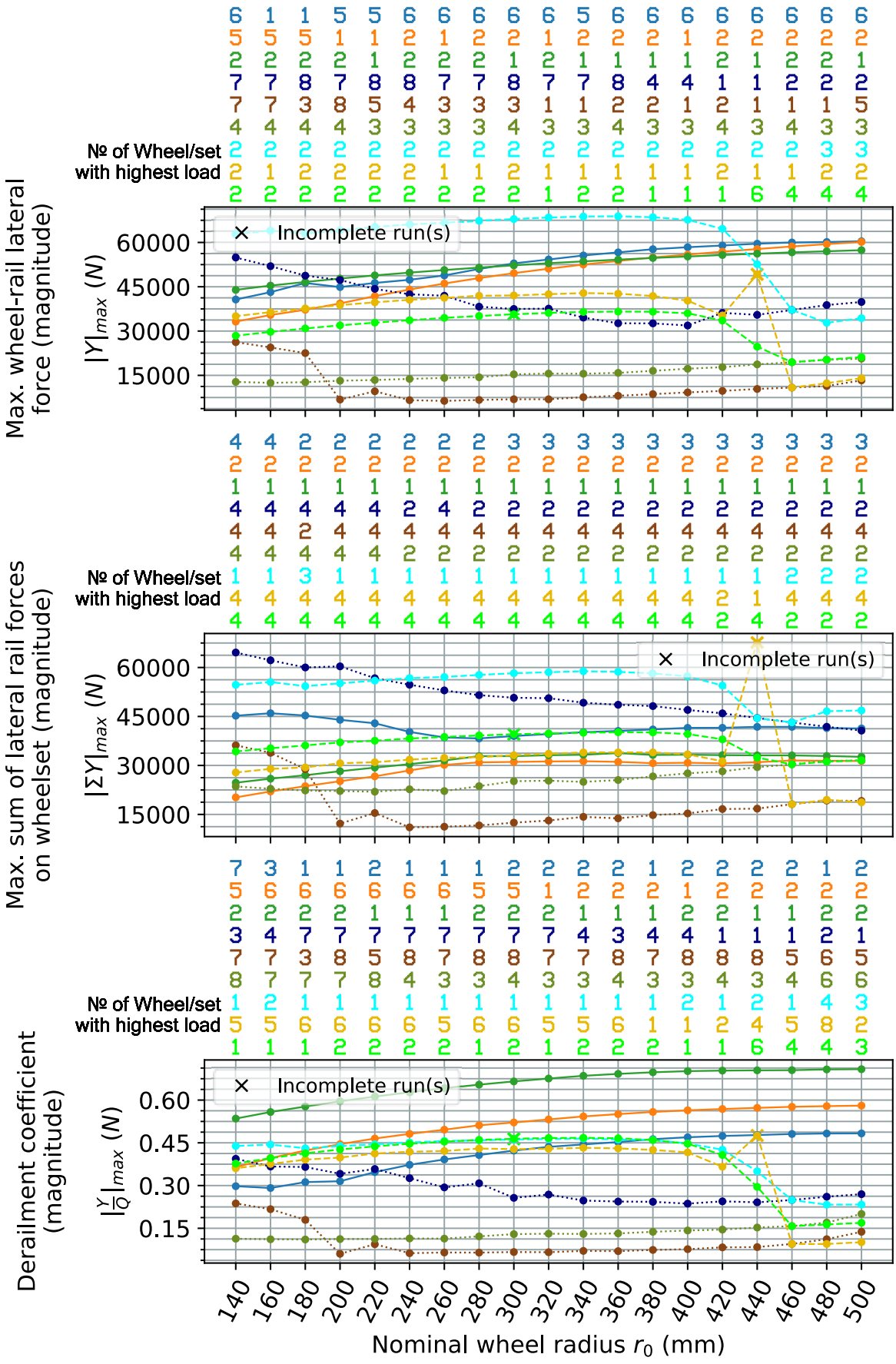

Figure G.29 Laden vehicle on a track with 1430 mm gauge and 1:40 rail cant, CAT4 curve

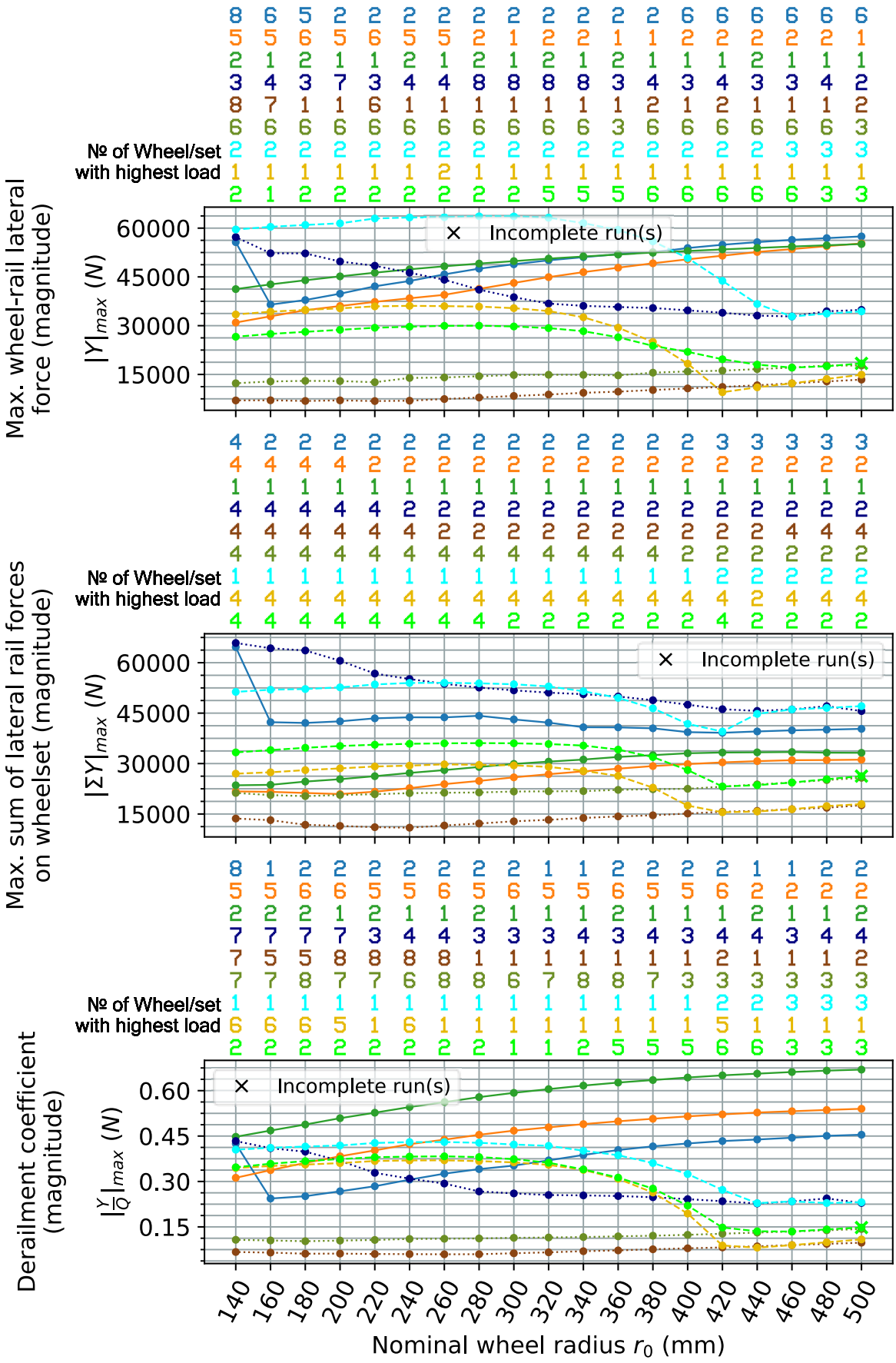

Figure G.30 Laden vehicle on a track with 1437 mm gauge and no rail cant, CAT4 curve

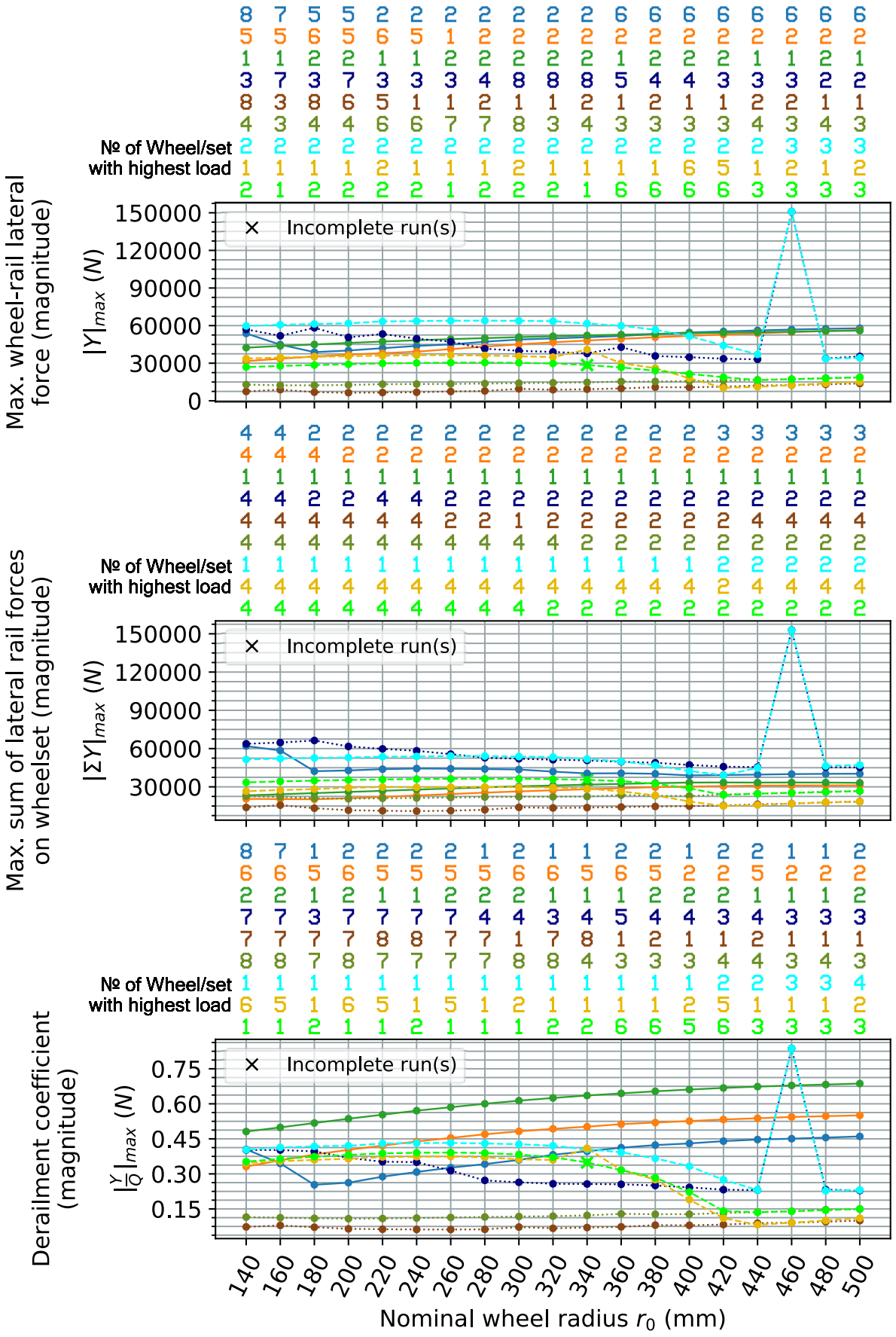

Figure G.31 Laden vehicle on a track with 1435 mm gauge and no rail cant, CAT4 curve

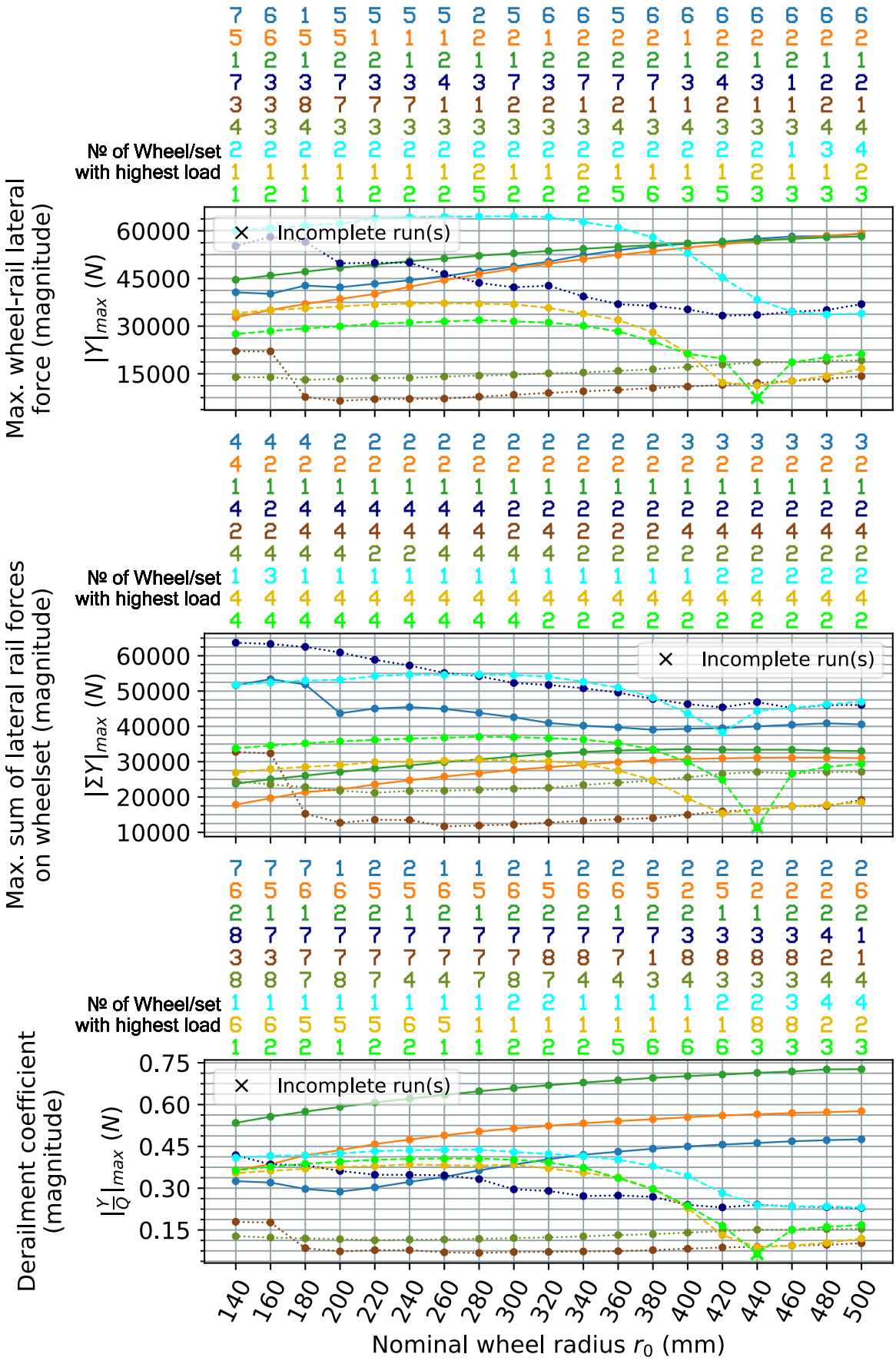

Figure G.32 Laden vehicle on a track with 1432 mm gauge and no rail cant, CAT4 curve

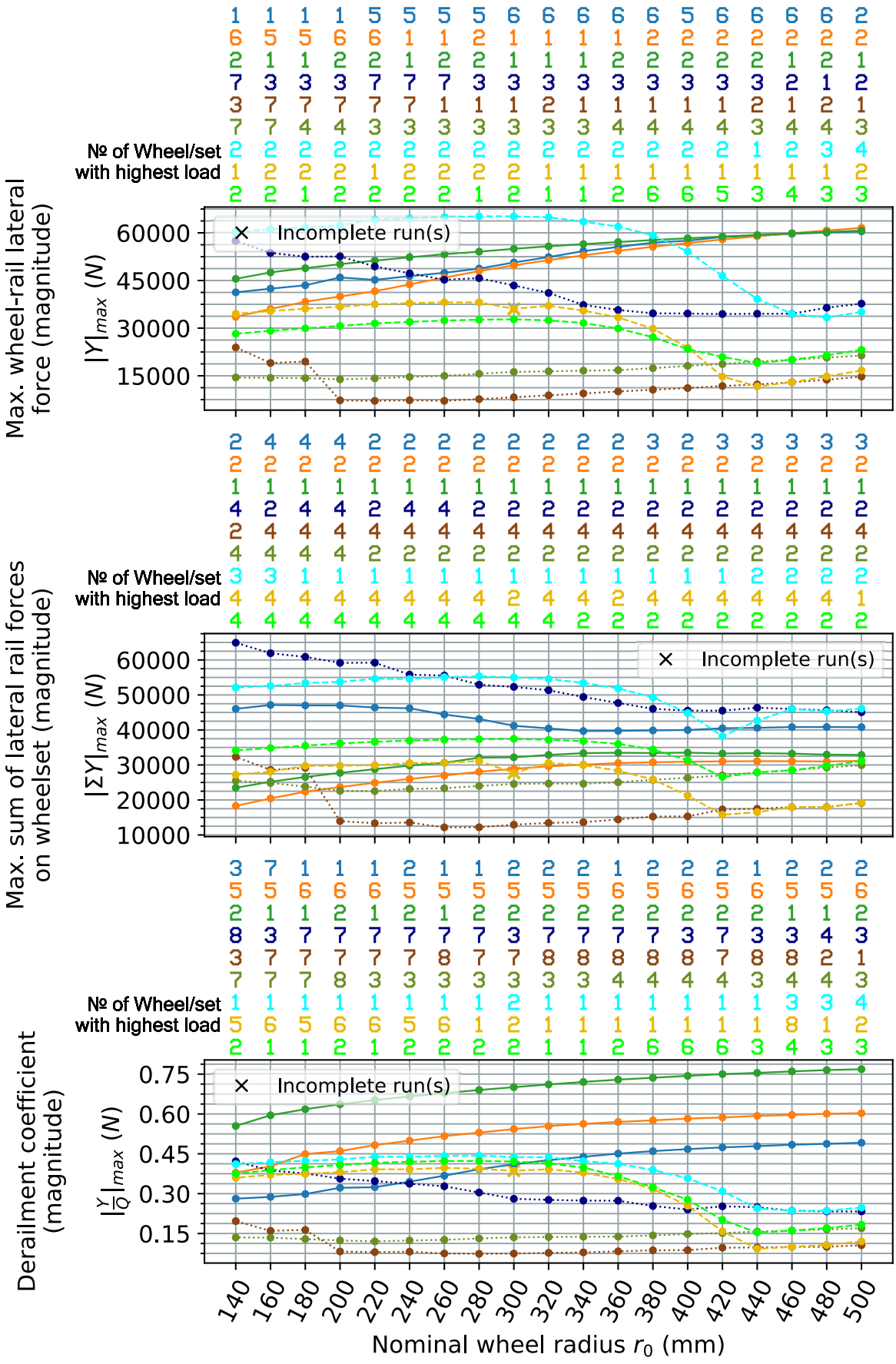

Figure G.33 Laden vehicle on a track with 1430 mm gauge and no rail cant, CAT4 curve

Appendix H Distance between nominal wheel-rail contact points on left and right wheels for each track gauge, rail cant and wheel profile

Table H.1 Lateral distance between left and right nominal wheel-rail contact points, e

Track gauge (mm)	Wheel profile	Corresponding nominal wheel radius in profile modification case MAT (mm)	Rail cant	
			1:40	None
			Lateral wheel-rail contact point distance *e* (m)	
1437	S1002	460	1.5103	1.4921
	Scaled 70%	--	1.5143	1.4983
	Scaled 108.7%	500	1.5079	1.4891
	Scaled 104.3%	480	1.5093	1.4907
	Scaled 95.7%	440	1.5112	1.4933
	Scaled 91.3%	420	1.5119	1.4943
	Scaled 87.0%	400	1.5125	1.4952
	Scaled 82.6%	380	1.5131	1.4961
	Scaled 78.3%	360	1.5135	1.4970
	Scaled 73.9%	340	1.5139	1.4977
	Scaled 69.6%	320	1.5143	1.4984
	Scaled 65.2%	300	1.5147	1.4991
	Scaled 60.9%	280	1.5150	1.4999
	Scaled 56.5%	260	1.5153	1.5006
	Scaled 52.2%	240	1.5156	1.5014
	Scaled 47.8%	220	1.5159	1.5021
	Scaled 43.5%	200	1.5161	1.5028
	Scaled 39.1%	180	1.5164	1.5035
	Scaled 34.8%	160	1.5166	1.5042
	Scaled 30.4%	140	1.5168	1.5049
1435	S1002	460	1.5051	1.4874
	Scaled 70%	--	1.5115	1.4953
	Scaled 108.7%	500	1.5010	1.4836
	Scaled 104.3%	480	1.5032	1.4856
	Scaled 95.7%	440	1.5066	1.4890
	Scaled 91.3%	420	1.5079	1.4904
	Scaled 87.0%	400	1.5089	1.4916
	Scaled 82.6%	380	1.5097	1.4927
	Scaled 78.3%	360	1.5104	1.4936
	Scaled 73.9%	340	1.5110	1.4945
	Scaled 69.6%	320	1.5115	1.4954
	Scaled 65.2%	300	1.5120	1.4961
	Scaled 60.9%	280	1.5124	1.4969
	Scaled 56.5%	260	1.5128	1.4977
	Scaled 52.2%	240	1.5132	1.4985

	Scaled 47.8%	220	1.5135	1.4993
	Scaled 43.5%	200	1.5138	1.5001
	Scaled 39.1%	180	1.5141	1.5009
	Scaled 34.8%	160	1.5144	1.5016
	Scaled 30.4%	140	1.5147	1.5024
1432	S1002	460	1.4954	1.4793
	Scaled 70%	--	1.5068	1.4904
	Scaled 108.7%	500	1.4917	1.4740
	Scaled 104.3%	480	1.4935	1.4768
	Scaled 95.7%	440	1.4975	1.4816
	Scaled 91.3%	420	1.4997	1.4836
	Scaled 87.0%	400	1.5017	1.4854
	Scaled 82.6%	380	1.5035	1.4869
	Scaled 78.3%	360	1.5048	1.4883
	Scaled 73.9%	340	1.5060	1.4895
	Scaled 69.6%	320	1.5068	1.4906
	Scaled 65.2%	300	1.5076	1.4916
	Scaled 60.9%	280	1.5083	1.4925
	Scaled 56.5%	260	1.5088	1.4933
	Scaled 52.2%	240	1.5093	1.4942
	Scaled 47.8%	220	1.5098	1.4951
	Scaled 43.5%	200	1.5102	1.4960
	Scaled 39.1%	180	1.5106	1.4969
	Scaled 34.8%	160	1.5110	1.4977
	Scaled 30.4%	140	1.5113	1.4986
1430	S1002	460	1.4899	1.4730
	Scaled 70%	--	1.5031	1.4871
	Scaled 108.7%	500	1.4860	1.4672
	Scaled 104.3%	480	1.4881	1.4700
	Scaled 95.7%	440	1.4917	1.4759
	Scaled 91.3%	420	1.4937	1.4784
	Scaled 87.0%	400	1.4958	1.4807
	Scaled 82.6%	380	1.4981	1.4827
	Scaled 78.3%	360	1.5001	1.4844
	Scaled 73.9%	340	1.5018	1.4859
	Scaled 69.6%	320	1.5032	1.4872
	Scaled 65.2%	300	1.5043	1.4883
	Scaled 60.9%	280	1.5052	1.4894
	Scaled 56.5%	260	1.5060	1.4904
	Scaled 52.2%	240	1.5066	1.4913
	Scaled 47.8%	220	1.5072	1.4922
	Scaled 43.5%	200	1.5077	1.4932
	Scaled 39.1%	180	1.5082	1.4942
	Scaled 34.8%	160	1.5086	1.4951
	Scaled 30.4%	140	1.5090	1.4960

References

1. Csiba J. Bogie Type Anniversary: The Bogie Type Y25 is Over 50 Years. In: Zobory I, editor. 10th International Conference on Railway Bogies and Running Gears; 12-15 September; Budapest, Hungary: Department of Rolling Stock, SSME/GTE; 2016. p. 253–262.
2. DIN EN 13715. Railway applications - Wheelsets and bogies - Wheels - Tread profile; German and French version. Berlin, Germany: Beuth Verlag, April 2015.
3. DIN EN 15273-2:2013. Railway applications - Gauges - Part 2: Rolling stock gauge; German version. Berlin, Germany: Beuth Verlag, September 2014.
4. Jahn H. Güterwagen-Drehgestelle: Clouth/Gummirollfeder - Talbot RoLa, BA 690 [Freight wagon bogie: Clouth/rubber roll spring - Talbot RoLa, BA 690; in German]. 2011. http://www.drehgestelle.de/6/gummi_rola690.html.
5. Lehmann D. Niederflurwagen für die "Rollende Landstraße Flachland": Saadkms 690 [Low-floor wagon for the "Rolling Highway Flatland": Saadkms 690; in German]. https://www.dybas.de/dybas/gw/gw_s_6/g690.html.
6. Rollende Landstraße 2019 [Rolling Highway 2019; in German]: Rail Cargo Operator - Austria GmbH; 2019.
7. Deutsche Bahn. Sylt Shuttle-Tarif [Sylt Shuttle tariff; in German], January 01, 2019.
8. Auto Abmessungen der europäischen Automobilmarkt mit Foto von jedem Neuwagen, Maße und seinen Dimensionen von Länge, Breite und Höhe [Automobile dimensions in the European automobile market with photos of each new vehicle, measurements and its dimensions of length, width and height; in German]. https://de.automobiledimension.com/.
9. Wandtke R. Neuentwicklungen der Stadler Pankow GmbH [New developments of Stadler Pankow GmbH; in German]; September 2011.
10. Künzel T. Triebwagen für den zukünftigen Nah- und Regionalverkehr in Deutschland [Multiple units for the short-distance and regional transport of future in Germany; in German] [Dissertation]. Berlin, Germany: Technical University of Berlin; 2019.
11. Holzborn I, Holzborn K-D. Kleine Typenkunde deutscher Triebfahrzeuge [Brief typology of powered railway vehicles in Germany; in German]: Betriebsfähige Lokomotiven und Triebwagen der Deutschen Bahn [Operational locomotives and multiple units of German Railway]. Berlin: Transpress; 1995.
12. Riechers D. Regionaltriebwagen: Neue Fahrzeuge für Deutschlands Nahverkehr [Regional multiple units: New vehicles for Germany's short-distance transport; in German]. 1st ed. Stuttgart: Transpress; 1998.
13. Deutscher Bahnkunden-Verband Brandenburg Regionalverband Havelland e.V. Aus Fahrgastsicht Regionaltriebwagen im Vergleich [Comparison of regional multiple units from passengers' viewpoint; in German]. Signal. 1997;1:21–3.
14. Klingel J. Ueber den Lauf der Eisenbahnwagen auf gerader Bahn [On the running of railway vehicles on straight railway track; in German]. Organ für die Fortschritte des Eisenbahnwesens in technischer Beziehung. 1883;20:16,114-123.

15. International Union of Railways UIC 510-2. Trailing stock: wheels and wheelsets. Conditions concerning the use of wheels of various diameters. 4th ed. Paris, France: International Union of Railways, May 2004.
16. DIN EN 14363-2016. Railway applications - Testing and simulation for the acceptance of running characteristics of railway vehicles - Running behaviour and stationary tests; German version. Berlin, Germany: Beuth Verlag, October 2016.
17. Yao J. 机车车辆动力学 [Dynamics of Locomotives and Rolling Stock; in Chinese]. Beijing, China: Science Press; 2014.
18. Standardization Administration of China GB 5599-85. Railway Vehicles - Specification for evaluation of the dynamic performance and accreditation test [in Chinese]. China: National Bureau of Standards, November 1985.
19. Spiryagin M, Cole C, Sun YQ, McClanachan M, Spiryagin V, McSweeney T. Design and simulation of rail vehicles. Boca Raton, Florida: CRC Press/Taylor and Francis; 2014.
20. International Union of Railways UIC 518. Testing and approval of railway vehicles from the point of view of their dynamic behaviour - Safety - Track fatigue - Ride quality. 3rd ed. Paris, France: International Union of Railways, October 2005.
21. European Commission Agency for Railways EU 321/2013. Technical specification for interoperability relating to the subsystem rolling stock — freight wagons of the rail system in the European Union and repealing Decision 2006/8 as well as61/EC, 13 March 2013.
22. Iwnicki S. Handbook of railway vehicle dynamics. Boca Raton: CRC/Taylor & Francis; 2006.
23. Wickens AH. The dynamics of railway vehicles—from Stephenson to Carter. Proceedings of the Institution of Mechanical Engineers, Part F: Journal of Rail and Rapid Transit. 1998;212:209–17. doi:10.1243/0954409981530805.
24. von Oeynhausen C. Ueber die Schienenwege in England: Bemerkungen gesammelt auf einer Reise in den Jahren 1826 und 1827 [On railroads in England: remarks collected from a trip in the years 1826 and 1827; in German]: G. Reimer; 1829.
25. Redtenbacher F. Die Gesetze des Lokomotiv-Baues [The laws locomotive construction; in German]. Mannheim: Verlag von Friedrich Bassermann; 1855.
26. Knothe K. Rail Vehicle Dynamics. Cham, Switzerland: Springer; 2016.
27. Wickens AH. Fundamentals of rail vehicle dynamics: Guidance and stability / A.H. Wickens. Lisse, The Netherlands, Exton, (PA): Swets & Zeitlinger Publishers; 2003.
28. Garg DP. Describing function techniques for the non-linear analysis of the dynamics of a rail vehicle wheelset. Springfield, Virginia, U.S.A.: U.S. Department of Transportation; July 1975.
29. Evans J, Berg M. Challenges in simulation of rail vehicle dynamics. Vehicle System Dynamics. 2009;47:1023–48. doi:10.1080/00423110903071674.
30. Dassault Systèmes. Simpack User Assistance; 2018.
31. Kisilowski J, editor. Advanced railway vehicle system dynamics. Warsaw: Wydawn. Naukowo-Techniczne; 1991.
32. Omale, D, Ojih, PB, Ogwo MO. Mathematical analysis of stiff and non-stiff initial value problems of ordinary differential equation using matlab. International Journal of Scientific & Engineering Research. 2014;5.

33. Vohla GKW. Werkzeuge zur realitätsnahen Simulation der Laufdynamik von Schienenfahrzeugen [Tools for realistic simulations of railway vehicle running dynamics; in German] [Dissertation]: ETH Zurich; 1995.
34. Bruni S, Vinolas J, Berg M, Polach O, Stichel S. Modelling of suspension components in a rail vehicle dynamics context. Vehicle System Dynamics. 2011;49:1021–72. doi:10.1080/00423114.2011.586430.
35. Kumbhalkar MA, Bhope DV, Vanalkar AV. Analysis of rail vehicle suspension spring with special emphasis on curving, tracking and tractive efforts. IOP Conf. Ser.: Mater. Sci. Eng. 2016;149:12131. doi:10.1088/1757-899X/149/1/012131.
36. Wittrick WH. On elastic wave propagation in helical springs. International Journal of Mechanical Sciences. 1966;8:25–47. doi:10.1016/0020-7403(66)90061-0.
37. Tang JS. Passive and semi-active airspring suspensions for rail passenger vehicles - theory and practice. Proceedings of the Institution of Mechanical Engineers, Part F: Journal of Rail and Rapid Transit. 1996;210:103–17. doi:10.1243/pime_proc_1996_210_333_02.
38. Quaglia G, Sorli M. Air suspension dimensionless analysis and design procedure. Vehicle System Dynamics. 2001;35:443–75. doi:10.1076/vesd.35.6.443.2040.
39. Ouyang Q, Shi Y. The non-linear mechanical properties of an airspring. Mechanical Systems and Signal Processing. 2003;17:705–11. doi:10.1006/mssp.2001.1434.
40. Doquier N. Multiphysics modelling of multibody systems – application to railway pneumatic suspensions [Ph. D. thesis]. Louvain-la-Neuve, Belgium: Université catholique de Louvain; November 2010.
41. Weidemann C, Mulski S. Modelling helical springs. SIMPACK News. 2007;11.
42. Presthus M. Derivation of air spring model parameters for train simulation [Master's thesis]: Luleå University of Technology; 2002.
43. Stiepel M, Zeipel S. Freight wagon running gears with leaf spring and ring suspension. In: Simpack User Group Meeting; 2004.
44. Piotrowski J. Model of the UIC link suspension for freight wagons. Archive of Applied Mechanics. 2003;73:517–32. doi:10.1007/s00419-003-0305-6.
45. van Kasteel R, Wang C-G, Qian L, Liu J-Z, Ye G-H. A new shock absorber model for use in vehicle dynamics studies. Vehicle System Dynamics. 2005;43:613–31. doi:10.1080/00423110420002667 20.
46. Garibaldi L, Onah HN. Viscoelastic material damping technology: Becchis Osiride; 1996.
47. Mellado AC, Gomez E, Vinolas J. Advances on railway yaw damper characterisation exposed to small displacements. International Journal of Heavy Vehicle Systems. 2006;13:263. doi:10.1504/ijhvs.2006.010583.
48. Freakley PK, Payne AR. Theory and practice of engineering with rubber: Applied Science Publishers; 1978.
49. Duym S, Stiens R, Reybrouck K. Evaluation of shock absorber models. Vehicle System Dynamics. 1997;27:109–27. doi:10.1080/00423119708969325.
50. Kaiser AB, Cusumano JP, Gardner JF. Modeling and Dynamics of Friction Wedge Dampers in Railroad Freight Trucks. Vehicle System Dynamics. 2002;38:55–82. doi:10.1076/vesd.38.1.55.3519.

51. Xia F. Modelling of a two-dimensional Coulomb friction oscillator. Journal of Sound and Vibration. 2003;265:1063–74. doi:10.1016/s0022-460x(02)01444-x.
52. Bruni S, Belforte P, Mancini G, Cera A, Hartwig H, Mazzola L. Experimental investigation of yaw damper performances: An improved and harmonised testing methodology developed within ModTrain EU project. In: WCRR'08 International Conference; May 18-22; Seoul, Korea; 2008.
53. Evans J. The modelling of railway passenger vehicles, the dynamics of vehicles on roads and tracks. In: 12th IAVSD Symposium; August 26-30, 1991; Lyon, France. Amsterdam/Lisse: Swets&Zeitlinger; 1992. p. 144–156.
54. Harder RF. Dynamic Modelling and Simulation of Three-Piece North American Freight Vehicle Suspensions with Non-linear Frictional Behaviour Using ADAMS/Rail. In: ; May10-12; Haarlem, the Netherlands; 2000.
55. Hertz H. Ueber die Berührung fester elastischer Körper [On the contact of elastic bodies; in German]. Journal für die reine und angewandte Mathematik [Journal for pure and applied mathematics]. 1881;92:156–71.
56. Kalker JJ. A Simplified Theory for Non-Hertzian Contact. Vehicle System Dynamics. 1983;12:43–5. doi:10.1080/00423118308968716.
57. Carter FW. The electric locomotive. Proceedings of the Institution of Civil Engineers. 1916:221–52.
58. Johnson KL. The effect of tangential contact force upon the rolling motion of an elastic sphere upon a plane. Journal of Applied Mechanics. 1958;80:339–46.
59. Johnson KL. The effect of spin upon the rolling motion of an elastic sphere upon a plane. Journal of Applied Mechanics. 1958;80:332–8.
60. Vermeulen PJ, Johnson KL. Contact of non-spherical elastic bodies transmitting tangential forces. Journal of Applied Mechanics. 1964;86:338–40.
61. Kalker JJ. On the rolling contact of two elastic bodies in the presence of dry friction [Doctoral thesis]. Delft, the Netherlands: TU Delft; 1967.
62. Kalker JJ. Three-dimensional elastic bodies in rolling contact. Dordrecht, London: Kluwer Academic Publishers; 1990.
63. Polach O. A fast wheel-rail forces calculation computer code. Vehicle System Dynamics. 1999;33:728–39. doi:10.1080/00423114.1999.12063125.
64. brilliant.org. Newton Raphson Method. https://brilliant.org/wiki/newton-raphson-method/.
65. Forsythe GE, Malcolm MA, Moler C. Computer methods for mathematical computations. Englewood Cliffs, London: Prentice-Hall; 1977.
66. Arnold M, Burgermeister B, Führer C, Hippmann G, Rill G. Numerical methods in vehicle system dynamics: state of the art and current developments. Vehicle System Dynamics. 2011;49:1159–207. doi:10.1080/00423114.2011.582953.
67. Petzold LR. Methods and software for differential-algebraic systems. In: Haug EJ, Deyo RC, editors; 1991; Berlin, Heidelberg. Berlin, Heidelberg: Springer Berlin Heidelberg; 1991. p. 127–140.
68. Brenan KE, Campbell SL, Petzold LR. Numerical solution of initial-value problems in differential-algebraic equations: Society for Industrial and Applied Mathematics; 1995.

69. Polach O. On non-linear methods of bogie stability assessment using computer simulations. Proceedings of the Institution of Mechanical Engineers, Part F: Journal of Rail and Rapid Transit. 2006;220:13–27. doi:10.1243/095440905X33251.
70. Alfi S, Mazzola L, Bruni S. Effect of motor connection on the critical speed of high-speed railway vehicles. Vehicle System Dynamics. 2008;46:201–14. doi:10.1080/00423110801935814.
71. Wang K, Huang C, Zhai W, Liu P, Wang S. Progress on wheel-rail dynamic performance of railway curve negotiation. Journal of Traffic and Transportation Engineering (English Edition). 2014;1:209–20. doi:10.1016/S2095-7564(15)30104-5.
72. Braghin F, Bruni S, Resta F. Active yaw damper for the improvement of railway vehicle stability and curving performances: simulations and experimental results. Vehicle System Dynamics. 2006;44:857–69. doi:10.1080/00423110600733972.
73. Sun YQ, Simson S. Nonlinear three-dimensional wagon–track model for the investigation of rail corrugation initiation on curved track. Vehicle System Dynamics. 2007;45:113–32. doi:10.1080/00423110600863407.
74. Mazzola L. Possibilities and challenges for the virtual homologation of the railway rolling stock; 2009.
75. Mazzola L, Bruni S, Alfi S. Virtual homologation of railway rolling stock: possibilities and challenges. In: ; July 8-12; St. Petersburg, Russia; 2009. p. 1–13.
76. Polach O, Böttcher A, Vannucci D, Sima J, Schelle H, Chollet H, et al. Validation of simulation models in the context of railway vehicle acceptance,. Proceedings of the Institution of Mechanical Engineers, Part F: Journal of Rail and Rapid Transit. 2015;229:729–54. doi:10.1177/0954409714554275.
77. Wilson N, Fries R, Witte M, Haigermoser A, Wrang M, Evans J, Orlova A. Assessment of safety against derailment using simulations and vehicle acceptance tests: a worldwide comparison of state-of-the-art assessment methods. Vehicle System Dynamics. 2011;49:1113–57. doi:10.1080/00423114.2011.586706.
78. Polach O, Evans J. Simulations of running dynamics for vehicle acceptance: application and validation. Int J Railw Tech. 2013;2:59–84. doi:10.4203/ijrt.2.4.4.
79. Dongfang S. 高速列车悬挂系统参数多目标优化 [Multiobjective optimization of suspension parameters of a high-speed railway coach; in Chinese] [Master thesis]. Beijing, China: Beijing Jiaotong University; 2015.
80. Liu Y, Liu X. Railway wheel profile optimization design based on NURBS curve. In: 2010 Second International Conference on Computer Modeling and Simulation (ICCMS); 1/22/2010 - 1/24/2010; Sanya, China. Piscataway, NJ: IEEE; 2010. p. 331–335. doi:10.1109/ICCMS.2010.439.
81. Bhushan B. Principles and applications of tribology. Chichester: Wiley; 2013.
82. Krause H, Poll G. Verschleiss bei gleitender und wälzender Relativbewegung - Vorschlag zur Berechnung und Versuch einer Synthese des energetischen Ansatzes und der Grenzflächentemperaturhypothese [Wear from sliding and rolling relative motion - suggestions on the simulation and testing of a synthesis of the energy method and the border area temperature hypothesis; in German]. Tribologie und Schmierungstechnik [Tribology and Lubrication Technology]. 1984;31:209–214, 285-289.

83. Smith A, Iwnicki S, Kaushal A, Odolinski K, Wheat P. Estimating the relative cost of track damage mechanisms: combining economic and engineering approaches. Proc Inst Mech Eng F J Rail Rapid Transit. 2017;231:620–36. doi:10.1177/0954409717698850.
84. Archard JF. Contact and rubbing of flat surfaces. Journal of Applied Physics. 1953;24:981–8. doi:10.1063/1.1721448.
85. Kettler G. Güterwagen-Laufwerke der Neubau-Güterwagen der Rail Cargo Austria AG [Freight wagon running gears of the newly constructed freight wagons of Rail Cargo Austria AG; in German]. Graz, Austria; April 7-10, 2013.
86. Karttunen K. Influence of rail, wheel and track geometries on wheel and rail degradation [Ph. D. thesis]. Göteborg, Sweden: Chalmers University of Technology; 2015.
87. Herrmann T. Methode zur Detektion von hohlgelaufenen Rädern an Güterwagen [Methods for detecting wheels with hollow wear on freight wagons; in German]. 1st ed. Herzogenrath: Shaker; 2017.
88. Tavakkoli H, Ghajar R, Alizadeh K. J. The influence of tread hollowing of the railway wheels on the hunting of a coach. In: ASME 2010 International Mechanical Engineering Congress and Exposition; 11/12/2010 - 11/18/2010; Vancouver, British Columbia, Canada. New York, N.Y.: ASME; 2012. p. 895–900. doi:10.1115/IMECE2010-37832.
89. Lu Y, Gao Z, Wang J. Study on influence of diversified parameters of vehicle and track on wheel hollow wear. Shock and Vibration. 2018;2018:1–11. doi:10.1155/2018/8972615.
90. Sawley K, Wu H. The formation of hollow-worn wheels and their effect on wheel/rail interaction. Wear. 2005;258:1179–86. doi:10.1016/j.wear.2004.03.029.
91. Cui D, Li L, Wang H, Wen Z, Xiong J. High-speed EMU wheel re-profiling threshold for complex wear forms from dynamics viewpoint. Wear. 2015;338-339:307–15. doi:10.1016/j.wear.2015.06.020.
92. Lari AA. Wheel wear prediction-comparison between analytical approaches and field tests. In: Joint Rail Conference; April 4-6; Atlanta, Georgia, USA; 2006. p. 45–54.
93. Markine VL, Shevtsov IY. Optimization of a wheel profile accounting for design robustness. Proceedings of the Institution of Mechanical Engineers, Part F: Journal of Rail and Rapid Transit. 2011;225:433–42. doi:10.1177/09544097JRRT305.
94. Cui D. Wheel-rail profiles matching design considering railway track parameters. Chinese Journal of Mechanical Engineering. 2010;23:410. doi:10.3901/CJME.2010.04.410.
95. Esveld C, Markine VL, Shevtsov IY. Shape optimisation of a railway wheel profile. 2006. https://www.globalrailwayreview.com/article/2222/shape-optimisation-of-a-railway-wheel-profile/.
96. Magel E, Kalousek J. Designing and assessing wheel/rail profiles for improved rolling contact fatigue and wear performance. Proceedings of the Institution of Mechanical Engineers, Part F: Journal of Rail and Rapid Transit. 2017;231:805–18. doi:10.1177/0954409717708079.
97. Lu Z, Zhang B, Wang H. Wheel reprofiling of a high-speed electric-multiple-unit train based on a multi-objective optimization strategy. Proceedings of the Institution of Mechanical Engineers, Part F: Journal of Rail and Rapid Transit. 2015;229:484–99. doi:10.1177/0954409713515858.

98. Grzyna M. Analiza konstrukcji nowoczesnych układów biegowych wagonów towarowych w aspekcie zamienności ze standardowymi wózkami Y25 [Analysis of the construction of modern running systems of freight wagons in terms of interchangeability with the standard Y25 bogies; in Polish]. Zeszyty Naukowe Państwowej Wyższej Szkoły Zawodowej im. Witelona w Legnicy [Scientific Papers of The Witelon State University of Applied Sciences in Legnica]. 2018;29:321–40.
99. Federal Ministry of Transport and Digital Infrastructure of Germany (Bundesministerium für Verkehr und digitale Infrastruktur). Eisenbahn-Bau- und Betriebsordnung [Ordinance on the Construction and Operation of Railways; in German], May 8, 1967.
100. Österreiche Bundesbahnen (ÖBB) (Austrian Federal Railways) ÖBB-Regelwerk 01/03. Entwerfen von Bahnanlagen: Linienführung von Gleisen [Design of railway facilities: course arrangement of the railway track; in German], Sept. 2, 2016.
101. Hecht M, Geike T, Schirmer A. Entgleisungsrechnung für einen Kesselwagen mit Y25-Drehgestellen bei Federbruch [Derailment calculation for a tank wagon with Y25 bogies in the case of spring failure; in German]. Berlin, Germany: Technical University of Berlin; 2002, 34/2002.
102. Hecht M, Keudel J. Entgleisungsuntersuchung für einen Kesselwagen mit Y25 Drehgestellen [Derailment calculation for a tank wagon with Y25 bogies; in German]. Berlin, Germany: Technical University of Berlin; 2003, 32/2003.
103. Hecht M, Keudel J. Exemplarische Entgleisungsuntersuchung für einen Kesselwagen mit Y25 Drehgestellen [An exemplary derailment investigation of a tank wagon with Y25 bogies; in German]. Berlin, Germany: Technical University of Berlin; 2005, 24/2005.
104. Hecht M, Keudel J. Numerische Simulation eines Schiebewandwagens Habbiins344 mit Y25 Drehgestellen Y−Kraft [Numerical simulation of a sliding-wall wagon Habbiins344 with Y25 bogies; in German]. Berlin, Germany: Technical University of Berlin; 2005, 03/2005.
105. Hecht M, Keudel J. Numerische Simulation eines Selbstentladewagensmit Y25-Drehgestellen [Numerical simulation of a self-dumping wagon with Y25 bogies; in German]. Berlin, Germany: Technical University of Berlin; 2005, 31/2005.
106. Molatefi H, Hecht M, Kadivar MH. Critical speed and limit cycles in the empty Y25-freight wagon. JRRT, Journal of Rail and Rapid Transit. 2006;220:347–59.
107. Keudel J. Messung der Charakteristik der Primärfesselung eines Güterwagendrehgestells der Bauart Y25 und deren Implementierung in eines MKS-Modell für die Simulationssoftware MEDYNA [Measurement of primary suspension characteristics of a Type Y25 freight wagon bogie and its interpretation in an MBS model for the simulation software MEDYNA; in German]. Berlin: Technical University of Berlin; March 2003.
108. Hecht M, Schelle H. Simulation von Kesselwagen mit Y25-Drehgestellen bei Gleislagefehlern [Simulation of tank wagons with Y25 bogies with track irregularities; in German]. Berlin, Germany: Technical University of Berlin; 2010, 16/2010.
109. Hecht M, Götz G. Energy reduction of the freight wagon bogie TVP2007 compared to the standard bogie Y25. Berlin, Germany: Technical University of Berlin; 2014, 23/2013.
110. Muñoz-Alicea R. Introduction to bifurcations and the Hopf bifurcation theorem for planar systems: Colorado State University; 2011.

111. DIN EN 13803:2017. Railway applications - Track - Track alignment design parameters - Track gauges 1 435 mm and wider; German version. Berlin, Germany: Beuth Verlag, September 2017.
112. Wickens AH, Goodall RM, Li J. Re-evaluation of the limitations of the railway wheelset: passive and active. Vehicle System Dynamics. 2006;44:14–23. doi:10.1080/00423110600867200.
113. Hanneforth W, Fischer W. Laufwerke [Running gears; in German]. 1st ed. Berlin: Transpress Verl. f. Verkehrswesen; 1986.
114. Scheffel H. Unconventional bogie designs - their practical basis and historical background. Vehicle System Dynamics. 1995;24:497–524. doi:10.1080/00423119508969106.
115. DIN EN 13775-1:2003. Railway applications - Measuring of new and modified freight wagons - Part 1: Measuring principles; German version. Berlin, Germany: Beuth Verlag, September 2004.